Faculty of Science and Engineering
School of Earth and Planetary Sciences

Decoding Mafic Dykes in Southern Yilgarn and East Antarctica: Implications for the Supercontinent Cycle

Jutta Camilla Stark

This thesis is presented for the Degree of
Doctor of Philosophy
of
Curtin University

November 2018

DECLARATION

To the best of my knowledge and belief this thesis contains no material previously published by any other person except where due acknowledgement has been made. This thesis contains no material which has been accepted for the award of any other degree or diploma in any university.

The author acknowledges that copyright of published works contained within this thesis resides with the copyright holder(s) of those works. I warrant that I have obtained, where necessary, permission from the copyright owners to use any third-party copyright material reproduced in the thesis (e.g. questionnaires, artwork, unpublished letters), or to use any of my own published work (e.g. journal articles) in which the copyright is held by another party (e.g. publisher, co-author).

22 November 2018

Jutta Camilla Stark

Date

ABSTRACT

Mafic dyke swarms are ubiquitous in cratons worldwide and preserve snapshots of their tectonic and magmatic evolution. Mafic dykes also provide important targets for paleomagnetic studies and act as barcodes in paleogeographic reconstructions. Their utility is often hampered by the lack of high precision geochronology because dating mafic rocks can be difficult due to their mineralogy. This PhD study applies a two-step U-Pb geochronology technique to date suboptimal samples and presents the discoveries of three previously unknown mafic dykes swarms in southwestern Yilgarn Craton and the first U-Pb age for a mafic dyke swarm at Bunger Hills in East Antarctica.

The discovery of the 2615 Ma Yandinilling dyke swarm provides the first evidence of Archean mafic dykes in the Yilgarn Craton. Their emplacement supports a model involving post-orogenic collapse and lithospheric delamination following a Neoarchean orogeny and cratonisation, possibly associated with assembly of Superia. Paleogeographic reconstructions suggest that the Yilgarn and Zimbabwe cratons may have been neighbours during the Neoarchean and coeval Stockford dykes in the Central Zone of the Limpopo Belt may thus have been produced by the same tectonic event. Mafic dykes of this age are rare worldwide and have so far only been reported from the Limpopo Belt and the São Francisco Craton in South America.

The newly identified 1888 Ma Boonadgin dyke swarm is synchronous with a global episode of major crustal growth. This event is present in most Archean cratons worldwide but has been unknown in the Yilgarn Craton until now. On a regional scale, the emplacement of the dyke swarm coincides with lithospheric extension in the northern and southern margins of the craton. Paleogeographic evidence suggests that the West Australian Craton was adjacent to India during the Paleoproterozoic and raises the possibility that the Boonadgin dykes are part of the 1890 Ma Bastar-Cuddapah LIP in India. However, new paleomagnetic evidence does not support

assembly of Nuna at 1890 Ma and indicates that whereas the West Australian Craton was adjacent to the India, it was separated from other free-drifting cratonic blocks by oceans. Preliminary geochemical analysis indicates involvement of a predominantly depleted mantle source with contribution from the subcontinental lithosphere and/or the lower crust.

The 1390 Ma Biberkine dyke swarm coincides with renewed subduction along the southern margin of the West Australian Craton after a prolonged period of tectonic quiescence. Whereas it is difficult to directly link the dykes to other tectonothermal episodes regionally, current models suggest that this was a direct consequence of plate reorganisation during transition from Nuna to Rodinia. Initial geochemical evidence indicates that the predominant source was the subcontinental lithospheric mantle and/or lower crust. The Biberkine dykes are synchronous with mafic dyke swarms in many other cratons worldwide.

The first U-Pb age of 1134 Ma for a major mafic dyke swarm at Bunger Hills in East Antarctica confirms a previous Rb-Sr age of ca. 1140 Ma. The Bunger Hills, and the Windmill Islands 400 km further east, have been interpreted as part of the Yilgarn Craton during the Mesoproterozoic and the dykes were emplaced during the final stages of the Albany-Fraser Orogeny, which marks the collision of the West Australian and Mawson cratons during assembly of Rodinia. Existing and new geochemical data suggest that the source of the dykes involved an EMORB-like source reservoir that was contaminated by a lower crust-like component. Similar but undated dykes at Windmill Islands may be of same age and if this is the case, the presence of a dyke swarm of at least 400 km in extent suggests a possible mantle plume source.

The new dyke swarm ages presented in this study fall in key periods of supercontinent assembly and breakup/reconfiguration between the Neoarchean and the Mesoproterozoic and make an important contribution to the global database of mafic dyke swarms.

ACKNOWLEDGMENTS

I would like to extend my heartfelt gratitude to the following people -

- My main supervisors Zheng-Xiang Li and Xuan-Ce Wang - thank you for your ongoing support and advice along the way - I am very grateful for being given the opportunity to work on this exciting project and to find my scientific feet
- My supervisors Sergei Pisarevskiy and Fred Jourdan - thank you for your help, encouragement and advice, and for reminding me to keep smiling when things were difficult; thank you also for the excellent and at times humorous discussions that helped lighten the day
- Collaborative researchers Jian-Wei Zi and Stephen Sheppard - I am truly grateful for the steady and unwavering support you provided throughout this project, regardless of how many times I asked for help, comments and feedback (this includes the SHRIMP mounts and the n^{th} iterations of the various manuscripts that landed in your inbox)
- Collaborative researcher Simon Wilde - thank you for your support, unwavering and inspiring enthusiasm about science and for all the excellent discussions on a such a wide range of topics
- Collaborative researchers Steven Denyszyn and Ulf Söderlund - thank you for the opportunity to work with you and for the excellent discussions on TIMS dating and the use of the Wilfley table on how to best extract those pesky minute grains
- John de Laeter Centre/SHRIMP personnel Cristina Talavera and Hao Gao - thank you so much for your assistance and support with the SHRIMP; all the times I needed help with setups and beam tuning or when the coater wasn't collaborating, you were always happy to assist nomatter what the time
- Technical staff at the Earth and Planetary Science Department: Celia Mayers, Zdenka Martinelli and Andrew Wieczorek - thank you for always being so happy to help and for being just the nicest bunch of people around

- My friends in Australia and in the various other parts of the world - thank you for your support and for listening to me for hours on end, and for putting up with me when I disappeared from the radar for weeks on end!
- My family back in Europe - thank you for your unconditional love, support and understanding, and for all the encouragement and humour that kept me going
- My husband Birger - it is needless to say that without your support, patience and love I would have never made it. Thank you from the bottom of my heart.

"Remember to look up at the stars and not down at your feet. Try to make sense of what you see and wonder about what makes the universe exist. Be curious. And however difficult life may seem, there is always something you can do and succeed at. It matters that you don't just give up."

Stephen Hawking

LIST OF PUBLICATIONS INCLUDED AS PART OF THIS THESIS

This thesis contains the following published research papers:

Paper 1: Stark, J.C., Wang, X.-C., Denyszyn, S.W., Li, Z.-X., Rasmussen, B., Zi, J.-W., Sheppard, S., Liu, Y., 2017. Newly identified 1.89 Ga mafic dyke swarm in the Archean Yilgarn Craton, Western Australia suggests a connection with India. **Precambrian Res.**, **In Press**. Available at http://10.1016/j.precamres.2017.12.036

Paper 2: Stark, J.C., Wang, X.-C., Li, Z.-X., Rasmussen, B., Sheppard, S., Xi, J.-W., Clark, C., Hand, M., Li, W.-X., 2018. In situ U-Pb geochronology and geochemistry of a 1.13 Ga mafic dyke suite at Bunger Hills, East Antarctica: the end of the Albany-Fraser Orogeny. **Precambrian Res. 310, 76–92.** Available at https://doi.org/10.1016/j.precamres.2018.02.023

Paper 3: Stark, J.C., Wilde, S.A., Söderlund, U., Li, Z.-X., Rasmussen, B., Zi, J.-W., 2018. First evidence of Archean mafic dykes at 2.62 Ga in the Yilgarn Craton, Western Australia: links to cratonisation and the Zimbabwe Craton. **Precambrian Res**. **317, 1-13.** Available at https://doi.org/10.1016/j.precamres.2018.08.004

Paper 4: Stark, J.C., Wang, X.-C., Li, Z.-X., Denyszyn, S.W., Rasmussen, B., Zi, J.-W., Sheppard, S., 2018. 1.39 Ga mafic dyke swarm in southwestern Yilgarn Craton marks Nuna to Rodinia transition in the West Australian Craton. **Precambrian Res**. **316, 291-304.** Available at https://doi.org/10.1016/j.precamres.2018.08.014

LIST OF RELEVANT CO-AUTHORED PUBLICATIONS AND CONFERENCE PRESENTATIONS

Paper 5: Liu, Y., Li, Z.-X., Pisarevsky, S.A., Kirscher, U., Mitchell, R.N., **Stark, J.C.,** 2018. Palaeomagnetism of the 1.89 Ga Boonadgin dykes of the Yilgarn Craton: Possible connection with India. **Precambrian Res., In Press**. Available at https://doi.org/10.1016/j.precamres.2018.05.021

Paper 6: Liu, Y., Li, Z.-X., Pisarevsky, S.A., Kirscher, U., Mitchell, R.N., Stark, J.C., Clark, C., Hand, M., **2018**. First Precambrian palaeomagnetic data from the Mawson Craton (East Antarctica) and tectonic implications. **Sci. Rep**. **8, 16403**.

Stark, J.C., Wang, X.-C., Li, Z.-X., Rasmussen, B., Zi, J.-W., Clark, C., Hand, M., **2016**. In situ SHRIMP U-Pb geochronology and geochemistry of mafic dykes in the Yilgarn Craton , Western Australia and Bunger Hills , East Antarctica, in: **Goldschmidt Conference** Abstracts. p. 2941.

Denyszyn, S., **Stark, J.C**., Liao, A.C.-Y., Shellnutt, J.G., Li, Z.-X., **2018**. ID-TIMS U-Pb Geochronology of Mafic Dykes from the Yilgarn Craton (Australia) and Bastar Craton (India): New Piercing Points for Paleogeographic Reconstruction, **15th Annual Meeting, Asia Oceania Geosciences Society** 2-8 June 2018 Honolulu, Hawaii.

TABLE OF CONTENTS

LIST OF FIGURES

LIST OF TABLES

Chapter 1 Introduction

Mafic dykes occur on every continent on Earth and are ubiquitous in Archean cratons, where their emplacement history may span several billion years. Because they preserve tectonic and magmatic snapshots of the evolution of the craton far back in time when other geological evidence may long have been eroded away, they are excellent targets for paleomagnetic studies (Ernst and Buchan, 1997; Buchan et al., 2001; Bleeker and Ernst, 2006; Halls, 2008; Teixeira et al., 2013) and can act as proxies for paleostress fields and pre-existing crustal weaknesses (Halls, 1982; Ernst et al., 1995b; Hoek and Seitz, 1995; Halls and Zhang, 1998; Hou, 2012; Ju et al., 2013). Moreover, mafic dyke swarms, which represent the plumbing systems of now eroded Large Igneous Provinces (LIPs) (Coffin and Eldholm, 1994), can be employed as unique magmatic barcodes and geological piercing points for paleogeographic reconstructions (e.g. Ernst and Buchan, 1997; Bleeker, 2004; Bleeker and Ernst, 2006; Ernst and Bleeker, 2010; Ernst et al., 2016). LIPs are commonly linked to breakup and rifting of supercontinents, which are thought to have formed through cyclical assembly and amalgamation of cratonic blocks since the late Paleoproterozoic (Yale and Carpenter, 1998; Zhong et al., 2007; Nance and Murphy, 2013; Meert, 2014; Nance et al., 2014; Pisarevsky et al., 2014a). The supercontinent cycle is a first-order planetary scale process that has profoundly influenced the mantle dynamics, surface processes, evolution of life and the compositions of the atmosphere and the hydrosphere on Earth (Worsley et al., 1984; Nance et al., 1986; Santosh, 2010; Bradley, 2011; Murphy and Nance, 2013). The utility of large igneous provinces and their mafic dyke swarms fundamentally depends on the availability of precise geochronology and for many cratons worldwide, this is still limited due to challenges presented by the mineralogical and petrological characteristics of mafic rocks.

This PhD project focusses on improving the magmatic barcode of the Yilgarn Craton of Western Australia and the Bunger Hills of East Antarctica in order to place them in the regional and wider tectonic context of the supercontinent cycle. This is achieved through systematic dating and, where possible, preliminary geochemical characterisation of mafic dykes in an area where dense dyke swarms are known to occur. Moreover, the improved magmatic barcode for the Yilgarn Craton and the Bunger Hills contributes to the ongoing effort to date and fingerprint mafic dyke swarms globally (Ernst and Buchan, 2001a; Bleeker and Ernst, 2006; Ernst et al., 2013). This study will demonstrate how targeted sampling of dykes and use of a combination of geochronology techniques may be applied to successfully overcome some of the difficulties in mafic dyke geochronology.

1.1 Study field areas

Unlike some Archean cratons worldwide, such as the Superior Craton in North America and the Kola-Karelia Craton in northern Europe (e.g. Ernst et al., 2010; Ernst and Bleeker, 2010), the magmatic barcode of the Yilgarn Craton (section 2.2) has been limited. For Antarctica, the record is even less defined due to obvious lack of outcrop and logistical difficulties for sampling. Prior to this study, two craton-wide mafic dyke swarms at 2408 Ma and 1210 Ma (e.g. Doehler and Heaman, 1998; Wingate et al., 2000; Pidgeon and Nemchin, 2001; Wingate, 2007) and minor occurrences of 1075 Ma and 735 Ma dykes (Wingate, 2002, 2017; Wingate et al., 2004; Spaggiari et al., 2009) were known in the Yilgarn Craton. At Bunger Hills (section 2.5), which has been interpreted as part of the Yilgarn Craton at least until the Mesoproterozoic (Sheraton et al., 1993, 1995; Clark et al., 2000; Fitzsimons, 2003; Aitken et al., 2016; Tucker et al., 2017), several geochemically distinctive mafic dyke suites have been identified but none have available precise geochronology (Sheraton et al., 1990). Mapping (Geological Survey of Western Australia) and aeromagnetic data (Geoscience Australia magnetic grid of Australia V6 2015 base reference) indicate that many different dyke orientations are present across the Yilgarn Craton and many of these have been assigned to the 1210 Ma Marnda Moorn LIP, which comprises a number of sub-swarms that extend along the craton margins in a variety of orientations. However, on the basis of aeromagnetic data and evidence from other Archean cratons worldwide, it is anticipated that other dyke generations could be present. Moreover, recent studies have demonstrated that dyke orientations alone may not be a reliable indicator between different dyke generations, especially near major tectonic boundaries and structures (e.g. Hanson et al., 2004; Wingate, 2007; French and Heaman, 2010; Belica et al., 2014).

1.2 Aims and objectives

The main aims of this PhD project were set out as follows:

1. Obtain high-precision geochronology from mafic dykes in south-western Yilgarn Craton to establish how many different dyke generations are present

2. Obtain first high-precision geochronology from mafic dykes at Bunger Hills in East Antarctica, which has been interpreted part of the Yilgarn Craton during the Mesoproterozoic

3. Where possible, undertake preliminary geochemical analyses for successfully dated dykes to characterise their mantle source

4. Based on these results, clarify the tectonic setting during emplacement of the dykes and establish how the timing of their emplacement is related to the supercontinent cycle

1.3 Thesis structure

The main body of this thesis consists of four papers on newly discovered or dated mafic dyke swarms in Western Australia and East Antarctica, with ages spanning from Neoarchean to the Mesoproterozoic. An introductory chapter outlining the project aims and the thesis structure is followed by a literature review in Chapter 2 and an overview of the key aspects of the geochronology techniques in Chapter 3. Chapters 5 to 7 comprise papers that have been published/accepted for publication in Precambrian Research. Chapter 8 presents conclusions of this study and discusses the significance of the newly discovered mafic dykes in the wider context of paleogeographic reconstructions and the supercontinent cycle. Copies of the published papers and the relevant co-author approvals are found in Appendix A. Brief outlines of each chapter are given below.

Chapter 2. Literature review. This chapter reviews the relevant literature and provides background for the results presented in the following chapters.

Chapter 3. Overview of the geochronology methods. This chapter outlines the geochronology techniques employed in this study, focussing on application of the *in situ* U-Pb ion microprobe dating on mafic dykes and how it has played a key role in the success of the project.

Chapter 4. First evidence of 2.62 Ga Archean mafic dykes in the Yilgarn Craton, Western Australia and links with the Zimbabwe Craton. This chapter reports the first evidence for Archean mafic dykes (named the Yandinilling dyke swarm) in the Yilgarn Craton and discusses their links with final stages of cratonisation and lithospheric delamination. A possible connection with the Zimbabwe Craton and the Limpopo Belt in southern Africa is proposed on the basis of coeval mafic dykes, paleomagnetic evidence and tectonothermal history.

Chapter 5. Newly discovered 1.89 Ga mafic dyke swarm in the Yilgarn Craton, Western Australia suggests a connection with India. This chapter reports the discovery of a new mafic dykes (named the Boonadgin dyke swarm) in southwestern Yilgarn Craton. Combined with recent paleomagnetic evidence, the paper proposes that the Boonadgin dyke swarm is part of the 1890 Ma Cuddapah Large Igneous Province in India.

Chapter 6. 1.39 Ga mafic dyke swarm in southwestern Yilgarn Craton marks Nuna to Rodinia transition in the West Australian Craton. This chapter discusses the discovery of 1.39 Ga mafic dykes (named the Biberkine dyke swarm) and argues that their emplacement marks the Nuna to Rodinia transition in the West Australian Craton after a hiatus of 200 m.y. in tectonic activity.

Chapter 7. First U-Pb geochronology for a 1.13 Ga Ma mafic dyke suite at Bunger Hills, East Antarctica marks the end of the Albany-Fraser Orogeny. This chapter presents the first U-Pb geochronology from a mafic dyke suite at Bunger Hills and links their emplacement with the final stages of the Mesoproterozoic Albany-Fraser Orogeny.

Chapter 8. Conclusions and the significance of mafic dykes as tectonic markers in the supercontinent cycle. This chapter discusses the application of mafic dykes in paleogeographic reconstructions with focus on the tectonic implications and presents conclusions from this PhD study.

1.4 References

Aitken, A.R.A., Betts, P.G., Young, D.A., Blankenship, D.D., Roberts, J.L., Siegert, M.J., 2016. The Australo-Antarctic Columbia to Gondwana transition. Gondwana Res. 29, 136–152.

Belica, M.E., Piispa, E.J., Meert, J.G., Pesonen, L.J., Plado, J., Pandit, M.K., Kamenov, G.D., Celestino, M., 2014. Paleoproterozoic mafic dyke swarms from the Dharwar craton; paleomagnetic poles for India from 2.37 to 1.88Ga and rethinking the Columbia supercontinent. Precambrian Res. 244, 100–122.

Bleeker, W., 2004. Taking the pulse of planet Earth: a proposal for a new multi-disciplinary flagship project in Canadian solid Earth sciences. Geosci. Canada 31.

Bleeker, W., Ernst, R., 2006. Short-lived mantle generated magmatic events and their dyke swarms: the key unlocking Earth's paleogeographic record back to 2.6 Ga, in: Hanski, E.J., Mertanen, S., Rämö, O.T., Vuollo, J. (Eds.), Dyke Swarms—time Markers of Crustal Evolution: Selected Papers of the Fifth International Dyke Conference in Finland, Rovaniemi, Finland, 31 July- 3 Aug 2005 & Fourth International Dyke Conference, Kwazulu-Natal, South Africa 26-29 June 2001. CRC Press, London, pp. 3–26.

Bradley, D.C., 2011. Secular trends in the geologic record and the supercontinent cycle. Earth-Science Rev. 108, 16–33.

Buchan, K.L., Ernst, R.E., Hamilton, M.A., Mertanen, S., Pesonen, L.J., Elming, S.-Å., 2001. Rodinia: the evidence from integrated palaeomagnetism and U–Pb geochronology. Precambrian Res. 110, 9–32.

Clark, D.J., Hensen, B.J., Kinny, P.D., 2000. Geochronological constraints for a two-stage history of the Albany – Fraser Orogen , Western Australia. Precambrian Res. 102, 155–183.

Coffin, M.F., Eldholm, O., 1994. Large igneous provinces: crustal structure, dimensions, and external consequences. Rev. Geophys. 32, 1–36.

Doehler, J.S., Heaman, L.M., 1998. 2.41 Ga U–Pb Baddeleyite ages for two gabbroic dykes from the Widgiemooltha swarm, Western Australia: a Yilgarn–Lewisian connection, in: Geological Society of America 1998 Annual Meeting, Abstracts with Programs. Geological Society of America, pp. 291–292.

Ernst, R., Bleeker, W., 2010. Large igneous provinces (LIPs), giant dyke swarms, and mantle plumes: significance for breakup events within Canada and adjacent regions from 2.5 Ga to the Present. Can. J. Earth Sci. 47, 695–739.

Ernst, R.E., Bleeker, W., Söderlund, U., Kerr, A.C., 2013. Large Igneous Provinces and supercontinents: Toward completing the plate tectonic revolution. Lithos 174, 1–14.

Ernst, R., Srivastava, R., Bleeker, W., Hamilton, M., 2010. Precambrian Large Igneous Provinces (LIPs) and their dyke swarms: New insights from high-precision geochronology integrated with paleomagnetism and geochemistry. Precambrian Res. 183, vii–xi.

Ernst, R.E., Buchan, K.L., 2001. Large mafic magmatic events through time and links to mantle-plume heads, in: Geological Society of America Special Paper 352. pp. 483–576.

Ernst, R.E., Buchan, K.L., 1997. Giant radiating dyke swarms: their use in identifying pre-Mesozoic large igneous provinces and mantle plumes, in: Large Igneous Provinces: Continental, Oceanic, and Planetary Flood Volcanism. American Geophysical Union Monograph 100, pp. 297–333.

Ernst, R.E., Hamilton, M.A., Soderlund, U., Hanes, J.A., Gladkochub, D.P., Okrugin, A. V, Kolotilina, T., Mekhonoshin, A.S., Bleeker, W., LeCheminant, A.N., Buchan, K.L., Chamberlain, K.R., Didenko, A.N., 2016. Long-lived connection between southern Siberia and northern Laurentia in the Proterozoic. Nat. Geosci 9, 464–469.

Ernst, R.E., Head, J.W., Parfitt, E., Grosfils, E., Wilson, L., 1995. Giant radiating dyke swarms on Earth and Venus. Earth-Science Rev. 39, 1–58.

Fitzsimons, I.C.W., 2003. Proterozoic basement provinces of southern and southwestern Australia, and their correlation with Antarctica. Geol. Soc. London, Spec. Publ. 206, 93–130.

French, J.E., Heaman, L.M., 2010. Precise U-Pb dating of Paleoproterozoic mafic dyke swarms of the Dharwar craton, India: Implications for the existence of the Neoarchean supercraton Sclavia. Precambrian Res. 183, 416–441.

Halls, H.C., Zhang, B., 1998. Uplift structure of the southern Kapuskasing zone from 2.45 Ga dike swarm displacement. Geology 26, 67–70.

Hanson, R.E., Gose, W.A., Crowley, J.L., Ramezani, J., Bowring, S.A., Bullen, D.S., Hall, R.P., Pancake, J.A., Mukwakwami, J., 2004. Paleoproterozoic intraplate magmatism and basin development on the Kaapvaal Craton: Age, paleomagnetism and geochemistry of~ 1.93 to~ 1.87 Ga post-Waterberg dolerites. South African J. Geol. 107, 233–254.

Hoek, J.D., Seitz, H.-M., 1995. Continental mafic dyke swarms as tectonic indicators: an example from the Vestfold Hills, Antarctica. Precambrian Res. 75, 121–139.

Hou, G., 2012. Mechanism for three types of mafic dyke swarms. Geosci. Front. 3, 217–223.

Ju, W., Hou, G., Hari, K.R., 2013. Mechanics of mafic dyke swarms in the Deccan Large Igneous Province: Palaeostress field modelling. J. Geodyn. 66, 79–91.

Meert, J.G., 2014. Strange attractors, spiritual interlopers and lonely wanderers: The search for pre-Pangean supercontinents. Geosci. Front. 5, 155–166.

Murphy, J.B., Nance, R.D., 2013. Speculations on the mechanisms for the formation and breakup of supercontinents. Geosci. Front. 4, 185–194.

Nance, R.D., Murphy, J.B., 2013. Origins of the supercontinent cycle. Geosci. Front. 4, 439–448.

Nance, R.D., Murphy, J.B., Santosh, M., 2014. The supercontinent cycle: A retrospective essay. Gondwana Res. 25, 4–29.

Nance, R.D., Worsley, T.R., Moody, J.B., 1986. Post -Archean biogeochemical cycles and long-term episodicity in tectonic processes. Geology 14, 514–518.

Pidgeon, R.T., Nemchin, A.A., 2001. 1.2 Ga Mafic dyke near York, southwestern Yilgarn Craton, Western Australia. Aust. J. Earth Sci. 48, 751–755.

Pisarevsky, S.A., Elming, S.-Å., Pesonen, L.J., Li, Z.-X., 2014. Mesoproterozoic paleogeography: Supercontinent and beyond. Precambrian Res. 244, 207–225.

Santosh, M., 2010. Supercontinent tectonics and biogeochemical cycle: A matter of “life and death.” Geosci. Front. 1, 21–30.

Sheraton, J.W., Black, L.P., McCulloch, M.T., Oliver, R.L., 1990. Age and origin of a compositionally varied mafic dyke swarm in the Bunger Hills, East Antarctica. Chem. Geol. 85, 215–246.

Sheraton, J.W., Tingey, R.J., Black, L.P., Oliver, R.L., 1993. Geology of the Bunger Hills area, Antarctica: implications for Gondwana correlations. Antarct. Sci. 5, 85–102.

Sheraton, J.W., Tingey, R.J., Oliver, R.L., Black, L.P., 1995. Geology of the Bunger Hills-Denman Glacier region, East Antarctica, BMR Bulletin 244. Australian Geological Survey Organisation.

Spaggiari, C. V, Bodorkos, S., Barquero-Molina, M., Tyler, I.M., Wingate, M.T.D., 2009. Interpreted bedrock geology of the South Yilgarn and of the South Yilgarn and Central Albany-Fraser Orogen, Western Australia, Geological Survey of Western Australia Record 2009/10.

Teixeira, W., D'Agrella-Filho, M.S., Hamilton, M.A., Ernst, R.E., Girardi, V.A.V., Mazzucchelli, M., Bettencourt, J.S., 2013. U–Pb (ID-TIMS) baddeleyite ages and paleomagnetism of 1.79 and 1.59Ga tholeiitic dyke swarms, and position of the Rio de la Plata Craton within the Columbia supercontinent. Lithos 174, 157–174.

Tucker, N.M., Payne, J.L., Clark, C., Hand, M., Taylor, R.J., Kylander-Clark, A.R.C., 2017. Proterozoic reworking of Archean (Yilgarn) basement in the Bunger Hills, east Antarctica. Precambrian Res. 298, 16–38.

Wingate, M.T.D., 2017. Mafic dyke swarms and large igneous provinces in Western Australia get a digital makeover, in: Geological Survey of Western Australia Record 2017/2. pp. 4–8.

Wingate, M.T.D., 2007. Proterozoic mafic dykes in the Yilgarn Craton, in: Proceedings of Geoconferences (WA) Inc. Kalgoorlie 2007 Conference, Kalgoorlie, Western Australia. pp. 80–84.

Wingate, M.T.D., 2002. Age and Paleomagnetism of Dolerite Sills Intruded Into the Bangemall Supergroup on the Edmund 1: 250 000 Map Sheet, Western Australia. Geological Survey of Western Australia.

Wingate, M.T.D., Campbell, I.H., Harris, L.B., 2000. SHRIMP baddeleyite age for the Fraser dyke swarm, southeast Yilgarn Craton, Western Australia. Aust. J. Earth Sci. 47, 309–313.

Wingate, M.T.D., Pirajno, F., Morris, P.A., 2004. Warakurna large igneous province: a new Mesoproterozoic large igneous province in west-central Australia. Geology 32, 105–108.

Worsley, T.R., Nance, D., Moody, J.B., 1984. Global tectonics and eustasy for the past 2 billion years. Mar. Geol. 58, 373–400.

Yale, L.B., Carpenter, S.J., 1998. Large igneous provinces and giant dike swarms: proxies for supercontinent cyclicity and mantle convection. Earth Planet. Sci. Lett. 163, 109–122.

Zhong, S., Zhang, N., Li, Z.-X., Roberts, J.H., 2007. Supercontinent cycles, true polar wander, and very long-wavelength mantle convection. Earth Planet. Sci. Lett. 261, 551–564.

Chapter 2 Mafic dykes and supercontinent cycles

This PhD project focusses on the identification and use of mafic dyke swarms as magmatic markers in the regional and wider tectonic context of the supercontinent cycle. This Chapter presents a literature review of Large Igneous Provinces and mafic dyke swarms, and their role in unravelling the supercontinent cycle. Regional geology for the areas involved, the Yilgarn Craton of Western Australia and the Bunger Hills of East Antarctica, is also reviewed. It should be noted that some overlap between this Chapter and Chapters 4-7 necessarily arises from the latter being self-contained publications. Specifically,

- Regional geology, tectonothermal evolution and mafic dykes of the Yilgarn Craton are discussed in sections 4.3.1, 5.3 and 6.3.

- Regional geology and mafic dykes of the Bunger Hills are discussed in section 7.3.

- The Albany-Fraser Orogen is discussed in sections 6.8.2 and 7.9.2.1.

2.1 Large Igneous Provinces

Large igneous provinces (LIPs; Coffin and Eldholm, 1994) are high-volume, short-duration, predominantly mafic intraplate magmatic events that occur throughout Earth's history (Figure 2.1) (Ernst and Buchan, 1997, 2001a; Isley and Abbott, 1999; Abbott and Isley, 2002a; Bryan and Ernst, 2008; Bryan et al., 2010; Ernst et al., 2010; Ernst, 2014). They are defined as magmatic provinces with areal extents > 0.1 Mkm^2 and maximum lifespans of ~50 Ma, and include continental and oceanic flood basalts, regional dyke swarms, sill provinces and associated silicic and ultramafic intrusives (Bryan and Ernst, 2008; Ernst, 2014). The origins of large igneous provinces are under debate and they have been variably associated with mantle plumes (Richards et al., 1989; Campbell and Griffiths, 1990; Ernst and Buchan, 2001a, 2001b; Courtillot et al., 2003; Ernst and Bleeker, 2010), back-arc extension (Smith, 1992; Rivers and Corrigan, 2000; Puffer, 2003), breakup of supercontinents

(Courtillot et al., 1999; Ernst and Bleeker, 2010; Ernst et al., 2013), lithospheric mantle delamination events (Elkins Tanton and Hager, 2000; Elkins-Tanton, 2005), Earth's deep volatile cycling (Wang et al., 2015, 2016), decompression melting during lithospheric extension and rifting (White and McKenzie, 1989), craton edge-driven convection (Anderson, 1995; King and Anderson, 1995) and meteorite impacts (Abbott and Isley, 2002b; Jones et al., 2002; Ingle and Coffin, 2004). Large igneous provinces are intimately connected with mantle dynamics and supercontinent cycles (e.g. Condie, 2004; Prokoph et al., 2004; Bleeker and Ernst, 2006; Ernst et al., 2008; Li and Zhong, 2009; Clowes et al., 2010; Goldberg, 2010), formation of major mineral deposits (e.g. Pirajno and Hoatson, 2012; Ernst and Jowitt, 2013) and the evolution of life and the compositions of the atmosphere and the hydrosphere (Worsley et al., 1984; Nance et al., 1986; Wignall, 2001; Jourdan et al., 2005; Santosh, 2010; Sobolev et al., 2011; Murphy and Nance, 2013; Young, 2013; Ernst and Youbi, 2017). The flood basalt members of Phanerozoic LIPs are preserved but only plumbing systems remain for the majority of Precambrian LIPs, represented by mafic dyke swarms (e.g. Bryan and Ernst, 2008; De Kock et al., 2014; Ernst, 2014 and references therein).

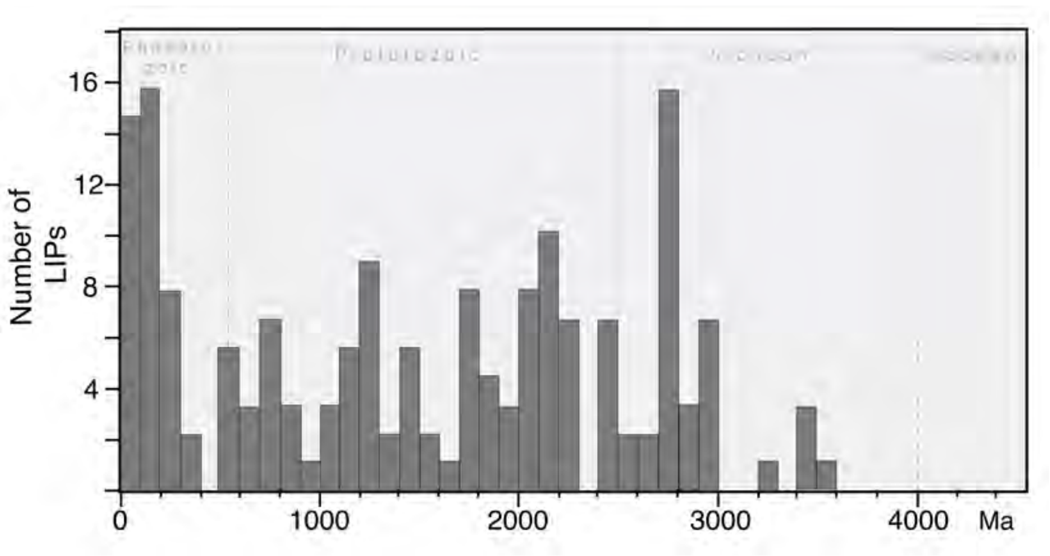

Figure 2.1 Age distribution of Large Igeous Provinces (LIPs) through time. After Prokoph et al. (2004).

2.1.1 Formation mechanisms of large igneous provinces

Most large igneous provinces have been linked to mantle plumes and their frequency and distribution is employed as a proxy of mantle plume events (Ernst and Buchan, 1997, 2001a; Bleeker and Ernst, 2006; Ernst and Bleeker, 2010; Condie et al., 2015). When a thermal buoyancy-driven mantle plume head rising from deep mantle and impinges upon the base of the lithosphere, tholeiitic flood basalts arise from the cooler regions of the plume head with a mixture of source mantle and entrained lower-mantle material (Figure 2.2) (Richards et al., 1989; Campbell and Griffiths, 1990; Ernst and Buchan, 2001a; Courtillot et al., 2003). Clusters of plumes, or superplumes, have been linked to breakup and rifting of supercontinents (Morgan, 1971; Cande and Stegman, 2011) including Rodinia (Li et al., 2003, 2008; Li and Zhong, 2009) and Pangea/Gondwana (Vaughan and Storey, 2007).

Other proposed mechanisms involve decompression melting of the mantle due to thinned lithosphere (Figure 2.2) (at depths greater than ca. 115 km, hydrostatic pressure prevents partial melting of fertile non-hydrous mantle). These include lithospheric extension during rifting without plume involvement (i.e. with ambient mantle potential temperature gradients; Wijk et al., 2001) and with plume involvement (White and McKenzie, 1989) and lithospheric delamination of gravitationally unstable lower lithosphere (Elkins Tanton and Hager, 2000; Elkins-Tanton, 2005). Instead of active thinning of the lithosphere, edge-driven convection involves decompression melting through focussed thermal upwelling of mantle along the edges of cratons, where the lithosphere is thinner (King and Anderson, 1995). This model also explains why most LIPs are found near craton margins. All these mechanisms would be expected to involve melting of the mantle source at relatively shallow depths (<115 km), however partial melting could be deeper if the source region was hydrous and/or metasomatically enriched (Hirschmann et al., 1999) such as in subduction zones. No lithospheric extension or plume is necessarily required if deep upwelling of hydrous mantle material displaced by stagnant subducted slabs at the 660 km mantle transition zone rise to the base of the lithosphere and fertilise the shallow mantle at the lithosphere-asthenosphere boundary (Figure 2.2) (Wang et al., 2015, 2016).

2.2 Mafic dyke swarms

2.2.1 Mafic dyke swarms as geodynamic and tectonic indicators

Mafic dykes are intrusive tabular bodies of mafic composition that intrude pre-existing crustal fractures and commonly have very high length to width ratios. They are excellent indicators of paleostress fields and pre-existing crustal weaknesses (Halls, 1982; Ernst et al., 1995b; Hoek and Seitz, 1995; Halls and Zhang, 1998; Hou, 2012; Ju et al., 2013), and provide good targets for paleomagnetic studies (Evans, 1968, 1999, Li et al., 1996, 2004; Wingate and Evans, 2003; Pesonen et al., 2003; Li and Evans, 2011; Piispa et al., 2011; Belica et al., 2014; Pisarevsky et al., 2015, 2014b; Liu et al., 2018). Mafic dyke swarms, which are considered to represent plumbing systems of now-eroded flood basalts, comprise a large number of parallel or radially oriented dykes and can act as important markers for paleogeographic reconstructions (Figure 2.3) (Ernst and Buchan, 1997; Buchan et al., 2001; Bleeker and Ernst, 2006; Ernst and Srivastava, 2008; Heaman, 2008; Ernst et al., 2010, 2013). Aerial extent of dyke swarms can be used as proxy of their volume (Ernst, 2014) and this is assisted by regional aeromagnetic data, where mafic dykes often form prominent and distinctive features (e.g. Tucker and Boyd, 1987; Boyd and Tucker, 1990; Goldberg, 2010). However, without comprehensive geochronology it is difficult to assess the actual size of a dyke swarm and its designation as a LIP can be preliminary pending further studies.

The LIP magmatic barcode method is based on systematic use of coeval dyke swarms to match conjugate margins of crustal blocks (Bleeker, 2003, 2004; Bleeker and Ernst, 2006; Ernst and Srivastava, 2008; Ernst et al., 2008, 2013, 2016; Söderlund et al., 2010). Giant dyke swarms are of particular importance because of they extend into the craton interior (preservation) and can provide unique piercing points (Halls, 1982; Bleeker and Ernst, 2006; Heaman, 2008). Presence of a dyke swarm may be the only preserved evidence for a major extensional or rifting event in the craton (Goldberg, 2010) and the magmatic barcode method can be employed to define the relative orientations of the now-dispersed crustal blocks and to constrain correlations in the absence of robust paleomagnetic poles. The LIP magmatic barcode method is critically dependent on the availability of robust high-precision

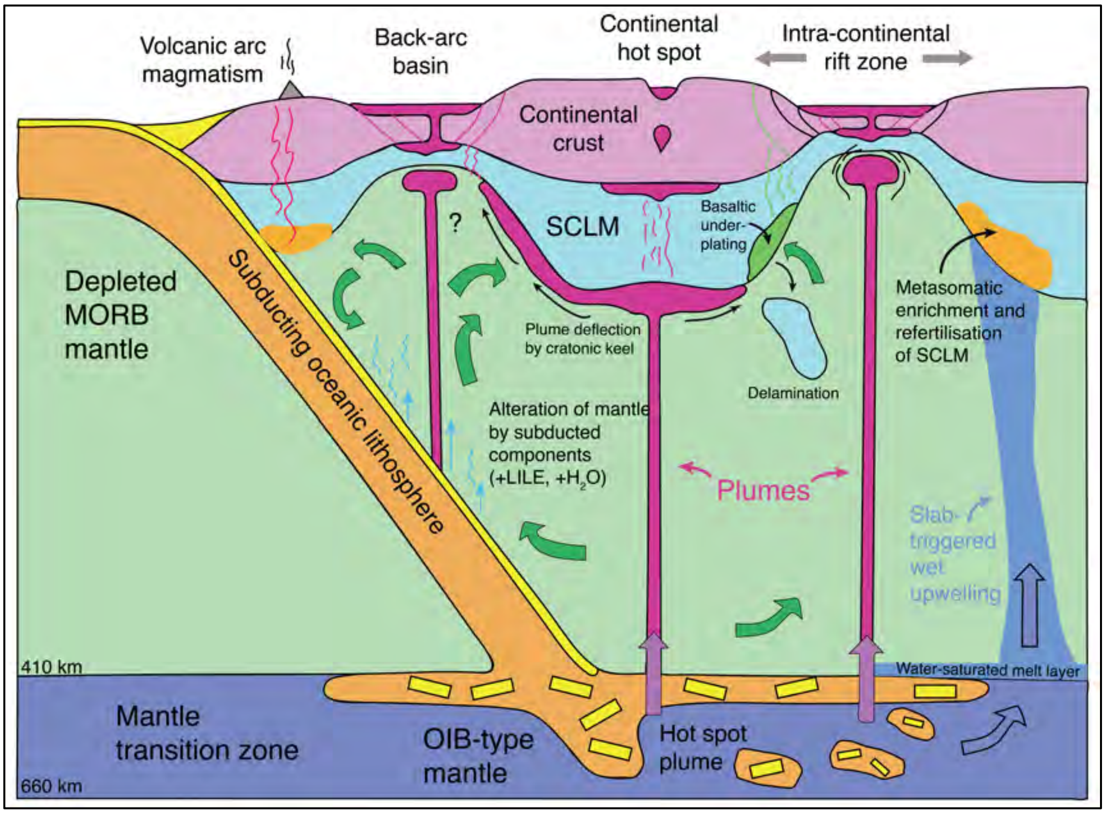

Figure 2.2 Various formation mechanisms of continental flood basalts. Redrafted and modified from Winter (2014)*. MORB = mid-ocean ridge basalt, OIB = ocean island basalt, SCLM = subcontinental lithospheric mantle. Slab-triggered wet upwelling after Wang et al. (2015, 2016).*

geochronology and to this end, global efforts to create a worldwide LIP database are ongoing (Ernst and Buchan, 2001a; Bleeker and Ernst, 2006). Some Archean cratons, such as the Superior Craton in North America and the Kola-Karelia Craton in northern Europe, have well characterised barcodes whereas others, including the Yilgarn Craton of Western Australia and the Zimbabwe Craton of southern Africa, still lack comprehensive high-precision geochronology (Ernst et al., 2013).

Dyke trends are important indicators of the tectonic setting during their emplacement. Dykes originating from the same magmatic event have been found to generally exhibit consistent linear trends or regional radiating patterns (e.g. Figure 2.3) (e.g. Halls, 1982; Tucker and Boyd, 1987; Buchan et al., 2010; Ernst, 2014). For example, giant mafic dyke swarms (>300 km long; Ernst et al., 1995) with typical average widths between 10 m and 40 m can be traced hundreds of kilometers (Ernst et al., 1995a; Ernst, 2014). In some cases, the dyke orientation alone cannot be reliably used to distinguish between different dyke generations, especially near major tectonic boundaries and craton scale structures such as continental rifts (e.g. Hanson et al., 2004; Wingate, 2007; French and Heaman, 2010; Belica et al., 2014). An example of this is the Marnda Moorn LIP of the Yilgarn Craton, which has been linked to a mantle plume (Dawson et al., 2003; Wang et al., 2014), and comprises several sub-swarms that extend along and often parallel to the craton margins (Isles and Cooke, 1990; Evans, 1999; Wingate et al., 2000; Pidgeon and Nemchin, 2001; Pidgeon and Cook, 2003; Wingate and Pidgeon, 2005; Wingate, 2007; Claoué-Long and Hoatson, 2009).

Figure 2.3 Enhanced Google Earth satellite image of the Vestfold Hills, East Antarctica, showing five different dyke generations. The NE trending dykes have been dated at ca. 1245 Ma, the north-trending dykes at ca. 1380 Ma, the NW trending dykes at ca. 1754 Ma, the WNW trending dykes at ca. 2400 Ma and the west-trending dykes at ca. 2240 Ma (Lanyon et al., 1993). *The centre of the image is approximately 68°30'41 S 78° 06'43 E at eye altitude of 1.5 km.*

Regional dyke swarms are generally emplaced parallel to the principal stress direction (i.e. parallel to the maximum compressive stress direction; Pollard, 1987;

Hou et al., 2006; Hou, 2012) and on a regional scale their emplacement is controlled by plate-boundary stresses (where plates interact, compressive stress during convergence and tensional stress during extension). This is demonstrated well by the ca. 1267 Ma Mackenzie LIP in North America (Heaman and Le Cheminant, 1988; LeCheminant and Heaman, 1989; Baragar et al., 1996; Ernst et al., 2008). The Mackenzie dyke swarm has a gently radiating geometry for over 2000 km and was emplaced from a deep mantle source, vertically near the plume centre and horizontally at distances > 1000 km under a uniform regional stress field acting on the craton margin (Ernst and Baragar, 1992; Hou et al., 2010). Moreover, at Vestfold Hills in East Antarctica, Hoek and Seitz (1995) used multiple generations of mafic dykes (Figure 2.3) to constrain the geodynamic and tectonothermal evolution of the region.

2.2.2 Geochemistry of mafic dyke swarms

Geochemistry of LIPs and mafic dykes reflects the diversity of their sources and their mechanisms of formation are under vigorous debate. Of particular interest is whether LIPs are mantle plume related because mantle plumes are thought to play a key role in the breakup and rifting of supercontinents. This aspect is discussed in more detail in section 2.3.2.

Heterogeneities of the subcontinental lithospheric mantle (SCLM), secular changes of the asthenospheric mantle composition and crustal contamination play a key role in petrogenesis of mafic rocks and complicate interpretation of geochemical data (Allègre et al., 1982; Hart, 1984; Zindler and Hart, 1986; Hawkesworth et al., 1990, 1995; Campbell, 2002; Stracke et al., 2005; Ernst et al., 2005; Jourdan et al., 2007; Wang et al., 2013, 2015, 2016; Li et al., 2014; Merle et al., 2014; Heinonen et al., 2014, 2016; Hughes et al., 2014). The mantle source of many LIPs has been interpreted to involve both a depleted asthenospheric component and heterogeneous SCLM whereas a mantle plume source has been inferred for others, such as the Matachewan (Ciborowski et al., 2015), Marnda Moorn (Wang et al., 2014) and Siberian LIPs (Sobolev et al., 2011). Many continental flood basalts display arc-like trace element signatures that are characterised by relative depletion of High Field Strength elements (HFSE) such as Nb-Ta-Ti and enrichment in Large Ion Lithophile

Elements (LILE) such as Rb, Sr and Ba. These are thought to originate from hydrated long-term SCLM reservoirs enriched by fluids released from subducted slabs (Hawkesworth et al., 1995; Puffer, 2001; Jourdan et al., 2007; Murphy and Dostal, 2007; Wang et al., 2008, 2014, 2016) or from crustal contamination or asthenospheric mantle melts (Hawkesworth et al., 1995; Jourdan et al., 2007; Xia, 2014). Recent studies have also raised the possibility that the fluids may originate at the mantle transition zone at ca. 660 km depth, where stagnated subducted slabs undergo dehydration and phase transitions (Bercovici and Karato, 2003; Ivanov and Litasov, 2014; Pearson et al., 2014). The Cenozoic Chifeng continental flood basalts have been associated with such deep wet upwelling (Wang et al., 2015). Identification of a plume source is not unambiguous but involvement of an ocean island basalt (OIB) type component, high mantle potential temperatures during partial melting of the source region and lack of HFSE depletion (e.g. Nb, Ta) are considered plume characteristics (Puffer, 2001). As discussed above, these can be masked if SCLM or crustal contamination is significant.

Geochemical characteristics of dykes emplaced during the same magmatic event can be very complex even in a limited geographic area, such as the Bunger Hills of East Antarctica (ca. 300 km^2 of outcrop) where at least six distinct mantle reservoirs are thought to be involved in the genesis of five compositionally distinct dyke groups (Sheraton et al., 1990; Condie, 1997). Previous studies have demonstrated that within a single dyke swarm, each dyke is a unique emplacement event with consistent geochemical composition (incompatible element ratios) and paleomagnetic direction along-strike, but these are nevertheless different from a nearby dyke of the same swarm (Halls, 1986; Buchan et al., 1993, 2007). This is also the case at Bunger Hills (Sheraton et al., 1990). Given the further possibility that in some cases the dyke trends are not unique within a dyke swarm, geochemical data for mafic dykes should ideally be accompanied by robust geochronology to ensure that the dykes belong to the same magmatic episode.

2.3 Supercontinent cycles

2.3.1 Supercontinents through time

The concept of what constitutes a supercontinent is not strictly defined but in general terms the term is applied to a large landmass that consists of an assembly of most, but not necessarily all, of Earth's continents (Hoffman, 1999; Gutiérrez-Alonso et al., 2008; Li et al., 2008; Meert, 2012; Evans et al., 2016). Worsley, Nance and others (Worsley et al., 1984, 1985; Nance et al., 1986) predicted the existence of five supercontinents at ca. 600 Ma, 1100 Ma, 1800-1600 Ma, 2000 Ma and 2600 Ma and there is current consensus on the existence of at least two Precambrian and two Phanerozoic supercontinents (Figure 2.4). Timing of Gondwana assembly is contentious but it is thought to have amalgamated between ca. 750 Ma and 500 Ma (Bradley, 2008, 2011; Li et al., 2008; Stampfli et al., 2013; Evans et al., 2016), overlapping with the final breakup of Rodinia at ca. 520 Ma (Bradley, 2008 and references therein) whereas Pangea formed by ca. 300 Ma, followed by breakup starting at ca. 180 Ma (Bradley, 2011; Stampfli et al., 2013). Rodinia assembled between ca. 1300 Ma and 900 Ma (Condie, 2003; Li et al., 2008) and disassembled between ca. 750 Ma and 550 Ma (Li et al., 2008), although Bradley (2011) argues for ca. 1000-850 Ma tenure on the basis of passive margin and detrital zircon records. Timing of pre-Rodinia supercontinents is less certain. Estimates for the assembly of Nuna (Hoffman, 1997) or Columbia (Rogers and Santosh, 2002) vary between ca. 1850 Ma and 1600 Ma, with breakup sometime between 1450 Ma and 1380 Ma (Rogers and Santosh, 2002; Zhao et al., 2002; Bradley, 2011; Pisarevsky et al., 2014a; Nordsvan et al., 2018), although Bradley (2011) suggests that Nuna remained intact until at least 1000 Ma. The oldest hypothesised supercontinents include Kenorland at ca. 2500 Ma (Williams et al., 1991) and Ur/expanded Ur between ca. 3000-1500 Ma (Rogers, 1996) with Arctica and Atlantica supercratons at ca. 2500-2000 Ma (Rogers, 1996). Moreover, supercratons Vaalbara, Sclavia and Superia have been proposed at ca. 3470-2700 Ma, ca. 2600-2200 Ma and ca. 2700-2100 Ma, respectively (Bleeker, 2003, 2004; Bleeker and Ernst, 2006; Ernst and Bleeker, 2010). Bradley (2008) argued for slightly different timings on the basis of passive margin ages, with Vaalbara at ca. 3470-2685 Ma, Superia at ca. 2700-2300 Ma and Sclavia at ca. 2600-2090 Ma.

2.3.2 Supercontinent cycles and LIPs

Cyclicity in the assembly, amalgamation and breakup of such continents was first proposed by Worsley et al. (Worsley et al., 1982, 1984), who argued that these would be manifested as episodic peaks in orogenic activity and rifting with associated mafic dyke swarms (LIPs). Increasing evidence suggests that assembly and breakup of supercontinents may have been a quasi-periodical phenomenon since at least the late Paleoproterozoic (Worsley et al., 1984, 1985, 1986, 1991, Nance et al., 1986, 2014; Worsley and Nance, 1989; Hoffman, 1998; Zhao et al., 2002; Rogers and Santosh, 2003, 2004; Zhong et al., 2007; Bradley, 2008, 2011; Santosh, 2010; Condie, 2011; Ernst et al., 2013; Murphy and Nance, 2013; Nance and Murphy, 2013; Pisarevsky et al., 2014a; Meert, 2014; Pastor-Galán et al., 2018). Hawkesworth et al. (2010, 2016) proposed that peaks of zircon U-Pb crystallization ages are associated with periods of crustal thickening, continental collision, and thereby also assembly of supercontinents. Similarly, the minima and maxima in U-Pb ages of zircons from granite (Condie et al., 2009) and from detrital zircon and passive margin abundances in both the Phanerozoic and the Precambrian have been linked with supercontinent cycles (Bradley, 2008, 2011).

LIPs and giant mafic dyke swarms have commonly been used as proxies for breakup and rifting of supercontinents (Figure 2.4) (Yale and Carpenter, 1998; Courtillot et al., 1999; Ernst and Bleeker, 2010; Ernst et al., 2013; Condie et al., 2015). Based on the LIP record, Yale and Carpenter (1998) defined seven possible supercontinents since 3000 Ma (2800-2700 Ma, 2550-2400 Ma, 2250-2000 Ma, 1900-1600 Ma, 1350-1000 Ma, 850-550 Ma and 350-0 Ma) and identified a 300-500 m.y. periodicity in the supercontinent cycle. Similarly, Prokoph et al. (2004) used the global LIP record (154 LIPs) to identify four LIP age distribution maxima (2800–2700 Ma, 2200–2100 Ma, 1800– 1700 Ma and 1300–1200 Ma) and four minima (2400–2300 Ma, 1600–1500 Ma, 900–800 Ma and 500–300 Ma). These minima correlate with zircon and passive margin records and coincide with some of the proposed tenures of Gondwana, Rodinia and Nuna (Bradley, 2011). Condie et al. (2015) found major periodicity at 250, 150, 100 and 50 million years in the LIP record and pointed out that not all LIP forming events are associated with zircon-producing events (granite formation), commonly linked to orogenic activity.

As discussed in section 2.2.1, the LIP method for paleogeographic reconstructions method utilises mafic dyke swarms as barcodes to match magmatic events on cratonic blocks (Bleeker, 2003; Ernst and Bleeker, 2010). The effectiveness of this approach depends on identification of the main (major) intraplate magmatic events within a craton and the extent and location of the magmatic event (must be large enough to extend across several cratons and not too far away from the craton margins). The magmatic barcode method benefits from the inherent characteristics of mafic dyke swarms (Bleeker, 2004; Bleeker and Ernst, 2006; Ernst et al., 2013), including rapid emplacement that can be dated precisely, typically large footprint across the craton, excellent paleostress and piercing point information and ability to yield high-quality paleomagnetic poles.

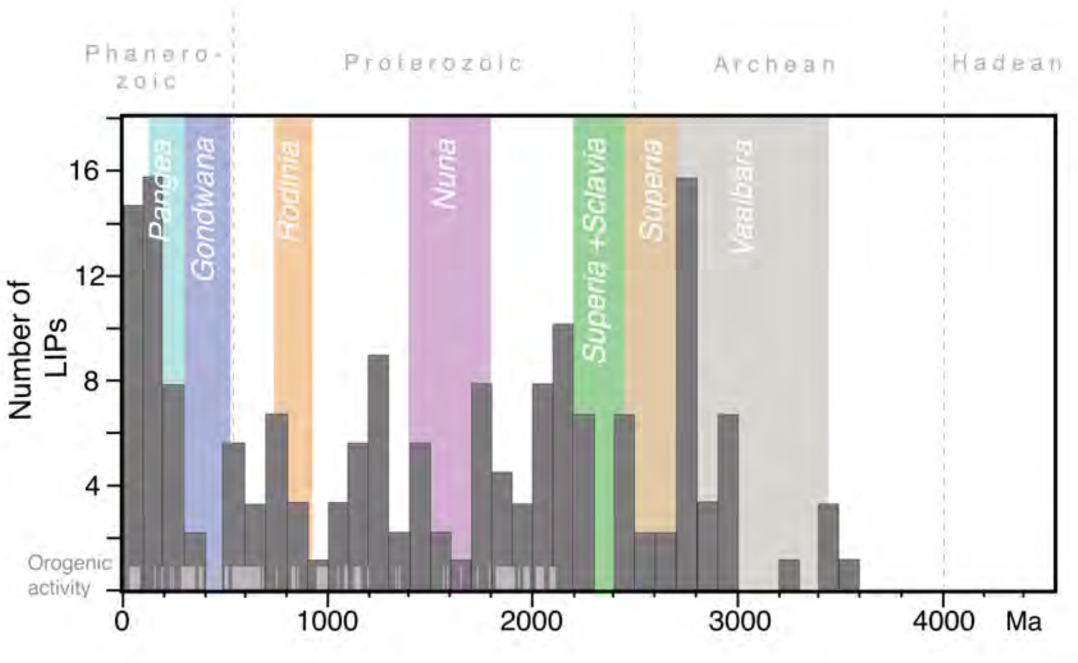

*Figure 2.4 Age distribution of Large Igneous Provinces showing hypothesised supercontinent tenures and orogenic activity. LIP data after Prokoph et al. (2004) and orogenic activity is from Condie and Aster (*2013, *Fig.3B). See section 2.3.1 for discussion on supercontinents.*

2.4 Mafic dykes of the Yilgarn Craton, Western Australia

2.4.1 Regional geology

The Archean Yilgarn Craton is a ca. 900 x 1000 km granite-greenstone crustal block that lies in the southern part of the West Australian Craton. It is divided into the South West, Narryer, Youanmi, Kalgoorlie, Kurnalpi and Burtville terranes, the latter three forming the Eastern Goldfields Superterrane (Figure 2.5) (Cassidy et al., 2006). The craton is bounded by three Proterozoic orogenic belts: the ca. 2005─570 Ma Capricorn Orogen in the north (Cawood and Tyler, 2004; Sheppard et al., 2010a; Johnson et al., 2011), the ca. 1815─1140 Ma Albany-Fraser Orogen in the south and east (Nelson et al., 1995a; Clark et al., 2000; Spaggiari et al., 2015), and the ca. 1090–525 Ma Pinjarra Orogen in the west (Myers, 1990; Wilde, 1999; Ksienzyk et al., 2012). Most of the terranes formed between ca. 3050 and 2550 Ma and whereas the South West and Narryer Terranes in the west comprise high-grade supracrustal rocks, granitic gneisses and granites, the Youanmi and Eastern Goldfields Terranes in the east are dominated by greenstone belts separated by granites and granitic gneisses (Figure 2.6) (e.g., Gee et al., 1981; Pidgeon and Wilde, 1990; Myers, 1993; Wilde et al., 1996; Nelson, 1997; Cassidy et al., 2002; Barley et al., 2003).

Amalgamation of the craton involved repeated collisions during a Neoarchean orogeny between ca. 2730 and 2625 Ma (Myers, 1993, 1995; Barley et al., 2003; Blewett and Hitchman, 2006; Korsch et al., 2011; Zibra et al., 2017a; Witt et al., 2018) with development of a stable cratonic lithosphere by ca. 2660 Ma (Zibra et al., 2017b). Cratonisation was accompanied by widespread granitic magmatism between ca. 2690 Ma and 2625 Ma (Compston et al., 1986; Wilde and Pidgeon, 1986; Champion and Sheraton, 1997; Nemchin and Pidgeon, 1997; Qiu et al., 1997; Smithies and Champion, 1999; Cassidy et al., 2002; Mole et al., 2012).

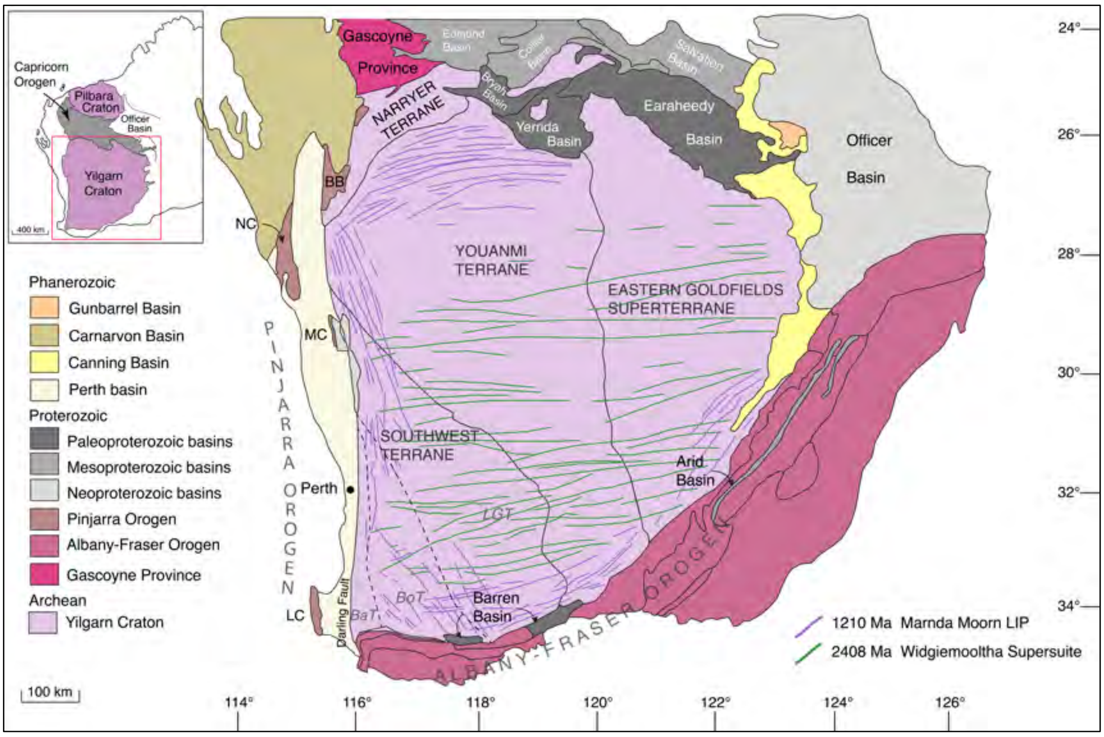

Figure 2.5 Map of the Yilgarn Craton showing major tectonic units. Inset shows the extent of the West Australian Craton (Pilbara Craton, Yilgarn Craton and Capricorn Orogen). From Geological Survey of Western Australia 1:2.5M Interpreted Bedrock Geology 2015 and 1:10M Tectonic Units 2016. Dashed lines are terrane boundaries within the southwestern Yilgarn Craton after Wilde et al. 1996: BaT = Balingup Terrane, BoT = Boddington Terrane and LGT = Lake Grace Terrane. For more details see Figure 2.6

2.4.2 Mafic dykes

The Yilgarn Craton hosts numerous dyke suites of different orientations, and dyke density increases towards the southern and western craton margins (Hallberg, 1987; Tucker and Boyd, 1987). The dykes are clearly discernible in aeromagnetic data but deep weathering and thick regolith cover make sampling difficult. Two craton-wide dyke swarms are well dated and limited occurrences of at least four others have been identified (Figure 2.5). The largest dykes belong to the E-W to NE-SW trending 2418–2408 Ma Widgiemooltha Supersuite (Sofoulis, 1965; Evans, 1968; Campbell et al., 1970; Hallberg, 1987; Doehler and Heaman, 1998; Nemchin and Pidgeon, 1998; Wingate, 1999, 2007; French et al., 2002), which includes the 2401 ±1 Ma Eraynia dykes in the eastern part of the craton (Pisarevsky et al., 2015). The Widgiemooltha dykes are up to 3.2 km wide, vertical to sub vertical and comprise predominantly massive olivine dolerite and gabbro or picrite (Myers, 1990). They extend up to 700 km across the craton and the largest intrusions, Jimberlana and

Binneringie, show well-developed igneous layering (Campbell et al., 1970; Lewis, 1994). McCall and Peers (1971) describe flow layering and laminar flow structures and stepping in the massive Binneringie dyke, dated at 2418 ± 3 Ma by Nemchin and Pidgeon (1998), which is 500-1000 m wide and continuous for over 585 km. Similarly, the Jimberlana dyke is ~180 km long, with up to 2.5 km wide funnel shaped layered intrusion with cumulate textures (Campbell et al., 1970; McClay and Campbell, 1976).

The most extensive dyke swarm in the craton is the 1210 Ma Marnda Moorn LIP (Figure 2.5), which was emplaced during stage 2 of the Albany-Fraser Orogeny (ca. 1214–1140 Ma; Clark et al., 2000) in association with intracratonic reactivation and extension (Clark et al., 2000). The Marnda Moorn LIP consists of several sub-swarms of different orientations intruding along the craton margins (Isles and Cooke, 1990; Evans, 1999; Wingate et al., 2000; Pidgeon and Nemchin, 2001; Pidgeon and Cook, 2003; Wingate and Pidgeon, 2005; Wingate, 2007; Claoué-Long et al., 2009). These include the the 1212 Ma Fraser suite in the east (Wingate et al., 2000), the 1203 Ma to 1218 Ma Gnowangerup suite in the south (Evans, 1999; Rasmussen and Fletcher, 2004), the 1204 Ma to 1214 Ma Boyagin suite in the south-southwest (Pidgeon and Nemchin, 2001; Pidgeon and Cook, 2003), the 1215-1216 Ma Wheatbelt suite in the central west (Evans, 1999; Qiu et al., 1999) and the 1211-1213 Ma Muggamurra suite (Wingate and Pidgeon, 2005) in the northwest of the craton. Few outcrops from the NE-SW trending Fraser swarm are known and only one exposure of an undeformed 30-35 m thick dyke in the Victory gold open pit mine has been identified by Wingate et al. (2000), who suggested that these dykes are probably continuous southward, extending to the Gnowangerup suite near Ravensthorpe. The Gnowangerup dykes trend E-NE to W-SW and are sub-parallel to the southern margin of the craton and progressively become more deformed and recrystallised as they approach the Albany Orogen (Myers, 1990b), implying that they are either pre- or syntectonic. Dykes within the Boyagin suite have variable

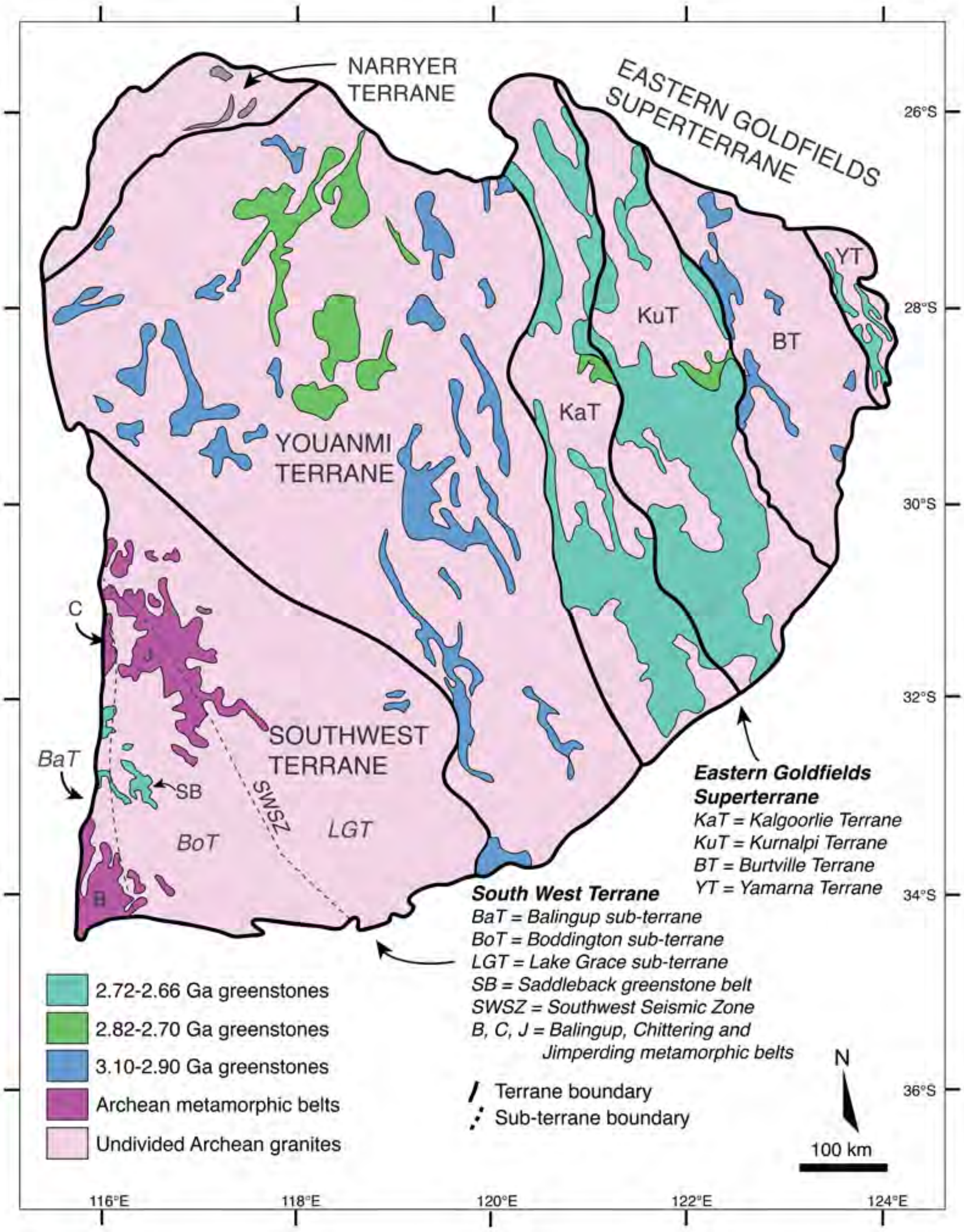

Figure 2.6 Map of the Yilgarn Craton showing terrane and sub-terrane boundaries and greenstone belt and granite distributions. Modified after Witt et al., 2018. South West Terrane: sub-terranes are from Wilde et al., 1996, and the boundary with the Youanmi Terrane is after Cassidy et al., 2006.

trends but most are oriented N-NW. The only in-depth geochemical study of mafic dykes in the Yilgarn Craton has been conducted on the Gnowangerup-Fraser dykes and suggests that the Marnda Moorn LIP was associated with a mantle plume (Wang et al., 2014).

Other limited occurrences include the SW-trending dykes of the 1075 Ma Warakurna LIP in the northern Yilgarn Craton (Wingate et al., 2004), the WNW-trending ca. 735 Ma Nindibillup dykes in the central and SE Yilgarn Craton (Spaggiari et al., 2009, 2011; Wingate, 2017), the NNE-trending ca. 735 Ma Northampton dykes in the far west (Embleton and Schmidt, 1985) and the undated (likely <1140 Ma) NW-trending Beenong dykes in the southeastern Yilgarn Craton (Wingate, 2007; Spaggiari et al., 2009, 2011).

2.5 Mafic dykes at Bunger Hills, East Antarctica

2.5.1 Regional geology

The Bunger Hills area forms a continuous low relief outcrop of about 300 km^2 along the coast in Wilkes Land near Shackleton Ice Shelf, approximately 400 km west of the Windmill Islands (Figure 2.7). Bunger Hills forms one of three geologically distinct regions in the immediate vicinity of the Denman and Scott Glaciers; the other two areas are the Obruchev Hills between Scott and Denman Glaciers and a group of smaller outcrops west of Denman Glacier. The Highjump Archipelago extends just north-northeast from Bunger Hills and comprises a ca. 93 km-long belt of small rocky islands.

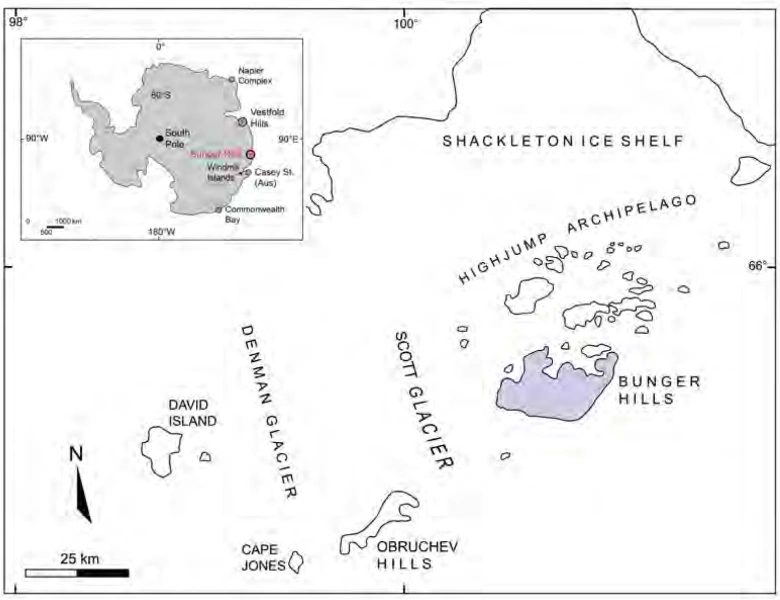

Figure 2.7 Location of Bunger Hills, Highjump Archipelago and Obruchev Hills in East Antarctica. After Sheraton et al. (1990, 1995).

The outcrop at Bunger Hills comprises predominantly granulite-facies mafic and felsic orthogneiss with subordinate paragneiss and voluminous charnockitic plutons intruded by several generations of mafic dykes (Figure 2.8) (Ravich et al., 1968; Sheraton et al., 1990, 1992, 1993, 1995; Sheraton and Tingey, 1994; Tucker et al., 2017). The presence of underlying Archean basement is inferred from a ca. 2800–2700 Ma zircon population from the mafic–felsic orthogneiss (Tucker et al., 2017), which is similar to the ca. 2640 Ma tonalitic orthogneiss at Obruchev Hills ca. 30 km to the southwest (Black et al., 1992). Zircon populations at ca. 1700–1500 Ma from granodioritic orthogneiss (Sheraton et al., 1993, 1995), ca. 1900–1500 Ma from the extensive metapelite sequence and ca. 1734 Ma and 1666 Ma from tonalitic orthogneiss suggest that these lithologies form a Paleoproterozoic cover to Archean basement (Sheraton et al., 1992, 1993; Tucker et al., 2017).

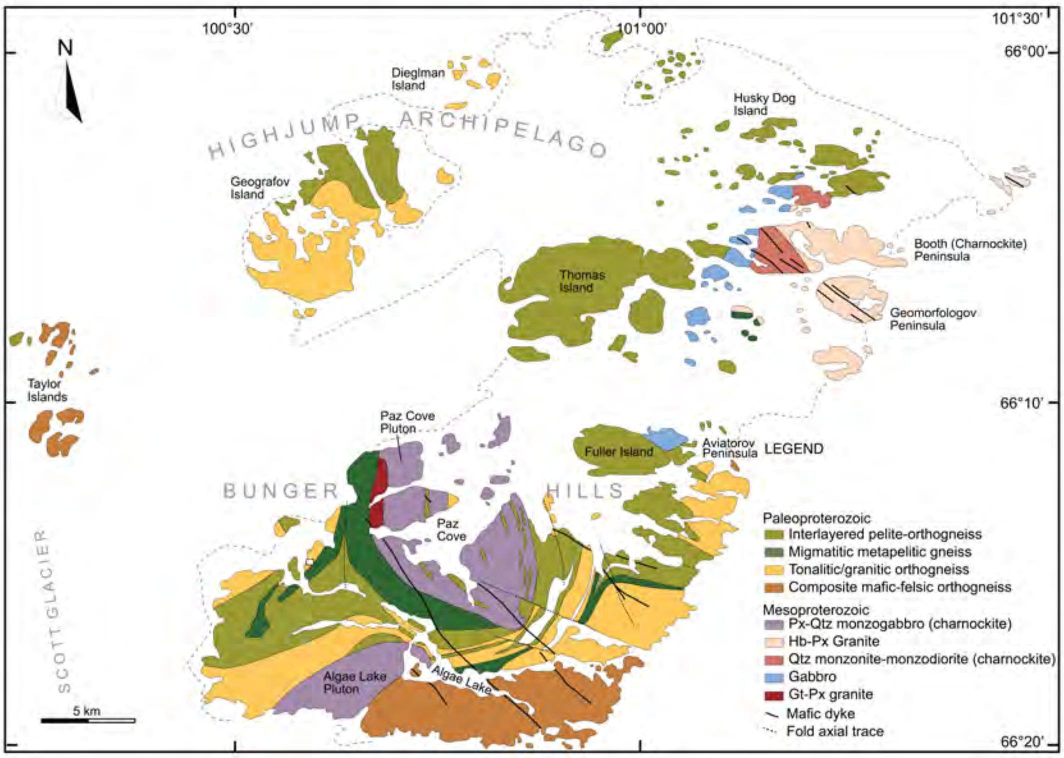

Figure 2.8 Geological Map of Bunger Hills and Highjump Archipelago showing sample locations and regional geology. Modified after Sheraton et al. (1994) and Tucker et al. (2017).

At least four metamorphic events have been identified at Bunger Hills (Stüwe and Powell, 1989; Stüwe and Wilson, 1990; Ding and James, 1991; Sheraton et al., 1993, 1995; Tucker et al., 2017). Peak granulite facies conditions of 850–900° C and 5–6 kbar were reached at 1183 ± 8 Ma in the Highjump Archipelago (Tucker and Hand, 2016), whereas conditions of 750–800°C and 5–6 kbar at 1190 ± 15 Ma were reported at Bunger Hills proper (Sheraton et al., 1993). Recent data also indicate metamorphic zircon growth peaks at ca. 1300–1270 Ma and ca. 1250 Ma, with minor peaks at ca. 1330 Ma and 1200 Ma (Tucker et al., 2017). Peak metamorphism at ca. 1190 Ma may have been associated with an extensional setting (Stüwe and Powell, 1989). This was followed by compressional NNW–SSE-directed deformation under granulite facies conditions by the final stage (ca. 1170 Ma) of deformation during uplift and cooling involving formation of extensive shear zones (Stüwe and Powell, 1989; Sheraton et al., 1992, 1993, 1995; Tucker et al., 2017).

2.5.2 Mafic dykes

Sheraton et al. (1990) identified five distinctive dyke suites at Bunger Hills based on their trace element compositions. Most dykes fall on the whole-rock Rb/Sr isochron giving an emplacement age of ~1140 Ma and a Sm/Nd whole-rock, clinopyroxene and isochron age of 1100 ± 330 Ma. Group 1 sill-like tholeiites are quartz-normative with relatively fractionated REE pattern and distinctive negative Th and Y anomalies. Group 2 SE-NW oriented olivine-bearing tholeiites are less evolved with higher Mg content and have high incompatible element contents and negative Nb, Sr and P anomalies. Group 3 and 4 NW-trending dolerites comprise at least 70% of all the dykes at Bunger Hills and have highly variable incompatible element compositions. Group 4 dolerites are more olivine-normative and have a higher Mg-number than group 3 dolerites, but all dykes within these groups are relatively fractionated with marked negative Sr and Nb anomalies. Alkaline and lamprophyric dykes and trachybasalts with a predominantly E-W orientation are the youngest suite with Rb/Sr crystallisation ages of ~502 Ma. Chemical variability between and within the five dyke groups suggests involvement of dynamic partial melting of variably enriched and metasomatised mantle regions (Sheraton et al., 1990).

2.6 Summary and conclusions

Large igneous provinces and their mafic dyke swarms, considered to be the plumbing systems of flood basalts, were emplaced throughout Earth's history. They are intimately connected with mantle dynamics and act as important tectonic and magmatic markers for paleogeographic reconstructions and as indicators of paleostress fields and pre-existing crustal weaknesses. Whereas their formation is commonly linked with mantle plumes and breakup of supercontinents, they have also been linked to other formation mechanisms such as back-arc extension, lithospheric delamination and decompression melting during passive rifting. Recent evidence has also linked modern flood basalts with the deep Earth volatile cycle and wet upwelling from the mantle transition zone. Geochemistry of mafic dykes is complex and reflects their varied sources, such as depleted asthenospheric mantle and variably metasomatised and isotopically enriched subcontinental lithospheric mantle. Many mafic dyke swarms display arc-like geochemical characteristics that may be imparted by the mantle source region or crustal contamination. Geochemical studies should be considered with precise geochronology and other constraints to correctly interpret the tectonic setting during their emplacement.

The Archean Yilgarn Craton of Western Australia and the Bunger Hills of East Antarctica share a Mesoproterozoic history, the latter being interpreted as a rifted remnant of the Albany-Fraser Orogen. The magmatic barcode for the Yilgarn Craton is limited and includes the craton-wide Paleoproterozoic Widgiemooltha Supersuite and the Mesoproterozoic Marnda Moorn LIP, with minor occurrences of other Proterozoic dykes in various parts of the craton. Mapping and aeromagnetic data suggest that many more dyke generations could be present. Comprehensive geochemical study is only available for the Marnda Moorn LIP, which is has been linked with a mantle plume. At Bunger Hills, at least three different dyke suites are present with imprecise age dates suggesting Meso-and Neoproterozoic mafic magmatism. Geochemistry indicates involvement of at least three sources in the genesis of the Mesoproterozoic dykes.

2.7 References

Abbott, D.H., Isley, A.E., 2002a. The intensity, occurrence, and duration of superplume events and eras over geological time. J. Geodyn. 34, 265–307.

Abbott, D.H., Isley, A.E., 2002b. Extraterrestrial influences on mantle plume activity. Earth Planet. Sci. Lett. 205, 53–62.

Allègre, C.J., Dupré, B., Richard, P., Rousseau, D., Brooks, C., 1982. Subcontinental versus suboceanic mantle, II. NdSrPb isotopic comparison of continental tholeiites with mid-ocean ridge tholeiites, and the structure of the continental lithosphere. Earth Planet. Sci. Lett. 57, 25–34. doi:10.1016/0012-821X(82)90170-4

Anderson, D.L., 1995. Lithosphere, asthenosphere, and perisphere. Rev. Geophys. 33, 125–149.

Baragar, W.R.A., Ernst, R.E., Hulbert, L., Peterson, T., 1996. Longitudinal petrochemical variation in the Mackenzie dyke swarm, northwestern Canadian Shield. J. Petrol. 37, 317–359.

Barley, M.E., Brown, S.J.A., Cas, R.A.F., Cassidy, K.F., Champion, D.C., Gardoll, S.J., Krapež, B., 2003. An integrated geological and metallogenic framework for the eastern Yilgarn Craton: developing geodynamic models of highly mineralised Archaean granite–greenstone terranes. AMIRA Project P624.

Belica, M.E., Piispa, E.J., Meert, J.G., Pesonen, L.J., Plado, J., Pandit, M.K., Kamenov, G.D., Celestino, M., 2014. Paleoproterozoic mafic dyke swarms from the Dharwar craton; paleomagnetic poles for India from 2.37 to 1.88Ga and rethinking the Columbia supercontinent. Precambrian Res. 244, 100–122. doi:10.1016/j.precamres.2013.12.005

Bercovici, D., Karato, S.-I., 2003. Whole-mantle convection and the transition-zone water filter. Nature 425, 39–44. doi:10.1038/nature01918

Black, L.P., Sheraton, J.W., Tingey, R.J., McCulloch, M.T., 1992. New U-Pb Zircon Ages From the Denman Glacier Area, East Antarctica, and Their Significance for Gondwana Reconstruction. Antarct. Sci. 4, 447–460. doi:10.1017/S095410209200066X

Bleeker, W., 2004. Taking the pulse of planet Earth: a proposal for a new multi-disciplinary flagship project in Canadian solid Earth sciences. Geosci. Canada 31.

Bleeker, W., 2003. The late Archean record: a puzzle in ca. 35 pieces. Lithos 71, 99–134.

Bleeker, W., Ernst, R., 2006. Short-lived mantle generated magmatic events and their dyke swarms: the key unlocking Earth's paleogeographic record back to 2.6 Ga, in: Hanski, E.J., Mertanen, S., Rämö, O.T., Vuollo, J. (Eds.), Dyke Swarms—time Markers of Crustal Evolution: Selected Papers of the Fifth International Dyke Conference in Finland, Rovaniemi, Finland, 31 July- 3 Aug 2005 & Fourth International Dyke Conference, Kwazulu-Natal, South Africa 26-29 June 2001. CRC Press, London, pp. 3–26.

Blewett, R.S., Hitchman, A.P., 2006. 3D Geological Models of the Eastern Yilgarn Craton: Final Report pmd* CRC Y2 Project September 2001–December 2004. Geoscience Australia Record 2006/05.

Boyd, D.M., Tucker, D.H., 1990. Australian magnetic dykes, in: Parker, A.J., Rickwood, P.C., Tucker, D.H. (Eds.), Mafic Dykes and Emplacement Mechanisms. A.A.Balkema, Rotterdam, pp. 391–399.

Bradley, D.C., 2011. Secular trends in the geologic record and the supercontinent cycle. Earth-Science Rev. 108, 16–33.

Bradley, D.C., 2008. Passive margins through earth history. Earth-Science Rev. 91, 1–26.

Bryan, S.E., Ernst, R.E., 2008. Revised definition of large igneous provinces (LIPs). Earth-Science Rev. 86, 175–202. doi:10.1016/j.earscirev.2007.08.008

Bryan, S.E., Peate, I.U., Peate, D.W., Self, S., Jerram, D.A., Mawby, M.R., Marsh, J.S., Miller, J.A., 2010. The largest volcanic eruptions on Earth. Earth-Science Rev. 102, 207–229.

Buchan, K.L., Ernst, R.E., Bleeker, W., Davies, W., Villeneuve, M., van Breemen, O., Hamilton, M., Söderlund, U., 2010. Proterozoic magmatic events of the Slave craton, Wopmay orogen and environs, in: Geological Survey of Canada, Open File 5985. Geological Survey of Canada.

Buchan, K.L., Ernst, R.E., Hamilton, M.A., Mertanen, S., Pesonen, L.J., Elming, S.-Å., 2001. Rodinia: the evidence from integrated palaeomagnetism and U–Pb geochronology. Precambrian Res. 110, 9–32.

Buchan, K.L., Goutier, J., Hamilton, M.A., Ernst, R.E., Matthews, W.A., 2007. Paleomagnetism, U–Pb geochronology, and geochemistry of Lac Esprit and other dyke swarms, James Bay area, Quebec, and implications for Paleoproterozoic deformation of the Superior Province. Can. J. Earth Sci. 44, 643–664.

Buchan, K.L., Mortensen, J.K., Card, K.D., 1993. Northeast-trending Early Proterozoic dykes of southern Superior Province: multiple episodes of emplacement recognized from integrated paleomagnetism and U–Pb geochronology. Can. J. Earth Sci. 30, 1286–1296.

Campbell, I.H., 2002. Implications of Nb / U , Th / U and Sm / Nd in plume magmas for the relationship between continental and oceanic crust formation and the development of the depleted mantle. Geochim. Cosmochim. Acta 66, 1651–1661. doi:10.1016/S0016-7037(01)00856-0

Campbell, I.H., Griffiths, R.W., 1990. Implications of mantle plume structure for the evolution of flood basalts. Earth Planet. Sci. Lett. 99, 79–93.

Campbell, I.H., McCall, G.J.H., Tyrwhitt, D.S., 1970. The Jimberlana Norite, Western Australia–a smaller analogue of the Great Dyke of Rhodesia. Geol. Mag. 107, 1–12.

Cande, S.C., Stegman, D.R., 2011. Indian and African plate motions driven by the push force of the Réunion plume head. Nature 475, 47–52. doi:10.1038/nature10174

Cassidy, K.F., Champion, D.C., Krapez, B., Barley, M.E., Brown, S.J.A., Blewett, R.S., Groenewald, Pb., Tyler, I.M., 2006. A revised geological framework for the Yilgarn Craton, Western Australia, in: Geological Survey of Western Australia Record 8/2006. Geological Survey of Western Australia.

Cassidy, K.F., Champion, D.C., McNaughton, N.J., Fletcher, I.R., Whitaker, A.J., Bastrakova, I. V, Budd, A.R., 2002. Characterisation and metallogenic significance of Archaean granitoids of the Yilgarn Craton, Western Australia, Minerals and Energy Research Institute of Western Australia (MERIWA) Report P482.

Cawood, P.A., Tyler, I.M., 2004. Assembling and reactivating the Proterozoic Capricorn Orogen: lithotectonic elements, orogenies, and significance. Precambrian Res. 128, 201–218. doi:10.1016/j.precamres.2003.09.001

Champion, D.C., Sheraton, J.W., 1997. Geochemistry and Nd isotope systematics of Archaean granites of the Eastern Goldfields, Yilgarn Craton, Australia:

implications for crustal growth processes. Precambrian Res. 83, 109–132.

Ciborowski, T.J.R., Kerr, A.C., Ernst, R.E., Mcdonald, I., Minifie, M.J., Harlan, S.S., Millar, I.L., 2015. The Early Proterozoic Matachewan Large Igneous Province : Geochemistry, Petrogenesis, and Implications for Earth Evolution 56. doi:10.1093/petrology/egv038

Claoué-Long, J.C., Hoatson, D.M., 2009. Guide to using the map of Australian Proterozoic large igneous provinces. Geoscience Australia.

Claoué-Long, J.C., Hoatson, D.M., Australia, G., 2009. Guide to using the Map of Australian Proterozoic Large Igneous Provinces. Geoscience Australia.

Clark, D.J., Hensen, B.J., Kinny, P.D., 2000. Geochronological constraints for a two-stage history of the Albany – Fraser Orogen , Western Australia. Precambrian Res. 102, 155–183.

Coffin, M.F., Eldholm, O., 1994. Large igneous provinces: crustal structure, dimensions, and external consequences. Rev. Geophys. 32, 1–36. doi:10.1029/93RG02508

Compston, W., Williams, I.S., McCulloch, M.T., 1986. Contrasting zircon U-Pb and model Sm-Nd ages for the Archaean Logue Brook Granite. Aust. J. Earth Sci. 33, 193–200. doi:10.1080/08120098608729359

Condie, K.C., 2011. The supercontinent cycle, in: Earth as an Evolving Planetary System. Academic Press, New York, pp. 317–355.

Condie, K.C., 2004. Supercontinents and superplume events: distinguishing signals in the geologic record. Phys. Earth Planet. Inter. 146, 319–332. doi:10.1016/j.pepi.2003.04.002

Condie, K.C., 2003. Supercontinents, superplumes and continental growth: the Neoproterozoic record. Geol. Soc. London, Spec. Publ. 206, 1–21.

Condie, K.C., 1997. Sources of Proterozoic mafic dyke swarms: constraints from ThTa and LaYb ratios. Precambrian Res. 81, 3–14. doi:http://dx.doi.org/10.1016/S0301-9268(96)00020-4

Condie, K.C., Aster, R.C., 2013. Refinement of the supercontinent cycle with Hf, Nd and Sr isotopes. Geosci. Front. 4, 667–680.

Condie, K.C., Belousova, E., Griffin, W.L., Sircombe, K.N., 2009. Granitoid events in space and time: Constraints from igneous and detrital zircon age spectra. Gondwana Res. 15, 228–242. doi:10.1016/j.gr.2008.06.001

Condie, K.C., Davaille, A., Aster, R.C., Arndt, N., 2015. Upstairs-downstairs: Supercontinents and large igneous provinces, are they related? Int. Geol. Rev. 57, 1341–1348. doi:10.1080/00206814.2014.963170

Courtillot, V., Davaille, A., Besse, J., Stock, J., 2003. Three distinct types of hotspots in the Earth's mantle. Earth Planet. Sci. Lett. 205, 295–308.

Courtillot, V., Jaupart, C., Manighetti, I., Tapponnier, P., Besse, J., 1999. On casual links between flood basalts and continental breakup. Earth Planet. Sci. Lett. 166, 177–195.

Dawson, G.C., Krapež, B., Fletcher, I.R., McNaughton, N.J., Rasmussen, B., 2003. 1.2 Ga thermal metamorphism in the Albany-Fraser Orogen of Western Australia: Consequence of collision or regional heating by dyke swarms? J. Geol. Soc. London. 160, 29–37. doi:10.1144/0166-764901-119

De Kock, M.O., Ernst, R., Söderlund, U., Jourdan, F., Hofmann, A., Le Gall, B., Bertrand, H., Chisonga, B.C., Beukes, N., Rajesh, H.M., Moseki, L.M., Fuchs, R., 2014. Dykes of the 1.11Ga Umkondo LIP, Southern Africa: Clues to a complex plumbing system. Precambrian Res. 249, 129–143. doi:10.1016/j.precamres.2014.05.006

Ding, P., James, P.R., 1991. Structural evolution of the Bunger Hills area of East Antarctica. Geol. Evol. Antarct. Cambridge Univ. Press. Cambridge 13–17.

Doehler, J.S., Heaman, L.M., 1998. 2.41 Ga U–Pb Baddeleyite ages for two gabbroic dykes from the Widgiemooltha swarm, Western Australia: a Yilgarn–Lewisian connection, in: Geological Society of America 1998 Annual Meeting, Abstracts with Programs. Geological Society of America, pp. 291–292.

Elkins-Tanton, L.T., 2005. Continental magmatism caused by lithospheric delamination. Geol. Soc. Am. Spec. Pap. 80301, 449–461. doi:10.1130/2005.2388(27).

Elkins Tanton, L.T., Hager, B.H., 2000. Melt intrusion as a trigger for lithospheric foundering and the eruption of the Siberian flood basalts. Geophys. Res. Lett. 27, 3937–3940.

Embleton, B.J.J., Schmidt, P.W., 1985. Age and significance of magnetizations in dolerite dykes from the Northampton Block, Western Australia. Aust. J. Earth Sci. 32, 279–286.

Ernst, R., Bleeker, W., 2010. Large igneous provinces (LIPs), giant dyke swarms, and mantle plumes: significance for breakup events within Canada and adjacent regions from 2.5 Ga to the Present. Can. J. Earth Sci. 47, 695–739. doi:10.1139/e10-025

Ernst, R., Jowitt, S., 2013. Large Igneous Provinces (LIPs) and Metallogeny. Soc. Econ. Geol. Inc. 17–51.

Ernst, R., Srivastava, R., Bleeker, W., Hamilton, M., 2010. Precambrian Large Igneous Provinces (LIPs) and their dyke swarms: New insights from high-precision geochronology integrated with paleomagnetism and geochemistry. Precambrian Res. 183, vii–xi.

Ernst, R.E., 2014. Large igneous provinces. Cambridge University Press.

Ernst, R.E., Baragar, W.R.A., 1992. Evidence from magnetic fabric for the flow pattern of magma in the Mackenzie giant radiating dyke swarm.

Ernst, R.E., Bleeker, W., Söderlund, U., Kerr, A.C., 2013. Large Igneous Provinces and supercontinents: Toward completing the plate tectonic revolution. Lithos 174, 1–14.

Ernst, R.E., Buchan, K.L., 2001a. Large mafic magmatic events through time and links to mantle-plume heads, in: Geological Society of America Special Paper 352. pp. 483–576.

Ernst, R.E., Buchan, K.L., 2001b. The use of mafic dike swarms in identifying and locating mantle plumes, in: Geological Society of America Special Paper 352. Geological Society of America, pp. 247–266.

Ernst, R.E., Buchan, K.L., 1997. Giant radiating dyke swarms: their use in identifying pre-Mesozoic large igneous provinces and mantle plumes, in: Large Igneous Provinces: Continental, Oceanic, and Planetary Flood Volcanism. American Geophysical Union Monograph 100, pp. 297–333.

Ernst, R.E., Buchan, K.L., Campbell, I.H., 2005. Frontiers in large igneous province research. Lithos 79, 271–297. doi:10.1016/j.lithos.2004.09.004

Ernst, R.E., Buchan, K.L., Palmer, H.C., 1995a. Physics and Chemistry of Dykes.

Ernst, R.E., Hamilton, M.A., Soderlund, U., Hanes, J.A., Gladkochub, D.P., Okrugin, A. V, Kolotilina, T., Mekhonoshin, A.S., Bleeker, W., LeCheminant, A.N., Buchan, K.L., Chamberlain, K.R., Didenko, A.N., 2016. Long-lived connection between southern Siberia and northern Laurentia in the Proterozoic. Nat. Geosci 9, 464–469.

doi:10.1038/ngeo2700\rhttp://www.nature.com/ngeo/journal/v9/n6/abs/ngeo2700.html#supplementary-information

Ernst, R.E., Head, J.W., Parfitt, E., Grosfils, E., Wilson, L., 1995b. Giant radiating dyke swarms on Earth and Venus. Earth-Science Rev. 39, 1–58.

Ernst, R.E., Srivastava, R.K., 2008. India's place in the Proterozoic world: constraints from the Large Igneous Province (LIP) record. Indian dykes. Ed. by RK Srivastava, Ch. Sivaji, NV Chalapathi Rao. Geochemistry, Geophys. Geochronology, Narosa Publ. House Pvt. Ltd, New Delhi, India 41–56.

Ernst, R.E., Wingate, M.T.D., Buchan, K.L., Li, Z.X., 2008. Global record of 1600–700Ma Large Igneous Provinces (LIPs): Implications for the reconstruction of the proposed Nuna (Columbia) and Rodinia supercontinents. Precambrian Res. 160, 159–178. doi:10.1016/j.precamres.2007.04.019

Evans, D.A.D., Li, Z., Murphy, J.B., 2016. Four-dimensional context of Earth ' s supercontinents. Geol. Soc. London 424, 1–14. doi:10.1144/SP424.12

Evans, M.E., 1968. Magnetization of dikes: a study of the paleomagnetism of the Widgiemooltha dike suite, Western Australia. J. Geophys. Res. 73, 3261–3270.

Evans, T., 1999. Extent and nature of the 1.2 Ga Wheatbelt dyke swarm, Yilgarn Craton, Western Australia. B.Sc. thesis, Univ. West. Aust. Perth.

French, J.E., Heaman, L.M., 2010. Precise U-Pb dating of Paleoproterozoic mafic dyke swarms of the Dharwar craton, India: Implications for the existence of the Neoarchean supercraton Sclavia. Precambrian Res. 183, 416–441. doi:10.1016/j.precamres.2010.05.003

French, J.E., Heaman, L.M., Chacko, T., 2002. Feasibility of chemical U-Th-total Pb baddeleyite dating by electron microprobe. Chem. Geol. 188, 85–104. doi:10.1016/S0009-2541(02)00074-8

French, J.E., Heaman, L.M., Chacko, T., Srivastava, R.K., 2008. 1891-1883 Ma Southern Bastar-Cuddapah mafic igneous events, India: A newly recognized large igneous province. Precambrian Res. 160, 308–322. doi:10.1016/j.precamres.2007.08.005

Gee, R.D., Baxter, J.L., Wilde, S.A., Williams, I.R., 1981. Crustal development in the Archaean Yilgarn Block, Western Australia. Spec. Publ. Geol. Soc. Aust 7, 43–56.

Goldberg, A.S., 2010. Dyke swarms as indicators of major extensional events in the

1.9–1.2 Ga Columbia supercontinent. J. Geodyn. 50, 176–190.

Gutiérrez-Alonso, G., Fernández-Suárez, J., Weil, A.B., Brendan Murphy, J., Damian Nance, R., Corf, F., Johnston, S.T., 2008. Self-subduction of the Pangaean global plate. Nat. Geosci. 1, 549–553. doi:10.1038/ngeo250

Hallberg, J.A., 1987. Postcratonization mafic and ultramafic dykes of the Yilgarn Block. Aust. J. Earth Sci. 34, 135–149. doi:10.1080/08120098708729398

Halls, H.C., 1986. Paleomagnetism, structure, and longitudinal correlation of Middle Precambrian dykes from northwestern Ontario and Minnesota. Can. J. Earth Sci. 23, 142–157.

Halls, H.C., 1982. The Importance and Potential of Mafic Dyke Swarms in Studies of Geodynamic Processes. Geosci. Canada. doi:10.12789/gs.v9i3.3309

Halls, H.C., Zhang, B., 1998. Uplift structure of the southern Kapuskasing zone from 2.45 Ga dike swarm displacement. Geology 26, 67–70. doi:10.1130/0091-7613(1998)026<0067:USOTSK>2.3.CO;2

Hanson, R.E., Gose, W.A., Crowley, J.L., Ramezani, J., Bowring, S.A., Bullen, D.S., Hall, R.P., Pancake, J.A., Mukwakwami, J., 2004. Paleoproterozoic intraplate magmatism and basin development on the Kaapvaal Craton: Age, paleomagnetism and geochemistry of~ 1.93 to~ 1.87 Ga post-Waterberg dolerites. South African J. Geol. 107, 233–254.

Hart, S.R., 1984. A large-scale isotope anomaly in the Southern Hemisphere mantle. Nature 309, 753–757.

Hawkesworth, C.J., Cawood, P.A., Dhuime, B., 2016. Tectonics and crustal evolution. GSA Today 26, 4–11. doi:10.1130/GSATG272A.1.4

Hawkesworth, C.J., Dhuime, B., Pietranik, A.B., Cawood, P.A., Kemp, A.I.S., Storey, C.D., 2010. The generation and evolution of the continental crust. J. Geol. Soc. London. 167, 229–248. doi:10.1144/0016-76492009-072

Hawkesworth, C.J., Kempton, P.D., Rogers, N.W., Ellam, R.M., Calsteren, P.W. van, 1990. Continental mantle lithosphere, and shallow level enrichment processes in the Earth's mantle. Earth Planet. Sci. Lett. 96, 256–268.

Hawkesworth, C.J., Lightfoot, P.C., Fedorenko, V.A., Blake, S., Naldrett, A.J., Doherty, W., Gorbachev, N.S., 1995. Magma differentiation and mineralisation in the Siberian continental flood basalts. LITHOS 34, 61–88. doi:10.1016/0024-4937(95)90011-X

Heaman, L.M., 2008. Precambrian Large Igneous Provinces: An Overview of Geochronology, Origins and Impact on Earth Evolution. J. Geol. Soc. India 72, 15–34.

Heaman, L.M., Le Cheminant, A.N., 1988. U-Pb baddeleyite ages of the Muskox Intrusion and Mackenzie Dyke Swarm. NWT, Canada 53.

Heinonen, J.S., Carlson, R.W., Riley, T.R., Luttinen, A. V., Horan, M.F., 2014. Subduction-modified oceanic crust mixed with a depleted mantle reservoir in the sources of the Karoo continental flood basalt province. Earth Planet. Sci. Lett. 394, 229–241. doi:10.1016/j.epsl.2014.03.012

Heinonen, J.S., Luttinen, A. V., Bohrson, W.A., 2016. Enriched continental flood basalts from depleted mantle melts: modeling the lithospheric contamination of Karoo lavas from Antarctica. Contrib. to Mineral. Petrol. 171, 9. doi:10.1007/s00410-015-1214-8

Hirschmann, M.M., Asimow, P.D., Ghiorso, M.S., Stolper, E.M., 1999. Calculation of peridotite partial melting from thermodynamic models of minerals and melts. III. Controls on isobaric melt production and the effect of water on melt production. J. Petrol. 40, 831–851.

Hoek, J.D., Seitz, H.-M., 1995. Continental mafic dyke swarms as tectonic indicators: an example from the Vestfold Hills, Antarctica. Precambrian Res. 75, 121–139.

Hoffman, P.F., 1999. The break-up of Rodinia, birth of Gondwana, true polar wander and the snowball Earth. J. African Earth Sci. 28, 17–33.

Hoffman, P.F., 1998. A Neoproterozoic Snowball Earth. Science (80-.). 281, 1342–1346. doi:10.1126/science.281.5381.1342

Hoffman, P.F., 1997. Tectonic genealogy of North America. Earth Struct. an Introd. to Struct. Geol. tectonics. McGraw-Hill, New York 459–464.

Hou, G., 2012. Mechanism for three types of mafic dyke swarms. Geosci. Front. 3, 217–223. doi:10.1016/j.gsf.2011.10.003

Hou, G., Kusky, T.M., Wang, C., Wang, Y., 2010. Mechanics of the giant radiating Mackenzie dyke swarm: A paleostress field modeling. J. Geophys. Res. Solid Earth 115. doi:10.1029/2007JB005475

Hou, G., Wang, C., Li, J., Qian, X., 2006. Late Paleoproterozoic extension and a paleostress field reconstruction of the North China Craton. Tectonophysics 422, 89–98.

Hughes, H.S.R., McDonald, I., Goodenough, K.M., Ciborowski, T.J.R., Kerr, A.C., Davies, J.H.F.L., Selby, D., 2014. Enriched lithospheric mantle keel below the Scottish margin of the North Atlantic Craton: Evidence from the Palaeoproterozoic Scourie Dyke Swarm and mantle xenoliths. Precambrian Res. 250, 97–126. doi:10.1016/j.precamres.2014.05.026

Ingle, S., Coffin, M.F., 2004. Impact origin for the greater Ontong Java Plateau? Earth Planet. Sci. Lett. 218, 123–134. doi:10.1016/S0012-821X(03)00629-0

Isles, D.J., Cooke, A.C., 1990. Spatial associations between post-cratonisation dykes and gold deposits in the Yilgarn Block, Western Australia, in: Parker, A.J., Rickwood, P.C., Tucker, D.H. (Eds.), Mafic Dykes and Emplacement Mechanisms. Balkema, Rotterdam, pp. 147–162.

Isley, A.E., Abbott, D.H., 1999. Plume-related mafic volcanism and the deposition of banded iron formation. J. Geophys. Res. Solid Earth 104, 15461–15477.

Ivanov, A. V, Litasov, K.D., 2014. The deep water cycle and flood basalt volcanism. Int. Geol. Rev. 56, 1–14.

Johnson, S.P., Sheppard, S., Rasmussen, B., Wingate, M.T.D., Kirkland, C.L., Muhling, J.R., Fletcher, I.R., Belousova, E.A., 2011. Two collisions, two sutures: Punctuated pre-1950Ma assembly of the West Australian Craton during the Ophthalmian and Glenburgh Orogenies. Precambrian Res. 189, 239–262. doi:10.1016/j.precamres.2011.07.011

Jones, A.P., Price, G.D., Price, N.J., DeCarli, P.S., Clegg, R.A., 2002. Impact induced melting and the development of large igneous provinces. Earth Planet. Sci. Lett. 202, 551–561. doi:10.1016/S0012-821X(02)00824-5

Jourdan, F., Bertrand, H., Schärer, U., Blichert-Toft, J., Féraud, G., Kampunzu, A.B., 2007. Major and trace element and Sr, Nd, Hf, and Pb isotope compositions of the Karoo large igneous province, Botswana - Zimbabwe: Lithosphere vs Mantle Plume Contribution. J. Petrol. 48, 1043–1077. doi:10.1093/petrology/egm010

Jourdan, F., Féraud, G., Bertrand, H., Kampunzu, A.B., Tshoso, G., Watkeys, M.K., Le Gall, B., 2005. Karoo large igneous province: Brevity, origin, and relation to mass extinction questioned by new 40Ar/39Ar age data. Geology 33, 745–748.

Ju, W., Hou, G., Hari, K.R., 2013. Mechanics of mafic dyke swarms in the Deccan

Large Igneous Province: Palaeostress field modelling. J. Geodyn. 66, 79–91. doi:10.1016/j.jog.2013.02.002

King, S.D., Anderson, D.L., 1995. An alternative mechanism of flood basalt formation. Earth Planet. Sci. Lett. 136, 269–279.

Korsch, R.J., Kositcin, N., Champion, D.C., 2011. Australian island arcs through time: Geodynamic implications for the Archean and Proterozoic. Gondwana Res. 19, 716–734. doi:10.1016/j.gr.2010.11.018

Ksienzyk, A.K., Jacobs, J., Boger, S.D., Kosler, J., Sircombe, K.N., Whitehouse, M.J., 2012. U-Pb ages of metamorphic monazite and detrital zircon from the Northampton Complex: Evidence of two orogenic cycles in Western Australia. Precambrian Res. 198–199, 37–50. doi:10.1016/j.precamres.2011.12.011

Lanyon, R., Black, L.P., Seitz, H.-M., 1993. U-Pb zircon dating of mafic dykes and its application to the Proterozoic geological history of the Vestfold Hills, East Antarctica. Contrib. to Mineral. Petrol. 115, 184–203.

LeCheminant, A.N., Heaman, L.M., 1989. Mackenzie igneous events, Canada: Middle Proterozoic hotspot magmatism associated with ocean opening. Earth Planet. Sci. Lett. 96, 38–48.

Lewis, J.D., 1994. Mafic dykes in the Williams–Wandering area, Western Australia. Geol. Surv. West. Aust. Rep. 37, 37–52.

Li, J., Wang, X.-C., Ren, Z.-Y., Xu, J.-F., He, B., Xu, Y.-G., 2014. Chemical heterogeneity of the Emeishan mantle plume: Evidence from highly siderophile element abundances in picrites. J. Asian Earth Sci. 79, 191–205. doi:10.1016/j.jseaes.2013.09.009

Li, Z.-X., Evans, D.A.D., 2011. Late Neoproterozoic 40 intraplate rotation within Australia allows for a tighter-fitting and longer-lasting Rodinia. Geology 39, 39–42.

Li, Z.-X., Zhong, S., 2009. Supercontinent–superplume coupling, true polar wander and plume mobility: Plate dominance in whole-mantle tectonics. Phys. Earth Planet. Inter. 176, 143–156. doi:10.1016/j.pepi.2009.05.004

Li, Z.X., Bogdanova, S. V, Collins, A.S., Davidson, A., De Waele, B., Ernst, R.E., Fitzsimons, I.C.W., Fuck, R.A., Gladkochub, D.P., Jacobs, J., Karlstrom, K.E., Lu, S., Natapov, L.M., Pease, V., Pisarevsky, S.A., Thrane, K., Vernikovsky, V., 2008. Assembly, configuration, and break-up history of Rodinia: A synthesis. Precambrian Res. 160, 179–210. doi:10.1016/j.precamres.2007.04.021

Li, Z.X., Evans, D.A.D., Zhang, S., 2004. A 90° spin on Rodinia: possible causal links between the Neoproterozoic supercontinent, superplume, true polar wander and low-latitude glaciation. Earth Planet. Sci. Lett. 220, 409–421. doi:10.1016/s0012-821x(04)00064-0

Li, Z.X., Li, X.H., Kinny, P.D., Wang, J., Zhang, S., Zhou, H., 2003. Geochronology of Neoproterozoic syn-rift magmatism in the Yangtze Craton, South China and correlations with other continents: evidence for a mantle superplume that broke up Rodinia. Precambrian Res. 122, 85–109. doi:10.1016/S0301-9268(02)00208-5

Li, Z.X., Zhang, L., Powell, C.M., 1996. Positions of the East Asian cratons in the Neoproterozoic supercontinent Rodinia. Aust. J. Earth Sci. 43, 593–604.

Liu, Y., Li, Z.-X., Pisarevsky, S.A., Kirscher, U., Mitchell, R.N., Stark, J.C., 2018. Palaeomagnetism of the 1.89 Ga Boonadgin dykes of the Yilgarn Craton: Possible connection with India. Precambrian Res. Press.

McCall, G.J.H., Peers, R., 1971. Geology of the Binneringie Dyke, Western Australia. Geol. Rundschau 60, 1174–1263. doi:10.1007/BF02046541

Meert, J.G., 2014. Strange attractors, spiritual interlopers and lonely wanderers: The search for pre-Pangean supercontinents. Geosci. Front. 5, 155–166.

Meert, J.G., 2012. What's in a name? The Columbia (Paleopangaea/Nuna) supercontinent. Gondwana Res. 21, 987–993.

Merle, R., Marzoli, A., Reisberg, L., Bertrand, H., Nemchin, A., Chiaradia, M., Callegaro, S., Jourdan, F., Bellieni, G., Kontak, D., Puffer, J., Gregory McHone, J., 2014. Sr, Nd, Pb and Os isotope systematics of CAMP tholeiites from Eastern North America (ENA): Evidence of a subduction-enriched mantle source. J. Petrol. 55, 133–180. doi:10.1093/petrology/egt063

Mole, D.R., Fiorentini, M.L., Thebaud, N., McCuaig, T.C., Cassidy, K.F., Kirkland, C.L., Wingate, M.T.D., Romano, S.S., Doublier, M.P., Belousova, E.A., 2012. Spatio-temporal constraints on lithospheric development in the southwest–central Yilgarn Craton, Western Australia. Aust. J. Earth Sci. 59, 625–656. doi:10.1080/08120099.2012.691213

Morgan, W.J., 1971. Convection Plumes in the Lower Mantle. Nature 230, 42–43.

doi:10.1038/230042a0

Murphy, J.B., Dostal, J., 2007. Continental mafic magmatism of different ages in the same terrane: Constraints on the evolution of an enriched mantle source. Geology 35, 335–338. doi:10.1130/G23072A.1

Murphy, J.B., Nance, R.D., 2013. Speculations on the mechanisms for the formation and breakup of supercontinents. Geosci. Front. 4, 185–194. doi:10.1016/j.gsf.2012.07.005

Myers, J.S., 1995. The generation and assembly of an Archaean supercontinent: evidence from the Yilgarn craton, Western Australia. Geol. Soc. London, Spec. Publ. 95, 143–154.

Myers, J.S., 1993. Precambrian Tectonic History of the West Australian Craton and Adjacent Orogens. Annu. Rev. Earth Planet. Sci. 21, 453–485.

Myers, J.S., 1990a. Pinjarra orogen, in: Geology and Mineral Resources of Western Australia. State Printing Division, pp. 264–274.

Myers, J.S., 1990b. Albany–Fraser Orogen, in: Geology and Mineral Resources of Western Australia. Geological Survey of Western Australia Memoir, pp. 255–263.

Nance, R.D., Murphy, J.B., 2013. Origins of the supercontinent cycle. Geosci. Front. 4, 439–448. doi:10.1016/j.gsf.2012.12.007

Nance, R.D., Murphy, J.B., Santosh, M., 2014. The supercontinent cycle: A retrospective essay. Gondwana Res. 25, 4–29. doi:10.1016/j.gr.2012.12.026

Nance, R.D., Worsley, T.R., Moody, J.B., 1986. Post -Archean biogeochemical cycles and long-term episodicity in tectonic processes. Geology 14, 514–518. doi:10.1130/0091-7613(1986)14<514

Nelson, D.R., 1997. Evolution of the Archaean granite-greenstone terranes of the Eastern Goldfields, Western Australia: SHRIMP U-Pb zircon constraints. Precambrian Res. 83, 57–81. doi:10.1016/S0301-9268(97)00005-3

Nelson, D.R., Myers, J.S., Nutman, A.P., 1995. Chronology and evolution of the Middle Proterozoic Albany-Fraser Orogen, Western Australia. Aust. J. Earth Sci. 42, 481–495. doi:10.1080/08120099508728218

Nemchin, A.A., Pidgeon, R.T., 1998. Precise conventional and SHRIMP baddeleyite U-Pb age for the Binneringie Dyke, near Narrogin, Western Australia. Aust. J. Earth Sci. 45, 673–675.

Nemchin, A.A., Pidgeon, R.T., 1997. Evolution of the Darling Range batholith, Yilgarn Craton, Western Australia: a SHRIMP zircon study. J. Petrol. 38, 625–649.

Nordsvan, A.R., Collins, W.C., Li, Z.-X., Spencer, C.J., Pourteau, A., Withnall, I.W., Betts, P.G., Volante, S., 2018. Laurentian crust in northeast Australia: Implications for the assembly of the supercontinent Nuna. Geology.

Pastor-Galán, D., Nance, R.D., Murphy, J.B., Spencer, C.J., 2018. Supercontinents: myths, mysteries, and milestones. Geol. Soc. London, Spec. Publ. 470, SP470-16.

Pearson, D.G., Brenker, F.E., Nestola, F., McNeill, J., Nasdala, L., Hutchison, M.T., Matveev, S., Mather, K., Silversmit, G., Schmitz, S., 2014. Hydrous mantle transition zone indicated by ringwoodite included within diamond. Nature 507, 221.

Pesonen, L.J., Elming, S.-Å., Mertanen, S., Pisarevsky, S., D'Agrella-Filho, M.S., Meert, J.G., Schmidt, P.W., Abrahamsen, N., Bylund, G., 2003. Palaeomagnetic configuration of continents during the Proterozoic. Tectonophysics 375, 289–324.

Pidgeon, R.T., Cook, T.J.F., 2003. 1214±5 Ma dyke from the Darling Range, southwestern Yilgarn Craton, Western Australia. Aust. J. Earth Sci. 50, 769–773.

Pidgeon, R.T., Nemchin, A.A., 2001. 1.2 Ga Mafic dyke near York, southwestern Yilgarn Craton, Western Australia. Aust. J. Earth Sci. 48, 751–755. doi:10.1046/j.1440-0952.2001.485895.x

Pidgeon, R.T., Wilde, S.A., 1990. The distribution of 3.0 Ga and 2.7 Ga volcanic episodes in the Yilgarn Craton of Western Australia. Precambrian Res. 48, 309–325.

Piispa, E.J., Smirnov, A. V, Pesonen, L.J., Lingadevaru, M., Anantha Murthy, K.S., Devaraju, T.C., 2011. An Integrated Study of Proterozoic Dykes, Dharwar Craton, Southern India 33–45. doi:10.1007/978-3-642-12496-9_3

Pirajno, F., Hoatson, D.M., 2012. A review of Australia's Large Igneous Provinces and associated mineral systems: implications for mantle dynamics through geological time. Ore Geol. Rev. 48, 2–54.

Pisarevsky, S.A., Elming, S.-Å., Pesonen, L.J., Li, Z.-X., 2014a. Mesoproterozoic paleogeography: Supercontinent and beyond. Precambrian Res. 244, 207–225. doi:10.1016/j.precamres.2013.05.014

Pisarevsky, S.A., Wingate, M.T.D., Li, Z.-X., Wang, X.-C., Tohver, E., Kirkland, C.L., 2014b. Age and paleomagnetism of the 1210Ma Gnowangerup–Fraser dyke swarm, Western Australia, and implications for late Mesoproterozoic paleogeography. Precambrian Res. 246, 1–15. doi:10.1016/j.precamres.2014.02.011

Pisarevsky, S., De Waele, B., Jones, S., Söderlund, U., Ernst, R.E., 2015. Paleomagnetism and U–Pb age of the 2.4Ga Erayinia mafic dykes in the south-western Yilgarn, Western Australia: Paleogeographic and geodynamic implications. Precambrian Res. 259, 222–231. doi:10.1016/j.precamres.2014.05.023

Pollard, D.D., 1987. Elementary fracture mechanics applied to the structural interpretation of dykes, in: Mafic Dyke Swarms. Geological Association of Canada Special Paper 34, pp. 5–24.

Prokoph, A., Ernst, R.E., Buchan, K.L., 2004. Time-Series Analysis of Large Igneous Provinces: 3500 Ma to Present. J. Geol. 112, 1–22.

Puffer, J.H., 2003. A Reactivated Back-Arc Source for CAMP Magma. Insights from Fragments of Pangea. AGU Monograph 136, 151–162.

Puffer, J.H., 2001. Contrasting high field strength element contents of continental flood basalts from plume versus reactivated-arc sources. Geology 29, 675–678.

Qiu, Y., Groves, D.I., McNaughton, N.J., 1997. Deep-seated granitoids: implications for Late Archaean subduction-collision-lithospheric delamination and gold mineralization in the Yilgarn Craton. Aust. Geol. Surv. Organ. Rec. 41, 65–69.

Qiu, Y., McNaughton, N.J., Groves, D.I., Dunphy, J.M., 1999. First record of 1.2 Ga quartz dioritic magmatism in the Archaean Yilgarn Craton, Western Australia, and its significance. Aust. J. Earth Sci. 46, 421–428. doi:10.1046/j.1440-0952.1999.00715.x

Rasmussen, B., Fletcher, I.R., 2004. Zirconolite: A new U-Pb chronometer for mafic igneous rocks. Geology 32, 785–788.

Ravich, M.G., Klimov, L. V, Solov′ev, D.S., 1968. The Pre-Cambrian of East Antarctica. Israel Program for Scientific Translations [available from the US Department of Commerce, Clearinghouse for Federal Scientific and Technical

Information, Springfield, Va.].

Richards, M.A., Duncan, R.A., Courtillot, V.E., 1989. Flood basalts and hot-spot tracks: plume heads and tails. Science 246, 103–107.

Rivers, T., Corrigan, D., 2000. Convergent margin on southeastern Laurentia during the Mesoproterozoic: tectonic implications. Can. J. Earth Sci. 37, 359–383.

Rogers, J.J.W., 1996. A History of Continents in the past Three Billion Years. J. Geol. 104, 91–107.

Rogers, J.J.W., Santosh, M., 2004. Continents and supercontinents. Oxford University Press.

Rogers, J.J.W., Santosh, M., 2003. Supercontinents in earth history. Gondwana Res. 6, 357–368. doi:10.1016/S1342-937X(05)70993-X

Rogers, J.J.W., Santosh, M., 2002. Configuration of Columbia, a Mesoproterozoic Supercontinent. Gondwana Res. 5, 5–22. doi:10.1016/s1342-937x(05)70883-2

Santosh, M., 2010. Supercontinent tectonics and biogeochemical cycle: A matter of “life and death.” Geosci. Front. 1, 21–30. doi:10.1016/j.gsf.2010.07.001

Sheppard, S., Bodorkos, S., Johnson, S.P., Wingate, M.T.D., Kirkland, C.L., 2010. The Paleoproterozoic Capricorn Orogeny: intracontinental reworking not continent–continent collision, Geological Survey of Western Australia Report 108. Geological Survey of Western Australia.

Sheraton, J.W., Black, L.P., McCulloch, M.T., Oliver, R.L., 1990. Age and origin of a compositionally varied mafic dyke swarm in the Bunger Hills, East Antarctica. Chem. Geol. 85, 215–246.

Sheraton, J.W., Black, L.P., Tindle, A.G., 1992. Petrogenesis of plutonic rocks in a Proterozoic granulite-facies terrane — the Bunger Hills, East Antarctica. Chem. Geol. 97, 163–198. doi:10.1016/0009-2541(92)90075-G

Sheraton, J.W., Tingey, R.J., 1994. Bedrock Geology of the Bunger Hills-Denman Glacier Region, Australian Antarctic Territory. Aust. Geol. Surv. Organ. 1250 000 Map Ser.

Sheraton, J.W., Tingey, R.J., Black, L.P., Oliver, R.L., 1993. Geology of the Bunger Hills area, Antarctica: implications for Gondwana correlations. Antarct. Sci. 5, 85–102. doi:10.1017/S0954102093000112

Sheraton, J.W., Tingey, R.J., Oliver, R.L., Black, L.P., 1995. Geology of the Bunger Hills-Denman Glacier region, East Antarctica, BMR Bulletin 244. Australian

Geological Survey Organisation.

Smith, A.D., 1992. Back-arc convection model for Columbia River basalt genesis. Tectonophysics 207, 269–285.

Smithies, R.H., Champion, D.C., 1999. Late Archaean felsic alkaline igneous rocks in the Eastern Goldfields, Yilgarn Craton, Western Australia: a result of lower crustal delamination? J. Geol. Soc. London. 156, 561–576.

Sobolev, S. V., Sobolev, A. V., Kuzmin, D. V., Krivolutskaya, N.A., Petrunin, A.G., Arndt, N.T., Radko, V.A., Vasiliev, Y.R., 2011. Linking mantle plumes, large igneous provinces and environmental catastrophes. Nature 477, 312–316. doi:10.1038/nature10385

Söderlund, U., Hofmann, A., Klausen, M.B., Olsson, J.R., Ernst, R.E., Persson, P.O., 2010. Towards a complete magmatic barcode for the Zimbabwe craton: Baddeleyite U-Pb dating of regional dolerite dyke swarms and sill complexes. Precambrian Res. 183, 388–398. doi:10.1016/j.precamres.2009.11.001

Sofoulis, J., 1965. Explanatory Notes on the Widgiemooltha 1: 250,000 Geological Sheet Western Australia. Geological Survey of Western Australia.

Spaggiari, C.V., Kirkland, C.L., Smithies, H.R., Wingate, M.T.D., Belousova, E.A., 2015. Transformation of an Archean craton margin during Proterozoic basin formation and magmatism: The Albany–Fraser Orogen, Western Australia. Precambrian Res. 266, 440–466. doi:10.1016/j.precamres.2015.05.036

Spaggiari, C. V, Bodorkos, S., Barquero-Molina, M., Tyler, I.M., Wingate, M.T.D., 2009. Interpreted bedrock geology of the South Yilgarn and of the South Yilgarn and Central Albany-Fraser Orogen, Western Australia, Geological Survey of Western Australia Record 2009/10.

Spaggiari, C. V, Kirkland, C.L., Pawley, M.J., Smithies, R.H., Wingate, M.T.D., Doyle, M.G., Blenkinsop, T.G., Clark, C., Oorschot, C.W., Fox, L.J., 2011. The geology of the east Albany-Fraser Orogen—a field guide, Geological Survey of Western Australia Record 2011/23.

Stampfli, G.M., Hochard, C., Vérard, C., Wilhem, C., 2013. The formation of Pangea. Tectonophysics 593, 1–19.

Stracke, A., Hofmann, A.W., Hart, S.R., 2005. FOZO, HIMU, and the rest of the mantle zoo. Geochemistry, Geophys. Geosystems 6, Q05007 doi:10.1029/2004GC000824

Stüwe, K., Powell, R., 1989. Metamorphic evolution of the Bunger Hills, East Antarctica: evidence for substantial post-metamorphic peak compression with minimal cooling in a Proterozoic orogenic event. J. Metamorph. Geol. 7, 449–464.

Stüwe, K., Wilson, C.J.L., 1990. Interaction between deformation and charnockite emplacement in the Bunger Hills, East Antarctica. J. Struct. Geol. 12, 767–783. doi:10.1016/0191-8141(90)90088-g

Tucker, D.H., Boyd, D.M., 1987. Dykes of Australia detected by airborne magnetic surveys, in: Fahrig, W.F., Halls, H.C. (Eds.), Mafic Dyke Swarms. Geological Association of Canada Special Paper 34, pp. 163–172.

Tucker, N.M., Hand, M., 2016. New constraints on metamorphism in the Highjump Archipelago, East Antarctica. Antarct. Sci. 28, 487–503. doi:10.1017/S095410201600033X

Tucker, N.M., Payne, J.L., Clark, C., Hand, M., Taylor, R.J., Kylander-Clark, A.R.C., 2017. Proterozoic reworking of Archean (Yilgarn) basement in the Bunger Hills, east Antarctica. Precambrian Res. 298, 16–38.

Vaughan, A.P.M., Storey, B.C., 2007. A new supercontinent self-destruct mechanism: evidence from the Late Triassic–Early Jurassic. J. Geol. Soc. London. 164, 383–392.

Wang, X.-C., Li, X.-H., Li, W.-X., Li, Z.-X., Liu, Y., Yang, Y.-H., Liang, X.-R., Tu, X.-L., 2008. The Bikou basalts in the northwestern Yangtze block, South China: Remnants of 820-810 Ma continental flood basalts? Geol. Soc. Am. Bull. 120, 1478–1492. doi:10.1130/B26310.1

Wang, X.-C., Li, Z.-X., Li, J., Pisarevsky, S.A., Wingate, M.T.D., 2014. Genesis of the 1.21 Ga Marnda Moorn large igneous province by plume–lithosphere interaction. Precambrian Res. 241, 85–103. doi:10.1016/j.precamres.2013.11.008

Wang, X.-C., Li, Z.-X., Li, X.-H., Li, J., Xu, Y.-G., Li, X.-H., 2013. Identification of an ancient mantle reservoir and young recycled materials in the source region of a young mantle plume: Implications for potential linkages between plume and plate tectonics. Earth Planet. Sci. Lett. 377–378, 248–259. doi:10.1016/j.epsl.2013.07.003

Wang, X.-C., Wilde, S.A., Li, Q.-L., Yang, Y.-N., 2015. Continental flood basalts derived from the hydrous mantle transition zone. Nat. Commun. 6, 7700. doi:http://dx.doi.org/10.1038/ncomms8700

Wang, X.-C., Wilde, S.A., Xu, B., Pang, C.-J., 2016. Origin of arc-like continental basalts: Implications for deep-Earth fluid cycling and tectonic discrimination. Lithos 261, 5–45. doi:10.1016/j.lithos.2015.12.014

White, R., McKenzie, D., 1989. Magmatism at rift zones: The generation of volcanic continental margins and flood basalts. J. Geophys. Res. 94, 7685. doi:10.1029/JB094iB06p07685

Wignall, P.B., 2001. Large igneous provinces and mass extinctions. Earth-Science Rev. 53, 1–33.

Wijk, J.W. van, Huismans, R.S., Ter Voorde, M., Cloetingh, S., 2001. Melt generation at volcanic continental margins: no need for a mantle plume? Geophys. Res. Lett. 28, 3995–3998.

Wilde, S.A., 1999. Evolution of the Western Margin of Australia during the Rodinian and Gondwanan Supercontinent Cycles. Gondwana Res. 2, 481–499. doi:10.1016/S1342-937X(05)70287-2

Wilde, S.A., Middleton, M.F., Evans, B.J., 1996. Terrane accretion in the southwestern Yilgarn Craton: evidence from a deep seismic crustal profile. Precambrian Res. 78, 179–196.

Wilde, S.A., Pidgeon, R.T., 1986. Geology and geochronology of the Saddleback greenstone belt in the Archaean Yilgarn Block, southwestern Australia. Aust. J. Earth Sci. 33, 491–501.

Williams, H., Hoffman, P.F., Lewry, J.F., Monger, J.W.H., Rivers, T., 1991. Anatomy of North America: thematic geologic portrayals of the continent. Tectonophysics 187, 117–134.

Wingate, M.T.D., 2017. Mafic dyke swarms and large igneous provinces in Western Australia get a digital makeover, in: Geological Survey of Western Australia Record 2017/2. pp. 4–8.

Wingate, M.T.D., 2007. Proterozoic mafic dykes in the Yilgarn Craton, in: Proceedings of Geoconferences (WA) Inc. Kalgoorlie 2007 Conference, Kalgoorlie, Western Australia. pp. 80–84.

Wingate, M.T.D., 1999. Ion microprobe baddeleyite and zircon ages for Late Archaean mafic dykes of the Pilbara Craton, Western Australia. Aust. J. Earth

Sci. 46, 493–500. doi:10.1046/j.1440-0952.1999.00726.x

Wingate, M.T.D., Campbell, I.H., Harris, L.B., 2000. SHRIMP baddeleyite age for the Fraser dyke swarm, southeast Yilgarn Craton, Western Australia. Aust. J. Earth Sci. 47, 309–313.

Wingate, M.T.D., Evans, D.A.D., 2003. Palaeomagnetic constraints on the Proterozoic tectonic evolution of Australia. Geol. Soc. London, Spec. Publ. 206, 77–91.

Wingate, M.T.D., Pidgeon, R.T., 2005. The Marnda Moorn LIP, a late Mesoproterozoic large igneous province in the Yilgarn craton, Western Australia. July 2005 LIP of the month [WWW Document]. (unpub). Large Igneous Prov. Comm. Int. Assoc. Volcanol. Chem. Earth's Inter. URL http://www.largeigneousprovinces.org/05jul

Wingate, M.T.D., Pirajno, F., Morris, P.A., 2004. Warakurna large igneous province: a new Mesoproterozoic large igneous province in west-central Australia. Geology 32, 105–108.

Winter, J.D., 2014. Principles of igneous and metamorphic petrology, Second edi. ed. Pearson Education.

Witt, W.K., Cassidy, K.F., Lu, Y.-J., Hagemann, S.G., 2018. The tectonic setting and evolution of the 2.7 Ga Kalgoorlie–Kurnalpi Rift, a world-class Archean gold province. Miner. Depos. doi:10.1007/s00126-017-0778-9

Worsley, T.R., Moody, J.B., Nance, R.D., 1985. Proterozoic to Recent Tectonic Tuning of Biogeochemical Cycles, in: The Carbon Cycle and Atmospheric CO2: Natural Variations Archean to Present. American Geophysical Union Monograph Series, pp. 561–572. doi:10.1029/GM032p0561

Worsley, T.R., Nance, D., Moody, J.B., 1984. Global tectonics and eustasy for the past 2 billion years. Mar. Geol. 58, 373–400. doi:10.1016/0025-3227(84)90209-3

Worsley, T.R., Nance, R.D., 1989. Carbon redox and climate control through Earth history: a speculative reconstruction. Glob. Planet. Change 1, 259–282.

Worsley, T.R., Nance, R.D., Moody, J.B., 1991. Tectonics, life, and climate for the last three billion years: a unified system?, in: Schneider, S.H., Boston, P.J. (Eds.), Scientists on Gaia. MIT Press, Cambridge, MA, pp. 200–210.

Worsley, T.R., Nance, R.D., Moody, J.B., 1986. Tectonic cycles and the history of the Earth's biogeochemical and paleoceanographic record. Paleoceanography 1, 233–263.

Worsley, T.R., Nance, R.D., Moody, J.B., 1982. Plate tectonic episodicity: a deterministic model for periodic "Pangeas." Eos, Trans. Am. Geophys. Union 65, 1104.

Xia, L.-Q., 2014. The geochemical criteria to distinguish continental basalts from arc related ones. Earth-Science Rev. 139, 195–212.

Yale, L.B., Carpenter, S.J., 1998. Large igneous provinces and giant dike swarms: proxies for supercontinent cyclicity and mantle convection. Earth Planet. Sci. Lett. 163, 109–122.

Young, G.M., 2013. Precambrian supercontinents, glaciations, atmospheric oxygenation, metazoan evolution and an impact that may have changed the second half of Earth history. Geosci. Front. 4, 247–261.

Zhao, G., Cawood, P.A., Wilde, S.A., Sun, M., 2002. Review of global 2.1-1.8 Ga orogens: implications for a pre-Rodinia supercontinent. Earth-Science Rev. 59, 125–162.

Zhong, S., Zhang, N., Li, Z.-X., Roberts, J.H., 2007. Supercontinent cycles, true polar wander, and very long-wavelength mantle convection. Earth Planet. Sci. Lett. 261, 551–564.

Zibra, I., Clos, F., Weinberg, R.F., Peternell, M., 2017a. The ~2730 Ma onset of the Neoarchean Yilgarn Orogeny. Tectonics 36, 1787–1813. doi:10.1002/2017TC004562

Zibra, I., Korhonen, F.J., Peternell, M., Weinberg, R.F., Romano, S.S., Braga, R., De Paoli, M.C., Roberts, M., 2017b. On thrusting, regional unconformities and exhumation of high-grade greenstones in Neoarchean orogens. The case of the Waroonga Shear Zone, Yilgarn Craton. Tectonophysics 712–713, 362–395. doi:10.1016/j.tecto.2017.05.017

Zindler, A., Hart, S., 1986. Chemical geodynamics. Annu. Rev. Earth Planet. Sci. 14, 493–571.

Chapter 3 U-Pb geochronology of mafic dykes

The key technique in this PhD project is the use of a combination of *in situ* secondary ion mass spectrometry (SIMS) and isotope dilution thermal ionisation mass spectrometry (ID-TIMS) U-Pb techniques on baddeleyite. The *in situ* SIMS U-Pb method was employed as a reconnaissance tool to obtain approximate ages from samples that are considered unsuitable for conventional dating techniques. Based on these results, selected samples were re-dated by ID-TIMS to obtain high-precision ages. This Chapter outlines the concept of the *in situ* technique, and the principles of SIMS and ID-TIMS U-Pb dating of baddeleyite. Chapters 4-7 (4.5.1, 4.5.2, 5.5.1, 5.5.2, 6.5.1, 6.5.2 and 7.7.1) include detailed descriptions of the analyses and data processing methods for both SIMS and ID-TIMS and are not discussed here.

3.1 Geochronology of mafic dykes

Mafic dykes comprise predominantly of pyroxene, plagioclase and amphibole with a wide array of accessory minerals such as micas, Fe-Ti oxides and apatite. The methods of choice for precise geochronology of mafic dykes most commonly involve the U-Th-Pb and the $^{40}Ar/^{39}Ar$ systems. Plagioclase, amphibole and K-bearing mica minerals are targeted by the $^{40}Ar/^{39}Ar$ method (Kelley, 2002 and references therein; Merrihue and Turner, 1966). However, plagioclase is sensitive to retrograde metamorphism and hydrothermal alteration, which hampers its use for dating most Precambrian dykes. Pyroxene is generally more resistant to alteration than plagioclase under the same conditions but so far has only been successfully used to date Phanerozoic dolerites (Ware and Jourdan, 2018). The $^{40}Ar/^{39}Ar$ method on pyroxene is currently being refined and may become a viable alternative for dating Precambrian mafic dykes in the future (Ware and Jourdan, 2018).

Target minerals for U-Pb geochronology must have high uranium and low initial lead contents and be resistant to the effects of weathering and alteration processes. The most commonly used mineral in U-Pb geochronology is zircon ($ZrSiO_2$), which is ubiquitous in intermediate and felsic rocks. However, mafic and tholeiitic magmas are silica-undersaturated and zircon preferentially precipitates from very late stage fractionated melts (e.g. Black et al., 1991; Niu et al., 2002; Schaltegger and Davies, 2017). Baddeleyite (ZrO_2) commonly crystallizes from mafic melts during late stages of fractional crystallisation and has been extensively used in U-Pb dating of mafic, ultramafic and alkaline rocks (Krogh et al., 1987; Heaman and LeCheminant, 1993; French et al., 2002; Wu et al., 2015; Schaltegger and Davies, 2017; Schoene and Baxter, 2017). Baddeleyite is ideal for dating of mafic rocks because it is common, rarely xenocrystic, enriched in uranium (200-1000 ppm; e.g. Heaman and LeCheminant, 1993) and has negligible common lead. Baddeleyite commonly has very low Th content with Th/U ratios <0.05 (e.g. Heaman and LeCheminant, 1993). Where both zircon and baddeleyite are found in the same sample, zircon typically has a higher uranium content and is more susceptible to Pb loss than baddeleyite due to radiation damage and metamictisation (Heaman and Machado, 1992; Heaman and LeCheminant, 1993). In contrast to zircon, baddeleyite is more susceptible to alteration and reaction with silica-rich fluids or melts, readily developing zircon rims or recrystallising to zircon under igneous and metamorphic conditions (Davidson and van Breemen, 1988; Heaman and LeCheminant, 1993; Söderlund et al., 2008; Wu et al., 2015; Schaltegger and Davies, 2017). As an alternative U-Pb mineral chronometer to zircon and baddeleyite, zirconolite ($CaZrTi_2O_7$), which is an accessory phase in mafic and ultramafic rocks (Heaman et al., 1992; Heaman and LeCheminant, 1993) yields excellent precision (Rasmussen and Fletcher, 2004) although it has not been widely used.

In addition to their silica-unsaturated mineralogy, further challenges for geochronology of mafic dykes arise from their grain size, which limits the choice of the techniques and instruments. Mafic dykes form as linear features with very high length to width ratios and unless the dyke width is large (>20 m), they generally crystallise as basalts and dolerites, in which baddeleyite crystals typically form euhedral thin blades and prisms <10-20 μm in length (e.g. French et al., 2002; Heaman and LeCheminant, 1993). Wider dykes, especially those with gabbroic central portions, and extremely fractionated late stage felsic segregations associated with mafic dykes are usually targeted for geochronology (e.g. Black et al., 1991). However, in many areas of the Yilgarn Craton, dykes form discontinuous and scattered outcrops of mafic boulders (Fig. 1.1). Most dykes are relatively thin, have undergone retrograde metamorphism (destroying plagioclase and pyroxene and preventing use of the $^{40}Ar/^{39}Ar$ method) and are fine- to medium-grained with no felsic segregations (making standard heavy mineral separations for zircon and baddeleyite ineffective). Many of these dykes would be very difficult to date using a conventional approach either with $^{40}Ar/^{39}Ar$ or U-Pb.

Figure 3.1 Large mafic dyke outcrop in an agriculturally cleared area in southwestern Yilgarn Craton. This dyke was dated at 2615 Ma (see Chapter 4).

3.2 The *in situ* method

The most common approach for separating minerals from a rock involves crushing of the bulk rock sample followed by separation of crystals based on their magnetic susceptibility and density using methods such as isodynamic magnetic separators, heavy liquids lines and water shaking tables (e.g. Jones, 1987; McClenaghan, 2011; Silva, 1986; Söderlund and Johansson, 2002; Towie and Seet, 1995). This method offers high sample throughput and the potential to extract a large number of crystals in one separation (if the dykes are coarse grained or contain felsic segregates). The disadvantages of this approach include the risk of cross contamination from equipment, mix-up of samples, loss of textural context and, especially for fine grained rocks, the damage or loss of exceedingly small crystals targeted for geochronology (no yield). Moreover, availability of large amounts of sample (several hundred grams to several kilograms) is not always possible although improvements in techniques for extraction of baddeleyite have been made (Söderlund and Johansson, 2002).

The *in situ* method offers an alternative approach, which avoids cross contamination, allows for identification and analysis of very small crystals and preserves the mineralogical and textural context of the analysed sample (Rasmussen and Fletcher, 2002, 2010, Rasmussen et al., 2004, 2008; Kröner, 2010; Wu et al., 2015; Zi et al., 2015; Schaltegger and Davies, 2017). This involves collecting a representative set of samples, identifying suitable chronometers from thin sections, obtaining a low-precision SIMS age to determine whether the dyke is of a previously unknown age and finally acquiring a high-precision ID-TIMS age for specifically selected samples. Identification of suitable crystals is undertaken using scanning electron microscopy (SEM) and energy-dispersive X-ray spectrometry (EDX). Suitable crystals are extracted by directly drilling them out of the thin sections using a micro-drill and mounting them in an epoxy disk which is coated in conductive material (Figure 3.2). Depending on the instrument, a minimum of 8-10 plugs can be embedded in a standard mount of ca. 25 mm in diameter but larger mount sizes (megamounts) are also available. Since the thin section is already polished, the surface of the mount containing the thin section plugs requires no further polishing. A separate mount with relevant standards is analysed with the sample mount throughout the session.

3.3 *In situ* SIMS U-Pb geochronology of baddeleyite

Techniques such as Laser Ablation-Inductively Coupled Plasma-Mass Spectrometry (LA-ICP-MS) generally requires crystals of >20 μm in size (e.g. French et al., 2002) and baddeleyite in mafic rocks typically forms as thin blades that are too small to apply typical laser spot sizes, although recent developments on LA-ICP-MS baddeleyite dating have reduced the spot size down to 10 μm (Ibanez-Mejia et al., 2014). The spot size of the primary ion beam of SIMS can be as small as 5-10 μm in size is possible using instruments such as the Sensitive High Resolution Ion Microprobe (SHRIMP) (Compston et al., 1984) and the CAMECA IMS 1270/1280 (Chamberlain et al., 2010; Schmitt et al., 2010; Liu et al., 2011).

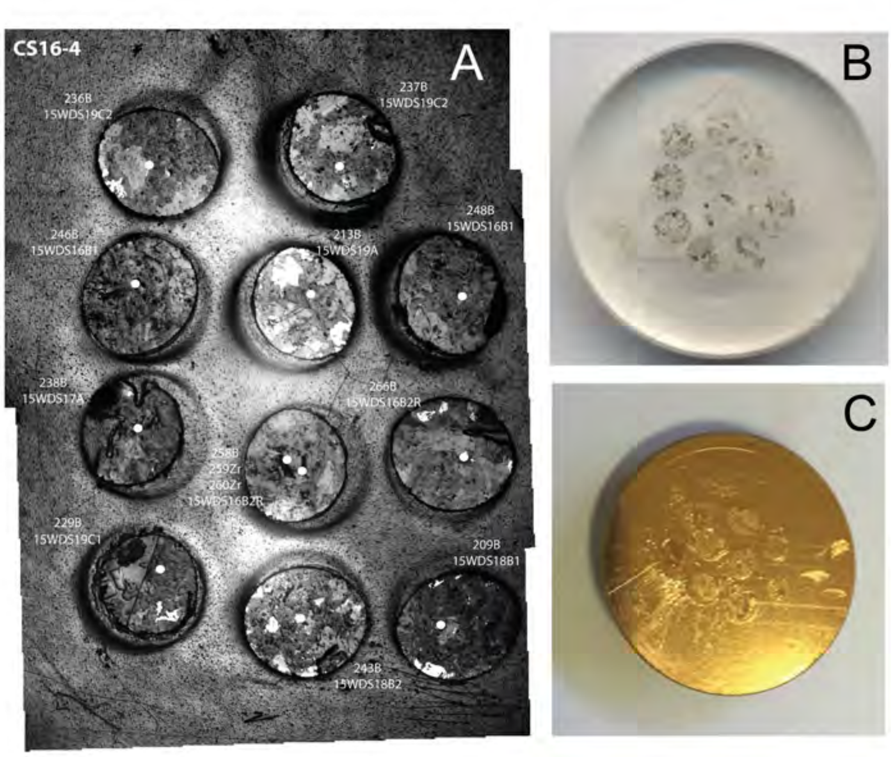

Figure 3.2 In situ U-Pb ion microprobe mounts ***(A)*** *Reflected light image of a mount showing plugs drilled out of the thin section. Note white dots denoting locations of baddeleyites identified suitable for ion microprobe analysis. FOV is approximately 15 mm* ***(B)*** *Uncoated epoxy mount showing 10 drilled out thin section plugs. Mount is ca. 25 mm in diameter* ***(C)*** *Gold coated epoxy mount.*

The SIMS U-Pb dating technique involves ablation of a small spot (~10-15 μm) with shallow pit depth (<2 μm) on the surface of the sample by a primary ion beam (commonly O^- or O^+) and double-focussing the resulting secondary ion beam into a mass spectrometer using an electrostatic analyser and a large-radius magnetic sector (Williams, 1998; Ireland and Williams, 2003; Schoene, 2013). The very high mass resolution (up to 10,000) and sensitivity of SIMS allows isobaric (equal mass) interferences between critical mass peaks such as ^{206}Pb to be distinguished at very low detection limits. The SHRIMP II is capable of mass resolution of 5000 at sensitivity of ≥20 counts/sec/ppm/nA for Pb from zircon (Williams, 1998).

Both Pb isotopic compositions and the Pb/U ratios must be measured accurately. Instrumentation effects and compositional differences in the analysed materials (matrix effects; e.g. Fletcher et al., 2010; Schoene, 2013) can lead to variability in the isotopic and elemental composition of the secondary ion beam during the analytical session. To counter this, standard samples are measured together with the unknowns, and measurements of the known Pb/U ratio of the standards are used to correct for fractionation between Pb and U during sputtering. This is possible because the UO^+/U^+ ratio can be measured directly and Pb^+/U co-varies with UO^+/U^+ during a session (Hinthorne et al., 1979). The average precision of single SIMS U-Pb dates is ca. 3%, which is due to elemental fractionation during slow sputtering (typically 20 min per spot), compositional changes in the analysed mineral and standard, and variability of the beam intensity during the session (Williams, 1998; Ireland and Williams, 2003; Schoene, 2013). Precision of standard measurements generally reflects the precision of the unknown measurements during the analytical session and between sessions (Stern and Amelin, 2003).

Baddeleyite crystals are twinned and exhibit crystal orientation effects (fractionation) in measured $^{206}Pb/^{238}U$ ratios under SIMS (Wingate and Compston, 2000; Schmitt et al., 2010). However, this does not affect the measured $^{207}Pb/^{206}Pb$ ratios and poses few problems when the radiogenic Pb content of the sample is high, i.e. in older (>1 Ga) rocks. For younger rocks the achievable accuracy and precision are low, and alternative techniques, such as LA-ICP-MS which do not appear to be affected by orientation effects on the measured $^{206}Pb/^{238}U$ ratios (e.g. Ibanez-Mejia et al., 2014), should be considered. The uncertainty in the isotopic composition of the common lead correction is greater than the analytical uncertainty of single measurments at low radiogenic Pb content (young rocks or rocks with low initial U content) and affects predominantly the $^{207}Pb/^{235}U$ system.

Generally, the precision of SIMS measurements from baddeleyite is lower than those from zircon mainly due to the their lower U content and their commonly small size of baddeleyite crystals, necessitating small spot size and consequently lower sensitivity (counts). Analysis of small baddeleyite crystals with SIMS can require a large number of measurements to reach acceptable precision. If the number of available samples is low, this may be a very difficult task. Better precision may be achieved by pooling a large number of analyses together and by applying statistical models, such as least-squares linear fit (isochron) and a weighted mean. The goodness of fit of the data to the model reflects the accuracy of the obtained age and can be evaluated using the mean square of weighted deviates (MSWD), which is 1 when there is a perfect match between the data and the model. However, if the geological uncertainties (e.g. Pb loss and mixing) are small compared with uncertainties of the individual data points (low precision dates), application of weighted mean can result in inaccurate but statistically robust ages (Schoene, 2013 and references therein).

3.4 Application of the *in situ* SIMS U-Pb method on mafic dykes in the Yilgarn Craton, Western Australia

In this study, sampling was undertaken in a targeted field area in the southwestern Yilgarn Craton, where mapping and aeromagnetic data indicated presence of many different dyke trends. In this area, most dyke contacts are not visible, the outcrop is limited and felsic segregations are rarely available. Most of the collected samples appeared suboptimal for geochronology due to alteration and/or fine grain size but they were nevertheless collected due to general scarcity of available outcrop. Out of the sampled dykes, SHRIMP dating identified three new but imprecise ages, which were followed up by re-dating with ID-TIMS.

Once collected, up to four thin sections per dyke were prepared for petrographic assessment to identify potential chronometers. Due to variable alteration of plagioclase (and pyroxene), use of the $^{40}Ar/^{39}Ar$ method was deemed unfeasible and alternative targets for U-Pb chronometers were searched using SEM-EDX. Zircon crystals were identified in some samples but all were unsuitable due to metamictisation. Baddeleyite was therefore selected as the only viable chronometer. Most baddeleyite crystals were too small (<10-15 μm in width) for SHRIMP dating and in average <10 % of identified crystals per thin section were suitable. The very small size of the baddeleyite crystals discounted use of standard bulk mineral separation techniques and the crystals were drilled out directly from the thin sections. They were then analysed *in situ* using the SHRIMP II to obtain an approximate age, which was adequate to determine whether the dyke was likely part of an already known dyke swarm. For each dyke with an indicated new age, samples with the best SHRIMP ages (presumed to have the highest probability of producing dateable crystals) were selected for bulk mineral separation using the water table method after

Söderlund et al. (2002). For two of the three dykes, only four baddeleyite crystals were successfully extracted from the bulk sample (Chapters 3 and 4).

3.5 ID-TIMS U-Pb geochronology

Isotope dilution thermal ionisation mass spectrometry of the U-Pb isotope system (Tilton et al., 1955; Wetherill, 1956) is based on measurement of the isotopic composition of U and Pb and is the highest precision dating method for zircon and baddeleyite. It can produce precision and accuracy better than of 0.1% (2σ) of the age for single crystals with extremely low concentration (picograms) of Pb (Schoene and Baxter, 2017 and references therein). This is mainly due to good ionisation efficiency, simple mass spectrum, high signal-to-noise ratio, low mass fractionation, negligible U and common Pb contamination and no requirement for standards (Parrish et al., 2003 and references therein). However, where high spatial resolution is required, e.g. for crystals with highly complex internal structure (multiple age domains), the *in situ* approach should be employed similar to the SIMS and LA-ICP-MS methods (as described in the previous sections). TIMS ion transmission from the source to the analyser is very high and combined with the ability to achieve a stable ion beam over periods of hours, allows for very high precision isotope ratios.

Unlike high-resolution SIMS, which has a mass resolution of ~5000, TIMS is not capable of resolving isobaric and polyatomic interferences due to its lower mass resolution of ~500, and chemical separation using a column with ion exchange resin is employed to separate elements based on their chemical properties. However, the method of Krogh (1973) allows for a simpler process for decomposition of zircon and baddeleyite, and U and Pb are isolated on a Teflon® anion exchange column and also permits an exact measurement of the amount of common Pb (Pb_c) contained in the analysed crystals. This method also uses a silica-gel loading technique, which provides stable emission for Pb for small samples and limits isotope fractionation during analysis by the mass spectrometer.

Isotope dilution technique, an isotope tracer solution containing concentrated parent and daughter element isotopes is added to the sample before the column processing and the unknown ratios can then be calculated from the known and calibrated ratios of the tracer (Wasserburg et al., 1981; Condon et al., 2015). Both the sample and the tracer are analysed simultaneously, eliminating the potential for variable parent/daughter fractionation. Since the initial Pb_c of zircon and baddeleyite is negligible, the Pb_c content of the laboratory blank must be extremely low to achieve high precision dates, i.e. the achievable precision is determined by the procedural blank. Similar to SIMS on zircon and baddelelyite, for young rocks the greatest source of uncertainty is the common Pb (Pb_c) correction because of low radiogenic Pb content of the crystal. For Proterozoic and Archean rocks, the sample size can be larger because of the higher radiogenic Pb in the sample.

Air abrasion is routinely employed to partially remove of the outer part of a zircon crystal, which is likely to have been exposed to Pb loss and would result in discordance in the measured compositions (Krogh, 1982). Chemical abrasion is an alternative technique involving partial leaching in HF or HF-HNO_3 mixtures where more soluble radiation-damaged parts of the crystal would be dissolved (Mattinson, 2005) but this has not been widely adopted. There are currently no established procedures to remove the effects of Pb loss in baddeleyite but a two-step HCl-HF chemical abrasion method has been developed to analyse composite grains containing zircon inter- and overgrowths due to metamorphism (Rioux et al., 2010).

Depending on the approach, after standard bulk separation and cleaning in distilled ultrapure HNO_3, or petrographic characterisation and extraction from a thin section (as discussed in the previous sections), the crystals are typically spiked with the isotope tracer and dissolved in Teflon® microcapsules in concentrated HF and HNO_3 and then placed in a pressure vessel in an oven at 200°C over three to six days. After the residue has been repeatedly dried and re-dissolved in H_3PO_4 and ultrapure HNO_3, they are re-dissolved in silica gel and loaded onto a thin metal filament (typically rhenium or tantalum). The filament is heated under carefully controlled conditions and the ionised sample is accelerated and focussed through the magnetic sectors into the analyzer for measurement of U and Pb isotope peak intensities.

3.6 References

Black, L.P., Kinny, P.D., Sheraton, J.W., 1991. The difficulties of dating mafic dykes: an Antarctic example. Contrib. to Mineral. Petrol. 109, 183–194. doi:10.1007/BF00306478

Chamberlain, K.R., Schmitt, A.K., Swapp, S.M., Harrison, T.M., Swoboda-Colberg, N., Bleeker, W., Peterson, T.D., Jefferson, C.W., Khudoley, A.K., 2010. In situ U–Pb SIMS (IN-SIMS) micro-baddeleyite dating of mafic rocks: method with examples. Precambrian Res. 183, 379–387.

Compston, W., Williams, I.S., Meyer, C., 1984. U-Pb geochronology of zircons from lunar breccia 73217 using a sensitive high mass-resolution ion microprobe. J. Geophys. Res. 89, B525. doi:10.1029/JB089iS02p0B525

Condon, D.J., Schoene, B., McLean, N.M., Bowring, S.A., Parrish, R.R., 2015. Metrology and traceability of U–Pb isotope dilution geochronology (EARTHTIME Tracer Calibration Part I). Geochim. Cosmochim. Acta 164, 464–480.

Davidson, A., van Breemen, O., 1988. Baddeleyite-zircon relationships in coronitic metagabbro, Grenville Province, Ontario: implications for geochronology. Contrib. to Mineral. Petrol. 100, 291–299. doi:10.1007/BF00379740

Fletcher, I.R., McNaughton, N.J., Davis, W.J., Rasmussen, B., 2010. Matrix effects and calibration limitations in ion probe U-Pb and Th-Pb dating of monazite. Chem. Geol. 270, 31–44. doi:10.1016/j.chemgeo.2009.11.003

French, J.E., Heaman, L.M., Chacko, T., 2002. Feasibility of chemical U-Th-total Pb baddeleyite dating by electron microprobe. Chem. Geol. 188, 85–104. doi:10.1016/S0009-2541(02)00074-8

Heaman, L.M., LeCheminant, A.N., 1993. Paragenesis and U-Pb systematics of baddeleyite (ZrO2). Chem. Geol. 110, 95–126. doi:10.1016/0009-2541(93)90249-I

Heaman, L.M., LeCheminant, A.N., Rainbird, R.H., 1992. Nature and timing of Franklin igneous events, Canada: implications for a Late Proterozoic mantle plume and the break-up of Laurentia. Earth Planet. Sci. Lett. 109, 117–131.

Heaman, L.M., Machado, N., 1992. Timing and origin of midcontinent rift alkaline magmatism, North America: evidence from the Coldwell Complex. Contrib. to Mineral. Petrol. 110, 289–303.

Hinthorne, J.R., Andersen, C.A., Conrad, R.L., Lovering, J.F., 1979. Single-grain 207Pb206Pb and U/Pb age determinations with a 10-µm spatial resolution using the ion microprobe mass analyzer (IMMA). Chem. Geol. 25, 271–303.

Ibanez-Mejia, M., Gehrels, G.E., Ruiz, J., Vervoort, J.D., Eddy, M.E., Li, C., 2014. Small-volume baddeleyite (ZrO2) U-Pb geochronology and Lu-Hf isotope geochemistry by LA-ICP-MS. Techniques and applications. Chem. Geol. 384, 149–167. doi:10.1016/j.chemgeo.2014.07.011

Ireland, T.R., Williams, I.S., 2003. Considerations in Zircon Geochronology by SIMS. Rev. Mineral. Geochemistry 53, 215–241. doi:10.2113/0530215

Jones, M.P., 1987. Applied mineralogy: a quantitative approach. Springer, London.

Kelley, S., 2002. K-Ar and Ar-Ar dating. Rev. Mineral. Geochemistry 47, 785–818. doi:10.2138/rmg.2002.47.17

Krogh, T.E., 1982. Improved accuracy of U-Pb zircon ages by the creation of more concordant systems using an air abrasion technique. Geochim. Cosmochim. Acta 46, 637–649.

Krogh, T.E., 1973. A low-contamination method for hydrothermal decomposition of zircon and extraction of U and Pb for isotopic age determinations. Geochim. Cosmochim. Acta 37, 485–494.

Krogh, T.E., Corfu, F., Davus, D.W., Dunning, G.R., Heaman, L.M., Kamo, S.L., Machado, N., 1987. Precise U–Pb Isotopic ages of diabase dykes and mafic to ultramafic rocks using trace amounts of baddeleyite and zircon, in: Halls, H.C., Fahrig, W.F. (Eds.), Mafic Dyke Swarms. Geological Association of Canada Special Paper 34, 147-152.

Kröner, A., 2010. The role of geochronology in understanding continental evolution. Geol. Soc. London, Spec. Publ. 338, 179–196. doi:10.1144/SP338.9

Liu, Y., Li, X.-H., Li, Q.-L., Tang, G.-Q., Yin, Q.-Z., 2011. Precise U–Pb zircon dating at a scale of <5 micron by the CAMECA 1280 SIMS using a Gaussian illumination probe. J. Anal. At. Spectrom. 26, 845. doi:10.1039/c0ja00113a

Mattinson, J.M., 2005. Zircon U–Pb chemical abrasion ("CA-TIMS") method: combined annealing and multi-step partial dissolution analysis for improved precision and accuracy of zircon ages. Chem. Geol. 220, 47–66.

McClenaghan, M.B., 2011. Overview of common processing methods for recovery of indicator minerals from sediment and bedrock in mineral exploration.

Geochemistry Explor. Environ. Anal. 11, 265–278. doi:10.1144/1467-7873/10-IM-025

Merrihue, C., Turner, G., 1966. Potassium-argon dating by activation with fast neutrons. J. Geophys. Res. 71, 2852–2857.

Niu, Y., Gilmore, T., Mackie, S., Greig, A., Bach, W., 2002. Mineral chemistry, whole-rock compositions, and petrogenesis of Leg 176 gabbros: data and discussion. Proc. Ocean Drill. Program, Sci. Results 176, 1–60.

Parrish, R.R., Parrish, R.R., Noble, S.R., 2003. Zircon U-Th-Pb geochronology by isotope dilution—thermal ionization mass spectrometry (ID-TIMS). Rev. Mineral. Geochemistry 53, 183–213.

Rasmussen, B., Fletcher, I.R., 2010. Dating sedimentary rocks using in situ U-Pb geochronology of syneruptive zircon in ash-fall tuff &lt 1 mm thick. Geology 38, 299–302. doi:10.1130/G30567.1

Rasmussen, B., Fletcher, I.R., 2004. Zirconolite: A new U-Pb chronometer for mafic igneous rocks. Geology 32, 785–788.

Rasmussen, B., Fletcher, I.R., 2002. Indirect dating of mafic intrusions by SHRIMP U-Pb analysis of monazite in contact metamorphosed shale: An example from the Palaeoproterozoic Capricorn Orogen, Western Australia. Earth Planet. Sci. Lett. 197, 287–299. doi:10.1016/S0012-821X(02)00501-0

Rasmussen, B., Fletcher, I.R., Bengtson, S., McNaughton, N.J., 2004. SHRIMP U-Pb dating of diagenetic xenotime in the Stirling Range Formation, Western Australia: 1.8 Billion year minimum age for the Stirling biota. Precambrian Res. 133, 329–337. doi:10.1016/j.precamres.2004.05.008

Rasmussen, B., Fletcher, I.R., Muhling, J.R., 2008. Pb/Pb geochronology, petrography and chemistry of Zr-rich accessory minerals (zirconolite, tranquillityite and baddeleyite) in mare basalt 10047. Geochim. Cosmochim. Acta 72, 5799–5818. doi:10.1016/j.gca.2008.09.010

Rioux, M., Bowring, S., Dudás, F., Hanson, R., 2010. Characterizing the U-Pb systematics of baddeleyite through chemical abrasion: Application of multi-step digestion methods to baddeleyite geochronology. Contrib. to Mineral. Petrol. 160, 777–801. doi:10.1007/s00410-010-0507-1

Schaltegger, U., Davies, J.H.F.L., 2017. Petrochronology of Zircon and Baddeleyite in Igneous Rocks: Reconstructing Magmatic Processes at High Temporal

Resolution. Rev. Mineral. Geochemistry 83, 297 LP-328.

Schmitt, A.K., Chamberlain, K.R., Swapp, S.M., Harrison, T.M., 2010. In situ U-Pb dating of micro-baddeleyite by secondary ion mass spectrometry. Chem. Geol. 269, 386–395. doi:10.1016/j.chemgeo.2009.10.013

Schoene, B., 2013. U-Th-Pb Geochronology, Treatise on Geochemistry: Second Edition. doi:10.1016/B978-0-08-095975-7.00310-7

Schoene, B., Baxter, E.F., 2017. Petrochronology and TIMS. Rev. Mineral. Geochemistry 83, 231 LP-260. doi:10.2138/rmg.2017.83.8

Silva, M.A., 1986. Placer gold recovery methods. Special Publication 87. California department of conservation, Division of Mines and Geology, Sacramento, California.

Söderlund, U., Hellström, F.A., Kamo, S.L., 2008. Geochronology of high‐pressure mafic granulite dykes in SW Sweden: tracking the P–T–t path of metamorphism using Hf isotopes in zircon and baddeleyite. J. Metamorph. Geol. 26, 539–560.

Söderlund, U., Johansson, L., 2002. A simple way to extract baddeleyite (ZrO_2). Geochemistry, Geophys. Geosystems 3. doi:10.1029/2001GC000212

Stern, R.A., Amelin, Y., 2003. Assessment of errors in SIMS zircon U-Pb geochronology using a natural zircon standard and NIST SRM 610 glass. Chem. Geol. 197, 111–142. doi:10.1016/S0009-2541(02)00320-0

Tilton, G.R., Patterson, C., Brown, H., Inghram, M., Hayden, R., Hess, D., Larsen Jr, E., 1955. Isotopic composition and distribution of lead, uranium, and thorium in a Precambrian granite. Geol. Soc. Am. Bull. 66, 1131–1148.

Towie, N.J., Seet, L.H., 1995. Diamond laboratory techniques. J. Geochemical Explor. 53, 205–212.

Ware, B., Jourdan, F., 2018. 40 Ar/39 Ar Geochronology of Terrestrial Pyroxene. Geochim. Cosmochim. Acta 230, 112-136.

Wasserburg, G.J., Jacobsen, S.B., DePaolo, D.J., McCulloch, M.T., Wen, T., 1981. Precise determination of Sm/Nd ratios, Sm and Nd isotopic abundances in standard solutions. Geochim. Cosmochim. Acta 45, 2311–2323.

Wetherill, G.W., 1956. Discordant uranium‐lead ages, I. Eos, Trans. Am. Geophys. Union 37, 320–326.

Williams, I.S., 1998. U-Th-Pb geochronology by ion microprobe. Rev. Econ. Geol. 7, 1–35.

Wingate, M.T.D., Compston, W., 2000. Crystal orientation effects during ion microprobe U–Pb analysis of baddeleyite. Chem. Geol. 168, 75–97. doi:10.1016/S0009-2541(00)00184-4

Wu, W.N., Schmitt, A.K., Pappalardo, L., 2015. U-Th baddeleyite geochronology and its significance to date the emplacement of silica undersaturated magmas†. Am. Mineral. 100, 2082–2090.

Zi, J.W., Rasmussen, B., Muhling, J.R., Fletcher, I.R., Thorne, A.M., Johnson, S.P., Cutten, H.N., Dunkley, D.J., Korhonen, F.J., 2015. In situ U-Pb geochronology of xenotime and monazite from the Abra polymetallic deposit in the Capricorn Orogen, Australia: Dating hydrothermal mineralization and fluid flow in a long-lived crustal structure. Precambrian Res. 260, 91–112. doi:10.1016/j.precamres.2015.01.010

Chapter 4 First evidence of Archean mafic dykes at 2.62 Ga in the Yilgarn Craton, Western Australia: links to cratonisation and the Zimbabwe Craton[1]

J. Camilla Stark, Simon A. Wilde, Ulf Söderlund, Zheng-Xiang Li,

Birger Rasmussen, Jian-Wei Zi

4.1 Abstract

The Archean Yilgarn Craton in Western Australia hosts at least five generations of Proterozoic mafic dykes, the oldest previously identified dykes belonging to the ca. 2408–2401 Ma Widgiemooltha Supersuite. We report here the first known Archean mafic dyke dated at 2615 ± 6 Ma by the ID-TIMS U-Pb method on baddeleyite and at 2607 ± 25 Ma using *in situ* SHRIMP U-Pb dating of baddeleyite. Aeromagnetic data suggest that the dyke is part of a series of NE-trending intrusions that potentially extend hundreds of kilometres in the southwestern part of the craton, here named the Yandinilling dyke swarm. Mafic magmatism at 2615 Ma was possibly related to delamination of the lower crust during the final stages of assembly and cratonisation, and was coeval with the formation of late-stage gold deposit at Boddington. Paleogeographic reconstructions suggest that the Yilgarn and Zimbabwe cratons may have been neighbours from ca. 2690 Ma to 2401 Ma and if the Zimbabwe and Kaapvaal cratons amalgamated at 2660-2610 Ma, the 2615 Ma mafic magmatism in the southwestern Yilgarn Craton may be associated with the same tectonic event that produced the ca. 2607–2604 Ma Stockford dykes in the Central Zone of the Limpopo Belt. Paleomagnetic evidence and a similar tectonothermal evolution, including coeval low-pressure high-temperature metamorphism, voluminous magmatism, and emplacement of mafic dykes, support a configuration where the northern part of the Zimbabwe Craton was adjacent to the western margin of the Yilgarn Craton during

[1] *This chapter is published as* Stark, J.C., Wilde, S.A., Soderlund, U., Li, Z.-X., Rasmussen, B., Zi, J.-W., 2018. First evidence of Archean mafic dykes at 2.62 Ga in the Yilgarn Craton, Western Australia: links to cratonisation and the Zimbabwe Craton. Precambrian Res. 317, 1-13.

the Neoarchean. Worldwide, reliably dated mafic dykes of this age have so far been reported from the Yilgarn Craton, the Limpopo Belt and the São Francisco Craton.

4.2 Introduction

Mafic dyke swarms are important markers for supercontinent reconstructions and mantle plumes (e.g., Ernst and Buchan, 1997; Buchan et al., 2001; Bleeker and Ernst, 2006; Ernst and Srivastava, 2008; Ernst et al., 2010, 2013) and act as indicators of local tectonic setting, including paleostress fields and pre-existing crustal weaknesses (Ernst et al., 1995b; Hoek and Seitz, 1995; Halls and Zhang, 1998; Hou, 2012; Ju et al., 2013). Throughout the geological evolution of the Earth, mafic dykes have been associated with processes causing intracratonic extension of the crust, such as subduction (back-arc extension), post-orogenic collapse, plumes and rifting during supercontinent breakup. However, mafic dykes may also be linked with early cratonisation history soon after amalgamation and stabilization of crustal blocks. A recent example is reported from the North China Craton, where emplacement of ca. 2516–2504 Ma dykes signifies the presence of a deep subcontinental lithosphere and constrains the time of final cratonisation during the Neoarchean (Li et al., 2010).

The Archean Yilgarn Craton of Western Australia hosts at least five generations of Proterozoic mafic dykes, including the 2408–2401 Ma Widgiemooltha Supersuite (Sofoulis, 1965; Evans, 1968; Hallberg, 1987; Doehler and Heaman, 1998; Nemchin and Pidgeon, 1998; Wingate, 1999; French et al., 2002; Pisarevsky et al., 2015), the 1888 Ma Boonadgin dykes (Stark et al., in press), the 1210 Ma Marnda Moorn Large Igneous Province (LIP; Wingate et al., 1998, 2000; Wingate, 2007), and limited occurrences of the 1075 Ma Warakurna LIP dykes (Wingate et al., 2002, 2004) and the 735 Ma Nindibillup dykes (Spaggiari et al., 2009, 2011; Wingate, 2017). The Widgiemooltha Supersuite has been linked with a mantle plume and rifting of an Archean supercraton (Heaman, 1997; Halls et al., 2007; Mohanty, 2015), the Boonadgin dykes with post-orogenic far-field extension or a mantle plume (Stark et al., in press) and the Marnda Moorn and Warakurna LIPs also with mantle plumes (Wingate et al., 2004; Wang et al., 2014). We present here *in situ* SHRIMP and ID-TIMS U-Pb results for the first known Archean mafic dyke within the Yilgarn Craton, emplaced during the final stages of cratonisation and marking one of the earliest tectonothermal events affecting the stabilized craton. We discuss the tectonic setting, timing of emplacement and the possible association of the mafic dykes with post-orogenic processes during final stages of cratonisation. We also consider evidence from paleogeographic reconstructions and coeval tectonothermal events that may link the evolution of the Yilgarn and Zimbabwe cratons during the Neoarchean.

4.3 Regional geology

4.3.1 The Yilgarn Craton

The Archean Yilgarn Craton of Western Australia is a ca. 900 x 1000 km granite-greenstone crustal block, which is divided into the South West, Narryer, Youanmi, Kalgoorlie, Kurnalpi and Burtville terranes, the latter three forming the Eastern Goldfields Superterrane (Figure 4.1) (Cassidy et al., 2006). The craton is bounded by three Proterozoic orogenic belts: the ca. 2005─570 Ma Capricorn Orogen in the north (Cawood and Tyler, 2004; Sheppard et al., 2010a; Johnson et al., 2011), the ca. 1815─1140 Ma Albany-Fraser Orogen in the south and east (Nelson et al., 1995a; Clark et al., 2000; Spaggiari et al., 2015), and the ca. 1600–525 Ma Pinjarra Orogen in the west (Myers, 1990; Wilde, 1999; Ksienzyk et al., 2012). Most of the terranes formed between ca. 3050 and 2550 Ma and whereas the South West and Narryer Terranes in the west comprise high-grade supracrustal rocks, granitic gneisses and granites, the Youanmi and Eastern Goldfields Terranes in the east are dominated by greenstone belts separated by granites and granitic gneisses (Figure 4.2) (e.g., Gee et al., 1981; Pidgeon and Wilde, 1990; Myers, 1993; Wilde et al., 1996; Nelson, 1997; Cassidy et al., 2002; Barley et al., 2003). Recent Sm-Nd isotopic mapping suggests the presence of an older western proto-craton comprising the Narryer, South West and Youanmi Terranes and a younger (more juvenile) eastern part, which comprises the Eastern Goldfields Superterrane (e.g. Champion and Cassidy, 2007; Mole et al., 2013; Witt et al., 2018).

Amalgamation of the Yilgarn Craton involved repeated collisions during a Neoarchean orogeny between ca. 2730 and 2625 Ma (Myers, 1993, 1995; Barley et al., 2003; Blewett and Hitchman, 2006; Korsch et al., 2011; Zibra et al., 2017a; Witt et al., 2018) with development of a stable cratonic lithosphere by ca. 2660 Ma (Zibra et al., 2017b). The Youanmi Terrane is considered to be the isotopically oldest nucleus of the Yilgarn Craton onto which other terranes accreted (Cassidy et al., 2002, 2006; Champion and Cassidy, 2008; David C Champion, 2013), with collisions between the Youanmi and Narryer terranes sometime between ca. 2780 and 2630 Ma (Myers, 1993, 1995; Nutman et al., 1993; Cassidy et al., 2002), the Youanmi and Kalgoorlie Terranes between ca. 2678 and 2658 Ma (Standing, 2008; Czarnota et al., 2010) and the Youanmi and the South West Terranes between ca. 2652 and 2625 Ma (Wilde and Pidgeon, 1987; Nemchin et al., 1994; Qiu et al., 1997a; Qiu and Groves, 1999; McFarlane, 2010). Cratonisation was accompanied by

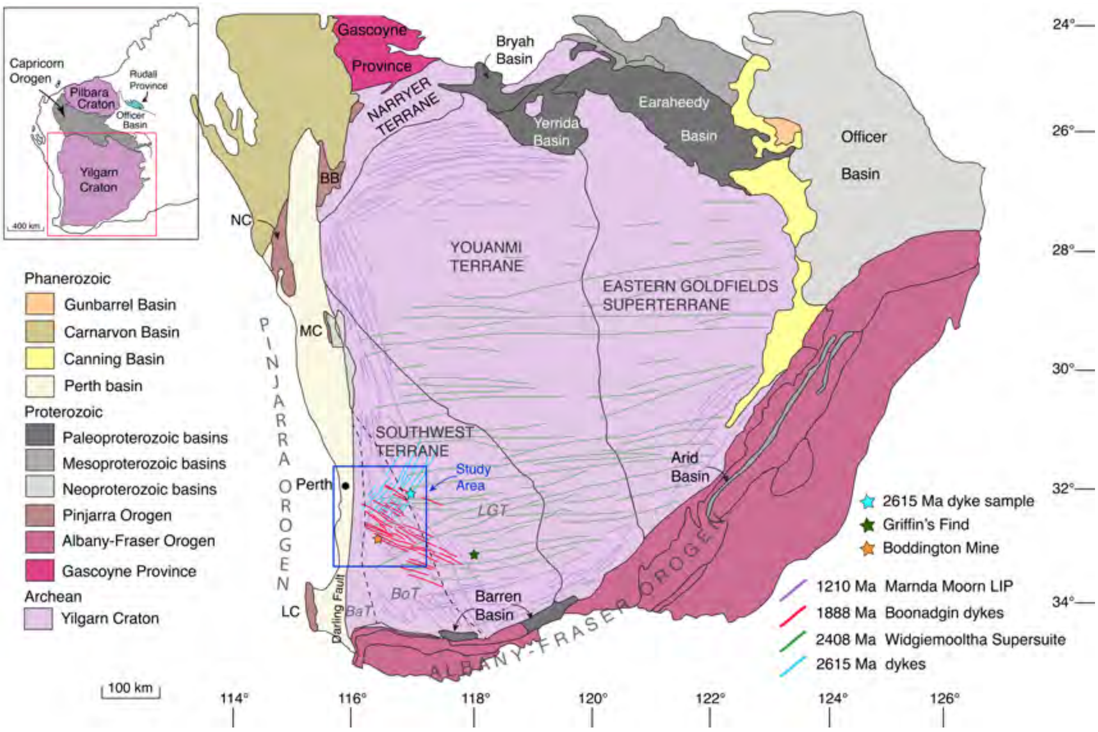

Figure 4.1 Map of the Yilgarn Craton showing major tectonic units. Inset shows the extent of the West Australian Craton (Pilbara Craton, Yilgarn Craton and Capricorn Orogen). From Geological Survey of Western Australia 1:2.5M Interpreted Bedrock Geology 2015 and 1:10M Tectonic Units 2016. Dashed lines are terrane boundaries within the southwestern Yilgarn Craton after Wilde et al. 1996: BaT = Balingup Terrane, BoT = Boddington Terrane and LGT = Lake Grace Terrane.

widespread granitic magmatism between ca. 2690 Ma and 2625 Ma (Compston et al., 1986; Wilde and Pidgeon, 1986; Champion and Sheraton, 1997; Nemchin and Pidgeon, 1997; Qiu et al., 1997; Smithies and Champion, 1999; Cassidy et al., 2002; Mole et al., 2012). Extensive gold mineralisation was associated with the late stages of cratonisation (Kent et al., 1996; McNaughton and Groves, 1996; Yeats et al., 1996; Allibone et al., 1998; Witt and Vanderhor, 1998; Qiu and Groves, 1999; Blewett et al., 2010).

4.3.2 The South West Terrane

Following the model of Wilde et al. (1996), the South West Terrane is divided (from west to east) into the Balingup, Boddington and Lake Grace sub-terranes (Figs. 1 and 2) based on U-Pb geochronology, deep crustal seismic data and re-evaluation of regional geology. It should be noted that Mole et al. (2012) proposed that the eastern part of the South West terrane could be part of the Youanmi Terrane crust on the basis of zircon U-Pb geochronology and spatial occurrence of granite pulses.

The Balingup Terrane comprises ca. 3070–2830 Ma amphibolite facies supracrustal rocks of the Balingup and Chittering metamorphic belts (Figure 4.2), interpreted as sedimentation at an evolving continental margin (Wilde, 1980, 1990; Gee et al., 1981; Fletcher et al., 1985). Granitoids emplaced in the central and northern part of the terrane include the ca. 2677–2626 Ma Darling Range batholith (Wilde and Low, 1978; Nieuwland and Compston, 1981; Nemchin and Pidgeon, 1997) and the ca. 2612 Ma Logue Brook Granite, although the latter may represent a recrystallisation age (Compston et al., 1986; Nemchin and Pidgeon, 1997).

The Boddington Terrane is separated from the Balingup Terrane by a ca. 2 km-wide shear zone and consists predominantly of granitoids of the Darling Range batholith, which enclose the greenschist facies Saddleback and Morangup greenstone belts and parts of the Jimperding metamorphic belt (Figure 4.2) (Wilde and Low, 1978; Wilde, 1980, 1990; Wilde et al., 1996). The ca. 3177 to 3100 Ma amphibolite facies Jimperding metamorphic belt consists of supracrustal rocks (Gee et al., 1981; Wilde, 1990) whereas the ca. 2714–2660 Ma Saddleback greenstone belt (Wilde, 1976; Wilde and Pidgeon, 1986; Pidgeon and Wilde, 1990; Allibone et al., 1998) within the Boddington domain has been interpreted as a remnant oceanic island or continental margin arc (Wilde et al., 1996; Korsch et al., 2011) and hosts the ca. 2675 to 2611 Ma Boddington Cu-Au deposit (e.g. Roth et al., 1990, 1991; Allibone et al., 1998). The greenschist facies Morangup greenstone belt in the northern part of the terrane is considered to be coeval with the Saddleback belt and comprises rocks with similar arc-type geochemical signatures (Wilde, 1990; Wilde and Pidgeon, 1990).

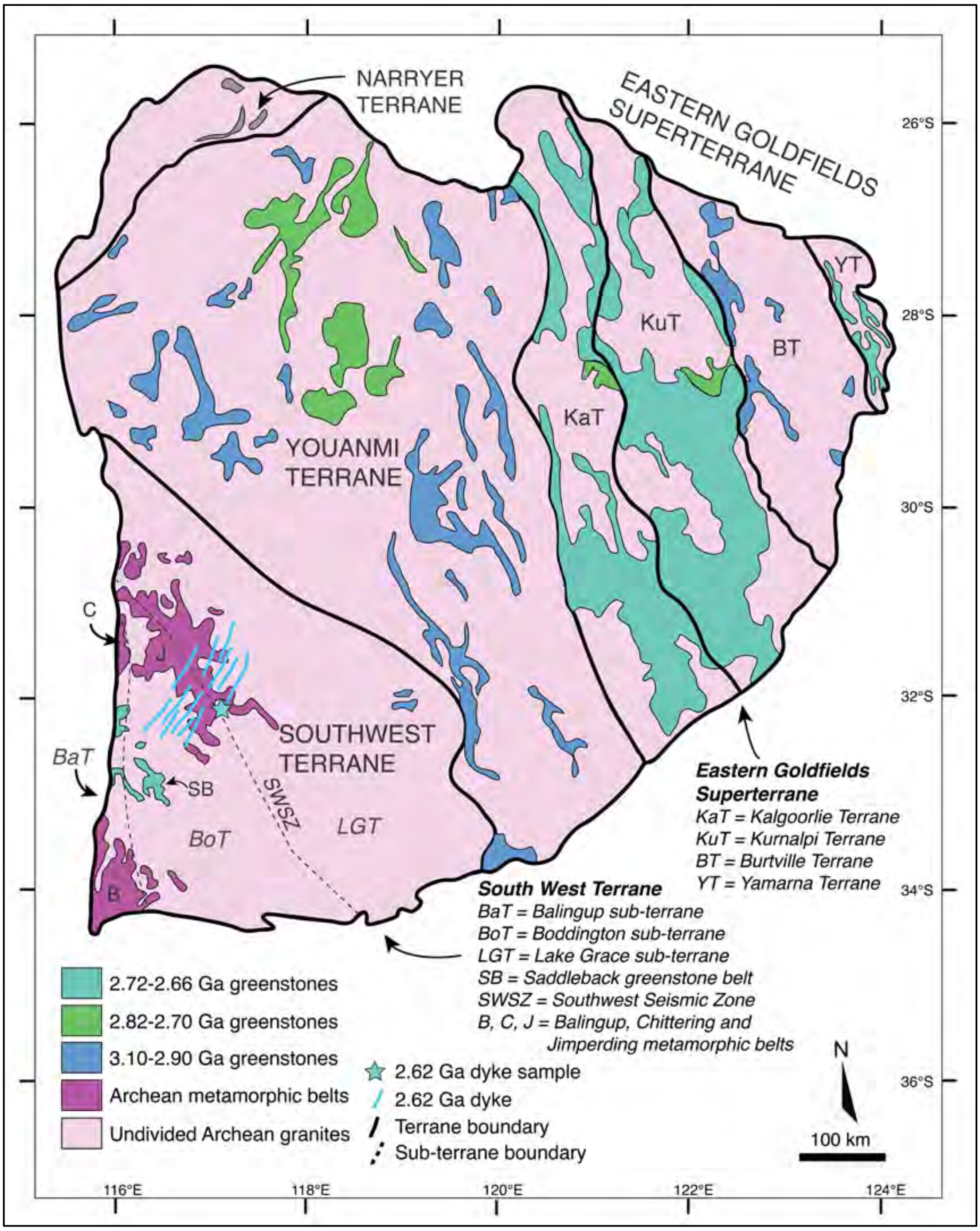

Figure 4.2 Map of the Yilgarn Craton showing terrane and sub-terrane boundaries and greenstone belt and granite distributions. Modified after Witt et al., 2018. South West Terrane sub-terranes are from Wilde et al., 1996 and the boundary with the Youanmi Terrane is after Cassidy et al., 2006.

The transition to the Lake Grace Terrane is marked by a change in structural style and increasing metamorphic grade (Wilde and Low, 1978; Wilde et al., 1996) across a major crustal discontinuity marked by the South West Seismic Zone (Figure 4.2) (Doyle, 1971; Dentith et al., 2000; Dentith and Featherstone, 2003). The terrane comprises deformed granitoids, felsic gneisses, several greenstone belt remnants and the eastern apart of the Jimperding metamorphic belt, all metamorphosed under low-pressure granulite facies conditions (Gee et al., 1981; Wilde, 1990; Wilde et al., 1996). Estimates of timing of peak metamorphism range between ca. 2649 and 2625 Ma (Wilde and Pidgeon, 1987; Nemchin et al., 1994; Qiu et al., 1997b; McFarlane, 2010) and lower amphibolite facies conditions may have been reached at ca. 2645 Ma (McFarlane, 2010). Griffin's Find, a small gold deposit ca. 175 km ESE of Boddington (Figure 4.1), records peak metamorphic conditions with temperatures of 820-870°C and at least 5.5 kbar (Tomkins and Grundy, 2009). Charnockites emplaced at ca. 2627 Ma have been interpreted as emplaced during syn-peak metamorphism (Wilde and Pidgeon, 1987; Wilde et al., 1996), although younger ca. 2587 Ma granitoids are also present (Wilde and Pidgeon, 1987).

4.3.3 Mafic dykes

The Yilgarn Craton hosts numerous dyke suites of different orientations and dyke density that increase towards the southern and western craton margins (Hallberg, 1987; Tucker and Boyd, 1987). The dykes are clearly discernible in aeromagnetic data but deep weathering and thick regolith cover make sampling difficult. The largest dykes belong to the E-W to NE-SW trending 2418–2408 Ma Widgiemooltha Supersuite (Sofoulis, 1965; Evans, 1968; Campbell et al., 1970; Hallberg, 1987; Doehler and Heaman, 1998; Nemchin and Pidgeon, 1998; Wingate, 1999, 2007; French et al., 2002), which includes the 2401 ± 1 Ma Eraynia dykes in the eastern part of the craton (Pisarevsky et al., 2015). The Widgiemooltha dykes are up to 3.2 km wide and extend up to 700 km across the craton, with the largest intrusions (Jimberlana and Binneringie) showing well-developed igneous layering (Campbell et al., 1970; Lewis, 1994). The most extensive dyke swarm in the craton is the 1210 Ma Marnda Moorn LIP which consists of several sub-swarms of different orientations intruding along the craton margins (Isles and Cooke, 1990; Evans, 1999; Wingate et al., 2000; Pidgeon and Nemchin, 2001; Pidgeon and Cook, 2003; Wingate and

Pidgeon, 2005; Wingate, 2007; Claoué-Long et al., 2009). Outcrops in the southeast are limited to a single occurrence, and the extent of the dykes in the northeast is unknown due to cover rocks, although one E-W oriented dioritic dyke dated at 1215 ± 11 Ma has been reported further inland (Qiu et al., 1999). Recently, a NW-trending 1888 Ma dyke swarm of unknown extent has been identified in the southwestern Yilgarn Craton and may be part of the Bastar-Cuddapah LIP of India (Stark et al., in press; Shellnutt et al., 2018). Other known dyke swarms with limited occurrences include the SW-trending dykes of the 1075 Ma Warakurna LIP in the northern Yilgarn Craton (Wingate et al., 2004), the WNW-trending ca. 735 Ma Nindibillup dykes in the central and SE Yilgarn Craton (Spaggiari et al., 2009, 2011; Wingate, 2017), the NNE-trending ca. 750 Ma Northampton dykes in the far west (Embleton and Schmidt, 1985) and the undated (likely <1140 Ma) NW-trending Beenong dykes in the southeastern Yilgarn Craton (Wingate, 2007; Spaggiari et al., 2009, 2011).

4.4 Samples

4.4.1 Field sampling

The field sampling area was selected using satellite imagery (Landsat/Copernicus or Astrium/CNES from Google Earth) and 1:250 000 geological maps from the Geological Survey of Western Australia (GSWA). The Corrigin map sheet (GSWA Corrigin 1:250,000 geological map, SI 50-3, 1985) shows several NE-trending mapped dykes in the area and the aeromagnetic data roughly coincides with some of these. Sample 16WDS13 (32 06.588 S, 117 09.072 E) was collected from a small ridge within an agriculturally cleared area adjacent to the main road (Figure 4.3), ca. 21 km east of the town of Beverley and is interpreted to be representative the NE-trending dykes in the area. Basement rocks are not exposed at the outcrop but geological mapping indicates that the dyke intrudes Archean metagranite at this location. The outcrop at the sample location is fresh and shows minor surficial weathering.

4.4.2 Sample description

Petrography indicates that the dyke is a fresh dolerite with intergranular ophitic to sub-ophitic texture, comprising ca. 45-50% plagioclase, 35-40% pyroxene, up to 5% ilmenite and magnetite, 1-2% sulfides (mainly pyrite and chalcopyrite) and <1%

chlorite, quartz and apatite (Figure 4.4). Plagioclase is slightly affected by sericitisation and most pyroxene grains have been altered to a variable degree. The main U- and Th-bearing accessory mineral is baddeleyite, only identifiable using an SEM due to small crystal size (typically ≤70 µm long and 20-30 µm wide). Rare zirconolite crystals are also present and form euhedral to subhedral prisms and laths up to 60 µm long and 10 µm wide.

Figure 4.3 Field photos of the dyke at the sample location (sample 16WDS13) ***Upper photo*** *looking NE and* ***lower photo*** *looking north. The dyke forms a wide NE-trending ridge, which extends along strike as a series of similar discontinuous ridges.*

4.5 U-Pb geochronology and geochemistry

4.5.1 SHRIMP U-Pb geochronology

Polished thin sections were scanned to identify baddeleyite, zircon and zirconolite with a Hitachi TM3030 scanning electron microscope (SEM) equipped with energy dispersive X-ray spectrometer (EDX) at Curtin University. For SHRIMP (Sensitive High Resolution Ion Microprobe) U-Pb dating, selected grains were drilled directly from the thin sections using a micro drill and mounted into epoxy disks, which were cleaned and coated with 40 nm of gold. Baddeleyite in thin sections forms subhedral to euhedral equant, prismatic and tabular grains and laths, some with thin zircon rims, and most are <70 μm long and up to 30 μm across. Only one crystal with suitable dimensions for SHRIMP dating was identified, closely associated with quartz (Figure 4.5).

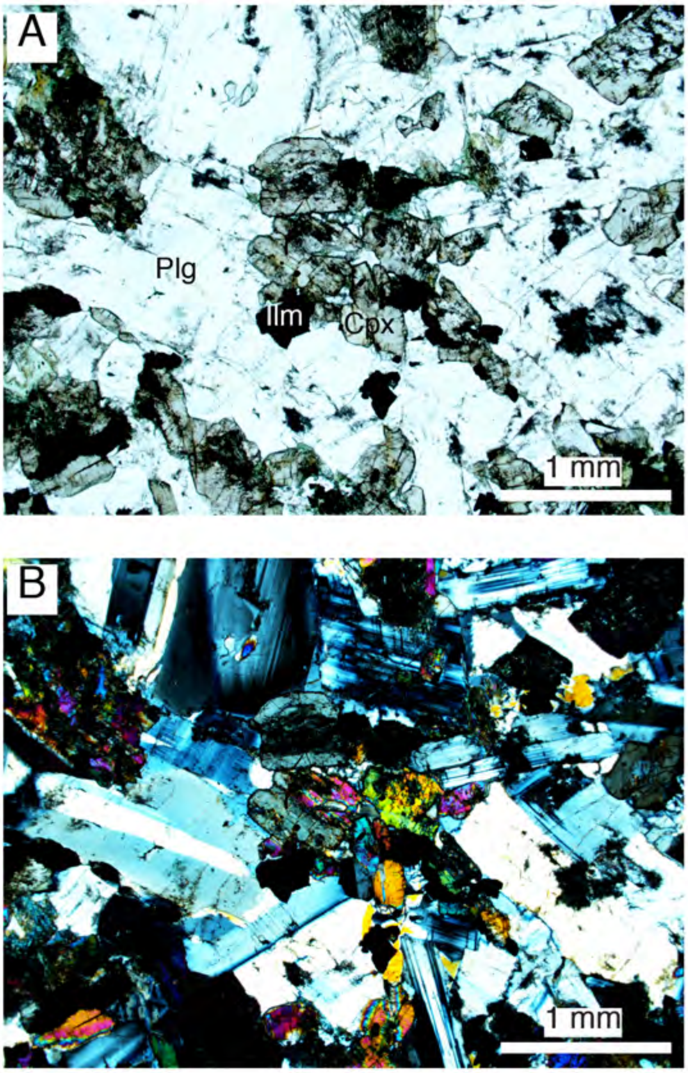

*Figure 4.4 Plane (**A**) and crossed polar (**B**) photomicrographs of sample 16WDS13E.*

Baddeleyite was analysed for U, Th and Pb using the SHRIMP II at the John de Laeter Centre at Curtin University in Perth, Australia, following standard operating procedures after Williams (1998). The SHRIMP analysis method for mounts with polished thin section plugs, as outlined in Rasmussen and Fletcher (2010), was modified for baddeleyite. Mass resolution for all analyses was ≥5000. During the session, 19 baddeleyite and 13 standard analyses were undertaken, with standard zircon OG1 (Stern et al., 2009) employed for monitoring of instrumental mass fractionation and BR266 zircon (Stern, 2001) for calibration of U and Th concentration and as an accuracy standard. Phalaborwa baddeleyite (Heaman, 2009) and NIST were analysed as additional standards. Spot size was ca. 11µm with primary O_2^- current at 0.5 nA and count times 10 s for ^{204}Pb, ^{206}Pb, ^{208}Pb and 30 seconds for ^{207}Pb. Data were processed with Squid version 2.50 (Ludwig, 2009) and Isoplot version 3.76.12 (Ludwig, 2012). For common Pb correction, common Pb isotopic composition was calculated from the Stacey and Kramers (1975) two-stage terrestrial Pb isotopic evolution model. The assigned 1σ external Pb/U error is 1% and analysis is given with 1σ error.

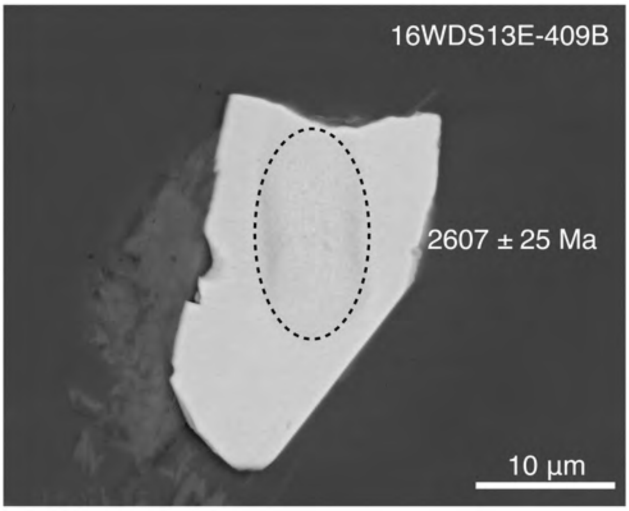

Figure 4.5 SEM backscatter image showing SHRIMP spot on baddeleyite crystal 16WDS13E-409B

4.5.2 ID-TIMS U-Pb geochronology

One block was sawn from the field bulk rock sample 16WDS13E to remove weathering and approximately 40 baddeleyite grains were separated using the technique of Söderlund and Johansson (2002). The best-quality baddeleyite grains were split into three fractions of 5-6 grains each and thereafter transferred into Teflon© capsules. The grains were carefully washed in several steps using ultrapure 3M HNO_3. A small amount of a ^{205}Pb-$^{233-236}$U tracer solution and 10 drops of concentrated HF and HNO_3 (in proportion 10:1) were added to the Teflon© capsules. The capsules were inserted into steel jackets and placed in an oven at 200°C for 3 days. After being dried down on a hotplate, 1 drop of 0.25M H_3PO_4 was added to each capsule along with 10 drops of 6.2 M ultra-pure HCl. The capsules were dried again on a hotplate at 100°C. Each sample was re-dissolved in 2 µl of silica gel and then loaded on an out-gassed, single Re filament.

The intensities of U and Pb isotopes were measured on a Finnigan Triton thermal ionization multi-collector mass spectrometer at the Swedish Museum of Natural History in Stockholm. The mass spectrometer is equipped with Faraday cups and an ETP Secondary Electron Multiplier. Lead was analysed at filament temperatures of 1210-1240°C, while the intensities of ^{233}U, ^{236}U and ^{238}U were recorded subsequently at filament temperatures exceeding 1320°C. The initial Pb composition was taken from Stacey and Kramers (1975), and the ^{238}U and ^{235}U decay constants are from Jaffey et al. (1971). Procedural blank level was 0.6 pg for Pb and 0.06 pg for U.

4.6 Results

4.6.1 SHRIMP U-Pb geochronology

As part of preliminary reconnaissance SHRIMP dating of several dykes sampled in the area, one analysis (Table 4.1) was obtained from one baddeleyite grain during the SHRIMP session (Figure 4.5). The analysed baddeleyite crystal had U and Th concentrations of 59.7 ppm and 1.4 ppm, respectively, and yielded a common Pb-corrected ^{207}Pb/^{206}Pb date of 2607 ± 25 Ma (1σ), which is interpreted as indicative of the crystallisation age of the dyke. Based on this preliminary result, TIMS U-Pb analysis was carried out on baddeleyite from the same sample. It should be noted that despite only having one analysis available, the decision to proceed with TIMS dating was based on the initial identification of a potentially new dyke age from SHRIMP dating.

4.6.2 ID-TIMS U-Pb geochronology

U-Pb data for the samples is presented in Table 4.2 and the calculated isotopic ages are shown in the concordia diagram in Figure 4.6. One fraction of five grains and two fractions of six grains yielded slightly discordant common Pb-corrected ^{207}Pb/^{206}Pb dates of 2615.7 ± 2.9 Ma, 2616.7 ± 3.1 Ma and 2611.3 ± 3.3 Ma, respectively, giving a weighted mean ^{207}Pb/^{206}Pb date of 2615 ± 6 Ma (MSWD = 2.8). Forced regression through 0 Ma yields an upper intercept date of 2615 ± 3 Ma. However, despite higher uncertainty, the weighted mean ^{207}Pb/^{206}Pb date is preferred due to slight discordance of the analyses. Thus, the $^{207}Pb/^{206}Pb$ age is interpreted as the best, though conservative, emplacement age of the mafic dyke.

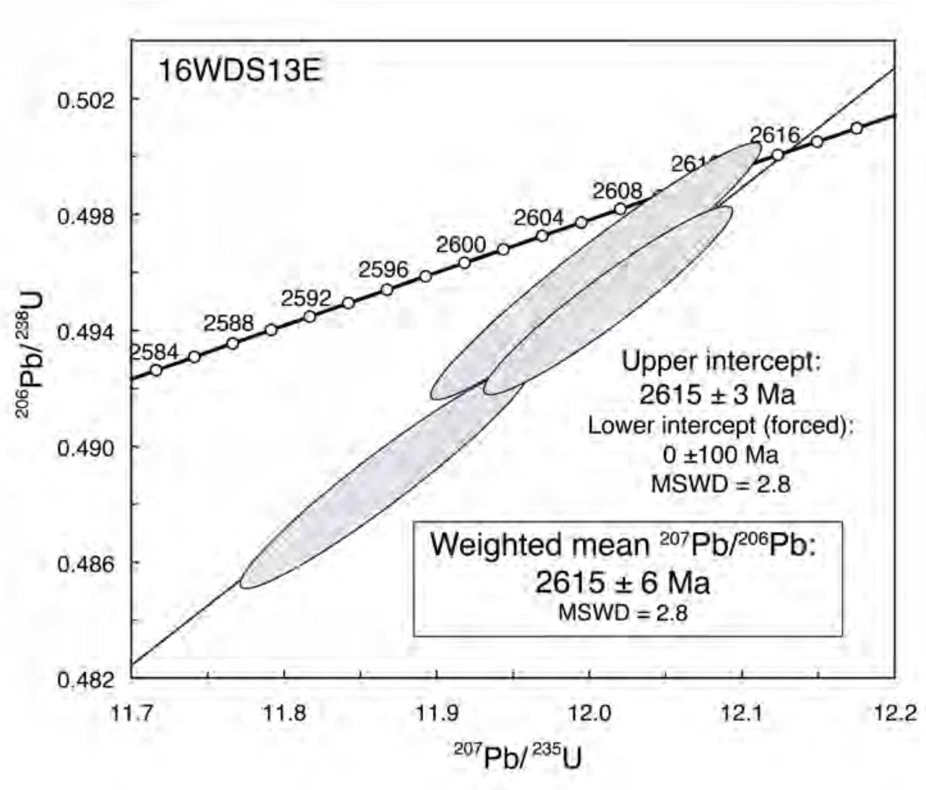

Figure 4.6 Concordia plot for analysed baddeleyite ID-TIMS U-Pb results from sample 16WDS13E

4.7 Discussion

We have identified the oldest known mafic dyke within the Yilgarn Craton, here informally named as the Yandinilling dyke. The extent of dykes of this age within the craton is currently unknown but aeromagnetic data (Geological Survey of Western Australia magnetic anomaly grids with 20-40 m cell size, Geoscience Australia magnetic grid of Australia V6 2015 base reference) show that linear NE-trending features interpreted as dykes extend at least 150 km northeast from Boddington and across the Boddington and Lake Grace terrane boundary. The dyke dated in this study lies on one of these features, suggesting it is part of a much longer intrusion that may belong to a major dyke swarm. The temporally closest known mafic magmatic event within the Yilgarn Craton produced the ca. 2410 Ma Widgiemooltha Supersuite (Sofoulis, 1965; Evans, 1968; Campbell et al., 1970; Hallberg, 1987; Doehler and Heaman, 1998; Nemchin and Pidgeon, 1998; Wingate, 1999, 2007; French et al., 2002). The E- to ENE-trending Widgiemooltha dykes traverse nearly the entire width of the craton approximately orthogonally to the regional structural grain, similar to the ca. 2480 - 2450 Ma Matachewan and Hearst dykes in North America (Heaman, 1997). Worldwide, mafic dykes of similar age to the Yandinilling dyke are found in the São Francisco Craton in Brazil, dated at 2624 ± 7 Ma (Oliveira et al., 2013), and in the high-grade Limpopo Belt between the Zimbabwe and Kaapvaal cratons in of southern Africa, where deformed dykes have been dated at 2559 ± 4 Ma, 2607 ± 5 Ma and 2604 ± 6 Ma (Xie et al., 2017). Evidence for a possible connection between the Yilgarn and Zimbabwe cratons is discussed in the following sections.

4.7.1 Assembly of the South West Terrane

Amalgamation of the South West Terrane is considered to have involved subduction in the west and continental collision in the east. The ca. 2715–2675 Ma Saddleback greenstone belt has been interpreted as an island or continental arc (Wilde, 1990; Wilde et al., 1996; Korsch et al., 2011). Subduction of the Balingup Terrane beneath the Boddington Terrane between ca. 2714 Ma and 2969 Ma (Korsch et al., 2011) and collision between ca**.** 2696 and 2675 Ma is constrained by calc-alkaline magmatism and granitic intrusions within the Saddleback Group (Allibone et al., 1998; Cassidy et al., 1998; Wilde and Pidgeon, 2006). Following their amalgamation, the Lake Grace Terrane was subducted under the newly formed Balingup-Boddington Terrane producing the pyroclastic and intrusive rocks of the upper Saddleback Group at ca. 2675–2650 Ma (Wilde and Pidgeon, 1986; Allibone et al., 1998; Zhao et al., 2006).

Collision and final formation of the South West Terrane along a suture now marked by the South West Seismic Zone (Doyle, 1971; Middleton et al., 1993; Wilde et al., 1996; Dentith et al., 2000) is uncertain but probably took place sometime between ca. 2649 and 2625 Ma, constrained by low-pressure amphibolite to granulite facies metamorphism at ca. 2649–2640 Ma (Nemchin et al., 1994; McFarlane, 2010),

Table 4.1 SHRIMP U-Pb data for baddeleyite from dyke sample 16WDS13E

Spot	f_{206} %	U ppm	Th ppm	Th/U	±%	Total $^{238}U/^{206}Pb$	±%	Total $^{207}Pb/^{206}Pb$	±%	$^{238}U/^{206}Pb^*$	±%	$^{207}Pb^*/^{206}Pb^*$	±%	$^{206}Pb^*/^{238}U$ Age (Ma)	± 1σ	$^{207}Pb^*/^{206}Pb^*$ Age (Ma)	± 1σ	Disc. %
16WDS13E.409B-1	0.22	89	2	0.02	2.3	1.80	1.90	0.177	1.3	1.8	1.9	0.175	1.5	2819	±43	2607	±25	-10

Notes **1)** f_{204} is the proportion of common Pb in ^{206}Pb, determined using the measured $^{204}Pb/^{206}Pb$ and the common Pb composition from the Stacey and Kramers (1975) model at the approximate age of the sample **2)** Disc. = $100(t[^{207}Pb^*/^{206}Pb^*] - t[^{238}U/^{206}Pb^*])/t[^{207}Pb^*/^{206}Pb^*]$

Table 4.2 ID-TIMS U-Pb data for baddeleyite from dyke sample 16WDS13E

Analysis no. (number of grains)	U/Th	Pb_c/Pb_{tot} 1)	$^{206}Pb/^{204}Pb$ Raw 2)	$^{207}Pb/^{235}U$ [Corr] 3)	± 2s % err	$^{206}Pb/^{238}U$ [Corr] 3)	± 2s % err	$^{207}Pb/^{235}U$ [Age, Ma]	± 2s	$^{206}Pb/^{238}U$ [Age, Ma]	± 2s	$^{207}Pb/^{206}Pb$ [Age, Ma]	± 2s	Concordance
Bd-1 (5 grains)	6.3	0.045	1280.3	12.0130	0.55	0.49498	0.54	2605.4	5.2	2592.2	11.4	2615.7	2.9	0.991
Bd-2 (6 grains)	6.0	0.039	1555.0	11.8670	0.65	0.48887	0.64	2594.0	6.1	2565.8	13.5	2616.1	3.1	0.981
Bd-3 (6 grains)	7.5	0.056	1062.7	12.0053	0.74	0.49599	0.73	2604.8	6.9	2596.6	15.6	2611.3	3.3	0.994

[1] Pb_c = common Pb; Pb_{tot} = total Pb (radiogenic + blank + initial).
[2] Measured ratio, corrected for fractionation and spike.
[3] Isotopic ratios corrected for fractionation (0.1% per amu for Pb), spike contribution, blank (0.6 pg Pb and 0.06 pg U), and initial common Pb. Initial common Pb corrected with isotopic compositions from the model of Stacey and Kramers (1975) at the age of the sample.

emplacement of charnockites at ca. 2627 Ma (Wilde and Pidgeon, 1987; Wilde et al., 1996) and monazite and zircon growth at ca. 2625 Ma (McFarlane, 2010) in the eastern Lake Grace Terrane.

4.7.2 Mechanism and timing of 2615 Ma mafic magmatism: post-orogenic lithospheric delamination beneath the Yilgarn Craton?

The nature of widespread granitic magmatism during the amalgamation of the Yilgarn Craton provides evidence for significant changes in tectonic setting during the Neoarchean. The ca. 2690–2650 Ma high-Ca granites (Champion and Sheraton, 1997) were associated with orogenic thickening of the crust and partial melting of an isotopically young, deep source of basaltic composition, whereas the ca. 2650–2625 Ma low-Ca granites were emplaced craton-wide and involved partial melting of a shallow, isotopically older tonalitic source (Champion and Sheraton, 1997; Qiu and Groves, 1999; Cassidy et al., 2002; Mole et al., 2012). Smithies and Champion (1999) proposed that emplacement of the low-Ca granites and syenites in the Eastern Goldfields (Figure 4.1) at ca. 2650–2630 Ma was a result of delamination or convective thinning of dense eclogitic lower crust ca. 10-15 m.y. after a major partial melting event. Cassidy et al. (2002) argued that the craton-wide extent of low-Ca magmatism at ca. 2650–2630 Ma indicates that the entire craton was undergoing extension or post-orogenic attenuation at this time, possibly associated with the end of a major compressional event in the Eastern Goldfields, as originally proposed by Smithies and Champion (1999). Geophysical investigations of the deep crustal architecture beneath the Eastern Goldfields Superterrane (Figure 4.2) are also consistent with delamination of the lower lithosphere (Nelson, 1992), including ca. 40 km thick crust underlain by a flat, east-dipping Moho and a high-velocity layer at 100–200 km (Blewett et al., 2010). Delamination of the lower lithosphere can occur through thermal, compositional or phase changes, which render it gravitationally unstable (denser than the underlying material) and viscous enough to allow flow (Schott and Schmeling, 1998; Elkins Tanton and Hager, 2000; Elkins-Tanton, 2005). Smithies and Champion (1999) advocate a model where the delamination (or convective thinning) was a direct result of partial melting and eclogitic restite formation in the lower crust due to orogenic thickening. The timing of the proposed delamination ca. 10-15 m.y. after the partial melting event, the consequent A-type syenitic and widespread low-Ca granitic magmatism and high-temperature metamorphism fit well with this scenario. An alternative mechanism could be the arrival of a mantle plume, which would cause the thickened lithospheric root to become less viscous and thermally unstable. Other workers have proposed that a mantle plume event at ca. 2700 Ma was responsible for komatiitic and felsic magmatism and a diachronous regional metamorphic peak at ca. 2690-2630 Ma (Campbell and Hill, 1988; Upton et al., 1997) but this model is not favoured by Smithies and Champion (1999) because it would be difficult to explain the timing and duration of the felsic alkaline and low-Ca granitic magmatism and the craton-wide E-W shortening at ca. 2690-2650 Ma.

In the western Yilgarn Craton, low-pressure granulite facies metamorphism at ca. 2649–2625 Ma, emplacement of charnockites at ca. 2652–2627 Ma within the Lake Grace Terrane (Wilde and Pidgeon, 1987; Nemchin et al., 1994; McFarlane, 2010) and the emplacement of the Darling Range batholith at ca. 2648–2626 Ma within the Boddington and Balingup Terranes (Nemchin and Pidgeon, 1997) are also consistent with the delamination model. Granites of ca. 2612 Ma age near the western margin of the South West Terrane have isotopic compositions of $\varepsilon Nd_{(2612)}$ = -2.9 and $\varepsilon Nd_{(2612)}$ = 0, respectively, suggesting that their source involved significant mixing of younger mantle-derived crust with older crust (Compston et al., 1986) or that the granitic magmas could have originated from partial melting of recently crystallised mafic rocks in the lower crust (e.g. Smithies et al., 2015). Qiu and Groves (1999) suggested that the geochemical characteristics of the ca. 2640–2630 Ma granites, the presence of igneous charnockites, and coeval widespread intrusion of other granitoids in the southern Lake Grace and Youanmi terranes collectively suggest massive melting of lower crust at high temperatures at ca. 2640–2630 Ma. They attributed the sudden significant increase in geothermal gradient over <10 m.y. and the lower partial melting pressures of the younger granites (indicating thinner crust) to lithospheric delamination during a late orogenic stage and suggested that the lack of known significant mafic intrusions of this age probably indicated partial, instead of complete, removal of the lower crust.

Collectively, these data and the newly discovered mafic magmatism in the South West Terrane are consistent with the presence of hot mantle material impinging on a thinned crust beneath most of the Yilgarn Craton, if not the entire Yilgarn Craton, between ca. 2652 Ma and 2615 Ma. Several lines of evidence suggest possible thermal effects that were associated with intrusion of the 2615 Ma mafic dykes, similar to the effects the Marnda Moorn LIP dykes in the middle Proterozoic Albany-Fraser Orogen (Dawson et al., 2003). Nemchin and Pidgeon (1997) reported extensive recrystallisation of zircon rims at 2628–2616 Ma and growth of titanite at ca. 2615 Ma within the Darling Range batholith. The 2615 ± 3 Ma titanite and the 2616 ± 21 Ma zircon recrystallisation ages are within uncertainty of the 2615 ± 6 Ma mafic dyke age reported here and strongly suggest that they are related. Moreover, zircons from a ca. 2612 Ma granite ca. 130 km southwest of the 2615 Ma dyke, yield dates of 2612 ± 5 Ma and 2613 ± 5 Ma, which could represent either the timing of recrystallisation or the emplacement (Nemchin and Pidgeon, 1997). Other coeval magmatism includes a felsic intrusive at ca. 2611 Ma within the Saddleback greenstone belt (Allibone et al., 1998) and a monzogranite dyke and a granodiorite at 2610 ± 6 Ma and 2610 ± 8 Ma, respectively, in the southern Boddington Terrane (Sircombe, 2007). The NE-SW trend of the Yandinilling dyke suggests NW-SE oriented regional extension, which is consistent with the inferred NE-SW oriented contraction and strike-slip movement in the eastern part of the craton, constrained by syn-kinematic emplacement of low-Ca granites at 2637 ± 7 Ma (Dunphy et al., 2003).

4.7.3 Timing of mafic magmatism and gold mineralisation

Craton-wide (> 400,000 km^2) gold mineralisation at ca. 2640–2630 Ma was associated with a major tectonothermal event (Groves, 1993; Kent et al., 1996; Yeats and McNaughton, 1997; Qiu and Groves, 1999 and references therein) involving a deep crustal fluid source (McNaughton and Groves, 1996; Qiu and Groves, 1999), which Qiu and Groves (1999) argued was driven by lithospheric delamination. The mafic magmatism dated at 2615 ± 6 Ma in the South West Terrane thus post-dates the main mineralisation event but may have been synchronous with formation of late-stage gold deposits. Gold mineralisation at Boddington may also have been synchronous with the ca. 2611 Ma felsic intrusives and movement along brittle shear zones (Allibone et al., 1998).

4.7.4 The Neoarchean tectonic and paleogeographic setting of the Yilgarn Craton: links with the Zimbabwe Craton

Using coeval mafic dyke swarms as a magmatic barcode (Bleeker and Ernst, 2006) between the Zimbabwe and Yilgarn cratons, Söderlund et al. (2010) proposed that both could have been part of the ca. 2510–2100 Ma Superia supercraton (Bleeker and Ernst, 2006; Ernst and Bleeker, 2010). Paleomagnetic data from the E- to ENE-trending ca. 2408 Ma Widgiemooltha and ca. 2401 Ma Erayinia dykes (Sofoulis, 1965; Evans, 1968; Campbell et al., 1970; Hallberg, 1987; Doehler and Heaman, 1998; Nemchin and Pidgeon, 1998; Wingate, 1999, 2007; French et al., 2002; Pisarevsky et al., 2015) and the NNW-trending ca. 2408 Ma Sebanga dyke swarm (Wilson et al., 1987; Mushayandebvu et al., 1995; Söderlund et al., 2010) permit a possible configuration where the western Yilgarn Craton is attached to the northern Zimbabwe Craton and the Sebanga dyke swarm could be a continuation of the Widgiemooltha/Erayinia dyke swarm (Figure 4.7A) (Pisarevsky et al., 2015). The Yandinilling dyke swarm is older than the 2575 Ma Great Dyke (Oberthür et al., 2002) and the Umvimeela satellite dyke (Söderlund et al., 2010), which are currently the oldest known mafic dykes with robust geochronology in the Zimbabwe Craton. However, the Sebanga dyke swarm includes two dyke generations at ca. 2512 Ma and 2470 Ma, both considered to be part of the same swarm (Söderlund et al., 2010). This suggests that if the Yilgarn and the Zimbabwe cratons were neighbours, yet to be identified mafic magmatism of these ages could be present in the Yilgarn Craton. If the configuration of Söderlund et al. (2010) and Pisarevsky et al. (2015) at ca. 2400 Ma is accepted and the Yandinilling dyke and the Umvimeela/Great Dyke are considered as part of the same swarm (despite their up to 40 m.y. age difference), the barcode between the two cratons does not match unless one of the cratons rotated significantly between ca. 2575 Ma and 2512 Ma (or their respective regional stress fields were very different) (Figure 4.7C). If the Yilgarn and Zimbabwe cratons were adjacent to each other between 2615 Ma and 2408 Ma, continuous but episodic mafic magmatism on these cratons lasting for more than 200 m.y. suggests that at least some of the dyke swarms could be associated with processes other than a mantle plume, or that several plumes were involved.

In contrast to the reconstructions of Söderlund et al. (2010), Smirnov et al. (2013) proposed that at ca. 2410 Ma, the eastern margin of the Yilgarn Craton was adjacent to the southern margin of the Zimbabwe Craton, forming the Zimgarn supercraton and aligning the Sebanga swarm approximately parallel to the Widgiemooltha dykes (Figure 4.7B). Whilst noting that the paleomagnetic data used for such a reconstruction were limited, these authors preferred the position of the Zimbabwe Craton north of the Yilgarn Craton because the juvenile eastern margin of the Yilgarn Craton was a better match with the progressive west to east cratonisation of the Zimbabwe Craton, and because offsets on major terrane-bounding shear zones in the eastern Yilgarn Craton could be restored to a feasible proto-Zimgarn configuration at ca. 2690 Ma (Figure 4.7D). In the ca. 2690 Ma configuration, Smirnov et al. (2013) aligned the southeastern margin of the Yilgarn Craton directly with the southwestern margin of the Zimbabwe Craton. Pisarevsky et al. (2015) noted that if the Zimgarn model of Smirnov et al. (2013) at ca. 2400 Ma is accepted, then paleomagnetic constraints imply that the Zimbabwe and Yilgarn cratons were not part of Superia. This does not preclude the Smirnov et al. (2013) configuration, but there is currently no evidence of mafic dykes or sills older than 2401 Ma in the eastern Yilgarn Craton.

Xie et al. (2017) recently obtained 2607 ± 5 Ma and 2604 ± 6 Ma SHRIMP U-Pb zircon ages for tholeiitic Stockford dykes within the Central Zone of the Limpopo Belt, which separates the Archean Kaapvaal and Zimbabwe cratons in South Africa. The Stockford dykes were deformed and metamorphosed under granulite facies conditions at ca. 2014 –2005 Ma (Xie et al., 2017) and intrude the Paleoarchean Sand River Gneiss, which records high-grade metamorphic events at ca. 2640 Ma and ca. 2025 Ma (Zeh et al., 2007, 2010; Gerdes and Zeh, 2009). The timing of the amalgamation of the Central Zone to the Zimbabwe Craton is uncertain, but is thought to have occurred during the collision and amalgamation between the Kaapvaal and Zimbabwe cratons at ca. 2660-2610 Ma (Burke et al., 1986; Kramers et al., 2011; Xie et al., 2017; Brandt et al., 2018) or at ca. 2020 Ma (e.g. Holzer et al., 1998; Söderlund et al., 2010). If the Zimbabwe and Kaapvaal Cratons amalgamated at this time, the 2615 Ma mafic magmatism in the southwestern Yilgarn Craton may be associated with the same tectonic event that produced the ca. 2607–2604 Ma Stockford dykes in the Central Zone of the Limpopo Belt. The South West Terrane and the Central Zone share a similar tectonothermal evolution in an orogenic setting that involved contemporaneous low-pressure granulite facies metamorphism associated with voluminous felsic magmatism, closely followed by mafic magmatism. Voluminous magmatism in the Central Zone at ca. 2650–2610 Ma includes the 2612 ± 7 Ma Bulai pluton and the 2613 ± 7 Ma Zanzibar gneiss

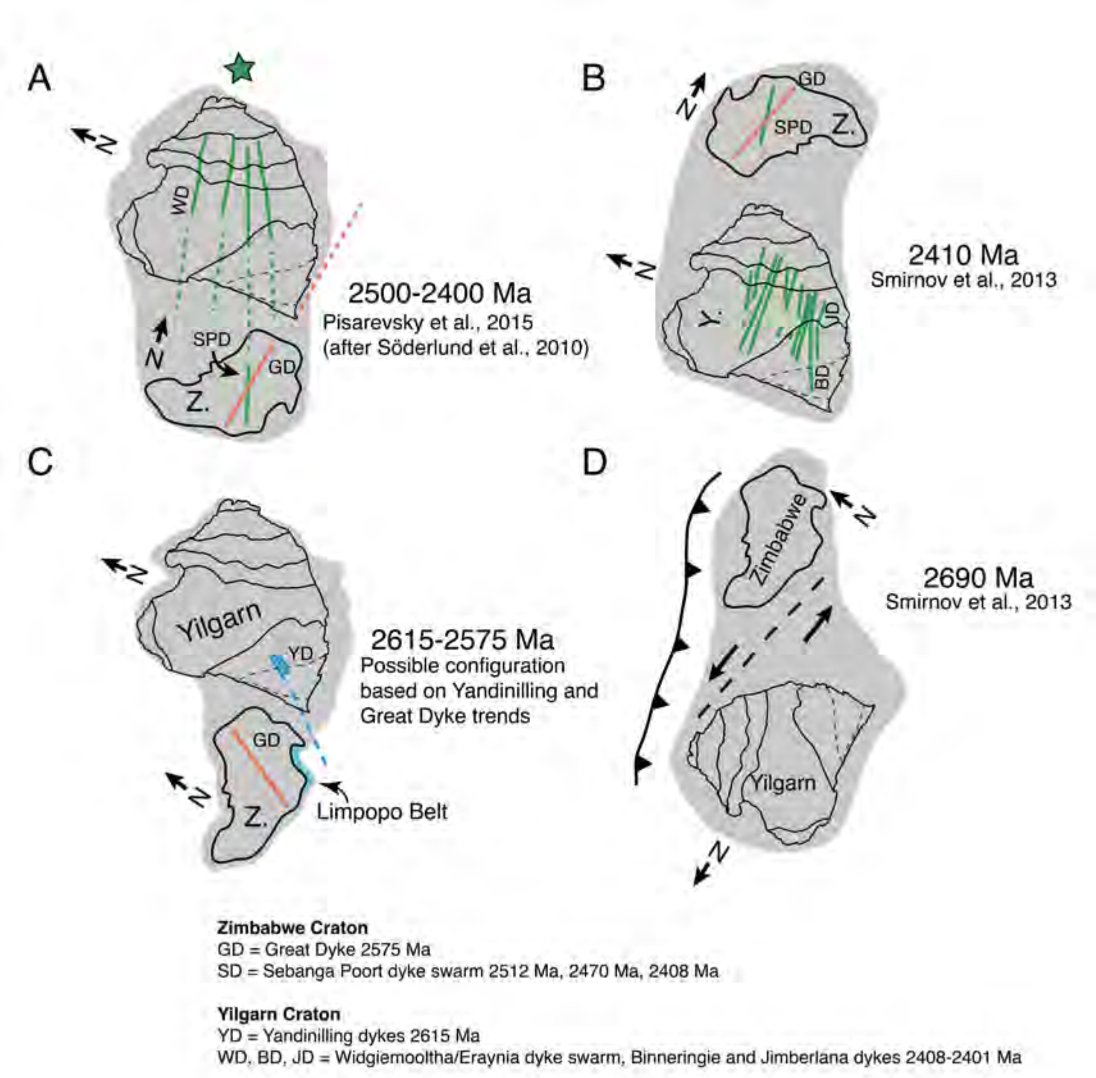

*Figure 4.7 Paleogeographic reconstructions of the Yilgarn and Zimbabwe cratons. (**A**) Superia configuration after Söderlund et al. (2010) and Pisarevsky et al. (2015) at ca. 2500–2400 Ma. Only the Yilgarn and Zimbabwe cratons are shown. (**B**) Reconstruction of Smirnov et al. (2013) at ca. 2410 Ma, (**C**) Relative orientations of the Yilgarn and Zimbabwe cratons rotated from (A) to an approximate alignment of the 2615 Ma Yandinilling swarm with the 2575 Ma Great Dyke. and (**D**) reconstruction of Smirnov et al. (2013) at ca. 2690 Ma. Yilgarn Craton: green = Widgiemooltha/ Eraynia dykes, BD = Binneringie Dyke and JD = Jimberlana Dyke (both part of the Widgiemooltha swarm), blue = Yandinilling swarm, green star = possible mantle plume location. Zimbabwe Craton: GD (orange) = the Great Dyke, SPD (green) = the Sebanga Poort Dyke, SD = Sebanga dykes*

(Zeh et al., 2007; Millonig et al., 2008), which are coeval with the ca. 2612–2611 Ma Logue Brook Granite (Compston et al., 1986; Nemchin and Pidgeon, 1997) and ca. 2611–2610 felsic magmatism elsewhere within the South West Terrane (Allibone et al., 1998; Sircombe, 2007). Moreover, a low-pressure high-grade tectonothermal event at ca. 2650–2644 Ma in the Central Zone of the Zimbabwe Craton (Holzer et al., 1998; Zeh et al., 2007, 2010; Millonig et al., 2008), possibly linked to magmatic underplating (e.g. Holzer et al., 1998), is coeval with the ca. 2650 Ma low-pressure granulite facies metamorphism in the Lake Grace Terrane and the timing of proposed lithospheric delamination beneath the Yilgarn Craton (section 4.7.2). Furthermore, Brandt et al. (2018) propose that the UHT metamorphic event in the Central Zone at ca. 2660-2610 was likely due to lithospheric delamination and Kröner et al. (1999), Kamber and Biino (1995) and Berger et al. (1995) favoured a lithospheric delamination (or mantle plume) model for the ca.2700-2600 Ma high-grade event in the Northern Marginal Zone. Similar to the Yandinilling swarm reported here, Xie et al. (2017) argued that the Stockford dykes may have formed in a post-collisional extensional environment during orogenic collapse, which they consider to represent the Neoarchean amalgamation of the Zimbabwe and Kaapvaal cratons. Alternatively, an upwelling mantle plume could explain the wide extent of magmatic underplating and low-pressure high-temperature metamorphism followed by the emplacement of mafic dykes. Such an event would be expected to show up as mafic magmatism in other nearby crustal blocks but reliably dated mafic dykes of ca. 2620–2600 Ma age are currently not known from other cratons. If the Zimbabwe and Kaapvaal cratons amalgamated at ca. 2660-2610 Ma, the Smirnov et al. (2013) reconstruction at ca. 2410 Ma (Figure 4.7B) would not be feasible and would require adjustment to accommodate the consolidated Zimbabwe-Kaapvaal Craton. This also raises the possibility that ca. 2615 Ma mafic magmatism coeval with the Yandinilling dyke may be present in the Kaapvaal Craton (Figure 4.7C).

4.8 Conclusions

We have identified the oldest known mafic dyke in the Yilgarn Craton of Western Australia, dated at 2615 ± 6 Ma by ID-TIMS on baddeleyite and at 2610 ± 25 Ma utilizing *in situ* SHRIMP U-Pb dating of baddeleyite. Aeromagnetic data suggest that the dyke is part of a series of NE-trending intrusions, here named the Yandinilling dyke swarm, that extend hundreds of kilometers within the southwestern part of the craton. The 2615 Ma mafic magmatism postdates the ca. 2650–2630 Ma craton-wide emplacement of low-Ca granites that have been linked with post-orogenic collapse and delamination of the lower crust beneath the Yilgarn Craton. The Yandinilling swarm also postdates the ca. 2640–2630 Ma craton-wide gold mineralisation event, but may be coeval with some late-stage gold mineralisation at Kambalda and Boddington. Paleogeographic reconstructions suggest that the Yilgarn and Zimbabwe cratons may have been neighbours between ca. 2690 Ma and 2401 Ma. If the Zimbabwe and Kaapvaal Cratons amalgamated at ca. 2660-2610 Ma, the 2615 Ma mafic magmatism in the southwestern Yilgarn Craton may be associated with the same tectonic event that produced the ca. 2607–2604 Ma Stockford dykes in the Central Zone of the Limpopo Belt. Paleomagnetic evidence, coeval granitic magmatism, high-grade metamorphism, and emplacement of mafic dykes support a configuration where the northern part of the Zimbabwe Craton may have been adjacent to the western margin of the Yilgarn Craton during the Neoarchean. Worldwide, reliably dated mafic dykes of this age have so far been reported from the Yilgarn Craton, the Limpopo Belt and the São Francisco Craton.

4.9 Acknowledgments

This work was funded by the Australian Research Council (ARC) Centre of Excellence for Core to Crust Fluid Systems Grant (CE110001017) and the ARC Laureate Fellowship (FL150100133) to Z.- X.L. JCS acknowledges support from a Curtin University Postgraduate Scholarship. We thank Gregory Shellnutt and Timothy Kusky for helpful and constructive reviews that greatly improved the manuscript. We also thank Cristina Talavera and Hao Gao for their generous support with SHRIMP analyses and Stephen Sheppard is thanked for helpful discussion and feedback on a previous version of the manuscript. Baddeleyite analyses were carried out on the Sensitive High Resolution Ion Micro Probe mass spectrometer (SHRIMP II) at the John de Laeter Centre, Curtin University, with the financial support of the Australian Research Council and Auscope NCRI. BSE imaging was undertaken at the Australian Microscopy and Microanalysis Research Facility at the Centre for Microscopy, Characterisation and Analysis (CMCA) at the University of Western Australia. This is a contribution to IGCP project 648.

4.10 References

Allibone, A.H., Windh, J., Etheridge, M.A., Burton, D., Anderson, G., Edwards, P.W., Miller, A., Graves, C., Fanning, C.M., Wysoczanski, R., 1998. Timing relationships and structural controls on the location of Au-Cu mineralization at the Boddington gold mine, Western Australia. Econ. Geol. 93, 245–270.

Barley, M.E., Brown, S.J.A., Cas, R.A.F., Cassidy, K.F., Champion, D.C., Gardoll, S.J., Krapež, B., 2003. An integrated geological and metallogenic framework for the eastern Yilgarn Craton: developing geodynamic models of highly mineralised Archaean granite–greenstone terranes. AMIRA Project P624.

Berger, M., Kramers, J.D., Nägler, T., 1995. Geochemistry and geochronology of charnoenderbites in the northern marginal zone of the Limpopo Belt, Southern Africa, and genetic models. Schweizerische Mineral. und Petrogr. Mitteilungen 75, 17–42.

Bleeker, W., Ernst, R., 2006. Short-lived mantle generated magmatic events and their dyke swarms: the key unlocking Earth's paleogeographic record back to 2.6 Ga, in: Hanski, E.J., Mertanen, S., Rämö, O.T., Vuollo, J. (Eds.), Dyke Swarms—time Markers of Crustal Evolution: Selected Papers of the Fifth International Dyke Conference in Finland, Rovaniemi, Finland, 31 July- 3 Aug 2005 & Fourth International Dyke Conference, Kwazulu-Natal, South Africa 26-29 June 2001. CRC Press, London, pp. 3–26.

Blewett, R.S., Henson, P.A., Roy, I.G., Champion, D.C., Cassidy, K.F., 2010. Scale-integrated architecture of a world-class gold mineral system: The Archaean eastern Yilgarn Craton, Western Australia. Precambrian Res. 183, 230–250.

Blewett, R.S., Hitchman, A.P., 2006. 3D Geological Models of the Eastern Yilgarn Craton: Final Report pmd* CRC Y2 Project September 2001–December 2004. Geoscience Australia Record 2006/05.

Brandt, S., Klemd, R., Li, Q., Kröner, A., Brandl, G., Fischer, A., Bobek, P., Zhou, T., 2018. Pressure-temperature evolution during two granulite-facies metamorphic events (2.62 and 2.02 Ga) in rocks from the Central Zone of the Limpopo Belt, South Africa. Precambrian Res. In Press.

Buchan, K.L., Ernst, R.E., Hamilton, M.A., Mertanen, S., Pesonen, L.J., Elming, S.-Å., 2001. Rodinia: the evidence from integrated palaeomagnetism and U–Pb geochronology. Precambrian Res. 110, 9–32.

Burke, K., Kidd, W.S.F., Kusky, T.M., 1986. Archean foreland basin tectonics in the

Witwatersrand, South Africa. Tectonics 5, 439–456.

Campbell, I.H., Hill, R.I., 1988. A two-stage model for the formation of the granite-greenstone terrains of the Kalgoorlie-Norseman area, Western Australia. Earth Planet. Sci. Lett. 90, 11–25.

Campbell, I.H., McCall, G.J.H., Tyrwhitt, D.S., 1970. The Jimberlana Norite, Western Australia–a smaller analogue of the Great Dyke of Rhodesia. Geol. Mag. 107, 1–12.

Cassidy, K.F., Champion, D.C., Krapez, B., Barley, M.E., Brown, S.J.A., Blewett, R.S., Groenewald, Pb., Tyler, I.M., 2006. A revised geological framework for the Yilgarn Craton, Western Australia, in: Geological Survey of Western Australia Record 8/2006. Geological Survey of Western Australia.

Cassidy, K.F., Champion, D.C., McNaughton, N.J., Fletcher, I.R., Whitaker, A.J., Bastrakova, I. V, Budd, A.R., 2002. Characterisation and metallogenic significance of Archaean granitoids of the Yilgarn Craton, Western Australia, Minerals and Energy Research Institute of Western Australia (MERIWA) Report P482.

Cassidy, K.F., Champion, D.C., Wyborn, L.A.I., 1998. A Geochemical Study of Granitoids of the Boddington Gold Mine: Final Report to SRK (Australasia) Ltd. Australian Geological Survey Organisation.

Cawood, P.A., Tyler, I.M., 2004. Assembling and reactivating the Proterozoic Capricorn Orogen: lithotectonic elements, orogenies, and significance. Precambrian Res. 128, 201–218.

Champion, D.C., 2013. Neodymium depleted mantle model age map of Australia: explanatory notes and user guide. Geoscience Australia Record 2013/44.

Champion, D.C., Cassidy, K.F., 2008. Geodynamics: Using geochemistry and isotopic signatures of granites to aid mineral systems studies: An example from the Yilgarn craton. Geoscience Ausralia Record 2008/9, 7–16.

Champion, D.C., Cassidy, K.F., 2007. An overview of the Yilgarn Craton and its crustal evolution, in: Geoscience Australia Record 2007/14, 8–13.

Champion, D.C., Sheraton, J.W., 1997. Geochemistry and Nd isotope systematics of Archaean granites of the Eastern Goldfields, Yilgarn Craton, Australia: implications for crustal growth processes. Precambrian Res. 83, 109–132.

Claoué-Long, J.C., Hoatson, D.M., Australia, G., 2009. Guide to using the Map of

Australian Proterozoic Large Igneous Provinces. Geoscience Australia.

Clark, D.J., Hensen, B.J., Kinny, P.D., 2000. Geochronological constraints for a two-stage history of the Albany – Fraser Orogen , Western Australia. Precambrian Res. 102, 155–183.

Compston, W., Williams, I.S., McCulloch, M.T., 1986. Contrasting zircon U-Pb and model Sm-Nd ages for the Archaean Logue Brook Granite. Aust. J. Earth Sci. 33, 193–200.

Czarnota, K., Champion, D.C., Goscombe, B., Blewett, R.S., Cassidy, K.F., Henson, P.A., Groenewald, P.B., 2010. Geodynamics of the eastern Yilgarn Craton. Precambrian Res. 183, 175–202.

Dawson, G.C., Krapež, B., Fletcher, I.R., McNaughton, N.J., Rasmussen, B., 2003. 1.2 Ga thermal metamorphism in the Albany-Fraser Orogen of Western Australia: Consequence of collision or regional heating by dyke swarms? J. Geol. Soc. London. 160, 29–37.

Dentith, M.C., Dent, V.F., Drummond, B.J., 2000. Deep crustal structure in the southwestern Yilgarn Craton , Western Australia. Tectonophysics 325, 227–255.

Dentith, M.C., Featherstone, W.E., 2003. Controls on intra-plate seismicity in southwestern Australia. Tectonophysics 376, 167–184.

Doehler, J.S., Heaman, L.M., 1998. 2.41 Ga U–Pb Baddeleyite ages for two gabbroic dykes from the Widgiemooltha swarm, Western Australia: a Yilgarn–Lewisian connection, in: Geological Society of America 1998 Annual Meeting, Abstracts with Programs. Geological Society of America, pp. 291–292.

Doyle, H.A., 1971. Seismicity and structure in Australia. Bull. R. Soc. New Zeal. 9, 149–152.

Dunphy, J.M., Fletcher, I.R., Cassidy, K.F., Champion, D.C., 2003. Compilation of SHRIMP U–Pb geochronological data, Yilgarn Craton, Western Australia, 2001–2002. Geosci. Aust. Rec. 15, 139.

Elkins-Tanton, L.T., 2005. Continental magmatism caused by lithospheric delamination. Geol. Soc. Am. Spec. Pap. 80301, 449–461.

Elkins Tanton, L.T., Hager, B.H., 2000. Melt intrusion as a trigger for lithospheric foundering and the eruption of the Siberian flood basalts. Geophys. Res. Lett. 27, 3937–3940.

Embleton, B.J.J., Schmidt, P.W., 1985. Age and significance of magnetizations in dolerite dykes from the Northampton Block, Western Australia. Aust. J. Earth Sci. 32, 279–286.

Ernst, R., Bleeker, W., 2010. Large igneous provinces (LIPs), giant dyke swarms, and mantle plumes: significance for breakup events within Canada and adjacent regions from 2.5 Ga to the Present. Can. J. Earth Sci. 47, 695–739.

Ernst, R., Srivastava, R., Bleeker, W., Hamilton, M., 2010. Precambrian Large Igneous Provinces (LIPs) and their dyke swarms: New insights from high-precision geochronology integrated with paleomagnetism and geochemistry. Precambrian Res. 183, vii–xi.

Ernst, R.E., Bleeker, W., Söderlund, U., Kerr, A.C., 2013. Large Igneous Provinces and supercontinents: Toward completing the plate tectonic revolution. Lithos 174, 1–14.

Ernst, R.E., Buchan, K.L., 1997. Giant radiating dyke swarms: their use in identifying pre-Mesozoic large igneous provinces and mantle plumes, in: Large Igneous Provinces: Continental, Oceanic, and Planetary Flood Volcanism. American Geophysical Union Monograph 100, pp. 297–333.

Ernst, R.E., Head, J.W., Parfitt, E., Grosfils, E., Wilson, L., 1995. Giant radiating dyke swarms on Earth and Venus. Earth-Science Rev. 39, 1–58.

Ernst, R.E., Srivastava, R.K., 2008. India's place in the Proterozoic world: constraints from the Large Igneous Province (LIP) record. Indian dykes. Ed. by RK Srivastava, Ch. Sivaji, NV Chalapathi Rao. Geochemistry, Geophys. Geochronology, Narosa Publ. House Pvt. Ltd, New Delhi, India 41–56.

Evans, M.E., 1968. Magnetization of dikes: a study of the paleomagnetism of the Widgiemooltha dike suite, Western Australia. J. Geophys. Res. 73, 3261–3270.

Evans, T., 1999. Extent and nature of the 1.2 Ga Wheatbelt dyke swarm, Yilgarn Craton, Western Australia. B.Sc. thesis, Univ. West. Aust. Perth.

Fletcher, I.R., Wilde, S.A., Rosman, K.J., 1985. Sm-Nd model ages across the margins of the Archaean Yilgarn block, Western Australia — III. The western margin. Aust. J. Earth Sci. 32, 73–82.

French, J.E., Heaman, L.M., Chacko, T., 2002. Feasibility of chemical U-Th-total Pb baddeleyite dating by electron microprobe. Chem. Geol. 188, 85–104.

Gee, R.D., Baxter, J.L., Wilde, S.A., Williams, I.R., 1981. Crustal development in the Archaean Yilgarn Block, Western Australia. Spec. Publ. Geol. Soc. Aust 7, 43–56.

Gerdes, A., Zeh, A., 2009. Zircon formation versus zircon alteration - New insights from combined U-Pb and Lu-Hf in-situ LA-ICP-MS analyses, and consequences for the interpretation of Archean zircon from the Central Zone of the Limpopo Belt. Chem. Geol. 261, 230–243.

Groves, D.I., 1993. The crustal continuum model for late-Archaean lode-gold deposits of the Yilgarn Block, Western Australia. Miner. Depos. 28, 366–374.

Hallberg, J.A., 1987. Postcratonization mafic and ultramafic dykes of the Yilgarn Block. Aust. J. Earth Sci. 34, 135–149.

Halls, H.C., Kumar, A., Srinivasan, R., Hamilton, M.A., 2007. Paleomagnetism and U-Pb geochronology of easterly trending dykes in the Dharwar craton, India: feldspar clouding, radiating dyke swarms and the position of India at 2.37 Ga. Precambrian Res. 155, 47–68.

Halls, H.C., Zhang, B., 1998. Uplift structure of the southern Kapuskasing zone from 2.45 Ga dike swarm displacement. Geology 26, 67–70.

Heaman, L.M., 2009. The application of U–Pb geochronology to mafic, ultramafic and alkaline rocks: An evaluation of three mineral standards. Chem. Geol. 261, 43–52.

Heaman, L.M., 1997. Global mafic magmatism at 2.45 Ga: Remnants of an ancient large igneous province? Geology 25, 299–302.

Hoek, J.D., Seitz, H.-M., 1995. Continental mafic dyke swarms as tectonic indicators: an example from the Vestfold Hills, Antarctica. Precambrian Res. 75, 121–139.

Holzer, L., Frei, R., Barton, J.M., Kramers, J.D., 1998. Unraveling the record of successive high grade events in the Central Zone of the Limpopo Belt using Pb single phase dating of metamorphic minerals. Precambrian Res. 87, 87–115.

Hou, G., 2012. Mechanism for three types of mafic dyke swarms. Geosci. Front. 3, 217–223.

Isles, D.J., Cooke, A.C., 1990. Spatial associations between post-cratonisation dykes and gold deposits in the Yilgarn Block, Western Australia, in: Parker, A.J., Rickwood, P.C., Tucker, D.H. (Eds.), Mafic Dykes and Emplacement Mechanisms. Balkema, Rotterdam, pp. 147–162.

Jaffey, A.H., Flynn, K.F., Glendenin, L.E., Bentley, W.C. t, Essling, A.M., 1971. Precision measurement of half-lives and specific activities of U 235 and U 238. Phys. Rev. C 4, 1889.

Johnson, S.P., Sheppard, S., Rasmussen, B., Wingate, M.T.D., Kirkland, C.L., Muhling, J.R., Fletcher, I.R., Belousova, E.A., 2011. Two collisions, two sutures: Punctuated pre-1950Ma assembly of the West Australian Craton during the Ophthalmian and Glenburgh Orogenies. Precambrian Res. 189, 239–262.

Ju, W., Hou, G., Hari, K.R., 2013. Mechanics of mafic dyke swarms in the Deccan Large Igneous Province: Palaeostress field modelling. J. Geodyn. 66, 79–91.

Kamber, B.S., Biino, G.G., 1995. The evolution of high T-low P granulites in the Northern Marginal Zone sensu stricto, Limpopo Belt, Zimbabwe-the case for petrography. Schweizerische Mineral. und Petrogr. Mitteilungen 75, 427–454.

Kent, A.J.R., Cassidy, K.F., Fanning, M.C., 1996. Archean gold mineralisation synchronous with the final stages of cratonization, Yilgarn Craton, Western Australia. Geology 96, 879–882.

Korsch, R.J., Kositcin, N., Champion, D.C., 2011. Australian island arcs through time: Geodynamic implications for the Archean and Proterozoic. Gondwana Res. 19, 716–734.

Kramers, J.D., McCourt, S., Roering, C., Smit, C.A., Van Reenen, D.D., 2011. Tectonic models proposed for the Limpopo Complex: Mutual compatibilities and constraints. Geol. Soc. Am. Mem. 207, 311–324.

Kröner, A., Jaeckel, P., Brandl, G., Nemchin, A.A., Pidgeon, R.T., 1999. Single zircon ages for granitoid gneisses in the Central Zone of the Limpopo Belt, Southern Africa and geodynamic significance. Precambrian Res. 93, 299–337.

Ksienzyk, A.K., Jacobs, J., Boger, S.D., Kosler, J., Sircombe, K.N., Whitehouse, M.J., 2012. U-Pb ages of metamorphic monazite and detrital zircon from the Northampton Complex: Evidence of two orogenic cycles in Western Australia. Precambrian Res. 198–199, 37–50.

Lewis, J.D., 1994. Mafic dykes in the Williams–Wandering area, Western Australia. Geol. Surv. West. Aust. Rep. 37, 37–52.

Li, T., Zhai, M., Peng, P., Chen, L., Guo, J., 2010. Ca. 2.5 billion year old coeval ultramafic-mafic and syenitic dykes in Eastern Hebei: Implications for cratonization of the North China Craton. Precambrian Res. 180, 143–155.

Ludwig, K., 2012. User's manual for Isoplot version 3.75–4.15: a geochronological toolkit for Microsoft. Berkeley Geochronological Cent. Spec. Publ.

Ludwig, K., 2009. Squid 2.50, A User's Manual (No. 2.50.11.02.03 Rev. 03 Feb 2011). Berkeley, California, USA.

McFarlane, C.R.M., 2010. Geodynamic constraints on mineralization and metamorphism at the Griffin's Find gold deposit, Western Australia, from calibrated Tt trajectories, in: GeoCanada 2010, Calgary May 10-14. Canadian Society of Petroleum Geoscientists, Calgary.

McNaughton, N.J., Groves, D.I., 1996. A review of Pb-isotope constraints on the genesis of lode-gold deposits in the Yilgarn Craton, Western Australia. J. R. Soc. West. Aust. 79, 123–129.

Middleton, M.F., Wilde, S.A., Evans, B.A., Long, A., Dentith, M., 1993. A preliminary interpretation of deep seismic reflection and other geophysical data from the Darling Fault Zone, Western Australia. Explor. Geophys. 24, 711–718.

Millonig, L., Zeh, A., Gerdes, A., Klemd, R., 2008. Neoarchaean high-grade metamorphism in the Central Zone of the Limpopo Belt (South Africa): Combined petrological and geochronological evidence from the Bulai pluton. Lithos 103, 333–351.

Mohanty, S., 2015. Precambrian continent assembly and dispersal events of South Indian and East Antarctic Shields. Int. Geol. Rev. 57, 1992–2027.

Mole, D.R., Fiorentini, M.L., Cassidy, K.F., Kirkland, C.L., Thebaud, N., McCuaig, T.C., Doublier, M.P., Duuring, P., Romano, S.S., Maas, R., Belousova, E.A., Barnes, S.J., Miller, J., 2015. Crustal evolution, intra-cratonic architecture and the metallogeny of an Archaean craton. Geol. Soc. London, Spec. Publ. 393, 23–80.

Mole, D.R., Fiorentini, M.L., Thebaud, N., McCuaig, T.C., Cassidy, K.F., Kirkland, C.L., Wingate, M.T.D., Romano, S.S., Doublier, M.P., Belousova, E.A., 2012. Spatio-temporal constraints on lithospheric development in the southwest–central Yilgarn Craton, Western Australia. Aust. J. Earth Sci. 59, 625–656.

Mushayandebvu, M.F., Jones, D.L., Briden, J.C., Baer, G., Heimann, A., 1995. Palaeomagnetic and geochronological results from Proterozoic mafic intrusions in southern Zimbabwe, in: Physics and Chemistry of Dykes. Balkema Rotterdam, pp. 293–303.

Myers, J.S., 1995. The generation and assembly of an Archaean supercontinent: evidence from the Yilgarn craton, Western Australia. Geol. Soc. London, Spec. Publ. 95, 143–154.

Myers, J.S., 1993. Precambrian Tectonic History of the West Australian Craton and Adjacent Orogens. Annu. Rev. Earth Planet. Sci. 21, 453–485.

Myers, J.S., 1990. Pinjarra orogen, in: Geology and Mineral Resources of Western Australia. State Printing Division, pp. 264–274.

Nelson, D.R., 1997. Evolution of the Archaean granite-greenstone terranes of the Eastern Goldfields, Western Australia: SHRIMP U-Pb zircon constraints. Precambrian Res. 83, 57–81.

Nelson, D.R., Myers, J.S., Nutman, A.P., 1995. Chronology and evolution of the Middle Proterozoic Albany-Fraser Orogen, Western Australia. Aust. J. Earth Sci. 42, 481–495.

Nelson, K.D., 1992. Are crustal thickness variations in old mountain belts like the Appalachians a consequence of lithospheric delamination? Geology 20, 498–502.

Nemchin, A.A., Pidgeon, R.T., 1998. Precise conventional and SHRIMP baddeleyite U-Pb age for the Binneringie Dyke, near Narrogin, Western Australia. Aust. J. Earth Sci. 45, 673–675.

Nemchin, A.A., Pidgeon, R.T., 1997. Evolution of the Darling Range batholith, Yilgarn Craton, Western Australia: a SHRIMP zircon study. J. Petrol. 38, 625–649.

Nemchin, A.A., Pidgeon, R.T., Wilde, S.A., 1994. Timing of Late Archaean granulite facies metamorphism in the southwestern Yilgarn Craton of Western Australia: evidence from U-Pb ages of zircons from mafic granulites. Precambrian Res. 68, 307–321.

Nieuwland, D.A., Compston, W., 1981. Crustal evolution in the Yilgarn block near Perth, Western Australia, in: Archean Geology, Second International Symposium (Perth 1980): Geological Society of Australia, Special Publication. pp. 159–171.

Nutman, A.P., Bennett, V.C., Kinny, P.D., Price, R., 1993. Large-scale crustal structure of the Northwestern Yilgarn Craton, western Australia: Evidence from Nd isotopic data and zircon geochronology. Tectonics 12, 971–981.

Oberthür, T., Davis, D.W., Blenkinsop, T.G., Höhndorf, A., 2002. Precise U–Pb mineral ages, Rb–Sr and Sm–Nd systematics for the Great Dyke, Zimbabwe—constraints on late Archean events in the Zimbabwe craton and Limpopo belt. Precambrian Res. 113, 293–305.

Oliveira, E.P., Silveira, E.M., Söderlund, U., Ernst, R.E., 2013. U-Pb ages and geochemistry of mafic dyke swarms from the Uauá Block, São Francisco Craton, Brazil: LIPs remnants relevant for Late Archaean break-up of a supercraton. Lithos 174, 308–322.

Pidgeon, R.T., Cook, T.J.F., 2003. 1214±5 Ma dyke from the Darling Range, southwestern Yilgarn Craton, Western Australia. Aust. J. Earth Sci. 50, 769–773.

Pidgeon, R.T., Nemchin, A.A., 2001. 1.2 Ga Mafic dyke near York, southwestern Yilgarn Craton, Western Australia. Aust. J. Earth Sci. 48, 751–755.

Pidgeon, R.T., Wilde, S.A., 1990. The distribution of 3.0 Ga and 2.7 Ga volcanic episodes in the Yilgarn Craton of Western Australia. Precambrian Res. 48, 309–325.

Pisarevsky, S., De Waele, B., Jones, S., Söderlund, U., Ernst, R.E., 2015. Paleomagnetism and U–Pb age of the 2.4 Ga Erayinia mafic dykes in the south-western Yilgarn, Western Australia: Paleogeographic and geodynamic implications. Precambrian Res. 259, 222–231.

Qiu, Y., Groves, D.I., 1999. Late Archean collision and delamination in the Southwest Yilgarn Craton; the driving force for Archean orogenic lode gold mineralization? Econ. Geol. 94, 115–122.

Qiu, Y., Groves, D.I., McNaughton, N.J., 1997a. Deep-seated granitoids: implications for Late Archaean subduction-collision-lithospheric delamination and gold mineralization in the Yilgarn Craton. Aust. Geol. Surv. Organ. Rec. 41, 65–69.

Qiu, Y., McNaughton, N.J., Groves, D., Dalstra, H.J., 1997b. Shrimp U-Pb in zircon and lead-isotope constraints on the timing and source of an Archaean granulite-hosted lode-gold deposit at Griffin's Find, Yilgarn craton, Western Australia. Chron. la Rech. Min. 91–104.

Qiu, Y., McNaughton, N.J., Groves, D.I., Dunphy, J.M., 1999. First record of 1.2 Ga quartz dioritic magmatism in the Archaean Yilgarn Craton, Western Australia, and its significance. Aust. J. Earth Sci. 46, 421–428.

Rasmussen, B., Fletcher, I.R., 2010. Dating sedimentary rocks using in situ U-Pb geochronology of syneruptive zircon in ash-fall tuff less than 1 mm thick. Geology 38, 299–302.

Roth, E., Bennett, J.M., Symons, P.M., 1990. Boddington and Black Flag: anomalous Archaean gold deposits. Geol. Dep. Univ. Extension, Univ. West. Aust. Publ. 20, 189–194.

Roth, E., Groves, D., Anderson, G., Daley, L., Staley, R., 1991. Primary mineralization at the Boddington gold mine, Western Australia: An Archean porphyry Cu-Au-Mo deposit, in: Brazil Gold. pp. 481–488.

Schott, B., Schmeling, H., 1998. Delamination and detachment of a lithospheric root. Tectonophysics 296, 225–247.

Shellnutt, J.G., Hari, K.R., Liao, A.C.-Y., Denyszyn, S.W., Vishwakarma, N., 2018. A 1.88 Ga giant radiating mafic dyke swarm across Southern India and Western Australia. Precambrian Res. 308, 58–74.

Sheppard, S., Bodorkos, S., Johnson, S.P., Wingate, M.T.D., Kirkland, C.L., 2010. The Paleoproterozoic Capricorn Orogeny: intracontinental reworking not continent–continent collision, Geological Survey of Western Australia Report 108. Geological Survey of Western Australia.

Sircombe, K.N., 2007. Compilation of SHRIMP U-Pb geochronological data, Yilgarn Craton, Western Australia, 2004-2006. Geoscience Australia Record 2007/1.

Smirnov, A. V, Evans, D.A.D., Ernst, R.E., Söderlund, U., Li, Z.-X., 2013. Trading partners: Tectonic ancestry of southern Africa and western Australia, in Archean supercratons Vaalbara and Zimgarn. Precambrian Res. 224, 11–22.

Smithies, R.H., Champion, D.C., 1999. Late Archaean felsic alkaline igneous rocks in the Eastern Goldfields, Yilgarn Craton, Western Australia: a result of lower crustal delamination? J. Geol. Soc. London. 156, 561–576.

Smithies, R.H., Howard, H.M., Kirkland, C.L., Korhonen, F.J., Medlin, C.C., Maier, W.D., de Gromard, R.Q., Wingate, M.T.D., Quentin De Gromard, R., Wingate, M.T.D., 2015. Piggy-back supervolcanoes-long-lived, voluminous, juvenile rhyolite volcanism in mesoproterozoic central Australia. J. Petrol. 56, egv015.

Söderlund, U., Hofmann, A., Klausen, M.B., Olsson, J.R., Ernst, R.E., Persson, P.O.,

2010. Towards a complete magmatic barcode for the Zimbabwe craton: Baddeleyite U-Pb dating of regional dolerite dyke swarms and sill complexes. Precambrian Res. 183, 388–398.

Söderlund, U., Johansson, L., 2002. A simple way to extract baddeleyite (ZrO_2). Geochemistry, Geophys. Geosystems 3, 1-7.

Sofoulis, J., 1965. Explanatory Notes on the Widgiemooltha 1: 250,000 Geological Sheet Western Australia. Geological Survey of Western Australia.

Spaggiari, C.V., Kirkland, C.L., Smithies, H.R., Wingate, M.T.D., Belousova, E.A., 2015. Transformation of an Archean craton margin during Proterozoic basin formation and magmatism: The Albany–Fraser Orogen, Western Australia. Precambrian Res. 266, 440–466.

Spaggiari, C. V, Bodorkos, S., Barquero-Molina, M., Tyler, I.M., Wingate, M.T.D., 2009. Interpreted bedrock geology of the South Yilgarn and of the South Yilgarn and Central Albany-Fraser Orogen, Western Australia, Geological Survey of Western Australia Record 2009/10.

Spaggiari, C. V, Kirkland, C.L., Pawley, M.J., Smithies, R.H., Wingate, M.T.D., Doyle, M.G., Blenkinsop, T.G., Clark, C., Oorschot, C.W., Fox, L.J., 2011. The geology of the east Albany-Fraser Orogen—a field guide, Geological Survey of Western Australia Record 2011/23.

Stacey, J.S., Kramers, J.D., 1975. Approximation of terrestrial lead isotope evolution by a two-stage model. Earth Planet. Sci. Lett. 26, 207–221.

Standing, J.G., 2008. Terrane amalgamation in the Eastern Goldfields Superterrane, Yilgarn Craton: evidence from tectonostratigraphic studies of the Laverton Greenstone Belt. Precambrian Res. 161, 114–134.

Stark, J.C., Wang, X.-C., Denyszyn, S.W., Li, Z.-X., Rasmussen, B., Zi, J.-W., Sheppard, S., Liu, Y., 2017. Newly identified 1.89 Ga mafic dyke swarm in the Archean Yilgarn Craton, Western Australia suggests a connection with India. Precambrian Res. Press.

Stern, R.A., 2001. A new isotopic and trace-element standard for the ion microprobe: preliminary thermal ionization mass spectrometry (TIMS) U-Pb and electron-microprobe data, Geological Survey of Canada Current Research 2001-F.

Stern, R.A., Bodorkos, S., Kamo, S.L., Hickman, A.H., Corfu, F., 2009. Measurement of SIMS instrumental mass fractionation of Pb isotopes during zircon dating. Geostand. Geoanalytical Res. 33, 145–168.

Tomkins, A.G., Grundy, C., 2009. Upper Temperature Limits of Orogenic Gold Deposit Formation : Constraints from the Granulite-Hosted Griffin's Find Deposit , Yilgarn Craton. Econ. Geol. 104, 669–685.

Tucker, D.H., Boyd, D.M., 1987. Dykes of Australia detected by airborne magnetic surveys, in: Fahrig, W.F., Halls, H.C. (Eds.), Mafic Dyke Swarms. Geological Association of Canada Special Paper 34, pp. 163–172.

Upton, P., Hobbs, B., Ord, A., Zhang, Y., Drummond, B., Archibald, N., 1997. Thermal and deformation modelling of the Yilgarn deep seismic transect, in: Geodynamics and Ore Deposits Conference Abstracts. pp. 22–25.

Wang, X.-C., Li, Z.-X., Li, J., Pisarevsky, S.A., Wingate, M.T.D., 2014. Genesis of the 1.21 Ga Marnda Moorn large igneous province by plume–lithosphere interaction. Precambrian Res. 241, 85–103.

Wilde, S.A., 1999. Evolution of the Western Margin of Australia during the Rodinian and Gondwanan Supercontinent Cycles. Gondwana Res. 2, 481–499.

Wilde, S.A., 1990. Geology and crustal evolution of the southwestern Yilgarn Craton, in: Third International Archaean Symposium, Perth. pp. 89–122.

Wilde, S.A., 1980. The Jimperding Metamorphic Belt in the Toodyay area and the Balingup Metamorphic Belt and associated granitic rocks in the southwestern Yilgarn Craton. Excursion Guide, in: 2nd International Archaean Symposium, Geological Society of Western Australia.

Wilde, S.A., 1976. The Saddleback Group–a newly discovered Archaean greenstone belt in the southwestern Yilgarn Block. Western Australia Geological Survey Annual Report, 92–95.

Wilde, S.A., Low, G.H., 1978. Perth, Western Australia, 1: 250 000 Geological Series Explanatory Notes. Western Australia Geological Survey

Wilde, S.A., Middleton, M.F., Evans, B.J., 1996. Terrane accretion in the southwestern Yilgarn Craton: evidence from a deep seismic crustal profile. Precambrian Res. 78, 179–196.

Wilde, S.A., Pidgeon, R.T., 2006. Nature and timing of Late Archaean arc magmatism along the western margin of the Yilgarn Craton. Geochim. Cosmochim. Acta 70, A701.

Wilde, S.A., Pidgeon, R.T., 1990. The Morangup Greenstone Belt: a further discovery of Late Archaean volcanic rocks in the southwest Yilgarn Craton, Western Australia. International Archaean Symposium, 3rd Perth 1990. Abstr. Geoconferences 205–206.

Wilde, S.A., Pidgeon, R.T., 1987. U-Pb. Geochronology, Geothermometry and Petrology of the Main Areas of Gold Mineralization in the Wheat Belt Region of Western Australia Project 30 Final Report. Western Australian Mining and Petroleum Research Institute.

Wilde, S.A., Pidgeon, R.T., 1986. Geology and geochronology of the Saddleback greenstone belt in the Archaean Yilgarn Block, southwestern Australia. Aust. J. Earth Sci. 33, 491–501.

Williams, I.S., 1998. U-Th-Pb geochronology by ion microprobe. Rev. Econ. Geol. 7, 1–35.

Wilson, J.F., Jones, D.L., Kramers, J.D., 1987. Mafic dyke swarms in Zimbabwe, in: Mafic Dyke Swarms. Geological Association of Canada Special Paper 34,.pp. 433–444.

Wingate, M.T.. D., Campbell, I.H., Compston, W., Gibson, G.M., 1998. Ion microprobe U–Pb ages for Neoproterozoic basaltic magmatism in south-central Australia and implications for the breakup of Rodinia. Precambrian Res. 87, 135–159.

Wingate, M.T.D., 2017. Mafic dyke swarms and large igneous provinces in Western Australia get a digital makeover, in: Geological Survey of Western Australia Record 2017/2. pp. 4–8.

Wingate, M.T.D., 2007. Proterozoic mafic dykes in the Yilgarn Craton, in: Proceedings of Geoconferences (WA) Inc. Kalgoorlie 2007 Conference, Kalgoorlie, Western Australia. pp. 80–84.

Wingate, M.T.D., 1999. Ion microprobe baddeleyite and zircon ages for Late Archaean mafic dykes of the Pilbara Craton, Western Australia. Aust. J. Earth Sci. 46, 493–500.

Wingate, M.T.D., Campbell, I.H., Harris, L.B., 2000. SHRIMP baddeleyite age for the Fraser dyke swarm, southeast Yilgarn Craton, Western Australia. Aust. J. Earth Sci. 47, 309–313.

Wingate, M.T.D., Pidgeon, R.T., 2005. The Marnda Moorn LIP, a late Mesoproterozoic large igneous province in the Yilgarn craton, Western

Australia. July 2005 LIP of the month [WWW Document]. (unpub). Large Igneous Prov. Comm. Int. Assoc. Volcanol. Chem. Earth's Inter. URL http://www.largeigneousprovinces.org/05jul

Wingate, M.T.D., Pirajno, F., Morris, P.A., 2004. Warakurna large igneous province: a new Mesoproterozoic large igneous province in west-central Australia. Geology 32, 105–108.

Wingate, M.T.D., Pisarevsky, S.A., Evans, D.A.D., 2002. Rodinia connections between Australia and Laurentia: no SWEAT, no AUSWUS? Terra Nov. 14, 121–128.

Witt, W.K., Cassidy, K.F., Lu, Y.-J., Hagemann, S.G., 2018. The tectonic setting and evolution of the 2.7 Ga Kalgoorlie–Kurnalpi Rift, a world-class Archean gold province. Miner. Depos. 1-31.

Witt, W.K., Vanderhor, F., 1998. Diversity within a unified model for Archaean gold mineralization in the Yilgarn Craton of Western Australia: an overview of the late-orogenic, structurally-controlled gold deposits. Ore Geol. Rev. 13, 29–64.

Xie, H., Kröner, A., Brandl, G., Wan, Y., 2017. Two orogenic events separated by 2.6 Ga mafic dykes in the Central Zone, Limpopo Belt, southern Africa. Precambrian Res. 289, 129–141.

Yeats, C.J., McNaughton, N.J., 1997. Significance of SHRIMP II U-Pb geochronology on lode-gold deposits of the Yilgarn craton. Aust. Geol. Surv. Organ. Rec. 41, 125–130.

Yeats, C.J., McNaughton, N.J., Groves, D.I., 1996. SHRIMP U-Pb geochronological constraints on Archean volcanic-hosted massive sulfide and lode gold mineralization at Mount Gibson, Yilgarn Craton, Western Australia. Econ. Geol. 91, 1354–1371.

Zeh, A., Gerdes, A., Barton Jr, J., Klemd, R., 2010. U–Th–Pb and Lu–Hf systematics of zircon from TTG's, leucosomes, meta-anorthosites and quartzites of the Limpopo Belt (South Africa): constraints for the formation, recycling and metamorphism of Palaeoarchaean crust. Precambrian Res. 179, 50–68.

Zeh, A., Gerdes, A., Klemd, R., Barton, J.M., 2007. Archaean to proterozoic crustal evolution in the central zone of the Limpopo Belt (South Africa-Botswana): Constraints from combined U-Pb and Lu-Hf isotope analyses of zircon. J. Petrol. 48, 1605–1639.

Zhao, G., Sun, M., Wilde, S.A., Li, S., Zhang, J., 2006. Some key issues in reconstructions of Proterozoic supercontinents. J. Asian Earth Sci. 28, 3–19.

Zibra, I., Clos, F., Weinberg, R.F., Peternell, M., 2017a. The ~2730 Ma onset of the Neoarchean Yilgarn Orogeny. Tectonics 36, 1787–1813.

Zibra, I., Korhonen, F.J., Peternell, M., Weinberg, R.F., Romano, S.S., Braga, R., De Paoli, M.C., Roberts, M., 2017b. On thrusting, regional unconformities and exhumation of high-grade greenstones in Neoarchean orogens. The case of the Waroonga Shear Zone, Yilgarn Craton. Tectonophysics 712–713, 362–395.

Chapter 5 Newly identified 1.89 Ga mafic dyke swarm in the Archean Yilgarn Craton, Western Australia, suggests a connection with India[2]

J. Camilla Stark, Xuan-Ce Wang, Steven W. Denyszyn, Zheng-Xiang Li, Birger Rasmussen, Jian-Wei Zi, Stephen Sheppard and Yebo Liu

5.1 Abstract

The Archean Yilgarn Craton in Western Australia is intruded by numerous mafic dykes of varying orientations, which are poorly exposed but discernible in aeromagnetic maps. Previous studies have identified two craton-wide dyke swarms, the 2408 Ma Widgiemooltha and the 1210 Ma Marnda Moorn Large Igneous Provinces (LIP), as well as limited occurrences of the 1075 Ma Warakurna LIP in the northern part of the craton. We report here a newly identified NW-trending mafic dyke swarm in southwestern Yilgarn Craton dated at 1888 ± 9 Ma with ID-TIMS U-Pb method on baddeleyite from a single dyke and at 1858 ± 54 Ma, 1881 ± 37 and 1911 ± 42 Ma with in situ SHRIMP U-Pb on baddeleyite from three dykes. Preliminary interpretation of aeromagnetic data indicates that the dykes form a linear swarm several hundred kilometers long, truncated by the Darling Fault in the west. This newly named Boonadgin dyke swarm is synchronous with post-orogenic extension and deposition of granular iron formations in the Earaheedy basin in the Capricorn Orogen and its emplacement may be associated with far field stresses. Emplacement of the dykes may also be related to initial stages of rifting and formation of the intracratonic Barren Basin in the Albany-Fraser Orogen, where the regional extensional setting prevailed for the following 300 million years. Recent studies and new paleomagnetic evidence raise the possibility that the dykes could be part of the coeval 1890 Ma Bastar-Cuddapah LIP in India. Globally, the Boonadgin dyke swarm is synchronous with a major orogenic episode and records of intracratonic mafic magmatism on many other Precambrian cratons.

---

[2] *This chapter is published as* Stark, J.C., Wang, X.-C., Denyszyn, S.W., Li, Z.-X., Rasmussen, B., Zi, J.-W., Sheppard, S., Liu, Y.,. Newly identified 1.89 Ga mafic dyke swarm in the Archean Yilgarn Craton, Western Australia suggests a connection with India. Precambrian Res. *In press*. https://doi.org/10.1016/j.precamres.2017.12.036, online on 19 December 2017

5.2 Introduction

Regardless of their proposed mechanism of formation (e.g. mantle plume, flux melting, passive rifting or global mantle warming), large igneous provinces (LIPs; Coffin and Eldholm, 1994), including mafic dyke swarms, appear to be intimately connected with deep-Earth dynamics and supercontinent cycles (e.g. Condie, 2004; Prokoph et al., 2004; Bleeker and Ernst, 2006; Ernst et al., 2008; Li and Zhong, 2009; Clowes et al., 2010; Goldberg, 2010). Mafic dyke swarms act as important markers for supercontinent reconstructions (e.g. Ernst and Buchan, 1997; Buchan et al., 2001; Bleeker and Ernst, 2006; Ernst and Srivastava, 2008; Ernst et al., 2010, 2013) and as indicators of paleostress fields and pre-existing crustal weaknesses (Ernst et al., 1995b; Hoek and Seitz, 1995; Halls and Zhang, 1998; Hou, 2012; Ju et al., 2013). Key to such application is the availability of high-precision geochronology for mafic dykes. Recent studies have shown that orientation alone cannot be reliably used to distinguish between different dyke generations, especially near major tectonic boundaries and craton scale structures such as continental rifts (e.g. Hanson et al., 2004; Wingate, 2007; French and Heaman, 2010; Belica et al., 2014).

Like many other Archean cratons worldwide, the Yilgarn Craton in Western Australia is intruded by many generations of dyke suites with different orientations. Currently, robust geochronology is only available for two craton-wide dyke swarms at 2408 Ma (Sofoulis, 1965; Evans, 1968; Hallberg, 1987; Doehler and Heaman, 1998; Nemchin and Pidgeon, 1998; Wingate, 1999; French et al., 2002) and at 1210 Ma (Marnda Moorn LIP; Wingate et al., 1998, 2000; Wingate, 2007), and for limited dyke occurrences at 1075 Ma (Warakurna LIP; Wingate et al., 2002, 2004) and ca. 735 Ma (Nindibillup dykes; Spaggiari et al., 2009, 2011; Wingate, 2017). The magmatic record ("barcode") for the Yilgarn Craton dyke swarms is very limited compared with other Archean cratons, such as the Superior and Kola-Karelia Cratons (Ernst and Bleeker, 2010; Ernst et al., 2010). The apparent absence of mafic magmatism in the Yilgarn Craton during the major global episode of juvenile magmatism and crustal growth at ca. 1890 Ma is surprising since this event is found on most other Precambrian cratons worldwide (Heaman et al., 1986, 2009; Hanson et al., 2004; French et al., 2008; Minifie et al., 2008; Buchan et al., 2010; Ernst and

Bell, 2010; Söderlund et al., 2010). The lack of geochronology and paleomagnetic data from the Yilgarn Craton between ca. 1900 Ma and 1300 Ma, the proposed time interval for the supercontinent Nuna/Columbia, is especially problematic for paleographic reconstructions.

Here we report *in situ* SHRIMP and ID-TIMS U-Pb results for a previously unidentified NW-trending Paleoproterozoic mafic dyke suite in the southwestern Yilgarn Craton and discuss the tectonic setting during its emplacement. A direct record of Paleoproterozoic tectonic events in the craton margins is largely absent due to extensive overprinting by younger events, so we also evaluate evidence from remnant Proterozoic sedimentary basins, which preserve a history of past tectonic setting, crustal architecture and lithospheric stress fields. In light of previous studies suggesting India-Yilgarn connection (Mohanty, 2012, 2015) and recent paleomagnetic data (Belica et al., 2014; Liu et al., 2016, 2018) we consider the possibility that the dykes may be associated with the coeval Bastar-Cuddapah LIP in India.

5.3 Regional geology

The Yilgarn Craton is a ca. 900 x 1000 km Archean crustal block comprising six accreted terranes: the Southwest, Narryer, Youanmi, Kalgoorlie, Kurnalpi and Burtville terranes, the latter three forming the Eastern Goldfields Superterrane (Figure 5.1). These comprise variably metamorphosed granites and volcanic and sedimentary rocks with protolith ages between ca. 3730 and 2620 Ma (Cassidy et al., 2005, 2006 and references therein) and are thought to represent a series of volcanic arcs, back arc basins and microcontinents, which amalgamated between ca. 2900 and 2700 Ma (Myers, 1993; Wilde et al., 1996). Abundant granites were emplaced between ca. 2760 Ma and 2630 Ma (Cassidy et al., 2006 and references therein) and the entire craton underwent intense metamorphism and hydrothermal activity between 2780 and 2630 Ma (Myers, 1993; Nemchin et al., 1994; Nelson et al., 1995a; Wilde et al., 1996). The Southwest Terrane comprises multiply deformed ca. 3200–2800 Ma high-grade metasedimentary rocks and ca. 2720─2670 Ma meta-igneous rocks intruded by 2750─2620 Ma granites (Myers, 1993; Wilde et al., 1996; Nemchin and Pidgeon, 1997).

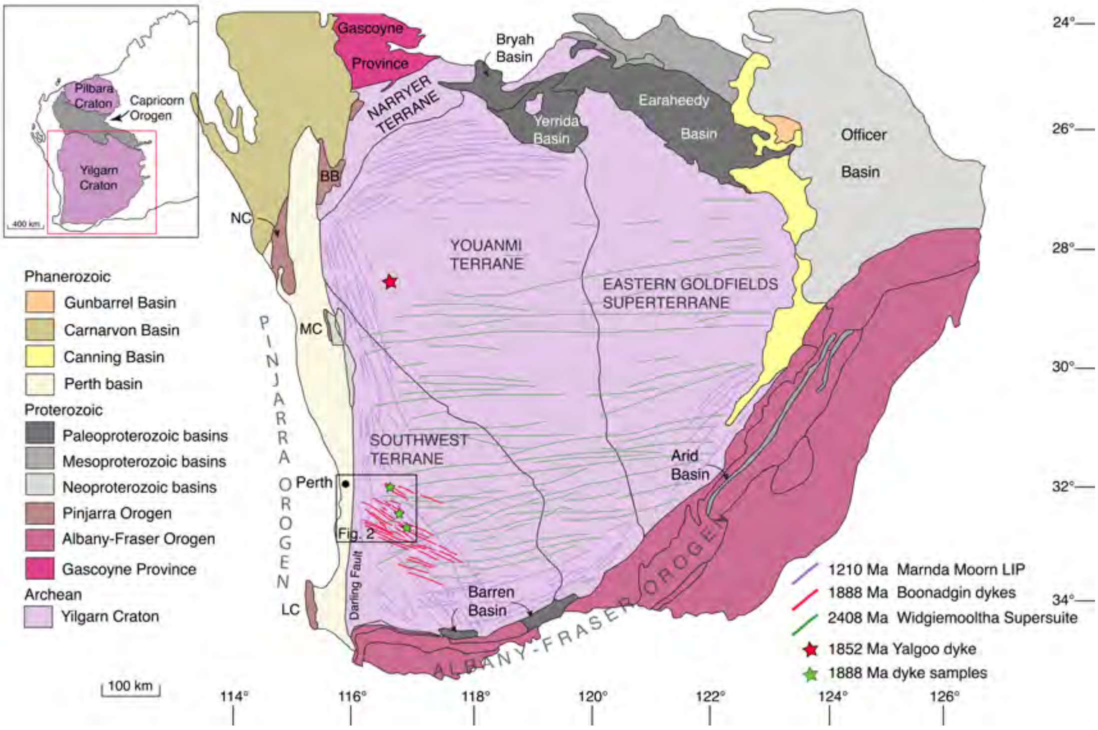

Figure 5.1 Map of the Yilgarn showing major tectonic units and the Capricorn and Albany-Fraser Orogens. Inset shows the extent of the West Australian Craton (Pilbara Craton, Yilgarn Craton and Capricorn Orogen). From Geological Survey of Western Australia 1:2.5M Interpreted Bedrock Geology 2015 and 1:10M Tectonic Units 2016

The Yilgarn Craton is bounded by three Proterozoic orogenic belts: the ca. 2005─570 Ma Capricorn Orogen in the north (Cawood and Tyler, 2004; Sheppard et al., 2010a; Johnson et al., 2011), the ca. 1815─1140 Ma Albany-Fraser Orogen in the south and east (Nelson et al., 1995a; Clark et al., 2000; Spaggiari et al., 2015), and the ca. 1090-525 Ma Pinjarra Orogen in the west (Myers, 1990; Wilde, 1999; Ksienzyk et al., 2012). Prolonged lateritic weathering has produced the modern denuded landscape and poor exposure of basement rocks (Anand and Paine, 2002).

Following cratonisation toward the end of the Archean, the Yilgarn Craton collided along the Capricorn Orogen with the combined Pilbara Craton-Glenburgh Terrane by 1950 Ma to form the West Australian Craton (WAC: Sheppard et al., 2004, 2010; Johnson et al., 2011). Four syn- to post-orogenic sedimentary basins developed along the southern Capricorn Orogen, including the Earaheedy Basin in the east (Pirajno et al., 2009). The Earaheedy succession was thought to be post-1800 Ma in age, but new dating (Rasmussen et al., 2012; Sheppard et al., 2016) shows that the basin comprises three unconformity-bound packages at ca. 1990–1950 Ma, ca. 1890 Ma and ca. 1890–1810 Ma.

The Yilgarn Craton is intruded by a large number of dykes of different orientations with the dyke density increasing towards the southern and western craton margins (Hallberg, 1987; Tucker and Boyd, 1987). The dykes are discernible in aeromagnetic data but difficult to sample due to deep weathering and thick regolith cover. The oldest known dykes belong to the E-W to NE-SW trending 2408 Ma Widgiemooltha Supersuite (Sofoulis, 1965; Evans, 1968; Campbell et al., 1970; Hallberg, 1987; Doehler and Heaman, 1998; Nemchin and Pidgeon, 1998; Wingate, 1999, 2007; French et al., 2002). The Widgiemooltha dykes are up to 3.2 km wide and extend up to 700 km across the craton, with the largest intrusions (Jimberlana and Binneringie) showing well developed igneous layering (Campbell et al., 1970; Lewis, 1994). The dykes exhibit dual magnetic polarity (Tucker and Boyd, 1987; Boyd and Tucker, 1990) and recent geochronology and paleomagnetic data suggest that their emplacement may have involved several pulses (Wingate, 2007; Pisarevsky et al., 2015). The second craton-wide suite is the 1210 Ma Marnda Moorn LIP which consists of several sub-swarms of different orientations intruding along the craton margins (Isles and Cooke, 1990; Evans, 1999; Wingate et al., 2000; Pidgeon and Nemchin, 2001; Pidgeon and Cook, 2003; Wingate and Pidgeon, 2005; Wingate, 2007; Claoué-Long and Hoatson, 2009). Outcrops in the southeast are limited to a single occurrence, and the extent of the dykes in the northeast is unknown due to cover rocks but one E-W oriented dioritic dyke dated at 1215 ± 11 Ma has been reported further inland (Qiu et al., 1999). Other identified dyke swarms with limited occurrences include the SW-trending dykes of the 1075 Ma Warakurna LIP in the northern Yilgarn Craton (Wingate et al., 2004), the WNW-trending ca. 735 Ma Nindibillup dykes in the central and SE Yilgarn Craton (Spaggiari et al., 2009, 2011; Wingate, 2017) and the undated (likely <1140 Ma) NW-trending Beenong dykes in the SE Yilgarn Craton (Wingate, 2007; Spaggiari et al., 2009, 2011).

5.4 Samples

5.4.1 Field sampling

Field sampling sites were targeted using satellite imagery (Landsat/Copernicus or Astrium/CNES from Google Earth), aeromagnetic data (20-40 m cell size, Geoscience Australia magnetic grid of Australia V6 2015 base reference) and 1:250 000 geological maps from the Geological Survey of Western Australia.

Four block samples were collected from outcrops within agriculturally cleared areas where the dykes stand out as small ridges. Sample WDS09 was collected from an outcrop ca. 18 km southwest of the town of Pingelly, sample 16WDS01 and 16WDS02 ca. 29 km northwest of Pingelly and sample 16WDS06 ca. 14 km southwest of the village of Gwambygine (Figure 5.2). Coordinates for sample locations are given in Table 5.1. Basement rocks are only exposed at the WDS09 outcrop where the dyke intrudes Archean migmatitic gneiss with a sharp chilled margin. At the 16WDS01/16WDS02 and 16WDS06 sites, geological mapping indicates that the country rocks to the dykes are mainly Archean granites. The outcrops are fresh with weathering forming a thin crust best visible along fractures.

5.4.2 Sample description

All samples are dolerites with intergranular ophitic to sub-ophitic texture, comprising ca. 50% plagioclase, 45% clinopyroxene, 1-2 % quartz, 2-3 % opaque minerals (ilmenite, magnetite and minor pyrite) and trace biotite and apatite. Sample WDS09 is relatively fresh but samples 16WDS01/02 and 16WDS06 in the northern part of the sampling area are more altered, with most clinopyroxene grains partially altered to chlorite and green amphibole. Plagioclase is affected by sericitisation but most grains still show twinning. Biotite is associated with the opaque minerals, forming corona like rims. The main U- and Th-bearing accessory minerals are baddeleyite and zirconolite, only identifiable under SEM due to their small size, typically ≤ 70 µm long and 20-30 µm across. Some crystals show thin zircon rims or alteration to zircon along fractures but most appear pristine.

5.5 U-Pb geochronology and geochemistry

5.5.1 SHRIMP U-Pb geochronology

Polished thin sections were scanned to identify baddeleyite, zircon and zirconolite with a Hitachi TM3030 scanning electron microscope (SEM) equipped with energy dispersive X-ray spectrometer (EDX) at Curtin University. For SHRIMP U-Pb dating, selected grains were drilled directly from the thin sections using a micro drill and mounted into epoxy disks, which were cleaned and coated with 40 nm of gold. Baddeleyite forms unaltered subhedral to euhedral equant and tabular grains and

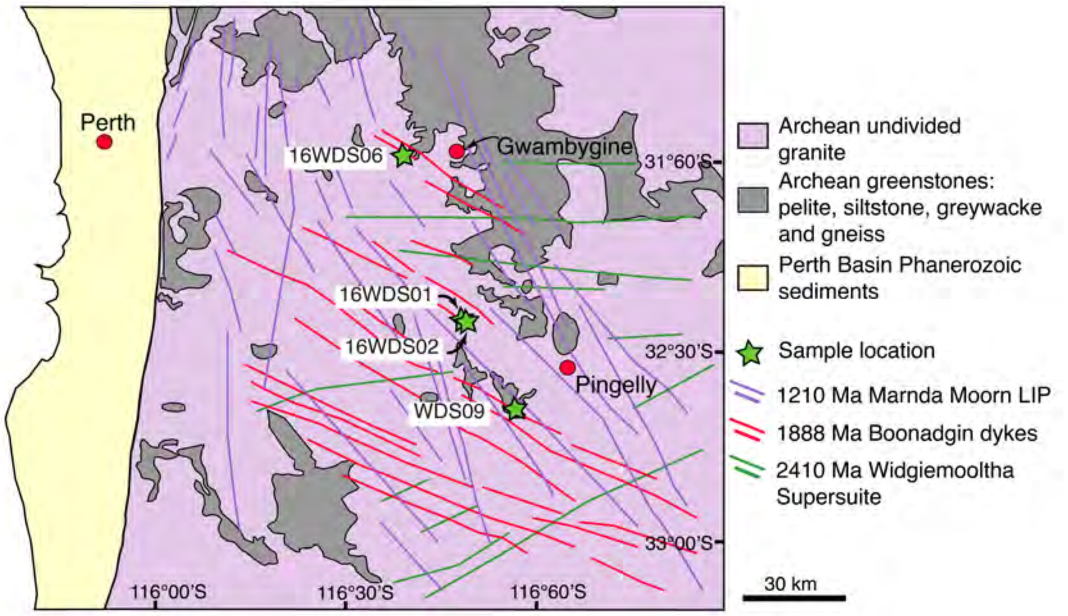

Figure 5.2 Sampling locations. See Table 5.1 for detailed information

Dyke ID	Dlat / Dlon	Samples	Comments
WDS09	32 39.339 S 116 57.132 E	WDS09M-N, WDS09RSA-B	NW trending dolerite dyke near West Pingelly
16WDS01	32 24.738 S 116 48.818 E	16WDS01A-D	NNW trending dolerite dyke west of Brookton, ridge
16WDS02	32 24.740 S 116 48.798 E	16WDS02A-D	NNW trending dolerite dyke west of Brookton. Same dyke as 16WDS01
16WDS06	31 59.973 S 116 39.699 E	16WDS06A-D	NW trending dyke near Talbot

Table 5.1 Sample locations. Datum WGS84, Dlat = decimal latitude, Dlon = decimal longitude

laths, some with thin zircon rims, and most are <60 μm long and up to 20-30 μm across (Figure 5.3).

Baddeleyite was analysed for U, Th and Pb using the sensitive high-resolution ion microprobe (SHRIMP II) at the John de Laeter Centre at Curtin University in Perth, Australia, following standard operating procedures after Compston et al. (1984). The

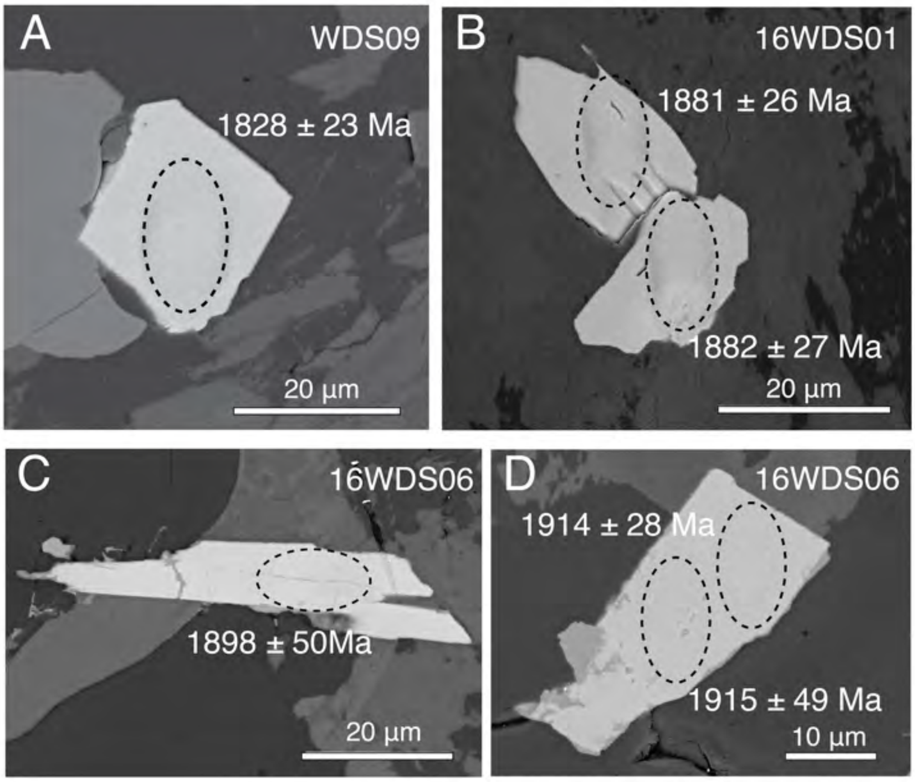

*Figure 5.3 SEM backscatter images showing SHRIMP baddeleyite spots and dates. (**A**) WDS09-2B (**B**) 16WDS01-372B (**C**) 16WDS06-405B (**D**) 16WDS06-406B*

SHRIMP analysis method for mounts with polished thin section plugs outlined in Rasmussen and Fletcher (2010) was modified for baddeleyite (SHRIMP operating parameters in Table 5.2. During each analysis session, standard zircon OG1 (Stern et al., 2009) was used to monitor instrumental mass fractionation and BR266 zircon (Stern, 2001) was used for calibrating U and Th concentration and as an accuracy standard. Phalaborwa baddeleyite (Heaman, 2009) was employed as an additional accuracy standard. Typical spot size with primary O_2^- current was 10-15 µm at 0.8-1.4 nA. Data were processed with Squid version 2.50 (Ludwig, 2009) and Isoplot version 3.76.12 (Ludwig, 2012). For common Pb correction, 1890 Ma common Pb isotopic compositions were calculated from the Stacey and Kramers (1975) two-stage terrestrial Pb isotopic evolution model. Analyses with >1% common Pb (in ^{206}Pb) or >10% discordance (see footnote in Table 5.3 for definition) are considered unreliable and were disregarded in age calculations. The assigned 1σ external Pb/U error for all analyses is 1%, except for 1.04% for 16WDS06. All weighted mean ages are given at 95% confidence level, whereas individual analyses are presented with 1σ error.

Mount	CS16-1	CS16-6	CS16-7
Dykes analysed	WDS09, WDS09RS	16WDS01	16WDS06
Date analysed	21-Jul-16	14-Sep-16	6-Sep-16
Kohler aperture (μm)	50	50	50
Spot size (micrometres)	11	9	7
O2- primary current (nA)	0.9	0.6	0.2
Number of scans per analysis	8	8	8
Total number of analyses	23	32	34
Number of standard analyses	13	13	14
Pb/U external precision % (1σ)	1.00	1.00	1.00
Raster time (seconds)	120	180	180
Raster aperture (μm)	90	90	80

Table 5.2 SHRIMP operating parameters. Notes ***1)*** *Mass resolution for all analyses ≥ 5000 at 1% peak height* ***2)*** *BR266, OGC, Phalaborwa and NIST used as standards for each session* ***3)*** *Count times for each scan: ^{204}Pb, ^{206}Pb, ^{208}Pb = 10 seconds, ^{207}Pb = 30 seconds*

5.5.2 ID-TIMS U-Pb geochronology

A sample for ID-TIMS U-Pb geochronology was selected based on results from the SHRIMP dating and the highest number of identified baddeleyites in thin section. A block sample was first sawn from the field sample to remove weathering, then crushed, powdered and processed using a mineral-separation technique amended from Söderlund and Johansson (2002). Baddeleyite grains were hand picked under ethanol under a stereographic optical microscope and selected grains were cleaned with concentrated distilled HNO_3 and HCl. Due to the small size of the grains, no chemical separation methods were required.

Samples were spiked with a University of Western Australia in-house ^{205}Pb-^{235}U tracer solution, which has been calibrated against SRM981, SRM982 (for Pb), and CRM 115 (for U), as well as an externally-calibrated U-Pb solution (the JMM solution from the EarthTime consortium). This tracer is regularly checked using "synthetic zircon" solutions that yield U-Pb ages of 500 Ma and 2000 Ma, provided by D. Condon (BGS). Dissolution and equilibration of spiked single crystals was by vapour transfer of HF, using Teflon microcapsules in a Parr pressure vessel placed in a 200°C oven for six days. The resulting residue was re-dissolved in HCl and H_3PO_4

and placed on an outgassed, zone-refined rhenium single filament with 5 µL of silicic acid gel. U–Pb isotope analyses were carried out using a Thermo Triton T1 mass spectrometer, in peak-jumping mode using a secondary electron multiplier. Uranium was measured as an oxide (UO_2). Fractionation and deadtime were monitored using SRM981 and SRM 982. Mass fractionation was 0.02 ± 0.07%/amu. Data were reduced and plotted using the software packages Tripoli (from CIRDLES.org) and Isoplot 4.15 (Ludwig, 2011). All uncertainties are reported at 2σ. U decay constants are from Jaffey et al. (1971). The weights of the baddeleyite crystals were calculated from measurements of photomicrographs and estimates of the third dimension. The weights are used to determine U and Pb concentrations and do not contribute to the age calculation. An uncertainty of ± 50% may be attributed to the concentration estimate.

5.6 Geochemistry

Slabs were sawn from block samples to remove weathering. After an initial crush, a small fraction of material was separated and chips with fresh fracture surfaces were hand picked under the microscope and pulverised in an agate mill for isotope analysis. Remaining material was pulverised in a low-Cr steel mill for major and trace element analysis.

Major element analysis was undertaken at Intertek Genalysis Laboratories in Perth, Western Australia using X-ray fluorescence (XRF) using the Geological Survey of Western Australia (GSWA) standard BB1 (Morris, 2007) and Genalysis laboratory internal standards SARM1 and SY-4. Trace element analysis was carried out at University of Queensland (UQ) on a Thermo XSeries 2 inductively coupled plasma mass spectrometer (ICP-MS) equipped with an ESI SC-4 DX FAST autosampler, following procedure for ICP-MS trace element analysis by Eggins et al. (1997) modified by the UQ Radiogenic Isotope Laboratory (Kamber et al., 2003). Sample solutions were diluted 4000 times and 12ppb ^{6}Li, 6ppb ^{61}Ni, Rh, In and Re, and 4.5ppb ^{235}U internal spikes were added. USGS W2 was used as reference standard and crossed checked with BIR-1, BHVO-2 or other reference materials. All major element analyses have precision better than 5 % and all trace element analyses have relative standard deviation (RSD) < 2%.

Rb-Sr and Sm-Nd isotope analyses were carried out at the University of Melbourne (e.g. Maas et al., 2005, 2015). Small splits (70 mg) of rock powders were spiked with ^{149}Sm-^{150}Nd and ^{85}Rb-^{84}Sr tracers, followed by dissolution at high pressure in an oven, using Krogh-type PTFE vessels with steel jackets. Sm, Nd and Sr were extracted using EICHROM Sr-, TRU- and LN-resin, and Rb was extracted using cation exchange (AG50-X8, 200-400 mesh resin). Isotopic analyses were carried out on a NU Plasma multi-collector ICP-MS coupled to a CETAC Aridus desolvation system operated in low-uptake mode. Raw data for spiked Sr and Nd fractions were corrected for instrumental mass bias by normalizing to $^{88}Sr/^{86}Sr$ = 8.37521 and $^{146}Nd/^{145}Nd$ = 2.0719425 (equivalent to $^{146}Nd/^{144}Nd$ = 0.7219), respectively, using the exponential law as part of an on-line iterative spike-stripping/internal normalization procedure. Sr and Nd isotope data are reported relative to SRM987 = 0.710230 and La Jolla Nd = 0.511860 and have typical in-run precisions (2sd) of ± 0.000020 (Sr) and ± 0.000012 (Nd). External precision (reproducibility, 2sd) is ± 0.000040 (Sr) and ± 0.000020 (Nd). External precisions for $^{87}Rb/^{86}Sr$ and $^{147}Sm/^{144}Nd$ obtained by isotope dilution are ± 0.5% and ± 0.2%, respectively.

5.7 Results

5.7.1 SHRIMP U-Pb geochronology

Seventeen analyses were obtained from thirteen baddeleyite grains (9 grains from WDS09, 1 grain from 16WDS01 and 3 grains from 16WDS06) during three SHRIMP sessions (Figure 5.4; detailed U-Pb data are given in Table 5.3. The analysed baddeleyites have low to moderate U concentrations varying from 47 to 449 ppm (median = 181 ppm) and low Th from 5 to 76 ppm, with Th/U ratios ranging from 0.02 to 0.47. Eight analyses were excluded based on their high common Pb (>1% ^{206}Pb) and/or >10% discordance. Sample WDS09 yielded a common Pb-corrected weighted mean $^{207}Pb/^{206}Pb$ date of 1858 ± 54 Ma (MSWD = 1.80, 4 analyses from 4 grains). If spot WDS09N5.29B-1, which is near-concordant (6% discordance) but contains slightly higher common Pb (1.45%) is included, the weighted mean is 1860 ± 41 Ma (MSWD = 1.4, n = 5). Two analyses on a single grain from 16WDS01 yield a $^{207}Pb/^{206}Pb$ weighted mean of 1881 ± 37 Ma (MSWD = 0.00075) and three analyses on 2 grains from 16WDS06 give a weighted mean of 1911 ± 42 Ma. Collectively, the 9 analyses on five baddeleyite grains from three samples give $^{207}Pb/^{206}Pb$ dates overlapping with each other within uncertainties;

combining them yields a weighted mean of 1874 ± 25 Ma (MSWD = 1.3), which is interpreted as the best approximation of the crystallisation age of the dykes.

5.7.2 ID-TIMS U-Pb geochronology

Four baddeleyite crystals were analyzed from sample WDS09 (Table 5.4, Figure 5.5). Calculated weights are on the order of 0.1 μg, with low calculated U concentrations, all below 50 ppm. One grain has an apparently very low U content (3 ppm) and a concomitant low $^{206}Pb/^{204}Pb$ ratio of 30. This results in a relatively

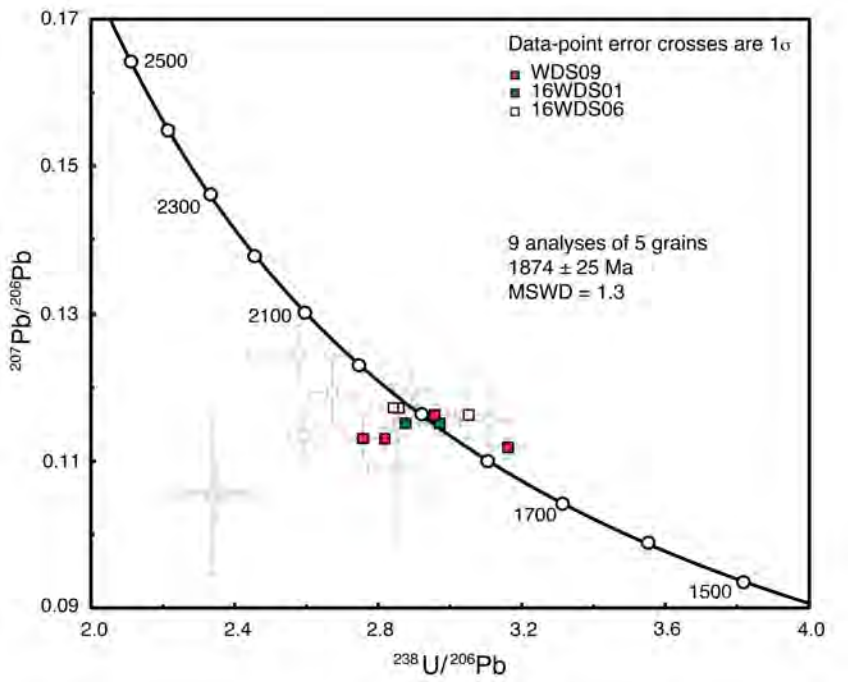

Figure 5.4 Tera-Wasserburg plot of SHRIMP U-Pb baddeleyite results for samples WDS09, 16WDS01 and 16WDS06. Grey squares denote excluded data (see section 5.7.1 for details)

imprecise age determination and large analytical uncertainties for all data are the result of very low radiogenic Pb concentrations. Calculated U concentrations are unusually low for baddeleyite; this may reflect an overestimate of the grain weights, but the low Pb abundance (both radiogenic and common Pb) also implies a low initial U concentration. Th/U ratios are <0.1, a typical value for baddeleyite. One datum is discordant but the coherence in $^{207}Pb/^{206}Pb$ age for all baddeleyite crystals

Table 5.3 SHRIMP U-Pb data for baddeleyite from dyke samples WDS09, 16WDS01 and 16WDS6.

Notes ***1)*** *f_{204} is the proportion of common Pb in ^{206}Pb, determined using the measured ^{204}Pb/^{206}Pb and a common Pb composition from the Stacey and Kramers (1975) model at the approximate age of the sample* ***2)*** *Disc. = 100(t[^{207}Pb*/^{206}Pb*] - t[^{238}U/^{206}Pb*])/t[^{207}Pb*/^{206}Pb*]*

Spot	f_{206} %	U ppm	Th ppm	Th/U	±%	Total ^{238}U/^{206}Pb	±%	Total ^{207}Pb/^{206}Pb	±%	^{238}U/^{206}Pb*	±%	^{207}Pb*/^{206}Pb*	±%	^{238}U/^{206}Pb* Age (Ma)	± 1σ	^{207}Pb*/^{206}Pb* Age (Ma)	± 1σ	Disc. %
WDS09N1.2B	0.40	206	5.0	0.024	1.0	3.15	1.2	0.1152	0.9	3.16	1.2	0.1117	1.3	1771	±19	1828	±23	+4
WDS09N5.38B-1	0.58	269	10.0	0.039	2.9	2.94	1.9	0.1213	0.8	2.96	1.9	0.1162	1.2	1877	±30	1899	±22	+1
WDS09RSB3.45B-1	0.72	449	76.0	0.174	7.3	2.80	1.5	0.1192	0.7	2.82	1.5	0.1129	1.3	1958	±25	1847	±23	-7
WDS09RSB1.54B-1	0.75	67	30.0	0.468	2.2	2.74	1.7	0.1196	1.5	2.76	1.7	0.1131	2.6	1994	±29	1849	±48	-9
16WDS6D.406B-1	0.08	247	23.5	0.098	1.0	2.9	1.7	0.118	1.4	2.9	1.7	0.117	1.5	1934	±29	1914	±28	-1
16WDS6D.406B-2	0.43	129	14.4	0.115	1.3	2.8	2.2	0.121	1.9	2.8	2.2	0.117	2.7	1944	±37	1915	±49	-2
16WDS6D.405B-1	0.67	251	23.9	0.098	3.9	3.0	1.8	0.122	1.7	3.1	1.8	0.116	2.8	1827	±29	1898	±50	+4
16WDS1C.372B-1	0.17	199	9.0	0.05	3.5	3.0	1.9	0.117	1.2	3.0	1.9	0.115	1.4	1870	±30	1881	±26	+1
16WDS1C.372B-2	0.07	181	6.0	0.03	2.7	2.9	1.9	0.116	1.4	2.9	1.9	0.115	1.5	1923	±32	1882	±27	-3
Excluded analyses																		
WDS09N3.18B1	2.12	117	47.0	0.414	1.2	2.62	2.3	0.1379	1.8	2.67	2.3	0.1193	3.7	2050	±40	1946	±67	-6
WDS09N5.29B-1	1.45	131	8.0	0.064	3.8	3.06	2.6	0.1283	2.1	3.11	2.6	0.1156	3.3	1799	±42	1890	±60	+6
WDS09N3.21B-1	2.17	373	35.0	0.098	1.8	2.83	2.0	0.1386	0.7	2.90	2.0	0.1196	1.9	1912	±33	1950	±34	+2
WDS09N1.4B-1	0.53	97	8.0	0.082	1.1	2.57	1.6	0.1180	1.5	2.59	1.7	0.1134	2.3	2106	±30	1854	±42	-16
WDS09N1.3B-1	1.79	205	19.0	0.096	2.5	2.53	5.7	0.1401	1.4	2.58	5.7	0.1243	3.2	2113	±102	2019	±56	-5
WDS09RSB3.45B-2	3.08	178	73.0	0.425	4.2	2.28	3.9	0.1324	1.1	2.35	3.9	0.1057	3.8	2286	±75	1726	±70	-39
16WDS6D.401B-1	2.75	83	4.3	0.053	2.5	2.8	2.7	0.133	2.7	2.9	2.8	0.109	8.3	1937	±47	1779	±151	-10
16WDS6D.401B-2	2.15	47	5.9	0.129	2.3	2.3	5.9	0.124	3.7	2.3	6.0	0.105	10.1	2296	±116	1720	±185	-40

Table 5.4 ID-TIMS U-Pb data for baddeleyite from dyke WDS09

Notes **1)** All uncertainties given at 2σ **2)** ρ = error correlation coefficient of radiogenic $^{207}Pb/^{235}U$ vs. $^{206}Pb/^{238}U$ **3)** Pb_c = Total common Pb including analytical blank (0.8±0.3 pg per analysis) **4)** Blank composition is: $^{206}Pb/^{204}Pb = 18.55 \pm 0.63$, $^{207}Pb/^{204}Pb = 15.50 \pm 0.55$, $^{208}Pb/^{204}Pb = 38.07 \pm 1.56$ (all 2σ), and a $^{206}Pb/^{204}Pb$ – $^{207}Pb/^{204}Pb$ correlation of 0.9. **5)** Th/U calculated from radiogenic $^{208}Pb/^{206}Pb$ and age of 1.88 Ga **6)** Sample weights are calculated from crystal dimensions and are associated with as much as 50% uncertainty (estimated) **7)** Measured isotopic ratios corrected for tracer contribution and mass fractionation (0.02 ± 0.06 %/amu) **8)** Ratios involving ^{206}Pb are corrected for initial disequilibrium in $^{230}Th/^{238}U$ using Th/U = 4 in the crystallization environment

Sample	wt. (µg)	U (ppm	Pb_c (pg)	mol% Pb*	$\frac{Th}{U}$	$\frac{^{206}Pb}{^{204}Pb}$	$\frac{^{207}Pb}{^{206}Pb}$	± (%)	$\frac{^{207}Pb}{^{235}U}$	± (%)	$\frac{^{206}Pb}{^{238}U}$	± (%)	ρ	$^{206}Pb/^{238}U$ Age (Ma)	± (Ma)	$^{207}Pb/^{206}Pb$ Age (Ma)	± (Ma)
1	0.1	38	0.8	58	0.03	98	0.11340	7.20	4.6180	8.34	0.29534	1.23	.94	1668.1	20.5	1854.7	130.1
2	0.2	3	0.4	19	0.13	30	0.11478	7.36	5.2167	10.50	0.32962	6.28	.72	1836.5	115.4	1876.4	132.6
3	0.1	21	0.6	56	0.01	87	0.11311	3.78	5.2972	4.46	0.33966	1.05	.71	1885.0	19.7	1850.0	68.4
4	0.2	36	0.8	59	0.07	104	0.11710	7.75	5.5091	9.03	0.34120	1.36	.95	1892.4	25.8	1912.5	139.1

supports our interpretation of the analyses representing a single magmatic crystallization age. The weighted-mean $^{207}Pb/^{206}Pb$ dates of the four single-crystal analyses is 1863 ± 50 Ma (2σ, MSWD = 0.24, n = 4), and the concordia age of the three concordant analyses is 1888.4 ± 8.8 Ma (2σ, decay-constant errors included).

5.8 Geochemistry

Due to limited age control, only three samples were available for geochemical analyses and clearly only preliminary conclusions about the geochemical characteristics of the dykes can be made based on these data. Two samples from WDS09 and one sample from 16WDS02 (same dyke as 16WDS01) were analysed for major and trace elements and for Sr and Nd isotopes. Data for the samples are

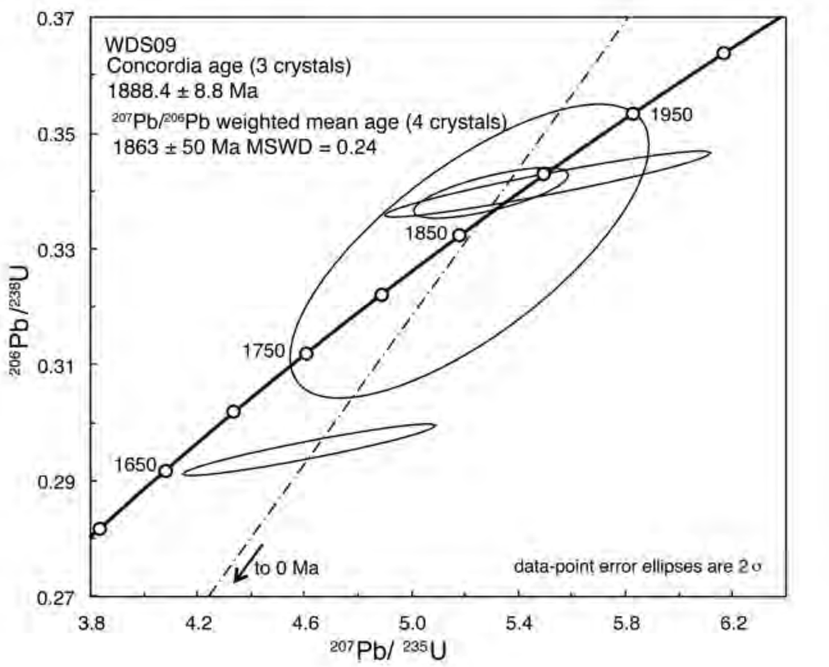

Figure 5.5 Concordia plot for analysed baddeleyite ID-TIMS U-Pb results from sample WDS09

presented together with major and trace element geochemistry from the 1210 Ma Marnda Moorn LIP dykes because the latter are the only known tholeiitic dyke swarm within the Yilgarn Craton with detailed studies available both in geochronology and geochemistry.

5.8.1 Major and trace elements

All samples have LOI <1.0 wt% and display low MgO (6.18-6.73 wt%), SiO_2 (50.12-50.43 wt%), relatively high iron (FeO_{tot} = 14.10-15.09 wt%), normal to intermediate CaO (10.71-11.28 wt%) and slightly high Al_2O_3 (13.37-13.87 wt%)(Table 5.5). The samples have low total alkalis (Na_2O+K_2O = 2.39-2.49 wt%) and high Na_2O/K_2O ratios (6.32-6.44), suggesting sodium enrichment. The

Boonadgin samples are classified as sub-alkaline basalts on the TAS diagram (Figure 5.6 A) and belong to tholeiitic series on the AFM diagram (Figure 5.6 B) similar to Group 1 of the Marnda Moorn dykes (Wang et al., 2014). The chondrite normalised rare earth element (REE) distribution patterns are relatively flat (Figure 5.6 C) with slight enrichment of light REE (LREE), as evidenced by La_N/Yb_N = 1.48 to 1.57 and La_N/Sm_N = 1.18 to 1.26. The low Tb_N/Yb_N ratios (1.16 to 1.18) are similar to the average N-MORB (1.0; Sun and McDonough, 1989) and the primitive mantle-normalised trace element patterns show strong enrichment of Cs, Rb, U and Pb and a prominent negative Nb anomaly (Figure 5.6 D). With the exception of these fluid-mobile elements and the negative Nb anomaly, the studied samples displayed a relative flat trace element distribution patterns without significant enrichment or depletion in specific elements.

5.8.2 Nd and Sr Isotopes

The same three samples were analysed for Nd and Sr isotopes (Table 5.5). Ratios of $^{147}Sm/^{144}Nd$ and $^{143}Nd/^{144}Nd$ are 0.1825–0.1848 and 0.512533–0.512562, respectively. The corresponding initial $\varepsilon Nd_{1.89Ga}$ values range from +1.3 to +1.6, suggesting a slightly depleted mantle component. The $^{87}Rb/^{86}Sr$ ratio ranges from 0.39999 to 0.5464, the $^{87}Sr/^{86}Sr$ ratio from 0.714588 to 0.716562, corresponding initial Sr isotopes of $(^{87}Sr/^{86}Sr)_i$ ratio varying from 0.70124 to 0.70391. The larger range of initial Sr isotope compositions is in contrast with the uniform initial Nd isotopes, and may reflect mobility of Rb. Therefore, the measured Sr isotope compositions of the studied samples may not accurately represent their primary signature.

Table 5.5 Major, trace element and isotope data for samples WDS09M, WDS09N and 16WDS02A

Notes **1)**Major elements (XRF) are given in wt % and trace elements (ICP-MS) in ppm **2)** Mg# = 100 x Mg/(Mg+Fe), Fe^{2+}/Fe_{total}=0.85
3) Crystallisation age t = 1890 Ma **4)** typical internal precision (2σ) is ±0.000015 for $^{87}Sr/^{86}Sr$ and ±0.000014 for $^{143}Nd/^{144}Nd$ **5)** Recent isotope dilution analyses for USGS basalt standard BCR-2 average 6.41 ppm Sm, 28.02 ppm Nd, $^{147}Sm/^{144}Nd$ 0.1381±0.0004 and $^{143}Nd/^{144}Nd$ 0.512635±0.000023 (n=6, ±2sd); 46.5 ppm Rb, 337.6 ppm Sr, $^{87}Rb/^{86}Sr$ 0.3982±0.0010, $^{87}Sr/^{86}Sr$ 0.704987±0.000015 (n=1, ±2se). These results are consistent with TIMS and MC-ICPMS reference values. e_{Nd} values are calculated relative to a modern chondritic mantle (CHUR) with $^{147}Sm/^{144}Nd$ = 0.1960 and $^{143}Nd/^{144}Nd$ = 0.512632 (Bouvier et al., 2008). Age-corrected initial e_{Nd} and $^{87}Sr/^{86}Sr$ have propagated uncertainties of ±0.5 units and ≤±0.00010 (assuming an age uncertainty of ±5 Ma), respectively. Decay constants are ^{87}Rb 1.395E^{-11}/yr and ^{147}Sm 6.54E^{-12}/yr.

	WDS09M	**WDS09M**	**16WDS02A**
SiO_2	49.68	50.42	49.91
TiO_2	1.14	1.31	1.25
Al_2O_3	13.75	13.42	13.26
CaO	10.65	10.71	11.19
Fe_2O_3(tot)	14.53	15.09	14.29
K_2O	0.32	0.34	0.32
MgO	6.67	6.18	6.59
MnO	0.23	0.24	0.23
Na_2O	2.05	2.15	2.06
P_2O_5	0.095	0.119	0.108
LOI	0.69	0.03	0.54
Total	99.81	100.01	99.75

	WDS09M	**WDS09N**	**16WDS02A**
Sm (ppm)	2.43	3.13	2.90
Nd (ppm)	7.93	10.37	9.54
$^{143}Nd/^{144}Nd$	0.512558	0.512533	0.512562
$^{147}Sm/^{144}Nd$	0.1848	0.1825	0.1837
$(^{143}Nd/^{144}Nd)_i$	0.510260	0.510263	0.510278
εNd(t)	1.3	1.3	1.6
Rb (ppm)	18.13	22.04	15.39
Sr (ppm)	102.10	116.80	111.40
$^{87}Rb/^{86}Sr$	0.514200	0.546400	0.399900
$^{87}Sr/^{86}Sr$	0.716562	0.715838	0.714588
$(^{87}Sr/^{86}Sr)_i$	0.702820	0.701240	0.703910

Table 5.5 *continued*

	WDS09M	WDS09M	16WDS02A
Mg#	51.22	48.36	51.33
Sc	45.80	46.80	47.80
V	302.00	310.00	315.00
Co	55.30	56.90	57.70
Ni	87.60	121.00	87.70
Ga	16.40	17.40	16.60
Ge	542.00	559.00	556.00
Rb	17.50	22.50	18.30
Sr	110.00	120.00	115.00
Y	22.60	28.40	26.70
Zr	59.00	80.50	72.40
Nb	3.11	4.07	3.67
Cs	0.56	1.02	0.19
Ba	53.90	59.40	56.80
La	4.92	6.04	5.42
Ce	11.90	15.00	13.10
Pr	1.75	2.20	2.00
Nd	8.35	10.50	9.61
Sm	2.53	3.18	2.96
Eu	0.96	1.12	1.05
Gd	3.27	4.09	3.80
Tb	0.58	0.73	0.68
Dy	3.79	4.73	4.45

	BCR-2	JND-1
$^{143}Nd/^{144}Nd$	0.512637	0.512112
	0.512640	0.512117
	0.512623	0.512102
	0.512633	
$^{87}Sr/^{86}Sr$	0.704987	
	0.705013	

Table 5.5 *continued*

	WDS09M	WDS09M	16WDS02A
Ho	0.83	1.05	0.98
Er	2.37	2.94	2.77
Tm	0.35	0.45	0.42
Yb	2.25	2.85	2.62
Lu	0.34	0.42	0.39
Hf	1.63	2.19	2.00
Ta	0.21	0.28	0.25
Pb	2.99	3.62	1.75
Th	0.83	1.05	0.91
U	0.30	0.38	0.30

5.9 Discussion

We have identified a previously unrecognized NNW-trending swarm of mafic dykes in the Yilgarn Craton, which, based on preliminary aeromagnetic interpretation, covers an area of ca. 33 000 km^2 in the southwestern part of the craton. However, until further sampling within the craton allows better delineation of the extent of the dykes, their designation as a swarm is preliminary. Emplacement of the Boonadgin dykes was synchronous with many 1890-1880 Ma LIPs worldwide, such as the Bastar-Cuddapah dykes in India (French et al., 2008; Belica et al., 2014), the Circum-Superior magmatism of the Superior Craton (Heaman et al., 1986; Halls and Heaman, 2000; Ernst and Bell, 2010), the Ghost-Mara dyke swarm of the Slave Craton (Buchan et al., 2010), the Uatuma dyke swarm of the Amazonian Craton (Klein et al., 2012; Antonio et al., 2017) and the Mashonaland sill province of the Zimbabwe Craton (Söderlund et al., 2010), the Soutpansperg sill province (Hanson et al., 2004) and the Black Hills dyke swarm (Olsson et al., 2016) of the Kaapvaal

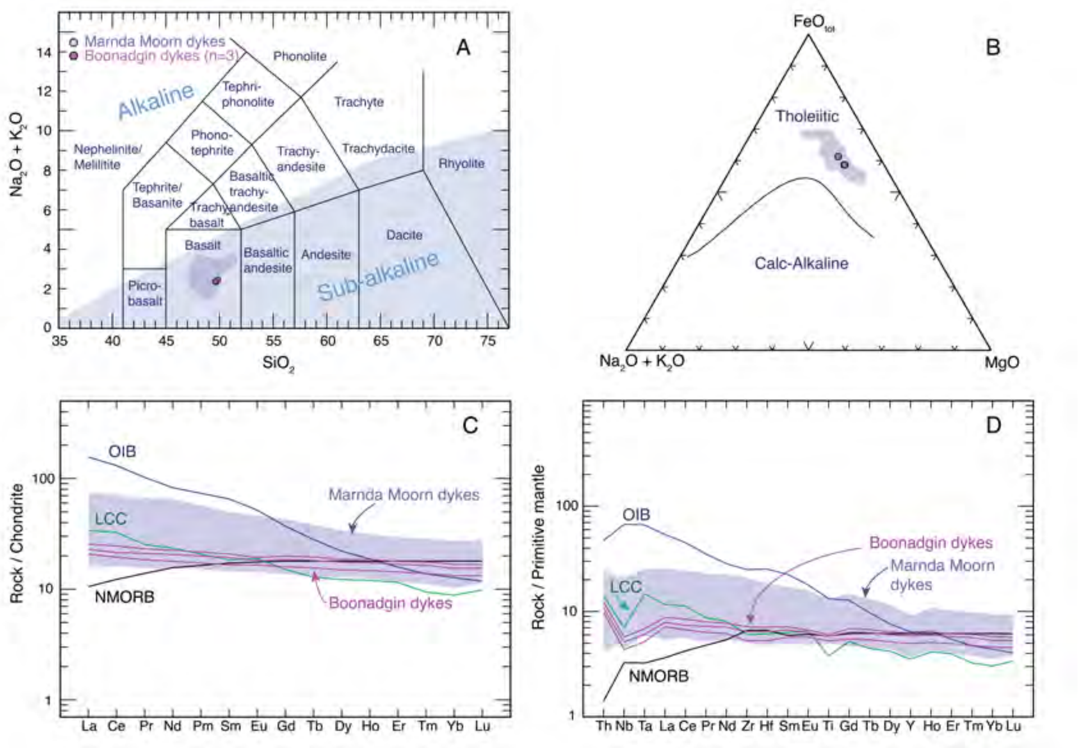

*Figure 5.6 (**A**) Total alkali-silica (TAS) plot after LeMaitre, 1989. Blue dots are Marnda Moorn group 1 dykes from Wang et al., 2014. (**B**) AFM plot after Irvine and Baragar, 1971. (**C**) Chondrite and (**D**) primitive mantle normalised multi- element lots for Boonadgin and Marnda Moorn group 1 dykes (Wang et al., 2014). LCC = lower continental crust after Rudnick and Gao, 2004; OIB = ocean island basalt and NMORB = mid ocean ridge basalt after Sun and McDonough, 1989.*

Craton. In the following sections, we discuss the emplacement of the dykes within the regional tectonic setting, coeval magmatism elsewhere in the region, and the implications for a recently proposed tectonic reconstruction, which raises the possibility that the dykes may be associated with the Bastar-Cuddapah LIP in India.

5.9.1 Coeval magmatism in Australia

No other mafic magmatism within uncertainty of the 1888 ± 9 Ma age for the Boonadgin dyke swarm is currently known in the WAC or elsewhere in Australia. However, felsic tuffs from a succession of granular iron formation (GIF) in the Frere Formation in the Earaheedy Basin have been dated at 1891 ± 8 Ma and 1885 ± 18 Ma, and linked to voluminous mantle input from an oceanic mafic source during a major global episode of mantle upwelling and crustal growth (Rasmussen et al., 2012). Evidence of synchronous magmatism elsewhere in the Capricorn Orogen is limited to a 1900 Ma zircon population peak from the Chiall Formation in the upper sequence of the Earaheedy Basin (Halilovic et al., 2004).

Ameen and Wilde (2006) reported WSW-trending mafic dykes with a zircon SHRIMP U-Pb age of 1852 ± 12 Ma from the Yalgoo greenstone belt in the Youanmi Terrane in the northwestern Yilgarn Craton (Figure 5.1), ca. 360 km NNE of Perth and ca. 350 km north of sample 16WDS06. Their emplacement suggests a further episode of lithospheric extension ca. 35 Ma after the Boonadgin dykes. The WSW orientation of the Yalgoo dykes may reflect a change in the regional stress field, the influence of local crustal architecture, or a change in the position of plume centre. There is limited, but suggestive, evidence of magmatism within the Capricorn Orogen coeval with the Yalgoo dykes. The age of the Yalgoo dykes is within uncertainty of an 1842 ± 5 Ma detrital zircon population from the Leake Spring Metamorphics, a predominantly siliciclastic sequence within the northern Gascoyne Province (Sheppard et al., 2010b) and a ca. 1860 Ma detrital zircon population from turbidites in the Ashburton Basin (Sircombe, 2002).

The temporally closest mafic magmatism in the North Australian Craton (NAC) consist of the predominantly mafic volcanic rocks of the Biscay Formation in the Halls Creek Orogen in northwestern Australia, which yielded a U-Pb zircon age of 1880 ± 3 Ma (Blake et al., 1999). The Woodward Dolerite, which comprises sills intruding the succession, has maximum and minimum ages, respectively, of ca. 1847 Ma and 1808 Ma (Blake et al., 1997) and its emplacement age is thus closer to the Yalgoo dykes. However, the Halls Creek bimodal volcanism has been associated with convergence of two cratons unrelated to the West Australian Craton, and pre-dates amalgamation of the West Australian Craton with other cratons (Bagas, 2004; Cawood and Korsch, 2008).

5.9.2 Tectonic and magmatic events in the WAC at ca. 1890 Ma

The Boonadgin dyke swarm was emplaced into the western margin of the WAC, about 60 million years after the WAC was assembled along the Capricorn Orogen during the Glenburgh Orogeny at 2005-1950 Ma (Sheppard et al., 2004, 2010a; Johnson et al., 2011). Following amalgamation of the WAC, the Capricorn Orogen was the site of episodic intracontinental reworking and reactivation for more than one billion years (Cawood and Tyler, 2004; Sheppard et al., 2010a; Johnson et al., 2011). At the time the Boonadgin dykes were emplaced, the WAC was under a period of tectonic quiescence. The ca. 1891-1885 Ma felsic volcanic rocks in the Earaheedy Basin (Rasmussen et al., 2012) were emplaced during limited rifting and suggest that at least the eastern part of the Capricorn Orogen underwent lithospheric extension at this time (Sheppard et al., 2016).

Emplacement of the NW-trending Boonadgin dykes indicates regional SW-NE oriented lithospheric extension, which is consistent with direction of coeval extension within the NW-trending Earaheedy basin. In aeromagnetic images the dykes are linear, appear to have a single magnetic polarity and extend across the southwestern craton before being apparently truncated by the Darling Fault in the west and by the Albany-Fraser Orogen in the south. The orientation of the dykes is roughly parallel to the regional NW-SE tectonic grain imparted by terrane accretion during the Archean (Middleton et al., 1993; Wilde et al., 1996; Dentith and Featherstone, 2003) and suggests that they intruded along existing crustal weaknesses controlled by a regional stress field (Hou et al., 2010; Hou, 2012; Ju et al., 2013). A seismic survey south of sample WDS09 identified a ca. 20° NE-dipping high-velocity zone, which was interpreted to represent a mafic-ultramafic body in the lower crust at ca. 30 km depth; this may be either a possible conduit for mafic magma that intruded along the suture, a zone of intrusions, or a fault-bounded terrane of possible oceanic affinity (Dentith et al., 2000; Dentith and Featherstone, 2003).

No direct Paleoproterozoic record along the western margin of Yilgarn Craton has been preserved due to younger orogenic and rifting events and it is uncertain whether it was an active plate boundary when the Boonadgin dykes were emplaced. Along the southern margin of the craton, the only known event coeval with emplacement of the Boonadgin dyke swarm could be deposition of the Stirling Range Formation in the Paleoproterozoic Barren Basin in the western Albany-Fraser Orogen. The Barren Basin comprises structural remnants of a much larger basin system deposited in an intra-continental rift or back-arc setting (Clark et al., 2000; Spaggiari et al., 2011, 2014b, 2015). Formation age of the basin is unclear, but detrital zircon and monazite dating suggests that it is younger than ca. 2016 Ma and possibly formed at ca. 1895 Ma (Rasmussen and Fletcher, 2002; Rasmussen et al., 2004). Given the uncertainty of timing of early rifting in the southwest, it is difficult to link emplacement of the Boonadgin dykes with any tectonic events adjacent to the southwestern part of the craton.

5.9.3 Source of the Boonadgin dykes

Ratios of incompatible trace elements sensitive to source composition and partial melting effects but insensitive to crystal fractionation can be used to investigate mantle source characteristics. Zirconium can be used to evaluate mobility of major and trace elements during alteration and metamorphism (e.g. Polat et al., 2002). The Nb, Ta, Hf, Th and REE concentrations in the samples show good correlation with Zr (not shown) suggesting that these elements represent the primary composition of the dykes. The primitive mantle-normalised profile of the Boonadgin dykes (Figure 5.6 D, Table 5.5) is remarkably similar to that of the lower continental crust (LCC; Rudnick and Gao, 2004) with average ratios of Nb/La = 0.66, Th/Nb = 0.26 and Ce/Pb = 5.20 (0.63, 0.24 and 5.0, respectively for LCC). Ratios of La/Sm = 1.89 and Sm/Nd = 0.30 are near-chondritic (1.55 and 0.33, respectively; Sun and McDonough, 1989) and close to the Marnda Moorn Group 1 dykes (ca. 1.70 and 0.28, respectively). The ratio of Nb/Ta = 14.75 is much higher than the lower crust (8.33) but close to that of depleted mantle (ca. 15; Salters and Stracke, 2004) and Marnda

Moorn Group 1 dykes (ca. 15; Wang et al., 2014). The ratio of Zr/Sm = 24.36 is similar to the lower crust (ca. 24) and much lower than depleted mantle (ca. 29).

The similarity of the trace element compositions of the studied samples to the average value of lower continental crust suggests the possibility of lower continental crust contamination. We conducted preliminary binary mixing modelling (Donald J. DePaolo, 1981) using data from the three Boonadgin dykes samples. If the primary melt had a N-MORB-like trace element composition and $\varepsilon Nd_{1.9Ga}$ = +8, incorporating 20-30% of mafic lower continental crust ($\varepsilon Nd_{1.9Ga}$ = -10, estimated by Nd isotope mapping of the Yilgarn (D C Champion, 2013) and the method proposed by DePaolo (1987)) into the primary melt can produce the observed Nd isotope and trace element compositions. The lack of prominent fractionation of HREE indicates that partial melting likely occurred within the spinel stability field (at <70 km depth). If this is correct, the sub-continental lithospheric mantle (SCLM) beneath the margin of the Yilgarn Craton may have been largely removed or thinned. This could be attributed to lithospheric extension, consistent with basin formation along the southern margin of the craton (section 5.9.2).

Another possible mechanism to produce the observed trace element compositions and slightly depleted Nd isotope signature is via melt-rock interaction with asthenospheric mantle. Because lower continental crust can founder into the convecting mantle (e.g. Gao et al., 2004), melts derived from recycled lower continental crust could interact with the ambient peridotite to form enriched pyroxenitic lithologies (Sobolev et al., 2005, 2007; Wang et al., 2014), imparting a lower continental crust signature and a slightly depleted Nd isotope signature on the resultant melts.

5.9.4 Was the WAC connected to other cratons at ca. 1890 Ma?

The position of WAC in Paleoproterozoic reconstruction models is highly debated partly due to the absence of robust paleomagnetic and high precision geochronological data for dyke swarms. For example, the WAC has been placed near India (Rogers and Santosh, 2002; Zhao et al., 2002; Mohanty, 2012, 2015), Kaapvaal and Zimbabwe Cratons (Zhao et al., 2002; Hou et al., 2008; Belica et al., 2014), or Siberia (Hou et al., 2008; Belica et al., 2014) in reconstructions for various

Paleoproterozoic time intervals. Halls et al. (2007) used paleomagnetic data to argue that India and Australia were at high paleolatitudes but ~2000 km apart at ca. 2400-2350 Ma. Similarly, Mohanty (2012, 2015) proposed a juxtaposition of the western margin of the WAC and the eastern margin of the Bastar-Dharwar craton at ca. 2400-2300 Ma (the South India-Western Australia SIWA supercraton; Figure 5.7) based on paleomagnetic data, synchronous mafic magmatism and matching dyke orientation but their relative positions by ca. 1900 Ma were unknown. Mohanty (2012, 2015) nonetheless noted that the lack of 2.0-1.8 Ga dykes in the Yilgarn Craton implies that the breakup of SIWA must have taken place during an earlier rifting event. Our discovery of the 1888 Ma Boonadgin dykes in the Yilgarn Craton makes such an early breakup unnecessary. With such a configuration at 1890 Ma, NE-SW extension and emplacement of the NW-oriented 1888 Ma Boonadgin dykes in the Yilgarn Craton is synchronous with E-W extension initiating the Cuddapah Basin and the associated 1890 Ma NW-oriented mafic dykes and ultramafic magmatism in the Dharwar Craton (Anand, 2003; French et al., 2008), as well as the emplacement of NW-oriented dykes in the Bastar Craton (French et al., 2008) as segments of a single radiating dyke swarm.

Liu et al. (2018) obtained a high quality paleomagnetic pole from the Boonadgin dykes and used available robust paleomagnetic data to test the SIWA connection and other possible configurations. The new Boonadgin dyke pole falls close to the Frere Formation (Capricorn Orogen) pole of Williams et al. (2004), which has been considered to be 1891-1885 Ma in age (e.g. Antonio et al., 2017; Klein et al., 2016) based on zircon data from tuffs within the basal Frere Formation (Rasmussen et al., 2012). However, Williams et al. (2004) sampled the upper part of the formation, implying that the actual magnetization age for their Frere Formation pole is likely younger than 1885 Ma. Consequently, Liu et al. (this volume) suggest that the ca. 1890 Ma Boonadgin pole is coeval with the 1888-1882 Ma Dharwar-Bastar pole (Belica et al., 2014) and that the age difference between the Boonadgin and the <1885 Ma Frere Formation poles may explain the slight difference in their positions. The Boonadgin and Dharwar-Bastar dyke poles are about 50° apart after restoration of the two continental blocks to the SIWA configuration (Figure 5.7 A), indicating that the SIWA fit is invalid at ca. 1890 Ma. In contrast, an alternative configuration juxtaposing the northern WAC (Pilbara) and north-eastern India (Singhbhum) is not only consistent with paleomagnetic data (Figure 5.7 B), but still allows the contemporaneous mafic dykes in India and the WAC to form a radiating dyke swarm. If this interpretation is correct, the 1888 Ma Boonadgin dykes in the Yilgarn Craton may be part of the Bastar-Cuddapah LIP event (French et al., 2008; Belica et al., 2014).

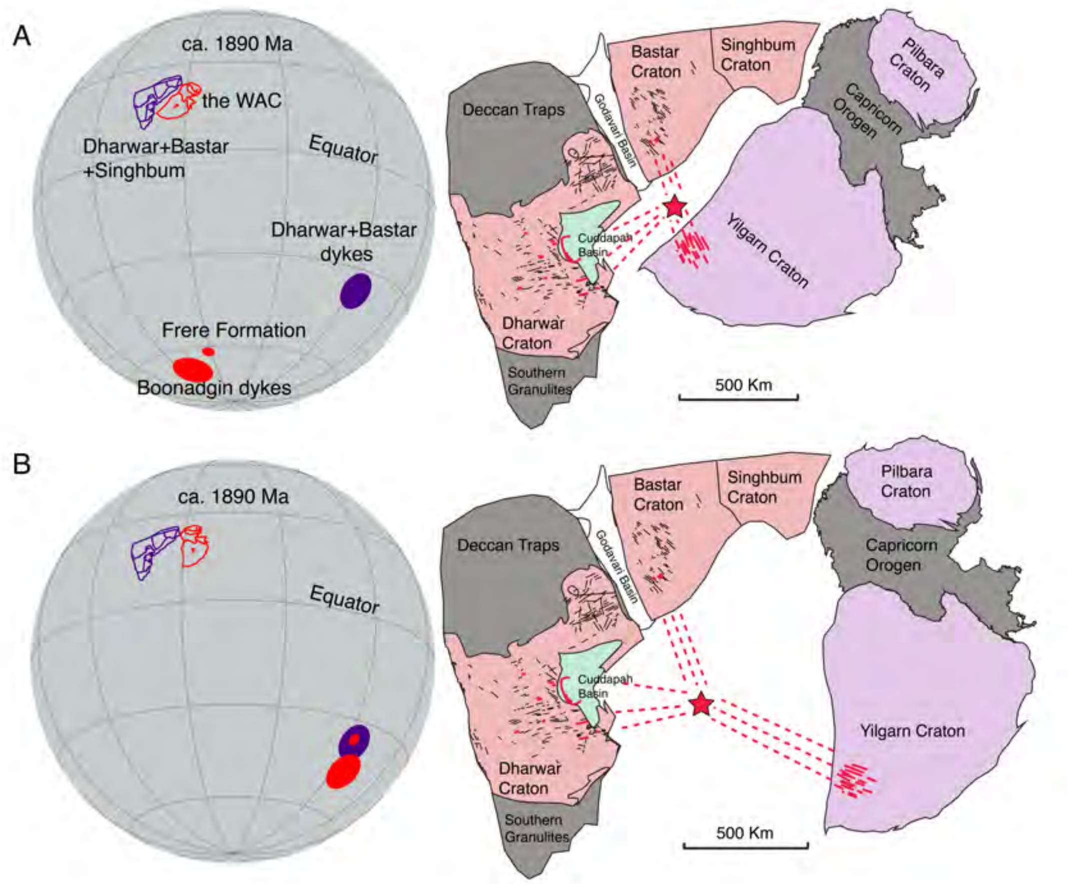

Figure 5.7 Possible configurations of the WAC and Dharwar, Bastar and Singhbum cratons tested with paleomagnetic data at ca. 1890 Ma. Coeval paleopoles are plotted on the left-hand side and color coded with the respective cratons. The WAC was rotated to the Indian coordinates and more detailed reconstructions are shown on the right side. Indian dykes shown in red have been dated with U-Pb or Ar-Ar methods at 1879-1894 Ma (Chatterjee and Bhattacharji, 2001; Halls et al., 2007; French et al., 2008; Belica et al., 2014). Black undated dykes in India are modified after French et al. (2008) and Srivastava et al. (2015). Red star denotes possible location of a mantle plume. ***(A)*** *SIWA configuration modified from ca. 2400 Ma reconstruction of Mohanty (2012);* ***(B)*** *Alternative onfiguration of Liu et al. (2018) supported by paleomagnetic data.*

5.9.5 Could the Boonadgin dyke swarm be part of the Bastar-Cuddapah LIP?

Abundant, predominantly NW-SE to NNW-ESE oriented 1890-1880 Ma Bastar-Cuddapah LIP dykes intrude the Bastar and Dharwar cratons and form a radiating dyke swarm over at least 90,000 km^2 (Anand, 2003; Halls et al., 2007; French et al., 2008; Belica et al., 2014). In the southern Bastar Craton, BD2 dykes are oriented predominantly NW-SE to WNW-ESE (French et al., 2008). In the Dharwar craton, baddeleyite from the Pulivendla sill in the Cuddapah basin yielded an ID-TIMS $^{207}Pb/^{206}Pb$ age of 1885 ± 3 Ma (French et al., 2008) and paleomagnetic data suggest that dykes of this age also have NW-SE, E-W and NE-SW orientations depending on their location within the craton (Halls et al., 2007; Belica et al., 2014). The NW-trending dykes appear to be sub-parallel to the regional Archean structural grain in both the Bastar and Dharwar cratons, suggesting that they may have intruded along pre-existing faults and fabrics (Crookshank, 1963; Chatterjee and Bhattacharji, 2001). New SHRIMP U-Pb dating of felsic tuffs from the lowermost succession of the Cuddapah Basin, the Tadpatri Formation, yielded ca. 1864 Ma and ca. 1858 Ma, and mafic-ultramafic sills intruding this stratigraphic level (and higher) indicate that mafic magmatism continued until after ca. 1860 Ma (Sheppard et al., 2017).. Dykes of <1900 Ma age are present in both Bastar and Dharwar Cratons but their ages are currently either poorly constrained or unknown (Murthy, 1987; Mallikharjuna et al., 1995; Meert et al., 2010), making any comparison highly speculative.

Extensive coeval mafic magmatism and intracontinental rifting in the Dharwar Craton at ca. 1899-1885 Ma have been linked to a mantle plume beneath India or east of the Cuddapah Basin (Ernst and Srivastava, 2008; Belica et al., 2014; Mishra, 2015), or to passive rifting associated with a short lived global mantle upwelling (Anand, 2003; French et al., 2008). Two models have been proposed for formation of the Cuddapah Basin, one arguing for failed rifting (Chaudhuri et al., 2002) and another for full rifting and opening of an ocean basin (Kumar and Leelanandam, 2008; Kumar et al., 2010). Dasgupta et al. (2013) proposed that formation of the Cuddapah Basin at ca. 1890 Ma was associated with continental rifting between India and another craton. If this was the WAC, no evidence of equivalent basins is preserved on the western or southern margin of the Yilgarn Craton.

In contrast to the Boonadgin dykes, the Cuddapah sills are more enriched and contain a more significant melt component from the Archean lithosphere, with La_N/Sm_N ratios between 1.4 and 2.5, La_N/Yb_N ratios between 2.4 and 4.3 (1.18-1.26 and 1.48-1.57 for Boonadgin dykes, respectively) and $\varepsilon Nd_{1.89Ga}$ values between +1 and -10 (+1.3 to +1.6 for Boonadgin dykes) (Anand, 2003). Modelling of the Cuddapah sills suggests that they were produced by 15-20% partial melting of a lherzolitic mantle with a potential temperature of ~1500°C, similar to ambient mantle of similar age and not necessarily indicative of a mantle plume (Anand, 2003). Current geochemical evidence is insufficient to determine whether the Boonadgin dykes and the Bastar-Cuddapah LIP are associated with the same mantle source.

Similar to the Yilgarn Craton where the Boonadgin and Yalgoo dykes are interpreted to be associated with discrete episodes of lithospheric extension, sills intruding the unconformity-bound sedimentary successions within the Cuddapah basin are coeval with episodes of lithospheric extension (Sheppard et al., 2017) In both cases, mafic magmatism appears to span 35-40 Ma (ca. 1890 to 1855 Ma) rather than comprising a very short-lived event.

5.10 Conclusions

The Archean Yilgarn Craton in Western Australia is intruded by multiple generations of Precambrian mafic dykes, identified by previous studies. Until now, evidence for mafic magmatism in the Yilgarn Craton at ca. 1890 Ma has been absent, surprising since mafic magmatism of this age is found on most other Precambrian cratons worldwide. The newly named, NW-trending 1888 Ma Boonadgin dyke swarm is interpreted to extend across an area of at least 33 000 km^2 in the southwestern Yilgarn Craton. The dykes were emplaced along the southwestern margin of the Yilgarn Craton more than 50 million years after it was amalgamated with the Pilbara Craton-Glenburgh Terrane along the Capricorn Orogen to form the West Australian Craton. Intrusion of the Boonadgin dyke swarm was synchronous with minor rifting, felsic volcanism and deposition of granular iron formation in the Earaheedy Basin at the southeastern end of the Capricorn Orogen. Evidence for another pulse of mafic magmatism at ca. 1852 Ma in the northern Yilgarn Craton was also coeval with magmatism in the Capricorn Orogen, suggesting that mafic magmatism spanned at least 35 million years. Emplacement of the Boonadgin dyke swarm is contemporaneous with the Bastar-Cuddapah LIP and opening of the Cuddapah Basin on the eastern margin of India, and the ca. 1852 Ma Yalgoo dykes in northern Yilgarn may be coeval with ca. 1860 mafic magmatism in the Cuddapah basin. Moreover, existing studies and recent paleomagnetic data suggest that the Yilgarn and Bastar-Cuddapah cratons were adjacent to each other at c. 1890 Ma, raising the possibility that the Boonadgin dyke swarm may be part of a wider Bastar-Cuddapah LIP. However, Meso- to Neoproterozoic orogenic activity and Phanerozoic rifting along the western margin in the Yilgarn Craton have obliterated stratigraphic successions equivalent to the Cuddapah Basin, and poor age control of extension and initial rifting in southern Yilgarn Craton do not provide reliable geological piercing points. In contrast to proposed rifting of the Yilgarn Craton from India at ca. 2300 Ma, new evidence presented in this paper suggests that the cratons may still have been neighbours at 1890 Ma.

5.11 Acknowledgments

This work was funded by ARC Centre for Core to Crust Fluid Systems CoE Grant (CE110001017) and ARC Laureate Fellowship Grant (FL150100133) to Z.-X.L. JCS was supported by Curtin University ORD Postgraduate Scholarship. We thank Cristina Talavera and Hao Gao for their invaluable support with SHRIMP U-Pb analyses at John de Laeter Centre, Curtin University. We also thank Roland Maas and Nenping Shen for their valuable assistance with geochemical analyses and Louise Heyworth for her help with sample preparation at UWA.

5.12 References

Ameen, S.M.M., Wilde, S.A., 2006. Identification of 1.85 Ga mafic dykes in the Northern Yilgarn Craton: a relationship to the Columbia supercontinent? IAGR Annu. Conv. Int. Symp. Hong Kong, 2006.

Anand, M., 2003. Early Proterozoic Melt Generation Processes beneath the Intra-cratonic Cuddapah Basin, Southern India. J. Petrol. 44, 2139–2171. doi:10.1093/petrology/egg073

Anand, R.R., Paine, M., 2002. Regolith geology of the Yilgarn Craton, Western Australia: implications for exploration. Aust. J. Earth Sci. 49, 3–162.

Antonio, P.Y.J., D'Agrella-Filho, M.S., Trindade, R.I.F., Nédélec, A., de Oliveira, D.C., da Silva, F.F., Roverato, M., Lana, C., 2017. Turmoil before the boring billion: Paleomagnetism of the 1880–1860Ma Uatumã event in the Amazonian craton. Gondwana Res. 49, 106–129.

Bagas, L., 2004. Proterozoic evolution and tectonic setting of the northwest Paterson Orogen, Western Australia. Precambrian Res. 128, 475–496. doi:10.1016/j.precamres.2003.09.011

Belica, M.E., Piispa, E.J., Meert, J.G., Pesonen, L.J., Plado, J., Pandit, M.K., Kamenov, G.D., Celestino, M., 2014. Paleoproterozoic mafic dyke swarms from the Dharwar craton; paleomagnetic poles for India from 2.37 to 1.88Ga and rethinking the Columbia supercontinent. Precambrian Res. 244, 100–122. doi:10.1016/j.precamres.2013.12.005

Blake, D.H., Tyler, I.M., Griffin, T.J., Sheppard, S., Thorne, A.M., Warren, R.G., 1999. Geology of the Halls Creek 1: 100 000 Sheet area (4461), Western Australia. Aust. Geol. Surv. Organ. Canberra.

Blake, D.H., Tyler, I.M., Sheppard, S., 1997. Geology of the Ruby Plains 1: 100 000 sheet area (4460), Western Australia. Australian Geological Survey Organisation.

Bleeker, W., Ernst, R., 2006. Short-lived mantle generated magmatic events and their dyke swarms: the key unlocking Earth's paleogeographic record back to 2.6 Ga, in: Hanski, E.J., Mertanen, S., Rämö, O.T., Vuollo, J. (Eds.), Dyke Swarms—time Markers of Crustal Evolution: Selected Papers of the Fifth International Dyke Conference in Finland, Rovaniemi, Finland, 31 July- 3 Aug 2005 & Fourth International Dyke Conference, Kwazulu-Natal, South Africa 26-29 June 2001. CRC Press, London, pp. 3–26.

Boyd, D.M., Tucker, D.H., 1990. Australian magnetic dykes, in: Parker, A.J., Rickwood, P.C., Tucker, D.H. (Eds.), Mafic Dykes and Emplacement Mechanisms. A.A.Balkema, Rotterdam, pp. 391–399.

Buchan, K.L., Ernst, R.E., Bleeker, W., Davies, W., Villeneuve, M., van Breemen, O., Hamilton, M., Söderlund, U., 2010. Proterozoic magmatic events of the Slave craton, Wopmay orogen and environs, in: Geological Survey of Canada, Open File 5985. Geological Survey of Canada.

Buchan, K.L., Ernst, R.E., Hamilton, M.A., Mertanen, S., Pesonen, L.J., Elming, S.-Å., 2001. Rodinia: the evidence from integrated palaeomagnetism and U–Pb geochronology. Precambrian Res. 110, 9–32.

Campbell, I.H., McCall, G.J.H., Tyrwhitt, D.S., 1970. The Jimberlana Norite, Western Australia–a smaller analogue of the Great Dyke of Rhodesia. Geol. Mag. 107, 1–12.

Cassidy, K.F., Champion, D.C., Huston, D.L., 2005. Crustal evolution constraints on the metallogeny of the Yilgarn Craton, in: Mineral Deposit Research: Meeting the Global Challenge. Springer, pp. 901–904.

Cassidy, K.F., Champion, D.C., Krapez, B., Barley, M.E., Brown, S.J.A., Blewett, R.S., Groenewald, Pb., Tyler, I.M., 2006. A revised geological framework for the Yilgarn Craton, Western Australia, in: Geological Survey of Western Australia Record 8/2006. Geological Survey of Western Australia.

Cawood, P.A., Korsch, R.J., 2008. Assembling Australia: Proterozoic building of a continent. Precambrian Res. 166, 1–35. doi:10.1016/j.precamres.2008.08.006

Cawood, P.A., Tyler, I.M., 2004a. Assembling and reactivating the Proterozoic Capricorn Orogen: lithotectonic elements, orogenies, and significance. Precambrian Res. 128, 201–218. doi:10.1016/j.precamres.2003.09.001

Cawood, P.A., Tyler, I.M., 2004b. Assembling and reactivating the Proterozoic Capricorn Orogen: lithotectonic elements, orogenies, and significance. Precambrian Res. 128, 201–218.

Champion, D.C., 2013. Neodymium depleted mantle model age map of Australia: explanatory notes and user guide. Geosci. Aust. Rec. 2013/44, 209. doi:10.11636/Record.2013.044

Chatterjee, N., Bhattacharji, S., 2001. Petrology, geochemistry and tectonic settings of the mafic dikes and sills associated with the evolution of the Proterozoic Cuddapah Basin of south India. J. Earth Syst. Sci. 110, 433–453.

Chaudhuri, A.K., Saha, D., Deb, G.K., Deb, S.P., Mukherjee, M.K., Ghosh, G., 2002. The Purana basins of southern cratonic province of India-a case for Mesoproterozoic fossil rifts. Gondwana Res. 5, 23–33.

Claoué-Long, J.C., Hoatson, D.M., 2009. Guide to using the map of Australian Proterozoic large igneous provinces. Geoscience Australia.

Clark, D.J., Hensen, B.J., Kinny, P.D., 2000. Geochronological constraints for a two-stage history of the Albany – Fraser Orogen , Western Australia. Precambrian Res. 102, 155–183.

Coffin, M.F., Eldholm, O., 1994. Large igneous provinces: crustal structure, dimensions, and external consequences. Rev. Geophys. 32, 1–36. doi:10.1029/93RG02508

Compston, W., Williams, I.S., Meyer, C., 1984. U-Pb geochronology of zircons from lunar breccia 73217 using a sensitive high mass-resolution ion microprobe. J. Geophys. Res. 89, B525. doi:10.1029/JB089iS02p0B525

Condie, K.C., 2004. Supercontinents and superplume events: distinguishing signals in the geologic record. Phys. Earth Planet. Inter. 146, 319–332. doi:10.1016/j.pepi.2003.04.002

Crookshank, H., 1963. Geology of southern Bastar and Jeypore from the Bailadila range to the Eastern Ghats, 87th ed.

Dasgupta, S., Bose, S., Das, K., 2013. Tectonic evolution of the Eastern Ghats Belt, India. Precambrian Res. 227, 247–258. doi:10.1016/j.precamres.2012.04.005

Dentith, M.C., Dent, V.F., Drummond, B.J., 2000. Deep crustal structure in the southwestern Yilgarn Craton , Western Australia. Tectonophysics 325, 227–255.

Dentith, M.C., Featherstone, W.E., 2003. Controls on intra-plate seismicity in southwestern Australia. Tectonophysics 376, 167–184. doi:10.1016/j.tecto.2003.10.002

Depaolo, D.J., 1981. Trace element and isotopic effects of combined wallrock assimilation and fractional crystallization. Earth Planet. Sci. Lett. 53, 189–202.

Doehler, J.S., Heaman, L.M., 1998. 2.41 Ga U–Pb Baddeleyite ages for two gabbroic dykes from the Widgiemooltha swarm, Western Australia: a Yilgarn–Lewisian connection, in: Geological Society of America 1998 Annual Meeting, Abstracts with Programs, pp. 291–292.

Eggins, S.M., Woodhead, J.D., Kinsley, L.P.J., Mortimer, G.E., Sylvester, P., McCulloch, M.T., Hergt, J.M., Handler, M.R., 1997. A simple method for the precise determination of≥ 40 trace elements in geological samples by ICPMS using enriched isotope internal standardisation. Chem. Geol. 134, 311–326.

Ernst, R., Bleeker, W., 2010. Large igneous provinces (LIPs), giant dyke swarms, and mantle plumes: significance for breakup events within Canada and adjacent regions from 2.5 Ga to the Present. Can. J. Earth Sci. 47, 695–739. doi:10.1139/e10-025

Ernst, R., Srivastava, R., Bleeker, W., Hamilton, M., 2010. Precambrian Large Igneous Provinces (LIPs) and their dyke swarms: New insights from high-precision geochronology integrated with paleomagnetism and geochemistry. Precambrian Res. 183, vii–xi.

Ernst, R.E., Bell, K., 2010. Large igneous provinces (LIPs) and carbonatites. Mineral. Petrol. 98, 55–76.

Ernst, R.E., Bleeker, W., Söderlund, U., Kerr, A.C., 2013. Large Igneous Provinces and supercontinents: Toward completing the plate tectonic revolution. Lithos 174, 1–14.

Ernst, R.E., Buchan, K.L., 1997. Giant radiating dyke swarms: their use in identifying pre-Mesozoic large igneous provinces and mantle plumes, in: Large Igneous Provinces: Continental, Oceanic, and Planetary Flood Volcanism. American Geophysical Union Monograph 100, pp. 297–333.

Ernst, R.E., Head, J.W., Parfitt, E., Grosfils, E., Wilson, L., 1995. Giant radiating dyke swarms on Earth and Venus. Earth-Science Rev. 39, 1–58.

Ernst, R.E., Srivastava, R.K., 2008. India's place in the Proterozoic world: constraints from the Large Igneous Province (LIP) record. Indian dykes. Ed. by RK Srivastava, Ch. Sivaji, NV Chalapathi Rao. Geochemistry, Geophys. Geochronology, Narosa Publ. House Pvt. Ltd, New Delhi, India 41–56.

Ernst, R.E., Wingate, M.T.D., Buchan, K.L., Li, Z.X., 2008. Global record of 1600–700Ma Large Igneous Provinces (LIPs): Implications for the reconstruction of the proposed Nuna (Columbia) and Rodinia supercontinents. Precambrian Res. 160, 159–178. doi:10.1016/j.precamres.2007.04.019

Evans, M.E., 1968. Magnetization of dikes: a study of the paleomagnetism of the Widgiemooltha dike suite, Western Australia. J. Geophys. Res. 73, 3261–3270.

Evans, T., 1999. Extent and nature of the 1.2 Ga Wheatbelt dyke swarm, Yilgarn Craton, Western Australia. B.Sc. thesis, Univ. West. Aust. Perth.

French, J.E., Heaman, L.M., 2010. Precise U-Pb dating of Paleoproterozoic mafic dyke swarms of the Dharwar craton, India: Implications for the existence of the

Neoarchean supercraton Sclavia. Precambrian Res. 183, 416–441. doi:10.1016/j.precamres.2010.05.003

French, J.E., Heaman, L.M., Chacko, T., 2002. Feasibility of chemical U-Th-total Pb baddeleyite dating by electron microprobe. Chem. Geol. 188, 85–104. doi:10.1016/S0009-2541(02)00074-8

French, J.E., Heaman, L.M., Chacko, T., Srivastava, R.K., 2008. 1891-1883 Ma Southern Bastar-Cuddapah mafic igneous events, India: A newly recognized large igneous province. Precambrian Res. 160, 308–322. doi:10.1016/j.precamres.2007.08.005

Gao, S., Rudnick, R.L., Yuan, H.-L., Liu, X.-M., Liu, Y.-S., Xu, W.-L., Ling, W.-L., Ayers, J., Wang, X.-C., Wang, Q.-H., 2004. Recycling lower continental crust in the North China craton. Nature 432, 892–897.

Goldberg, A.S., 2010. Dyke swarms as indicators of major extensional events in the 1.9–1.2 Ga Columbia supercontinent. J. Geodyn. 50, 176–190.

Halilovic, J., Cawood, P.A., Jones, J.A., Pirajno, F., Nemchin, A.A., 2004. Provenance of the Earaheedy Basin: implications for assembly of the Western Australian Craton. Precambrian Res. 128, 343–366.

Hallberg, J.A., 1987. Postcratonization mafic and ultramafic dykes of the Yilgarn Block. Aust. J. Earth Sci. 34, 135–149. doi:10.1080/08120098708729398

Halls, H.C., Heaman, L.M., 2000. The paleomagnetic significance of new U-Pb age data from the Molson dyke swarm, Cauchon Lake area, Manitoba. Can. J. Earth Sci. 37, 957–966.

Halls, H.C., Kumar, a., Srinivasan, R., Hamilton, M. a., 2007. Paleomagnetism and U-Pb geochronology of easterly trending dykes in the Dharwar craton, India: feldspar clouding, radiating dyke swarms and the position of India at 2.37 Ga. Precambrian Res. 155, 47–68. doi:10.1016/j.precamres.2007.01.007

Halls, H.C., Zhang, B., 1998. Uplift structure of the southern Kapuskasing zone from 2.45 Ga dike swarm displacement. Geology 26, 67–70. doi:10.1130/0091-7613(1998)026<0067:USOTSK>2.3.CO;2

Hanson, R.E., Gose, W.A., Crowley, J.L., Ramezani, J., Bowring, S.A., Bullen, D.S., Hall, R.P., Pancake, J.A., Mukwakwami, J., 2004. Paleoproterozoic intraplate magmatism and basin development on the Kaapvaal Craton: Age, paleomagnetism and geochemistry of~ 1.93 to~ 1.87 Ga post-Waterberg dolerites. South African J. Geol. 107, 233–254.

Heaman, L.M., 2009. The application of U–Pb geochronology to mafic, ultramafic and alkaline rocks: An evaluation of three mineral standards. Chem. Geol. 261, 43–52. doi:10.1016/j.chemgeo.2008.10.021

Heaman, L.M., Machado, N., Krogh, T.E., Weber, W., 1986. Precise U-Pb zircon ages for the Molson dyke swarm and the Fox River sill: constraints for Early Proterozoic crustal evolution in northeastern Manitoba, Canada. Contrib. to Mineral. Petrol. 94, 82–89.

Heaman, L.M., Peck, D., Toope, K., 2009. Timing and geochemistry of 1.88 Ga Molson Igneous Events, Manitoba: Insights into the formation of a craton-scale magmatic and metallogenic province. Precambrian Res. 172, 143–162.

Hoek, J.D., Seitz, H.-M., 1995. Continental mafic dyke swarms as tectonic indicators: an example from the Vestfold Hills, Antarctica. Precambrian Res. 75, 121–139.

Hou, G., 2012. Mechanism for three types of mafic dyke swarms. Geosci. Front. 3, 217–223. doi:10.1016/j.gsf.2011.10.003

Hou, G., Kusky, T.M., Wang, C., Wang, Y., 2010. Mechanics of the giant radiating Mackenzie dyke swarm: A paleostress field modeling. J. Geophys. Res. Solid Earth 115. doi:10.1029/2007JB005475

Hou, G., Santosh, M., Qian, X., Lister, G.S., Li, J., 2008. Configuration of the Late Paleoproterozoic supercontinent Columbia: Insights from radiating mafic dyke swarms. Gondwana Res. 14, 395–409. doi:10.1016/j.gr.2008.01.010

Isles, D.J., Cooke, A.C., 1990. Spatial associations between post-cratonisation dykes and gold deposits in the Yilgarn Block, Western Australia, in: Parker, A.J., Rickwood, P.C., Tucker, D.H. (Eds.), Mafic Dykes and Emplacement Mechanisms. Balkema, Rotterdam, pp. 147–162.

Jaffey, A.H., Flynn, K.F., Glendenin, L.E., Bentley, W.C. t, Essling, A.M., 1971. Precision measurement of half-lives and specific activities of U 235 and U 238. Phys. Rev. C 4, 1889.

Johnson, S.P., Sheppard, S., Rasmussen, B., Wingate, M.T.D., Kirkland, C.L., Muhling, J.R., Fletcher, I.R., Belousova, E.A., 2011. Two collisions, two sutures: Punctuated pre-1950Ma assembly of the West Australian Craton during the Ophthalmian and Glenburgh Orogenies. Precambrian Res. 189, 239–262. doi:10.1016/j.precamres.2011.07.011

Ju, W., Hou, G., Hari, K.R., 2013. Mechanics of mafic dyke swarms in the Deccan Large Igneous Province: Palaeostress field modelling. J. Geodyn. 66, 79–91. doi:10.1016/j.jog.2013.02.002

Kamber, B.S., Greig, A., Schoenberg, R., Collerson, K.D., 2003. A refined solution to Earth's hidden niobium: implications for evolution of continental crust and mode of core formation. Precambrian Res. 126, 289–308.

Klein, E.L., Almeida, M.E., Rosa-Costa, L.T., 2012. The 1.89-1.87 Ga Uatumã Silicic Large Igneous Province, northern South America. November LIP of the Month [WWW Document]. URL http://www.largeigneousprovinces.org/12nov

Klein, R., Pesonen, L.J., Mänttäri, I., Heinonen, J.S., 2016. A late Paleoproterozoic key pole for the Fennoscandian Shield: A paleomagnetic study of the Keuruu diabase dykes, Central Finland. Precambrian Res. 286, 379–397. doi:10.1016/j.precamres.2016.10.013

Ksienzyk, A.K., Jacobs, J., Boger, S.D., Kosler, J., Sircombe, K.N., Whitehouse, M.J., 2012. U-Pb ages of metamorphic monazite and detrital zircon from the Northampton Complex: Evidence of two orogenic cycles in Western Australia. Precambrian Res. 198–199, 37–50. doi:10.1016/j.precamres.2011.12.011

Kumar, K.V., Ernst, W.G., Leelanandam, C., Wooden, J.L., Grove, M.J., 2010. First Paleoproterozoic ophiolite from Gondwana: Geochronologic-geochemical documentation of ancient oceanic crust from Kandra, SE India. Tectonophysics 487, 22–32. doi:10.1016/j.tecto.2010.03.005

Kumar, K.V., Leelanandam, C., 2008. Evolution of the Eastern Ghats belt, India: a plate tectonic perspective. Geol. Soc. India 72, 720–749.

Lewis, J.D., 1994. Mafic dykes in the Williams–Wandering area, Western Australia. Geol. Surv. West. Aust. Rep. 37, 37–52.

Li, Z.-X., Zhong, S., 2009. Supercontinent–superplume coupling, true polar wander and plume mobility: Plate dominance in whole-mantle tectonics. Phys. Earth Planet. Inter. 176, 143–156. doi:10.1016/j.pepi.2009.05.004

Liu, Y., Li, Z.-X., Pisarevsky, S.A., Kirscher, U., Mitchell, R.N., Stark, J.C., 2018. Palaeomagnetism of the 1.89 Ga Boonadgin dykes of the Yilgarn Craton:

Possible connection with India. Precambrian Res. Precambrian Res. In Press, https://doi.org/10.1016/j.precamres.2018.05.021

Liu, Y., Li, Z.-X., Pisarevsky, S.A., Stark, J.C., 2016. Paleomagnetic investigation of mafic dykes in the southwestern Yilgarn Craton, Western Australia, in: Australian Earth Sciences Convention 2016 Abstracts. Geological Society of Australia, p. 277.

Ludwig, K., 2012. User's manual for Isoplot version 3.75–4.15: a geochronological toolkit for Microsoft. Berkeley Geochronological Cent. Spec. Publ.

Ludwig, K., 2009. Squid 2.50, A User's Manual (No. 2.50.11.02.03 Rev. 03 Feb 2011). Berkeley, California, USA.

Maas, R., Grew, E.S., Carson, C.J., 2015. Isotopic constraints (Pb, Rb-Sr, Sm-Nd) on the sources of early Cambrian pegmatites with Boron and Beryllium minerals in the Larsemann Hills, Prydz Bay, Antarctica. Can. Mineral. 53, 249–272.

Maas, R., Kamenetsky, M.B., Sobolev, A. V, Kamenetsky, V.S., Sobolev, N. V, 2005. Sr, Nd, and Pb isotope evidence for a mantle origin of alkali chlorides and carbonates in the Udachnaya kimberlite, Siberia. Geology 33, 549–552.

Mallikharjuna, R.J., Bhattacharji, S., Rao, M.N., Hermes, O.D., 1995. 40Ar–39Ar ages and geochemical characteristics of dolerite dykes around the Proterozoic Cuddapah Basin, South India, in: Geological Society of India Memoir 33. pp. 307–328.

Meert, J.G., Pandit, M.K., Pradhan, V.R., Banks, J., Sirianni, R., Stroud, M., Newstead, B., Gifford, J., 2010. Precambrian crustal evolution of Peninsular India: A 3.0 billion year odyssey. J. Asian Earth Sci. 39, 483–515. doi:10.1016/j.jseaes.2010.04.026

Middleton, M.F., Wilde, S.A., Evans, B.A., Long, A., Dentith, M., 1993. A preliminary interpretation of deep seismic reflection and other geophysical data from the Darling Fault Zone, Western Australia. Explor. Geophys. 24, 711–718.

Minifie, M., Kerr, A.C., Ernst, R.E., Pearce, J.A., 2008. The origin, nature and consequences of the Circum-Superior 1880 Ma Large Igneous Province. Geochim. Cosmochim. Acta Suppl. 72, A633.

Mishra, D.C., 2015. Plume and Plate Tectonics Model for Formation of some Proterozoic Basins of India along Contemporary Mobile Belts: Mahakoshal – Bijawar, Vindhyan and Cuddapah Basins. J. Geol. Soc. India 85, 525–536.

Mohanty, S., 2015. Precambrian continent assembly and dispersal events of South Indian and East Antarctic Shields. Int. Geol. Rev. 57, 1992–2027. doi:10.1080/00206814.2015.1048751

Mohanty, S., 2012. Spatio-temporal evolution of the Satpura Mountain Belt of India: A comparison with the Capricorn Orogen of Western Australia and implication for evolution of the supercontinent Columbia. Geosci. Front. 3, 241–267. doi:10.1016/j.gsf.2011.10.005

Morris, P.A., 2007. Composition of the Bunbury Basalt (BB1) and Kerba Monzogranite (KG1) geochemical reference materials, and assessing the contamination effects of mill heads, in: Geological Survey of Western Australia Record 2007/14. Geological Survey of Western Australia Record 2007/14.

Murthy, N.G.K., 1987. Mafic dyke swarms of the Indian shield, in: Fahrig, W.F., Halls, H.C. (Eds.), Mafic Dyke Swarms. Geological Association of Canada Special Paper 34, pp. 393–400.

Myers, J.S., 1993. Precambrian Tectonic History of the West Australian Craton and Adjacent Orogens. Annu. Rev. Earth Planet. Sci. 21, 453–485.

Myers, J.S., 1990. Pinjarra orogen, in: Geology and Mineral Resources of Western Australia. State Printing Division, pp. 264–274.

Nelson, D.R., Myers, J.S., Nutman, A.P., 1995. Chronology and evolution of the Middle Proterozoic Albany-Fraser Orogen, Western Australia. Aust. J. Earth Sci. 42, 481–495. doi:10.1080/08120099508728218

Nemchin, A.A., Pidgeon, R.T., 1998. Precise conventional and SHRIMP baddeleyite U□Pb age for the Binneringie Dyke, near Narrogin, Western Australia. Aust. J. Earth Sci. 45, 673–675.

Nemchin, A.A., Pidgeon, R.T., 1997. Evolution of the Darling range batholith, Yilgarn craton, western Australia: a SHRIMP zircon study. J. Petrol. 38, 625–649.

Nemchin, A.A., Pidgeon, R.T., Wilde, S.A., 1994. Timing of Late Archaean granulite facies metamorphism in the southwestern Yilgarn Craton of Western Australia: evidence from U-Pb ages of zircons fro mafic granulites. Precambrian Res. 68, 307–321.

Olsson, J.R., Klausen, M.B., Hamilton, M.A., März, N., Söderlund, U., Roberts, R.J., 2016. Baddeleyite U–Pb ages and gechemistry of the 1875–1835 Ma Black

Hills Dyke Swarm across north-eastern South Africa: part of a trans-Kalahari Craton back-arc setting? GFF 138, 183–202.

Pidgeon, R.T., Cook, T.J.F., 2003. 1214±5 Ma dyke from the Darling Range, southwestern Yilgarn Craton, Western Australia. Aust. J. Earth Sci. 50, 769–773.

Pidgeon, R.T., Nemchin, A.A., 2001. 1.2 Ga Mafic dyke near York, southwestern Yilgarn Craton, Western Australia. Aust. J. Earth Sci. 48, 751–755. doi:10.1046/j.1440-0952.2001.485895.x

Pisarevsky, S. a., De Waele, B., Jones, S., Söderlund, U., Ernst, R.E., 2015. Paleomagnetism and U–Pb age of the 2.4Ga Erayinia mafic dykes in the south-western Yilgarn, Western Australia: Paleogeographic and geodynamic implications. Precambrian Res. 259, 222–231. doi:10.1016/j.precamres.2014.05.023

Polat, a., Hofmann, a. W., Rosing, M.T., 2002. Boninite-like volcanic rocks in the 3.7-3.8 Ga isua greenstone belt, West Greenland: Geochemical evidence for intra-oceanic subduction zone processes in the early earth. Chem. Geol. 184, 231–254. doi:10.1016/S0009-2541(01)00363-1

Prokoph, A., Ernst, R.E., Buchan, K.L., 2004. Time-Series Analysis of Large Igneous Provinces: 3500 Ma to Present. J. Geol. 112, 1–22. doi:10.1086/379689

Qiu, Y., McNaughton, N.J., Groves, D.I., Dunphy, J.M., 1999. First record of 1.2 Ga quartz dioritic magmatism in the Archaean Yilgarn Craton, Western Australia, and its significance. Aust. J. Earth Sci. 46, 421–428. doi:10.1046/j.1440-0952.1999.00715.x

Rasmussen, B., Fletcher, I.R., 2010. Dating sedimentary rocks using in situ U-Pb geochronology of syneruptive zircon in ash-fall tuff less than 1 mm thick. Geology 38, 299–302. doi:10.1130/G30567.1

Rasmussen, B., Fletcher, I.R., 2002. Indirect dating of mafic intrusions by SHRIMP U-Pb analysis of monazite in contact metamorphosed shale: An example from the Palaeoproterozoic Capricorn Orogen, Western Australia. Earth Planet. Sci. Lett. 197, 287–299. doi:10.1016/S0012-821X(02)00501-0

Rasmussen, B., Fletcher, I.R., Bekker, A., Muhling, J.R., Gregory, C.J., Thorne, A.M., 2012. Deposition of 1.88-billion-year-old iron formations as a consequence of rapid crustal growth. Nature 484, 498–501.

Rasmussen, B., Fletcher, I.R., Bengtson, S., McNaughton, N.J., 2004. SHRIMP U-Pb dating of diagenetic xenotime in the Stirling Range Formation, Western Australia: 1.8 Billion year minimum age for the Stirling biota. Precambrian Res. 133, 329–337. doi:10.1016/j.precamres.2004.05.008

Rogers, J.J.W., Santosh, M., 2002. Configuration of Columbia, a Mesoproterozoic Supercontinent. Gondwana Res. 5, 5–22. doi:10.1016/s1342-937x(05)70883-2

Rudnick, R.L., Gao, S., 2003. Composition of the continental crust, in: Holland, H.D., Turekian, K.K. (Eds.), The Crust Vol. 3. Treatise on Geochemistry. pp. 1–64.

Salters, V.J.M., Stracke, A., 2004. Composition of the depleted mantle. Geochemistry, Geophys. Geosystems 5, Q05B07. doi:10.1029/2003GC000597

Sheppard, S., Bodorkos, S., Johnson, S.P., Wingate, M.T.D., Kirkland, C.L., 2010. The Paleoproterozoic Capricorn Orogeny: intracontinental reworking not continent–continent collision, Geological Survey of Western Australia Report 108. Geological Survey of Western Australia.

Sheppard, S., Fletcher, I.R., Rasmussen, B., Zi, J.-W., Muhling, J.R., Occhipinti, S.A., Wingate, M.T.D., Johnson, S.P., 2016. A new Paleoproterozoic tectonic history of the eastern Capricorn Orogen, Western Australia, revealed by U–Pb zircon dating of micro-tuffs. Precambrian Res. 286, 1–19. doi:10.1016/j.precamres.2016.09.026

Sheppard, S., Johnson, S.P., Wingate, M.T.D., Kirkland, C.L., Pirajno, F., 2010b. Explanatory notes for the Gascoyne Province. Geol. Surv. West. Aust. 336.

Sheppard, S., Occhipinti, S.A., Tyler, I.M., 2004. A 2005–1970 Ma Andean-type batholith in the southern Gascoyne Complex, Western Australia. Precambrian Res. 128, 257–277. doi:10.1016/j.precamres.2003.09.003

Sheppard, S., Rasmussen, B., Zi, J.-W., Soma, V.S., Sarma, S., Mohan, M.R., Krapez, B., Wilde, S.A., McNaughton, N.J., 2017. Sedimentation and mafic magmatism in the Paleoproterozoic Cuddapah Basin, India, as a consequence of lithospheric extension. Gondwana Res. 48, 153–163. doi:10.1016/j.gr.2017.04.024

Sircombe, K.N., 2002. Reconnaissance detrital zircon geochronology provenance of the Palaeoproterozoic Ashburton Formation: implications for Pilbara and

Yilgarn amalgamation, 16th Australian Geological Convention Abstract, 1-5 July 2002, Adelaide, South Australia. Geological Society of Australia.

Sobolev, A. V., Hofmann, A.W., Kuzmin, D. V., Yaxley, G.M., Arndt, N.T., Chung, S.-L., Danyushevsky, L. V., Elliott, T., Frey, F.A., Garcia, M.O., Gurenko, A.A., Kamenetsky, V.S., Kerr, A.C., Krivolutskaya, N.A., Matvienkov, V. V., Nikogosian, I.K., Rocholl, A., Sigurdsson, I.A., Sushchevskaya, N.M., Teklay, M., 2007. The amount of recycled crust in sources of mantle-derived melts. Science 316, 412–417.

Sobolev, A. V, Hofmann, A.W., Sobolev, S. V, Nikogosian, I.K., 2005. An olivine-free mantle source of Hawaiian shield basalts. Nature 434, 590–597.

Söderlund, U., Hofmann, A., Klausen, M.B., Olsson, J.R., Ernst, R.E., Persson, P.O., 2010. Towards a complete magmatic barcode for the Zimbabwe craton: Baddeleyite U-Pb dating of regional dolerite dyke swarms and sill complexes. Precambrian Res. 183, 388–398. doi:10.1016/j.precamres.2009.11.001

Söderlund, U., Johansson, L., 2002. A simple way to extract baddeleyite (ZrO_2). Geochemistry, Geophys. Geosystems 3. doi:10.1029/2001GC000212

Sofoulis, J., 1965. Explanatory Notes on the Widgiemooltha 1: 250,000 Geological Sheet Western Australia. Geological Survey of Western Australia.

Spaggiari, C.V., Kirkland, C.L., Smithies, H.R., Wingate, M.T.D., Belousova, E.A., 2015. Transformation of an Archean craton margin during Proterozoic basin formation and magmatism: The Albany–Fraser Orogen, Western Australia. Precambrian Res. 266, 440–466. doi:10.1016/j.precamres.2015.05.036

Spaggiari, C.V., Kirkland, C.L., Smithies, R.H., Wingate, M.T.D., 2014. Tectonic links between Proterozoic sedimentary cycles, basin formation and magmatism in the Albany-Fraser Orogen, Western Australia, Geological Survey of Western Australia Report 133.

Spaggiari, C. V, Bodorkos, S., Barquero-Molina, M., Tyler, I.M., Wingate, M.T.D., 2009. Interpreted bedrock geology of the South Yilgarn and of the South Yilgarn and Central Albany-Fraser Orogen, Western Australia, Record 2009/10.

Spaggiari, C. V, Kirkland, C.L., Pawley, M.J., Smithies, R.H., Wingate, M.T.D., Doyle, M.G., Blenkinsop, T.G., Clark, C., Oorschot, C.W., Fox, L.J., 2011. The geology of the east Albany-Fraser Orogen—a field guide. Geol. Surv. West. Aust. Rec. 2011/23 23, 97.

Stacey, J.S. t, Kramers, 1JD, 1975. Approximation of terrestrial lead isotope evolution by a two-stage model. Earth Planet. Sci. Lett. 26, 207–221.

Stern, R.A., 2001. A new isotopic and trace-element standard for the ion microprobe: preliminary thermal ionization mass spectrometry (TIMS) U-Pb and electron-microprobe data, Geological Survey of Canada Report 14, Current Research 2001-F.

Stern, R.A., Bodorkos, S., Kamo, S.L., Hickman, A.H., Corfu, F., 2009. Measurement of SIMS instrumental mass fractionation of Pb isotopes during zircon dating. Geostand. Geoanalytical Res. 33, 145–168. doi:10.1111/j.1751-908X.2009.00023.x

Sun, S. -s., McDonough, W.F., 1989. Chemical and isotopic systematics of oceanic basalts: implications for mantle composition and processes. Geol. Soc. London, Spec. Publ. 42, 313–345. doi:10.1144/GSL.SP.1989.042.01.19

Tucker, D.H., Boyd, D.M., 1987. Dykes of Australia detected by airborne magnetic surveys. Mafic Dyke Swarms. Geol. Assoc. Canada Spec. Pap. 34, 163–172.

Wang, X.-C., Li, Z.-X., Li, J., Pisarevsky, S.A., Wingate, M.T.D., 2014. Genesis of the 1.21 Ga Marnda Moorn large igneous province by plume–lithosphere interaction. Precambrian Res. 241, 85–103. doi:10.1016/j.precamres.2013.11.008

Wilde, S.A., Middleton, M.F., Evans, B.J., 1996. Terrane accretion in the southwestern Yilgarn Craton: evidence from a deep seismic crustal profile. Precambrian Res. 78, 179–196.

Wilde, S. a., 1999. Evolution of the Western Margin of Australia during the Rodinian and Gondwanan Supercontinent Cycles. Gondwana Res. 2, 481–499. doi:10.1016/S1342-937X(05)70287-2

Williams, G.E., Schmidt, P.W., Clark, D.A., 2004. Palaeomagnetism of iron-formation from the late Palaeoproterozoic Frere Formation, Earaheedy Basin, Western Australia: palaeogeographic and tectonic implications. Precambrian Res. 128, 367–383. doi:10.1016/j.precamres.2003.09.008

Wingate, M.T.. D., Campbell, I.H., Compston, W., Gibson, G.M., 1998. Ion microprobe U–Pb ages for Neoproterozoic basaltic magmatism in south-central Australia and implications for the breakup of Rodinia. Precambrian Res. 87, 135–159. doi:10.1016/S0301-9268(97)00072-7

Wingate, M.T.D., 2017. Mafic dyke swarms and large igneous provinces in Western Australia get a digital makeover, in: Geological Survey of Western Australia Record 2017/2. Geological Survey of Western Australia, pp. 4–8.

Wingate, M.T.D., 2007. Proterozoic mafic dykes in the Yilgarn Craton, in: Proceedings of Geoconferences (WA) Inc. Kalgoorlie 2007 Conference, Kalgoorlie, Western Australia. pp. 80–84.

Wingate, M.T.D., 1999. Ion microprobe baddeleyite and zircon ages for Late Archaean mafic dykes of the Pilbara Craton, Western Australia. Aust. J. Earth Sci. 46, 493–500.

Wingate, M.T.D., Campbell, I.H., Harris, L.B., 2000. SHRIMP baddeleyite age for the Fraser dyke swarm, southeast Yilgarn Craton, Western Australia. Aust. J. Earth Sci. 47, 309–313.

Wingate, M.T.D., Pidgeon, R.T., 2005. The Marnda Moorn LIP, a late Mesoproterozoic large igneous province in the Yilgarn craton, Western Australia. July 2005 LIP of the month [WWW Document]. URL http://www.largeigneousprovinces.org/05jul

Wingate, M.T.D., Pirajno, F., Morris, P.A., 2004. Warakurna large igneous province: a new Mesoproterozoic large igneous province in west-central Australia. Geology 32, 105–108.

Wingate, M.T.D., Pisarevsky, S.A., Evans, D.A.D., 2002. Rodinia connections between Australia and Laurentia: no SWEAT, no AUSWUS? Terra Nov. 14, 121–128.

Zhao, G., Cawood, P.A., Wilde, S.A., Sun, M., 2002. Review of global 2.1-1.8 Ga orogens: implications for a pre-Rodinia supercontinent. Earth-Science Rev. 59, 125–162.

Chapter 6 1.39 Ga mafic dyke swarm in southwestern Yilgarn Craton marks Nuna to Rodinia transition in the West Australian Craton[3]

J. Camilla Stark, Xuan-Ce Wang, Zheng-Xiang Li, Steven W. Denyszyn, Birger Rasmussen and Jian-Wei Zi

6.1 Abstract

The Archean Yilgarn Craton in Western Australia hosts at least five generations of mafic dykes ranging from Archean to Neoproterozoic in age, including the craton-wide ca. 2408 Ma Widgiemooltha and the 1210 Ma Marnda Moorn Large Igneous Provinces (LIP), the 1888 Ma Boonadgin dykes in the southwest and the 1075 Ma Warakurna LIP in the northern part of the craton. We report here a newly identified NNW-trending mafic dyke swarm, here named the Biberkine dyke swarm, in the southwestern Yilgarn Craton dated at 1390 ± 3 Ma by ID-TIMS U-Pb geochronology of baddeleyite. The regional extent of the dyke swarm is uncertain but aeromagnetic data suggest that the dykes are part of a linear swarm several hundred kilometers long, truncated by the Mesoproterozoic Albany-Fraser Orogen to the south. Geochemical data indicate that the dykes have tholeiitic compositions with a significant contribution from metasomatically enriched subcontinental lithospheric mantle and/or lower continental crust. Paleogeographic reconstructions suggest that a prolonged tectonic quiescence in the Yilgarn Craton from ca. 1600 Ma was interrupted by renewed subduction along the southern and southeastern margin at ca. 1400 Ma, reflecting a transition from Nuna to Rodinia configuration. The 1390 Ma Biberkine dykes are likely a direct consequence of this transition and mark the change from a passive to active tectonic setting, which culminated in the Albany-Fraser Orogeny at ca. 1330 Ma. The Biberkine dykes are coeval with a number of other mafic dyke swarms worldwide and provide an important target for paleomagnetic studies.

[3] *This chapter is published as* Stark, J.C., Wang, X.-C., Li, Z.-X., Denyszyn, S.W., Rasmussen, B., Zi, J.-W., Sheppard, S., 2018. 1.39 Ga mafic dyke swarm in southwestern Yilgarn Craton marks Nuna to Rodinia transition in the West Australian Craton. Precambrian Res. 316, 291-304.

6.2 Introduction

Mafic dyke swarms act as important markers for supercontinent reconstructions (e.g. Ernst and Buchan, 1997; Buchan et al., 2001; Bleeker and Ernst, 2006; Ernst and Srivastava, 2008; Ernst et al., 2010, 2013) and as indicators of paleostress fields and pre-existing crustal weaknesses (Ernst et al., 1995b; Hoek and Seitz, 1995; Halls and Zhang, 1998; Hou, 2012; Ju et al., 2013). They appear to be intimately connected with deep-Earth dynamics and supercontinent cycles (e.g. Condie, 2004; Prokoph et al., 2004; Bleeker and Ernst, 2006; Ernst et al., 2008; Li and Zhong, 2009; Clowes et al., 2010; Goldberg, 2010) and their presence acts as a tectonic fingerprint of intracratonic crustal extension associated with processes such as subduction (back-arc extension), mantle plumes and rifting during supercontinent breakup.

The Archean Yilgarn Craton in Western Australia shared a large part of its tectonic evolution with Antarctica during the Mesoproterozoic and is thus an important component in reconstructions for the Nuna and Rodinia supercontinents (Dalziel, 1991; Meert, 2002; Rogers and Santosh, 2002; Wingate et al., 2002; Li et al., 2008; Nance et al., 2014; Pisarevsky et al., 2014a; Meert and Santosh, 2017). The transition from Nuna to Rodinia likely occurred after ca. 1400 Ma (Li et al., 2008; Evans and Mitchell, 2011; Pisarevsky et al., 2014a; Aitken et al., 2016), after an interval of apparent tectonic quiescence in the Yilgarn Craton since ca. 1600 Ma. Here we report the discovery of a Mesoproterozoic (1390 Ma) NNW-trending mafic dyke swarm in the southwestern Yilgarn Craton, identified by U-Pb geochronology using a combination of *in situ* SHRIMP and ID-TIMS methodologies. We also present results from a preliminary geochemical analysis and discuss the tectonic setting during emplacement of the dykes and implications for regional tectonic models.

6.3 Regional geology

The Yilgarn Craton is a ca. 900 x 1000 km Archean crustal block comprising six accreted terranes: the Southwest, Narryer, Youanmi, Kalgoorlie, Kurnalpi and Burtville terranes, the latter three forming the Eastern Goldfields Superterrane (Figure 6.1). These comprise variably metamorphosed granites and volcanic and sedimentary rocks with protolith ages between ca. 3730 and 2620 Ma (Cassidy et al., 2005, 2006 and references therein) and are thought to represent a series of volcanic arcs and back- arc basins, which amalgamated during a Neoarchean orogeny between ca. 2730 and 2625 Ma (Myers, 1993, 1995; Wilde et al., 1996; Barley et al., 2003; Blewett and Hitchman, 2006; Korsch et al., 2011; Witt et al., 2018). Abundant granites were emplaced between ca. 2760 Ma and 2630 Ma (Cassidy et al., 2006 and references therein) and the entire craton underwent intense metamorphism and hydrothermal activity between 2780 and 2630 Ma (Myers, 1993; Nemchin et al., 1994; Nelson et al., 1995a; Wilde et al., 1996). The Southwest Terrane comprises multiply deformed ca. 3200–2800 Ma high-grade metasedimentary rocks and ca. 2720─2670 Ma meta-igneous rocks intruded by 2750─2620 Ma granites (Myers, 1993; Wilde et al., 1996; Nemchin and Pidgeon, 1997).

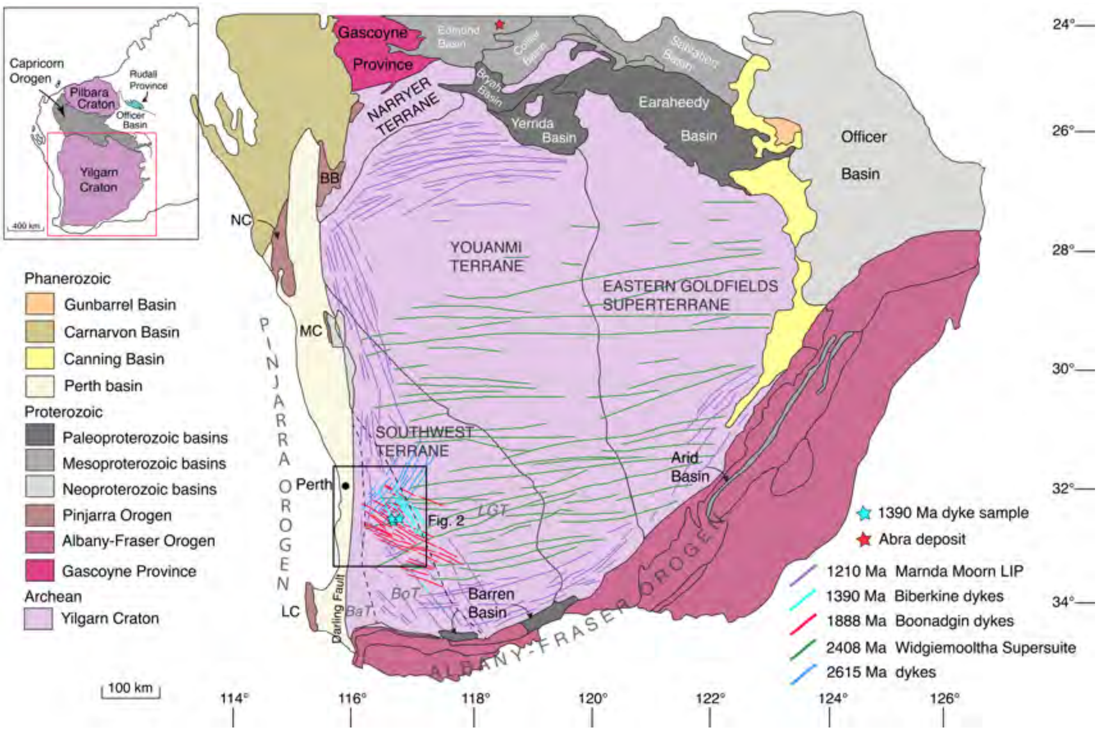

Figure 6.1 Map of the Yilgarn Craton showing major tectonic units and the Capricorn and Albany-Fraser orogens. Inset shows the extent of the West Australian Craton (Pilbara Craton, Yilgarn Craton and Capricorn Orogen). From Geological Survey of Western Australia 1:2.5M Interpreted Bedrock Geology 2015 and 1:10M Tectonic Units 2016.

The Yilgarn Craton is bounded by three Proterozoic orogenic belts: the ca. 2005─570 Ma Capricorn Orogen in the north (Cawood and Tyler, 2004; Sheppard et al., 2010a; Johnson et al., 2011), the ca. 1815─1140 Ma Albany-Fraser Orogen in the south and east (Nelson et al., 1995a; Clark et al., 2000; Spaggiari et al., 2015), and the ca. 1090-525 Ma Pinjarra Orogen in the west (Myers, 1990; Wilde, 1999; Ksienzyk et al., 2012). Following cratonisation toward the end of the Archean, the

Yilgarn Craton collided along the Capricorn Orogen with the combined Pilbara Craton-Glenburgh Terrane by 1950 Ma to form the West Australian Craton (WAC) (Sheppard et al., 2004, 2010; Johnson et al., 2011). Prolonged lateritic weathering has produced the modern denuded landscape and poor exposure of basement rocks (Anand and Paine, 2002).

The Yilgarn Craton hosts a large number of mafic dykes of different orientations with the dyke density increasing towards the southern and western craton margins (Hallberg, 1987; Tucker and Boyd, 1987). The dykes are discernible in aeromagnetic data but outcrops are difficult to identify and sample due to deep weathering and thick regolith cover. The oldest known mafic dyke in the Yilgarn Craton is the NE-trending ca. 2620 Ma Yandinilling dyke, which has been dated from one outcrop 120 km east of Perth but is probably part of a large dyke swarm that extends at least across the South West Terrane (Stark et al., 2018). The oldest mafic dykes with craton-wide extent belong to the E- to NE-trending 2418-2408 Ma Widgiemooltha dyke swarm (Sofoulis, 1965; Evans, 1968; Campbell et al., 1970; Hallberg, 1987; Doehler and Heaman, 1998; Nemchin and Pidgeon, 1998; Wingate, 1999, 2007; French et al., 2002; Pisarevsky et al., 2015). The Widgiemooltha dykes are up to 3.2 km wide and extend up to 700 km across the craton, with the largest intrusions (Jimberlana and Binneringie) showing well-developed igneous layering (Campbell et al., 1970; Lewis, 1994). The dykes exhibit dual magnetic polarity (Tucker and Boyd, 1987; Boyd and Tucker, 1990) and recent geochronology and paleomagnetic data suggest that their emplacement may have involved several pulses (Wingate, 2007; Smirnov et al., 2013; Pisarevsky et al., 2015). The second craton-wide suite is the 1210 Ma Marnda Moorn LIP, which consists of several sub-swarms of different orientations intruding along the craton margins (Isles and Cooke, 1990; Evans, 1999; Wingate et al., 2000; Pidgeon and Nemchin, 2001; Pidgeon and Cook, 2003; Rasmussen and Fletcher, 2004; Wingate and Pidgeon, 2005; Wingate, 2007; Claoué-Long and Hoatson, 2009). Outcrops in the southeast are limited to a single occurrence, and the extent of the dykes in the northeast is unknown due to cover rocks but one E-trending dioritic dyke dated at 1215 ±11 Ma has been reported further inland (Qiu et al., 1999). Other identified dyke swarms include the NW-trending ca. 1888 Ma Boonadgin dyke swarm in the southwest (Stark et al., 2017) the SW-trending dykes of the 1075 Ma Warakurna LIP in the northern Yilgarn Craton (Wingate et al., 2004), the WNW-trending ca. 735 Ma Nindibillup dykes in the central and southeast Yilgarn Craton (Spaggiari et al., 2009, 2011; Wingate, 2017) and the undated (likely <1140 Ma) NW-trending Beenong dykes in the southeast Yilgarn Craton (Wingate, 2007; Spaggiari et al., 2009; 2011).

6.4 Samples

6.4.1 Field sampling

Field sampling sites were targeted using satellite imagery (Landsat/Copernicus or Astrium/CNES from Google Earth), aeromagnetic data (20-40 m cell size, Geoscience Australia magnetic grid of Australia V6 2015 base reference) and 1:250 000 geological maps from the Geological Survey of Western Australia.

Three block samples were collected from outcrops SW to WSW of the town of Pingelly from outcrops within agriculturally cleared areas near accessible roads (Figure 6.2 and Table 6.1). Basement rocks are not exposed at any of the sampling sites but geological mapping indicates that the country rocks to the dykes are Archean granites (Baxter et al., 1980). Dykes form gentle ridges often associated with large trees, where farming is difficult due to concentrations of large boulders of dolerite (Figure 6.3). Due to the lack of exposed contacts, the widths of the dykes are unknown, however at WDS10 the dyke is probably more than 60 m wide, based on the extents of partially exposed rock. All outcrops appear relatively fresh and weathering forms a light red-brown crust of varying thickness that is best visible along fractures (Figure 6.3).

6.4.2 Sample description

All samples are dolerites with intergranular ophitic to sub-ophitic texture, comprising 45-50% plagioclase, 25-35% pyroxene, up to 10% quartz and 10-15% opaque minerals (magnetite and ilmenite) and trace apatite. The samples are relatively fresh apart from uralitic alteration of pyroxene and variable but relatively minor sericitisation of plagioclase (Figure 6.4). Most clinopyroxene grains have been

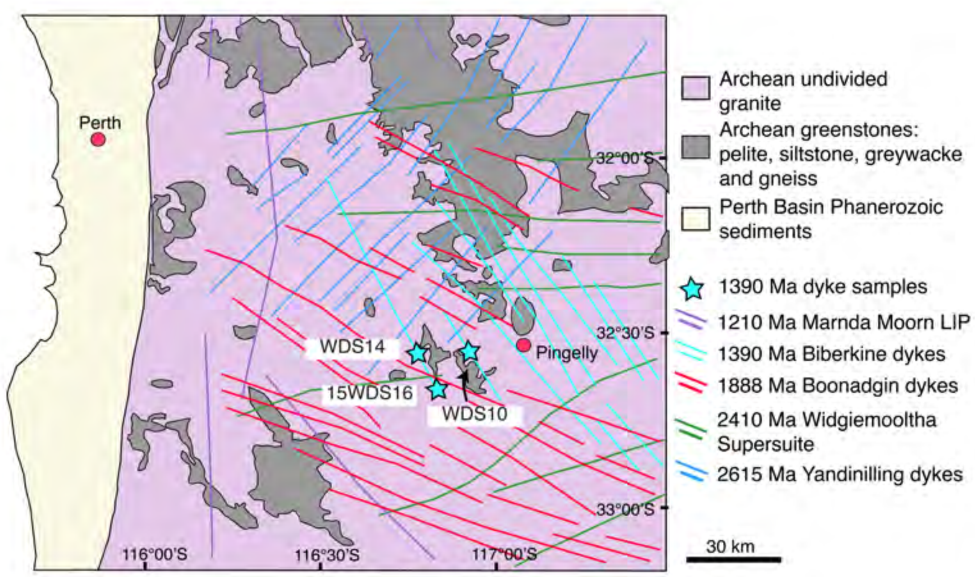

Figure 6.2 Sample localities. See Table 1 for detailed information

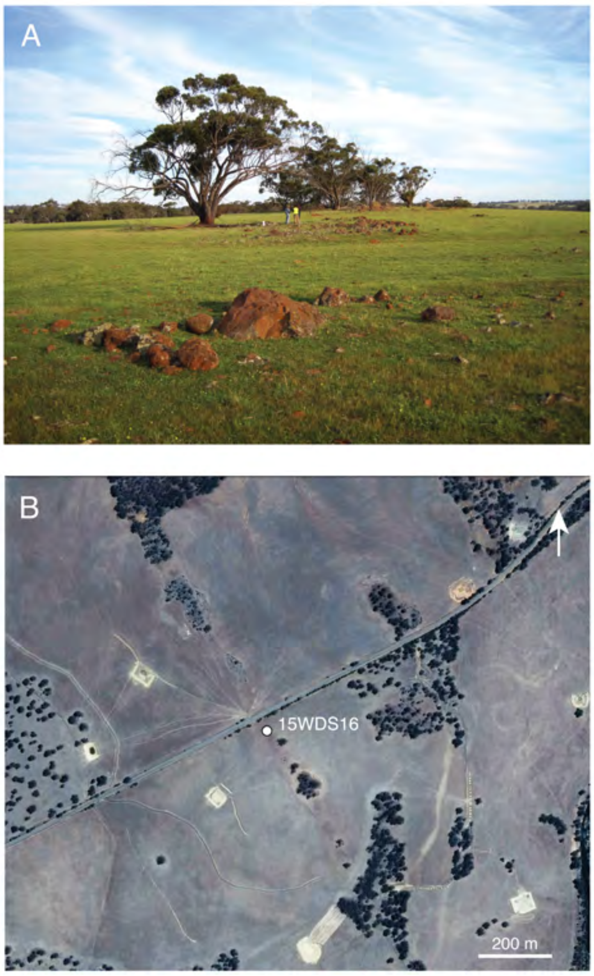

Figure 6.3 ***(A)*** *15WDS16 sample location, looking SSE.* ***(B)*** *Satellite image showing the location of sample 15WDS16. Note the faint but visible NNW trending trace of the dyke, associated with clusters of trees.*

affected by alteration, ranging in intensity from the growth of brown amphibole near grain boundaries to pervasive alteration of the entire grain into a mixture of brown and green amphibole. Plagioclase preserves original twinning and some zoned grains exhibit weak alteration along fractures. Abundant opaque minerals appear as subhedral to euhedral grains in the groundmass but also as extremely fine-grained masses within altered pyroxene and along grain boundaries.

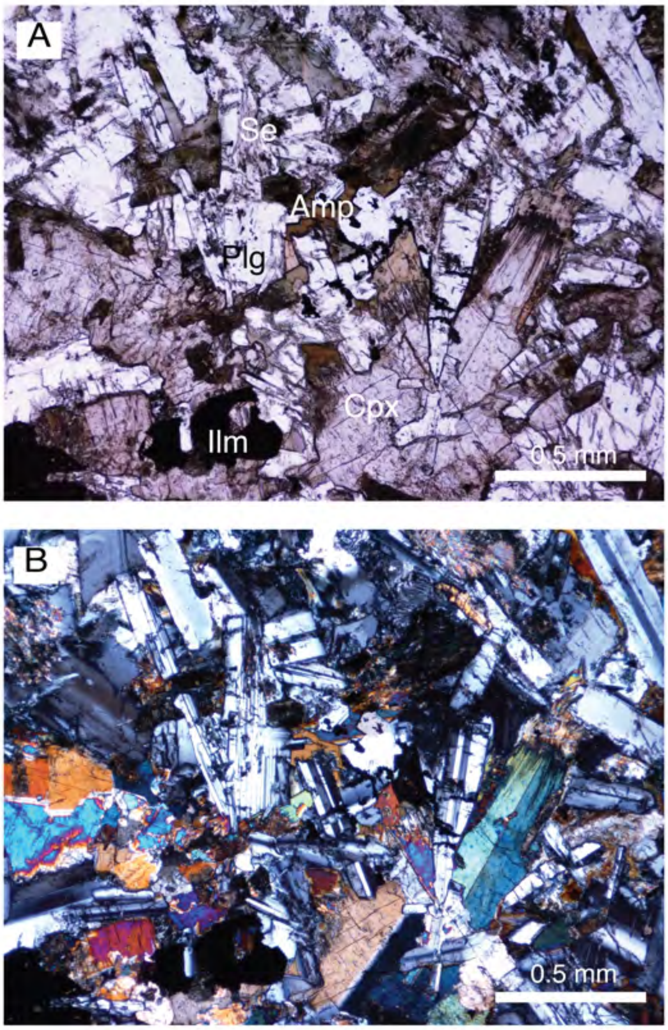

Figure 6.4 Photomicrograph of sample WDS10C. ***(A)*** *Plane polarised light (PPL) image showing subophitic growth of plagioclase within clinopyroxene in the lower right quadrant and the growth of brown and green amphibole near and within intercumulus grain boundaries.* ***(B)*** *Cross-polarized light (XPL) image showing twinning in the poikilitic clinopyroxene in the lower right quadrant. Plg = plagioclase, Cpx = clinopyroxene, Amp = amphibole, Se = sericite, Ilm = ilmenite.*

6.5 U-Pb geochronology and geochemistry

6.5.1 SHRIMP U-Pb geochronology

Polished thin sections were scanned to identify baddeleyite, zircon and zirconolite with a Hitachi TM3030 scanning electron microscope (SEM) equipped with energy dispersive X-ray spectrometer (EDX) at Curtin University. For SHRIMP U-Pb dating, selected grains were drilled directly from the thin sections using a micro drill and mounted into epoxy disks, which were cleaned and coated with 40 nm of gold. Baddeleyite forms mostly unaltered, subhedral to euhedral equant and tabular grains, some with thin zircon rims. Most baddeleyite grains are up to 100 µm long and up to 30 µm across (Figure 6.5).

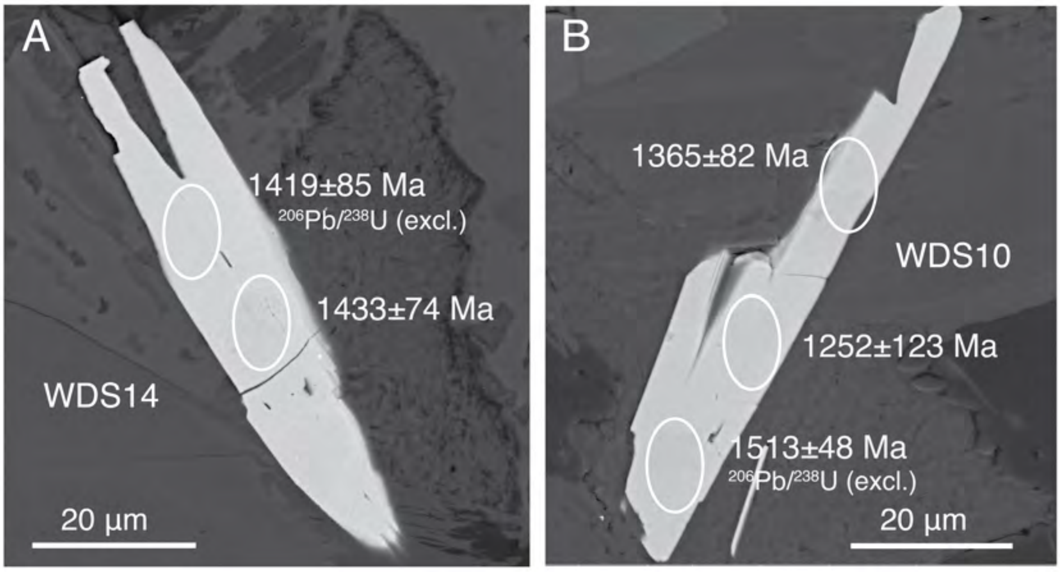

*Figure 6.5 SEM backscatter images showing SHRIMP baddeleyite spots and dates. (**A**) WDS09-2B (**B**) 16WDS01-372B (**C**) 16WDS06-405B (**D**) 16WDS06-406B*

Baddeleyite was analysed for U, Th and Pb using the sensitive high-resolution ion microprobe (SHRIMP II) at the John de Laeter Centre at Curtin University in Perth, Australia, following standard operating procedures after Williams (1998). The SHRIMP analysis method for mounts with polished thin section plugs outlined in Rasmussen and Fletcher (2010) was modified for baddeleyite (SHRIMP operating parameters in Table 6.2). During each analytical session, standard zircon OG1 (Stern et al., 2009) was used to monitor instrumental mass fractionation and BR266 zircon (Stern, 2001) was used for calibrating U and Th concentration and as an accuracy standard. Phalaborwa baddeleyite (Heaman, 2009) was employed as an additional accuracy standard. Typical spot size with primary O_2^- current was 10-15 µm at 0.1-0.2 nA. Data were processed with Squid version 2.50 (Ludwig, 2009) and Isoplot version 3.76.12 (Ludwig, 2012). For common Pb correction, 1390 Ma common Pb isotopic compositions were calculated from the Stacey and Kramers (1975) two-stage terrestrial Pb isotopic evolution model. Analyses with >1% common Pb (in

Dyke ID	Dlat / Dlon	Samples	Comments
WDS09	32 39.339 S 116 57.132 E	WDS09M-N, WDS09RSA-B	NW trending dolerite dyke near West Pingelly
16WDS01	32 24.738 S 116 48.818 E	16WDS01A-D	NNW trending dolerite dyke west of Brookton, ridge
16WDS02	32 24.740 S 116 48.798 E	16WDS02A-D	NNW trending dolerite dyke west of Brookton. Same dyke as 16WDS01
16WDS06	31 59.973 S 116 39.699 E	16WDS06A-D	NW trending dyke near Talbot

Table 6.1 Sample locations. Datum WGS84, Dlat = decimal latitude, Dlon = decimal longitude

^{206}Pb) or >10% discordance (see footnote in Table 6.3 for definition) are considered unreliable and were disregarded in age calculations. The assigned 1σ external Pb/U error for all analyses is 1%. All weighted mean ages are given at 95% confidence level, except 15WDS16 where 2σ internal error is used. All individual analyses are presented with 1σ error.

6.5.2 ID-TIMS U-Pb geochronology

A sample for ID-TIMS U-Pb geochronology was selected based on results from the SHRIMP dating and the highest number of identified baddeleyite crystals in thin section. A block sample was first sawn from the field sample to remove weathering, then crushed, powdered and processed using a mineral-separation technique modified after Söderlund and Johansson (2002). Baddeleyite grains were hand picked under ethanol under a stereographic optical microscope and selected grains were cleaned with concentrated distilled HNO_3 and HCl. Due to the small size of the separated fractions, no chemical separation methods were required.

Samples were spiked with a University of Western Australia in-house ^{205}Pb-^{235}U tracer solution, which has been calibrated against SRM981, SRM982 (for Pb), and CRM 115 (for U), as well as an externally-calibrated U-Pb solution (the JMM solution from the EarthTime consortium). This tracer is regularly checked using "synthetic zircon" solutions that yield U-Pb ages of 500 Ma and 2000 Ma, provided by D. Condon (British Geological Survey). Dissolution and equilibration of spiked

Mount	CS16-1	CS16-6	CS16-7
Dykes analysed	WDS09, WDS09RS	16WDS01	16WDS06
Date analysed	21-Jul-16	14-Sep-16	6-Sep-16
Kohler aperture (μm)	50	50	50
Spot size (micrometres)	11	9	7
O2- primary current (nA)	0.9	0.6	0.2
Number of scans per analysis	8	8	8
Total number of analyses	23	32	34
Number of standard analyses	13	13	14
Pb/U external precision % (1σ)	1.00	1.00	1.00
Raster time (seconds)	120	180	180
Raster aperture (μm)	90	90	80

Table 6.2 SHRIMP operating parameters. Notes ***1)*** *Mass resolution for all analyses ≥ 5000 at 1% peak height* ***2)*** *BR266, OGC, Phalaborwa and NIST used as standards for each session* ***3)*** *Count times for each scan:* ^{204}Pb, ^{206}Pb, ^{208}Pb *= 10 seconds,* ^{207}Pb *= 30 seconds*

single crystals was by vapour transfer of HF, using Teflon microcapsules in a Parr pressure vessel placed in a 200°C oven for six days. The resulting residue was re-dissolved in HCl and H_3PO_4 and placed on an outgassed, zone-refined rhenium single filament with 5 µL of silicic acid gel. U–Pb isotope analyses were carried out using a Thermo Triton T1 mass spectrometer, in peak-jumping mode using a secondary electron multiplier. Uranium was measured as an oxide (UO_2). Fractionation and deadtime were monitored using SRM981 and SRM 982. Mass fractionation was 0.02 ± 0.06%/amu. Data were reduced and plotted using the software packages Tripoli (from CIRDLES.org) and Isoplot 4.15 (Ludwig, 2011). All uncertainties are reported at 2σ. U decay constants are from Jaffey et al. (1971). The weights of the baddeleyite crystals were calculated from measurements of photomicrographs and estimates of the third dimension. The weights are used to determine U and Pb concentrations and do not contribute to the age calculation. An uncertainty of ± 50% may be attributed to the concentration estimate.

6.6 Geochemistry

Slabs were sawn from block samples to remove weathering. After an initial crush, a small fraction of material was separated and chips with fresh fracture surfaces were hand picked under the microscope and pulverised in an agate mill for isotope analysis. Remaining material was pulverised in a low-Cr steel mill for major and trace element analysis.

Major element analysis was undertaken at Intertek Genalysis Laboratories in Perth, Western Australia using X-ray fluorescence (XRF) using the Geological Survey of Western Australia (GSWA) standard BB1 (Morris, 2007) and Genalysis laboratory internal standards SARM1 and SY-4. Trace element analysis was carried out at University of Queensland (UQ) on a Thermo XSeries 2 inductively coupled plasma mass spectrometer (ICP-MS) equipped with an ESI SC-4 DX FAST autosampler, following procedure for ICP-MS trace element analysis by Eggins et al. (1997) modified by the UQ Radiogenic Isotope Laboratory (Kamber et al., 2003). Sample solutions were diluted 4,000 times, and 12 ppb ^{6}Li, 6ppb ^{61}Ni, Rh, In and Re, and 4.5 ppb ^{235}U internal spikes were added. USGS W2 was used as reference standard and crossed checked with BIR-1, BHVO-2 or other reference materials. All major element analyses have precision better than 5% and all trace element analyses have relative standard deviation (RSD) $<2\%$.

Rb-Sr and Sm-Nd isotope analyses were carried out at the University of Melbourne (e.g. Maas et al., 2005, 2015). Small splits (70 mg) of rock powders were spiked with ^{149}Sm-^{150}Nd and ^{85}Rb-^{84}Sr tracers, followed by dissolution at high pressure in an oven, using Krogh-type PTFE vessels with steel jackets. Sm, Nd and Sr were extracted using EICHROM Sr-, TRU- and LN-resin, and Rb was extracted using cation exchange (AG50-X8, 200-400 mesh resin). Isotopic analyses were carried out on a NU Plasma multi-collector ICP-MS coupled to a CETAC Aridus desolvation system operated in low-uptake mode. Raw data for spiked Sr and Nd fractions were corrected for instrumental mass bias by normalizing to ^{88}Sr/^{86}Sr = 8.37521 and ^{146}Nd/^{145}Nd = 2.0719425 (equivalent to ^{146}Nd/^{144}Nd = 0.7219), respectively, using the exponential law as part of an on-line iterative spike-stripping/internal normalization procedure. Sr and Nd isotope data are reported relative to SRM987 = 0.710230 and La Jolla Nd = 0.511860 and have typical in-run precisions (2sd) of ± 0.000020 (Sr) and ± 0.000012 (Nd). External precision (reproducibility, 2sd) is ± 0.000040 (Sr) and ± 0.000020 (Nd). External precisions for ^{87}Rb/^{86}Sr and ^{147}Sm/^{144}Nd obtained by isotope dilution are ± 0.5% and ± 0.2%, respectively.

6.7 Results

6.7.1 SHRIMP U-Pb geochronology

Twenty-three analyses were obtained from 13 baddeleyite crystals (4 grains from WDS10, 5 grains from WDS14 and 4 grains from 15WDS16) during two SHRIMP sessions (Figure 6.6; detailed U-Pb data are given in Table 6.3). The analysed baddeleyite crystals have low to moderate U concentrations varying from 40 to 330 ppm (median = 163 ppm) and low Th concentrations ranging from 1 to 89 ppm, with Th/U ratios ranging from 0.23 to 0.28. Fourteen analyses were excluded based on their high common Pb (>1.58% ^{206}Pb) and/or >18% discordance. The small size and narrow shape of the baddeleyite crystals made it difficult to place the ion beam without overlapping onto adjacent minerals (e.g. Figure 6.5 B). Crystal orientation dependent Pb/U fractionation effects in baddeleyite during secondary ion mass spectrometry (SIMS) can lead to biased ^{206}Pb/^{238}U ages but this is not necessarily the case for all crystals (e.g. Wingate and Compston, 2000; Schmitt et al., 2010), and in some instances, the ^{204}Pb-corrected ^{206}Pb/^{238}U dates were more precise than the ^{204}Pb-corrected ^{207}Pb/^{206}Pb dates (Table 3). Four analyses from three grains from sample WDS10 yielded a common Pb-corrected ^{207}Pb/^{206}Pb weighted mean of 1442 ± 250 Ma (MSWD = 3.3), four analyses from two grains from 15WDS16 gave a common Pb-corrected ^{207}Pb/^{206}Pb weighted mean of 1470 ± 58 Ma (MSWD = 2.11, 2σ internal error) and one analysis from one grain from WDS14 gave 1433 ± 74 Ma. Despite the low precision of the individual analyses, we consider the age difference between the dykes insignificant relative to the analytical uncertainty. Combining all valid analyses from WDS10, WDS14 and 15WDS16 yields a ^{207}Pb/^{206}Pb weighted mean age of 1458 ± 76 Ma (MSWD = 2.09; n = 9, six grains).

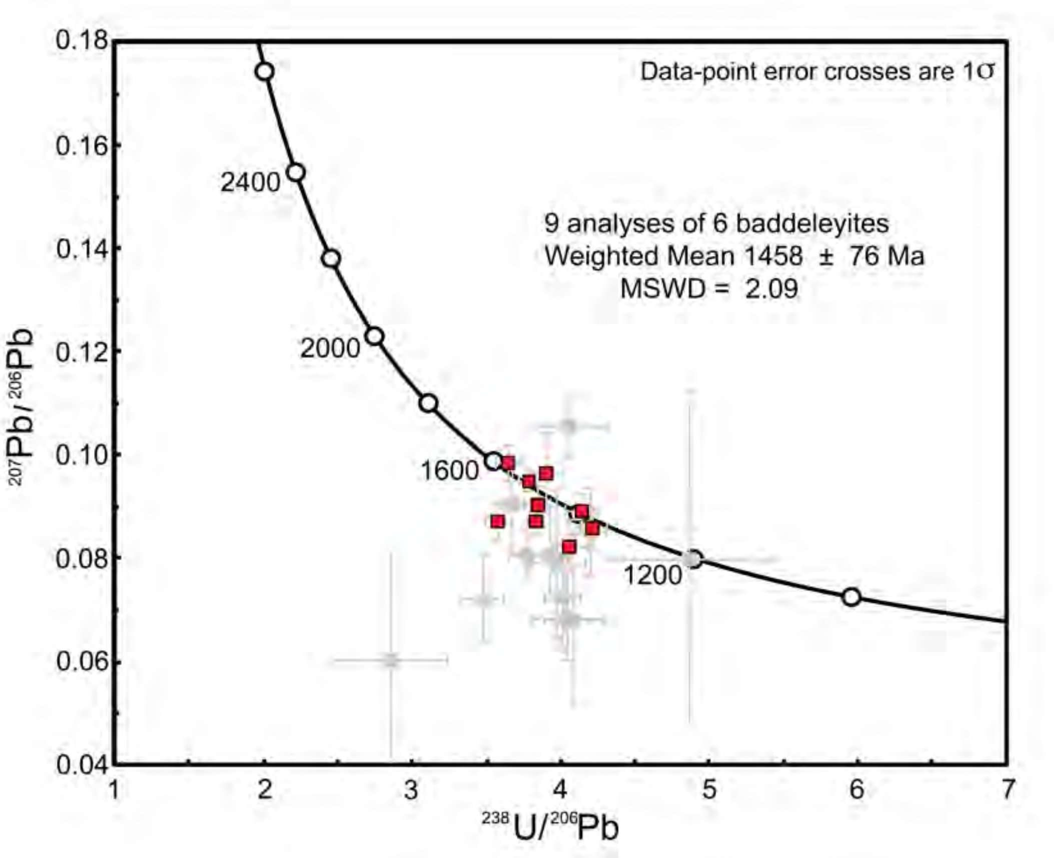

Figure 6.6 Tera-Wasserburg plot of SHRIMP U-Pb baddeleyite results for samples WDS10, WDS14 and 15WDS16. Grey squares denote excluded data (see section 5.7.1 and Table 6.3 for details)

6.7.2 ID-TIMS U-Pb geochronology

Four baddeleyite crystals were analyzed from sample WDS10 (Table 6.4, Figure 6.7). Calculated weights are on the order of 0.1 µg, with low calculated U concentrations between 21 ppm and 80 ppm. Calculated U concentrations are unusually low for baddeleyite and this may reflect an overestimate of the grain weights, but the low Pb abundance (both radiogenic and common Pb) also implies a low initial U concentration. Th/U ratios are <0.1, a typical value for baddeleyite. Coherence in age of all measured baddeleyite crystals supports our interpretation of the analyses representing a single magmatic crystallization age. The weighted mean $^{207}Pb/^{206}Pb$ age of the four concordant single-crystal analyses is 1389 ± 14 Ma (2σ, n = 4, MSWD = 0.57) and the weighted mean $^{206}Pb/^{238}U$ age of these analyses is 1389.9 ± 3.0 Ma (2σ, n = 4, MSWD = 1.4). This precise 1390 ± 3 Ma age is within the uncertainty of our baddeleyite SHRIMP U-Pb $^{207}Pb/^{206}Pb$ date of 1458 ± 76 Ma, and is therefore considered as the best estimate of the crystallisation age of the sampled dykes.

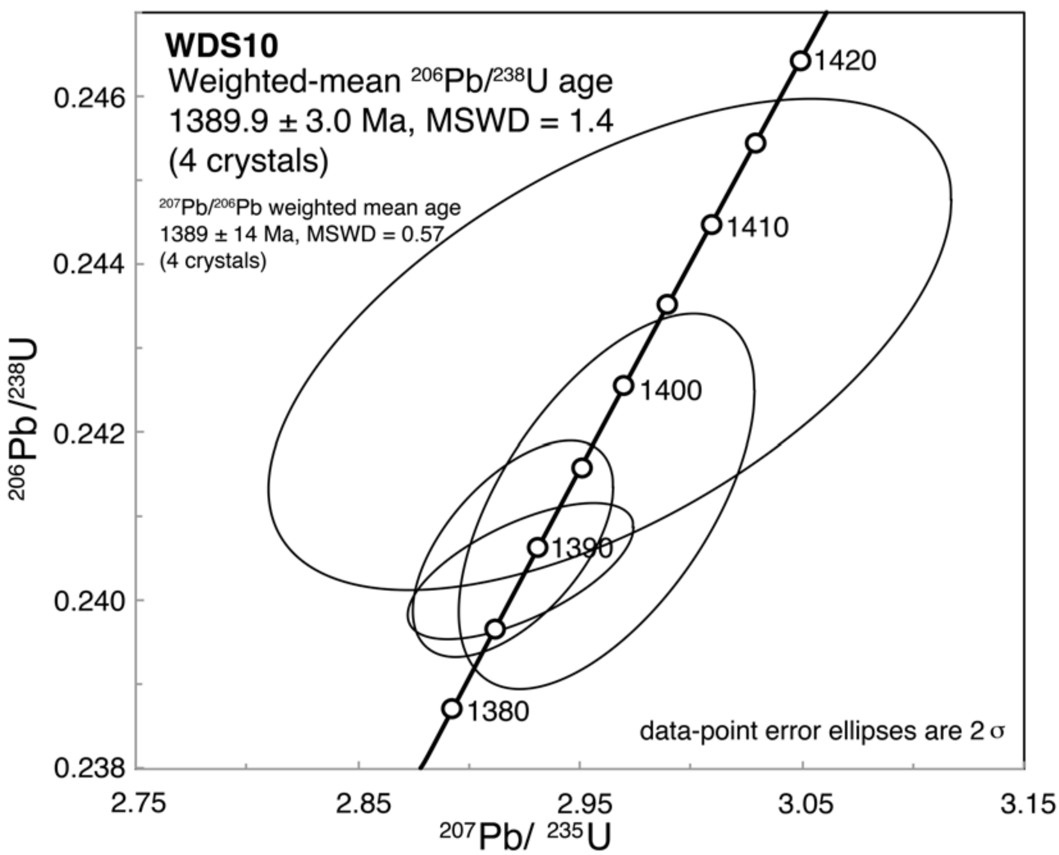

Figure 6.7 Concordia plot for analysed baddeleyite ID-TIMS U-Pb results from sample WDS10

6.7.3 Geochemistry

Due to limited age control, only four samples from three dykes were available for geochemical analyses. Consequently, only preliminary conclusions about the geochemical characteristics of the dykes can be made. Two samples from WDS10, one sample from WDS14 and one sample from 15WDS16 were analysed for major and trace elements and for Sr and Nd isotopes. Data for the samples are presented together with major and trace element geochemistry from the 1210 Ma Marnda Moorn and the 1888 Ma Boonadgin dykes.

6.7.3.1 Major and trace elements

Three samples have LOI <1.0 wt% and one (15WDS16A) has LOI of 1.63%. All samples display low MgO (5.99-6.90 wt%), moderate SiO_2 (49.02-50.84 wt%), FeO_{tot} (12.92-14.55 wt%) and CaO (9.55-10.48 wt%), and moderate to high Al_2O_3

(13.31-14.29 wt%) (Table 6.5). All samples have moderate total alkalis (Na_2O + K_2O = 2.79-3.08 wt%) and Na_2O/K_2O ratios (2.54-3.81). The sampled dykes are classified as sub-alkaline basalts on the TAS diagram (Figure 6.8A; Irvine and Baragar, 1971; Le Maitre et al., 1989) and belong to the tholeiitic series on the AFM diagram (Figure 6.8B; Irvine and Baragar, 1971), similar to Group 1 of the ca. 1210 Ma Marnda Moorn LIP (Wang et al., 2014) and the ca. 1888 Ma Boonadgin dykes (Stark et al., in press). The chondrite-normalised rare earth element patterns (Figure 6.8C) shows moderate enrichment of light REE (LREE) with La_N/Yb_N = 4.50 to 4.80 and La_N/Sm_N = 2.40 to 2.51, whereas the heavy REE (HREE) profiles are flat, with low Tb_N/Yb_N ratios (1.32 to 1.37) slightly higher than the average values of N-MORB and E-MORB (1.0; Sun and McDonough, 1989). The primitive mantle-normalised trace element patterns show depletion of high field strength elements (HFSE) with prominent negative Nb-Ta and slightly negative Zr-Hf and Ti anomalies (Figure 6.8D) and enrichment in Cs, Rb and Ba (large ion lithophile elements LILEs, not shown).

6.7.3.2 Nd and Sr Isotopes

All four samples were analysed for Nd and Sr isotopes (Table 6.5). Ratios of $^{147}Sm/^{144}Nd$ and $^{143}Nd/^{144}Nd$ are 0.1355–0.1380 and 0.511845–0.511877, respectively. The corresponding initial εNd_{1389Ma}values range from -4.4 to -4.5, which are much lower than the inferred lower estimate of εNd_{DM} = +4.8 for the contemporaneous depleted mantle (calculated using the method of DePaolo, 1981), suggesting involvement of an enriched reservoir (crustal component or enriched subcontinent lithospheric mantle). The $^{87}Rb/^{86}Sr$ ratio ranges from 0.2398 to 0.8046 and the $^{87}Sr/^{86}Sr$ ratio from 0.710143 to 0.726251, the corresponding initial ratios $(^{87}Sr/^{86}Sr)_{1390\ Ma}$ varying from 0.70497 to 0.71050. The latter are significantly higher than 0.7017 estimated for contemporaneous mantle (calculated using $^{87}Rb/^{86}Sr$ = 0.046 and $^{87}Sr/^{86}Sr$ = 0.7026 for modern depleted mantle; Taylor and McLennan, 1985) and also suggest involvement of an enriched reservoir or an effect of alteration of the Rb-Sr isotope system. In contrast with the uniform initial Nd isotopes, the wide range of initial Sr isotope compositions and positive correlation between LOI and the initial $^{87}Sr/^{86}Sr$ ratios (not shown) suggest mobility of Rb during alteration, leading to disturbance of the Rb-Sr isotope system. Consequently, Sr isotope data are excluded from the following discussion.

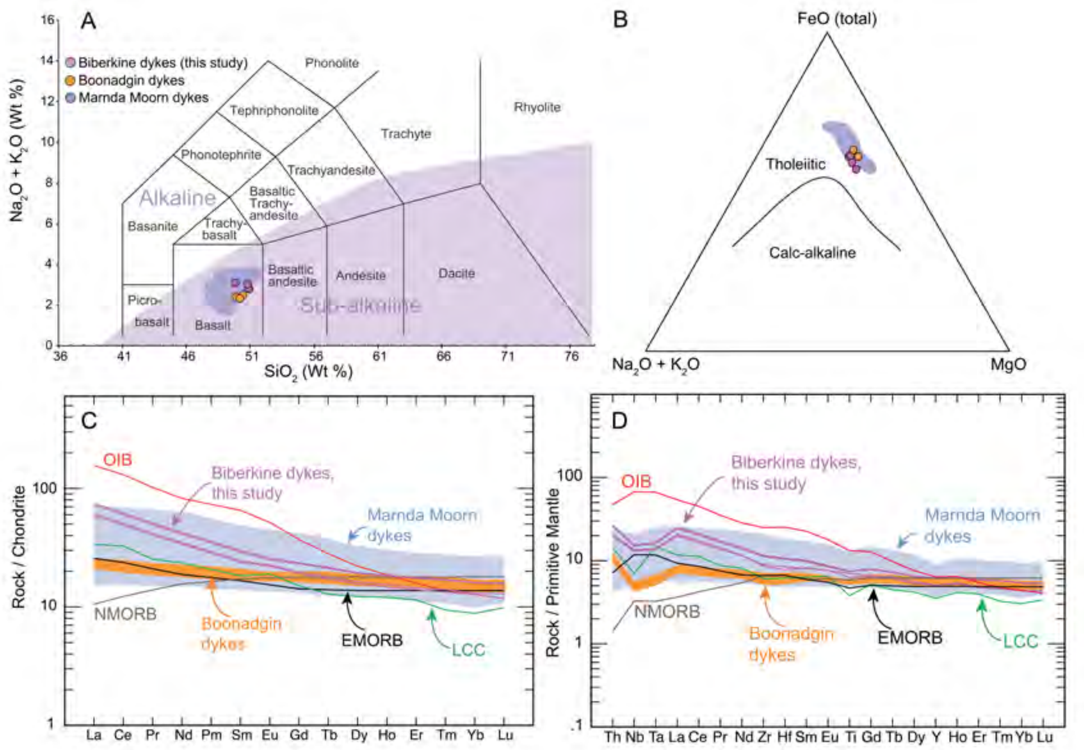

*Figure 6.8 (**A**) Total alkali-silica (TAS) plot after LeMaitre (1989) with alkaline-sub-alkaline boundary after Irvine and Baragar (1971). Orange dots denote ca. 1888 Ma Boonadgin dykes from Stark at al. (in press) and blue field the ca. 1210 Ma Marnda Moorn group 1 dykes from Wang et al. (2014). (**B**) AFM plot after Irvine and Baragar (1971). (**C**) Chondrite and (**D**) primitive mantle normalised multi-element plots for Biberkine, Boonadgin and Marnda Moorn group 1 dykes. LCC = lower continental crust after Rudnick and Gao (2004); OIB = ocean island basalt, NMORB = mid ocean ridge basalt and EMORB = enriched MORB after Sun and McDonough (1989).*

6.8 Discussion

We have identified a previously unknown Mesoproterozoic NNW-trending mafic dyke swarm in the southwestern Yilgarn Craton, here named the Biberkine dykes. Aeromagnetic data suggest that the dyke swarm extends several hundred kilometers across the South West Terrane, truncated by the Albany-Fraser Orogen in the south and the Darling Fault in the west (Figure 6.1). However, until further sampling

Table 6.3 SHRIMP U-Pb data for baddeleyite from dyke samples WDS10, WDS14 and 15WDS16. Note common Pb and discordance thresholds of 1.58 % and 18 %, respectively, for accepted analyses.

Spot	f_{206} %	U ppm	Th ppm	Th/U	±%	Total $^{238}U/^{206}Pb$	±%	Total $^{207}Pb/^{206}Pb$	±%	$^{238}U/^{206}Pb^*$	±%	$^{207}Pb^*/^{206}Pb^*$	±%	$^{206}Pb^*/^{238}U$ Age (Ma) ± 1σ		$^{207}Pb^*/^{206}Pb^*$ Age (Ma) ± 1σ		Disc. %
WDS10C1.11B-1	0.25	246	21.5	0.090	5.8	3.64	2.3	0.101	2.7	3.65	2.3	0.098	3.5	1563	±32	1595	±66	+2
WDS10C2.44B-1	0.83	256	37.4	0.151	1.3	4.19	2.1	0.093	2.5	4.22	2.2	0.086	4.9	1371	±27	1336	±96	-3
WDS10C4.177B-2	1.04	151	7.3	0.050	5.1	4.02	2.9	0.091	2.8	4.06	2.9	0.082	6.3	1418	±37	1252	±123	-15
WDS10C4.177B-3	0.60	203	10.0	0.051	2.5	3.56	2.5	0.092	2.4	3.58	2.5	0.087	4.3	1588	±35	1365	±82	-18
WDS14B1.109B-1	0.26	181	13.6	0.078	1.9	3.84	2.3	0.093	2.9	3.85	2.3	0.090	3.9	1489	±30	1433	±74	-4
15WDS16B2R.258B-1	1.35	53	1.2	0.023	5.0	3.85	3.1	0.108	3.5	3.91	3.2	0.096	8.1	1470	±42	1557	±152	+6
15WDS16B2R.258B-2	0.18	231	11.5	0.052	1.5	3.78	1.7	0.097	1.7	3.78	1.7	0.095	2.1	1512	±22	1527	±39	+1
15WDS16B1.248B-1	1.58	308	52.0	0.175	2.9	4.08	2.6	0.103	1.2	4.14	2.6	0.089	3.6	1394	±33	1407	±68	+1
15WDS16B1.248B-2	1.21	330	88.9	0.279	1.9	3.79	1.5	0.098	1.9	3.84	1.5	0.087	3.1	1493	±20	1365	±61	-10
Excluded analyses																		
WDS10C1.10B-1	3.20	119	9.3	0.081	5.2	3.88	2.9	0.099	3.7	4.01	3.1	0.072	14.5	1435	±40	995	±294	-49
WDS10C1.10B-2	9.72	155	20.8	0.139	9.0	2.58	13.2	0.140	3.4	2.85	13.5	0.060	34.7	1936	±225	615	±749	-250
WDS10C4.177B-1	1.31	175	8.9	0.053	3.9	3.73	3.5	0.092	2.5	3.78	3.5	0.081	6.4	1513	±48	1211	±126	-28
WDS14B2.187B-1	6.23	114	6.9	0.063	2.9	3.84	4.7	0.120	3.5	4.09	5.1	0.068	24.4	1409	±64	870	±505	-69
WDS14B2.187B-2	3.03	222	18.1	0.084	2.0	3.37	4.1	0.097	2.7	3.47	4.2	0.072	11.6	1631	±61	988	±235	-74
WDS14B3.191B-1	3.81	314	50.1	0.165	2.8	3.89	5.6	0.100	2.5	4.04	5.7	0.068	12.3	1426	±73	882	±254	-69
WDS14B1.109B-2	--	163	12.0	0.076	2.6	4.08	6.7	0.102	5.0	4.06	6.7	0.106	5.8	1419	±85	1724	±107	+20

Table 6.3 *continued*

Spot	f_{206} %	U ppm	Th ppm	Th/U	±%	Total ^{238}U / ^{206}Pb	±%	Total ^{207}Pb / ^{206}Pb	±%	^{238}U / $^{206}Pb^*$	±%	$^{207}Pb^*$ / $^{206}Pb^*$	±%	$^{206}Pb^*/^{238}U$ Age (Ma) ± 1σ		$^{207}Pb^*/^{206}Pb^*$ Age (Ma) ± 1σ		Disc. %
WDS14B2.184B-1	5.88	81	5.8	0.074	2.9	3.99	3.4	0.103	5.2	4.24	3.8	0.055	27.4	1366	±47	427	±610	-245
WDS14B3.192B-1	24.75	47	5.2	0.116	3.9	3.66	8.1	0.169	5.8	4.87	11.6	0.080	40.6	1204	±127	1196	±801	-1
WDS14B3.192B-2	8.42	40	2.3	0.059	5.4	4.35	5.2	0.085	11.3	4.75	7.0	0.016	239.4	1231	±78			
15WDS16B2R.266B-1	2.24	68	6.0	0.092	2.3	4.11	2.7	0.104	3.2	4.20	2.8	0.085	10.2	1376	±35	1320	±197	-5
15WDS16B2R.266B-2	6.53	94	6.7	0.073	4.6	3.72	4.4	0.134	2.8	3.98	4.7	0.079	17.9	1445	±61	1170	±355	-26
15WDS16B2R.266B-3	2.56	71	6.2	0.091	2.1	3.83	2.7	0.102	3.1	3.93	2.9	0.081	11.2	1460	±37	1215	±220	-22
15WDS16B1.246B-1	4.26	297	29.4	0.102	1.3	3.52	1.8	0.127	4.8	3.68	2.0	0.090	10.7	1551	±27	1436	±204	-9

Notes **1)** f_{204} is the proportion of common Pb in ^{206}Pb, determined using the measured $^{204}Pb/^{206}Pb$ and a common Pb composition from the Stacey and Kramers (1975) model at the approximate age of the sample **2)** Disc. = 100(t[$^{207}Pb^*/^{206}Pb^*$] - t[$^{238}U/^{206}Pb^*$/])/t[$^{207}Pb^*/^{206}Pb^*$]

Table 6.4 ID-TIMS U-Pb data for baddeleyite from dyke WDS10

Notes **1)** All uncertainties given at 2σ **2)** ρ = error correlation coefficient of radiogenic $^{207}Pb/^{235}U$ vs. $^{206}Pb/^{238}U$ **3)** Pb_c = Total common Pb including analytical blank (0.8±0.3 pg per analysis) **4)** Blank composition is: $^{206}Pb/^{204}Pb = 18.55 \pm 0.63$, $^{207}Pb/^{204}Pb = 15.50 \pm 0.55$, $^{208}Pb/^{204}Pb = 38.07 \pm 1.56$ (all 2σ), and a $^{206}Pb/^{204}Pb$ – $^{207}Pb/^{204}Pb$ correlation of 0.9. **5)** Th/U calculated from radiogenic $^{208}Pb/^{206}Pb$ age **6)** Sample weights are calculated from crystal dimensions and are associated with as much as 50% uncertainty (estimated) **7)** Measured isotopic ratios corrected for tracer contribution and mass fractionation (0.02 ± 0.06 %/amu) **8)** Ratios involving ^{206}Pb are corrected for initial disequilibrium in $^{230}Th/^{238}U$ using Th/U = 4 in the crystallization environment

Sampl	wt. (µg)	U (ppm	Pb_c (pg)	mol%_Pb*	$\frac{Th}{U}$	$\frac{^{206}Pb}{^{204}Pb}$	$\frac{^{207}Pb}{^{206}Pb}$	± (%)	$\frac{^{207}Pb}{^{235}U}$	± (%)	$\frac{^{206}Pb}{^{238}U}$	± (%)	ρ	$^{206}Pb/^{238}U$ Age (Ma)	± (Ma)	$^{207}Pb/^{206}Pb$ Age (Ma)	± (Ma)
1	0.3	80	1.6	53	0.04	90	0.08821	1.26	2.9233	1.42	0.24036	0.28	.65	1388.5	3.8	1387.0	24.2
2	0.1	21	1.9	20	0.02	35	0.08842	3.75	2.9635	4.24	0.24305	0.98	.59	1402.5	13.8	1391.7	71.9
3	0.1	44	0.8	54	0.01	88	0.08801	1.07	2.9199	1.26	0.24062	0.44	.57	1389.9	6.1	1382.7	20.6
4	0.3	25	0.9	39	0.03	56	0.08907	1.52	2.9620	1.84	0.24118	0.76	.59	1392.8	10.5	1405.6	29.1

Table 6.5 Major, trace element and isotope data for samples

Notes **1)**Major elements (XRF) are given in wt % and trace elements (ICP-MS) in ppm **2)** Mg# = 100 x Mg/(Mg+Fe), Fe^{2+}/Fe_{total}=0.85
3) Crystallisation age t = 1890 Ma **4)** typical internal precision (2σ) is ±0.000015 for $^{87}Sr/^{86}Sr$ and ±0.000014 for $^{143}Nd/^{144}Nd$ **5)** Recent isotope dilution analyses for USGS basalt standard BCR-2 average 6.41 ppm Sm, 28.02 ppm Nd, $^{147}Sm/^{144}Nd$ 0.1381±0.0004 and $^{143}Nd/^{144}Nd$ 0.512635±0.000023 (n=6, ±2sd); 46.5 ppm Rb, 337.6 ppm Sr, $^{87}Rb/^{86}Sr$ 0.3982±0.0010, $^{87}Sr/^{86}Sr$ 0.704987±0.000015 (n=1, ±2se). These results are consistent with TIMS and MC-ICPMS reference values. e_{Nd} values are calculated relative to a modern chondritic mantle (CHUR) with $^{147}Sm/^{144}Nd$ = 0.1960 and $^{143}Nd/^{144}Nd$ = 0.512632 (Bouvier et al., 2008). Age-corrected initial e_{Nd} and $^{87}Sr/^{86}Sr$ have propagated uncertainties of ±0.5 units and ≤±0.00010 (assuming an age uncertainty of ±5 Ma), respectively. Decay constants are ^{87}Rb 1.395E^{-11}/yr and ^{147}Sm 6.54E^{-12}/yr.

	WDS10D	WDS10E	WDS14B	15WDS16A
SiO_2	50.61	50.63	50.84	49.02
TiO_2	1.63	1.64	1.38	1.51
Al_2O_3	13.65	13.65	14.29	13.31
CaO	10.1	9.9	10.48	9.55
$Fe_2O_{3(tot)}$	14.36	14.47	12.92	14.55
K_2O	0.68	0.85	0.58	0.73
MgO	5.99	6.01	6.79	6.9
MnO	0.21	0.22	0.21	0.24
Na_2O	2.16	2.16	2.21	2.35
P_2O_5	0.185	0.186	0.152	0.161
LOI	0.46	0.39	0.3	1.63

Table 6.5 *continued*

ID-TIMS	WDS10D	WDS10E	WDS14B	15WDS16A
Sm (ppm)	4.29	4.33	3.62	3.51
Nd (ppm)	18.86	19.07	16.12	15.34
$^{143}Nd/^{144}Nd$	0.511868	0.511864	0.511845	0.511877
$^{147}Sm/^{144}Nd$	0.1375	0.1372	0.1355	0.138
$(^{143}Nd/^{144}Nd)_i$	0.510612	0.510611	0.510607	0.510616
εNd(t)	-4.5	-4.5	-4.6	-4.4
Rb (ppm)	27.55	35.78	19.02	49.05
Sr (ppm)	189.8	189.8	229.5	176.7
$^{87}Rb/^{86}Sr$	0.4201	0.4201	0.2398	0.8046
$^{87}Sr/^{86}Sr$	0.713193	0.713193	0.710143	0.726251
$(^{87}Sr/^{86}Sr)_i$	0.70496648	0.70497	0.70545	0.7105

	WDS10D	WDS10E	WDS14B	15WDS16A
Total	100.04	100.11	100.15	99.96
Mg#	49.30	49.19	55.06	52.50
Sc	41.2	41.2	40.4	41
V	337	335	296	306
Co	50.5	50.9	48.6	50.4
Ni	55	57.2	69.4	65.8
Ga	18.2	18.5	17.5	17.2
Ge	533	529	529	522
Rb	27.9	37.2	19.8	43.1
Sr	193	203	236	188
Y	28	28.5	22.7	23.4
Zr	127	131	103	97.1
Nb	10.7	11.1	9.27	9.37
Cs	1.83	1.7	1.38	1.83
Ba	212	227	209	165
La	16.9	17.5	14.4	13.8
Ce	36.5	37.7	31.1	29.7
Pr	4.64	4.78	3.94	3.81
Nd	19.1	19.6	16.2	15.9
Sm	4.4	4.52	3.7	3.71
Eu	1.43	1.48	1.28	1.3
Gd	4.71	4.8	3.89	4.01
Tb	0.782	0.8	0.641	0.661

Table 6.5 *continued*

ID-TIMS	BCR-2	JND-1
$^{143}Nd/^{144}Nd$	0.512637	0.512112
	0.512640	0.512117
	0.512623	0.512102
	0.512633	
$^{87}Sr/^{86}Sr$	0.704987	
	0.705013	

	WDS10D	WDS10E	WDS14B	15WDS16A
Dy	4.83	4.89	3.95	4.12
Ho	1.03	1.04	0.829	0.866
Er	2.85	2.91	2.3	2.38
Tm	0.426	0.431	0.342	0.354
Yb	2.69	2.72	2.15	2.2
Lu	0.398	0.401	0.319	0.325
Hf	3.25	3.34	2.63	2.43
Ta	0.658	0.682	0.565	0.567
Pb	4.61	3.34	3.44	3.69
Th	2.24	2.32	1.81	1.68
U	0.461	0.484	0.377	0.365

within the craton allows a better delineation of the extent of the dykes, their designation as a swarm is preliminary. The Biberkine dykes are coeval with several mafic magmatic events worldwide, such as the ca. 1386-1380 Ma Hart River dykes (Abbott, 1997) and the ca. 1379 Ma Salmon River Arch sills (Doughty and Chamberlain, 1996) in North America, the ca. 1384 Ma Chieress dykes in Siberia (Okrugin et al., 1990; Ernst et al., 2000), the ca. 1380 Ma dykes at Vestfold Hills in East Antarctica (Lanyon et al., 1993), the ca. 1382 Ma Zig Zag Dal Formation in Greenland (Upton et al., 2005), the giant Lake Victoria dyke swarm in east Africa (Mäkitie et al., 2014) and the ca. 1385 Ma Mashak igneous event (Ronkin et al., 2005; Ernst et al., 2006). No other mafic magmatism within uncertainty of the 1390 ± 3 Ma age for the Biberkine dykes is currently known in the WAC or elsewhere in Australia and the temporally closest magmatic events within the WAC are the ca. 1360 Ma Gifford Creek carbonatite in the Edmund Basin of the Capricorn Orogen (Zi et al., 2017) and the ca. 1465 Ma mafic sills of the Narimbunna dolerite (Wingate, 2002; Morris and Pirajno, 2005; Sheppard et al., 2010b).

6.8.1 Nature of the mantle source of the Biberkine dykes

Zirconium can be used to evaluate mobility of major and trace elements during alteration and metamorphism (e.g. Polat et al., 2002; Wang et al., 2008, 2014). The Nb, Ta, Hf, Th and REE concentrations in the samples display good correlation with Zr (not shown) indicating that these elements have been unaffected by post-magmatic processes and reflect the primary composition of the magma. The Biberkine dykes display arc-like geochemical characteristics, including depletion of HFSE, unradiogenic initial Nd isotopes and enrichment of LILE and radiogenic Sr isotopes, which may have been imparted either by crustal contamination or inherited from heterogeneous metasomatically enriched source region, or both (Hawkesworth et al., 1990; Hawkesworth, 1993; Puffer, 2001; Zhao et al., 2013; Wang et al., 2016). Crustal contamination during magma ascent would produce synchronous changes between major and trace elements and radiogenic isotope compositions (Brandon et al., 1993; Hawkesworth et al., 1995; Wang et al., 2008, 2014). Relative to rocks sourced from asthenospheric mantle, crustal material is characterised by high La/Sm and Th/La and low Sm/Nd, Nb/La and εNd, and crustal contamination during magma ascent would therefore produce negative and positive correlations, respectively, with Mg# (e.g. Wang et al., 2008, 2014). No such correlations are evident in the data or in the Sm/Nd and Nb/La ratios. The nearly constant initial $\varepsilon Nd_{(t)}$ values, near uniform SiO_2 contents (49.02-50.84 wt%) and incompatible trace element ratios (Sm/Nd = 0.23 and La/Sm = 3.9-3.7) with a large range of Mg# values (49-55) do not support significant crustal contamination in the generation of these dykes. This is supported further by primitive mantle–like trace element ratios of Nb/Ta (16.3-16.5), Zr/Hf (39.1-40.0) and Zr/Sm (26.2-28.9) of the dykes (primitive mantle: Nb/Ta = 17.39, Zr/Hf = 36.25 and Zr/Sm = 25.23; Sun and McDonough, 1989), which are also similar to typical asthenospheric mantle-derived melts, such as MORB (Sun and McDonough, 1989). Although significant crustal contamination appears unlikely, the dykes display arc-like trace element signatures such as depletion of HFSE and enrichment of LILE. These characteristics may be attributed to Earth deep volatile cycling (e.g. Wang et al., 2016) or partial melting of SCLM enriched by previous subduction processes or recycled components (Wang et al., 2008, 2014). On the basis of the above evidence and the unradiogenic initial Nd isotopes, we prefer an interpretation where the predominant source of the dykes is an enriched SCLM. Geochemical analysis of a much larger number of samples across the dyke swarm is required to further constrain the nature of the source of the Biberkine dykes.

The flat HREE profiles of the 1390 Ma Biberkine, 1888 Ma Boonadgin and 1210 Ma Marnda Moorn dykes indicate that partial melting likely occurred within the spinel stability field (at <75 km depth), suggesting that the SCLM at least beneath and near the margin of the Yilgarn Craton may have been largely removed or thinned sometime before 1888 Ma. Smithies et al. (1999) argued for a craton-wide delamination of the lower crust at ca. 2650 Ma during the final stages of cratonisation and seismic data from eastern Yilgarn Craton supports presence of a delaminated lower crustal layer that foundered in the upper mantle (Blewett et al., 2010). Moreover, evidence for a mafic-ultramafic layer in the lower crust beneath the southwestern Yilgarn Craton may be related to underplating during crustal extension (Dentith et al., 2000). The Biberkine and Boonadgin dykes, although separated by ca. 500 m.y. in age, were emplaced through the same SCLM because they were sampled in areas where they outcrop close to each other (Figure 6.2). Whereas the Boonadgin dykes have similar primitive mantle-normalised profiles and LCC-like trace element ratios, they have significantly higher $\varepsilon Nd_{(t)}$ values of +1.3 to +1.6 (Stark et al., in press) than the Biberkine dykes, suggesting that their source involved a higher proportion of depleted mantle with less contribution from the enriched component. The enriched LREE, LILE and isotopic compositions of both the Biberkine and the Boonadgin dykes could have been produced either via mixing of lower crust and depleted asthenospheric mantle, or through interaction between asthenospheric mantle and metasomatically enriched regions within the SCLM (and possibly the lower crust) that formed during earlier subduction events.

6.8.2 Tectonic setting of the WAC at 1390 Ma

The interval between ca. 1600-1350 Ma is considered a period of relative tectonic quiescence in the West Australian Craton, characterised by the formation of extensive basins in a passive margin setting along the southern and southeastern margins of the craton (Spaggiari et al., 2015). Aitken et al. (2016) argued that reorganization of Nuna to Rodinia occurred between ca. 1500 Ma and 1300 Ma and involved relative motion and rotation between the South Australian/Mawson cratons and the West and North Australian cratons. They suggested that this adjustment was responsible for the renewed subduction along the southern and southeastern margins of the craton. If this model is correct, and the subduction was west dipping, the Biberkine dykes may be a direct consequence of the plate movement during this transition. Alternatively, regional dyke swarms may be associated with laterally injected magma propagating from a distal plume (Baragar et al., 1996; Ernst and Buchan, 1997, 2001a). If this were the case, the trace element profiles of the Biberkine dykes could reflect compositional variation in the SCLM and the lower crust at a much greater distance.

Paleogeographic reconstructions at ca. 1400 Ma suggest that the southern and southeastern margins of the West Australian Craton were in a back-arc setting, converging with the northwestern margin of the Mawson Craton (Figure 6.9) (Boger, 2011; Kirkland et al., 2011; Spaggiari et al., 2011, 2014b, 2015, Aitken et al., 2014, 2016). This NW-SE movement led to Albany-Fraser Orogeny stage 1 at ca. 1345 Ma with continent-continent collision inferred at ca. 1310-1290 Ma (Clark et al., 2000; Bodorkos and Clark, 2004a, 2004b; Aitken et al., 2016), although some workers suggest that this represents a west-directed soft collision at ca. 1310 Ma involving accretion of the oceanic Loongana arc (Madura Province; Figure 6.9 and Figure 6.10) to the southeastern margin of the West Australian Craton (Spaggiari et al., 2015). Aitken et al. (2016) argue that after predominantly east-dipping subduction and clockwise rotation of the Mawson Craton until ca. 1400 Ma, a switch in polarity

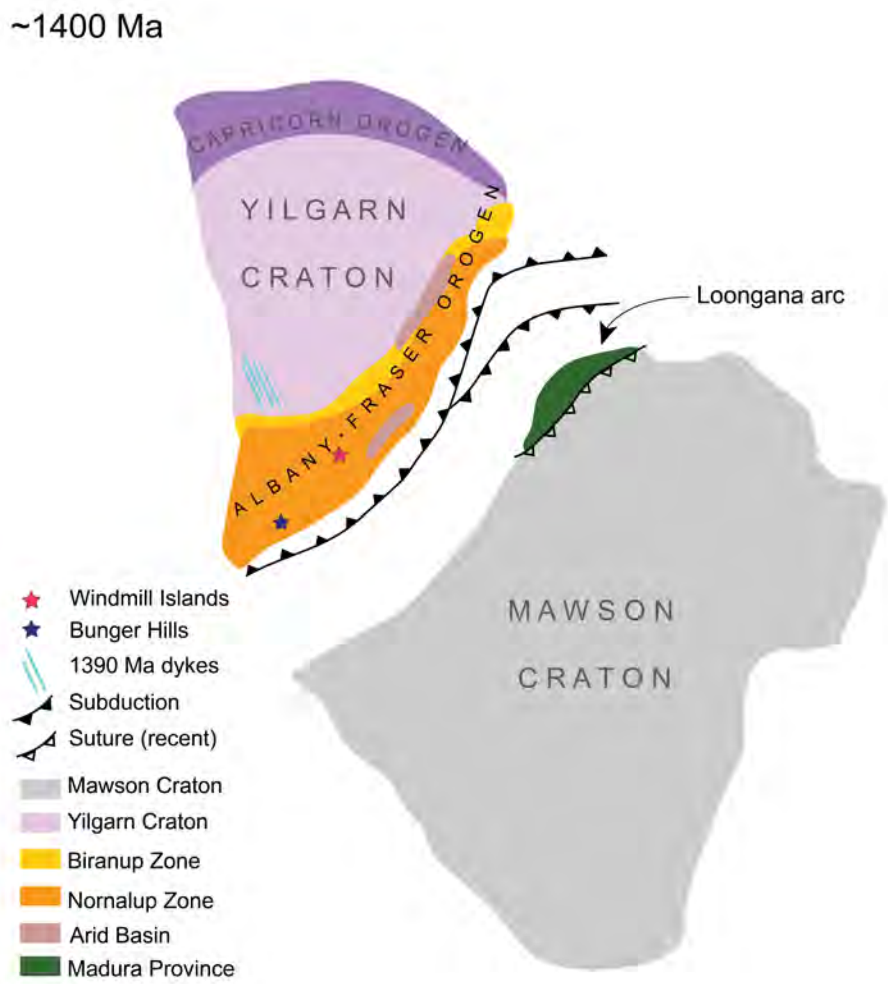

Figure 6.9 Simplified paleogeographic reconstruction of the Yilgarn and Mawson cratons at ca. 1400 Ma. Modified after Aitken et al. (2016), only the Yilgarn Craton and Capricorn Orogen of the WAC and the northern part of the Mawson Craton are shown. Note stars denoting the inferred original locations of Bunger Hills and Windmill Islands (based on interpretations of Tucker et al., 2017 and Morrissey et al., 2017, respectively).

to west-dipping subduction beneath the West Australian Craton ended in hard collision at ca. 1290 Ma. Further evidence for a change in tectonic setting from passive to a convergent margin is recorded in the Arid Basin in eastern Albany-Fraser Orogen (Figure 6.9 and Figure 6.10), where detritus previously sourced predominantly from the Yilgarn Craton became dominated by input from the approaching Loongana arc at ca. 1425 Ma (Spaggiari et al., 2014b, 2015).

It is difficult to link the 1390 Ma mafic magmatism in the southwestern Yilgarn Craton directly with known contemporaneous tectonic or magmatic events within the West Australian Craton because there is limited evidence for tectonic activity between ca. 1400 Ma and 1345 Ma (Aitken et al., 2016). However, a small ca. 1388 Ma detrital zircon population in the Fraser Complex in southeastern Albany-Fraser Orogen suggests coeval active magmatism (Clark et al., 1999; Spaggiari et al., 2009). Furthermore, ca. 1390-1370 Ma inherited and detrital zircon populations have been identified at the Windmill Islands and zircon rim growth at ca. 1397-1368 Ma at Bunger Hills in East Antarctica, both of which have been interpreted as part of the Albany-Fraser Orogen during the Mesoproterozoic (Figure 6.9 and Figure 6.10) (Zhang et al., 2012; Morrissey et al., 2017; Tucker et al., 2017). At ca. 1410 Ma, the Arid Basin (ca. 1600-1305 Ma, Figure 6.9 and Figure 6.10) likely formed in a passive margin setting with east-dipping subduction of the Yilgarn Craton crust beneath the Loongana oceanic arc (Spaggiari et al., 2011, 2014b, 2015) or as a back-arc basin with west-dipping subduction of the approaching Loongana arc from the east beneath the Yilgarn Craton (Morrissey et al., 2017). The ca. 1415-1400 Ma magmatism in the Madura Province (Figure 6.9 and Figure 6.10) has also been interpreted as evidence for subduction (Kirkland et al., 2013; Spaggiari et al., 2014b; Aitken et al., 2016). Collectively, this evidence suggests the presence of an active subduction zone and NW-directed convergence along the southeastern (and possibly southern) margin of the Yilgarn Craton at ca. 1410-1310 Ma. If the Biberkine dykes are associated with subduction (back-arc extension or intracontinental rifting), this implies presence of a west dipping subduction zone as suggested by Morrissey et al. (2017) and Aitken et al. (2016). Alternatively, if the dykes intruded through lateral propagation of magma from a distal source, their emplacement could be due to intracontinental rifting and lithospheric extension associated with a mantle plume.

The Capricorn Orogen north of the Yilgarn Craton (Figure 6.1) formed during assembly of the West Australian Craton during the Glenburgh Orogeny at 2005-1950 Ma and was subjected to repeated episodic intracontinental reworking and reactivation over the following billion years (Cawood and Tyler, 2004; Sheppard et al., 2004, 2010a; Johnson et al., 2011). Hydrothermal monazite in the Abra polymetallic deposit in the Edmund Basin (Figure 6.1) records a tectonothermal event at 1375 ± 14 Ma, possibly a regional-scale episode of intracontinental reworking (Zi et al., 2015). The ca. 1360 Ma Gifford Creek carbonatite complex, also in the Edmund Basin, occurs within a major crustal suture, and may have formed in response to reactivation of this suture during far field stresses associated with plate reorganization (Zi et al., 2017). The ca. 1888 Ma Boonadgin dyke swarm in the southwestern Yilgarn Craton has also been linked with possible far-field tectonic stresses and lithospheric extension in the eastern Capricorn Orogen (Stark et al., in press), where coeval felsic volcanic rocks were emplaced during limited rifting at ca. 1891-1885 Ma (Rasmussen et al., 2012; Sheppard et al., 2016).

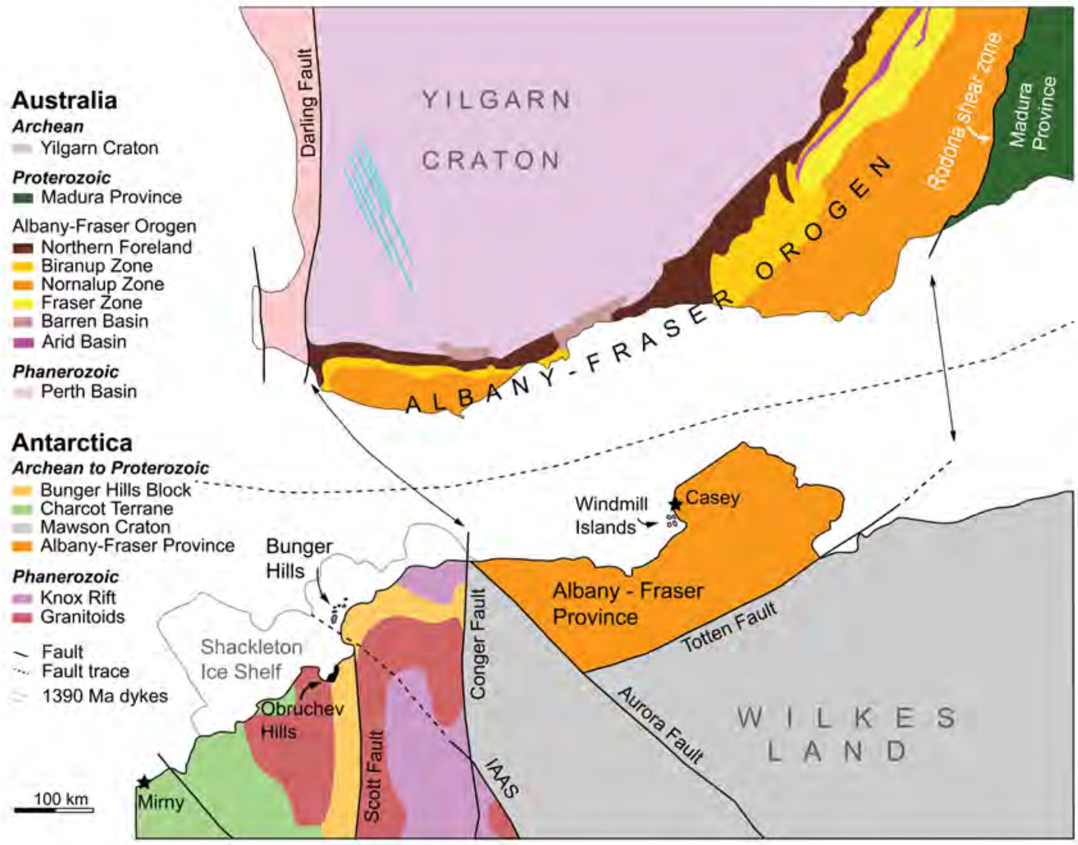

Figure 6.10 Possible configuration of the Yilgarn and Mawson cratons during the Mesoproterozoic showing common tectonic elements between the Yilgarn Craton, Bunger Hills and Windmill Islands. Modified after Aitken et al. (2016) and Tucker et al. (2017, 2015). Interpreted bedrock geology of Western Australia (Geological Survey of Western Australia, 2015). Piercing points of between the Darling–Conger and Rodona–Totten Faults are from Aitken et al. (2014, 2016).

Emplacement of the NNW-trending Biberkine dykes indicates regional SSW-NNE oriented lithospheric extension, which is consistent with interpreted NW-trending convergence and subduction along the southeastern craton margin. The orientation of the dykes is roughly parallel to the regional NW-SE tectonic grain imparted by terrane accretion during the Archean (Middleton et al., 1993; Wilde et al., 1996; Dentith and Featherstone, 2003) and suggests that, like the NW-trending 1889 Ma Boonadgin dyke swarm (Stark et al., in press), they intruded along existing crustal weaknesses controlled by a regional stress field (Hou et al., 2010; Hou, 2012; Ju et al., 2013). This may be supported by the presence of a ca. 20° NE-dipping high-velocity zone at ca. 30 km depth south of sample 15WDS16, interpreted as a mafic-ultramafic body in the lower crust that could represent a conduit for mafic magma that intruded along the suture (Dentith et al., 2000; Dentith and Featherstone, 2003).

6.9 Conclusions

Newly discovered NNW-trending ca. 1390 Ma mafic dykes, here named the Biberkine dykes, have been identified in the southwestern Yilgarn Craton in Western Australia using *in situ* SHRIMP and ID-TIMS U-Pb methods. The extent of the dyke swarm is unknown but in aeromagnetic data they appear to extend several hundred kilometres across the South West Terrane. The Biberkine dykes are coeval with a number of other mafic dyke swarms worldwide and thus provide an important target for paleomagnetic studies. Preliminary geochemical analysis indicates that the dykes have tholeiitic compositions with a significant contribution from metasomatically enriched subcontinental lithosphere and/or lower crust. Current models for the Yilgarn Craton infer a tectonically quiescent period between ca. 1600 Ma and 1345 Ma but indirect evidence from the Albany-Fraser Orogen and from Windmill Islands and Bunger Hills in East Antarctica support renewed subduction along the southeastern and possibly southern margin of the craton by ca. 1410 Ma. Paleogeographic reconstructions suggest that this was a result of relative motion and rotation between the West Australian, South Australian and Mawson cratons and represents transition from Nuna to Rodinia configuration for the three cratons. The 1390 Ma Biberkine dykes are likely a direct consequence of this transition and mark the change from passive to active tectonic setting, which culminated in the Albany-Fraser Orogeny at ca. 1330 Ma.

6.10 Acknowledgments

This work was funded by ARC Centre for Core to Crust Fluid Systems CoE Grant (CE110001017) and ARC Laureate Fellowship Grant (FL150100133) to Z.-X.L. JCS was supported by Curtin University ORD Postgraduate Scholarship. We thank Cristina Talavera and Hao Gao for their support with SHRIMP U-Pb analyses at John de Laeter Centre, Curtin University. We also thank Roland Maas and Nenping Shen for their valuable assistance with geochemical analyses and Louise Heyworth for her help with sample preparation at UWA.

6.11 References

Abbott, G., 1997. Geology of the Upper Hart River Area, Eastern Ogilvie Mountains, Yukon Territory (9116A/10, 116A/11) Bulletin 9. Indian and Northern Affairs Canada, Exploration and Geological Services Division.

Aitken, A.R.A., Betts, P.G., Young, D.A., Blankenship, D.D., Roberts, J.L., Siegert, M.J., 2016. The Australo-Antarctic Columbia to Gondwana transition. Gondwana Res. 29, 136–152.

Aitken, A.R.A., Young, D.A., Ferraccioli, F., Betts, P.G., Greenbaum, J.S., Richter, T.G., Roberts, J.L., Blankenship, D.D., Siegert, M.J., 2014. The subglacial geology of Wilkes Land, East Antarctica. Geophys. Res. Lett. 41, 2390–2400.

Anand, R.R., Paine, M., 2002. Regolith geology of the Yilgarn Craton, Western Australia: implications for exploration. Aust. J. Earth Sci. 49, 3–162.

Barley, M.E., Brown, S.J.A., Cas, R.A.F., Cassidy, K.F., Champion, D.C., Gardoll, S.J., Krapež, B., 2003. An integrated geological and metallogenic framework for the eastern Yilgarn Craton: developing geodynamic models of highly mineralised Archaean granite–greenstone terranes. AMIRA Project P624.

Baxter, J.L., Lipple, S.L., Playford, P.E., Low, G.H., Lowry, D.C., 1980. Pinjarra, WA Sheet SI 50-2, Geological Survey of Western Australia 1:250 000 Geological Series Maps.

Bleeker, W., Ernst, R., 2006. Short-lived mantle generated magmatic events and their dyke swarms: the key unlocking Earth's paleogeographic record back to 2.6 Ga, in: Hanski, E.J., Mertanen, S., Rämö, O.T., Vuollo, J. (Eds.), Dyke Swarms—time Markers of Crustal Evolution: Selected Papers of the Fifth International Dyke Conference in Finland, Rovaniemi, Finland, 31 July- 3 Aug 2005 & Fourth International Dyke Conference, Kwazulu-Natal, South Africa 26-29 June

2001. CRC Press, London, pp. 3–26.

Blewett, R.S., Henson, P.A., Roy, I.G., Champion, D.C., Cassidy, K.F., 2010. Scale-integrated architecture of a world-class gold mineral system: The Archaean eastern Yilgarn Craton, Western Australia. Precambrian Res. 183, 230–250.

Blewett, R.S., Hitchman, A.P., 2006. 3D Geological Models of the Eastern Yilgarn Craton: Final Report pmd* CRC Y2 Project September 2001–December 2004. Geoscience Australia Record 2006/05.

Bodorkos, S., Clark, D.J., 2004a. Evolution of a crustal-scale transpressive shear zone in the Albany-Fraser Orogen, SW Australia: 2. Tectonic history of the Coramup Gneiss and a kinematic framework for Mesoproterozoic collision of the West Australian and Mawson cratons. J. Metamorph. Geol. 22, 713–731.

Bodorkos, S., Clark, D.J., 2004b. Evolution of a crustal-scale transpressive shear zone in the Albany-Fraser Orogen, SW Australia: 1. P-T conditions of Mesoproterozoic metamorphism in the Coramup Gneiss. J. Metamorph. Geol. 22, 691–711.

Boger, S.D., 2011. Antarctica—before and after Gondwana. Gondwana Res. 19, 335–371.

Boyd, D.M., Tucker, D.H., 1990. Australian magnetic dykes, in: Parker, A.J., Rickwood, P.C., Tucker, D.H. (Eds.), Mafic Dykes and Emplacement Mechanisms. A.A.Balkema, Rotterdam, pp. 391–399.

Brandon, A.D., Hooper, P.R., Goles, G.G., Lambert, R.S.J., 1993. Evaluating crustal contamination in continental basalts: the isotopic composition of the Picture Gorge Basalt of the Columbia River Basalt Group. Contrib. to Mineral. Petrol. 114, 452–464.

Buchan, K.L., Ernst, R.E., Hamilton, M.A., Mertanen, S., Pesonen, L.J., Elming, S.-Å., 2001. Rodinia: the evidence from integrated palaeomagnetism and U–Pb geochronology. Precambrian Res. 110, 9–32.

Campbell, I.H., McCall, G.J.H., Tyrwhitt, D.S., 1970. The Jimberlana Norite, Western Australia–a smaller analogue of the Great Dyke of Rhodesia. Geol. Mag. 107, 1–12.

Cassidy, K.F., Champion, D.C., Huston, D.L., 2005. Crustal evolution constraints on the metallogeny of the Yilgarn Craton, in: Mineral Deposit Research: Meeting the Global Challenge: Proceedings of the Eight Biennia SGA Meeting.

Springer, Berlin, pp. 901–904.

Cassidy, K.F., Champion, D.C., Krapez, B., Barley, M.E., Brown, S.J.A., Blewett, R.S., Groenewald, Pb., Tyler, I.M., 2006. A revised geological framework for the Yilgarn Craton, Western Australia, in: Geological Survey of Western Australia Record 8/2006. Geological Survey of Western Australia.

Cawood, P.A., Tyler, I.M., 2004. Assembling and reactivating the Proterozoic Capricorn Orogen: lithotectonic elements, orogenies, and significance. Precambrian Res. 128, 201–218.

Claoué-Long, J.C., Hoatson, D.M., Australia, G., 2009. Guide to using the Map of Australian Proterozoic Large Igneous Provinces. Geoscience Australia Record 2009/44.

Clark, D.J., Hensen, B.J., Kinny, P.D., 2000. Geochronological constraints for a two-stage history of the Albany – Fraser Orogen , Western Australia. Precambrian Res. 102, 155–183.

Clark, D.J., Kinny, P.D., Post, N.J., 1999. Relationships between magmatism, metamorphism and deformation in the Fraser Complex, Western Australia: constraints from new SHRIMP U–Pb zircon geochronology. Aust. J. Earth Sci. 46, 923–932.

Condie, K.C., 2004. Supercontinents and superplume events: distinguishing signals in the geologic record. Phys. Earth Planet. Inter. 146, 319–332.

Dalziel, I.W.D., 1991. Pacific margins of Laurentia and East Antarctica-Australia as a conjugate rift pair: Evidence and implications for an Eocambrian supercontinent. Geology 19, 598–601.

Dentith, M.C., Dent, V.F., Drummond, B.J., 2000. Deep crustal structure in the southwestern Yilgarn Craton , Western Australia. Tectonophysics 325, 227–255.

Dentith, M.C., Featherstone, W.E., 2003. Controls on intra-plate seismicity in southwestern Australia. Tectonophysics 376, 167–184.

DePaolo, D.J., 1981. Neodymium isotopes in the Colorado Front Range and crust–mantle evolution in the Proterozoic. Nature 291, 193–196.

Doehler, J.S., Heaman, L.M., 1998. 2.41 Ga U–Pb Baddeleyite ages for two gabbroic dykes from the Widgiemooltha swarm, Western Australia: a Yilgarn–Lewisian connection, in: Geological Society of America 1998 Annual Meeting, Abstracts with Programs. Geological Society of America, pp. 291–292.

Doughty, P.T., Chamberlain, K.R., 1996. Salmon River Arch revisited: New evidence for 1370 Ma rifting near the end of deposition in the Middle Proterozoic Belt basin. Can. J. Earth Sci. 33, 1037–1052.

Eggins, S.M., Woodhead, J.D., Kinsley, L.P.J., Mortimer, G.E., Sylvester, P., McCulloch, M.T., Hergt, J.M., Handler, M.R., 1997. A simple method for the precise determination of≥ 40 trace elements in geological samples by ICPMS using enriched isotope internal standardisation. Chem. Geol. 134, 311–326.

Ernst, R., Bleeker, W., 2010. Large igneous provinces (LIPs), giant dyke swarms, and mantle plumes: significance for breakup events within Canada and adjacent regions from 2.5 Ga to the Present. Can. J. Earth Sci. 47, 695–739.

Ernst, R., Srivastava, R., Bleeker, W., Hamilton, M., 2010. Precambrian Large Igneous Provinces (LIPs) and their dyke swarms: New insights from high-precision geochronology integrated with paleomagnetism and geochemistry. Precambrian Res. 183, vii–xi.

Ernst, R.E., Bleeker, W., Söderlund, U., Kerr, A.C., 2013. Large Igneous Provinces and supercontinents: Toward completing the plate tectonic revolution. Lithos 174, 1–14.

Ernst, R.E., Buchan, K.L., 1997. Giant radiating dyke swarms: their use in identifying pre-Mesozoic large igneous provinces and mantle plumes, in: Large Igneous Provinces: Continental, Oceanic, and Planetary Flood Volcanism. American Geophysical Union Monograph 100, pp. 297–333.

Ernst, R.E., Buchan, K.L., Hamilton, M.A., Okrugin, A. V, Tomshin, M.D., 2000. Integrated paleomagnetism and U-Pb geochronology of mafic dikes of the eastern Anabar Shield region, Siberia: Implications for Mesoproterozoic paleolatitude of Siberia and comparison with Laurentia. J. Geol. 108, 381–401.

Ernst, R.E., Head, J.W., Parfitt, E., Grosfils, E., Wilson, L., 1995. Giant radiating dyke swarms on Earth and Venus. Earth-Science Rev. 39, 1–58.

Ernst, R.E., Pease, V., Puchkov, V.N., Kozlov, V.I., Sergeeva, N.D., Hamilton, M.,

2006. Geochemical characterization of Precambrian magmatic suites of the Southeastern margin of the East European Craton, Southern Urals, Russia. Geol. Sb. 5, 119–161.

Ernst, R.E., Srivastava, R.K., 2008. India's place in the Proterozoic world: constraints from the Large Igneous Province (LIP) record. Indian dykes. Ed. by RK Srivastava, Ch. Sivaji, NV Chalapathi Rao. Geochemistry, Geophys. Geochronology, Narosa Publ. House Pvt. Ltd, New Delhi, India 41–56.

Ernst, R.E., Wingate, M.T.D., Buchan, K.L., Li, Z.X., 2008. Global record of 1600–700Ma Large Igneous Provinces (LIPs): Implications for the reconstruction of the proposed Nuna (Columbia) and Rodinia supercontinents. Precambrian Res. 160, 159–178.

Evans, D.A.D., Mitchell, R.N., 2011. Assembly and breakup of the core of Paleoproterozoic–Mesoproterozoic supercontinent Nuna. Geology 39, 443–446.

Evans, M.E., 1968. Magnetization of dikes: a study of the paleomagnetism of the Widgiemooltha dike suite, Western Australia. J. Geophys. Res. 73, 3261–3270.

Evans, T., 1999. Extent and nature of the 1.2 Ga Wheatbelt dyke swarm, Yilgarn Craton, Western Australia. B.Sc. thesis, Univ. West. Aust. Perth.

French, J.E., Heaman, L.M., Chacko, T., 2002. Feasibility of chemical U-Th-total Pb baddeleyite dating by electron microprobe. Chem. Geol. 188, 85–104.

Goldberg, A.S., 2010. Dyke swarms as indicators of major extensional events in the 1.9–1.2 Ga Columbia supercontinent. J. Geodyn. 50, 176–190.

Hallberg, J.A., 1987. Postcratonization mafic and ultramafic dykes of the Yilgarn Block. Aust. J. Earth Sci. 34, 135–149.

Halls, H.C., Zhang, B., 1998. Uplift structure of the southern Kapuskasing zone from 2.45 Ga dike swarm displacement. Geology 26, 67–70.

Hawkesworth, C., 1993. Mantle and Slab Contribution in Arc Magmas. Annu. Rev. Earth Planet. Sci. 21, 175–204.

Hawkesworth, C.J., Kempton, P.D., Rogers, N.W., Ellam, R.M., Calsteren, P.W. van, 1990. Continental mantle lithosphere, and shallow level enrichment processes in the Earth's mantle. Earth Planet. Sci. Lett. 96, 256–268.

Hawkesworth, C.J., Lightfoot, P.C., Fedorenko, V.A., Blake, S., Naldrett, A.J., Doherty, W., Gorbachev, N.S., 1995. Magma differentiation and mineralisation in the Siberian continental flood basalts. Lithos 34, 61–88.

Heaman, L.M., 2009. The application of U–Pb geochronology to mafic, ultramafic and alkaline rocks: An evaluation of three mineral standards. Chem. Geol. 261, 43–52.

Hoek, J.D., Seitz, H.-M., 1995. Continental mafic dyke swarms as tectonic indicators: an example from the Vestfold Hills, Antarctica. Precambrian Res. 75, 121–139.

Hou, G., 2012. Mechanism for three types of mafic dyke swarms. Geosci. Front. 3, 217–223.

Hou, G., Kusky, T.M., Wang, C., Wang, Y., 2010. Mechanics of the giant radiating Mackenzie dyke swarm: A paleostress field modeling. J. Geophys. Res. Solid Earth 115.

Irvine, T.N.J., Baragar, W., 1971. A guide to the chemical classification of the common volcanic rocks. Can. J. Earth Sci. 8, 523–548.

Isles, D.J., Cooke, A.C., 1990. Spatial associations between post-cratonisation dykes and gold deposits in the Yilgarn Block, Western Australia, in: Parker, A.J., Rickwood, P.C., Tucker, D.H. (Eds.), Mafic Dykes and Emplacement Mechanisms. Balkema, Rotterdam, pp. 147–162.

Jaffey, A.H., Flynn, K.F., Glendenin, L.E., Bentley, W.C. t, Essling, A.M., 1971. Precision measurement of half-lives and specific activities of U 235 and U 238. Phys. Rev. C 4, 1889.

Johnson, S.P., Sheppard, S., Rasmussen, B., Wingate, M.T.D., Kirkland, C.L., Muhling, J.R., Fletcher, I.R., Belousova, E.A., 2011. Two collisions, two sutures: Punctuated pre-1950Ma assembly of the West Australian Craton during the Ophthalmian and Glenburgh Orogenies. Precambrian Res. 189, 239–262.

Ju, W., Hou, G., Hari, K.R., 2013. Mechanics of mafic dyke swarms in the Deccan Large Igneous Province: Palaeostress field modelling. J. Geodyn. 66, 79–91.

Kamber, B.S., Greig, A., Schoenberg, R., Collerson, K.D., 2003. A refined solution to Earth's hidden niobium: implications for evolution of continental crust and mode of core formation. Precambrian Res. 126, 289–308.

Kirkland, C.L., Smithies, R.H., Woodhouse, A.J., Howard, H.M., Wingate, M.T.D., Belousova, E.A., Cliff, J.B., Murphy, R.C., Spaggiari, C. V, 2013. Constraints and deception in the isotopic record; the crustal evolution of the west Musgrave Province, central Australia. Gondwana Res. 23, 759–781.

Kirkland, C.L., Spaggiari, C. V, Pawley, M.J., Wingate, M.T.D., Smithies, R.H., Howard, H.M., Tyler, I.M., Belousova, E.A., Poujol, M., 2011. On the edge: U–Pb, Lu–Hf, and Sm–Nd data suggests reworking of the Yilgarn craton margin during formation of the Albany-Fraser Orogen. Precambrian Res. 187, 223–247.

Korsch, R.J., Kositcin, N., Champion, D.C., 2011. Australian island arcs through time: Geodynamic implications for the Archean and Proterozoic. Gondwana Res. 19, 716–734.

Ksienzyk, A.K., Jacobs, J., Boger, S.D., Kosler, J., Sircombe, K.N., Whitehouse, M.J., 2012. U-Pb ages of metamorphic monazite and detrital zircon from the Northampton Complex: Evidence of two orogenic cycles in Western Australia. Precambrian Res. 198–199, 37–50.

Lanyon, R., Black, L.P., Seitz, H.-M., 1993. U-Pb zircon dating of mafic dykes and its application to the Proterozoic geological history of the Vestfold Hills, East Antarctica. Contrib. to Mineral. Petrol. 115, 184–203.

Le Maitre, R.W.B., Dudek, P., Keller, A., Lameyre, J., Le Bas, J., Sabine, M.J., Schmid, P.A., Sorensen, R., Streckeisen, H., Woolley, A., 1989. A classification of igneous rocks and glossary of terms: Recommendations of the International Union of Geological Sciences, Subcommission on the Systematics of Igneous Rocks. International Union of Geological Sciences, Blackwell Scientific.

Lewis, J.D., 1994. Mafic dykes in the Williams–Wandering area, Western Australia. Geol. Surv. West. Aust. Rep. 37, 37–52.

Li, Z.-X., Zhong, S., 2009. Supercontinent–superplume coupling, true polar wander and plume mobility: Plate dominance in whole-mantle tectonics. Phys. Earth Planet. Inter. 176, 143–156.

Li, Z.X., Bogdanova, S. V, Collins, A.S., Davidson, A., De Waele, B., Ernst, R.E., Fitzsimons, I.C.W., Fuck, R.A., Gladkochub, D.P., Jacobs, J., Karlstrom, K.E., Lu, S., Natapov, L.M., Pease, V., Pisarevsky, S.A., Thrane, K., Vernikovsky, V., 2008. Assembly, configuration, and break-up history of Rodinia: A synthesis. Precambrian Res. 160, 179–210.

Ludwig, K., 2012. User's manual for Isoplot version 3.75–4.15: a geochronological toolkit for Microsoft. Berkeley Geochronological Cent. Spec. Publ.

Ludwig, K., 2009. Squid 2.50, A User's Manual (No. 2.50.11.02.03 Rev. 03 Feb 2011). Berkeley, California, USA.

Maas, R., Grew, E.S., Carson, C.J., 2015. Isotopic constraints (Pb, Rb-Sr, Sm-Nd) on the sources of early Cambrian pegmatites with Boron and Beryllium minerals in the Larsemann Hills, Prydz Bay, Antarctica. Can. Mineral. 53, 249–272.

Maas, R., Kamenetsky, M.B., Sobolev, A. V, Kamenetsky, V.S., Sobolev, N. V, 2005. Sr, Nd, and Pb isotope evidence for a mantle origin of alkali chlorides and carbonates in the Udachnaya kimberlite, Siberia. Geology 33, 549–552.

Mäkitie, H., Data, G., Isabirye, E., Mänttäri, I., Huhma, H., Klausen, M.B., Pakkanen, L., Virransalo, P., 2014. Petrology, geochronology and emplacement model of the giant 1.37 Ga arcuate Lake Victoria Dyke Swarm on the margin of a large igneous province in eastern Africa. J. African Earth Sci. 97, 273–296.

Meert, J.G., 2002. Paleomagnetic evidence for a Paleo-Mesoproterozoic supercontinent Columbia. Gondwana Res. 5, 207–215.

Meert, J.G., Santosh, M., 2017. The Columbia supercontinent revisited. Gondwana Res. 50, 67–83.

Middleton, M.F., Wilde, S.A., Evans, B.A., Long, A., Dentith, M., 1993. A preliminary interpretation of deep seismic reflection and other geophysical data from the Darling Fault Zone, Western Australia. Explor. Geophys. 24, 711–718.

Morris, P.A., 2007. Composition of the Bunbury Basalt (BB1) and Kerba Monzogranite (KG1) geochemical reference materials, and assessing the contamination effects of mill heads, in: Geological Survey of Western Australia Record 2007/14. Geological Survey of Western Australia Record 2007/14.

Morris, P.A., Pirajno, F., 2005. Mesoproterozoic sill complexes in the Bangemall Supergroup, Western Australia: geology, geochemistry and mineralization potential. Geological Survey of Western Australia Report 99.

Morrissey, L.J., Payne, J.L., Hand, M., Clark, C., Taylor, R., Kirkland, C.L., Kylander-Clark, A., 2017. Linking the Windmill Islands, east Antarctica and the Albany–Fraser Orogen: Insights from U–Pb zircon geochronology and Hf isotopes. Precambrian Res. 293, 131–149.

Myers, J.S., 1995. The generation and assembly of an Archaean supercontinent: evidence from the Yilgarn craton, Western Australia. Geol. Soc. London, Spec. Publ. 95, 143–154.

Myers, J.S., 1993. Precambrian Tectonic History of the West Australian Craton and Adjacent Orogens. Annu. Rev. Earth Planet. Sci. 21, 453–485.

Myers, J.S., 1990. Pinjarra Orogen, in: Geology and Mineral Resources of Western Australia. Geological Survey of Western Australia Memoir 3, pp. 264–274.

Nance, R.D., Murphy, J.B., Santosh, M., 2014. The supercontinent cycle: A retrospective essay. Gondwana Res. 25, 4–29.

Nelson, D.R., Myers, J.S., Nutman, A.P., 1995. Chronology and evolution of the Middle Proterozoic Albany-Fraser Orogen, Western Australia. Aust. J. Earth Sci. 42, 481–495.

Nemchin, A.A., Pidgeon, R.T., 1998. Precise conventional and SHRIMP baddeleyite U-Pb age for the Binneringie Dyke, near Narrogin, Western Australia. Aust. J. Earth Sci. 45, 673–675.

Nemchin, A.A., Pidgeon, R.T., 1997. Evolution of the Darling Range batholith, Yilgarn Craton, Western Australia: a SHRIMP zircon study. J. Petrol. 38, 625–649.

Nemchin, A.A., Pidgeon, R.T., Wilde, S.A., 1994. Timing of Late Archaean granulite facies metamorphism in the southwestern Yilgarn Craton of Western Australia: evidence from U-Pb ages of zircons fro mafic granulites. Precambrian Res. 68, 307–321.

Okrugin, A. V, Oleinikov, B. V, Savvinov, V.T., Tomshin, M.D., 1990. Late Precambrian dyke swarms of the Anabar massif, Siberian platform, USSR, in: Parker, A.J., Rickwood, P.C., Tucker, D.H. (Eds.), Mafic Dykes and Emplacement Mechanisms. Balkema, Rotterdam, pp. 529–533.

Pidgeon, R.T., Cook, T.J.F., 2003. 1214±5 Ma dyke from the Darling Range, southwestern Yilgarn Craton, Western Australia. Aust. J. Earth Sci. 50, 769–773.

Pidgeon, R.T., Nemchin, A.A., 2001. 1.2 Ga Mafic dyke near York, southwestern Yilgarn Craton, Western Australia. Aust. J. Earth Sci. 48, 751–755.

Pisarevsky, S.A., Elming, S.-Å., Pesonen, L.J., Li, Z.-X., 2014. Mesoproterozoic paleogeography: Supercontinent and beyond. Precambrian Res. 244, 207–225.

Pisarevsky, S., De Waele, B., Jones, S., Söderlund, U., Ernst, R.E., 2015. Paleomagnetism and U–Pb age of the 2.4Ga Erayinia mafic dykes in the south-western Yilgarn, Western Australia: Paleogeographic and geodynamic implications. Precambrian Res. 259, 222–231.

Polat, a., Hofmann, a. W., Rosing, M.T., 2002. Boninite-like volcanic rocks in the 3.7-3.8 Ga isua greenstone belt, West Greenland: Geochemical evidence for intra-oceanic subduction zone processes in the early earth. Chem. Geol. 184, 231–254.

Prokoph, A., Ernst, R.E., Buchan, K.L., 2004. Time-Series Analysis of Large Igneous Provinces: 3500 Ma to Present. J. Geol. 112, 1–22.

Puffer, J.H., 2001. Contrasting high field strength element contents of continental flood basalts from plume versus reactivated-arc sources. Geology 29, 675–678.

Qiu, Y., McNaughton, N.J., Groves, D.I., Dunphy, J.M., 1999. First record of 1.2 Ga quartz dioritic magmatism in the Archaean Yilgarn Craton, Western Australia, and its significance. Aust. J. Earth Sci. 46, 421–428.

Rasmussen, B., Fletcher, I.R., 2010. Dating sedimentary rocks using in situ U-Pb geochronology of syneruptive zircon in ash-fall tuff &lt 1 mm thick. Geology 38, 299–302.

Rasmussen, B., Fletcher, I.R., 2004. Zirconolite: A new U-Pb chronometer for mafic igneous rocks. Geology 32, 785–788.

Rasmussen, B., Fletcher, I.R., Bekker, A., Muhling, J.R., Gregory, C.J., Thorne, A.M., 2012. Deposition of 1.88-billion-year-old iron formations as a consequence of rapid crustal growth. Nature 484, 498–501.

Rogers, J.J.W., Santosh, M., 2002. Configuration of Columbia, a Mesoproterozoic Supercontinent. Gondwana Res. 5, 5–22.

Ronkin, Y.L., Maslov, A. V, Matukov, D.I., Lepikhina, O.P., Popova, O.Y., 2005. The Mashak riftogenic event of the Riphean type region (southern Urals): new isotopic-geochronological framework. Struct. Geodyn. Mineral. Process. Lithosphere. Geoprint, Syktyvkar 305–307.

Schmitt, A.K., Chamberlain, K.R., Swapp, S.M., Harrison, T.M., 2010. In situ U-Pb dating of micro-baddeleyite by secondary ion mass spectrometry. Chem. Geol. 269, 386–395.

Sheppard, S., Bodorkos, S., Johnson, S.P., Wingate, M.T.D., Kirkland, C.L., 2010a. The Paleoproterozoic Capricorn Orogeny: intracontinental reworking not continent–continent collision, Geological Survey of Western Australia Report 108. Geological Survey of Western Australia.

Sheppard, S., Fletcher, I.R., Rasmussen, B., Zi, J.-W., Muhling, J.R., Occhipinti, S.A., Wingate, M.T.D., Johnson, S.P., 2016. A new Paleoproterozoic tectonic history of the eastern Capricorn Orogen, Western Australia, revealed by U–Pb zircon dating of micro-tuffs. Precambrian Res. 286, 1–19.

Sheppard, S., Johnson, S.P., Wingate, M.T.D., Kirkland, C.L., Pirajno, F., 2010b. Explanatory notes for the Gascoyne Province, Geological Survey of Western Australia Report 336.

Sheppard, S., Occhipinti, S.A.A., Tyler, I.M.M., 2004. A 2005-1970 Ma Andean-type batholith in the southern Gascoyne Complex, Western Australia. Precambrian Res. 128, 257–277.

Smirnov, A. V, Evans, D.A.D., Ernst, R.E., Söderlund, U., Li, Z.-X., 2013. Trading partners: Tectonic ancestry of southern Africa and western Australia, in Archean supercratons Vaalbara and Zimgarn. Precambrian Res. 224, 11–22.

Smithies, R.H., Champion, D.C., 1999. Late Archaean felsic alkaline igneous rocks in the Eastern Goldfields, Yilgarn Craton, Western Australia: a result of lower crustal delamination? J. Geol. Soc. London. 156, 561–576.

Söderlund, U., Johansson, L., 2002. A simple way to extract baddeleyite (ZrO_2). Geochemistry, Geophys. Geosystems 3.

Sofoulis, J., 1965. Explanatory Notes on the Widgiemooltha 1: 250,000 Geological Sheet Western Australia. Geological Survey of Western Australia Record 1965/10.

Spaggiari, C.V., Kirkland, C.L., Smithies, H.R., Wingate, M.T.D., Belousova, E.A., 2015. Transformation of an Archean craton margin during Proterozoic basin formation and magmatism: The Albany–Fraser Orogen, Western Australia. Precambrian Res. 266, 440–466.

Spaggiari, C.V., Kirkland, C.L., Smithies, R.H., Wingate, M.T.D., 2014. Tectonic links between proterozoic sedimentary cycles, basin formation and magmatism in the Albany-Fraser Orogen, Western Australia, Geological Survey of Western Australia Report 133.

Spaggiari, C. V, Bodorkos, S., Barquero-Molina, M., Tyler, I.M., Wingate, M.T.D., 2009. Interpreted bedrock geology of the South Yilgarn and of the South Yilgarn and Central Albany-Fraser Orogen, Western Australia, Geological Survey of Western Australia Record 2009/10.

Spaggiari, C. V, Kirkland, C.L., Pawley, M.J., Smithies, R.H., Wingate, M.T.D., Doyle, M.G., Blenkinsop, T.G., Clark, C., Oorschot, C.W., Fox, L.J., 2011. The geology of the east Albany-Fraser Orogen—a field guide, Geological Survey of Western Australia Record 2011/23.

Stacey, J.S., Kramers, J.D., 1975. Approximation of terrestrial lead isotope evolution by a two-stage model. Earth Planet. Sci. Lett. 26, 207–221.

Stark, J.C., Wang, X.-C., Denyszyn, S.W., Li, Z.-X., Rasmussen, B., Zi, J.-W., Sheppard, S., Liu, Y., 2017. Newly identified 1.89 Ga mafic dyke swarm in the Archean Yilgarn Craton, Western Australia suggests a connection with India. Precambrian Res. Press.

Stark, J.C., Wilde, S.A., Söderlund, U., Li, Z.-X., Rasmussen, B., Zi, J.-W., 2018. First evidence of Archean mafic dykes at 2.62 Ga in the Yilgarn Craton, Western Australia: links to cratonisation and the Zimbabwe Craton. Precambrian Res. 317, 1–13.

Stern, R.A., 2001. A new isotopic and trace-element standard for the ion microprobe: preliminary thermal ionization mass spectrometry (TIMS) U-Pb and electron-microprobe data, Geological Survey of Canada Current Research 2001-F.

Stern, R.A., Bodorkos, S., Kamo, S.L., Hickman, A.H., Corfu, F., 2009. Measurement of SIMS instrumental mass fractionation of Pb isotopes during zircon dating. Geostand. Geoanalytical Res. 33, 145–168.

Sun, S. -s., McDonough, W.F., 1989. Chemical and isotopic systematics of oceanic basalts: implications for mantle composition and processes. Geol. Soc. London, Spec. Publ. 42, 313–345.

Taylor, S.R., McLennan, S.M., 1985. The continental crust: its composition and evolution, 1st ed. Blackwell Scientific Publishers, Palo Alto, CA.

Tucker, D.H., Boyd, D.M., 1987. Dykes of Australia detected by airborne magnetic surveys, in: Fahrig, W.F., Halls, H.C. (Eds.), Mafic Dyke Swarms. Geological Association of Canada, pp. 163–172.

Tucker, N.M., Payne, J.L., Clark, C., Hand, M., Taylor, R.J., Kylander-Clark, A.R.C., 2017. Proterozoic reworking of Archean (Yilgarn) basement in the Bunger Hills, east Antarctica. Precambrian Res. 298, 16–38.

Upton, B.G.J., Rämö, O.T., Heaman, L.M., Blichert-Toft, J., Kalsbeek, F., Barry, T.L., Jepsen, H.F., 2005. The Mesoproterozoic Zig-Zag Dal basalts and associated intrusions of eastern North Greenland: Mantle plume-lithosphere interaction. Contrib. to Mineral. Petrol. 149, 40–56.

Wang, X.-C., Li, X.-H., Li, W.-X., Li, Z.-X., Liu, Y., Yang, Y.-H., Liang, X.-R., Tu, X.-L., 2008. The Bikou basalts in the northwestern Yangtze block, South China: Remnants of 820-810 Ma continental flood basalts? Geol. Soc. Am. Bull. 120, 1478–1492.

Wang, X.-C., Li, Z.-X., Li, J., Pisarevsky, S.A., Wingate, M.T.D., 2014. Genesis of the 1.21 Ga Marnda Moorn large igneous province by plume–lithosphere interaction. Precambrian Res. 241, 85–103.

Wang, X.-C., Wilde, S.A., Xu, B., Pang, C.-J., 2016. Origin of arc-like continental basalts: Implications for deep-Earth fluid cycling and tectonic discrimination. Lithos 261, 5–45.

Wilde, S.A., 1999. Evolution of the Western Margin of Australia during the Rodinian and Gondwanan Supercontinent Cycles. Gondwana Res. 2, 481–499.

Wilde, S.A., Middleton, M.F., Evans, B.J., 1996. Terrane accretion in the southwestern Yilgarn Craton: evidence from a deep seismic crustal profile. Precambrian Res. 78, 179–196.

Williams, I.S., 1998. U-Th-Pb geochronology by ion microprobe. Rev. Econ. Geol. 7, 1–35.

Wingate, M.T.D., 2017. Mafic dyke swarms and large igneous provinces in Western Australia get a digital makeover, in: Geological Survey of Western Australia Record 2017/2. pp. 4–8.

Wingate, M.T.D., 2007. Proterozoic mafic dykes in the Yilgarn Craton, in:

Proceedings of Geoconferences (WA) Inc. Kalgoorlie 2007 Conference, Kalgoorlie, Western Australia. pp. 80–84.

Wingate, M.T.D., 2002. Age and Paleomagnetism of Dolerite Sills Intruded Into the Bangemall Supergroup on the Edmund 1: 250 000 Map Sheet, Western Australia. Geological Survey of Western Australia Record 2002/4.

Wingate, M.T.D., 1999. Ion microprobe baddeleyite and zircon ages for Late Archaean mafic dykes of the Pilbara Craton, Western Australia. Aust. J. Earth Sci. 46, 493–500.

Wingate, M.T.D., Campbell, I.H., Harris, L.B., 2000. SHRIMP baddeleyite age for the Fraser dyke swarm, southeast Yilgarn Craton, Western Australia. Aust. J. Earth Sci. 47, 309–313.

Wingate, M.T.D., Compston, W., 2000. Crystal orientation effects during ion microprobe U–Pb analysis of baddeleyite. Chem. Geol. 168, 75–97.

Wingate, M.T.D., Pidgeon, R.T., 2005. The Marnda Moorn LIP, a late Mesoproterozoic large igneous province in the Yilgarn craton, Western Australia. July 2005 LIP of the month [WWW Document]. (unpub). Large Igneous Prov. Comm. Int. Assoc. Volcanol. Chem. Earth's Inter. URL http://www.largeigneousprovinces.org/05jul

Wingate, M.T.D., Pirajno, F., Morris, P.A., 2004. Warakurna large igneous province: a new Mesoproterozoic large igneous province in west-central Australia. Geology 32, 105–108.

Wingate, M.T.D., Pisarevsky, S.A., Evans, D.A.D., 2002. Rodinia connections between Australia and Laurentia: no SWEAT, no AUSWUS? Terra Nov. 14, 121–128.

Witt, W.K., Cassidy, K.F., Lu, Y.-J., Hagemann, S.G., 2018. The tectonic setting and evolution of the 2.7 Ga Kalgoorlie–Kurnalpi Rift, a world-class Archean gold province. Miner. Depos. 1–31.

Zhang, S.H., Zhao, Y., Liu, X.C., Liu, Y.S., Hou, K.J., Li, C.F., Ye, H., 2012. U-Pb geochronology and geochemistry of the bedrocks and moraine sediments from the Windmill Islands: Implications for Proterozoic evolution of East Antarctica. Precambrian Res. 206–207, 52–71.

Zhao, Z.-F., Dai, L.-Q., Zheng, Y.-F., 2013. Postcollisional mafic igneous rocks record crust-mantle interaction during continental deep subduction. Nat. Sci. Reports 3, 3413.

Zi, J.W., Gregory, C.J., Rasmussen, B., Sheppard, S., Muhling, J.R., 2017. Using monazite geochronology to test the plume model for carbonatites: The example of Gifford Creek Carbonatite Complex, Australia. Chem. Geol. 463, 50–60.

Zi, J.W., Rasmussen, B., Muhling, J.R., Fletcher, I.R., Thorne, A.M., Johnson, S.P., Cutten, H.N., Dunkley, D.J., Korhonen, F.J., 2015. In situ U-Pb geochronology of xenotime and monazite from the Abra polymetallic deposit in the Capricorn Orogen, Australia: Dating hydrothermal mineralization and fluid flow in a long-lived crustal structure. Precambrian Res. 260, 91–112.

Chapter 7 In situ U-Pb geochronology and geochemistry of a 1.13 Ga mafic dyke suite at Bunger Hills, East Antarctica: the end of the Albany-Fraser Orogeny[4]

J. Camilla Stark, Xuan-Ce Wang, Zheng-Xiang Li, Birger Rasmussen[4], Stephen Sheppard, Jian-Wei Zi, Christopher Clark, Martin Hand, Wu-Xian Li

7.1 Abstract

Antarctica contains continental fragments of Australian, Indian and African affinities, and is one of the key elements in the reconstruction of Nuna, Rodinia and Gondwana. The Bunger Hills region in East Antarctica is widely interpreted as a remnant of the Mesoproterozoic Albany–Fraser Orogen, which formed during collision between the West Australian and Mawson cratons and is linked with the assembly of Rodinia. Previous studies have suggested that several generations of mafic dyke suites are present at Bunger Hills but an understanding of their origin and tectonic context is limited by the lack of precise age constraints. New *in situ* SHRIMP U-Pb zircon and baddeleyite dates of, respectively, 1134 ± 9 Ma and 1131± 16 Ma confirm an earlier Rb-Sr whole-rock age estimate of ca. 1140 Ma for emplacement of a major mafic dyke suite in the area. Existing and new geochemical data suggest that the source of the dyke involved an EMORB-like source reservoir that was contaminated by a lower crust-like component. The new age constraint indicates that the dykes post-date the last known phase of plutonism at Bunger Hills by ca. 20 million years and were emplaced at the end of Stage 2 of the Albany-Fraser Orogeny. In current models, post-orogenic uplift and progressive tectonic thinning of the lithosphere were associated with melting and reworking of lower and middle

---

[4] *This chapter is published as* Stark, J.C., Wang, X.-C., Li, Z.-X., Rasmussen, B., Sheppard, S., Xi, J.-W., Clark, C., Hand, M., Li, W.-X., 2018. In situ U-Pb geochronology and geochemistry of a 1.13 Ga mafic dyke suite at Bunger Hills, East Antarctica: the end of the Albany-Fraser Orogeny. Precambrian Res. 310, 76–92.

crust that produced abundant plutonic rocks at Bunger Hills. A major episode of mafic dyke emplacement following uplift, cooling, and plutonic activity with increasing mantle input, suggests that the dykes mark the end of a prolonged interval of thermal weakening of the lithosphere that may have been associated with continued mafic underplating during orogenic collapse. If the undated olivine gabbro dykes with similar trend, geochemistry and petrology at Windmill Islands are coeval with the ca. 1134 Ma dyke at Bunger Hills, this would suggest the presence of a major dyke swarm at least 400 km in extent. In such case, the dykes could have been emplaced laterally from a much more distant mantle source, possibly a plume, and interacted with the locally heterogeneous and variably metasomatised lithosphere.

7.2 Introduction

Mafic dykes are products of lithospheric extension that was sufficient to allow propagation of mantle-derived magma through rigid lithosphere. Emplacement of mafic dykes therefore acts as a proxy for paleostress fields and pre-existing crustal weaknesses (Ernst et al., 1995b; Hoek and Seitz, 1995; Halls and Zhang, 1998; Hou, 2012; Ju et al., 2013). Mafic dykes are also important targets of paleomagnetic analyses for continent reconstructions (e.g., Ernst and Buchan, 1997; Buchan et al., 2001; Bleeker and Ernst, 2006; Teixeira et al., 2013) and precisely dated dyke swarms, which represent the plumbing systems of now eroded Large Igneous Provinces (LIPs) (Coffin and Eldholm, 1994), can provide a unique magmatic barcode and geological piercing points (Ernst and Buchan, 1997; Bleeker, 2004; Bleeker and Ernst, 2006; Ernst and Bleeker, 2010; Ernst et al., 2016).

Antarctica contains key elements of the supercontinents Nuna, Rodinia and Pangea that existed since ca. 2000 Ma. Some of these elements are fragments that share close affinities to the Australian, Indian and African continental blocks (Fitzsimons, 2000a, 2000b, 2003; Boger, 2011; Harley et al., 2013). Mafic dykes are widespread in Archean cratonic blocks in East Antarctica, being readily identifiable in the field and satellite imagery in ice-free areas. Several generations of Precambrian mafic dykes have been identified at Vestfold Hills (Collerson and Sheraton, 1986; John W Sheraton et al., 1987; Black et al., 1991; Lanyon et al., 1993; Sheraton et al., 1993), Bunger Hills (Sheraton et al., 1990; Sheraton et al., 1993), Windmill Islands (Blight and Oliver, 1977; Post et al., 1997; Post, 2000; Zhang et al., 2012), Commonwealth Bay (Sheraton et al., 1989) and the Napier Complex (Sheraton et al., 1980; Sheraton and Black, 1982; J. W. Sheraton et al., 1987; Suzuki et al., 2008). However, with the exception of the Vestfold Hills where U-Pb geochronology has permitted precise dating of five different dyke generations (Black et al., 1991; Lanyon et al., 1993), only Rb–Sr and/or Sm–Nd isotope ages are available for most dykes in Antarctica, which is problematic since these isotope systems are often disturbed by younger tectonothermal events.

The Bunger Hills, a short coastal segment outcropping in Wilkes Land in East Antarctica, have long been proposed to represent a fragment of the Mesoproterozoic Albany-Fraser Orogen in Western Australia (e.g., Sheraton et al., 1990, 1993; Black et al., 1992; Fitzsimons, 2000a; Duebendorfer, 2002). The Windmill Islands, ca. 400 km east of Bunger Hills, appear to preserve a similar tectonothermal and magmatic history (Sheraton et al., 1993; Post et al., 1997; Post, 2000; Morrissey et al., 2017). Data from the Bunger Hills were first obtained during field campaigns in 1956–57 (Ravich et al., 1968) and 1986 (Sheraton et al., 1990, 1992, 1993, 1995; Stüwe and Wilson, 1990; Ding and James, 1991). In 2016, another field campaign was undertaken to study the crustal evolution at Bunger Hills (Tucker and Hand, 2016; Tucker et al., 2017) and Windmill Islands (Morrissey et al., 2017) and has led to improved tectonic models. However, current models and derived continent reconstructions have not incorporated mafic dykes in this part of Antarctica due to the imprecise age constraints for the dykes (Blight and Oliver, 1977; Sheraton et al., 1990, 1995; Post et al., 1997; Post, 2000; Zhang et al., 2012; Morrissey et al., 2017).

We present here the first baddeleyite and zircon U-Pb geochronology obtained from one of the largest and widest dykes at Bunger Hills sampled during the 2016 field campaign. We investigate the nature of the mantle source using existing and new major-trace element and isotope data, followed by a discussion on a possible tectonic setting during dyke emplacement at Bunger Hills in the wider context of the Albany–Fraser Orogen.

7.3 Regional geology

The Bunger Hills area forms a continuous low relief outcrop of about 300 km^2 along the coast in Wilkes Land near Shackleton Ice Shelf, approximately 400 km west of the Windmill Islands (Figure 7.1). Bunger Hills forms one of three geologically distinct regions in the immediate vicinity of the Denman and Scott Glaciers; the other two areas are the Obruchev Hills between Scott and Denman Glaciers

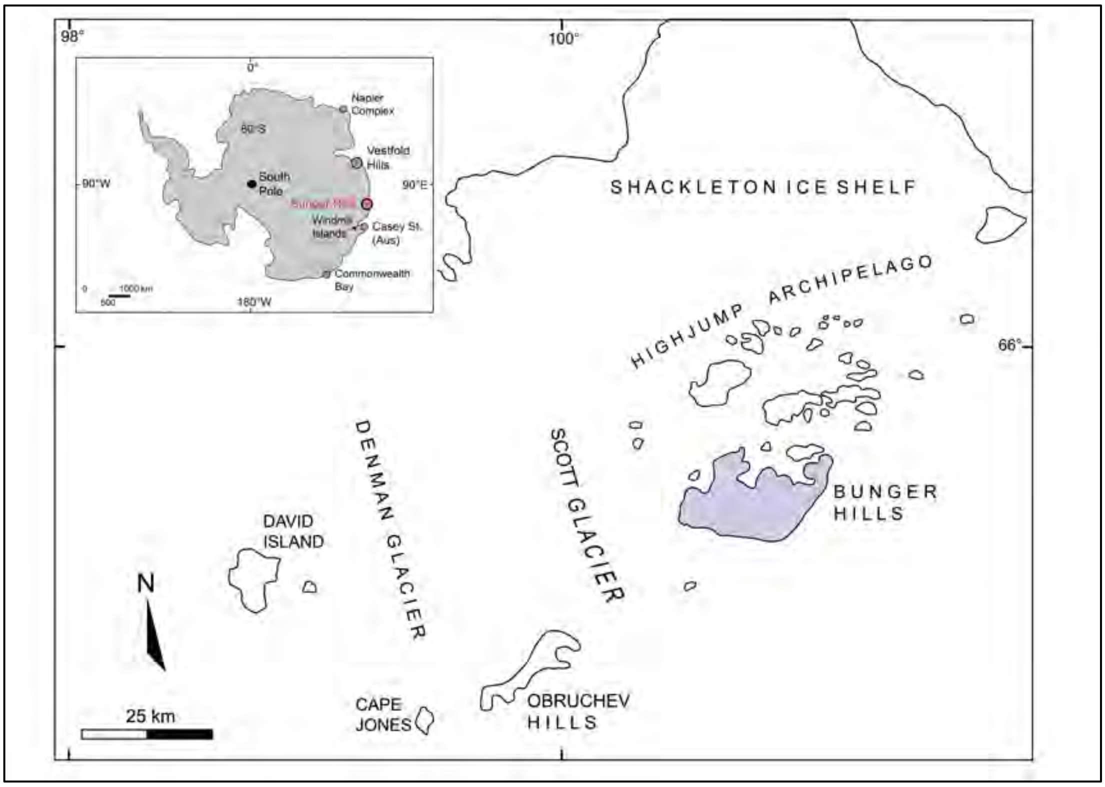

Figure 7.1 Location of Bunger Hills, Highjump Archipelago and Obruchev Hills in East Antarctica. After Sheraton et al. (1990, 1995).

and a group of smaller outcrops west of Denman Glacier. The Highjump Archipelago extends just north-northeast from Bunger Hills and comprises a ca. 93 km-long belt of small rocky islands.

7.4 Basement lithology

At least four metamorphic events have been identified at Bunger Hills (Stüwe and Powell, 1989; Stüwe and Wilson, 1990; Ding and James, 1991; Sheraton et al., 1993, 1995; Tucker et al., 2017). Peak granulite facies conditions of 850–900° C and 5–6 kbar were reached at 1183 ± 8 Ma in the Highjump Archipelago (Tucker and Hand, 2016), whereas conditions of 750–800°C and 5–6 kbar at 1190 ± 15 Ma were reported at Bunger Hills proper (Sheraton et al., 1993). Recent data also indicate metamorphic zircon growth peaks at ca. 1300–1270 Ma and ca. 1250 Ma, with minor peaks at ca. 1330 Ma and 1200 Ma (Tucker et al., 2017).

Peak metamorphism at ca. 1190 Ma may have been associated with an extensional setting (Stüwe and Powell, 1989). This was followed by compressional NNW–SSE-directed deformation under granulite facies conditions by ca. 1170 Ma (Stüwe and Powell, 1989; Sheraton et al., 1992, 1993, 1995; Tucker et al., 2017), the final stage of deformation during uplift and cooling involving formation of extensive shear zones.

7.5 Plutonism and mafic dykes

Three major mafic to felsic intrusive units - the Algae Lake pluton and the Paz Cove and Booth (Charnockite) Peninsula batholiths (Figure 7.1and Figure 7.2) - outcrop in the Bunger Hills area. Their compositions range from subalkaline gabbro to quartz monzogabbro and they were likely emplaced at deep crustal levels (ca. 20 km) as a series of small intrusions syn- to post-peak metamorphism and deformation, between ca. 1203 Ma and 1151 Ma (Ravich et al., 1968; Sheraton et al., 1992, 1993, 1995; Tucker et al., 2017). Late-stage felsic dykes are uncommon and may be genetically related to the plutonic rocks (Sheraton et al., 1992, 1995). Several generations of mafic dyke suites have been identified at Bunger Hills (Stüwe and Powell, 1989; Sheraton et al., 1990; Stüwe and Wilson, 1990; Sheraton et al., 1993) but mafic dykes are rare west of Denman Glacier (L P Black et al., 1992; Sheraton et al., 1995).

The oldest identifiable dykes are mafic granulites of unknown age and comprise boudinaged and deformed (proto-)olivine or quartz tholeiites within the plutons as well as mafic layers in basement gneisses. Most of the undeformed dykes cut both the basement and plutonic rocks and have a maximum age limit of ca. 1203 Ma, defined by the youngest dated pluton intruded by the dykes (Sheraton et al., 1990, 1992, 1993; Tucker et al., 2017).

The undeformed dykes comprise five compositionally distinctive groups ranging from olivine tholeiites and slightly alkaline dolerites to picrites–ankaramites

(Sheraton et al., 1990, 1995). Group 1 tholeiitic dykes are <2 m thick, relatively uncommon and found mainly in the southwestern part of Bunger Hills. Rare NW to NNW trending group 2 high-Mg dolerites have varying thicknesses whereas the most common dykes belong to groups 3 and 4, trend NW and have thicknesses up to 50 m. The youngest dykes are EW-trending alkali basalt dykes, which are generally <1m thick. Whole-rock Rb–Sr and Sm–Nd mineral isochron data suggest emplacement of Group 3 and 4 dykes at ca. 1140 Ma (the former group possibly slightly older) and alkali dykes at ca. 502 Ma (Sheraton et al., 1990, 1992, 1995). Group 1 dykes appear

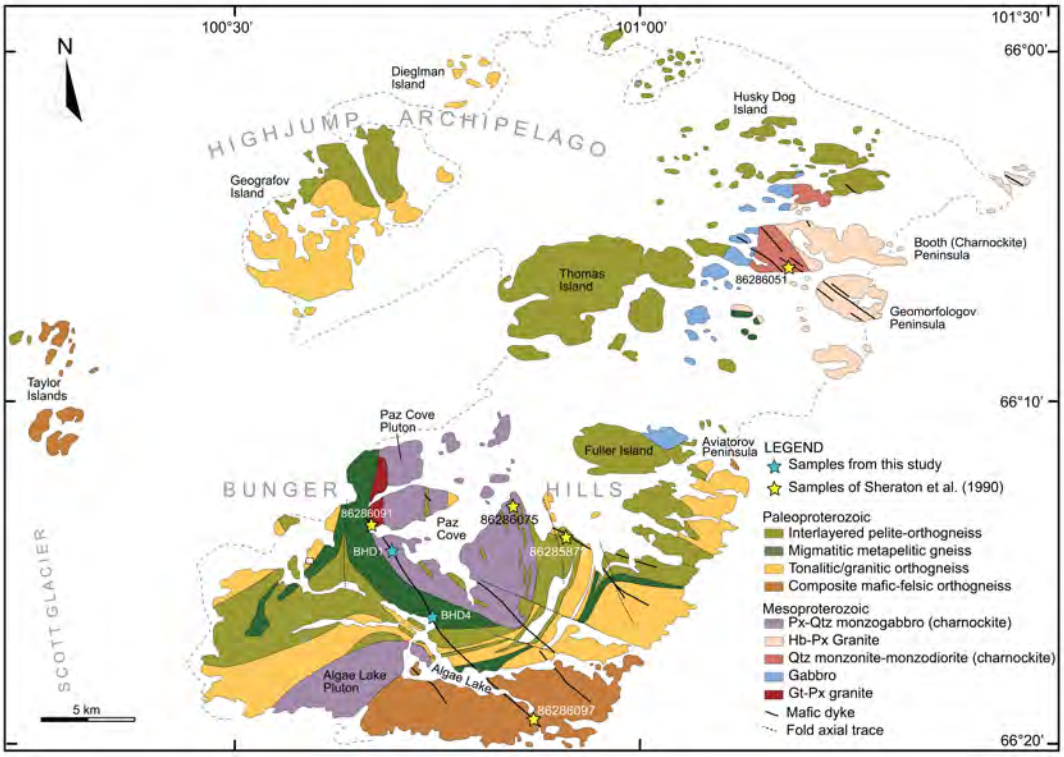

Figure 7.2 Geological Map of Bunger Hills and Highjump Archipelago showing sample locations and regional geology. Modified after Sheraton et al. (1994) and Tucker et al. (2017). Samples in this study are from locations BHD1 and BHD4 (blue stars), the 8-digit numbers (yellow stars) denote samples of Sheraton et al. (1990).

to be the oldest of the undeformed dyke suites and may be coeval with the ca. 1151 Ma Booth Peninsula monzodiorite. Mineral Rb–Sr analyses from the tholeiites and dolerites also reveal partial resetting events at ca. 907 Ma and 514 Ma. Sheraton et al. (1990) interpreted the variation in incompatible element ratios between and within the ca. 1140 Ma dyke groups (3 and 4) as lateral and vertical source heterogeneity in at least six distinctive mantle source regions. Group 1 dykes probably originated from an enriched lithospheric mantle source with an OIB-like component, whereas other dyke groups likely had at least two source components ranging from slightly depleted (Sr_i = 0.7029, εNd = +6.3) to moderately enriched (Sr_i = 0.7046 - 0.7053, εNd = +6.3) in composition. It was proposed that the source of group 3 and 4 dykes consisted of a depleted mantle component and Archean or Paleoproterozoic long-term enriched lithospheric mantle containing subducted crustal materials.

7.6 Samples

7.6.1 Field sampling

Fourteen block samples were collected from two locations along the largest dyke on the island Figure 7.2 and Figure 7.3). Seven samples were collected from each location: six samples from the mafic component for geochemistry and one sample from the associated leucocratic segregation for geochronology (Table 7.1).

Figure 7.3 Sampled dyke at Algae Lake near sampling location of BHD4, looking SSW.

Sample locality BHD1 is near Paz Cove where the dyke is ca. 50 m wide and intrudes the Paz Cove batholith. Chilled margins up to 10 cm wide are visible along the contact with the charnockite. Sample locality BHD4 is at the shore of Algae Lake, just south of the old Polish station Dobrowolski (Figure 7.3). Here the dyke is still ca. 50 m wide and intrudes migmatitic pelitic gneiss. Samples BHD1-4, BHD1-

5, and BHD1-6 (Paz Cove), and BHD4-3, BHD4-5, and BHD4-6 (Algae Lake) are gabbroic and were collected from the center of the dyke. Samples BHD1-1, BHD1-2, and BHD1-3 (Paz Cove), and BHD4-1 and BHD4-2 (Algae Lake) are doleritic and were collected closer to the edges of the dyke. Samples BHD1-7 and BHD4-7 were collected from associated leucocratic segregations. The dyke has a visible strike length of >10 km from Algae Lake to Paz Cove and is identical to the major dyke crossing the entire Bunger Hills in a NW–SE direction that was mapped by Sheraton and Tingey (1994).

Location	Dlat	Lon	Easting	Northing	Zone	Samples	Comments
BHD1	66 14 43.001 S	100 42 13.312 E	576574	2651708	47D	BHD1-1 to BHD1-6 (mafic) BHD1-7 (felsic segregation)	Near Paz Cove, cross-cuts Paz Cove batholith
BHD4	66 16 36.626 S	100 45 21.554 E	578825	2648126	47D	BHD4-1 to BHD4-6 (mafic) BHD4-7 (felsic segregation)	Shore of Algae Lake, intrudes migmatitic pelitic gneiss

Table 7.1 Sampling locations. Samples were collected along strike and across the dyke. Datum WGS84, Dlat = decimal latitude, Dlon = decimal longitude

7.6.2 Sample descriptions

The dyke is an olivine gabbro with intergranular to sub-ophitic and ophitic (poikilitic) texture (Figure 7.4). The gabbroic samples comprise ca. 55– 60% plagioclase, 15–25% augitic clinopyroxene, 5–10% olivine, up to 5% of orthopyroxene, 3-5% biotite, accessory opaques (ilmenite, magnetite and hematite) and apatite. Clinopyroxene is commonly poikilitic and encloses olivine and plagioclase crystals. Olivine crystals are rimmed by a thin reaction corona where in contact with plagioclase. Most plagioclase grains are strongly clouded by minute inclusions of black and brown particles (likely Fe–Ti oxides) and larger, green spherical to needle shaped grains, possibly amphiboles, and both inclusion types appear to grow preferentially, possibly along twin planes. Post-magmatic alteration appears minimal but growth of the inclusions in the plagioclase crystals may be due to emplacement and slow cooling at depth or a later thermal event (Halls and Palmer, 1990; Halls et al., 2007). Apatite forms acicular colourless needles. Brown biotite is associated with, and grows around, ilmenite, possibly due to late stage reaction with magmatic fluids common in gabbros. Leucocratic segregations comprise 75-80%

plagioclase, 5-10% quartz and green amphibole, 5% brown biotite and accessory apatite, zircon and chevkinite.

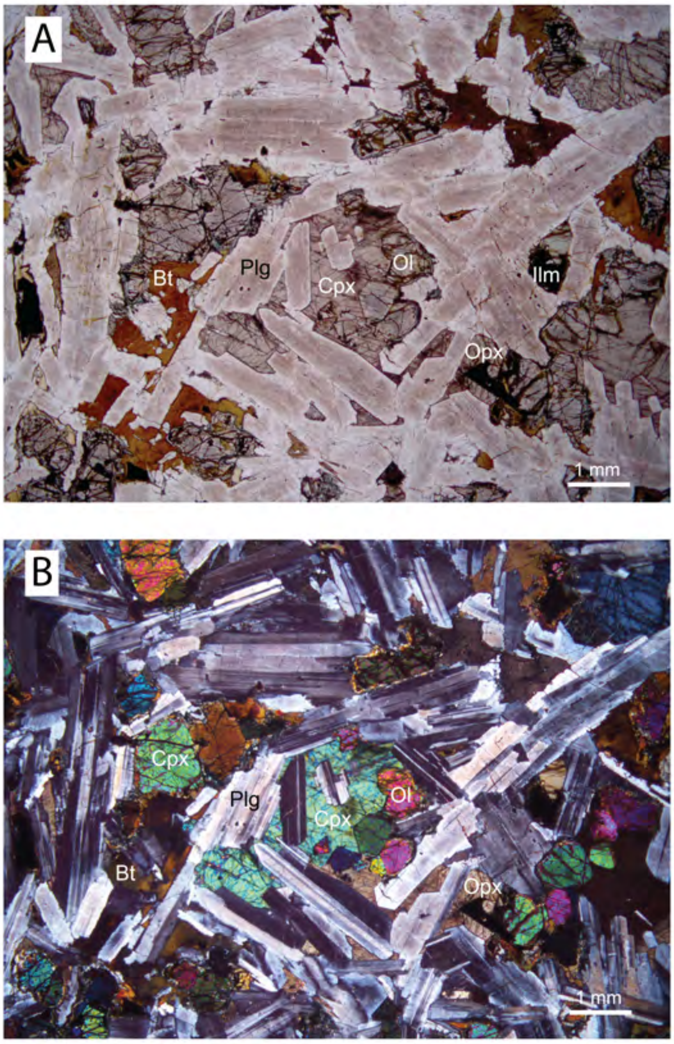

*Figure 7.4 Thin sections of sample BHD1-5. Note plagioclase and olivine poikilitically enclosed in clinopyroxene, biotite associated with ilmenite and abundant minute inclusions clouding the plagioclase. (**A**) Plane polarised light (**B**) Crossed polars.*

No petrography was available from Sheraton et al. (1990) samples 86286091 and 86286097, which they obtained from the same dyke. However, samples from BHD1 and BHD4 are petrographically similar to samples 86286075 and 86285872 (dyke Group 4B), which Sheraton et al. (1990, 1995) collected from a NW-trending dyke east of Paz Cove. They comprise fine- to medium-grained intergranular to sub-ophitic dolerite with olivine, clinopyroxene, plagioclase and minor reddish-brown biotite associated with Fe-Ti oxides.

7.7 U-Pb geochronology and geochemistry

7.7.1 SHRIMP U-Pb geochronology

Polished thin sections were scanned for baddeleyite (ZrO_2) and zircon with a Hitachi TM3030 scanning electron microscope (SEM) equipped with energy dispersive X-ray spectrometer (EDX) at Curtin University, Perth, Australia. For SHRIMP U-Pb dating, selected grains were drilled directly from the thin sections using a micro drill and then mounted into epoxy disks, which were cleaned and coated with 40 nm of pure gold. Standards used for the SHRIMP sessions were mounted in one separate epoxy disk and coated at the same time with the sample mounts.

In the leucocratic segregation samples from BHD1 and BHD4, zircon crystals are predominantly subhedral, prismatic to elongate ranging between 100 µm and 2 mm long, and many show thin, non-radial fractures (Figure 7.5 A and C). Some crystals have sharply delineated metasomatic zones but most are free from alteration. Many crystals appear skeletal or incomplete and some have quench-like textures, indicating rapid growth, consistent with their formation in a late-stage leucocratic segregation of the dyke. All crystals appear bright and unzoned under backscattered electron (BSE) microscopy and most are weakly zoned under cathodoluminescence (CL) imaging, brighter CL being associated with rims and fractures (Figure 7.5 B and D). Collectively, these characteristics support an igneous origin for the zircon (e.g. Corfu et al., 2003). Baddeleyite crystals form predominantly euhedral laths between 50 and 70 µm long (Figure 7.5 E and F). Thin zircon rims are common but fracture-associated alteration appears insignificant.

Zircon and baddeleyite were analysed for U, Th and Pb using the sensitive high-resolution ion microprobe (SHRIMP II) at the John de Laeter Centre at Curtin University, following standard operating procedures after Compston et al. (1984). The SHRIMP analysis method for mounts with polished thin section plugs outlined in Rasmussen and Fletcher (2010) was modified for baddeleyite (SHRIMP operating parameters are given in Table 7.2). BR266 zircon ($^{206}Pb/^{238}U$ age of 559 Ma, U concentration of 903 ppm; Stern, 2001) was used as a primary standard for calibrating Pb/U ratio and U concentration, and OG1 zircon with a $^{207}Pb/^{206}Pb$ age of 3465 Ma (Stern et al., 2009) was used to monitor the instrumental mass fractionation

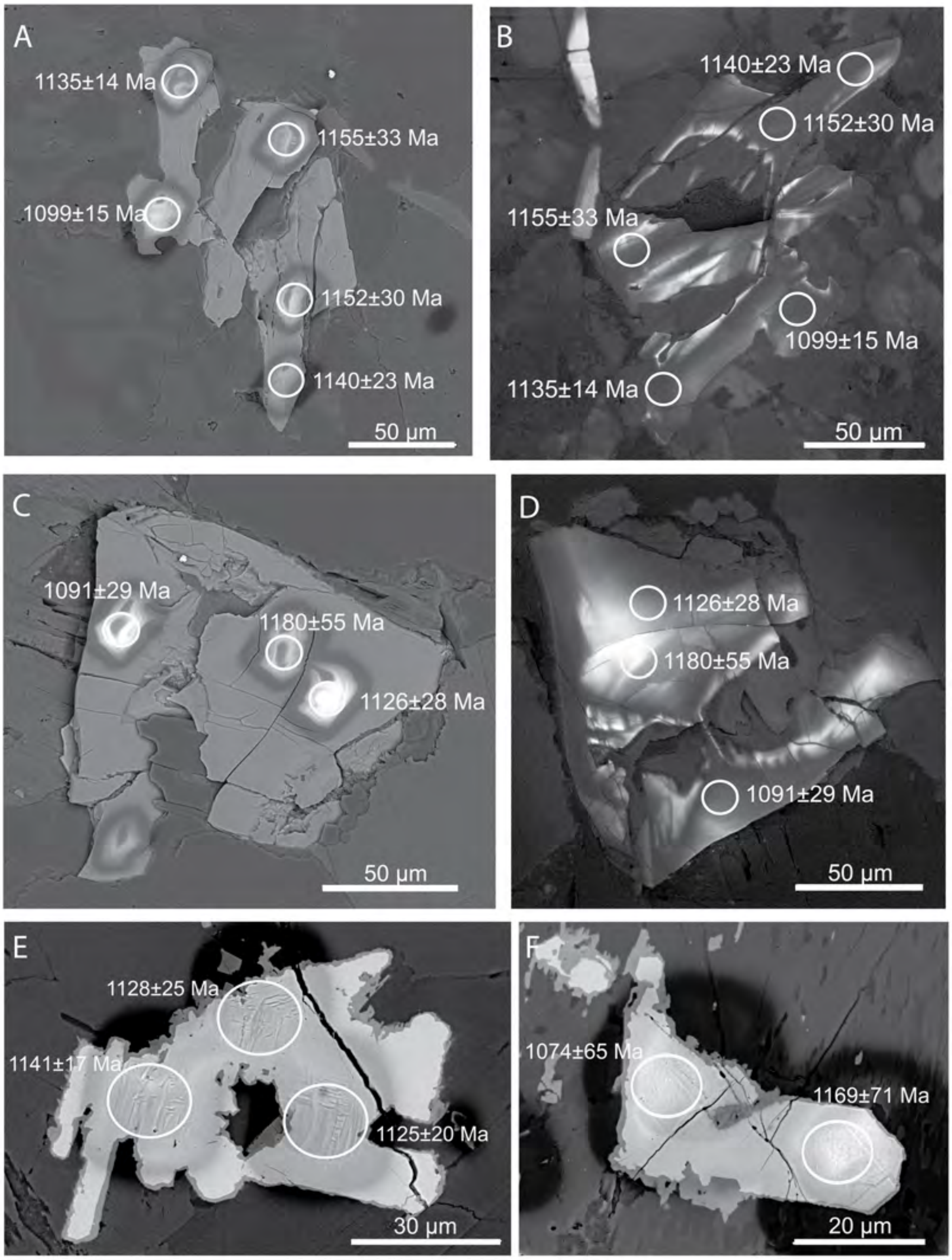

*Figure 7.5 SEM backscatter (BSE) and cathodoluminescence (CL) images showing SHRIMP spots and $^{207}Pb/^{206}Pb$ dates with 1$\boldsymbol{\sigma}$ error. (**A**) BSE and (**B**) CL images of zircons from BHD4-7B (note the rotation of the CL image). (**C**) BSE and (**D**) CL images of zircons from BHD4-7A. (**E**) and (**F**) SEM images of baddeleyite from BHD1-4.*

Mount	CS15-5	CS15-6
Samples analysed	BHD1-7, BHD4-7	BHD1-4, BHD4-1, BHD4-5
Date analysed	25-Nov-15	20-Oct-15
Kohler aperture (µm)	70	50
Spot size (micrometres)	20	13
O2- primary current (nA)	1.3	1.5
Number of scans per analysis	6	8
Total number of analyses	27	23
Number of standard analyses	22	21
Pb/U external 1σ precision % (assigned minimum 1%)	1.0	1.0
Raster time (seconds)	120	120
Raster aperture (µm)	90	90

Notes **1)** Mass resolution for all analyses ≥ 5000 at 1% peak height **2)** BR266, OGC, Phalaborwa and NIST 611 used as standards **3)** Count times for each scan for baddeleyite: ^{204}Pb, ^{206}Pb, ^{208}Pb = 10 seconds, ^{207}Pb = 30 seconds; count times for zircon: ^{204}Pb, ^{208}Pb = 10 seconds, ^{206}Pb = 20 seconds, ^{207}Pb = 30 seconds

Table 7.2 SHRIMP operating parameters

(IMF) in ^{207}Pb/^{206}Pb. For the baddeleyite analyses, the Phalaborwa baddeleyite (ca. 2060 Ma; Heaman, 2009) was employed as an additional standard. Typical spot size of the primary O_2^- beam was 13-20 µm with 1.3-1.5 nA current.

Data were processed with Squid version 2.50 (Ludwig, 2009) and Isoplot version 3.76.12 (Ludwig, 2012). For common Pb correction, 1134 Ma common Pb isotopic compositions were calculated from the Stacey and Kramers (1975) two-stage terrestrial Pb isotopic evolution model. Analyses with >1% common Pb (in ^{206}Pb) or >10% discordance for baddeleyite or >5% discordance for zircon (see footnote in Table 7.3 for definition of discordance) are considered unreliable and were disregarded in age calculations. All weighted mean ages are given at 95% confidence level and individual analyses are presented with 1σ error.

7.7.2 Geochemistry

Twelve blocks (BHD1-1 to BHD1-6 and BHD4-1 to BHD4-6) were cut from the hand specimens to remove weathered and altered parts. After initial crushing, approximately one quarter of the chips was split from each sample and the remaining material was pulverised in a chrome steel mill with quartz wash between each sample. From the quarter sample, chips with fresh fracture surfaces were picked under the microscope, washed and pulverised manually in an agate mill for isotope analysis.

Major elements were analysed at Intertek Genalysis Laboratories, Perth using X-ray fluorescence (XRF) and Genalysis laboratory internal standards SARM1 and SY-4. Trace elements were analysed with a Perkin-Elmex Sciex ELAN 6000 inductively coupled plasma mass spectrometer (ICP-MS) at Guangzhou Institute of Geochemistry, Chinese Academy of Sciences, following analytical procedures as described in Li (1997) and Liu et al. (1996). Sample powders were dissolved in high-pressure Teflon bombs using HF-HNO_3 mixture and an internal standard solution with Rh was used to monitor instrumental drift. A set of USGS standards including BHVO-2, AGV-2, GSR-3, W-2 and SARM4 were used for calibration of element concentrations. The uncertainty for major element analyses is <5% and most trace element analyses have relative standard deviation (RSD) < 3%.

Sr, Nd and Hf isotope analyses for six samples (three samples from BHD1 and BHD4 each) were carried out at the Earth and Planetary Sciences Geoanalytical Unit at Macquarie University, Sydney (e.g., Genske et al., 2016). Whole-rock samples and USGS reference material BHVO-2 (~100 mg) were digested in Teflon beakers and loaded onto Teflon columns. Hafnium was collected with the matrix after 5.4 mL and Sr after 34.9 mL, followed by Nd. Neodymium was further separated from Sm, Ba, La, Ce using a second column and Hf was separated from the matrix using two further columns. Isotopic analyses of Sr and Nd were obtained using a Thermo Finnigan Triton thermal ionisation mass spectrometer (TIMS). Samples for Sr isotope analysis were loaded onto single rhenium filaments and analysed (1380–1430°C, 1–11 V). Ratios were normalised to $^{86}Sr/^{88}Sr = 0.1194$ to correct for mass fractionation. Samples for Nd isotope analysis were loaded onto double rhenium filaments and analysed (1200–1600 °C, 0.5–10 V). Ratios were normalised to $^{146}Nd/^{144}Nd = 0.7219$ to correct for mass fractionation. Hafnium isotope analyses were obtained using a Nu Instruments multi-collector (MC) ICP-MS Nu034 and ratios were normalised to $^{176}Hf/^{177}Hf = 0.7325$ to correct for mass fractionation.

7.8 Results

7.8.1 SHRIMP U-Pb geochronology

Twenty-seven analyses were obtained from seven zircon crystals (four from BHD1 and three from BHD4) in one SHRIMP session (Figure 7.6 A and Table 7.3). The U and Th concentrations in most analyses are, respectively, <500 ppm (59–1551 ppm, median 385 ppm) and <850 ppm (40–4390 ppm, median 565 ppm). All Th/U ratios are >0.5 (0.55–2.83, median 1.55). Seven analyses were excluded on the basis of >5% discordance (all analyses had <0.55% common ^{206}Pb). The remaining twenty analyses (from seven crystals) yielded a weighted mean ^{206}Pb*/^{238}U (Pb* denotes radiogenic Pb) date of 1133 ± 7 Ma (MSWD = 1.2) and a weighted mean ^{207}Pb*/^{206}Pb* date of 1134 ± 9 Ma (MSWD = 0.87).

Twenty-three analyses were obtained from eleven baddeleyite crystals (six grains from BHD1 and five grains from BHD4) in one SHRIMP session (Figure 7.6 B and Table 7.3). The U and Th concentrations range from, respectively, 56–703 ppm (median 135 ppm) and from 1–83 ppm (median 13 ppm). All Th/U ratios are <0.13 (0.014–0.126, median 0.075). Twelve analyses were excluded due to >1% common ^{206}Pb or >10% discordance, or both. The remaining eleven analyses (from eight crystals) yielded a weighted mean ^{207}Pb*/^{206}Pb* date of 1131 ± 16 Ma (MSWD = 0.95). Only ^{207}Pb*/^{206}Pb* results are discussed here because ^{206}Pb*/^{238}U ratios measured with an ion microprobe may be significantly affected by orientation effects in baddeleyite crystals (Wingate, 1997; Wingate et al., 1998; Wingate and Compston, 2000; Schmitt et al., 2010).

The respective zircon and baddeleyite ^{207}Pb*/^{206}Pb* weighted mean dates of 1134 ± 9 Ma and 1131 ± 16 Ma are within analytical uncertainty of each other, indicating that the leucocratic segregation from which the zircons were sampled is part of the dyke. The more precise date of 1134 ± 9 Ma for zircons extracted from the leucocratic segregation (samples BHD1-7 and BHD4-7) is therefore considered to be the best estimate of the crystallisation age of the dyke. At BHD1, the dyke intrudes the Paz Cove charnockite, which has yielded U-Pb zircon dates of 1170 ± 4 Ma (Sheraton et al., 1992) and 1200 ± 6 Ma (Tucker et al., 2017). The pelites and orthogneisses contain zircon populations, respectively, between 1900 and 1500 Ma and between ca. 1700 and 1500 Ma, and are underlain by (unexposed) basement of Archean age (Tucker et al., 2017). These data further support the interpretation that the analysed zircons are not xenocrysts originating from the basement. The previously estimated emplacement age of ca. 1140 Ma for most of the group 3 and 4 dykes was based on Rb–Sr whole-rock and limited Sm–Nd isochron analyses by Sheraton et al. (1990) and is confirmed by our geochronology results. The most precise ages from their study were 1220 ± 80 Ma for group 3A dykes, 1120 ± 40 Ma for group 4D dykes (Sm–Nd mineral isochron) and 1160 ± 160 Ma for group 4E dykes. It is notable that the group 4D age is within uncertainty of the U-Pb ages reported here. Close agreement between the Rb-Sr (and some Sm-Nd) ages obtained from a number of NW-trending group 3 and 4 dykes by Sheraton et al. (1990) and the new U-Pb ages from the single NW-trending dyke in this study suggests that most group 3 and 4 dykes, and possibly other NW-trending dykes at Bunger Hills may be coeval and belong to the same dyke swarm.

7.8.2 Geochemistry

7.8.2.1 Major and trace elements

The results for geochemical analyses of 12 samples, collected along strike from the same dyke, are listed in Table 7.4. All samples have loss on ignition (LOI) <1 wt%, consistent with petrographic evidence for insignificant alteration. They display a wide range in MgO (6.15–9.27 wt%; Mg# = 47.37–63.66), low but near-constant SiO_2 (45.52–47.32 wt%) and relatively low CaO (7.69–9.23 wt%). They are also characterized by enrichment in FeO_{total} (12.03–15.94 wt%) and Al_2O_3 (15.82 to 19.30 wt%). The total alkali contents ($Na_2O + K_2O$ = 3.52–4.06 wt%) and Na_2O/K_2O ratios (3.43 to 5.14) are high, indicating alkali and sodium enrichment. All samples plot just outside the sub-alkaline field, in the alkaline corner of the basaltic field on the TAS diagram (Figure 7.7 A) (Irvine and Baragar, 1971; Le Maitre et al., 2002) and despite their alkaline character, display a tholeiitic trend on the AFM diagram (Irvine and Baragar, 1971; Figure 7.7 B). Modal calculations (Johannsen, 1931) indicate that all samples are hypersthene-normative with up to 5% olivine, 50–60% plagioclase, up to 5% orthoclase, 4–10% diopside, 5–16% hypersthene, up to 20%

Table 7.3 SHRIMP U-Pb data for zircon and baddeleyite from dyke samples BHD1 and BHD4

Notes **1)** f_{204} is the proportion of common Pb in ^{206}Pb, determined using the measured ^{204}Pb/^{206}Pb and a common Pb composition from the Stacey and Kramers (1975) model at the approximate age of the sample **2)** Disc. = 100(t[^{207}Pb*/^{206}Pb*] - t[^{238}U/^{206}Pb*/])/t[^{207}Pb*/^{206}Pb*]

Spot	f_{206} %	U ppm	Th ppm	^{232}Th/^{238}U	±%	Total ^{238}U/^{206}Pb	±%	Total ^{207}Pb/$_{206}$Pb	±%	^{238}U/^{206}Pb*	±%	^{207}Pb*/^{206}Pb*	±%	^{206}Pb/^{238}U Age (Ma)	± 1σ	^{207}Pb/^{206}Pb Age (Ma)	± 1σ	Disc. %
Zircons																		
BHD1-7A.21Z-1	0.03	846	1527.07	1.86	0.54	5.16	1.3	0.07806	0.65	5.16	1.3	0.0778	0.7	1142	±14	1142	±14	+0
BHD1-7A.21Z-3	0.13	365	565.30	1.60	0.77	5.30	1.2	0.07786	1.00	5.31	1.2	0.0767	1.3	1112	±13	1115	±25	+0
BHD4-7A.104Z-1	0.00	188	102.90	0.57	0.95	5.29	1.4	0.07718	1.39	5.29	1.4	0.0772	1.4	1117	±15	1126	±28	+1
BHD4-7A.104Z-2	0.16	286	328.79	1.19	2.88	5.30	1.3	0.07716	1.10	5.31	1.3	0.0758	1.4	1112	±13	1090	±29	-2
BHD4-7A.104Z-3	--	106	96.38	0.94	0.47	5.22	1.7	0.07640	1.87	5.20	1.7	0.0793	2.8	1134	±18	1180	±55	+4
BHD1-7A.19Z-1	0.05	518	856.57	1.71	0.29	5.27	1.2	0.07806	0.83	5.27	1.2	0.0777	0.9	1120	±12	1139	±18	+2
BHD1-7A.19Z-3	--	209	281.15	1.39	0.74	5.35	1.9	0.07786	2.05	5.35	1.9	0.0783	2.1	1105	±19	1155	±42	+5
BHD4-7B.81Z-1	0.07	634	1429.42	2.33	0.48	5.16	1.2	0.07812	0.73	5.17	1.2	0.0775	0.8	1141	±12	1135	±16	-1

Spot	f_{206} %	U ppm	Th ppm	$^{232}Th/^{238}U$	±%	Total $^{238}U/^{206}Pb$	±%	Total $^{207}Pb/_{206}Pb$	±%	$^{238}U/^{206}Pb^{*}$	±%	$^{207}Pb^{*}/^{206}Pb^{*}$	±%	$^{206}Pb/^{238}U$ Age (Ma) ± 1σ		$^{207}Pb/^{206}Pb$ Age (Ma) ± 1σ		Disc. %
BHD4-7B.81Z-2	--	387	712.09	1.90	0.57	5.07	1.2	0.07877	0.97	5.07	1.2	0.0793	1.1	1161	±13	1180	±21	+2
BHD4-7B.81Z-3	--	510	1265.53	2.56	0.32	5.20	1.2	0.07786	0.93	5.20	1.2	0.0779	0.9	1134	±13	1143	±19	+1
BHD1-7B.36Z-1	0.10	550	914.92	1.72	0.82	5.27	1.6	0.07812	0.79	5.28	1.6	0.0772	1.0	1119	±17	1127	±19	+1
BHD4-7B.66Z-1	0.18	491	843.71	1.78	0.61	5.22	1.2	0.07923	0.87	5.23	1.2	0.0777	1.2	1129	±12	1140	±23	+1
BHD4-7B.66Z-2	0.54	541	832.11	1.59	1.12	5.18	1.2	0.08276	0.82	5.21	1.2	0.0782	1.5	1132	±12	1152	±30	+2
BHD4-7B.66Z-3	0.05	445	920.72	2.14	0.38	5.17	1.2	0.07871	1.59	5.18	1.2	0.0783	1.6	1139	±12	1155	±33	+1
BHD1-7B.41Z-2	0.20	987	2046.35	2.14	0.89	5.08	1.4	0.07914	0.60	5.09	1.4	0.0774	0.8	1156	±15	1132	±16	-2
BHD1-7B.41Z-3	--	385	390.48	1.05	0.42	5.26	1.3	0.07778	1.01	5.26	1.3	0.0781	1.1	1121	±13	1149	±21	+3
BHD1-7A.19Z-4	0.22	170	216.48	1.31	0.58	5.25	1.5	0.07899	1.47	5.26	1.5	0.0772	2.0	1122	±15	1125	±41	+0
BHD1-7B.66Z-4	0.03	701	1288.08	1.90	0.25	5.19	1.1	0.07641	0.69	5.19	1.1	0.0761	0.7	1136	±12	1099	±15	-4
BHD1-7B.66Z-5	0.09	971	2197.97	2.34	1.24	5.12	1.1	0.07829	0.62	5.13	1.1	0.0775	0.7	1148	±12	1135	±14	-1
BHD1-7B.36Z-4	0.15	305	475.12	1.61	0.60	5.12	1.3	0.07859	1.08	5.12	1.3	0.0773	1.4	1149	±14	1129	±28	-2
Baddeleyites																		
BHD1-4.164B-1	0.21	480	37.31	0.08	0.56	5.13	1.7	0.07959	0.92	5.14	1.7	0.0778	1.2	1146	±18	1142	±25	-0
BHD1-4.167B-1	0.53	92	1.28	0.01	1.92	5.15	1.4	0.08336	2.02	5.18	1.4	0.0789	3.6	1138	±15	1169	±71	+3
BHD1-4.167B-2	0.93	168	2.25	0.01	5.34	5.05	1.2	0.08300	1.42	5.09	1.3	0.0752	3.2	1155	±13	1074	±65	-8
BHD1-4.181B-1	0.04	690	61.52	0.09	0.54	5.21	1.1	0.07830	0.82	5.21	1.1	0.0779	0.9	1132	±11	1146	±18	+1
BHD4-1.209B-2	0.45	683	58.82	0.09	1.55	5.17	1.3	0.07805	0.96	5.19	1.3	0.0742	1.6	1136	±14	1048	±33	-9
BHD4-1.209B-3	0.35	703	62.16	0.09	0.70	5.17	1.4	0.08004	0.86	5.19	1.4	0.0771	1.3	1137	±14	1123	±27	-1
BHD4-5.115B-1	0.87	72	4.92	0.07	6.93	5.03	1.4	0.08752	1.99	5.08	1.5	0.0802	4.1	1159	±16	1201	±81	+4

Spot	f_{206} %	U ppm	Th ppm	$^{232}Th/^{238}U$	±%	Total $^{238}U/^{206}Pb$	±%	Total $^{207}Pb/_{206}Pb$	±%	$^{238}U/^{206}Pb^*$	±%	$^{207}Pb^*/^{206}Pb^*$	±%	$^{206}Pb/^{238}U$ Age (Ma)	± 1σ	$^{207}Pb/^{206}Pb$ Age (Ma)	± 1σ	Disc. %
BHD1-4.157B-1	0.11	368	28.52	0.08	0.63	5.15	1.1	0.07806	0.82	5.15	1.1	0.0772	1.0	1143	±12	1125	±20	-2
BHD1-4.157B-2	0.07	409	29.82	0.08	0.37	5.15	1.1	0.07840	0.77	5.15	1.1	0.0778	0.9	1143	±11	1141	±17	-0
BHD1-4.157B-3	0.25	388	34.33	0.09	0.40	5.30	1.6	0.07941	0.90	5.31	1.6	0.0773	1.3	1112	±16	1128	±25	+2
BHD4-1.205B-3	0.36	69	2.71	0.04	24.77	5.32	1.5	0.08056	2.44	5.34	1.6	0.0775	3.8	1107	±16	1134	±75	+3
Excluded analyses																		
Zircons																		
BHD1-7A.21Z-2	--	101	91.76	0.94	0.46	5.34	1.7	0.07832	1.76	5.31	1.7	0.0819	2.7	1111	±18	1243	±54	+12
BHD1-7A.19Z-2	0.15	76	50.35	0.68	1.01	5.45	1.9	0.08025	2.12	5.46	1.9	0.0790	2.7	1085	±19	1172	±53	+8
BHD1-7B.36Z-2	--	184	219.94	1.23	0.71	5.34	1.5	0.07920	1.44	5.33	1.5	0.0804	1.8	1108	±15	1206	±34	+9
BHD1-7B.36Z-3	--	222	302.89	1.41	0.29	5.17	1.4	0.08062	1.25	5.17	1.4	0.0811	1.4	1140	±14	1223	±27	+7
BHD1-7B.41Z-1	0.01	1551	4390.02	2.92	0.85	4.99	1.4	0.07639	0.46	4.99	1.4	0.0763	0.5	1177	±15	1104	±9	-7
BHD1-7A.19Z-5	--	128	131.72	1.06	0.43	5.35	1.7	0.07935	1.76	5.33	1.7	0.0820	2.5	1109	±17	1246	±50	+12
BHD1-7A.19Z-6	--	59	40.27	0.71	1.03	5.50	2.1	0.08099	2.45	5.47	2.2	0.0860	4.1	1082	±21	1339	±79	+21
Baddeleyites																		
BHD1-4.193B-1	2.30	67	1.13	0.02	2.13	5.42	3.5	0.08587	2.60	5.55	3.6	0.0668	9.8	1068	±35	832	±205	-31
BHD1-4.193B-2	0.45	76	1.10	0.01	2.22	5.90	2.2	0.08066	3.93	5.92	2.3	0.0769	5.4	1006	±21	1118	±108	+11
BHD4-1.205B-1	2.86	107	5.96	0.06	1.06	5.10	1.5	0.10447	2.04	5.25	1.6	0.0803	7.8	1123	±17	1204	±154	+7
BHD4-1.205B-2	6.27	81	4.54	0.06	5.98	4.70	2.6	0.12921	1.85	5.01	2.9	0.0764	12.8	1173	±31	1107	±256	-7
BHD1-4.179B-1	1.38	110	2.37	0.02	2.85	4.60	1.3	0.08508	2.64	4.67	1.4	0.0735	5.1	1251	±16	1028	±102	-24

Spot	f_{206} %	U ppm	Th ppm	$^{232}Th/^{238}U$	±%	Total $^{238}U/^{206}Pb$	±%	Total $^{207}Pb/_{206}Pb$	±%	$^{238}U/^{206}Pb^*$	±%	$^{207}Pb^*/^{206}Pb^*$	±%	$^{206}Pb/^{238}U$ Age (Ma)	± 1σ	$^{207}Pb/^{206}Pb$ Age (Ma)	± 1σ	Disc. %
BHD1-4.179B-2	0.26	692	63.33	0.09	0.86	4.69	1.3	0.07995	0.65	4.70	1.3	0.0778	0.9	1243	±15	1141	±18	-10
BHD1-4.181B-2	0.27	679	83.00	0.13	3.91	4.59	2.0	0.07661	0.81	4.60	2.0	0.0744	1.2	1268	±23	1052	±24	-23
BHD4-1.209B-1	2.42	135	13.46	0.10	3.31	4.55	1.4	0.08223	2.95	4.66	1.5	0.0623	7.6	1253	±17	686	±161	-91
BHD4-5.115B-2	4.49	56	4.32	0.08	1.02	4.71	1.6	0.12511	1.89	4.93	1.8	0.0868	9.0	1190	±20	1357	±174	+13
BHD4-5.117B-1	0.12	343	20.19	0.06	0.79	5.62	1.4	0.08045	0.97	5.62	1.4	0.0794	1.2	1055	±13	1183	±23	+12
BHD4-5.125B-1	1.78	95	2.93	0.03	1.19	4.78	2.2	0.08727	2.94	4.87	2.2	0.0724	6.2	1205	±25	996	±127	-23
BHD4-1.209B-4	2.08	127	12.54	0.10	2.36	4.95	1.4	0.08383	1.83	5.06	1.5	0.0666	6.5	1163	±16	826	±135	-45

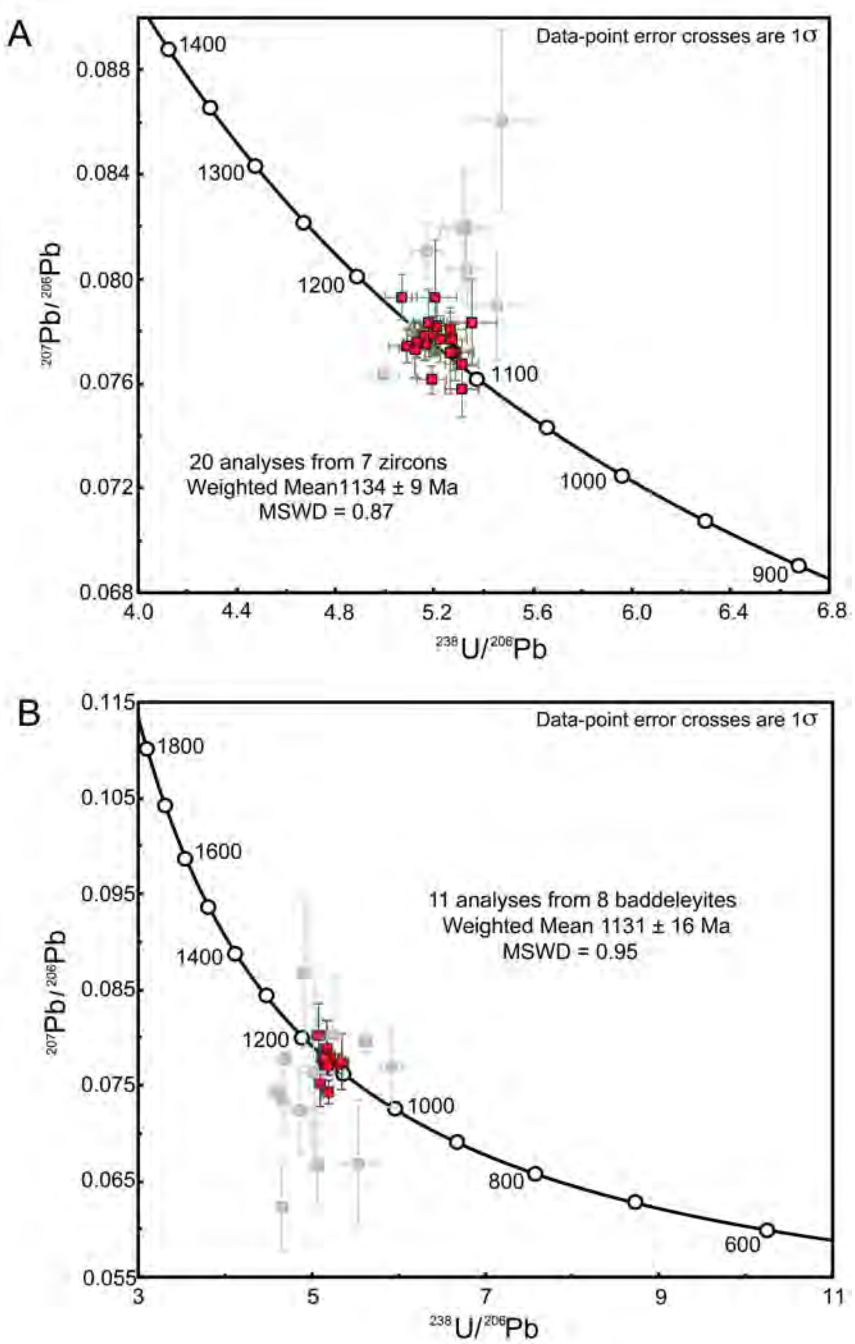

*Figure 7.6 Tera-Wasserburg plot of SHRIMP U-Pb results for **(A)** zircon and **(B)** baddeleyite analyses. Grey squares denote excluded data (see section 7.8.1 for details).*

Fe–Ti oxides (ilmenite and hematite), <1% quartz and traces of apatite, spinel and zircon. Samples from BHD4 (central part of Bunger Hills) contain more normative olivine and no quartz.

Trace element profiles on a chondrite-normalised plot show moderate enrichment of light rare earth elements (LREE) with $(La/Sm)_{CN}$ = 1.44–1.68 and $(La/Yb)_{CN}$ = 3.15–4.17 and slight fractionation of heavy rare earth elements (HREEs) with $(Sm/Yb)_{CN}$

= 1.98–2.31, $(Gd/Yb)_{CN}$ = 1.53–1.79 and $(Tb/Yb)_{CN}$ = 1.47–1.59 (Sun and McDonough, 1989, Figure 7.7 C). Most samples display a positive Eu anomaly (Figure 7.7 C, Table 7.4). The primitive mantle-normalised patterns show negative Nb and Ta and negative to positive Ti anomalies, elevated large ion lithophile elements (LILE) and elevated Th (Figure 7.7 D).

Some samples also display a Zr and Hf trough. Aside from the positive Ti anomalies of the samples, the overall trace element profile of the samples is very similar to that of lower continental crust (Rudnick and Gao, 2003). BHD1 samples have higher incompatible element contents than those of BHD4 samples, and the doleritic samples (BHD1-1 to BHD1-3) are higher in most incompatible elements. Two samples from the same dyke were collected by Sheraton et al. (1990), who classified sample 86286097 in the southeastern part of Bunger Hills as part of group 4A (Mg # = 47.5) and sample 86286091 in the northwestern part as a less evolved variant of Group 4A. The latter has a higher Mg number of 63.33, consistent with the highest Mg number of 63.66 of the BHD1 samples nearby. Major element data in this study are consistent with compositions of samples 86286091 and 86286097 of Sheraton et al. (1990). Previous studies have shown that major element compositions and trace element ratios of a single dyke belonging to a major regional swarm (>10 m in width) will be consistent along strike but may be different from an adjacent dyke, suggesting that each dyke represents a single magmatic pulse injected laterally from a magmatic chamber (Halls, 1986; Buchan et al., 2007; Ernst, 2014).

7.8.2.2 Nd and Sr isotopes

Six samples were analysed for Nd and Sr isotopes (Table 7.5). Measured ratios of $^{147}Sm/^{144}Nd$ and $^{143}Nd/^{144}Nd$ are, respectively, 0.1451–0.1602 and 0.5124390–0.5124560. Calculated initial ratios $^{143}Nd/^{144}Nd$ at 1134 Ma yielded 0.51125–0.51134, corresponding to εNd_{1134Ma} = +1.51 to +3.32, which is lower than the inferred lower estimate of εNd_{DM} = +5.4 for contemporaneous depleted mantle, calculated using the method of DePaolo (1981). The $^{87}Rb/^{86}Sr$ and $^{87}Sr/^{86}Sr$ ratios are, respectively, 0.1246–0.1771 and 0.7035–0.7071, with corresponding initial ratios $(^{87}Sr/^{86}Sr)_{1134Ma}$ = 0.703625–0.7043372. These values are higher than the contemporaneous depleted mantle (ca. 0.7019; Taylor and McLennan, 1985) and compatible with those expected in lower crust, which is strongly depleted in Rb

(Rudnick and Fountain, 1995; Rudnick and Gao, 2003; Hacker et al., 2015) and thus has low initial $^{87}Sr/^{86}Sr$ ratios similar to depleted mantle (Weaver and Tarney, 1980; Rollinson, 1993).

7.9 Discussion

7.9.1 Petrogenesis of the dykes

7.9.1.1 Fractional crystallisation

The range of Mg# (47–63) and low concentrations of compatible elements (Cr = 80.63-210.50 ppm, Ni = 88.9–220.0 ppm and MgO = 6.15-9.27 wt%) indicate that the dyke is evolved. The strong positive co-variation between Mg# and Ni ($r^2 = 0.90$) suggests olivine fractionation, consistent with presence of early (poikilitic) olivine in thin section (Figure 7.4). Elevated Al_2O_3 (15.82–19.30 wt%) can be attributed to a hydrous source (e.g. Wang et al., 2016) or accumulation of plagioclase. The latter is supported by low Rb/Sr ratios (0.03–0.06) and marked positive Eu anomalies mainly in the gabbroic samples. The degree of the Eu anomaly can be estimated using $Eu/Eu^* = Eu_{CN}/[(Sm_{CN}+Gd_{CN})]^{1/2}$ where Eu* is the expected extrapolated Eu concentration (Taylor and McLennan, 1985). Magmas evolving along liquid line of descent will have Eu/Eu* ≤1, assuming that there was no initial Eu/Eu* anomaly. All studied samples have Eu/Eu* >1 (1.04–1.28) with doleritic samples showing the smallest anomalies. The presence of positive Eu anomalies thus suggests that plagioclase is a cumulate mineral in the gabbroic samples.

The lack of correlation between Mg# and CaO ($r^2 = 0.07$) and Mg# and Sc/V ($r^2 = 0.02$) suggests that clinopyroxene fractionation may have been insignificant during magma evolution. Similarly, the presence of a strong negative covariance between Mg# and FeO_{tot} ($r^2 = 0.83$) and TiO_2 ($r^2 = 0.83$) indicates that fractionation of Fe-Ti oxides was insignificant as this would have resulted in strong depletion of these two elements.

Table 7.4 Major and trace element and isotope data for samples BHD1-1 to BHD1-6 and BHD4-1 to BHD4-6

Notes **1)**Major elements (XRF) are given in wt % and trace elements (ICP-MS) in ppm **2)** Mg# = 100 x Mg/(Mg+Fe), Fe^{2+}/Fe_{total}=0.85

	BHD1-1	BHD1-2A	BHD1-3	BHD1-4	BHD1-5	BHD1-6	BHD4-1B	BHD4-2	BHD4-3	BHD4-4	BHD4-5	BHD4-6
SiO_2	45.81	45.51	45.76	46.99	47.05	46.69	45.36	45.49	46.44	46.38	47.20	45.51
TiO_2	3.10	3.13	3.20	1.57	1.40	1.43	2.20	2.37	1.91	1.85	1.74	3.29
Al_2O_3	15.83	15.79	15.83	17.91	17.47	17.59	17.33	16.45	18.01	17.50	19.25	16.32
CaO	8.51	8.47	8.58	8.58	8.53	7.88	7.70	7.88	8.04	7.63	8.70	9.23
$Fe_2O_{3(tot)}$	15.63	15.60	15.95	12.36	12.35	13.15	15.21	15.26	13.37	13.95	12.00	14.59
K_2O	0.90	0.89	0.89	0.76	0.67	0.78	0.65	0.70	0.67	0.69	0.66	0.63
MgO	6.13	6.16	6.16	7.92	9.28	8.90	7.59	8.20	6.96	7.65	6.42	7.08
MnO	0.21	0.21	0.22	0.16	0.17	0.17	0.18	0.19	0.15	0.18	0.15	0.19
Na_2O	3.11	3.10	3.05	2.99	2.86	3.02	3.05	3.02	3.16	3.11	3.39	2.88
P_2O_5	0.43	0.43	0.44	0.31	0.29	0.38	0.26	0.27	0.26	0.27	0.23	0.25
LOI	0.22	0.21	-0.01	-0.06	-0.14	0.03	0.40	-0.05	0.95	0.59	0.03	0.08
Total	99.66	99.29	100.08	99.55	100.07	99.99	99.53	99.83	98.97	99.21	99.74	99.97
Mg#	47.76	47.93	47.37	59.90	63.66	61.20	53.77	55.61	54.82	56.11	55.50	53.08
Sc	27.03	26.44	26.45	16.17	16.47	11.96	14.66	17.91	14.87	13.47	13.38	29.48
V	239.40	233.20	244.30	158.60	100.80	125.60	231.60	201.10	178.10	152.80	161.00	251.60
Co	57.01	55.42	57.36	59.43	63.30	65.35	67.96	68.50	70.45	69.09	55.23	60.63
Ni	93.96	90.67	94.56	189.10	213.60	220.00	167.20	169.30	191.10	181.70	147.70	145.60
Ga	21.26	20.94	21.34	18.83	17.57	18.32	18.96	18.44	18.76	18.17	19.28	19.18

Table 7.4 *continued*

	BHD1-1	BHD1-2A	BHD1-3	BHD1-4	BHD1-5	BHD1-6	BHD4-1B	BHD4-2	BHD4-3	BHD4-4	BHD4-5	BHD4-6
Ge	3.99	3.56	3.98	3.18	2.81	3.20	3.40	3.27	3.25	3.25	2.71	3.23
Rb	18.82	17.88	17.97	17.06	14.46	17.53	12.91	13.72	12.76	13.79	11.98	12.60
Sr	293.90	289.10	293.60	317.90	305.10	306.50	309.10	303.70	333.20	320.40	365.00	292.20
Y	39.34	34.21	39.38	26.61	22.19	27.85	20.92	20.98	21.43	21.64	19.36	25.88
Zr	203.00	199.70	196.30	155.40	123.70	139.00	73.06	117.70	117.80	78.80	76.15	102.00
Nb	12.60	10.74	12.82	8.15	6.88	8.65	7.10	6.94	7.12	7.62	6.70	9.11
Cs	0.28	0.23	0.39	0.31	0.22	0.32	0.23	0.20	0.23	0.25	0.21	0.23
Ba	318.30	314.40	320.20	265.20	242.20	262.70	239.40	245.90	239.90	252.90	243.50	236.10
La	16.29	16.61	16.10	12.14	11.72	13.72	10.06	10.97	10.00	10.69	9.34	9.98
Ce	39.00	38.29	39.32	28.40	27.89	32.34	23.30	25.34	23.49	24.72	21.64	23.93
Pr	5.51	5.13	5.47	3.90	3.53	4.43	3.20	3.32	3.24	3.40	2.98	3.40
Nd	25.63	23.31	26.10	18.09	15.64	20.33	14.89	14.91	14.99	15.54	13.74	16.15
Sm	6.41	6.25	6.43	4.37	4.15	4.88	3.51	3.94	3.60	3.73	3.28	4.15
Eu	2.23	2.20	2.25	1.61	1.51	1.70	1.38	1.50	1.42	1.46	1.38	1.60
Gd	6.64	6.65	6.72	4.52	4.36	4.92	3.67	4.09	3.73	3.82	3.32	4.43
Tb	1.16	1.03	1.19	0.79	0.67	0.85	0.64	0.64	0.64	0.65	0.59	0.76
Dy	7.09	6.23	7.21	4.70	4.03	5.04	3.75	3.81	3.83	3.96	3.46	4.70
Ho	1.46	1.28	1.49	0.98	0.82	1.04	0.78	0.79	0.79	0.81	0.71	0.96
Er	3.98	3.40	4.02	2.66	2.22	2.83	2.08	2.10	2.15	2.20	1.94	2.60
Tm	0.58	0.49	0.59	0.40	0.32	0.41	0.30	0.31	0.32	0.32	0.28	0.39
Yb	3.58	3.07	3.60	2.40	2.02	2.57	1.82	1.90	1.92	1.95	1.70	2.27

Table 7.4 *continued*

	BHD1-1	BHD1-2A	BHD1-3	BHD1-4	BHD1-5	BHD1-6	BHD4-1B	BHD4-2	BHD4-3	BHD4-4	BHD4-5	BHD4-6
Lu	0.52	0.47	0.52	0.36	0.30	0.37	0.27	0.29	0.28	0.28	0.25	0.33
Hf	5.22	4.63	5.05	3.91	2.88	3.52	1.92	2.78	2.94	2.07	1.96	2.82
Ta	0.77	0.67	0.79	0.48	0.41	0.52	0.43	0.44	0.45	0.46	0.44	0.57
Pb	4.96	4.44	5.05	4.42	3.46	4.21	4.32	3.50	3.68	3.73	3.46	3.62
Th	2.01	2.00	1.82	1.75	1.47	1.84	1.34	1.44	1.22	1.34	1.18	1.27
U	0.35	0.36	0.37	0.39	0.27	0.34	0.24	0.25	0.24	0.24	0.23	0.22

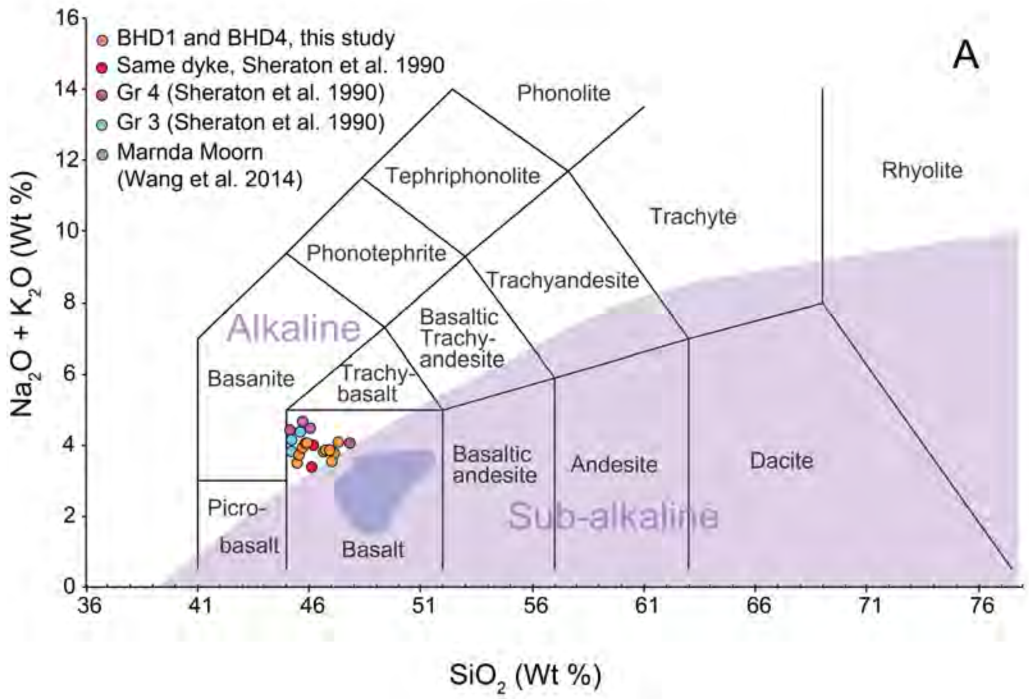

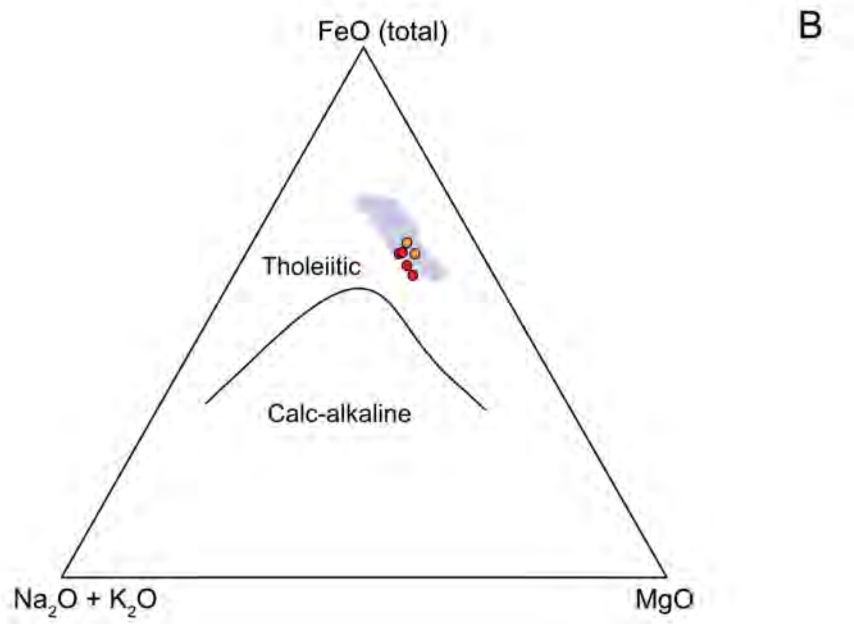

*Figure 7.7 (**A**) Total alkali-silica (TAS) plot after LeMaitre, 1989. Blue field denotes 1.21 Ga Marnda Moorn LIP dykes from Wang et al., 2014. (**B**) AFM plot after Irvine and Baragar, 1971. (**C**) Chondrite and (**D**) primitive mantle normalised multi-element plots with blue shaded area denoting range of Marnda Moorn dykes (Wang et al., 2014). LCC = lower continental crust after Rudnick and Gao, 2004; OIB = ocean island basalt, NMORB = mid ocean ridge basalt and EMORB = enriched MORB after Sun and McDonough, 1989*

.

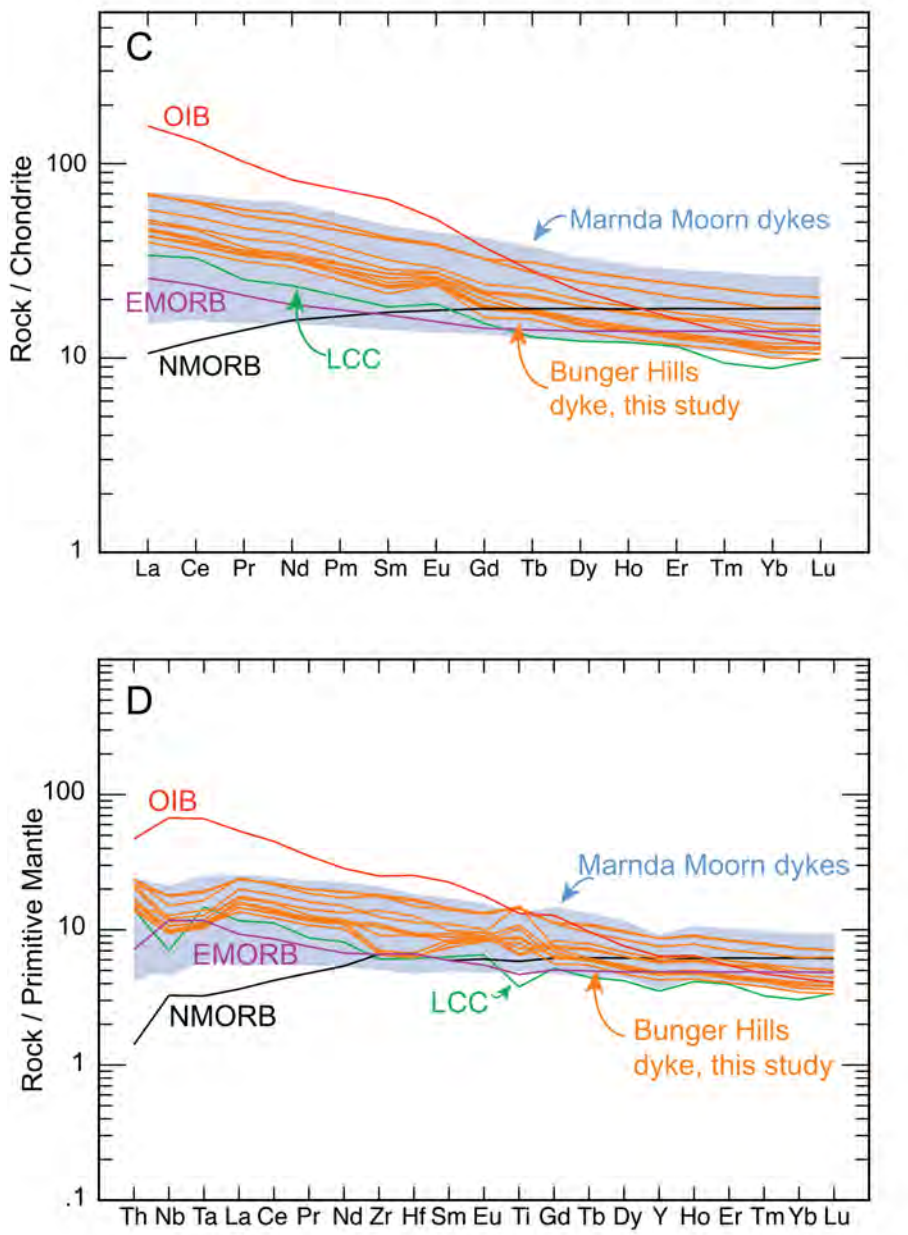

Figure 7.7 Continued.

7.9.1.2 Crustal contamination

Arc-like characteristics, such as negative Nb-Ta and Zr-Hf (HFSE) anomalies and elevated LILE contents on primitive mantle-normalised plots, may be due to subduction-related metasomatic enrichment, crustal contamination, or both (e.g. Saunders et al., 1992; Puffer, 2001; Wang et al., 2016). Relative to mantle, crust has high SiO_2, La/Sm, Th/La and $^{87}Sr/^{86}Sr_i$ but low εNd_t, MgO, Sm/Nd and Nb/La.

Contamination by (upper or middle) crustal material would produce positive correlations between Mg# and εNd_t, Nb/La and Sm/Nd and negative correlations between Mg# and La/Sm, Th/La and $^{87}Sr/^{86}Sr_i$ (e.g., Wang et al., 2012, 2014, 2016). Such predicted covariance is not observed in the analysed samples. Despite variations in the Mg number, the εNd_t values are nearly constant and the range of $^{87}Sr/^{86}Sr_i$ values is relatively small. In addition, ratios of La/Sm and Th/La are nearly constant and show weak positive correlation whereas ratios of Nb/La and Sm/Nd are nearly constant with a weak negative correlation. This implies that crustal contamination was not a significant process during magma evolution.

Trace element and isotope results from this study are consistent with those of Sheraton et al. (1990), who reported $^{87}Sr/^{86}Sr_i$ of 0.704 ± 0.002 for Group 4A dolerites (which includes the dyke sampled in this study) and εNd_{1140} between +2.9 and +6.3 for groups 4B, 4D and 4E, which have similar trace element profiles to group 4A. In addition, samples 86285833 from Geomorfologov Peninsula and 86286075 from the north-eastern part of Paz Cove (Group 4D and 4B dykes, respectively) have similar Sr_i (0.7044 and 0.7030, respectively) and εNd_t values (+2.9 and +3.9, respectively) as the dyke in this study. Sheraton et al. (1990) proposed that crustal contamination was significant only in Group 3A dykes and significant variability in trace element abundances and isotope compositions between dyke groups 1 to 4 was attributed to source heterogeneity.

As discussed above, crustal contamination was probably insignificant and the observed geochemical diversity likely reflects the source characteristics. As shown in Figs. 6C and 6D, the trace element composition of the samples is very similar to the lower continental crust (Rudnick and Gao, 2003) and the εNd_t values of the samples (+1.5 to +3.3) show slight but clear enrichment relative to the contemporary depleted mantle at 1134 Ma (+5.4; DePaolo, 1981). These characteristics suggest that the source probably involved a depleted mantle type component that interacted with material that had a lower εNd_t, slightly higher (but NMORB-like) $^{87}Sr/^{86}Sr_i$ and a lower crust-like trace element composition.

7.9.1.3 Nature of the mantle source

Mantle source characteristics in mafic systems can be investigated using ratios of incompatible trace elements that are sensitive to source composition and partial melting processes but insensitive to crystal fractionation. Ratios of Nb/La, Nb/Ta, Th/Nb, La/Sm, La/Yb, La/Ba, Sm/Nd and Th/U in the analysed samples are near constant despite a wide range of Mg#, indicating that they behaved in an essentially incompatible manner during fractional crystallisation and likely reflect their source composition. The average ratio of Nb/La = 0.71 falls between average depleted mantle values (0.90–0.93; Sun and McDonough, 1989; Salters and Stracke, 2004) and lower crust (0.63; Rudnick and Gao, 2003) whereas the ratio of Nb/Ta = 16.23 is close to that of NMORB or enriched MORB (EMORB) (17.65/17.66; Sun and McDonough, 1989). The ratio of Th/Nb = 0.18 is close to lower crust (0.24; Rudnick and Gao, 2003) and much higher than NMORB/EMORB or OIB (0.05/0.07 and 0.08, respectively; Sun and McDonough, 1989). The average ratios of La/Sm = 2.72, Sm/Nd = 0.25 and Th/U = 5.38 are all very close to lower crustal values (2.83, 0.25 and 6.0, respectively; Rudnick and Gao, 2003). The ratio of La/Yb = 5.82 is slightly higher than the lower crust (5.33) but much higher than MORB (0.82) and much lower than typical OIB (17.13).

The composition of the source region may also be constrained by using ratios of incompatible trace elements with identical bulk partition coefficients (D) (Sims and DePaolo, 1997; Willbold and Stracke, 2006; Wang et al., 2014). In log-log plots, slopes plot near unity if the ratios of two such elements remain constant. In the studied samples, calculated slopes are near unity for Tb/Yb (log(Tb) - log(Yb) = 1.05 ± 0.02 (1se), r^2 = 1.0), Lu/Yb (log(Lu) - log(Yb) = 1.01 ± 0.02 (1se), r^2 = 0.99), Gd/Yb (log(Gd) - log(Yb) = 1.03 ± 0.07 (1se), r^2 = 0.95), Zr/Hf (log(Zr) - log(Hf) = 0.94 ± 0.04 (1se), r^2 = 0.98) and Nb/Ta (log(Nb) - log(Ta) = 0.98 ± 0.04 (1se), r^2 = 0.98). The unit slopes of correlation between Tb and Yb, Gd and Yb, and Yb and Lu indicate that the bulk partition coefficients of middle REE and HREE are identical during partial melting and magma evolution (e.g. Wang et al., 2012). Because $D_{Tb/Yb}$, $D_{Gd/Yb}$ and $D_{Yb/Lu}$ are >1 between melt and garnet (e.g., Irving and Frey, 1978; Weaver and Tarney, 1981; Van Westrenen et al., 2001), this suggests that garnet is not the dominant phase in the residual mineral assemblage (e.g., Wang et al., 2012).

However, the observed slight overall HREE depletion could be due to a phase with a more uniform K_D for HREE, such as clinopyroxene. The slope of log (Nb) versus log (La) (0.77, r^2 = 0.74) indicates $D_{Nb/La}$ <1, which is a typical characteristic of partial melts of peridotitic dominant source (Wang et al., 2014). However, the near-unity slopes of log (Nb)-log(Ta) and log (Zr)-log (Hf) indicate presence of rutile in the source (e.g., Foley et al., 2000; Münker et al., 2004; Wang et al., 2014) because the calculated bulk partition coefficients $D_{Zr/Hf}$ and $D_{Nb/Ta}$ for peridotitic sources are less than one ($D_{Nb/Ta}$ ~ 0.4 ; Münker et al., 2004; Salters and Stracke, 2004; Pfänder et al., 2007; Wang et al., 2012; Zr/Hf ($D_{Zr/Hf}$ = 0.3 - 0.4; Wang et al. 2012 and references therein). These observations support a predominantly peridotitic source composition with at least one other rutile-bearing component.

The studied samples have elevated Th/Yb ratios similar to lower continental crust (LCC), Nb/Yb ratios close to both LCC and EMORB (Figure 7.8A) and, apart from elevated Th and enrichment in LILEs (Cs, Rb, K, Pb and Sr), the overall trace element distribution profiles of the samples share similarities with EMORB of Sun and McDonough (1989; Figure 7.8B). All samples lie near a binary mixing line between EMORB and LCC rather than assimilation and fractional crystallisation trajectories (AFC; Depaolo, 1981; Figure 7.8C). Binary mixing of EMORB with a depleted mantle-like εNd_t (+5.4) and $^{87}Sr/^{86}Sr_i$ (0.7030) and 20–30% of LCC -like component (εNd_t = -3.5, same as sample 86285815 of Charnockite Peninsula pluton) would require the latter to have $^{87}Sr/^{86}Sr_i$ ≤0.705 (sample 86285815 has $^{87}Sr/^{86}Sr_i$ = 0.708) to produce a reasonable mixing line between the two end member components (not shown in Figure 7.8C). The above evidence is consistent with the interpretation of Sheraton et al. (1990) who on the basis of isotope data proposed that the source of group 3 and 4 dykes involved a depleted mantle component, which was probably mixed with a lithospheric component enriched in subducted crustal material and/or long-term enriched late Archean or Paleoproterozoic mantle. However, Sheraton et al. (1990) also argued that significant differences in incompatible element ratios between the various dyke groups (presumed to be of similar age) preclude simple two-component mixing, requiring a more complex source and suggesting that the source region of the dykes was both laterally and vertically heterogeneous.

7.9.1.4 Relationship between plutonic rocks and mafic dykes at Bunger Hills

Emplacement of the plutons at Bunger Hills pre-dates the unmetamorphosed mafic dykes by 20 myr (and possibly less), although syn-plutonic dykes have also been reported (Sheraton et al., 1990, 1992, 1995). Compositions of the plutons range from subalkaline gabbro to quartz monzogabbro with tholeiitic affinity, and have primitive mantle-like HFSE ratios and LREE and LILE enrichment (Sheraton et al., 1992). The parental magmas of the gabbroic rocks had a high $^{87}Sr/^{86}Sr_i$ (0.7091 - 0.7147) and low εNd_t (-9.4) composition that likely originated from a common heterogeneous, long-term LILE- and LREE-enriched, Nb-poor mantle source. Compared to the Nb/La ratios of the older plutonic rocks at Bunger Hills, the Nb/La ratio (0.81, sample 86286051) of the youngest known pluton, the 1151 ± 4 Ma Booth Peninsula batholith, is much higher and comparable to the average Nb/La ratio (0.71) of the dyke in this study. In addition, the higher εNd (-3.5) and lower $^{87}Sr/^{86}Sr_i$ (0.7082, sample 86285815) of the Booth Peninsula batholith suggest a larger contribution from asthenospheric mantle than is the case for the older plutons (Nb/La = 0.19–0.25, Paz Cove sample 86286082; εNd = -9.4 and $^{87}Sr/^{86}Sr_i$ = 0.71435, Algae Lake sample 86265962, Sheraton et al., 1992). Moreover, probable syn-plutonic mafic granulite dykes with high Nb contents have been reported in the Booth Peninsula batholith (Sheraton et al., 1995).

Sheraton et al. (1992) suggested that Group 1 mafic dykes and the Charnockite Peninsula pluton could be coeval and originate from long-term (strongly) enriched lithospheric mantle with an OIB-like Nb-enriched component, whereas mafic dyke groups 3 and 4 tapped varying proportions of depleted asthenospheric mantle and only moderately enriched lithospheric mantle. Group 3 dykes have higher $^{87}Sr/^{86}Sr_i$ (0.7043) than most Group 4 dykes, which results in an older apparent whole-rock Rb-Sr isochron age (1220 ± 80 Ma; Sheraton et al., 1990). If correct, this would suggest a time-progressive increase in contribution from less enriched, more depleted mantle material in the dykes, which in turn is consistent with a similar trend observed in the plutonic rocks.

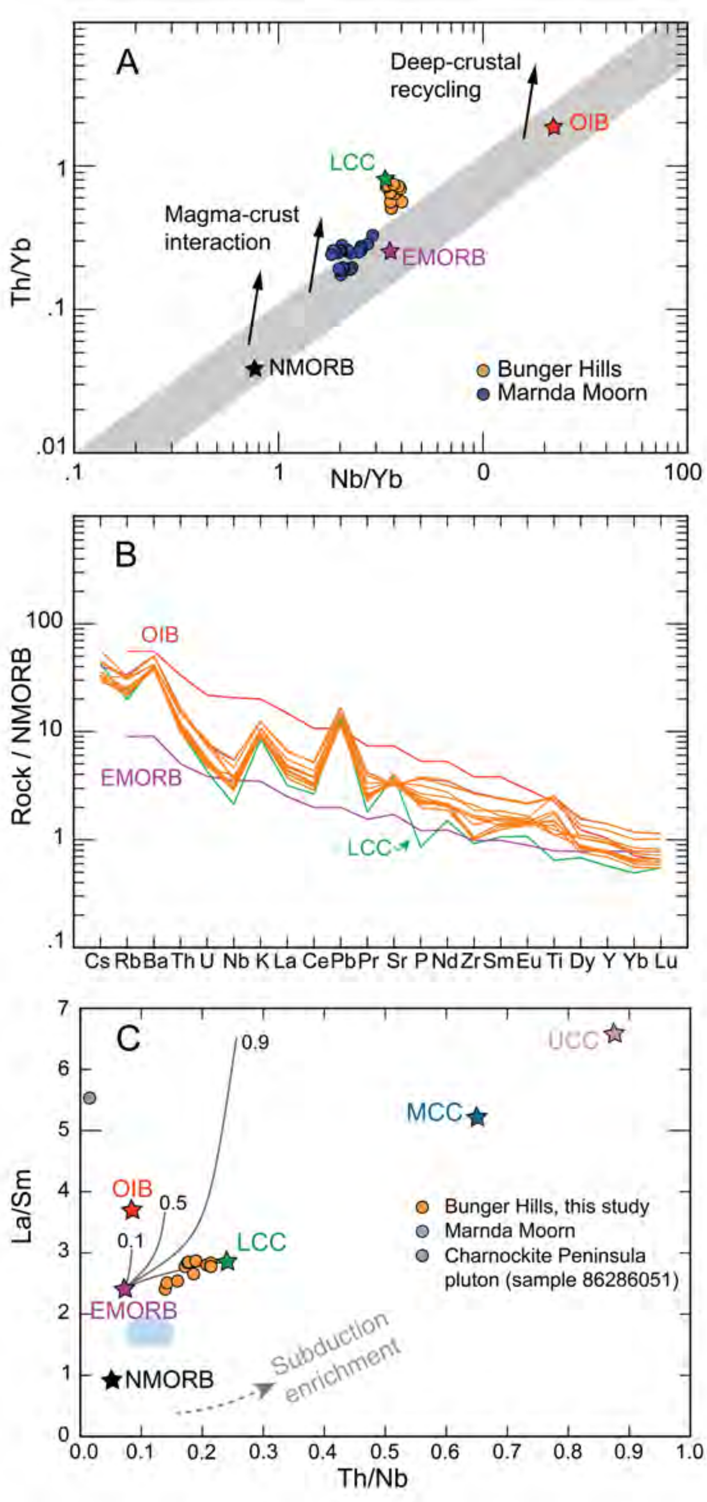

Figure 7.8 Incompatible trace element plots for samples from this study and from Marnda Moorn LIP dykes (Wang et al., 2014). NMORB, EMORB and OIB data are from McDonough, 1989 and lower crust (LCC) from Rudnick and Gao, 2004. MCC denotes middle continental crust and UCC upper continent crust.

***(A)** Nb/Yb vs Th/Yb after Pearce (2008)*

***(B)** NMORB-normalised incompatible trace element profile of samples from BHD1 and BHD4*

***(C)** Th/Nb vs La/Sm plot showing assimilation-fractional crystallisation (AFC; after DePaolo, 1981) and binary mixing between EMORB of Sun and McDonough (1989) and lower crust of Rudnick and Gao (2004). Numbers denote r values. Bulk partition coefficients D_{Th} = 0.01, D_{Nb} = 0.02, D_{La} = 0.11 and D_{Sm} = 0.19 after Rollinson (1993) assuming for 5% olivine, 35% clinopyroxene, 4% orthopyroxene, 55% plagioclase and 1% magnetite.*

7.9.2 Tectonic setting of Bunger Hills at ca. 1130 Ma

7.9.2.1 Bunger Hills as part of the Albany-Fraser Orogen

The Mesoproterozoic Albany-Fraser Orogen records two major tectonothermal events. The first stage at ca. 1340–1260 Ma was associated with the initial collision between the Western Australian and Mawson Cratons and the second at ca. 1214–1140 Ma with intracratonic reactivation and extension (Clark et al., 2000), both stages involving NW-directed compression in a transpressional setting (Myers, 1993; Nelson et al., 1995b; Bodorkos and Clark, 2004b). The Bunger Hills have widely been interpreted as a rifted fragment of the Albany–Fraser Orogen on the basis of similarities in lithology, structural style, kinematics, timing and degree of metamorphism (Black et al., 1992; Sheraton et al., 1993, 1995; Nelson et al., 1995; Clark et al., 2000; Duebendorfer, 2002; Fitzsimons, 2003; Boger, 2011; Tucker et al., 2017) and more recently geophysical evidence (Aitken et al., 2014, 2016). The Windmill Islands, ca. 400 km east along strike of Bunger Hills, have also been proposed as an along-strike extension of the Albany–Fraser Orogen through similar arguments (Paul et al., 1995; Post et al., 1997; Zhang et al., 2012; Morrissey et al., 2017). In the recent reconstruction of Aitken et al. (2014, 2016), at ca. 1150 Ma the Bunger Hills are directly aligned with the southwestern Albany-Fraser Orogen (Figure 7.9).

Tucker et al. (2017) proposed a revised model for the tectonic evolution of the Bunger Hills during the Paleo- and Mesoproterozoic, suggesting that they evolved as part of the Biranup and/or Nornalup zones of the Albany–Fraser Orogen. At ca. 1815–1650 Ma, Bunger Hills (then part of the southern margin of the Yilgarn Craton) was part of a back-arc (Biranup Zone) above a north-dipping subduction zone along the southern margin of the Yilgarn Craton (Kirkland et al., 2011; Spaggiari et al., 2015; Aitken et al., 2016). The period between ca. 1710 and 1650 Ma in the Albany-Fraser Orogen coincides with widespread magmatism, formation of a series of sedimentary basins and high-temperature metamorphism associated with the Biranup Orogeny (Kirkland et al., 2011; Spaggiari et al., 2011). Consistent with this scenario, isotope evidence suggests that recycling of an Archean basement source beneath the Bunger Hills was diluted by significant formation of new crust at ca. 1700 Ma (Tucker et al., 2017).

The ca. 1700 Ma volcaniclastic sequence at Bunger Hills described by Tucker et al. (2017) formed as part of the Biranup Zone during extension and voluminous magmatism in a back-arc setting, likely isolating the area as a basement high. The extensive metapelite sequence was deposited between ca. 1700 and 1500 Ma during uplift and erosion, possibly in a passive margin setting some distance away from the Yilgarn Craton margin (Tucker et al., 2017). After a relative period of quiescence, intense deformation and metamorphism at ca. 1330-1150 Ma followed during the two-stage Albany–Fraser Orogeny and collision of the Western Australian and Mawson cratons with peak metamorphic conditions at ca. 1200–1150 Ma associated with emplacement of voluminous isotopically evolved charnockites produced mainly by crustal reworking and varying contributions from depleted mantle. The revised model is in agreement with the interpreted location of Bunger Hills in the model of Aitken et al. (2014, 2016) and consistent with evidence for back-arc setting at Windmill Islands at ca. 1410 Ma (Morrissey et al., 2017).

7.9.2.2 Mesoproterozoic mafic magmatism within the Albany-Fraser Orogen

The interpreted location of Bunger Hills as part of the south-western Albany–Fraser Orogen (now Nornalup Zone) at ca. 1134 Ma suggests that dykes of this age could also be present further east within the orogen. Moreover, probable syn-plutonic mafic granulite dykes reported from the ca. 1151 Ma Booth Peninsula batholith at Bunger Hills (Sheraton et al., 1995) implies that dykes of this age may also be present elsewhere within the Albany–Fraser Orogen. Mafic dykes at Windmill Islands are undated, the only available age constraint being from a late aplite dyke dated at 1138 ± 9 Ma with zircon U-Pb (Post, 2000). Post et al. (1997, 2000) proposed that the up to 50 m-wide unmetamorphosed WNW–NW-trending olivine gabbro dykes at Windmill Islands were emplaced after peak metamorphism between ca. 1160 Ma and 1138 Ma, postdating the Ardery charnockite and the aplite dykes.

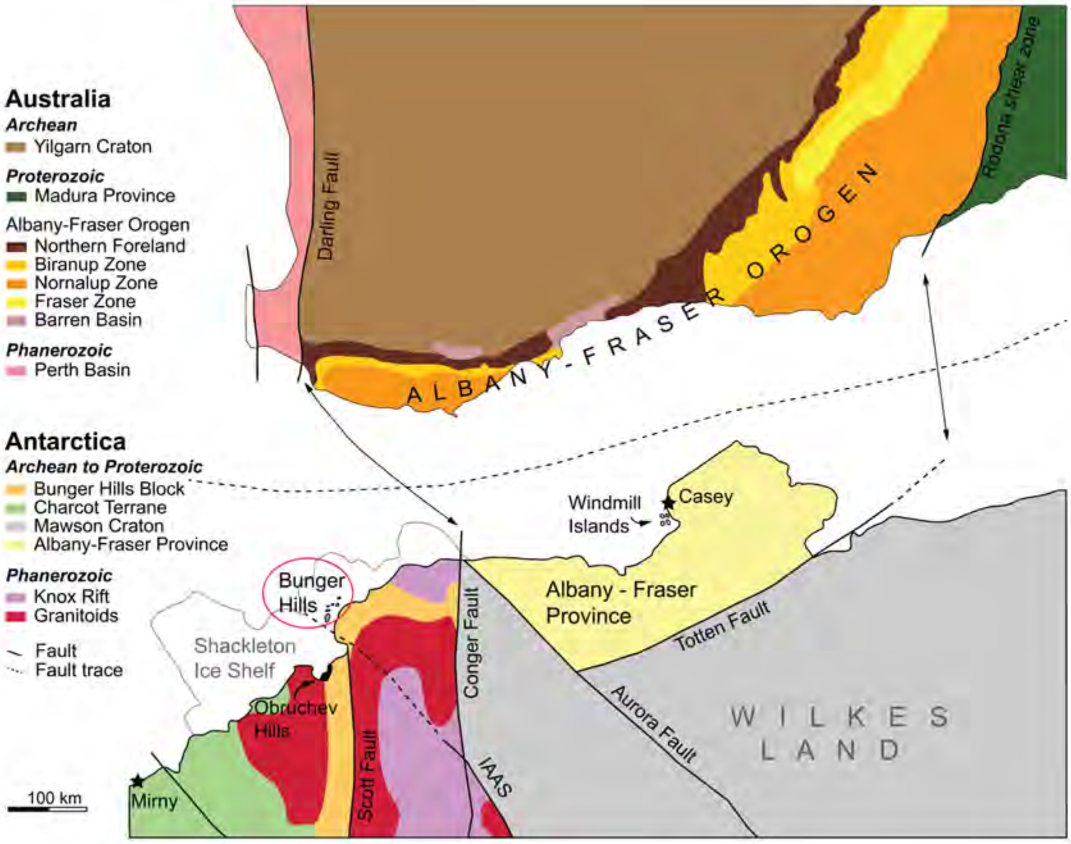

Figure 7.9 Approximate reconstructed configuration of the Yilgarn Craton, Bunger Hills and Windmill Islands at ca. 1150 Ma. Modified after Tucker et al. (2017, 2015), Aitken et al. (2014, 2016), Boger (2011), Spaggiari et al. (2009) and 1:2 500 000 interpreted bedrock geology of Western Australia (Geological Survey of Western Australia, 2015). Piercing points of between the Darling–Conger and Rodona–Totten Faults are from Aitken et al. (2014, 2016).

Similarly to the studied dyke at Bunger Hills, the olivine gabbro dykes at Windmill Islands post-date syn- to late-tectonic charnockites and appear to have similar chemical and mineralogical characteristics (Sheraton et al., 1995). The consistencies in trend, geochemistry and petrology between dyke groups 3 and 4 at Bunger Hills, the olivine gabbro dykes at Windmill Islands and the dyke in this study suggest that these dykes could be part of the same NW trending swarm with a >400 km lateral extent.

Mafic dykes of similar age are not known within the Albany–Fraser Orogen or elsewhere in the Yilgarn Craton. The youngest identified Gnowangerup dykes of the Marnda Moorn LIP are 1203 ± 15 Ma (Evans, 1999) and the oldest known Warakurna LIP dykes in north-western Yilgarn are 1075 ± 10 Ma (Wingate, 2003).

However, undated NE-trending dykes in the Tropicana region (Spaggiari et al., 2011) and NW-trending Beenong dykes in the south-east Yilgarn Craton are visible in aeromagnetic imagery and cross-cut all structures in the orogen (Wingate, 2007; Spaggiari et al., 2009, 2011). Field evidence indicates that the NE-trending undeformed amphibolitic dykes formed after deformation had ceased but before cooling, suggesting that they are younger than ca. 1140 Ma and may have formed late in stage II of the Albany–Fraser Orogeny (Spaggiari et al., 2011). Whilst these dykes may belong to the Warakurna LIP, or another as yet unidentified event, it is equally possible that they could be part of the same magmatic event that produced the 1134 Ma mafic dykes at Bunger Hills and possibly the olivine gabbro dykes at Windmill Islands. If so, the Bunger Hills and the Windmill Islands must have cooled much more rapidly after peak metamorphism because the dykes there are unmetamorphosed. Many dykes within the Albany–Fraser Orogen that have trends similar to the Gnowangerup and Fraser dykes of the Marnda Moorn LIP have been ascribed as belonging to the Marnda Moorn suite. However, as demonstrated by evidence from other mafic dyke studies in the Yilgarn and elsewhere, it cannot always be assumed that similarly oriented dykes in a region are part of the same magmatic event (Hanson et al., 2004; Wingate, 2007; French and Heaman, 2010; Stark et al., 2017).

If the Bunger Hills and Windmill Islands areas were juxtaposed with the Albany-Fraser Orogen at the time, the NW trend of the ca. 1134 Ma dykes in both areas (assuming they are coeval) probably also reflects the regional tectonic setting of the Albany-Fraser Orogen. The structural style and kinematics between the Albany-Fraser Orogen and the Bunger Hills area have been correlated (Duebendorfer, 2002) and peak metamorphism at Bunger Hills area corresponds closely with stage 2 of the Albany Fraser Orogeny (Sheraton et al., 1993; Clark et al., 2000; Tucker and Hand, 2016; Tucker et al., 2017). The NW-trending Bunger Hills dykes were emplaced during the final phase of stage 2, which within the Albany-Fraser Orogen has been interpreted as an episode of intracratonic reactivation, metamorphism and significant extension in a NNW to NW oriented transpressional setting (Bodorkos and Clark, 2004b; Kirkland et al., 2011). Moreover, the ca. 1214–1203 Ma Marnda Moorn dykes emplaced early during stage 2, have a similar NW to NNW orientation in the southwestern part of the Albany-Fraser Orogen (Wingate and Pidgeon, 2005; Wingate et al., 2005; Wingate, 2007, 2017)

7.9.2.3 Tectonic setting during emplacement of the 1134 Ma mafic dykes at Bunger Hills

As discussed in section 6.1.4, clues to the tectonic evolution leading to mafic dyke emplacement at Bunger Hills may come from the plutonic rocks in the area. Mesoproterozoic charnockites in East Antarctica have been attributed to continental collision, their formation resulting from high temperature decompression melting of dehydrated but fertile granulites in the lower crust during post-collisional exhumation and decompression (Young et al., 1997; Zhao et al., 1997; Mikhalsky et al., 2006). The presence of abundant, largely unmetamorphosed late-tectonic charnockites and clockwise P–T paths at Bunger Hills and Windmill Islands is consistent with this scenario. The ca. 1203–1151 Ma Bunger Hills charnockites are synchronous with the ca. 1200–1140 Ma Esperance Supersuite of the Albany–Fraser Orogen, the ca. 1205–1163 Ma Ardery charnockite, and the youngest known Marnda Moorn LIP dykes (the Gnowangerup suite) dated at 1203 ±15 Ma (Evans, 1999; Post, 2000; Zhang et al., 2012; Morrissey et al., 2017). Coeval emplacement of orogen-wide plutonic rocks and the Marnda Moorn LIP dykes (Wang et al., 2014) suggests that extensive melting of lower crust and the lithospheric mantle was synchronous with emplacement of vast amounts of mafic magma along the southern, western and eastern margins of the Yilgarn Craton. Emplacement of the Marnda Moorn dykes required lithospheric extension along the entire length of the orogen (Wingate et al., 2000) and probably caused the elevated regional thermal gradient that produced metamorphic monazite growth at ca. 1205 Ma (Dawson et al., 2003). Onset of rapid uplift and cooling between 1169 Ma and 1159 Ma in the western Albany–Fraser Orogen (Scibiorski et al., 2015) coincides with ca. 1170 Ma plutonic magmatism at Bunger Hills, followed by an increase in (depleted and/or less enriched) mantle input in the Ardery charnockite at Windmill Islands by ca. 1163 Ma (Morrissey et al., 2017) and in the Booth Peninsula batholith by ca. 1151 Ma (Sheraton et al., 1992).

The source of the ca. 1203–1170 Ma Bunger Hills plutons probably involved a heterogeneous, highly enriched mantle region with contributions from the lower crust and metasomatised SCLM (Sheraton et al., 1992; Zhang et al., 2012; Morrissey et al., 2017; Tucker et al., 2017) similar to the Esperance Supersuite granites, which were derived mainly by crustal recycling (Kirkland et al., 2011; R. Smithies et al., 2015; Tucker et al., 2017). In contrast, the Booth Peninsula batholith and the Ardery charnockite at Windmill Islands had a distinctively less enriched source (Sheraton et al., 1992; Morrissey et al., 2017). The apparent age-progressive increase of asthenospheric mantle input in the Bunger Hills and Windmill Islands charnockites is consistent with mafic underplating associated with orogenic collapse or rapid uplift interpreted as syn-tectonic active transpression (Scibiorski et al., 2015). This uplift appears to have affected both the Bunger Hills and Windmill Islands regions and may have been long-lived, with first plutonic activity commencing by ca. 1203 Ma and continuing at least until ca. 1151 Ma. Following cooling, at the latest by 1134 Ma, the crust was brittle enough to allow emplacement of the mafic dykes.

Geochemical evidence is consistent with a depleted or slightly enriched mantle source which interacted with a component of the sub-continental lithospheric mantle (SCLM) and/or lower crust that was metasomatically enriched and hybridized by an earlier subduction event or events during the Paleoproterozoic, and possibly in the Neoarchean (Sheraton et al., 1990, 1995). At Bunger Hills, formation of orthogneisses and the mantle extraction ages of the studied dyke all fall within the ca. 1815–1650 Ma interval, which is coeval with basin formation in a back-arc setting along the southern margin of the Yilgarn Craton during active subduction. During Paleoproterozoic arc activity, the mantle wedge would have been hybridized by addition of slab-derived fluids and/or melts and later incorporated into the continental lithospheric mantle during the Biranup and Albany-Fraser orogenies. The metasomatised and highly heterogeneous (at least in part, long-term enriched) sub-arc mantle was later tapped by parent magmas to the various plutons and dykes during active tectonic uplift and cooling associated with the final stages of the Albany–Fraser Orogeny. The emplacement of the 1134 Ma mafic dyke suite could thus mark the final phase of a prolonged episode of post-orogenic uplift which was associated with continued mafic underplating, decompression melting of the SCLM and lower crust that produced the plutonic rocks and, lastly, a thinned and thermally weakened lithosphere that permitted (asthenospheric) mantle material to dominate and intrude to at least middle crustal levels.

An alternative mechanism for the formation of the dykes could involve a mantle source much further away. If the NW-trending Windmill Island dykes are coeval with the NW-trending dykes at Bunger Hills, the extent of such a dyke swarm of at least 400 km could suggest a possible plume-like mantle source, similar to the giant ca. 1270 Ma Mackenzie (e.g. Ernst and Baragar, 1992; Baragar et al., 1996; Hou et al., 2010) and the ca. 2500-2540 Ma Matachewan dyke swarms (e.g. Ernst and Bleeker, 2010; Ciborowski et al., 2015). Moreover, dyke widths more than 10 m are characteristic of regional dyke swarms that acted as plumbing systems for LIPs (e.g. Ernst and Bell, 1992; Ernst, 2014). In this scenario, the dykes could have been emplaced laterally from a distant source, interacting with the locally heterogeneous and variably metasomatised continental lithosphere. If this is the case, dykes of ca. 1134 Ma age could also be present within the Albany-Fraser Orogen.

7.9.3 Conclusions

New U-Pb geochronology for the largest NW-trending olivine gabbro dyke at Bunger Hills yields a 1134 ± 9 Ma age, which is interpreted as the crystallisation age of the dyke. The new age constraint indicates that, according to current tectonic models, the dykes were emplaced in a late- to post-orogenic extensional setting that followed the collision of the West Australian and Mawson cratons during the final stage of the Mesoproterozoic Albany-Fraser Orogeny. Post-orogenic uplift and thinning of the lithosphere was associated with at least 50 million years of episodic crustal melting and reworking that produced the abundant plutonic rocks at Bunger Hills. Geochemical evidence suggests that the source of the dyke contained at least two distinctive components: a significant proportion of material with depleted mantle-like $^{143}Nd/^{144}Nd_i$ composition and a minor lower crust-like, metasomatically enriched lithospheric contaminant. A progressive increase in mantle-derived material in the plutonic rocks suggests that lithospheric extension was accompanied by mafic underplating. Uplift, extension and continued thermal weakening of the lithosphere by 1134 Ma culminated in the emplacement of several generations of mafic dykes within a relatively short period of time, which appear to carry variable imprints of the reworked lower crust underlying Bunger Hills. The undated WNW-NW trending olivine gabbro dykes at Windmill Islands also appear to post-date syn- to late-tectonic charnockites there and similarities in trend, geochemistry and petrology with the dykes at Bunger Hills suggest that these dykes could all be part of the same NW trending swarm at least 400 km in extent. This suggests an alternative mechanism of dyke formation involving a distant mantle source, potentially a plume, with the laterally propagating magma interacting locally with the heterogeneous lithosphere.

7.10 Acknowledgments

Cristina Talavera and Hao Gao are thanked for their generous assistance with SHRIMP analyses and Ian Fitzsimons for his valuable feedback on an earlier draft. We thank Richard Ernst for his constructive and thoughtful review that greatly improved the manuscript. This work was supported by the Australian Research Council Centre of Excellence for Core to Crust Fluid Systems (CE110001017), Laureate Fellowship grant to ZXL (FL150100133), ARC future fellowship grant to XCW (FT140100826), Australian Antarctic Science Project 4191 to MH and CC and Curtin University ORD postgraduate scholarship to JCS. Zircon and baddeleyite analyses were carried out on the Sensitive High Resolution Ion Micro Probe mass spectrometer (SHRIMP II) at the John de Laeter Centre, Curtin University, with the financial support of the Australian Research Council and Auscope NCRIS.

7.11 References

Aitken, A.R.A., Betts, P.G., Young, D.A., Blankenship, D.D., Roberts, J.L., Siegert, M.J., 2016. The Australo-Antarctic Columbia to Gondwana transition. Gondwana Res. 29, 136–152. doi:10.1016/j.gr.2014.10.019

Aitken, A.R.A., Young, D.A., Ferraccioli, F., Betts, P.G., Greenbaum, J.S., Richter, T.G., Roberts, J.L., Blankenship, D.D., Siegert, M.J., 2014. The subglacial geology of Wilkes Land, East Antarctica. Geophys. Res. Lett. 41, 2390–2400.

Baragar, W.R.A., Ernst, R.E., Hulbert, L., Peterson, T., 1996. Longitudinal petrochemical variation in the Mackenzie dyke swarm, northwestern Canadian Shield. J. Petrol. 37, 317–359.

Black, L.P., Harris, L.B., Delor, C.P., 1992. Reworking of Archaean and Early Proterozoic components a progressive, Middle Proterozoic tectonothermal event in the Albany Mobile Belt, Western Australia. Precambrian Res. 59, 95–123.

Black, L.P., Kinny, P.D., Sheraton, J.W., 1991. The difficulties of dating mafic dykes: an Antarctic example. Contrib. to Mineral. Petrol. 109, 183–194. doi:10.1007/BF00306478

Black, L.P., Sheraton, J.W., Tingey, R.J., McCulloch, M.T., 1992. New U-Pb Zircon Ages From the Denman Glacier Area, East Antarctica, and Their Significance for Gondwana Reconstruction. Antarct. Sci. 4, 447–460. doi:10.1017/S095410209200066X

Bleeker, W., 2004. Taking the pulse of planet Earth: a proposal for a new multi-disciplinary flagship project in Canadian solid Earth sciences. Geosci. Canada 31, 179–190.

Bleeker, W., Ernst, R., 2006. Short-lived mantle generated magmatic events and their dyke swarms: the key unlocking Earth's paleogeographic record back to 2.6 Ga, in: Hanski, E.J., Mertanen, S., Rämö, O.T., Vuollo, J. (Eds.), Dyke Swarms—time Markers of Crustal Evolution: Selected Papers of the Fifth International Dyke Conference in Finland, Rovaniemi, Finland, 31 July- 3 Aug 2005 & Fourth International Dyke Conference, Kwazulu-Natal, South Africa 26-29 June 2001. CRC Press, London, pp. 3–26.

Blight, D.F., Oliver, R.L., 1977. The metamorphic geology of the Windmill Islands, Antarctica: A preliminary account. J. Geol. Soc. Aust. 24, 239–262. doi:10.1080/00167617708728986

Bodorkos, S., Clark, D.J., 2004. Evolution of a crustal-scale transpressive shear zone in the Albany-Fraser Orogen, SW Australia: 1. P-T conditions of Mesoproterozoic metamorphism in the Coramup Gneiss. J. Metamorph. Geol. 22, 691–711. doi:10.1111/j.1525-1314.2004.00543.x

Boger, S.D., 2011. Antarctica—before and after Gondwana. Gondwana Res. 19, 335–371.

Buchan, K.L., Ernst, R.E., Hamilton, M.A., Mertanen, S., Pesonen, L.J., Elming, S.-Å., 2001. Rodinia: the evidence from integrated palaeomagnetism and U–Pb geochronology. Precambrian Res. 110, 9–32.

Buchan, K.L., Goutier, J., Hamilton, M.A., Ernst, R.E., Matthews, W.A., 2007. Paleomagnetism, U–Pb geochronology, and geochemistry of Lac Esprit and other dyke swarms, James Bay area, Quebec, and implications for Paleoproterozoic deformation of the Superior Province. Can. J. Earth Sci. 44, 643–664.

Ciborowski, T.J.R., Kerr, A.C., Ernst, R.E., Mcdonald, I., Minifie, M.J., Harlan, S.S., Millar, I.L., 2015. The Early Proterozoic Matachewan Large Igneous Province : Geochemistry, Petrogenesis, and Implications for Earth Evolution 56, 1459–1494.

Clark, D.J., Hensen, B.J., Kinny, P.D., 2000. Geochronological constraints for a two-stage history of the Albany – Fraser Orogen , Western Australia. Precambrian Res. 102, 155–183.

Coffin, M.F., Eldholm, O., 1994. Large igneous provinces: crustal structure, dimensions, and external consequences. Rev. Geophys. 32, 1–36. doi:10.1029/93RG02508

Collerson, K.D., Sheraton, J.W., 1986. Age and geochemical characteristics of a mafic dyke swarm in the Archaean Vestfold Block, Antarctica: inferences about Proterozoic dyke emplacement in Gondwana. J. Petrol. 27, 853–886.

Compston, W., Williams, I.S., Meyer, C., 1984. U-Pb geochronology of zircons from lunar breccia 73217 using a sensitive high mass-resolution ion microprobe. J. Geophys. Res. 89, B525. doi:10.1029/JB089iS02p0B525

Corfu, F., Hanchar, J.M., Hoskin, P.W.O., Kinny, P., 2003. Atlas of Zircon Textures. Rev. Mineral. Geochemistry 53, 469–500. doi:10.2113/0530469

Dawson, G.C., Krapež, B., Fletcher, I.R., McNaughton, N.J., Rasmussen, B., 2003. 1.2 Ga thermal metamorphism in the Albany-Fraser Orogen of Western Australia: Consequence of collision or regional heating by dyke swarms? J. Geol. Soc. London. 160, 29–37. doi:10.1144/0166-764901-119

DePaolo, D.J., 1981. Neodymium isotopes in the Colorado Front Range and crust–mantle evolution in the Proterozoic. Nature 291, 193–196. doi:10.1038/291193a0

DePaolo, D.J., 1981. Trace element and isotopic effects of combined wallrock assimilation and fractional crystallization. Earth Planet. Sci. Lett. 53, 189–202.

Ding, P., James, P.R., 1991. Structural evolution of the Bunger Hills area of East Antarctica. Geol. Evol. Antarct. Cambridge Univ. Press. Cambridge 13–17.

Duebendorfer, E.M., 2002. Regional correlation of mesoproterozoic structures and deformational events in the Albany-Fraser orogen, Western Australia. Precambrian Res. 116, 129–154. doi:10.1016/S0301-9268(02)00017-7

Ernst, R., Bleeker, W., 2010. Large igneous provinces (LIPs), giant dyke swarms, and mantle plumes: significance for breakup events within Canada and adjacent regions from 2.5 Ga to the Present. Can. J. Earth Sci. 47, 695–739. doi:10.1139/e10-025

Ernst, R.E., 2014. Large igneous provinces. Cambridge University Press.

Ernst, R.E., Baragar, W.R.A., 1992. Evidence from magnetic fabric for the flow pattern of magma in the Mackenzie giant radiating dyke swarm. Nature 356, 511–513.

Ernst, R.E., Bell, K., 1992. Petrology of the Great Abitibi Dyke, Superior Province, Canada. J. Petrol. 33, 423–469.

Ernst, R.E., Buchan, K.L., 1997. Giant radiating dyke swarms: their use in identifying pre□Mesozoic large igneous provinces and mantle plumes, in: Large Igneous Provinces: Continental, Oceanic, and Planetary Flood Volcanism. American Geophysical Union Monograph 100, pp. 297–333.

Ernst, R.E., Hamilton, M.A., Soderlund, U., Hanes, J.A., Gladkochub, D.P., Okrugin, A. V, Kolotilina, T., Mekhonoshin, A.S., Bleeker, W., LeCheminant, A.N., Buchan, K.L., Chamberlain, K.R., Didenko, A.N., 2016. Long-lived connection between southern Siberia and northern Laurentia in the Proterozoic. Nat. Geosci 9, 464–469. doi:10.1038/ngeo2700\rhttp://www.nature.com/ngeo/journal/v9/n6/abs/ngeo2700.html#supplementary-information

Ernst, R.E., Head, J.W., Parfitt, E., Grosfils, E., Wilson, L., 1995. Giant radiating dyke swarms on Earth and Venus. Earth-Science Rev. 39, 1–58.

Evans, T., 1999. Extent and nature of the 1.2 Ga Wheatbelt dyke swarm, Yilgarn Craton, Western Australia. B.Sc. thesis, Univ. West. Aust. Perth.

Fitzsimons, I.C.W., 2003. Proterozoic basement provinces of southern and southwestern Australia, and their correlation with Antarctica. Geol. Soc. London, Spec. Publ. 206, 93–130.

Fitzsimons, I.C.W., 2000a. Grenville-age basement provinces in East Antarctica: evidence for three separate collisional orogens. Geology 28, 879–882.

Fitzsimons, I.C.W., 2000b. A review of tectonic events in the East Antarctic Shield and their implications for Gondwana and earlier supercontinents. J. African Earth Sci. 31, 3–23.

Foley, S.F., Barth, M.G., Jenner, G.A., 2000. Rutile/melt partition coefficients for trace elements and an assessment of the influence of rutile on the trace element characteristics of subduction zone magmas. Geochim. Cosmochim. Acta 64, 933–938.

French, J.E., Heaman, L.M., 2010. Precise U-Pb dating of Paleoproterozoic mafic dyke swarms of the Dharwar craton, India: Implications for the existence of the Neoarchean supercraton Sclavia. Precambrian Res. 183, 416–441. doi:10.1016/j.precamres.2010.05.003

Genske, F.S., Beier, C., Stracke, A., Turner, S.P., Pearson, N.J., Hauff, F., Schaefer, B.F., Haase, K.M., 2016. Comparing the nature of the western and eastern Azores mantle. Geochim. Cosmochim. Acta 172, 76–92. doi:10.1016/j.gca.2015.08.019

Hacker, B.R., Kelemen, P.B., Behn, M.D., 2015. Continental Lower Crust. Annu. Rev. Earth Planet. Sci. 43, 167–205. doi:10.1146/annurev-earth-050212-124117

Halls, H.C., 1986. Paleomagnetism, structure, and longitudinal correlation of Middle Precambrian dykes from northwestern Ontario and Minnesota. Can. J. Earth Sci. 23, 142–157.

Halls, H.C., Kumar, a., Srinivasan, R., Hamilton, M. a., 2007. Paleomagnetism and U-Pb geochronology of easterly trending dykes in the Dharwar craton, India: feldspar clouding, radiating dyke swarms and the position of India at 2.37 Ga. Precambrian Res. 155, 47–68. doi:10.1016/j.precamres.2007.01.007

Halls, H.C., Palmer, H.C., 1990. The tectonic relationship of two Early Proterozoic dyke swarms to the Kapuskasing Structural Zone: a paleomagnetic and petrographic study. Can. J. Earth Sci. 27, 87–103. doi:10.1139/e90-007

Halls, H.C., Zhang, B., 1998. Uplift structure of the southern Kapuskasing zone from 2.45 Ga dike swarm displacement. Geology 26, 67–70. doi:10.1130/0091-7613(1998)026<0067:USOTSK>2.3.CO;2

Hanson, R.E., Gose, W.A., Crowley, J.L., Ramezani, J., Bowring, S.A., Bullen, D.S., Hall, R.P., Pancake, J.A., Mukwakwami, J., 2004. Paleoproterozoic intraplate magmatism and basin development on the Kaapvaal Craton: Age, paleomagnetism and geochemistry of~ 1.93 to~ 1.87 Ga post-Waterberg dolerites. South African J. Geol. 107, 233–254.

Harley, S.L., Fitzsimons, I.C.W., Zhao, Y., 2013. Antarctica and supercontinent evolution: historical perspectives, recent advances and unresolved issues. Geol. Soc. London, Spec. Publ. 383, 1–34.

Heaman, L.M., 2009. The application of U–Pb geochronology to mafic, ultramafic and alkaline rocks: An evaluation of three mineral standards. Chem. Geol. 261, 43–52. doi:10.1016/j.chemgeo.2008.10.021

Hoek, J.D., Seitz, H.-M., 1995. Continental mafic dyke swarms as tectonic indicators: an example from the Vestfold Hills, Antarctica. Precambrian Res. 75, 121–139.

Hou, G., 2012. Mechanism for three types of mafic dyke swarms. Geosci. Front. 3, 217–223. doi:10.1016/j.gsf.2011.10.003

Hou, G., Kusky, T.M., Wang, C., Wang, Y., 2010. Mechanics of the giant radiating Mackenzie dyke swarm: A paleostress field modeling. J. Geophys. Res. Solid Earth 115, B02402, doi:10.1029/2007JB005475.

Irvine, T.N.J., Baragar, W., 1971. A guide to the chemical classification of the common volcanic rocks. Can. J. Earth Sci. 8, 523–548.

Irving, A.J., Frey, F.A., 1978. Distribution of trace elements between garnet megacrysts and host volcanic liquids of kimberlitic to rhyolitic composition. Geochim. Cosmochim. Acta 42, 771–787.

Johannsen, A., 1931. A Descriptive Petrography Of The Igneous Rocks. Vol-I. The University of Chicago Press; Chicago.

Ju, W., Hou, G., Hari, K.R., 2013. Mechanics of mafic dyke swarms in the Deccan Large Igneous Province: Palaeostress field modelling. J. Geodyn. 66, 79–91. doi:10.1016/j.jog.2013.02.002

Kirkland, C.L., Spaggiari, C. V, Pawley, M.J., Wingate, M.T.D., Smithies, R.H., Howard, H.M., Tyler, I.M., Belousova, E.A., Poujol, M., 2011. On the edge: U–Pb, Lu–Hf, and Sm–Nd data suggests reworking of the Yilgarn craton margin during formation of the Albany-Fraser Orogen. Precambrian Res. 187, 223–247.

Lanyon, R., Black, L.P., Seitz, H.-M., 1993. U-Pb zircon dating of mafic dykes and its application to the Proterozoic geological history of the Vestfold Hills, East Antarctica. Contrib. to Mineral. Petrol. 115, 184–203.

Le Maitre, R.W., Streckeisen, A., Zanettin, B., Le Bas, M.J., Bonin, B., Bateman, P., Bellieni, G., Dudek, A., Efremova, S., Keller, J., Lameyre, J., Sabine, P.A., Schmid, R., Sørensen, H., Woolley, A.R., 2002. Igneous rocks: a classification and glossary of terms: recommendations of the International Union of Geological Sciences Subcommission on the Systematics of Igneous Rocks, 2nd ed. Cambridge University Press, New York.

Li, X.-H., 1997. Geochemistry of the Longsheng Ophiolite from the southern margin of Yangtze Craton, SE China. Geochem. J. 31, 323–337. doi:10.2343/geochemj.31.323

Liu, Y., Liu, H., Li, X., 1996. Simultaneous and precise determination of 40 trace elements in rock samples using ICP-MS [J]. Geochemia 25(6), 552.

Ludwig, K., 2012. User's manual for Isoplot version 3.75–4.15: a geochronological toolkit for Microsoft. Berkeley Geochronological Cent. Spec. Publ.

Ludwig, K., 2009. Squid 2.50, A User's Manual (No. 2.50.11.02.03 Rev. 03 Feb 2011). Berkeley, California, USA.

Mikhalsky, E. V, Sheraton, J.W., Hahne, K., Prince, N., Mountains, C., Coast, M., 2006. Charnockite composition in relation to the tectonic evolution of East Antarctica. Gondwana Res. 9, 379–397. doi:10.1016/j.gr.2005.11.007

Morrissey, L.J., Payne, J.L., Hand, M., Clark, C., Taylor, R., Kirkland, C.L., Kylander-Clark, A., 2017. Linking the Windmill Islands, east Antarctica and the Albany–Fraser Orogen: Insights from U–Pb zircon geochronology and Hf isotopes. Precambrian Res. 293, 131–149. doi:10.1016/j.precamres.2017.03.005

Münker, C., Wörner, G., Yogodzinski, G., Churikova, T., 2004. Behaviour of high field strength elements in subduction zones: constraints from Kamchatka–Aleutian arc lavas. Earth Planet. Sci. Lett. 224, 275–293. doi:10.1016/j.epsl.2004.05.030

Myers, J.S., 1993. Precambrian Tectonic History of the West Australian Craton and Adjacent Orogens. Annu. Rev. Earth Planet. Sci. 21, 453–485.

Nelson, D.R., Myers, J.S., Nutman, A.P., 1995. Chronology and evolution of the Middle Proterozoic Albany□Fraser Orogen, Western Australia. Aust. J. Earth Sci. 42, 481–495.

Paul, E., Stuwe, K., Teasdale, J., Worley, B., 1995. Structural and Metamorphic Geology of the Windmill-Islands, East Antarctica - Field Evidence for Repeated Tectonothermal Activity. Aust. J. Earth Sci. 42, 453–469. doi:10.1080/08120099508728216

Pearce, J.A., 2008. Geochemical fingerprinting of oceanic basalts with applications to ophiolite classification and the search for Archean oceanic crust. Lithos 100, 14–48. doi:10.1016/j.lithos.2007.06.016

Pfänder, J. a., Münker, C., Stracke, A., Mezger, K., 2007. Nb/Ta and Zr/Hf in ocean island basalts — Implications for crust–mantle differentiation and the fate of Niobium. Earth Planet. Sci. Lett. 254, 158–172. doi:10.1016/j.epsl.2006.11.027

Post, N.J., 2000. Unravelling Gondwana fragments: an integrated structural, isotopic and petrographic investigation of the Windmill Islands, Antarctica. University of New South Wales PhD Thesis.

Post, N.J., Hensen, B.J., Kinny, P.D., 1997. Two metamorphic episodes during a 1340–1180 Ma convergent tectonic event in the Windmill Islands, East Antarctica. Antarct. Reg. Geol. Evol. Process. Terra Antarct. Sienna 157–161.

Puffer, J.H., 2001. Contrasting high field strength element contents of continental flood basalts from plume versus reactivated-arc sources. Geology 29, 675–678. doi:10.1130/0091-7613(2001)029<0675:CHFSEC>2.0.CO

Rasmussen, B., Fletcher, I.R., 2010. Dating sedimentary rocks using in situ U-Pb geochronology of syneruptive zircon in ash-fall tuff &lt 1 mm thick. Geology 38, 299–302. doi:10.1130/G30567.1

Ravich, M.G., Klimov, L. V, Solov′ev, D.S., 1968. The Pre-Cambrian of East Antarctica. Israel Program for Scientific Translations [available from the US Department of Commerce, Clearinghouse for Federal Scientific and Technical Information, Springfield, Va.].

Rollinson, H.R., 1993. Using geochemical data: evaluation, presentation, interpretation. Longman Scientific & Technical; Copublished in the US with J. Wiley & Sons.

Rudnick, R.L., Fountain, D.M., 1995. Nature and composition of the continental crust: A lower crustal perspective. Rev. Geophys. 33, 267. doi:10.1029/95RG01302

Rudnick, R.L., Gao, S., 2003. Composition of the continental crust, in: Holland, H.D., Turekian, K.K. (Eds.), The Crust Vol. 3. Treatise on Geochemistry. pp. 1–64.

Salters, V.J.M., Stracke, A., 2004. Composition of the depleted mantle. Geochemistry, Geophys. Geosystems 5, Q05B07. doi:10.1029/2003GC000597

Saunders, A.D.A.D., Storey, M., Kent, R.W.W., Norry, M.J., Norrry, M.J., 1992. Consequences of plume-lithosphere interactions. Geol. Soc. Spec. Publ. London 68, 41–60.

Schmitt, A.K., Chamberlain, K.R., Swapp, S.M., Harrison, T.M., 2010. In situ U-Pb dating of micro-baddeleyite by secondary ion mass spectrometry. Chem. Geol. 269, 386–395. doi:10.1016/j.chemgeo.2009.10.013

Scibiorski, E., Tohver, E., Jourdan, F., 2015. Rapid cooling and exhumation in the western part of the Mesoproterozoic Albany-Fraser Orogen, Western Australia. Precambrian Res. 265, 232–248.

Sheraton, J.W., Black, L.P., 1982. Geochemistry and geochronology of Proterozoic tholeiite dykes of East Antarctica: evidence for mantle metasomatism. Contrib. to Mineral. Petrol. 78, 305–317.

Sheraton, J.W., Black, L.P., McCulloch, M.T., Oliver, R.L., 1990. Age and origin of a compositionally varied mafic dyke swarm in the Bunger Hills, East Antarctica. Chem. Geol. 85, 215–246.

Sheraton, J.W., Black, L.P., Tindle, A.G., 1992. Petrogenesis of plutonic rocks in a Proterozoic granulite-facies terrane — the Bunger Hills, East Antarctica. Chem. Geol. 97, 163–198. doi:10.1016/0009-2541(92)90075-G

Sheraton, J.W., Offe, L.A., Tingey, R.J., Ellis, D.J., 1980. Enderby land, Antarctica—an unusual Precambrian high□grade metamorphic terrain. J. Geol. Soc. Aust. 27, 1–18.

Sheraton, J.W., Oliver, R.L., Stüwe, K., 1989. Geochemistry of Proterozoic Amphibolite dykes of Commonwealth Bay, Antarctica, and possible correlations with mafic dyke swarms elsewhere in Gondwanaland. Precambrian Res. 44, 353–361. doi:10.1016/0301-9268(89)90052-1

Sheraton, J.W., Thomson, J.W., Collerson, K.D., 1987. Mafic dyke swarms of Antarctica, in: Halls, H.C., Fahrig, W.F. (Eds.), Mafic Dyke Swarms. Geological Association of Canada Special Paper 34, pp. 419–432.

Sheraton, J.W., Tingey, R.J., 1994. Bedrock Geology of the Bunger Hills-Denman Glacier Region, Australian Antarctic Territory. Aust. Geol. Surv. Organ. 1250 000 Map Ser.

Sheraton, J.W., Tingey, R.J., Black, L.P., Offe, L.A., Ellis, D.J., 1987. Geology of Enderby Land and western Kemp Land, Antarctica. BMR Bull. 233 51p.

Sheraton, J.W., Tingey, R.J., Black, L.P., Oliver, R.L., 1993. Geology of the Bunger Hills area, Antarctica: implications for Gondwana correlations. Antarct. Sci. 5, 85–102. doi:10.1017/S0954102093000112

Sheraton, J.W., Tingey, R.J., Oliver, R.L., Black, L.P., 1995. Geology of the Bunger Hills-Denman Glacier region, East Antarctica, BMR Bulletin 244. Australian Geological Survey Organisation.

Sims, K.W.W., DePaolo, D.J., 1997. Inferences about mantle magma sources from incompatible element concentration ratios in oceanic basalts. Geochim. Cosmochim. Acta 61, 765–784. doi:10.1016/S0016-7037(96)00372-9

Smithies, R., Spaggiari, C., Kirkland, C., 2015. Building the crust of the Albany-Fraser Orogen: Constraints from granite geochemistry, in: GSWA 2015 Extended Abstracts-Promoting the Prospectivity of Western Australia. Geological Survey of Western Australia, pp. 31–35.

Spaggiari, C.V., Kirkland, C.L., Smithies, H.R., Wingate, M.T.D., Belousova, E.A., 2015. Transformation of an Archean craton margin during Proterozoic basin formation and magmatism: The Albany–Fraser Orogen, Western Australia. Precambrian Res. 266, 440–466. doi:10.1016/j.precamres.2015.05.036

Spaggiari, C. V, Bodorkos, S., Barquero-Molina, M., Tyler, I.M., Wingate, M.T.D., 2009. Interpreted bedrock geology of the South Yilgarn and of the South Yilgarn and Central Albany-Fraser Orogen, Western Australia, Record 2009/10.

Spaggiari, C. V, Kirkland, C.L., Pawley, M.J., Smithies, R.H., Wingate, M.T.D., Doyle, M.G., Blenkinsop, T.G., Clark, C., Oorschot, C.W., Fox, L.J., 2011. The geology of the east Albany-Fraser Orogen—a field guide. Geol. Surv. West. Aust. Rec. 2011/23 23, 97.

Stacey, J.S. t, Kramers, 1JD, 1975. Approximation of terrestrial lead isotope evolution by a two-stage model. Earth Planet. Sci. Lett. 26, 207–221.

Stark, J.C., Wang, X.-C., Denyszyn, S.W., Li, Z.-X., Rasmussen, B., Zi, J.-W., Sheppard, S., Liu, Y., 2017. Newly identified 1.89 Ga mafic dyke swarm in the Archean Yilgarn Craton, Western Australia suggests a connection with India. Precambrian Res. In Press. doi:10.1016/j.precamres.2017.12.036

Stern, R.A., 2001. A new isotopic and trace-element standard for the ion microprobe: preliminary thermal ionization mass spectrometry (TIMS) U-Pb and electron-microprobe data, Geological Survey of Canada Current Research 2001-F. Geological Survey of Canada.

Stern, R.A., Bodorkos, S., Kamo, S.L., Hickman, A.H., Corfu, F., 2009. Measurement of SIMS instrumental mass fractionation of Pb isotopes during zircon dating. Geostand. Geoanalytical Res. 33, 145–168. doi:10.1111/j.1751-908X.2009.00023.x

Stüwe, K., Powell, R., 1989. Metamorphic evolution of the Bunger Hills, East Antarctica: evidence for substantial post-metamorphic peak compression with minimal cooling in a Proterozoic orogenic event. J. Metamorph. Geol. 7, 449–464.

Stüwe, K., Wilson, C.J.L., 1990. Interaction between deformation and charnockite emplacement in the Bunger Hills, East Antarctica. J. Struct. Geol. 12, 767–783. doi:10.1016/0191-8141(90)90088-g

Sun, S. -s., McDonough, W.F., 1989. Chemical and isotopic systematics of oceanic basalts: implications for mantle composition and processes. Geol. Soc. London, Spec. Publ. 42, 313–345. doi:10.1144/GSL.SP.1989.042.01.19

Suzuki, S., Ishizuka, H., Kagami, H., 2008. Early to middle Proterozoic dykes in the Mt. Riiser-Larsen area of the Napier Complex, East Antarctica: tectonic implications as deduced from geochemical studies. Geol. Soc. London, Spec. Publ. 308, 195–210.

Taylor, S.R., McLennan, S.M., 1985. The continental crust: its composition and evolution, 1st ed. Blackwell Scientific Publishers, Palo Alto, CA.

Teixeira, W., D'Agrella-Filho, M.S., Hamilton, M.A., Ernst, R.E., Girardi, V.A.V., Mazzucchelli, M., Bettencourt, J.S., 2013. U–Pb (ID-TIMS) baddeleyite ages and paleomagnetism of 1.79 and 1.59Ga tholeiitic dyke swarms, and position of the Rio de la Plata Craton within the Columbia supercontinent. Lithos 174, 157–174. doi:10.1016/j.lithos.2012.09.006

Tucker, N.M., Hand, M., 2016. New constraints on metamorphism in the Highjump Archipelago, East Antarctica. Antarct. Sci. 28, 487–503. doi:10.1017/S095410201600033X

Tucker, N.M., Payne, J.L., Clark, C., Hand, M., Taylor, R.J., Kylander-Clark, A.R.C., 2017. Proterozoic reworking of Archean (Yilgarn) basement in the Bunger Hills, east Antarctica. Precambrian Res. 298, 16–38.

Van Westrenen, W., Blundy, J.D., Wood, B.J., 2001. High field strength element/rare earth element fractionation during partial melting in the presence of garnet: Implications for identification of mantle heterogeneities. Geochemistry, Geophys. Geosystems 2. doi:10.1029/2000GC000133

Wang, X.-C., Li, Z.-X., Li, J., Pisarevsky, S.A., Wingate, M.T.D., 2014. Genesis of the 1.21 Ga Marnda Moorn large igneous province by plume–lithosphere interaction. Precambrian Res. 241, 85–103. doi:10.1016/j.precamres.2013.11.008

Wang, X.-C., Wilde, S.A., Xu, B., Pang, C.-J., 2016. Origin of arc-like continental basalts: Implications for deep-Earth fluid cycling and tectonic discrimination. Lithos 261, 5–45.

Wang, X.C., Li, Z.X., Li, X.H., Li, J., Liu, Y., Long, W.G., Zhou, J.B., Wang, F., 2012. Temperature, Pressure, and Composition of the Mantle Source Region of Late Cenozoic Basalts in Hainan Island, SE Asia: a Consequence of a Young Thermal Mantle Plume close to Subduction Zones? J. Petrol. 53, 177–233. doi:10.1093/petrology/egr061

Weaver, B.L., Tarney, J., 1981. The Scourie dyke suite: Petrogenesis and geochemical nature of the Proterozoic sub-continental mantle. Contrib. to Mineral. Petrol. 78, 175–188. doi:10.1007/BF00373779

Weaver, B.L., Tarney, J., 1980. Continental crust composition and nature of the lower crust: constraints from mantle Nd-Sr isotope correlation. Nature 286, 342–346.

Willbold, M., Stracke, A., 2006. Trace element composition of mantle end-members: Implications for recycling of oceanic and upper and lower continental crust. Geochemistry, Geophys. Geosystems 7, n/a-n/a. doi:10.1029/2005GC001005

Wingate, M.T.. D., Campbell, I.H., Compston, W., Gibson, G.M., 1998. Ion microprobe U–Pb ages for Neoproterozoic basaltic magmatism in south-central Australia and implications for the breakup of Rodinia. Precambrian Res. 87, 135–159. doi:10.1016/S0301-9268(97)00072-7

Wingate, M.T.D., 2017. Mafic dyke swarms and large igneous provinces in Western Australia get a digital makeover, in: Geological Survey of Western Australia Record 2017/2. Geological Survey of Western Australia, pp. 4–8.

Wingate, M.T.D., 2007. Proterozoic mafic dykes in the Yilgarn Craton, in: Proceedings of Geoconferences (WA) Inc. Kalgoorlie 2007 Conference, Kalgoorlie, Western Australia. pp. 80–84.

Wingate, M.T.D., 2003. Age and Palaeomagnetism of Dolerite Sills Intrusions of the Southeastern Collier Basin, and the Earaheedy and Yerrida Basins, Western Australia, in: Western Australian Geological Survey Record, 2003/3. Geological Survey of Western Australia, p. 35.

Wingate, M.T.D., 1997. Testing Precambrian continental reconstructions using ion microprobe U-Pb baddeleyite geochronology and paleomagnetism of mafic igneous rocks. Australian National University PhD Thesis.

Wingate, M.T.D., Campbell, I.H., Harris, L.B., 2000. SHRIMP baddeleyite age for the Fraser dyke swarm, southeast Yilgarn Craton, Western Australia. Aust. J. Earth Sci. 47, 309–313.

Wingate, M.T.D., Compston, W., 2000. Crystal orientation effects during ion microprobe U–Pb analysis of baddeleyite. Chem. Geol. 168, 75–97. doi:10.1016/S0009-2541(00)00184-4

Wingate, M.T.D., Morris, P.A., Pirajno, F., Pidgeon, R.T., 2005. Two large igneous provinces in Late Mesoproterozoic Australia, in: Supercontinents and Earth Evolution Symposium. Geological Society of Australia Abstracts, p. 151.

Wingate, M.T.D., Pidgeon, R.T., 2005. The Marnda Moorn LIP, a late Mesoproterozoic large igneous province in the Yilgarn craton, Western Australia. July 2005 LIP of the month [WWW Document]. (unpub). Large Igneous Prov. Comm. Int. Assoc. Volcanol. Chem. Earth's Inter. URL http://www.largeigneousprovinces.org/05jul

Young, D.N., Zhao, J., Ellis, D.J., McCulloch, M.T., 1997. Geochemical and Sr-Nd isotopic mapping of source provinces for the Mawson charnockites, east Antarctica: implications for Proterozoic tectonics and Gondwana reconstruction. Precambrian Res. 86, 1–19. doi:10.1016/S0301-9268(97)00030-2

Zhang, S.H., Zhao, Y., Liu, X.C., Liu, Y.S., Hou, K.J., Li, C.F., Ye, H., 2012. U-Pb geochronology and geochemistry of the bedrocks and moraine sediments from the Windmill Islands: Implications for Proterozoic evolution of East Antarctica. Precambrian Res. 206–207, 52–71. doi:10.1016/j.precamres.2012.02.019

Zhao, J., Ellis, D.J., Kilpatrick, J.A., McCulloch, M.T., 1997. Geochemical and Sr-Nd isotopic study of charnockites and related rocks in the northern Prince Charles Mountains, East Antarctica: implications for charnockite petrogenesis and proterozoic crustal evolution. Precambrian Res. 81, 37–66. doi:http://dx.doi.org/10.1016/S0301-9268(96)00022-8

Chapter 8 Thesis Conclusions

This PhD project has extended the number of known mafic dyke swarms in the Yilgarn Craton from five to eight and provided the first U-Pb age for a mafic dyke swarm at Bunger Hills in East Antarctica (Figure 8.1). As discussed in Chapter 3, the the success of the project was based on the use of two different U-Pb geochronology techniques (*in situ* SIMS followed by TIMS), which used in tandem allowed suboptimal samples of mafic dyke to be dated. The new data presented in Chapters 4-7 demonstrate the importance and application of mafic dyke swarms as magmatic and tectonic markers that position the Yilgarn Craton and the Bunger Hills in the wider context of regional and global tectonic evolution. The new ages fall in key periods of supercontinent assembly and breakup/reconfiguration between the Neoarchean and the Mesoproterozoic, and facilitate their use in paleomagnetic studies to refine paleogeographic reconstructions for this period.

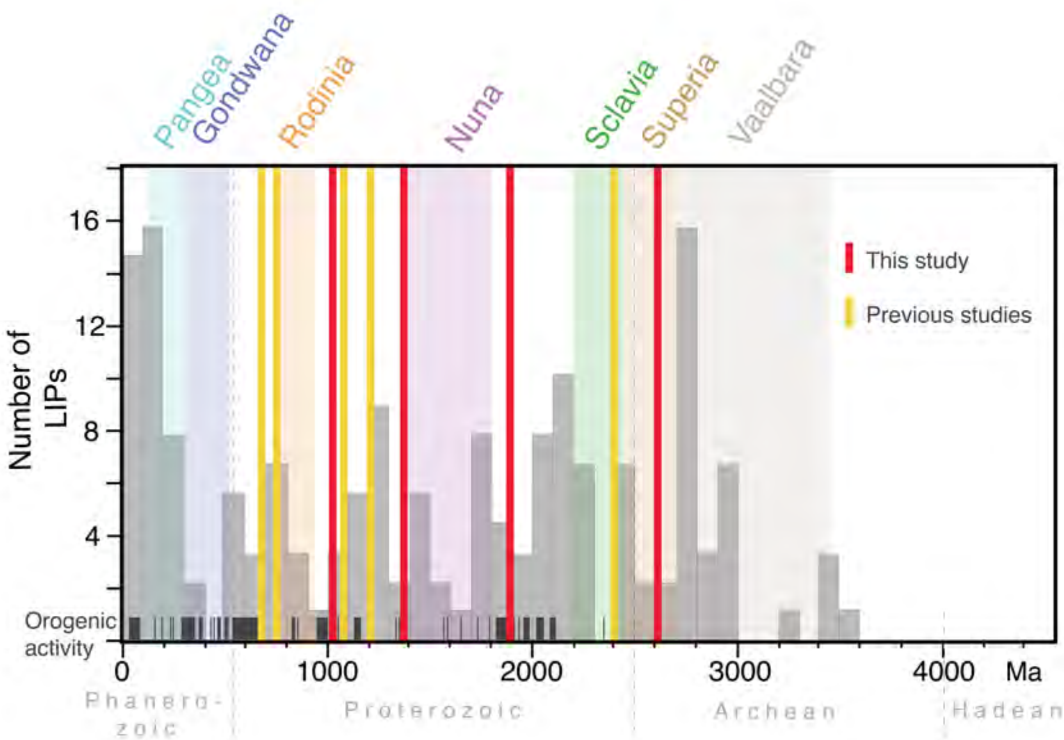

Figure 8.1 Mafic dyke swarms of the Yilgarn Craton plotted against worldwide age distribution of LIPs (after Prokoph et al., 2004)*, orogenic activity (from* (Condie and Aster, 2013) *and proposed supercontinents. Yellow lines denote previously known dyke swarms and red lines are new dyke ages presented in this study. See Chapter 2 for discussion on supercontinent tenures.*

8.1 The Neoarchean: cratonisation, lithospheric delamination and Superia

The discovery of the 2.62 Ga Yandinilling dyke (Chapter 4) provides the first evidence for Archean mafic dykes in the Yilgarn Craton. The dykes were emplaced during the final stages of its cratonisation during a Neoarchean orogeny. The emplacement of the dykes supports the previously proposed lithospheric delamination event at ca. 2.65 Ga (Smithies and Champion, 1999) and is consistent with impingement of hot mantle material at the base of the lithosphere that resulted in craton-wide, high-temperature metamorphism, voluminous felsic magmatism and late-stage gold mineralisation (Qiu and Groves, 1999). Globally, mafic dykes of this age have only been reported from the Limpopo Belt of southern Africa (Xie et al., 2017) and the So Francisco Craton of South America (Oliveira et al., 2013). Current paleogeographic reconstructions suggest that the Zimbabwe Craton was adjacent to the Yilgarn Craton at this time and because the Limpopo Belt is thought to represent the collision between the Zimbabwe and Kaapvaal cratons at ca. 2.66-2.61 Ga (Brandt et al., 2018), the Limpopo and Yandinilling dykes could be related to the same tectonic event.

Based on paleomagnetic data from the 2.40 Ga Widgiemooltha and Erayinia dykes, Pisarevsky et al. (2015) proposed that the Yilgarn and Zimbabwe cratons were part of the ca. 2.70-2.10 Ga Superia supercontinent (Bleeker, 2003; Bleeker and Ernst, 2006; Ernst and Bleeker, 2010), consistent with the interpretation of Söderlund et al. (2010) (Figure 8.2). This suggests that the Neoarchean orogeny between ca. 2.73 and 2.63 Ga, which led to amalgamation of the Yilgarn Craton (Myers, 1993, 1995; Barley et al., 2003; Blewett and Hitchman, 2006; Korsch et al., 2011; Zibra et al., 2017a; Witt et al., 2018) may be related to assembly of Superia. Moreover, Condie (2002) suggested that the delamination rate should be highest during supercontinent formation when many collisions occur between cratons, and it is notable that the ca. 2.70-2.60 Ga high-temperature thermal events in the Yilgarn Craton and the Limpopo Belt have both been linked to orogenic collapse and lithospheric delamination (Smithies and Champion, 1999; Moller et al., 2003; Brandt et al., 2018). Recent seismic studies also suggest that widespread lateral crustal flow in the

Yilgarn Craton at ca. 2.70-2.60 Ga resulted from collapse of thickened but weak early continental crust (Calvert and Doublier, 2018).

.

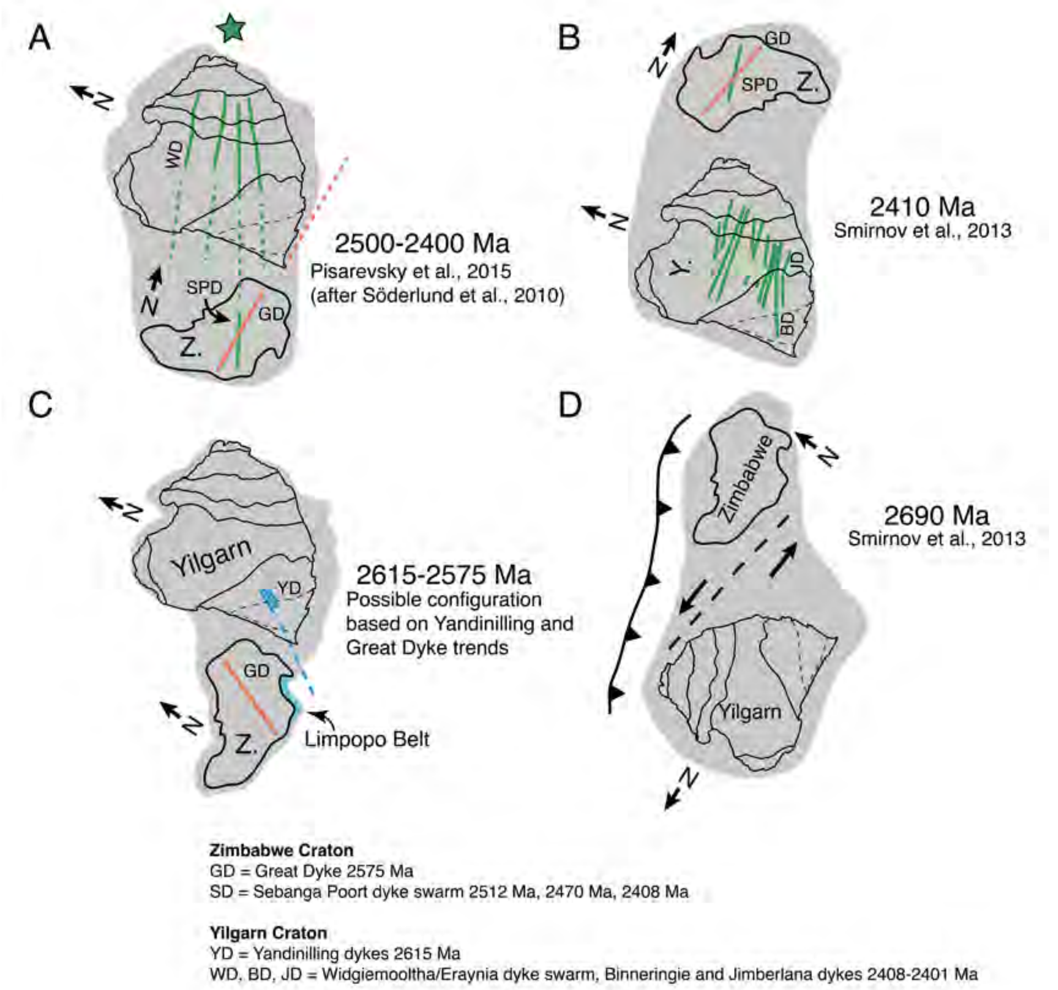

*Figure 8.2 Paleogeographic reconstructions of the Yilgarn and Zimbabwe cratons. (**A**) Superia configuration after Söderlund et al. (2010) and Pisarevsky et al. (2015) at ca. 2500–2400 Ma. Only the Yilgarn and Zimbabwe cratons are shown. (**B**) Reconstruction of Smirnov et al. (2013) at ca. 2410 Ma, (**C**) Relative orientations of the Yilgarn and Zimbabwe cratons rotated from (A) to an approximate alignment of the 2615 Ma Yandinilling swarm with the 2575 Ma Great Dyke. and (**D**) reconstruction of Smirnov et al. (2013) at ca. 2690 Ma. See Chapter 4 for details.*

No geochemical data for the 2.62 Ga Yandinilling dykes are yet available but they appear to be related to upwelling and impingement of asthenospheric mantle at the base of a thinned lithosphere, which could be due to a mantle plume. Extensive komatiitic flows at ca. 2.72 Ga in the Eastern Goldfields and in the Kaapvaal and Pilbara cratons have been linked to mantle plumes during a global-scale magmatic eruption (Campbell and Hill, 1988; Nelson, 1998; Barnes et al., 2012) and it is possible that the lithospheric delamination beneath the Yilgarn Craton and the Limpopo Belt at ca. 2.65 Ga was also expedited by such upwelling.

8.2 The Paleoproterozoic: India, the Bastar-Cuddapah LIP but no Nuna

The discovery of the NW-trending 1.89 Ga Boonadgin dyke swarm (Chapter 5) presents the first evidence for this global magmatic event in the Yilgarn Craton and importantly, provides a precise date to support paleomagnetic data (Liu et al., 2018) and a matching barcode with the Bastar-Cuddapah LIP in India (French and Heaman, 2010; Sheppard et al., 2017) (Figure 8.3). The dykes were emplaced soon after amalgamation of the West Australian Craton, which involved collision of the Pilbara Craton-Glenburgh Terrane and the Yilgarn Craton during the ca. 2.01-1.95 Ga Glenburgh Orogeny (Cawood and Tyler, 2004; Sheppard et al., 2010a; Johnson et al., 2011). Current tectonic models suggest active subduction along the southern margin of the Yilgarn Craton between ca. 1.82 Ga and 1.65 Ga (Kirkland et al., 2011; Spaggiari et al., 2014b; Aitken et al., 2016) and on a regional scale, the 1.89 Ga Boonadgin dyke swarm is linked to lithospheric extension that was synchronous with basin formation in northern and southern parts of the West Australian Craton (the Capricorn Orogen and the Barren Basin, respectively). Collectively, this evidence is consistent with NW-SE oriented compression, subduction along the southern margin and extension both near the margin and 1000 km away within the newly formed Capricorn Orogen. It has been proposed that subduction related processes can result in far-field intracratonic effect that propagates 1500 km into the plate interior (Giles et al., 2002). The Boonadgin dykes may be an expression of a similar process.

The 1.90-1.85 Ga worldwide crustal growth event has been linked to planetary-scale mantle upwelling or increased mantle plume (superplume) activity (Condie, 2002; French et al., 2008), which was associated with voluminous intraplate and plate margin mafic magmatism, basin development and the return of iron formations (e.g. Condie, 2002; Rasmussen et al., 2012). A plume origin for the 1.89 Ga Boonadgin dykes is possible, especially if it is confirmed that they are part of coeval Bastar-Cuddapah LIP in India, which is supported by paleomagnetic data (Liu et al., 2018).

The 1.9-1.85 Ga event has also been linked to amalgamation of arc systems to cratonic blocks during assembly of Nuna (Condie, 2002) sometime between ca. 2.10 Ga and 1.7 Ga (Condie, 2002; Zhao et al., 2002; Rogers and Santosh, 2003; Bradley, 2011; Pisarevsky et al., 2014a). However, new paleomagnetic data from the Boonadgin dykes (Liu et al., 2018) do not support assembly of Nuna at 1.89 Ga and indicate that whereas the West Australian Craton was adjacent to the India, it was

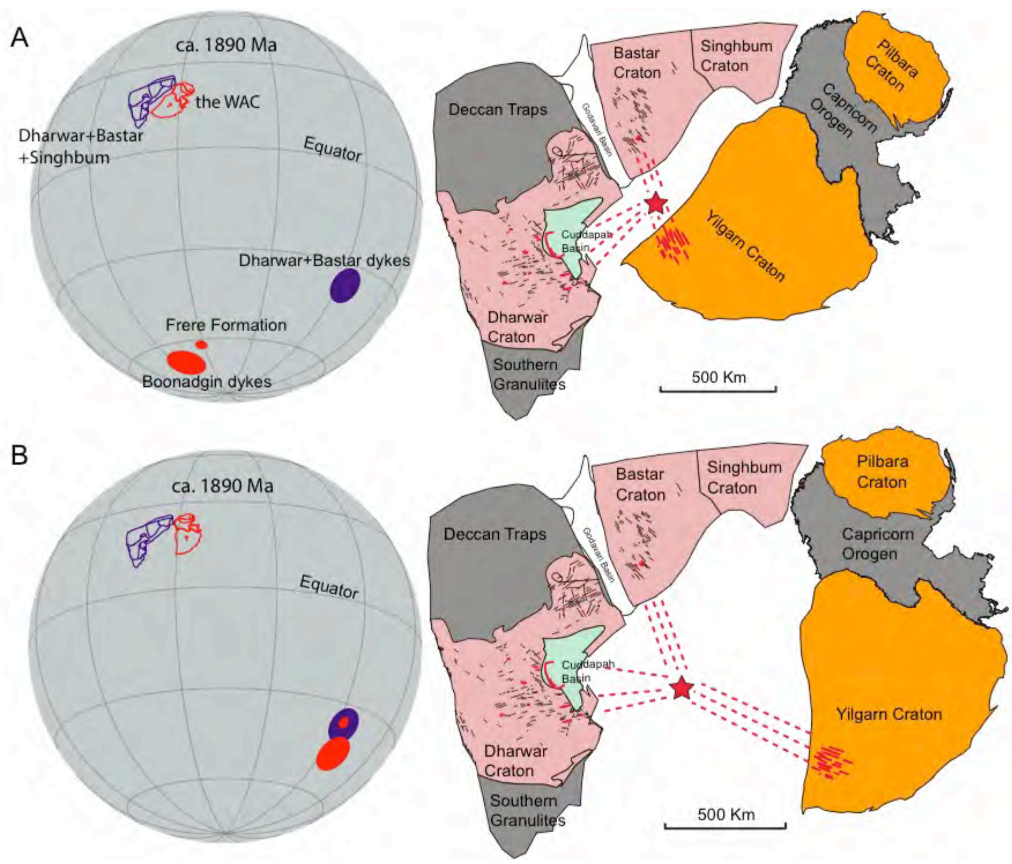

Figure 8.3 Possible configurations of the WAC and Dharwar, Bastar and Singhbum cratons tested with paleomagnetic data at ca. 1890 Ma. Coeval paleopoles are plotted on the left-hand side and color coded with the respective cratons. The WAC was rotated to the Indian coordinates and more detailed reconstructions are shown on the right side. Indian dykes shown in red have been dated with U-Pb or Ar-Ar methods at 1879-1894 Ma (Chatterjee and Bhattacharji, 2001; Halls et al., 2007; French et al., 2008; Belica et al., 2014). Black undated dykes in India are modified after French et al. (2008) and Srivastava et al. (2015). Red star denotes possible location of a mantle plume. ***(A)*** *SIWA configuration modified from ca. 2400 Ma reconstruction of Mohanty (2012);* ***(B)*** *Alternative configuration of Liu et al. (2018) supported by paleomagnetic data. See Chapter 5 for details.*

separated from other free-drifting cratonic blocks by oceans. The new paleogeographic configuration thus excludes the West Australian Craton from Nuna at 1.89 Ga.

8.3 The Mesoproterozoic: renewed subduction and Nuna to Rodinia transition

The discovery of the 1.39 Ga Biberkine dykes (Chapter 6) is very interesting because few tectonothermal or magmatic events of this age are currently known in the West Australian Craton but dykes of similar age are common in other cratons worldwide. In the Capricorn Orogen there is some evidence for a thermal event at 1.38 Ga, interpreted to result from regional-scale intracontinental reworking (Zi et al., 2015). Indirect evidence for tectonic activity in the southern part of the Yilgarn Craton is represented by a small 1.39 Ga detrital zircon population in the Fraser Complex in southeastern Albany-Fraser Orogen suggesting coeval magmatism there (Clark et al., 1999; Spaggiari et al., 2009). Moreover, ca. 1390-1370 Ma inherited and detrital zircon populations at Windmill Islands and zircon rim growth at ca. 1397-1368 Ma at Bunger Hills in East Antarctica (both of which have been interpreted as part of the Albany-Fraser Orogen during the Mesoproterozoic) indicate that the orogen was active (Zhang et al., 2012; Morrissey et al., 2017; Tucker et al., 2017). It is interesting to note that the emplacement of both the 1.89 Ga Boonadgin and the 1.39 Ga Biberkine dykes coincided with synchronous, although minor, tectonothermal events in the Capricorn Orogen, which is known to have been repeated reactivated over nearly one billion years following its formation (Sheppard et al., 2010a; Johnson et al., 2011).

Current models suggest a period of relative tectonic quiescence from ca. 1.60 Ga until ca. 1.40 Ga, when NW-oriented convergence with the northwestern margin of the Mawson Craton led to rejuvenated subduction and placed the southern margin of the craton in a back-arc setting (Boger, 2011; Kirkland et al., 2011; Spaggiari et al., 2011, 2014b, 2015, Aitken et al., 2014, 2016) (Figure 8.4). Aitken et al. (2016) argued that this was due to relative motion and rotation between the South Australian/Mawson the West and North Australian cratons during reorganization of Nuna to Rodinia and the NNW trend of the Boonadgin dykes is consistent with the inferred NW-directed compression. The paleogeographic reconstruction of Pisarevsky et al. (2014) is also compatible with this model.

Preliminary geochemistry of the dykes indicates significant involvement of a subcontinental lithospheric mantle and possibly lower crustal component. This is compatible with a scenario where upwelling asthenospheric mantle interacts with a metasomatised subcontinental lithospheric mantle in a back-arc setting. The Biberkine dykes could also represent a prelude to the 1.21 Ga mantle plume event that produced the Marnda Moorn LIP (Dawson et al., 2003; Goldberg, 2010; Wang et al., 2014) and if this is the case, the latter would represent a repeated plume event 180 million years later.

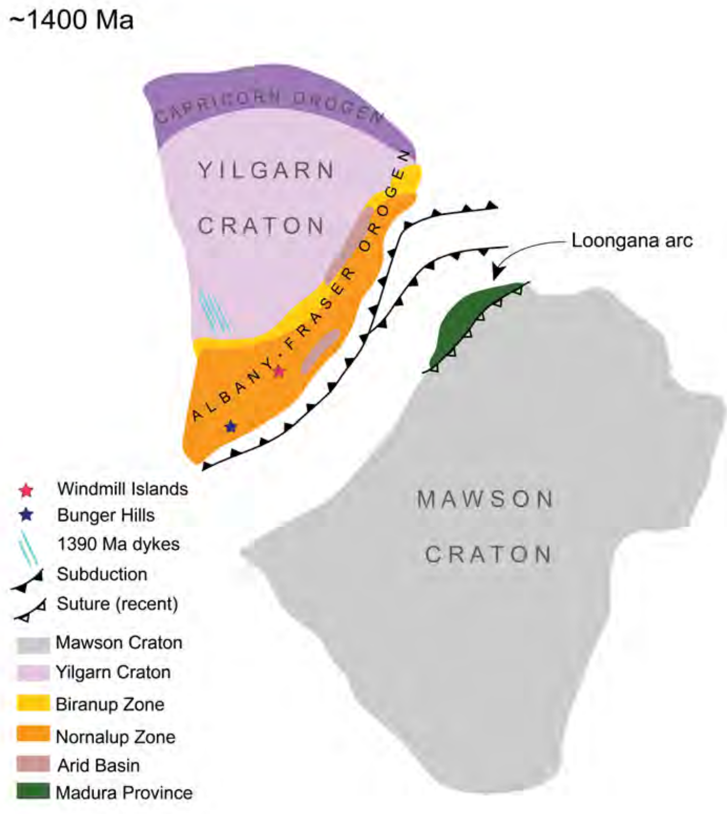

Figure 8.4 Simplified paleogeographic reconstruction of the Yilgarn and Mawson cratons at ca. 1400 Ma. Modified after Aitken et al. (2016), only the Yilgarn Craton and Capricorn Orogen of the WAC and the northern part of the Mawson Craton are shown. Note stars denoting the inferred original locations of Bunger Hills and Windmill Islands (based on interpretations of Tucker et al., 2017 and Morrissey et al., 2017, respectively). See Chapter 6 for details.

8.4 The Mesoproterozoic Albany-Fraser Orogeny: continental collision, mantle plume and a second LIP?

Because the Bungers Hills of East Antarctica, and the Windmill Islands 400 km further east along the coast, have both been interpreted as part of the Albany-Fraser Orogen during the Mesoproterozoic (e.g. Morrissey et al., 2017; Tucker et al., 2017), their tectonic evolution is closely linked to that of the Yilgarn Craton. The new U-Pb geochronology (Chapter 7) dates a widespread dyke swarm at Bunger Hills at 1.13 Ga and confirms a previous 1.14 Ga Rb-Sr age by Sheraton et al. (1990). The dated Bunger Hills olivine gabbro dyke matches a similarly oriented but undated olivine gabbro dyke at Windmill Islands raising a possibility that they are part of a LIP.

The new age for the Bunger Hills dykes indicates that they were emplaced during the final stages of the Albany-Fraser Orogeny. The first stage of the orogeny at ca. 1.35-1.26 Ga is linked to collision of the Mawson and West Australian Cratons whereas the second stage at ca. 1.22-1.14 Ga was mainly a thermal event linked to reactivation of the Orogen and emplacement of the 1.21 Ga Marnda Moorn LIP (Clark et al., 2000, 2014; Wingate et al., 2000; Dawson et al., 2003; Bodorkos and Clark, 2004b; Spaggiari et al., 2011, 2014a; Scibiorski et al., 2015) (Figure 8.5). Mesoproterozoic plutonic magmatism has commonly been associated with continental collision and high-temperature decompression melting during post-collisional exhumation (Young et al., 1997; Zhao et al., 1997; Mikhalsky et al., 2006) and this is consistent with the onset of plutonic magmatism at Bunger Hills at ca. 1.20 Ga and at ca. 1.21 Ga at Windmill Islands (Sheraton et al., 1992; Post, 2000; Zhang et al., 2012; Morrissey et al., 2017). The Bunger Hills dykes were emplaced soon after the onset of rapid uplift and cooling between 1.17 Ga and 1.16 Ga in the western Albany–Fraser Orogen (Scibiorski et al., 2015), which also coincides with increase in (depleted and/or less enriched) mantle input in the plutonic rocks at Windmill Islands by ca. 1.16 Ga (Morrissey et al., 2017) and at Bunher Hills by ca. 1151 Ma (Sheraton et al., 1992). The Marnda Moorn LIP, which is linked to a mantle plume (Wang et al., 2014), was emplaced 80 million years earlier and if the Bunger Hills and Windmill Islands dykes are part of a 1.13 Ga LIP, their wide extent may suggest a third plume event in the region between 1.39 Ga (Biberkine dykes) and 1.13 Ga. If correct, dykes of this age may also be present in southern Yilgarn Craton.

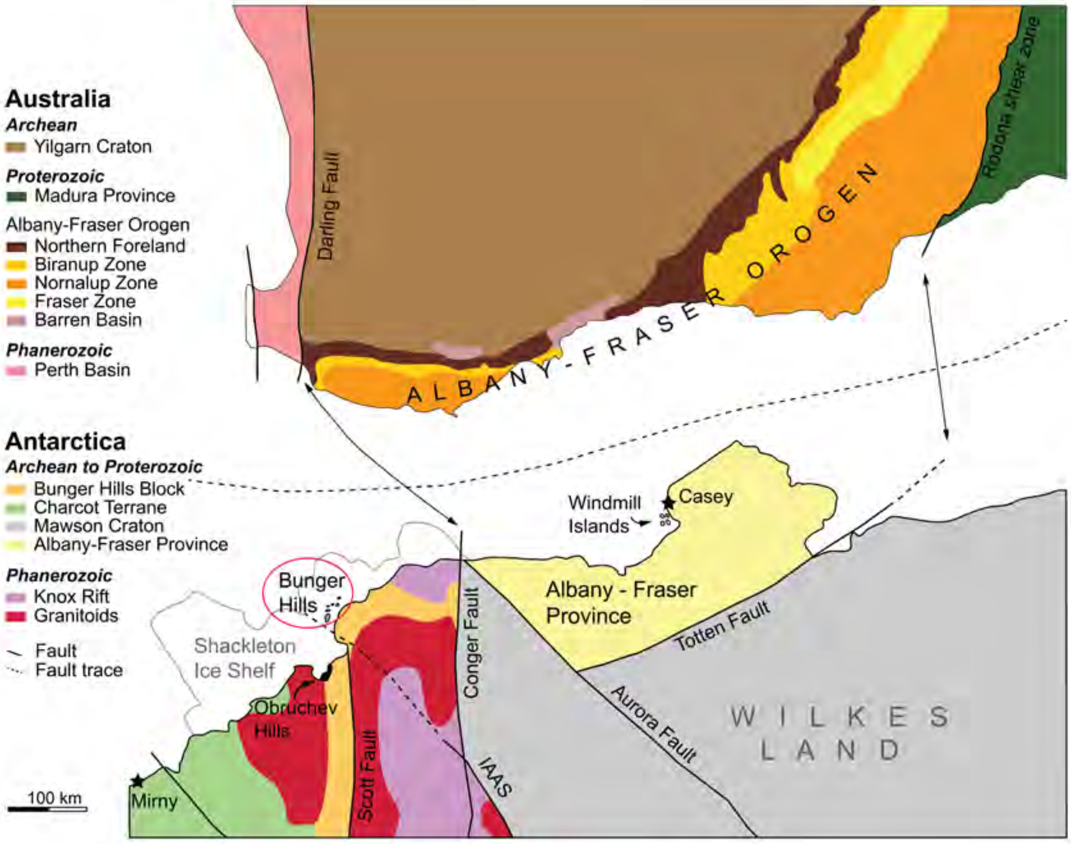

Figure 8.5 Approximate reconstructed configuration of the Yilgarn Craton, Bunger Hills and Windmill Islands at ca. 1150 Ma. Modified after Tucker et al. (2017, 2015), Aitken et al. (2014, 2016), Boger (2011), Spaggiari et al. (2009) and 1:2 500 000 interpreted bedrock geology of Western Australia (Geological Survey of Western Australia, 2015). Piercing points of between the Darling–Conger and Rodona–Totten Faults are from Aitken et al. (2014, 2016). See Chapter 7 for details.

8.5 Outlook and further studies

Fundamental questions in LIP research include the determination of their age and mantle source. Dating of mafic dykes is often challenging (Chapter 3) and without precise geochronology, it is also difficult to conduct comprehensive geochemical studies because dykes with similar trends may not be part of the same dyke swarm (Chapter 2). The main limitation of this study is that each new dyke age is based on dating of 1-3 dykes, which were sampled in a relatively small, targeted area. Consequently, the size estimate for each new swarm is based mainly on aeromagnetic data and mapping, and geochemical analysis necessarily only presents a preliminary characterisation of the mantle source. Whereas outcrop (and drill core) availability naturally determine the quality of the samples, continuous refinement of dating techniques should be the main focus for improvement in LIP research. This study has shown that a combination of *in situ* SIMS and TIMS is an effective way to obtain precise ages from difficult samples but these techniques have not changed significantly since their introduction, and future studies should focus on the development and refinement of small-grain baddeleyite dating. Promising new techniques currently include SIMS dating of microbaddeleyite (Chamberlain et al., 2010; Schmitt et al., 2010; Liu et al., 2011), improvements in the spot size achieved by LA-ICP-MS (Ibanez-Mejia et al., 2014) and $^{40}Ar/^{39}Ar$ dating of pyroxene (Ware and Jourdan, 2018), although the latter may be difficult in old and/or altered rocks.

8.6 Conclusions

This study has demonstrated the successful application of a two-step U-Pb geochronology technique to dating of mafic dykes. Three new dyke swarm ages for the Yilgarn Craton and the first U-Pb age for a mafic dyke swarm at Bunger Hills of East Antarctica fall in key time periods in the tectonic evolution of the Yilgarn Craton and the supercontinent cycle between the Neoarchean and the Mesoproterozoic. The 2.62 Ga Yandinilling dykes support the previously proposed ca. 2.65 Ga lithospheric delamination event following post-orogenic collapse of the newly amalgamated craton and together with paleomagnetic evidence, providing a possible barcode match with the Zimbabwe Craton and the Limpopo Belt of southern Africa. The 1.89 Ga Boonadgin dykes incorporate the Yilgarn Craton as part of the global ca. 1.89 Ga crustal growth event and together with associated paleomagnetic evidence indicate that while neighbours with India, it was not part of a supercontinent Nuna at this time. Emplacement of the 1.39 Ga Biberkine dykes is consistent with a back-arc setting and supports models where active subduction along the southern margin of the West Australian Craton was associated with plate movement during the transition from the Nuna to Rodinia configuration. The Biberkine dykes may also represent a prelude to the 1.21 Ga mantle plume event that produced the Marnda Moorn LIP but the time gap requires an explanation. The confirmed 1.13 Ga age of a dyke swarm at Bunger Hills links their emplacement to the final stages of the Albany-Fraser Orogen during rapid cooling and uplift. Similar but undated dykes at Windmill Islands 400 km away raise the possibility that both could be part of a LIP, which was emplaced ca. 80 million years after the plume-associated Marnda Moorn LIP. Collectively, the existing and new mafic dykes of the Yilgarn Craton now extend the magmatic barcode from 2620 Ma to ca. 735 Ma.

8.7 References

Aitken, A.R.A., Betts, P.G., Young, D.A., Blankenship, D.D., Roberts, J.L., Siegert, M.J., 2016. The Australo-Antarctic Columbia to Gondwana transition. Gondwana Res. 29, 136–152.

Aitken, A.R.A., Young, D.A., Ferraccioli, F., Betts, P.G., Greenbaum, J.S., Richter, T.G., Roberts, J.L., Blankenship, D.D., Siegert, M.J., 2014. The subglacial geology of Wilkes Land, East Antarctica. Geophys. Res. Lett. 41, 2390–2400.

Barley, M.E., Brown, S.J.A., Cas, R.A.F., Cassidy, K.F., Champion, D.C., Gardoll, S.J., Krapež, B., 2003. An integrated geological and metallogenic framework for the eastern Yilgarn Craton: developing geodynamic models of highly mineralised Archaean granite–greenstone terranes. AMIRA Project P624.

Bleeker, W., 2003. The late Archean record: a puzzle in ca. 35 pieces. Lithos 71, 99–134.

Bleeker, W., Ernst, R., 2006. Short-lived mantle generated magmatic events and their dyke swarms: the key unlocking Earth's paleogeographic record back to 2.6 Ga, in: Hanski, E.J., Mertanen, S., Rämö, O.T., Vuollo, J. (Eds.), Dyke Swarms—time Markers of Crustal Evolution: Selected Papers of the Fifth International Dyke Conference in Finland, Rovaniemi, Finland, 31 July- 3 Aug 2005 & Fourth International Dyke Conference, Kwazulu-Natal, South Africa 26-29 June 2001. CRC Press, London, pp. 3–26.

Blewett, R.S., Hitchman, A.P., 2006. 3D Geological Models of the Eastern Yilgarn Craton: Final Report pmd* CRC Y2 Project September 2001–December 2004. Geoscience Australia Record 2006/05.

Bodorkos, S., Clark, D.J., 2004. Evolution of a crustal-scale transpressive shear zone in the Albany-Fraser Orogen, SW Australia: 1. P-T conditions of Mesoproterozoic metamorphism in the Coramup Gneiss. J. Metamorph. Geol. 22, 691–711.

Boger, S.D., 2011. Antarctica—before and after Gondwana. Gondwana Res. 19, 335–371.

Bradley, D.C., 2011. Secular trends in the geologic record and the supercontinent cycle. Earth-Science Rev. 108, 16–33.

Brandt, S., Klemd, R., Li, Q., Kröner, A., Brandl, G., Fischer, A., Bobek, P., Zhou, T., 2018. Pressure-temperature evolution during two granulite-facies metamorphic events (2.62 and 2.02 Ga) in rocks from the Central Zone of the Limpopo Belt, South Africa. Precambrian Res. 310, 471–506.

Calvert, A., Doublier, M., 2018. Archaean continental spreading inferred from seismic images of the Yilgarn Craton, Nature Geoscience.

Campbell, I.H., Hill, R.I., 1988. A two-stage model for the formation of the granite-greenstone terrains of the Kalgoorlie-Norseman area, Western Australia. Earth Planet. Sci. Lett. 90, 11–25.

Cawood, P.A., Tyler, I.M., 2004. Assembling and reactivating the Proterozoic Capricorn Orogen: lithotectonic elements, orogenies, and significance. Precambrian Res. 128, 201–218.

Chamberlain, K.R., Schmitt, A.K., Swapp, S.M., Harrison, T.M., Swoboda-Colberg, N., Bleeker, W., Peterson, T.D., Jefferson, C.W., Khudoley, A.K., 2010. In situ U–Pb SIMS (IN-SIMS) micro-baddeleyite dating of mafic rocks: method with examples. Precambrian Res. 183, 379–387.

Clark, C., Kirkland, C.L., Spaggiari, C. V., Oorschot, C., Wingate, M.T.D.D., Taylor, R.J., 2014. Proterozoic granulite formation driven by mafic magmatism: An example from the Fraser Range Metamorphics, Western Australia. Precambrian Res. 240, 1–21.

Clark, D.J., Hensen, B.J., Kinny, P.D., 2000. Geochronological constraints for a two-stage history of the Albany – Fraser Orogen , Western Australia. Precambrian Res. 102, 155–183.

Clark, D.J., Kinny, P.D., Post, N.J., 1999. Relationships between magmatism, metamorphism and deformation in the Fraser Complex, Western Australia: constraints from new SHRIMP U–Pb zircon geochronology. Aust. J. Earth Sci. 46, 923–932.

Condie, K.C., 2002. Continental growth during a 1.9-Ga superplume event. J. Geodyn. 34, 249–264.

Condie, K.C., Aster, R.C., 2013. Refinement of the supercontinent cycle with Hf, Nd and Sr isotopes. Geosci. Front. 4, 667–680.

Dawson, G.C., Krapež, B., Fletcher, I.R., McNaughton, N.J., Rasmussen, B., 2003. 1.2 Ga thermal metamorphism in the Albany-Fraser Orogen of Western Australia: Consequence of collision or regional heating by dyke swarms? J. Geol. Soc. London. 160, 29–37.

Ernst, R., Bleeker, W., 2010. Large igneous provinces (LIPs), giant dyke swarms, and mantle plumes: significance for breakup events within Canada and adjacent regions from 2.5 Ga to the Present. Can. J. Earth Sci. 47, 695–739.

French, J.E., Heaman, L.M., 2010. Precise U-Pb dating of Paleoproterozoic mafic dyke swarms of the Dharwar craton, India: Implications for the existence of the Neoarchean supercraton Sclavia. Precambrian Res. 183, 416–441.

French, J.E., Heaman, L.M., Chacko, T., Srivastava, R.K., 2008. 1891-1883 Ma Southern Bastar-Cuddapah mafic igneous events, India: A newly recognized large igneous province. Precambrian Res. 160, 308–322.

Giles, D., Betts, P., Lister, G., 2002. Far-field continental backarc setting for the 1.80-1.67 Ga basins of northeastern Australia. Geology 30, 823–826.

Goldberg, A.S., 2010. Dyke swarms as indicators of major extensional events in the 1.9–1.2 Ga Columbia supercontinent. J. Geodyn. 50, 176–190.

Ibanez-Mejia, M., Gehrels, G.E., Ruiz, J., Vervoort, J.D., Eddy, M.E., Li, C., 2014. Small-volume baddeleyite (ZrO2) U-Pb geochronology and Lu-Hf isotope geochemistry by LA-ICP-MS. Techniques and applications. Chem. Geol. 384, 149–167.

Johnson, S.P., Sheppard, S., Rasmussen, B., Wingate, M.T.D., Kirkland, C.L., Muhling, J.R., Fletcher, I.R., Belousova, E.A., 2011. Two collisions, two sutures: Punctuated pre-1950Ma assembly of the West Australian Craton during the Ophthalmian and Glenburgh Orogenies. Precambrian Res. 189, 239–262.

Kirkland, C.L., Spaggiari, C. V, Pawley, M.J., Wingate, M.T.D., Smithies, R.H., Howard, H.M., Tyler, I.M., Belousova, E.A., Poujol, M., 2011. On the edge: U–Pb, Lu–Hf, and Sm–Nd data suggests reworking of the Yilgarn craton margin during formation of the Albany-Fraser Orogen. Precambrian Res. 187, 223–247.

Korsch, R.J., Kositcin, N., Champion, D.C., 2011. Australian island arcs through time: Geodynamic implications for the Archean and Proterozoic. Gondwana

Res. 19, 716–734.

Liu, Y., Li, X.-H., Li, Q.-L., Tang, G.-Q., Yin, Q.-Z., 2011. Precise U–Pb zircon dating at a scale of <5 micron by the CAMECA 1280 SIMS using a Gaussian illumination probe. J. Anal. At. Spectrom. 26, 845.

Liu, Y., Li, Z.-X., Pisarevsky, S.A., Kirscher, U., Mitchell, R.N., Stark, J.C., 2018. Palaeomagnetism of the 1.89 Ga Boonadgin dykes of the Yilgarn Craton: Possible connection with India. Precambrian Res. In Press.

Mikhalsky, E. V, Sheraton, J.W., Hahne, K., Prince, N., Mountains, C., Coast, M., 2006. Charnockite composition in relation to the tectonic evolution of East Antarctica. Gondwana Res. 9, 379–397.

Moller, A., O'Brien, P.J., Kennedy, A., Kroner, A., 2003. Linking growth episodes of zircon and metamorphic textures to zircon chemistry: an example from the ultrahigh-temperature granulites of Rogaland (SW Norway). Geol. Soc. London, Spec. Publ. 220, 65–81.

Morrissey, L.J., Payne, J.L., Hand, M., Clark, C., Taylor, R., Kirkland, C.L., Kylander-Clark, A., 2017. Linking the Windmill Islands, east Antarctica and the Albany–Fraser Orogen: Insights from U–Pb zircon geochronology and Hf isotopes. Precambrian Res. 293, 131–149.

Myers, J.S., 1995. The generation and assembly of an Archaean supercontinent: evidence from the Yilgarn craton, Western Australia. Geol. Soc. London, Spec. Publ. 95, 143–154.

Myers, J.S., 1993. Precambrian Tectonic History of the West Australian Craton and Adjacent Orogens. Annu. Rev. Earth Planet. Sci. 21, 453–485.

Nelson, D.R., 1998. Granite-greenstone crust formation on the Archaean Earth: a consequence of two superimposed processes. Earth Planet. Sci. Lett. 158, 109–119.

Oliveira, E.P., Silveira, E.M., Söderlund, U., Ernst, R.E., 2013. U-Pb ages and geochemistry of mafic dyke swarms from the Uauá Block, São Francisco Craton, Brazil: LIPs remnants relevant for Late Archaean break-up of a supercraton. Lithos 174, 308–322.

Pisarevsky, S.A., Elming, S.-Å., Pesonen, L.J., Li, Z.-X., 2014. Mesoproterozoic paleogeography: Supercontinent and beyond. Precambrian Res. 244, 207–225.

Pisarevsky, S., De Waele, B., Jones, S., Söderlund, U., Ernst, R.E., 2015.

Paleomagnetism and U–Pb age of the 2.4Ga Erayinia mafic dykes in the south-western Yilgarn, Western Australia: Paleogeographic and geodynamic implications. Precambrian Res. 259, 222–231.

Post, N.J., 2000. Unravelling Gondwana fragments: an integrated structural, isotopic and petrographic investigation of the Windmill Islands, Antarctica. University of New South Wales PhD Thesis.

Prokoph, A., Ernst, R.E., Buchan, K.L., 2004. Time‐Series Analysis of Large Igneous Provinces: 3500 Ma to Present. J. Geol. 112, 1–22.

Qiu, Y., Groves, D.I., 1999. Late Archean collision and delamination in the Southwest Yilgarn Craton; the driving force for Archean orogenic lode gold mineralization? Econ. Geol. 94, 115–122.

Rasmussen, B., Fletcher, I.R., Bekker, A., Muhling, J.R., Gregory, C.J., Thorne, A.M., 2012. Deposition of 1.88-billion-year-old iron formations as a consequence of rapid crustal growth. Nature 484, 498–501.

Rogers, J.J.W., Santosh, M., 2003. Supercontinents in earth history. Gondwana Res. 6, 357–368.

Schmitt, A.K., Chamberlain, K.R., Swapp, S.M., Harrison, T.M., 2010. In situ U-Pb dating of micro-baddeleyite by secondary ion mass spectrometry. Chem. Geol. 269, 386–395.

Scibiorski, E., Tohver, E., Jourdan, F., 2015. Rapid cooling and exhumation in the western part of the Mesoproterozoic Albany-Fraser Orogen, Western Australia. Precambrian Res. 265, 232–248.

Sheppard, S., Bodorkos, S., Johnson, S.P., Wingate, M.T.D., Kirkland, C.L., 2010. The Paleoproterozoic Capricorn Orogeny: intracontinental reworking not continent–continent collision, Geological Survey of Western Australia Report 108. Geological Survey of Western Australia.

Sheppard, S., Rasmussen, B., Zi, J.-W., Soma, V.S., Sarma, S., Mohan, M.R., Krapez, B., Wilde, S.A., McNaughton, N.J., 2017. Sedimentation and mafic magmatism in the Paleoproterozoic Cuddapah Basin, India, as a consequence of lithospheric extension. Gondwana Res. 48, 153–163.

Sheraton, J.W., Black, L.P., McCulloch, M.T., Oliver, R.L., 1990. Age and origin of a compositionally varied mafic dyke swarm in the Bunger Hills, East Antarctica. Chem. Geol. 85, 215–246.

Sheraton, J.W., Black, L.P., Tindle, A.G., 1992. Petrogenesis of plutonic rocks in a Proterozoic granulite-facies terrane — the Bunger Hills, East Antarctica. Chem. Geol. 97, 163–198.

Smithies, R.H., Champion, D.C., 1999. Late Archaean felsic alkaline igneous rocks in the Eastern Goldfields, Yilgarn Craton, Western Australia: a result of lower crustal delamination? J. Geol. Soc. London. 156, 561–576.

Söderlund, U., Hofmann, A., Klausen, M.B., Olsson, J.R., Ernst, R.E., Persson, P.O., 2010. Towards a complete magmatic barcode for the Zimbabwe craton: Baddeleyite U-Pb dating of regional dolerite dyke swarms and sill complexes. Precambrian Res. 183, 388–398.

Spaggiari, C.V., Kirkland, C.L., Smithies, H.R., Wingate, M.T.D., Belousova, E.A., 2015. Transformation of an Archean craton margin during Proterozoic basin formation and magmatism: The Albany–Fraser Orogen, Western Australia. Precambrian Res. 266, 440–466.

Spaggiari, C.V., Kirkland, C.L., Smithies, R., Occhipinti, S., Wingate, M., 2014a. Geological framework of the Albany-Fraser orogen, in: Spaggiari, C. V., Tyler, I.M. (Eds.), Albany-Fraser Orogen Seismic and Magnetotelluric (MT) Workshop 2014: Extended Abstracts. Geological Survey of Western Australia, Record 2014/6. pp. 12–27.

Spaggiari, C.V., Kirkland, C.L., Smithies, R.H., Wingate, M.T.D., 2014b. Tectonic links between proterozoic sedimentary cycles, basin formation and magmatism in the Albany-Fraser Orogen, Western Australia, Geological Survey of Western Australia Report 133.

Spaggiari, C. V, Bodorkos, S., Barquero-Molina, M., Tyler, I.M., Wingate, M.T.D., 2009. Interpreted bedrock geology of the South Yilgarn and of the South Yilgarn and Central Albany-Fraser Orogen, Western Australia, Geological Survey of Western Australia Record 2009/10.

Spaggiari, C. V, Kirkland, C.L., Pawley, M.J., Smithies, R.H., Wingate, M.T.D., Doyle, M.G., Blenkinsop, T.G., Clark, C., Oorschot, C.W., Fox, L.J., 2011. The geology of the east Albany-Fraser Orogen—a field guide, Geological Survey of Western Australia Record 2011/23.

Tucker, N.M., Payne, J.L., Clark, C., Hand, M., Taylor, R.J., Kylander-Clark, A.R.C., 2017. Proterozoic reworking of Archean (Yilgarn) basement in the

Bunger Hills, east Antarctica. Precambrian Res. 298, 16–38.

Wang, X.-C., Li, Z.-X., Li, J., Pisarevsky, S.A., Wingate, M.T.D., 2014. Genesis of the 1.21 Ga Marnda Moorn large igneous province by plume–lithosphere interaction. Precambrian Res. 241, 85–103.

Ware, B., Jourdan, F., 2018. 40 Ar/39 Ar Geochronology of Terrestrial Pyroxene. Geochim. Cosmochim. Acta 230, 112-136.

Wingate, M.T.D., Campbell, I.H., Harris, L.B., 2000. SHRIMP baddeleyite age for the Fraser dyke swarm, southeast Yilgarn Craton, Western Australia. Aust. J. Earth Sci. 47, 309–313.

Witt, W.K., Cassidy, K.F., Lu, Y.-J., Hagemann, S.G., 2018. The tectonic setting and evolution of the 2.7 Ga Kalgoorlie–Kurnalpi Rift, a world-class Archean gold province. Miner. Depos. 1–31.

Xie, H., Kröner, A., Brandl, G., Wan, Y., 2017. Two orogenic events separated by 2.6 Ga mafic dykes in the Central Zone, Limpopo Belt, southern Africa. Precambrian Res. 289, 129–141.

Young, D.N., Zhao, J., Ellis, D.J., McCulloch, M.T., 1997. Geochemical and Sr-Nd isotopic mapping of source provinces for the Mawson charnockites, east Antarctica: implications for Proterozoic tectonics and Gondwana reconstruction. Precambrian Res. 86, 1–19.

Zhang, S.H., Zhao, Y., Liu, X.C., Liu, Y.S., Hou, K.J., Li, C.F., Ye, H., 2012. U-Pb geochronology and geochemistry of the bedrocks and moraine sediments from the Windmill Islands: Implications for Proterozoic evolution of East Antarctica. Precambrian Res. 206–207, 52–71.

Zhao, G., Cawood, P.A., Wilde, S.A., Sun, M., 2002. Review of global 2.1-1.8 Ga orogens: implications for a pre-Rodinia supercontinent. Earth-Science Rev. 59, 125–162.

Zhao, J., Ellis, D.J., Kilpatrick, J.A., McCulloch, M.T., 1997. Geochemical and Sr-Nd isotopic study of charnockites and related rocks in the northern Prince Charles Mountains, East Antarctica: implications for charnockite petrogenesis and proterozoic crustal evolution. Precambrian Res. 81, 37–66.

Zi, J.W., Rasmussen, B., Muhling, J.R., Fletcher, I.R., Thorne, A.M., Johnson, S.P., Cutten, H.N., Dunkley, D.J., Korhonen, F.J., 2015. In situ U-Pb geochronology of xenotime and monazite from the Abra polymetallic deposit in the Capricorn

Orogen, Australia: Dating hydrothermal mineralization and fluid flow in a long-lived crustal structure. Precambrian Res. 260, 91–112.

Zibra, I., Clos, F., Weinberg, R.F., Peternell, M., 2017. The ~2730 Ma onset of the Neoarchean Yilgarn Orogeny. Tectonics 36, 1787–1813.

Chapter 9 Bibliography

Abbott, D.H., Isley, A.E., 2002a. The intensity, occurrence, and duration of superplume events and eras over geological time. J. Geodyn. 34, 265–307.

Abbott, D.H., Isley, A.E., 2002b. Extraterrestrial influences on mantle plume activity. Earth Planet. Sci. Lett. 205, 53–62.

Abbott, G., 1997. Geology of the Upper Hart River Area, Eastern Ogilvie Mountains, Yukon Territory (9116A/10, 116A/11) Bulletin 9. Indian and Northern Affairs Canada, Exploration and Geological Services Division.

Aitken, A.R.A., Betts, P.G., Young, D.A., Blankenship, D.D., Roberts, J.L., Siegert, M.J., 2016. The Australo-Antarctic Columbia to Gondwana transition. Gondwana Res. 29, 136–152. doi:10.1016/j.gr.2014.10.019

Aitken, A.R.A., Young, D.A., Ferraccioli, F., Betts, P.G., Greenbaum, J.S., Richter, T.G., Roberts, J.L., Blankenship, D.D., Siegert, M.J., 2014. The subglacial geology of Wilkes Land, East Antarctica. Geophys. Res. Lett. 41, 2390–2400.

Allègre, C.J., Dupré, B., Richard, P., Rousseau, D., Brooks, C., 1982. Subcontinental versus suboceanic mantle, II. NdSrPb isotopic comparison of continental tholeiites with mid-ocean ridge tholeiites, and the structure of the continental lithosphere. Earth Planet. Sci. Lett. 57, 25–34. doi:10.1016/0012-821X(82)90170-4

Allibone, A.H., Windh, J., Etheridge, M.A., Burton, D., Anderson, G., Edwards, P.W., Miller, A., Graves, C., Fanning, C.M., Wysoczanski, R., 1998. Timing relationships and structural controls on the location of Au-Cu mineralization at the Boddington gold mine, Western Australia. Econ. Geol. 93, 245–270.

Ameen, S.M.M., Wilde, S.A., 2006. Identification of 1.85 Ga mafic dykes in the Northern Yilgarn Craton: a relationship to the Columbia supercontinent? IAGR Annu. Conv. Int. Symp. 2006, Hong Kong.

Anand, M., 2003. Early Proterozoic Melt Generation Processes beneath the Intra-cratonic Cuddapah Basin, Southern India. J. Petrol. 44, 2139–2171. doi:10.1093/petrology/egg073

Anand, R.R., Paine, M., 2002. Regolith geology of the Yilgarn Craton, Western Australia: implications for exploration. Aust. J. Earth Sci. 49, 3–162.

Anderson, D.L., 1995. Lithosphere, asthenosphere, and perisphere. Rev. Geophys.

33, 125–149.

Antonio, P.Y.J., D'Agrella-Filho, M.S., Trindade, R.I.F., Nédélec, A., de Oliveira, D.C., da Silva, F.F., Roverato, M., Lana, C., 2017. Turmoil before the boring billion: Paleomagnetism of the 1880–1860Ma Uatumã event in the Amazonian craton. Gondwana Res. 49, 106–129.

Bagas, L., 2004. Proterozoic evolution and tectonic setting of the northwest Paterson Orogen, Western Australia. Precambrian Res. 128, 475–496. doi:10.1016/j.precamres.2003.09.011

Baragar, W.R.A., Ernst, R.E., Hulbert, L., Peterson, T., 1996. Longitudinal petrochemical variation in the Mackenzie dyke swarm, northwestern Canadian Shield. J. Petrol. 37, 317–359.

Barley, M.E., Brown, S.J.A., Cas, R.A.F., Cassidy, K.F., Champion, D.C., Gardoll, S.J., Krapež, B., 2003. An integrated geological and metallogenic framework for the eastern Yilgarn Craton: developing geodynamic models of highly mineralised Archaean granite–greenstone terranes. AMIRA Project P624.

Barnes, S.J., Van Kranendonk, M.J., Sonntag, I., 2012. Geochemistry and tectonic setting of basalts from the Eastern Goldfields Superterrane. Aust. J. Earth Sci. 59, 707–735.

Baxter, J.L., Lipple, S.L., Playford, P.E., Low, G.H., Lowry, D.C., 1980. Pinjarra, WA Sheet SI 50-2, Geological Survey of Western Australia 1:250 000 Geological Series Maps.

Belica, M.E., Piispa, E.J., Meert, J.G., Pesonen, L.J., Plado, J., Pandit, M.K., Kamenov, G.D., Celestino, M., 2014. Paleoproterozoic mafic dyke swarms from the Dharwar craton; paleomagnetic poles for India from 2.37 to 1.88Ga and rethinking the Columbia supercontinent. Precambrian Res. 244, 100–122. doi:10.1016/j.precamres.2013.12.005

Bercovici, D., Karato, S.-I., 2003. Whole-mantle convection and the transition-zone water filter. Nature 425, 39–44. doi:10.1038/nature01918

Berger, M., Kramers, J.D., Nägler, T., 1995. Geochemistry and geochronology of charnoenderbites in the northern marginal zone of the Limpopo Belt, Southern Africa, and genetic models. Schweizerische Mineral. und Petrogr. Mitteilungen 75, 17–42.

Black, L.P., Harris, L.B., Delor, C.P., 1992. Reworking of Archaean and Early

Proterozoic components a progressive, Middle Proterozoic tectonothermal event in the Albany Mobile Belt, Western Australia. Precambrian Res. 59, 95–123.

Black, L.P., Kinny, P.D., Sheraton, J.W., 1991. The difficulties of dating mafic dykes: an Antarctic example. Contrib. to Mineral. Petrol. 109, 183–194. doi:10.1007/BF00306478

Black, L.P., Sheraton, J.W., Tingey, R.J., McCulloch, M.T., 1992. New U-Pb Zircon Ages From the Denman Glacier Area, East Antarctica, and Their Significance for Gondwana Reconstruction. Antarct. Sci. 4, 447–460. doi:10.1017/S095410209200066X

Blake, D.H., Tyler, I.M., Griffin, T.J., Sheppard, S., Thorne, A.M., Warren, R.G., 1999. Geology of the Halls Creek 1: 100 000 Sheet area (4461), Western Australia. Australian Geological Survey Organisation.

Blake, D.H., Tyler, I.M., Sheppard, S., 1997. Geology of the Ruby Plains 1: 100 000 sheet area (4460), Western Australia. Australian Geological Survey Organisation.

Bleeker, W., 2004. Taking the pulse of planet Earth: a proposal for a new multi-disciplinary flagship project in Canadian solid Earth sciences. Geosci. Canada 31, 179–190.

Bleeker, W., 2003. The late Archean record: a puzzle in ca. 35 pieces. Lithos 71, 99–134.

Bleeker, W., Ernst, R., 2006. Short-lived mantle generated magmatic events and their dyke swarms: the key unlocking Earth's paleogeographic record back to 2.6 Ga, in: Hanski, E.J., Mertanen, S., Rämö, O.T., Vuollo, J. (Eds.), Dyke Swarms—time Markers of Crustal Evolution: Selected Papers of the Fifth International Dyke Conference in Finland, Rovaniemi, Finland, 31 July- 3 Aug 2005 & Fourth International Dyke Conference, Kwazulu-Natal, South Africa 26-29 June 2001. CRC Press, London, pp. 3–26.

Blewett, R.S., Henson, P.A., Roy, I.G., Champion, D.C., Cassidy, K.F., 2010. Scale-integrated architecture of a world-class gold mineral system: The Archaean eastern Yilgarn Craton, Western Australia. Precambrian Res. 183, 230–250. doi:10.1016/j.precamres.2010.06.004

Blewett, R.S., Hitchman, A.P., 2006. 3D Geological Models of the Eastern Yilgarn Craton: Final Report pmd* CRC Y2 Project September 2001–December 2004.

Geoscience Australia Record 2006/05.

Blight, D.F., Oliver, R.L., 1977. The metamorphic geology of the Windmill Islands, Antarctica: A preliminary account. J. Geol. Soc. Aust. 24, 239–262. doi:10.1080/00167617708728986

Bodorkos, S., Clark, D.J., 2004a. Evolution of a crustal-scale transpressive shear zone in the Albany-Fraser Orogen, SW Australia: 2. Tectonic history of the Coramup Gneiss and a kinematic framework for Mesoproterozoic collision of the West Australian and Mawson cratons. J. Metamorph. Geol. 22, 713–731. doi:10.1111/j.1525-1314.2004.00544.x

Bodorkos, S., Clark, D.J., 2004b. Evolution of a crustal-scale transpressive shear zone in the Albany-Fraser Orogen, SW Australia: 1. P-T conditions of Mesoproterozoic metamorphism in the Coramup Gneiss. J. Metamorph. Geol. 22, 691–711. doi:10.1111/j.1525-1314.2004.00543.x

Boger, S.D., 2011. Antarctica—before and after Gondwana. Gondwana Res. 19, 335–371.

Boyd, D.M., Tucker, D.H., 1990. Australian magnetic dykes, in: Parker, A.J., Rickwood, P.C., Tucker, D.H. (Eds.), Mafic Dykes and Emplacement Mechanisms. A.A.Balkema, Rotterdam, pp. 391–399.

Bradley, D.C., 2011. Secular trends in the geologic record and the supercontinent cycle. Earth-Science Rev. 108, 16–33.

Bradley, D.C., 2008. Passive margins through earth history. Earth-Science Rev. 91, 1–26.

Brandon, A.D., Hooper, P.R., Goles, G.G., Lambert, R.S.J., 1993. Evaluating crustal contamination in continental basalts: the isotopic composition of the Picture Gorge Basalt of the Columbia River Basalt Group. Contrib. to Mineral. Petrol. 114, 452–464. doi:10.1007/BF00321750

Brandt, S., Klemd, R., Li, Q., Kröner, A., Brandl, G., Fischer, A., Bobek, P., Zhou, T., 2018. Pressure-temperature evolution during two granulite-facies metamorphic events (2.62 and 2.02 Ga) in rocks from the Central Zone of the Limpopo Belt, South Africa. Precambrian Res. 310, 471–506. doi:10.1016/j.precamres.2018.03.002

Bryan, S.E., Ernst, R.E., 2008. Revised definition of large igneous provinces (LIPs). Earth-Science Rev. 86, 175–202. doi:10.1016/j.earscirev.2007.08.008

Bryan, S.E., Peate, I.U., Peate, D.W., Self, S., Jerram, D.A., Mawby, M.R., Marsh, J.S., Miller, J.A., 2010. The largest volcanic eruptions on Earth. Earth-Science Rev. 102, 207–229.

Buchan, K.L., Ernst, R.E., Bleeker, W., Davies, W., Villeneuve, M., van Breemen, O., Hamilton, M., Söderlund, U., 2010. Proterozoic magmatic events of the Slave craton, Wopmay orogen and environs, in: Geological Survey of Canada, Open File 5985. Geological Survey of Canada.

Buchan, K.L., Ernst, R.E., Hamilton, M.A., Mertanen, S., Pesonen, L.J., Elming, S.-Å., 2001. Rodinia: the evidence from integrated palaeomagnetism and U–Pb geochronology. Precambrian Res. 110, 9–32.

Buchan, K.L., Goutier, J., Hamilton, M.A., Ernst, R.E., Matthews, W.A., 2007. Paleomagnetism, U–Pb geochronology, and geochemistry of Lac Esprit and other dyke swarms, James Bay area, Quebec, and implications for Paleoproterozoic deformation of the Superior Province. Can. J. Earth Sci. 44, 643–664.

Buchan, K.L., Mortensen, J.K., Card, K.D., 1993. Northeast-trending Early Proterozoic dykes of southern Superior Province: multiple episodes of emplacement recognized from integrated paleomagnetism and U–Pb geochronology. Can. J. Earth Sci. 30, 1286–1296.

Burke, K., Kidd, W.S.F., Kusky, T.M., 1986. Archean foreland basin tectonics in the Witwatersrand, South Africa. Tectonics 5, 439–456.

Calvert, A., Doublier, M., 2018. Archaean continental spreading inferred from seismic images of the Yilgarn Craton. Nat. Geosci. 11, 526–530. doi:10.1038/s41561-018-0138-0

Campbell, I.H., 2002. Implications of Nb / U , Th / U and Sm / Nd in plume magmas for the relationship between continental and oceanic crust formation and the development of the depleted mantle. Geochim. Cosmochim. Acta 66, 1651–1661. doi:10.1016/S0016-7037(01)00856-0

Campbell, I.H., Griffiths, R.W., 1990. Implications of mantle plume structure for the evolution of flood basalts. Earth Planet. Sci. Lett. 99, 79–93.

Campbell, I.H., Hill, R.I., 1988. A two-stage model for the formation of the granite-greenstone terrains of the Kalgoorlie-Norseman area, Western Australia. Earth Planet. Sci. Lett. 90, 11–25.

Campbell, I.H., McCall, G.J.H., Tyrwhitt, D.S., 1970. The Jimberlana Norite, Western Australia–a smaller analogue of the Great Dyke of Rhodesia. Geol. Mag. 107, 1–12.

Cande, S.C., Stegman, D.R., 2011. Indian and African plate motions driven by the push force of the Réunion plume head. Nature 475, 47–52. doi:10.1038/nature10174

Cassidy, K.F., Champion, D.C., Huston, D.L., 2005. Crustal evolution constraints on the metallogeny of the Yilgarn Craton, in: Mineral Deposit Research: Meeting the Global Challenge: Proceedings of the Eight Biennia SGA Meeting. Springer, Berlin, pp. 901–904.

Cassidy, K.F., Champion, D.C., Krapez, B., Barley, M.E., Brown, S.J.A., Blewett, R.S., Groenewald, Pb., Tyler, I.M., 2006. A revised geological framework for the Yilgarn Craton, Western Australia, in: Geological Survey of Western Australia Record 8/2006. Geological Survey of Western Australia.

Cassidy, K.F., Champion, D.C., McNaughton, N.J., Fletcher, I.R., Whitaker, A.J., Bastrakova, I. V, Budd, A.R., 2002. Characterisation and metallogenic significance of Archaean granitoids of the Yilgarn Craton, Western Australia, Minerals and Energy Research Institute of Western Australia (MERIWA) Report P482.

Cassidy, K.F., Champion, D.C., Wyborn, L.A.I., 1998. A Geochemical Study of Granitoids of the Boddington Gold Mine: Final Report to SRK (Australasia) Ltd. Australian Geological Survey Organisation.

Cawood, P.A., Korsch, R.J., 2008. Assembling Australia: Proterozoic building of a continent. Precambrian Res. 166, 1–35. doi:10.1016/j.precamres.2008.08.006

Cawood, P.A., Tyler, I.M., 2004. Assembling and reactivating the Proterozoic Capricorn Orogen: lithotectonic elements, orogenies, and significance. Precambrian Res. 128, 201–218. doi:10.1016/j.precamres.2003.09.001

Chamberlain, K.R., Schmitt, A.K., Swapp, S.M., Harrison, T.M., Swoboda-Colberg, N., Bleeker, W., Peterson, T.D., Jefferson, C.W., Khudoley, A.K., 2010. In situ U–Pb SIMS (IN-SIMS) micro-baddeleyite dating of mafic rocks: method with examples. Precambrian Res. 183, 379–387.

Champion, D.C., 2013. Neodymium depleted mantle model age map of Australia: explanatory notes and user guide. Geosci. Aust. Rec. 2013/44, 209.

doi:10.11636/Record.2013.044

Champion, D.C., 2013. Neodymium depleted mantle model age map of Australia: explanatory notes and user guide. Geosci. Aust. Rec. 2013/44, 209. doi:10.11636/Record.2013.044

Champion, D.C., Cassidy, K.F., 2008. Geodynamics: Using geochemistry and isotopic signatures of granites to aid mineral systems studies: An example from the Yilgarn craton. Geosci. Aust. Rec. 9, 7–16.

Champion, D.C., Cassidy, K.F., 2007. An overview of the Yilgarn Craton and its crustal evolution, in: Geoscience Australia Record. pp. 8–13.

Champion, D.C., Sheraton, J.W., 1997. Geochemistry and Nd isotope systematics of Archaean granites of the Eastern Goldfields, Yilgarn Craton, Australia: implications for crustal growth processes. Precambrian Res. 83, 109–132.

Chatterjee, N., Bhattacharji, S., 2001. Petrology, geochemistry and tectonic settings of the mafic dikes and sills associated with the evolution of the Proterozoic Cuddapah Basin of south India. J. Earth Syst. Sci. 110, 433–453.

Chaudhuri, A.K., Saha, D., Deb, G.K., Deb, S.P., Mukherjee, M.K., Ghosh, G., 2002. The Purana basins of southern cratonic province of India-a case for Mesoproterozoic fossil rifts. Gondwana Res. 5, 23–33.

Ciborowski, T.J.R., Kerr, A.C., Ernst, R.E., Mcdonald, I., Minifie, M.J., Harlan, S.S., Millar, I.L., 2015. The Early Proterozoic Matachewan Large Igneous Province : Geochemistry, Petrogenesis, and Implications for Earth Evolution 56, 1459–1494. doi:10.1093/petrology/egv038

Claoué-Long, J.C., Hoatson, D.M., 2009. Guide to using the map of Australian Proterozoic large igneous provinces. Geoscience Australia.

Claoué-Long, J.C., Hoatson, D.M., Australia, G., 2009. Guide to using the Map of Australian Proterozoic Large Igneous Provinces. Geoscience Australia Record 2009/44.

Clark, C., Kirkland, C.L., Spaggiari, C. V., Oorschot, C., Wingate, M.T.D.D., Taylor, R.J., 2014. Proterozoic granulite formation driven by mafic magmatism: An example from the Fraser Range Metamorphics, Western Australia. Precambrian Res. 240, 1–21. doi:10.1016/j.precamres.2013.07.024

Clark, D.J., Hensen, B.J., Kinny, P.D., 2000. Geochronological constraints for a two-stage history of the Albany – Fraser Orogen , Western Australia. Precambrian

Res. 102, 155–183.

Clark, D.J., Kinny, P.D., Post, N.J., 1999. Relationships between magmatism, metamorphism and deformation in the Fraser Complex, Western Australia: constraints from new SHRIMP U–Pb zircon geochronology. Aust. J. Earth Sci. 46, 923–932.

Coffin, M.F., Eldholm, O., 1994. Large igneous provinces: crustal structure, dimensions, and external consequences. Rev. Geophys. 32, 1–36. doi:10.1029/93RG02508

Collerson, K.D., Sheraton, J.W., 1986. Age and geochemical characteristics of a mafic dyke swarm in the Archaean Vestfold Block, Antarctica: inferences about Proterozoic dyke emplacement in Gondwana. J. Petrol. 27, 853–886.

Compston, W., Williams, I.S., McCulloch, M.T., 1986. Contrasting zircon U-Pb and model Sm-Nd ages for the Archaean Logue Brook Granite. Aust. J. Earth Sci. 33, 193–200. doi:10.1080/08120098608729359

Compston, W., Williams, I.S., Meyer, C., 1984. U-Pb geochronology of zircons from lunar breccia 73217 using a sensitive high mass-resolution ion microprobe. J. Geophys. Res. 89, B525. doi:10.1029/JB089iS02p0B525

Condie, K.C., 2011. The supercontinent cycle, in: Earth as an Evolving Planetary System. Academic Press, New York, pp. 317–355.

Condie, K.C., 2004. Supercontinents and superplume events: distinguishing signals in the geologic record. Phys. Earth Planet. Inter. 146, 319–332. doi:10.1016/j.pepi.2003.04.002

Condie, K.C., 2003. Supercontinents, superplumes and continental growth: the Neoproterozoic record. Geol. Soc. London, Spec. Publ. 206, 1–21.

Condie, K.C., 2002. Continental growth during a 1.9-Ga superplume event. J. Geodyn. 34, 249–264. doi:10.1016/S0264-3707(02)00023-6

Condie, K.C., 1997. Sources of Proterozoic mafic dyke swarms: constraints from ThTa and LaYb ratios. Precambrian Res. 81, 3–14. doi:http://dx.doi.org/10.1016/S0301-9268(96)00020-4

Condie, K.C., Aster, R.C., 2013. Refinement of the supercontinent cycle with Hf, Nd and Sr isotopes. Geosci. Front. 4, 667–680.

Condie, K.C., Belousova, E., Griffin, W.L., Sircombe, K.N., 2009. Granitoid events in space and time: Constraints from igneous and detrital zircon age spectra.

Gondwana Res. 15, 228–242. doi:10.1016/j.gr.2008.06.001

Condie, K.C., Davaille, A., Aster, R.C., Arndt, N., 2015. Upstairs-downstairs: Supercontinents and large igneous provinces, are they related? Int. Geol. Rev. 57, 1341–1348. doi:10.1080/00206814.2014.963170

Condon, D.J., Schoene, B., McLean, N.M., Bowring, S.A., Parrish, R.R., 2015. Metrology and traceability of U–Pb isotope dilution geochronology (EARTHTIME Tracer Calibration Part I). Geochim. Cosmochim. Acta 164, 464–480.

Corfu, F., Hanchar, J.M., Hoskin, P.W.O., Kinny, P., 2003. Atlas of Zircon Textures. Rev. Mineral. Geochemistry 53, 469–500. doi:10.2113/0530469

Courtillot, V., Davaille, A., Besse, J., Stock, J., 2003. Three distinct types of hotspots in the Earth's mantle. Earth Planet. Sci. Lett. 205, 295–308.

Courtillot, V., Jaupart, C., Manighetti, I., Tapponnier, P., Besse, J., 1999. On casual links between flood basalts and continental breakup. Earth Planet. Sci. Lett. 166, 177–195.

Crookshank, H., 1963. Geology of southern Bastar and Jeypore from the Bailadila range to the Eastern Ghats, 87th ed.

Czarnota, K., Champion, D.C., Goscombe, B., Blewett, R.S., Cassidy, K.F., Henson, P.A., Groenewald, P.B., 2010. Geodynamics of the eastern Yilgarn Craton. Precambrian Res. 183, 175–202. doi:10.1016/j.precamres.2010.08.004

Dalziel, I.W.D., 1991. Pacific margins of Laurentia and East Antarctica-Australia as a conjugate rift pair: Evidence and implications for an Eocambrian supercontinent. Geology 19, 598–601.

Dasgupta, S., Bose, S., Das, K., 2013. Tectonic evolution of the Eastern Ghats Belt, India. Precambrian Res. 227, 247–258. doi:10.1016/j.precamres.2012.04.005

Davidson, A., van Breemen, O., 1988. Baddeleyite-zircon relationships in coronitic metagabbro, Grenville Province, Ontario: implications for geochronology. Contrib. to Mineral. Petrol. 100, 291–299. doi:10.1007/BF00379740

Dawson, G.C., Krapež, B., Fletcher, I.R., McNaughton, N.J., Rasmussen, B., 2003. 1.2 Ga thermal metamorphism in the Albany-Fraser Orogen of Western Australia: Consequence of collision or regional heating by dyke swarms? J. Geol. Soc. London. 160, 29–37. doi:10.1144/0166-764901-119

De Kock, M.O., Ernst, R., Söderlund, U., Jourdan, F., Hofmann, A., Le Gall, B., Bertrand, H., Chisonga, B.C., Beukes, N., Rajesh, H.M., Moseki, L.M., Fuchs, R., 2014. Dykes of the 1.11Ga Umkondo LIP, Southern Africa: Clues to a complex plumbing system. Precambrian Res. 249, 129–143. doi:10.1016/j.precamres.2014.05.006

Dentith, M.C., Dent, V.F., Drummond, B.J., 2000. Deep crustal structure in the southwestern Yilgarn Craton , Western Australia. Tectonophysics 325, 227–255.

Dentith, M.C., Featherstone, W.E., 2003. Controls on intra-plate seismicity in southwestern Australia. Tectonophysics 376, 167–184. doi:10.1016/j.tecto.2003.10.002

DePaolo, D.J., 1981. Trace element and isotopic effects of combined wallrock assimilation and fractional crystallization. Earth Planet. Sci. Lett. 53, 189–202.

DePaolo, D.J., 1981. Neodymium isotopes in the Colorado Front Range and crust–mantle evolution in the Proterozoic. Nature 291, 193–196. doi:10.1038/291193a0

Ding, P., James, P.R., 1991. Structural evolution of the Bunger Hills area of East Antarctica. Geol. Evol. Antarct. Cambridge Univ. Press. Cambridge 13–17.

Doehler, J.S., Heaman, L.M., 1998. 2.41 Ga U–Pb Baddeleyite ages for two gabbroic dykes from the Widgiemooltha swarm, Western Australia: a Yilgarn–Lewisian connection, in: Geological Society of America 1998 Annual Meeting, Abstracts with Programs. Geological Society of America, pp. 291–292.

Doughty, P.T., Chamberlain, K.R., 1996. Salmon River Arch revisited: New evidence for 1370 Ma rifting near the end of deposition in the Middle Proterozoic Belt basin. Can. J. Earth Sci. 33, 1037–1052.

Doyle, H.A., 1971. Seismicity and structure in Australia. Bull. R. Soc. New Zeal. 9, 149–152.

Duebendorfer, E.M., 2002. Regional correlation of mesoproterozoic structures and deformational events in the Albany-Fraser orogen, Western Australia. Precambrian Res. 116, 129–154. doi:10.1016/S0301-9268(02)00017-7

Dunphy, J.M., Fletcher, I.R., Cassidy, K.F., Champion, D.C., 2003. Compilation of SHRIMP U–Pb geochronological data, Yilgarn Craton, Western Australia, 2001–2002. Geosci. Aust. Rec. 15, 139.

Eggins, S.M., Woodhead, J.D., Kinsley, L.P.J., Mortimer, G.E., Sylvester, P., McCulloch, M.T., Hergt, J.M., Handler, M.R., 1997. A simple method for the precise determination of≥ 40 trace elements in geological samples by ICPMS using enriched isotope internal standardisation. Chem. Geol. 134, 311–326.

Elkins-Tanton, L.T., 2005. Continental magmatism caused by lithospheric delamination. Geol. Soc. Am. Spec. Pap. 80301, 449–461. doi:10.1130/2005.2388(27).

Elkins Tanton, L.T., Hager, B.H., 2000. Melt intrusion as a trigger for lithospheric foundering and the eruption of the Siberian flood basalts. Geophys. Res. Lett. 27, 3937–3940.

Embleton, B.J.J., Schmidt, P.W., 1985. Age and significance of magnetizations in dolerite dykes from the Northampton Block, Western Australia. Aust. J. Earth Sci. 32, 279–286.

Ernst, R., Bleeker, W., 2010. Large igneous provinces (LIPs), giant dyke swarms, and mantle plumes: significance for breakup events within Canada and adjacent regions from 2.5 Ga to the Present. Can. J. Earth Sci. 47, 695–739. doi:10.1139/e10-025

Ernst, R., Jowitt, S., 2013. Large Igneous Provinces (LIPs) and Metallogeny. Soc. Econ. Geol. Inc. 17–51.

Ernst, R., Srivastava, R., Bleeker, W., Hamilton, M., 2010. Precambrian Large Igneous Provinces (LIPs) and their dyke swarms: New insights from high-precision geochronology integrated with paleomagnetism and geochemistry. Precambrian Res. 183, vii–xi.

Ernst, R.E., 2014. Large igneous provinces. Cambridge University Press.

Ernst, R.E., Baragar, W.R.A., 1992. Evidence from magnetic fabric for the flow pattern of magma in the Mackenzie giant radiating dyke swarm. Nature 356, 511–513.

Ernst, R.E., Bell, K., 2010. Large igneous provinces (LIPs) and carbonatites. Mineral. Petrol. 98, 55–76.

Ernst, R.E., Bell, K., 1992. Petrology of the Great Abitibi Dyke, Superior Province, Canada. J. Petrol. 33, 423–469.

Ernst, R.E., Bleeker, W., Söderlund, U., Kerr, A.C., 2013. Large Igneous Provinces and supercontinents: Toward completing the plate tectonic revolution. Lithos 174, 1–14.

Ernst, R.E., Buchan, K.L., 2001a. Large mafic magmatic events through time and links to mantle-plume heads, in: Geological Society of America Special Paper 352. pp. 483–576.

Ernst, R.E., Buchan, K.L., 2001b. The use of mafic dike swarms in identifying and locating mantle plumes, in: Geological Society of America Special Paper 352. Geological Society of America, pp. 247–266.

Ernst, R.E., Buchan, K.L., 1997. Giant radiating dyke swarms: their use in identifying pre-Mesozoic large igneous provinces and mantle plumes, in: Large Igneous Provinces: Continental, Oceanic, and Planetary Flood Volcanism. American Geophysical Union Monograph 100, pp. 297–333.

Ernst, R.E., Buchan, K.L., Campbell, I.H., 2005. Frontiers in large igneous province research. Lithos 79, 271–297. doi:10.1016/j.lithos.2004.09.004

Ernst, R.E., Buchan, K.L., Hamilton, M.A., Okrugin, A. V, Tomshin, M.D., 2000. Integrated paleomagnetism and U-Pb geochronology of mafic dikes of the eastern Anabar Shield region, Siberia: Implications for Mesoproterozoic paleolatitude of Siberia and comparison with Laurentia. J. Geol. 108, 381–401.

Ernst, R.E., Buchan, K.L., Palmer, H.C., 1995a. Physics and Chemistry of Dykes.

Ernst, R.E., Hamilton, M.A., Soderlund, U., Hanes, J.A., Gladkochub, D.P., Okrugin, A. V, Kolotilina, T., Mekhonoshin, A.S., Bleeker, W., LeCheminant, A.N., Buchan, K.L., Chamberlain, K.R., Didenko, A.N., 2016. Long-lived connection between southern Siberia and northern Laurentia in the Proterozoic. Nat. Geosci 9, 464–469. doi:10.1038/ngeo2700\rhttp://www.nature.com/ngeo/journal/v9/n6/abs/ngeo2700.html#supplementary-information

Ernst, R.E., Head, J.W., Parfitt, E., Grosfils, E., Wilson, L., 1995b. Giant radiating dyke swarms on Earth and Venus. Earth-Science Rev. 39, 1–58.

Ernst, R.E., Pease, V., Puchkov, V.N., Kozlov, V.I., Sergeeva, N.D., Hamilton, M., 2006. Geochemical characterization of Precambrian magmatic suites of the Southeastern margin of the East European Craton, Southern Urals, Russia. Geol. Sb. 119–161.

Ernst, R.E., Srivastava, R.K., 2008. India’s place in the Proterozoic world: constraints from the Large Igneous Province (LIP) record. Indian dykes. Ed. by RK Srivastava, Ch. Sivaji, NV Chalapathi Rao. Geochemistry, Geophys.

Geochronology, Narosa Publ. House Pvt. Ltd, New Delhi, India 41–56.

Ernst, R.E., Wingate, M.T.D., Buchan, K.L., Li, Z.X., 2008. Global record of 1600–700Ma Large Igneous Provinces (LIPs): Implications for the reconstruction of the proposed Nuna (Columbia) and Rodinia supercontinents. Precambrian Res. 160, 159–178. doi:10.1016/j.precamres.2007.04.019

Ernst, R.E., Youbi, N., 2017. How Large Igneous Provinces affect global climate, sometimes cause mass extinctions, and represent natural markers in the geological record. Palaeogeogr. Palaeoclimatol. Palaeoecol. 478, 30–52. doi:10.1016/j.palaeo.2017.03.014

Evans, D.A.D., Li, Z., Murphy, J.B., 2016. Four-dimensional context of Earth ’ s supercontinents. Geol. Soc. London 424, 1–14. doi:10.1144/SP424.12

Evans, D.A.D., Mitchell, R.N., 2011. Assembly and breakup of the core of Paleoproterozoic–Mesoproterozoic supercontinent Nuna. Geology 39, 443–446.

Evans, M.E., 1968. Magnetization of dikes: a study of the paleomagnetism of the Widgiemooltha dike suite, Western Australia. J. Geophys. Res. 73, 3261–3270.

Evans, T., 1999. Extent and nature of the 1.2 Ga Wheatbelt dyke swarm, Yilgarn Craton, Western Australia. B.Sc. thesis, Univ. West. Aust. Perth.

Fitzsimons, I.C.W., 2003. Proterozoic basement provinces of southern and southwestern Australia, and their correlation with Antarctica. Geol. Soc. London, Spec. Publ. 206, 93–130.

Fitzsimons, I.C.W., 2000a. Grenville-age basement provinces in East Antarctica: evidence for three separate collisional orogens. Geology 28, 879–882.

Fitzsimons, I.C.W., 2000b. A review of tectonic events in the East Antarctic Shield and their implications for Gondwana and earlier supercontinents. J. African Earth Sci. 31, 3–23.

Fletcher, I.R., McNaughton, N.J., Davis, W.J., Rasmussen, B., 2010. Matrix effects and calibration limitations in ion probe U-Pb and Th-Pb dating of monazite. Chem. Geol. 270, 31–44. doi:10.1016/j.chemgeo.2009.11.003

Fletcher, I.R., Wilde, S.A., Rosman, K.J., 1985. Sm-Nd model ages across the margins of the Archaean Yilgarn block, Western Australia — III. The western margin. Aust. J. Earth Sci. 32, 73–82. doi:10.1080/08120098508729314

Foley, S.F., Barth, M.G., Jenner, G.A., 2000. Rutile/melt partition coefficients for trace elements and an assessment of the influence of rutile on the trace element characteristics of subduction zone magmas. Geochim. Cosmochim. Acta 64, 933–938.

French, J.E., Heaman, L.M., 2010. Precise U-Pb dating of Paleoproterozoic mafic dyke swarms of the Dharwar craton, India: Implications for the existence of the Neoarchean supercraton Sclavia. Precambrian Res. 183, 416–441. doi:10.1016/j.precamres.2010.05.003

French, J.E., Heaman, L.M., Chacko, T., 2002. Feasibility of chemical U-Th-total Pb baddeleyite dating by electron microprobe. Chem. Geol. 188, 85–104. doi:10.1016/S0009-2541(02)00074-8

French, J.E., Heaman, L.M., Chacko, T., Srivastava, R.K., 2008. 1891-1883 Ma Southern Bastar-Cuddapah mafic igneous events, India: A newly recognized large igneous province. Precambrian Res. 160, 308–322. doi:10.1016/j.precamres.2007.08.005

Gao, S., Rudnick, R.L., Yuan, H.-L., Liu, X.-M., Liu, Y.-S., Xu, W.-L., Ling, W.-L., Ayers, J., Wang, X.-C., Wang, Q.-H., 2004. Recycling lower continental crust in the North China craton. Nature 432, 892–897.

Gee, R.D., Baxter, J.L., Wilde, S.A., Williams, I.R., 1981. Crustal development in the Archaean Yilgarn Block, Western Australia. Spec. Publ. Geol. Soc. Aust 7, 43–56.

Genske, F.S., Beier, C., Stracke, A., Turner, S.P., Pearson, N.J., Hauff, F., Schaefer, B.F., Haase, K.M., 2016. Comparing the nature of the western and eastern Azores mantle. Geochim. Cosmochim. Acta 172, 76–92. doi:10.1016/j.gca.2015.08.019

Gerdes, A., Zeh, A., 2009. Zircon formation versus zircon alteration - New insights from combined U-Pb and Lu-Hf in-situ LA-ICP-MS analyses, and consequences for the interpretation of Archean zircon from the Central Zone of the Limpopo Belt. Chem. Geol. 261, 230–243. doi:10.1016/j.chemgeo.2008.03.005

Giles, D., Betts, P., Lister, G., 2002. Far-field continental backarc setting for the 1.80-1.67 Ga basins of northeastern Australia. Geology 30, 823–826.

Goldberg, A.S., 2010. Dyke swarms as indicators of major extensional events in the 1.9–1.2 Ga Columbia supercontinent. J. Geodyn. 50, 176–190.

Groves, D.I., 1993. The crustal continuum model for late-Archaean lode-gold deposits of the Yilgarn Block, Western Australia. Miner. Depos. 28, 366–374.

Gutiérrez-Alonso, G., Fernández-Suárez, J., Weil, A.B., Brendan Murphy, J., Damian Nance, R., Corf, F., Johnston, S.T., 2008. Self-subduction of the Pangaean global plate. Nat. Geosci. 1, 549–553. doi:10.1038/ngeo250

Hacker, B.R., Kelemen, P.B., Behn, M.D., 2015. Continental Lower Crust. Annu. Rev. Earth Planet. Sci. 43, 167–205. doi:10.1146/annurev-earth-050212-124117

Halilovic, J., Cawood, P.A., Jones, J.A., Pirajno, F., Nemchin, A.A., 2004. Provenance of the Earaheedy Basin: implications for assembly of the Western Australian Craton. Precambrian Res. 128, 343–366.

Hallberg, J.A., 1987. Postcratonization mafic and ultramafic dykes of the Yilgarn Block. Aust. J. Earth Sci. 34, 135–149. doi:10.1080/08120098708729398

Halls, H.C., 2008. The importance of integrating paleomagnetic studies of Proterozoic dykes with U–Pb geochronology and geochemistry. Indian Dykes Geochemistry, Geophys. Geochronol. 19–40.

Halls, H.C., 1986. Paleomagnetism, structure, and longitudinal correlation of Middle Precambrian dykes from northwestern Ontario and Minnesota. Can. J. Earth Sci. 23, 142–157.

Halls, H.C., 1982. The Importance and Potential of Mafic Dyke Swarms in Studies of Geodynamic Processes. Geosci. Canada. doi:10.12789/gs.v9i3.3309

Halls, H.C., Heaman, L.M., 2000. The paleomagnetic significance of new U-Pb age data from the Molson dyke swarm, Cauchon Lake area, Manitoba. Can. J. Earth Sci. 37, 957–966.

Halls, H.C., Kumar, A., Srinivasan, R., Hamilton, M.A., 2007. Paleomagnetism and U-Pb geochronology of easterly trending dykes in the Dharwar craton, India: feldspar clouding, radiating dyke swarms and the position of India at 2.37 Ga. Precambrian Res. 155, 47–68. doi:10.1016/j.precamres.2007.01.007

Halls, H.C., Palmer, H.C., 1990. The tectonic relationship of two Early Proterozoic dyke swarms to the Kapuskasing Structural Zone: a paleomagnetic and petrographic study. Can. J. Earth Sci. 27, 87–103. doi:10.1139/e90-007

Halls, H.C., Zhang, B., 1998. Uplift structure of the southern Kapuskasing zone from 2.45 Ga dike swarm displacement. Geology 26, 67–70. doi:10.1130/0091-7613(1998)026<0067:USOTSK>2.3.CO;2

Hanson, R.E., Gose, W.A., Crowley, J.L., Ramezani, J., Bowring, S.A., Bullen, D.S., Hall, R.P., Pancake, J.A., Mukwakwami, J., 2004. Paleoproterozoic intraplate magmatism and basin development on the Kaapvaal Craton: Age, paleomagnetism and geochemistry of~ 1.93 to~ 1.87 Ga post-Waterberg dolerites. South African J. Geol. 107, 233–254.

Harley, S.L., Fitzsimons, I.C.W., Zhao, Y., 2013. Antarctica and supercontinent evolution: historical perspectives, recent advances and unresolved issues. Geol. Soc. London, Spec. Publ. 383, 1–34.

Hart, S.R., 1984. A large-scale isotope anomaly in the Southern Hemisphere mantle. Nature 309, 753–757.

Hawkesworth, C., 1993. Mantle and Slab Contribution in Arc Magmas. Annu. Rev. Earth Planet. Sci. 21, 175–204. doi:10.1146/annurev.earth.21.1.175

Hawkesworth, C.J., Cawood, P.A., Dhuime, B., 2016. Tectonics and crustal evolution. GSA Today 26, 4–11. doi:10.1130/GSATG272A.1.4

Hawkesworth, C.J., Dhuime, B., Pietranik, A.B., Cawood, P.A., Kemp, A.I.S., Storey, C.D., 2010. The generation and evolution of the continental crust. J. Geol. Soc. London. 167, 229–248. doi:10.1144/0016-76492009-072

Hawkesworth, C.J., Kempton, P.D., Rogers, N.W., Ellam, R.M., Calsteren, P.W. van, 1990. Continental mantle lithosphere, and shallow level enrichment processes in the Earth's mantle. Earth Planet. Sci. Lett. 96, 256–268.

Hawkesworth, C.J., Lightfoot, P.C., Fedorenko, V.A., Blake, S., Naldrett, A.J., Doherty, W., Gorbachev, N.S., 1995. Magma differentiation and mineralisation in the Siberian continental flood basalts. Lithos 34, 61–88. doi:10.1016/0024-4937(95)90011-X

Heaman, L.M., 2009. The application of U–Pb geochronology to mafic, ultramafic and alkaline rocks: An evaluation of three mineral standards. Chem. Geol. 261, 43–52. doi:10.1016/j.chemgeo.2008.10.021

Heaman, L.M., 2008. Precambrian Large Igneous Provinces: An Overview of Geochronology, Origins and Impact on Earth Evolution. J. Geol. Soc. India 72, 15–34.

Heaman, L.M., 1997. Global mafic magmatism at 2.45 Ga: Remnants of an ancient large igneous province? Geology 25, 299–302.

Heaman, L.M., Le Cheminant, A.N., 1988. U-Pb baddeleyite ages of the Muskox Intrusion and Mackenzie Dyke Swarm. NWT, Canada 53.

Heaman, L.M., LeCheminant, A.N., 1993. Paragenesis and U-Pb systematics of baddeleyite (ZrO2). Chem. Geol. 110, 95–126. doi:10.1016/0009-2541(93)90249-I

Heaman, L.M., LeCheminant, A.N., Rainbird, R.H., 1992. Nature and timing of Franklin igneous events, Canada: implications for a Late Proterozoic mantle plume and the break-up of Laurentia. Earth Planet. Sci. Lett. 109, 117–131.

Heaman, L.M., Machado, N., 1992. Timing and origin of midcontinent rift alkaline magmatism, North America: evidence from the Coldwell Complex. Contrib. to Mineral. Petrol. 110, 289–303.

Heaman, L.M., Machado, N., Krogh, T.E., Weber, W., 1986. Precise U-Pb zircon ages for the Molson dyke swarm and the Fox River sill: constraints for Early Proterozoic crustal evolution in northeastern Manitoba, Canada. Contrib. to Mineral. Petrol. 94, 82–89.

Heaman, L.M., Peck, D., Toope, K., 2009. Timing and geochemistry of 1.88 Ga Molson Igneous Events, Manitoba: Insights into the formation of a craton-scale magmatic and metallogenic province. Precambrian Res. 172, 143–162.

Heinonen, J.S., Carlson, R.W., Riley, T.R., Luttinen, A. V., Horan, M.F., 2014. Subduction-modified oceanic crust mixed with a depleted mantle reservoir in the sources of the Karoo continental flood basalt province. Earth Planet. Sci. Lett. 394, 229–241. doi:10.1016/j.epsl.2014.03.012

Heinonen, J.S., Luttinen, A. V., Bohrson, W.A., 2016. Enriched continental flood basalts from depleted mantle melts: modeling the lithospheric contamination of Karoo lavas from Antarctica. Contrib. to Mineral. Petrol. 171, 9. doi:10.1007/s00410-015-1214-8

Hinthorne, J.R., Andersen, C.A., Conrad, R.L., Lovering, J.F., 1979. Single-grain 207Pb206Pb and U/Pb age determinations with a 10-µm spatial resolution using the ion microprobe mass analyzer (IMMA). Chem. Geol. 25, 271–303.

Hirschmann, M.M., Asimow, P.D., Ghiorso, M.S., Stolper, E.M., 1999. Calculation of peridotite partial melting from thermodynamic models of minerals and melts. III. Controls on isobaric melt production and the effect of water on melt production. J. Petrol. 40, 831–851.

Hoek, J.D., Seitz, H.-M., 1995. Continental mafic dyke swarms as tectonic indicators: an example from the Vestfold Hills, Antarctica. Precambrian Res.

75, 121–139.

Hoffman, P.F., 1999. The break-up of Rodinia, birth of Gondwana, true polar wander and the snowball Earth. J. African Earth Sci. 28, 17–33.

Hoffman, P.F., 1998. A Neoproterozoic Snowball Earth. Science (80-.). 281, 1342–1346. doi:10.1126/science.281.5381.1342

Hoffman, P.F., 1997. Tectonic genealogy of North America. Earth Struct. an Introd. to Struct. Geol. tectonics. McGraw-Hill, New York 459–464.

Holzer, L., Frei, R., Barton, J.M., Kramers, J.D., 1998. Unraveling the record of successive high grade events in the Central Zone of the Limpopo Belt using Pb single phase dating of metamorphic minerals. Precambrian Res. 87, 87–115. doi:10.1016/S0301-9268(97)00058-2

Hou, G., 2012. Mechanism for three types of mafic dyke swarms. Geosci. Front. 3, 217–223. doi:10.1016/j.gsf.2011.10.003

Hou, G., Kusky, T.M., Wang, C., Wang, Y., 2010. Mechanics of the giant radiating Mackenzie dyke swarm: A paleostress field modeling. J. Geophys. Res. Solid Earth 115, B02402, doi:10.1029/2007JB005475. doi:10.1029/2007JB005475

Hou, G., Santosh, M., Qian, X., Lister, G.S., Li, J., 2008. Configuration of the Late Paleoproterozoic supercontinent Columbia: Insights from radiating mafic dyke swarms. Gondwana Res. 14, 395–409. doi:10.1016/j.gr.2008.01.010

Hou, G., Wang, C., Li, J., Qian, X., 2006. Late Paleoproterozoic extension and a paleostress field reconstruction of the North China Craton. Tectonophysics 422, 89–98.

Hughes, H.S.R., McDonald, I., Goodenough, K.M., Ciborowski, T.J.R., Kerr, A.C., Davies, J.H.F.L., Selby, D., 2014. Enriched lithospheric mantle keel below the Scottish margin of the North Atlantic Craton: Evidence from the Palaeoproterozoic Scourie Dyke Swarm and mantle xenoliths. Precambrian Res. 250, 97–126. doi:10.1016/j.precamres.2014.05.026

Ibanez-Mejia, M., Gehrels, G.E., Ruiz, J., Vervoort, J.D., Eddy, M.E., Li, C., 2014. Small-volume baddeleyite (ZrO2) U-Pb geochronology and Lu-Hf isotope geochemistry by LA-ICP-MS. Techniques and applications. Chem. Geol. 384, 149–167. doi:10.1016/j.chemgeo.2014.07.011

Ingle, S., Coffin, M.F., 2004. Impact origin for the greater Ontong Java Plateau? Earth Planet. Sci. Lett. 218, 123–134. doi:10.1016/S0012-821X(03)00629-0

Ireland, T.R., Williams, I.S., 2003. Considerations in Zircon Geochronology by SIMS. Rev. Mineral. Geochemistry 53, 215–241. doi:10.2113/0530215

Irvine, T.N.J., Baragar, W., 1971. A guide to the chemical classification of the common volcanic rocks. Can. J. Earth Sci. 8, 523–548.

Irving, A.J., Frey, F.A., 1978. Distribution of trace elements between garnet megacrysts and host volcanic liquids of kimberlitic to rhyolitic composition. Geochim. Cosmochim. Acta 42, 771–787.

Isles, D.J., Cooke, A.C., 1990. Spatial associations between post-cratonisation dykes and gold deposits in the Yilgarn Block, Western Australia, in: Parker, A.J., Rickwood, P.C., Tucker, D.H. (Eds.), Mafic Dykes and Emplacement Mechanisms. Balkema, Rotterdam, pp. 147–162.

Isley, A.E., Abbott, D.H., 1999. Plume-related mafic volcanism and the deposition of banded iron formation. J. Geophys. Res. Solid Earth 104, 15461–15477.

Ivanov, A. V, Litasov, K.D., 2014. The deep water cycle and flood basalt volcanism. Int. Geol. Rev. 56, 1–14.

Jaffey, A.H., Flynn, K.F., Glendenin, L.E., Bentley, W.C. t, Essling, A.M., 1971. Precision measurement of half-lives and specific activities of U 235 and U 238. Phys. Rev. C 4, 1889.

Johannsen, A., 1931. A Descriptive Petrography Of The Igneous Rocks. Vol-I. The University of Chicago Press; Chicago.

Johnson, S.P., Sheppard, S., Rasmussen, B., Wingate, M.T.D., Kirkland, C.L., Muhling, J.R., Fletcher, I.R., Belousova, E.A., 2011. Two collisions, two sutures: Punctuated pre-1950Ma assembly of the West Australian Craton during the Ophthalmian and Glenburgh Orogenies. Precambrian Res. 189, 239–262. doi:10.1016/j.precamres.2011.07.011

Jones, A.P., Price, G.D., Price, N.J., DeCarli, P.S., Clegg, R.A., 2002. Impact induced melting and the development of large igneous provinces. Earth Planet. Sci. Lett. 202, 551–561. doi:10.1016/S0012-821X(02)00824-5

Jones, M.P., 1987. Applied mineralogy: a quantitative approach. Springer, London.

Jourdan, F., Bertrand, H., Schärer, U., Blichert-Toft, J., Féraud, G., Kampunzu, A.B., 2007. Major and trace element and Sr, Nd, Hf, and Pb isotope compositions of the Karoo large igneous province, Botswana - Zimbabwe: Lithosphere vs Mantle Plume Contribution. J. Petrol. 48, 1043–1077.

doi:10.1093/petrology/egm010

Jourdan, F., Féraud, G., Bertrand, H., Kampunzu, A.B., Tshoso, G., Watkeys, M.K., Le Gall, B., 2005. Karoo large igneous province: Brevity, origin, and relation to mass extinction questioned by new 40Ar/39Ar age data. Geology 33, 745–748.

Ju, W., Hou, G., Hari, K.R., 2013. Mechanics of mafic dyke swarms in the Deccan Large Igneous Province: Palaeostress field modelling. J. Geodyn. 66, 79–91. doi:10.1016/j.jog.2013.02.002

Kamber, B.S., Biino, G.G., 1995. The evolution of high T-low P granulites in the Northern Marginal Zone sensu stricto, Limpopo Belt, Zimbabwe-the case for petrography. Schweizerische Mineral. und Petrogr. Mitteilungen 75, 427–454.

Kamber, B.S., Greig, A., Schoenberg, R., Collerson, K.D., 2003. A refined solution to Earth's hidden niobium: implications for evolution of continental crust and mode of core formation. Precambrian Res. 126, 289–308.

Kelley, S., 2002. K-Ar and Ar-Ar dating. Rev. Mineral. Geochemistry 47, 785–818. doi:10.2138/rmg.2002.47.17

Kent, A.J.R., Cassidy, K.F., Fanning, M.C., 1996. Archean gold mineralisation synchronous with the final stages of cratonization, Yilgarn Craton, Western Australia. Geology 96, 879–882. doi:10.1130/0091-7613(1996)024<0879

King, S.D., Anderson, D.L., 1995. An alternative mechanism of flood basalt formation. Earth Planet. Sci. Lett. 136, 269–279.

Kirkland, C.L., Smithies, R.H., Woodhouse, A.J., Howard, H.M., Wingate, M.T.D., Belousova, E.A., Cliff, J.B., Murphy, R.C., Spaggiari, C. V, 2013. Constraints and deception in the isotopic record; the crustal evolution of the west Musgrave Province, central Australia. Gondwana Res. 23, 759–781.

Kirkland, C.L., Spaggiari, C. V, Pawley, M.J., Wingate, M.T.D., Smithies, R.H., Howard, H.M., Tyler, I.M., Belousova, E.A., Poujol, M., 2011. On the edge: U–Pb, Lu–Hf, and Sm–Nd data suggests reworking of the Yilgarn craton margin during formation of the Albany-Fraser Orogen. Precambrian Res. 187, 223–247.

Klein, E.L., Almeida, M.E., Rosa-Costa, L.T., 2012. The 1.89-1.87 Ga Uatumã Silicic Large Igneous Province, northern South America. November LIP of the Month [WWW Document]. URL http://www.largeigneousprovinces.org/12nov

Klein, R., Pesonen, L.J., Mänttäri, I., Heinonen, J.S., 2016. A late Paleoproterozoic key pole for the Fennoscandian Shield: A paleomagnetic study of the Keuruu diabase dykes, Central Finland. Precambrian Res. 286, 379–397. doi:10.1016/j.precamres.2016.10.013

Korsch, R.J., Kositcin, N., Champion, D.C., 2011. Australian island arcs through time: Geodynamic implications for the Archean and Proterozoic. Gondwana Res. 19, 716–734. doi:10.1016/j.gr.2010.11.018

Kramers, J.D., McCourt, S., Roering, C., Smit, C.A., Van Reenen, D.D., 2011. Tectonic models proposed for the Limpopo Complex: Mutual compatibilities and constraints. Geol. Soc. Am. Mem. 207, 311–324.

Krogh, T.E., 1982. Improved accuracy of U-Pb zircon ages by the creation of more concordant systems using an air abrasion technique. Geochim. Cosmochim. Acta 46, 637–649.

Krogh, T.E., 1973. A low-contamination method for hydrothermal decomposition of zircon and extraction of U and Pb for isotopic age determinations. Geochim. Cosmochim. Acta 37, 485–494.

Krogh, T.E., Corfu, F., Davus, D.W., Dunning, G.R., Heaman, L.M., Kamo, S.L., Machado, N., 1987. Precise U–Pb Isotopic ages of diabase dykes and mafic to ultramafic rocks using trace amounts of baddeleyite and zircon, in: Halls, H.C., Fahrig, W.F. (Eds.), Mafic Dyke Swarms. Geological Association of Canada Special Paper 34. pp. 147–152.

Kröner, A., 2010. The role of geochronology in understanding continental evolution. Geol. Soc. London, Spec. Publ. 338, 179–196. doi:10.1144/SP338.9

Kröner, A., Jaeckel, P., Brandl, G., Nemchin, A.A., Pidgeon, R.T., 1999. Single zircon ages for granitoid gneisses in the Central Zone of the Limpopo Belt, Southern Africa and geodynamic significance. Precambrian Res. 93, 299–337. doi:10.1016/S0301-9268(98)00102-8

Ksienzyk, A.K., Jacobs, J., Boger, S.D., Kosler, J., Sircombe, K.N., Whitehouse, M.J., 2012. U-Pb ages of metamorphic monazite and detrital zircon from the Northampton Complex: Evidence of two orogenic cycles in Western Australia. Precambrian Res. 198–199, 37–50. doi:10.1016/j.precamres.2011.12.011

Kumar, K.V., Ernst, W.G., Leelanandam, C., Wooden, J.L., Grove, M.J., 2010. First Paleoproterozoic ophiolite from Gondwana: Geochronologic-geochemical documentation of ancient oceanic crust from Kandra, SE India. Tectonophysics 487, 22–32. doi:10.1016/j.tecto.2010.03.005

Kumar, K.V., Leelanandam, C., 2008. Evolution of the Eastern Ghats belt, India: a plate tectonic perspective. Geol. Soc. India 72, 720–749.

Lanyon, R., Black, L.P., Seitz, H.-M., 1993. U-Pb zircon dating of mafic dykes and its application to the Proterozoic geological history of the Vestfold Hills, East Antarctica. Contrib. to Mineral. Petrol. 115, 184–203.

Le Maitre, R.W., Streckeisen, A., Zanettin, B., Le Bas, M.J., Bonin, B., Bateman, P., Bellieni, G., Dudek, A., Efremova, S., Keller, J., Lameyre, J., Sabine, P.A., Schmid, R., Sørensen, H., Woolley, A.R., 2002. Igneous rocks: a classification and glossary of terms: recommendations of the International Union of Geological Sciences Subcommission on the Systematics of Igneous Rocks, 2nd ed. Cambridge University Press, New York.

Le Maitre, R.W.B., Dudek, P., Keller, A., Lameyre, J., Le Bas, J., Sabine, M.J., Schmid, P.A., Sorensen, R., Streckeisen, H., Woolley, A., 1989. A classification of igneous rocks and glossary of terms: Recommendations of the International Union of Geological Sciences, Subcommission on the Systematics of Igneous Rocks. International Union of Geological Sciences, Blackwell Scientific.

LeCheminant, A.N., Heaman, L.M., 1989. Mackenzie igneous events, Canada: Middle Proterozoic hotspot magmatism associated with ocean opening. Earth Planet. Sci. Lett. 96, 38–48.

Lewis, J.D., 1994. Mafic dykes in the Williams–Wandering area, Western Australia. Geol. Surv. West. Aust. Rep. 37, 37–52.

Li, J., Wang, X.-C., Ren, Z.-Y., Xu, J.-F., He, B., Xu, Y.-G., 2014. Chemical heterogeneity of the Emeishan mantle plume: Evidence from highly siderophile element abundances in picrites. J. Asian Earth Sci. 79, 191–205. doi:10.1016/j.jseaes.2013.09.009

Li, T., Zhai, M., Peng, P., Chen, L., Guo, J., 2010. Ca. 2.5 billion year old coeval ultramafic-mafic and syenitic dykes in Eastern Hebei: Implications for cratonization of the North China Craton. Precambrian Res. 180, 143–155. doi:10.1016/j.precamres.2010.04.001

Li, X.-H., 1997. Geochemistry of the Longsheng Ophiolite from the southern margin of Yangtze Craton, SE China. Geochem. J. 31, 323–337. doi:10.2343/geochemj.31.323

Li, Z.-X., Evans, D.A.D., 2011. Late Neoproterozoic 40 intraplate rotation within

Australia allows for a tighter-fitting and longer-lasting Rodinia. Geology 39, 39–42.

Li, Z.-X., Zhong, S., 2009. Supercontinent–superplume coupling, true polar wander and plume mobility: Plate dominance in whole-mantle tectonics. Phys. Earth Planet. Inter. 176, 143–156. doi:10.1016/j.pepi.2009.05.004

Li, Z.X., Bogdanova, S. V, Collins, A.S., Davidson, A., De Waele, B., Ernst, R.E., Fitzsimons, I.C.W., Fuck, R.A., Gladkochub, D.P., Jacobs, J., Karlstrom, K.E., Lu, S., Natapov, L.M., Pease, V., Pisarevsky, S.A., Thrane, K., Vernikovsky, V., 2008. Assembly, configuration, and break-up history of Rodinia: A synthesis. Precambrian Res. 160, 179–210. doi:10.1016/j.precamres.2007.04.021

Li, Z.X., Evans, D.A.D., Zhang, S., 2004. A 90° spin on Rodinia: possible causal links between the Neoproterozoic supercontinent, superplume, true polar wander and low-latitude glaciation. Earth Planet. Sci. Lett. 220, 409–421. doi:10.1016/s0012-821x(04)00064-0

Li, Z.X., Li, X.H., Kinny, P.D., Wang, J., Zhang, S., Zhou, H., 2003. Geochronology of Neoproterozoic syn-rift magmatism in the Yangtze Craton, South China and correlations with other continents: evidence for a mantle superplume that broke up Rodinia. Precambrian Res. 122, 85–109. doi:10.1016/S0301-9268(02)00208-5

Li, Z.X., Zhang, L., Powell, C.M., 1996. Positions of the East Asian cratons in the Neoproterozoic supercontinent Rodinia. Aust. J. Earth Sci. 43, 593–604.

Liu, Y., Li, X.-H., Li, Q.-L., Tang, G.-Q., Yin, Q.-Z., 2011. Precise U–Pb zircon dating at a scale of <5 micron by the CAMECA 1280 SIMS using a Gaussian illumination probe. J. Anal. At. Spectrom. 26, 845. doi:10.1039/c0ja00113a

Liu, Y., Li, Z.-X., Pisarevsky, S.A., Kirscher, U., Mitchell, R.N., Stark, J.C., 2018. Palaeomagnetism of the 1.89 Ga Boonadgin dykes of the Yilgarn Craton: Possible connection with India. Precambrian Res. Press.

Liu, Y., Li, Z.-X., Pisarevsky, S.A., Stark, J.C., 2016. Paleomagnetic investigation of mafic dykes in the southwestern Yilgarn Craton, Western Australia, in: Australian Earth Sciences Convention 2016 Abstracts. Geological Society of Australia, p. 277.

Liu, Y., Liu, H., Li, X., 1996. Simultaneous and precise determination of 40 trace elements in rock samples using ICP-MS. Geochemia (in Chinese) 25(6), 552.

Ludwig, K., 2012. User's manual for Isoplot version 3.75–4.15: a geochronological toolkit for Microsoft. Berkeley Geochronological Cent. Spec. Publ.

Ludwig, K., 2009. Squid 2.50, A User's Manual (No. 2.50.11.02.03 Rev. 03 Feb 2011). Berkeley, California, USA.

Maas, R., Grew, E.S., Carson, C.J., 2015. Isotopic constraints (Pb, Rb-Sr, Sm-Nd) on the sources of early Cambrian pegmatites with Boron and Beryllium minerals in the Larsemann Hills, Prydz Bay, Antarctica. Can. Mineral. 53, 249–272.

Maas, R., Kamenetsky, M.B., Sobolev, A. V, Kamenetsky, V.S., Sobolev, N. V, 2005. Sr, Nd, and Pb isotope evidence for a mantle origin of alkali chlorides and carbonates in the Udachnaya kimberlite, Siberia. Geology 33, 549–552.

Mäkitie, H., Data, G., Isabirye, E., Mänttäri, I., Huhma, H., Klausen, M.B., Pakkanen, L., Virransalo, P., 2014. Petrology, geochronology and emplacement model of the giant 1.37 Ga arcuate Lake Victoria Dyke Swarm on the margin of a large igneous province in eastern Africa. J. African Earth Sci. 97, 273–296.

Mallikharjuna, R.J., Bhattacharji, S., Rao, M.N., Hermes, O.D., 1995. 40Ar–39Ar ages and geochemical characteristics of dolerite dykes around the Proterozoic Cuddapah Basin, South India, in: Geological Society of India Memoir 33. pp. 307–328.

Mattinson, J.M., 2005. Zircon U–Pb chemical abrasion ("CA-TIMS") method: combined annealing and multi-step partial dissolution analysis for improved precision and accuracy of zircon ages. Chem. Geol. 220, 47–66.

McCall, G.J.H., Peers, R., 1971. Geology of the Binneringie Dyke, Western Australia. Geol. Rundschau 60, 1174–1263. doi:10.1007/BF02046541

McClenaghan, M.B., 2011. Overview of common processing methods for recovery of indicator minerals from sediment and bedrock in mineral exploration. Geochemistry Explor. Environ. Anal. 11, 265–278. doi:10.1144/1467-7873/10-IM-025

McFarlane, C.R.M., 2010. Geodynamic constraints on mineralization and metamorphism at the Griffin's Find gold deposit, Western Australia, from calibrated Tt trajectories, in: GeoCanada 2010, Calgary May 10-14. Canadian Society of Petroleum Geoscientists, Calgary.

McNaughton, N.J., Groves, D.I., 1996. A review of Pb-isotope constraints on the genesis of lode-gold deposits in the Yilgarn Craton, Western Australia. J. R. Soc. West. Aust. 79, 123–129.

Meert, J.G., 2014. Strange attractors, spiritual interlopers and lonely wanderers: The search for pre-Pangean supercontinents. Geosci. Front. 5, 155–166.

Meert, J.G., 2012. What's in a name? The Columbia (Paleopangaea/Nuna) supercontinent. Gondwana Res. 21, 987–993.

Meert, J.G., 2002. Paleomagnetic evidence for a Paleo-Mesoproterozoic supercontinent Columbia. Gondwana Res. 5, 207–215.

Meert, J.G., Pandit, M.K., Pradhan, V.R., Banks, J., Sirianni, R., Stroud, M., Newstead, B., Gifford, J., 2010. Precambrian crustal evolution of Peninsular India: A 3.0 billion year odyssey. J. Asian Earth Sci. 39, 483–515. doi:10.1016/j.jseaes.2010.04.026

Meert, J.G., Santosh, M., 2017. The Columbia supercontinent revisited. Gondwana Res. 50, 67–83. doi:10.1016/j.gr.2017.04.011

Merle, R., Marzoli, A., Reisberg, L., Bertrand, H., Nemchin, A., Chiaradia, M., Callegaro, S., Jourdan, F., Bellieni, G., Kontak, D., Puffer, J., Gregory McHone, J., 2014. Sr, Nd, Pb and Os isotope systematics of CAMP tholeiites from Eastern North America (ENA): Evidence of a subduction-enriched mantle source. J. Petrol. 55, 133–180. doi:10.1093/petrology/egt063

Merrihue, C., Turner, G., 1966. Potassium-argon dating by activation with fast neutrons. J. Geophys. Res. 71, 2852–2857.

Middleton, M.F., Wilde, S.A., Evans, B.A., Long, A., Dentith, M., 1993. A preliminary interpretation of deep seismic reflection and other geophysical data from the Darling Fault Zone, Western Australia. Explor. Geophys. 24, 711–718.

Mikhalsky, E. V, Sheraton, J.W., Hahne, K., Prince, N., Mountains, C., Coast, M., 2006. Charnockite composition in relation to the tectonic evolution of East Antarctica. Gondwana Res. 9, 379–397. doi:10.1016/j.gr.2005.11.007

Millonig, L., Zeh, A., Gerdes, A., Klemd, R., 2008. Neoarchaean high-grade metamorphism in the Central Zone of the Limpopo Belt (South Africa): Combined petrological and geochronological evidence from the Bulai pluton. Lithos 103, 333–351. doi:10.1016/j.lithos.2007.10.001

Minifie, M., Kerr, A.C., Ernst, R.E., Pearce, J.A., 2008. The origin, nature and consequences of the Circum-Superior 1880 Ma Large Igneous Province.

Geochim. Cosmochim. Acta Suppl. 72, A633.

Mishra, D.C., 2015. Plume and Plate Tectonics Model for Formation of some Proterozoic Basins of India along Contemporary Mobile Belts: Mahakoshal – Bijawar, Vindhyan and Cuddapah Basins. J. Geol. Soc. India 85, 525–536.

Mohanty, S., 2015. Precambrian continent assembly and dispersal events of South Indian and East Antarctic Shields. Int. Geol. Rev. 57, 1992–2027. doi:10.1080/00206814.2015.1048751

Mohanty, S., 2012. Spatio-temporal evolution of the Satpura Mountain Belt of India: A comparison with the Capricorn Orogen of Western Australia and implication for evolution of the supercontinent Columbia. Geosci. Front. 3, 241–267. doi:10.1016/j.gsf.2011.10.005

Mole, D.R., Fiorentini, M.L., Cassidy, K.F., Kirkland, C.L., Thebaud, N., McCuaig, T.C., Doublier, M.P., Duuring, P., Romano, S.S., Maas, R., Belousova, E.A., Barnes, S.J., Miller, J., 2015. Crustal evolution, intra-cratonic architecture and the metallogeny of an Archaean craton. Geol. Soc. London, Spec. Publ. 393, 23–80. doi:10.1144/SP393.8

Mole, D.R., Fiorentini, M.L., Thebaud, N., McCuaig, T.C., Cassidy, K.F., Kirkland, C.L., Wingate, M.T.D., Romano, S.S., Doublier, M.P., Belousova, E.A., 2012. Spatio-temporal constraints on lithospheric development in the southwest–central Yilgarn Craton, Western Australia. Aust. J. Earth Sci. 59, 625–656. doi:10.1080/08120099.2012.691213

Moller, A., O’Brien, P.J., Kennedy, A., Kroner, A., 2003. Linking growth episodes of zircon and metamorphic textures to zircon chemistry: an example from the ultrahigh-temperature granulites of Rogaland (SW Norway). Geol. Soc. London, Spec. Publ. 220, 65–81. doi:10.1144/GSL.SP.2003.220.01.04

Morgan, W.J., 1971. Convection Plumes in the Lower Mantle. Nature 230, 42–43. doi:10.1038/230042a0

Morris, P.A., 2007. Composition of the Bunbury Basalt (BB1) and Kerba Monzogranite (KG1) geochemical reference materials, and assessing the contamination effects of mill heads, in: Geological Survey of Western Australia Record 2007/14. Geological Survey of Western Australia Record 2007/14.

Morris, P.A., Pirajno, F., 2005. Mesoproterozoic sill complexes in the Bangemall Supergroup, Western Australia: geology, geochemistry and mineralization potential. Geological Survey of Western Australia Report 99.

Morrissey, L.J., Payne, J.L., Hand, M., Clark, C., Taylor, R., Kirkland, C.L., Kylander-Clark, A., 2017. Linking the Windmill Islands, east Antarctica and the Albany–Fraser Orogen: Insights from U–Pb zircon geochronology and Hf isotopes. Precambrian Res. 293, 131–149. doi:10.1016/j.precamres.2017.03.005

Münker, C., Wörner, G., Yogodzinski, G., Churikova, T., 2004. Behaviour of high field strength elements in subduction zones: constraints from Kamchatka–Aleutian arc lavas. Earth Planet. Sci. Lett. 224, 275–293. doi:10.1016/j.epsl.2004.05.030

Murphy, J.B., Dostal, J., 2007. Continental mafic magmatism of different ages in the same terrane: Constraints on the evolution of an enriched mantle source. Geology 35, 335–338. doi:10.1130/G23072A.1

Murphy, J.B., Nance, R.D., 2013. Speculations on the mechanisms for the formation and breakup of supercontinents. Geosci. Front. 4, 185–194. doi:10.1016/j.gsf.2012.07.005

Murthy, N.G.K., 1987. Mafic dyke swarms of the Indian shield, in: Fahrig, W.F., Halls, H.C. (Eds.), Mafic Dyke Swarms. Geological Association of Canada Special Paper 34, pp. 393–400.

Mushayandebvu, M.F., Jones, D.L., Briden, J.C., Baer, G., Heimann, A., 1995. Palaeomagnetic and geochronological results from Proterozoic mafic intrusions in southern Zimbabwe, in: Physics and Chemistry of Dykes. Balkema Rotterdam, pp. 293–303.

Myers, J.S., 1995. The generation and assembly of an Archaean supercontinent: evidence from the Yilgarn craton, Western Australia. Geol. Soc. London, Spec. Publ. 95, 143–154.

Myers, J.S., 1993. Precambrian Tectonic History of the West Australian Craton and Adjacent Orogens. Annu. Rev. Earth Planet. Sci. 21, 453–485.

Myers, J.S., 1990a. Pinjarra Orogen, in: Geology and Mineral Resources of Western Australia. Geological Survey of Western Australia Memoir 3, pp. 264–274.

Myers, J.S., 1990b. Albany–Fraser Orogen, in: Geology and Mineral Resources of Western Australia. Geological Survey of Western Australia Memoir 3, pp. 255–263.

Nance, R.D., Murphy, J.B., 2013. Origins of the supercontinent cycle. Geosci. Front.

4, 439–448. doi:10.1016/j.gsf.2012.12.007

Nance, R.D., Murphy, J.B., Santosh, M., 2014. The supercontinent cycle: A retrospective essay. Gondwana Res. 25, 4–29. doi:10.1016/j.gr.2012.12.026

Nance, R.D., Worsley, T.R., Moody, J.B., 1986. Post -Archean biogeochemical cycles and long-term episodicity in tectonic processes. Geology 14, 514–518. doi:10.1130/0091-7613(1986)14<514

Nelson, D.R., 1998. Granite-greenstone crust formation on the Archaean Earth: a consequence of two superimposed processes. Earth Planet. Sci. Lett. 158, 109–119. doi:10.1016/S0012-821X(98)00049-1

Nelson, D.R., 1997. Evolution of the Archaean granite-greenstone terranes of the Eastern Goldfields, Western Australia: SHRIMP U-Pb zircon constraints. Precambrian Res. 83, 57–81. doi:10.1016/S0301-9268(97)00005-3

Nelson, D.R., Myers, J.S., Nutman, A.P., 1995a. Chronology and evolution of the Middle Proterozoic Albany-Fraser Orogen, Western Australia. Aust. J. Earth Sci. 42, 481–495. doi:10.1080/08120099508728218

Nelson, D.R., Myers, J.S., Nutman, A.P., 1995b. Chronology and evolution of the Middle Proterozoic Albany-Fraser Orogen, Western Australia. Aust. J. Earth Sci. 42, 481–495.

Nelson, K.D., 1992. Are crustal thickness variations in old mountain belts like the Appalachians a consequence of lithospheric delamination? Geology 20, 498–502.

Nemchin, A.A., Pidgeon, R.T., 1998. Precise conventional and SHRIMP baddeleyite U-Pb age for the Binneringie Dyke, near Narrogin, Western Australia. Aust. J. Earth Sci. 45, 673–675.

Nemchin, A.A., Pidgeon, R.T., 1997. Evolution of the Darling Range batholith, Yilgarn Craton, Western Australia: a SHRIMP zircon study. J. Petrol. 38, 625–649.

Nemchin, A.A., Pidgeon, R.T., Wilde, S.A., 1994. Timing of Late Archaean granulite facies metamorphism in the southwestern Yilgarn Craton of Western Australia: evidence from U-Pb ages of zircons from mafic granulites. Precambrian Res. 68, 307–321.

Nieuwland, D.A., Compston, W., 1981. Crustal evolution in the Yilgarn block near Perth, Western Australia, in: Archean Geology, Second International

Symposium (Perth 1980): Geological Society of Australia, Special Publication. pp. 159–171.

Niu, Y., Gilmore, T., Mackie, S., Greig, A., Bach, W., 2002. Mineral chemistry, whole-rock compositions, and petrogenesis of Leg 176 gabbros: data and discussion. Proc. Ocean Drill. Program, Sci. Results 176, 1–60.

Nordsvan, A.R., Collins, W.C., Li, Z.-X., Spencer, C.J., Pourteau, A., Withnall, I.W., Betts, P.G., Volante, S., 2018. Laurentian crust in northeast Australia: Implications for the assembly of the supercontinent Nuna. Geology.

Nutman, A.P., Bennett, V.C., Kinny, P.D., Price, R., 1993. Large-scale crustal structure of the Northwestern Yilgarn Craton, western Australia: Evidence from Nd isotopic data and zircon geochronology. Tectonics 12, 971–981. doi:10.1029/93TC00377

Oberthür, T., Davis, D.W., Blenkinsop, T.G., Höhndorf, A., 2002. Precise U–Pb mineral ages, Rb–Sr and Sm–Nd systematics for the Great Dyke, Zimbabwe—constraints on late Archean events in the Zimbabwe craton and Limpopo belt. Precambrian Res. 113, 293–305.

Okrugin, A. V, Oleinikov, B. V, Savvinov, V.T., Tomshin, M.D., 1990. Late Precambrian dyke swarms of the Anabar massif, Siberian platform, USSR, in: Parker, A.J., Rickwood, P.C., Tucker, D.H. (Eds.), Mafic Dykes and Emplacement Mechanisms. Balkema, Rotterdam, pp. 529–533.

Oliveira, E.P., Silveira, E.M., Söderlund, U., Ernst, R.E., 2013. U-Pb ages and geochemistry of mafic dyke swarms from the Uauá Block, São Francisco Craton, Brazil: LIPs remnants relevant for Late Archaean break-up of a supercraton. Lithos 174, 308–322. doi:10.1016/j.lithos.2012.05.025

Olsson, J.R., Klausen, M.B., Hamilton, M.A., März, N., Söderlund, U., Roberts, R.J., 2016. Baddeleyite U–Pb ages and gechemistry of the 1875–1835 Ma Black Hills Dyke Swarm across north-eastern South Africa: part of a trans-Kalahari Craton back-arc setting? GFF 138, 183–202.

Parrish, R.R., Parrish, R.R., Noble, S.R., 2003. Zircon U-Th-Pb geochronology by isotope dilution—thermal ionization mass spectrometry (ID-TIMS). Rev. Mineral. Geochemistry 53, 183–213.

Pastor-Galán, D., Nance, R.D., Murphy, J.B., Spencer, C.J., 2018. Supercontinents: myths, mysteries, and milestones. Geol. Soc. London, Spec. Publ. 470, SP470-

16.

Paul, E., Stuwe, K., Teasdale, J., Worley, B., 1995. Structural and Metamorphic Geology of the Windmill-Islands, East Antarctica - Field Evidence for Repeated Tectonothermal Activity. Aust. J. Earth Sci. 42, 453–469. doi:10.1080/08120099508728216

Pearce, J.A., 2008. Geochemical fingerprinting of oceanic basalts with applications to ophiolite classification and the search for Archean oceanic crust. Lithos 100, 14–48. doi:10.1016/j.lithos.2007.06.016

Pearson, D.G., Brenker, F.E., Nestola, F., McNeill, J., Nasdala, L., Hutchison, M.T., Matveev, S., Mather, K., Silversmit, G., Schmitz, S., 2014. Hydrous mantle transition zone indicated by ringwoodite included within diamond. Nature 507, 221.

Pesonen, L.J., Elming, S.-Å., Mertanen, S., Pisarevsky, S., D'Agrella-Filho, M.S., Meert, J.G., Schmidt, P.W., Abrahamsen, N., Bylund, G., 2003. Palaeomagnetic configuration of continents during the Proterozoic. Tectonophysics 375, 289–324.

Pfänder, J. a., Münker, C., Stracke, A., Mezger, K., 2007. Nb/Ta and Zr/Hf in ocean island basalts — Implications for crust–mantle differentiation and the fate of Niobium. Earth Planet. Sci. Lett. 254, 158–172. doi:10.1016/j.epsl.2006.11.027

Pidgeon, R.T., Cook, T.J.F., 2003. 1214±5 Ma dyke from the Darling Range, southwestern Yilgarn Craton, Western Australia. Aust. J. Earth Sci. 50, 769–773.

Pidgeon, R.T., Nemchin, A.A., 2001. 1.2 Ga Mafic dyke near York, southwestern Yilgarn Craton, Western Australia. Aust. J. Earth Sci. 48, 751–755. doi:10.1046/j.1440-0952.2001.485895.x

Pidgeon, R.T., Wilde, S.A., 1990. The distribution of 3.0 Ga and 2.7 Ga volcanic episodes in the Yilgarn Craton of Western Australia. Precambrian Res. 48, 309–325.

Piispa, E.J., Smirnov, A. V, Pesonen, L.J., Lingadevaru, M., Anantha Murthy, K.S., Devaraju, T.C., 2011. An Integrated Study of Proterozoic Dykes, Dharwar Craton, Southern India 33–45. doi:10.1007/978-3-642-12496-9_3

Pirajno, F., Hoatson, D.M., 2012. A review of Australia's Large Igneous Provinces and associated mineral systems: implications for mantle dynamics through geological time. Ore Geol. Rev. 48, 2–54.

Pisarevsky, S.A., Elming, S.-Å., Pesonen, L.J., Li, Z.-X., 2014a. Mesoproterozoic paleogeography: Supercontinent and beyond. Precambrian Res. 244, 207–225. doi:10.1016/j.precamres.2013.05.014

Pisarevsky, S.A., Wingate, M.T.D., Li, Z.-X., Wang, X.-C., Tohver, E., Kirkland, C.L., 2014b. Age and paleomagnetism of the 1210Ma Gnowangerup–Fraser dyke swarm, Western Australia, and implications for late Mesoproterozoic paleogeography. Precambrian Res. 246, 1–15. doi:10.1016/j.precamres.2014.02.011

Pisarevsky, S., De Waele, B., Jones, S., Söderlund, U., Ernst, R.E., 2015. Paleomagnetism and U–Pb age of the 2.4 Ga Erayinia mafic dykes in the south-western Yilgarn, Western Australia: Paleogeographic and geodynamic implications. Precambrian Res. 259, 222–231. doi:10.1016/j.precamres.2014.05.023

Polat, a., Hofmann, a. W., Rosing, M.T., 2002. Boninite-like volcanic rocks in the 3.7-3.8 Ga isua greenstone belt, West Greenland: Geochemical evidence for intra-oceanic subduction zone processes in the early earth. Chem. Geol. 184, 231–254. doi:10.1016/S0009-2541(01)00363-1

Pollard, D.D., 1987. Elementary fracture mechanics applied to the structural interpretation of dykes, in: Mafic Dyke Swarms. Geological Association of Canada, pp. 5–24.

Post, N.J., 2000. Unravelling Gondwana fragments: an integrated structural, isotopic and petrographic investigation of the Windmill Islands, Antarctica. University of New South Wales PhD Thesis.

Post, N.J., Hensen, B.J., Kinny, P.D., 1997. Two metamorphic episodes during a 1340–1180 Ma convergent tectonic event in the Windmill Islands, East Antarctica. Antarct. Reg. Geol. Evol. Process. Terra Antarct. Sienna 157–161.

Prokoph, A., Ernst, R.E., Buchan, K.L., 2004. Time-Series Analysis of Large Igneous Provinces: 3500 Ma to Present. J. Geol. 112, 1–22. doi:10.1086/379689

Puffer, J.H., 2003. A Reactivated Back-Arc Source for CAMP Magma. Cent. Atl. Magmat. Prov. Insights from Fragm. Pangea 151–162.

Puffer, J.H., 2001. Contrasting high field strength element contents of continental flood basalts from plume versus reactivated-arc sources. Geology 29, 675–678.

Qiu, Y., Groves, D.I., 1999. Late Archean collision and delamination in the Southwest Yilgarn Craton; the driving force for Archean orogenic lode gold mineralization? Econ. Geol. 94, 115–122.

Qiu, Y., Groves, D.I., McNaughton, N.J., 1997a. Deep-seated granitoids: implications for Late Archaean subduction-collision-lithospheric delamination and gold mineralization in the Yilgarn Craton. Aust. Geol. Surv. Organ. Rec. 41, 65–69.

Qiu, Y., McNaughton, N.J., Groves, D., Dalstra, H.J., 1997b. Shrimp U-Pb in zircon and lead-isotope constraints on the timing and source of an Archaean granulite-hosted lode-gold deposit at Griffin's Find, Yilgarn craton, Western Australia. Chron. la Rech. Min. 91–104.

Qiu, Y., McNaughton, N.J., Groves, D.I., Dunphy, J.M., 1999. First record of 1.2 Ga quartz dioritic magmatism in the Archaean Yilgarn Craton, Western Australia, and its significance. Aust. J. Earth Sci. 46, 421–428. doi:10.1046/j.1440-0952.1999.00715.x

Rasmussen, B., Fletcher, I.R., 2010. Dating sedimentary rocks using in situ U-Pb geochronology of syneruptive zircon in ash-fall tuff less than 1 mm thick. Geology 38, 299–302. doi:10.1130/G30567.1

Rasmussen, B., Fletcher, I.R., 2004. Zirconolite: A new U-Pb chronometer for mafic igneous rocks. Geology 32, 785–788.

Rasmussen, B., Fletcher, I.R., 2002. Indirect dating of mafic intrusions by SHRIMP U-Pb analysis of monazite in contact metamorphosed shale: An example from the Palaeoproterozoic Capricorn Orogen, Western Australia. Earth Planet. Sci. Lett. 197, 287–299. doi:10.1016/S0012-821X(02)00501-0

Rasmussen, B., Fletcher, I.R., Bekker, A., Muhling, J.R., Gregory, C.J., Thorne, A.M., 2012. Deposition of 1.88-billion-year-old iron formations as a consequence of rapid crustal growth. Nature 484, 498–501.

Rasmussen, B., Fletcher, I.R., Bengtson, S., McNaughton, N.J., 2004. SHRIMP U-Pb dating of diagenetic xenotime in the Stirling Range Formation, Western Australia: 1.8 Billion year minimum age for the Stirling biota. Precambrian Res. 133, 329–337. doi:10.1016/j.precamres.2004.05.008

Rasmussen, B., Fletcher, I.R., Muhling, J.R., 2008. Pb/Pb geochronology, petrography and chemistry of Zr-rich accessory minerals (zirconolite, tranquillityite and baddeleyite) in mare basalt 10047. Geochim. Cosmochim. Acta 72, 5799–5818. doi:10.1016/j.gca.2008.09.010

Ravich, M.G., Klimov, L. V, Solov′ev, D.S., 1968. The Pre-Cambrian of East Antarctica. Israel Program for Scientific Translations [available from the US Department of Commerce, Clearinghouse for Federal Scientific and Technical Information, Springfield, Va.].

Richards, M.A., Duncan, R.A., Courtillot, V.E., 1989. Flood basalts and hot-spot tracks: plume heads and tails. Science (80-.). 246, 103–107.

Rioux, M., Bowring, S., Dudás, F., Hanson, R., 2010. Characterizing the U-Pb systematics of baddeleyite through chemical abrasion: Application of multi-step digestion methods to baddeleyite geochronology. Contrib. to Mineral. Petrol. 160, 777–801. doi:10.1007/s00410-010-0507-1

Rivers, T., Corrigan, D., 2000. Convergent margin on southeastern Laurentia during the Mesoproterozoic: tectonic implications. Can. J. Earth Sci. 37, 359–383.

Rogers, J.J.W., 1996. A History of Continents in the past Three Billion Years. J. Geol. 104, 91–107.

Rogers, J.J.W., Santosh, M., 2004. Continents and supercontinents. Oxford University Press.

Rogers, J.J.W., Santosh, M., 2003. Supercontinents in earth history. Gondwana Res. 6, 357–368. doi:10.1016/S1342-937X(05)70993-X

Rogers, J.J.W., Santosh, M., 2002. Configuration of Columbia, a Mesoproterozoic Supercontinent. Gondwana Res. 5, 5–22. doi:10.1016/s1342-937x(05)70883-2

Rollinson, H.R., 1993. Using geochemical data: evaluation, presentation, interpretation. Longman Scientific & Technical; Copublished in the US with J. Wiley & Sons.

Ronkin, Y.L., Maslov, A. V, Matukov, D.I., Lepikhina, O.P., Popova, O.Y., 2005. The Mashak riftogenic event of the Riphean type region (southern Urals): new isotopic-geochronological framework. Struct. Geodyn. Mineral. Process. Lithosphere. Geoprint, Syktyvkar 305–307.

Roth, E., Bennett, J.M., Symons, P.M., 1990. Boddington and Black Flag: anomalous Archaean gold deposits. Geol. Dep. Univ. Extension, Univ. West. Aust. Publ. 20, 189–194.

Roth, E., Groves, D., Anderson, G., Daley, L., Staley, R., 1991. Primary mineralization at the Boddington gold mine, Western Australia: An Archean porphyry Cu-Au-Mo deposit, in: Brazil Gold. pp. 481–488.

Rudnick, R.L., Fountain, D.M., 1995. Nature and composition of the continental crust: A lower crustal perspective. Rev. Geophys. 33, 267. doi:10.1029/95RG01302

Rudnick, R.L., Gao, S., 2003. Composition of the continental crust, in: Holland, H.D., Turekian, K.K. (Eds.), The Crust Vol. 3. Treatise on Geochemistry. pp. 1–64.

Salters, V.J.M., Stracke, A., 2004. Composition of the depleted mantle. Geochemistry, Geophys. Geosystems 5, Q05B07. doi:10.1029/2003GC000597

Santosh, M., 2010. Supercontinent tectonics and biogeochemical cycle: A matter of "life and death." Geosci. Front. 1, 21–30. doi:10.1016/j.gsf.2010.07.001

Saunders, A.D.A.D., Storey, M., Kent, R.W.W., Norry, M.J., Norrry, M.J., 1992. Consequences of plume-lithosphere interactions. Geol. Soc. Spec. Publ. London 68, 41–60.

Schaltegger, U., Davies, J.H.F.L., 2017. Petrochronology of Zircon and Baddeleyite in Igneous Rocks: Reconstructing Magmatic Processes at High Temporal Resolution. Rev. Mineral. Geochemistry 83, 297 LP-328.

Schmitt, A.K., Chamberlain, K.R., Swapp, S.M., Harrison, T.M., 2010. In situ U-Pb dating of micro-baddeleyite by secondary ion mass spectrometry. Chem. Geol. 269, 386–395. doi:10.1016/j.chemgeo.2009.10.013

Schoene, B., 2013. U-Th-Pb Geochronology, Treatise on Geochemistry: Second Edition. doi:10.1016/B978-0-08-095975-7.00310-7

Schoene, B., Baxter, E.F., 2017. Petrochronology and TIMS. Rev. Mineral. Geochemistry 83, 231 LP-260. doi:10.2138/rmg.2017.83.8

Schott, B., Schmeling, H., 1998. Delamination and detachment of a lithospheric root. Tectonophysics 296, 225–247.

Scibiorski, E., Tohver, E., Jourdan, F., 2015. Rapid cooling and exhumation in the western part of the Mesoproterozoic Albany-Fraser Orogen, Western Australia. Precambrian Res. 265, 232–248. doi:10.1016/j.precamres.2015.02.005

Shellnutt, J.G., Hari, K.R., Liao, A.C.-Y., Denyszyn, S.W., Vishwakarma, N., 2018. A 1.88 Ga giant radiating mafic dyke swarm across Southern India and Western Australia. Precambrian Res. 308, 58–74.

Sheppard, S., Bodorkos, S., Johnson, S.P., Wingate, M.T.D., Kirkland, C.L., 2010a. The Paleoproterozoic Capricorn Orogeny: intracontinental reworking not continent–continent collision, Geological Survey of Western Australia Report 108. Geological Survey of Western Australia.

Sheppard, S., Fletcher, I.R., Rasmussen, B., Zi, J.-W., Muhling, J.R., Occhipinti, S.A., Wingate, M.T.D., Johnson, S.P., 2016. A new Paleoproterozoic tectonic history of the eastern Capricorn Orogen, Western Australia, revealed by U–Pb zircon dating of micro-tuffs. Precambrian Res. 286, 1–19. doi:10.1016/j.precamres.2016.09.026

Sheppard, S., Johnson, S.P., Wingate, M.T.D., Kirkland, C.L., Pirajno, F., 2010b. Explanatory notes for the Gascoyne Province, Geological Survey of Western Australia Report 336.

Sheppard, S., Occhipinti, S.A.A., Tyler, I.M.M., 2004. A 2005-1970 Ma Andean-type batholith in the southern Gascoyne Complex, Western Australia. Precambrian Res. 128, 257–277. doi:10.1016/j.precamres.2003.09.003

Sheppard, S., Rasmussen, B., Zi, J.-W., Soma, V.S., Sarma, S., Mohan, M.R., Krapez, B., Wilde, S.A., McNaughton, N.J., 2017. Sedimentation and mafic magmatism in the Paleoproterozoic Cuddapah Basin, India, as a consequence of lithospheric extension. Gondwana Res. 48, 153–163. doi:10.1016/j.gr.2017.04.024

Sheraton, J.W., Black, L.P., 1982. Geochemistry and geochronology of Proterozoic tholeiite dykes of East Antarctica: evidence for mantle metasomatism. Contrib. to Mineral. Petrol. 78, 305–317.

Sheraton, J.W., Black, L.P., McCulloch, M.T., Oliver, R.L., 1990. Age and origin of a compositionally varied mafic dyke swarm in the Bunger Hills, East Antarctica. Chem. Geol. 85, 215–246.

Sheraton, J.W., Black, L.P., Tindle, A.G., 1992. Petrogenesis of plutonic rocks in a Proterozoic granulite-facies terrane — the Bunger Hills, East Antarctica. Chem. Geol. 97, 163–198. doi:10.1016/0009-2541(92)90075-G

Sheraton, J.W., Offe, L.A., Tingey, R.J., Ellis, D.J., 1980. Enderby land, Antarctica—an unusual Precambrian high-grade metamorphic terrain. J. Geol. Soc. Aust. 27, 1–18.

Sheraton, J.W., Oliver, R.L., Stüwe, K., 1989. Geochemistry of Proterozoic

Amphibolite dykes of Commonwealth Bay, Antarctica, and possible correlations with mafic dyke swarms elsewhere in Gondwanaland. Precambrian Res. 44, 353–361. doi:10.1016/0301-9268(89)90052-1

Sheraton, J.W., Thomson, J.W., Collerson, K.D., 1987. Mafic dyke swarms of Antarctica, in: Halls, H.C., Fahrig, W.F. (Eds.), Mafic Dyke Swarms. Geological Association of Canada Special Paper 34, pp. 419–432.

Sheraton, J.W., Tingey, R.J., 1994. Bedrock Geology of the Bunger Hills-Denman Glacier Region, Australian Antarctic Territory. Aust. Geol. Surv. Organ. 1250 000 Map Ser.

Sheraton, J.W., Tingey, R.J., Black, L.P., Offe, L.A., Ellis, D.J., 1987. Geology of Enderby Land and western Kemp Land, Antarctica. BMR Bull. 233 51p.

Sheraton, J.W., Tingey, R.J., Black, L.P., Oliver, R.L., 1993. Geology of the Bunger Hills area, Antarctica: implications for Gondwana correlations. Antarct. Sci. 5, 85–102. doi:10.1017/S0954102093000112

Sheraton, J.W., Tingey, R.J., Oliver, R.L., Black, L.P., 1995. Geology of the Bunger Hills-Denman Glacier region, East Antarctica, BMR Bulletin 244. Australian Geological Survey Organisation.

Silva, M.A., 1986. Placer gold recovery methods. Special Publication 87. California department of conservation, Division of Mines and Geology, Sacramento, California.

Sims, K.W.W., DePaolo, D.J., 1997. Inferences about mantle magma sources from incompatible element concentration ratios in oceanic basalts. Geochim. Cosmochim. Acta 61, 765–784. doi:10.1016/S0016-7037(96)00372-9

Sircombe, K.N., 2007. Compilation of SHRIMP U-Pb geochronological data, Yilgarn Craton, Western Australia, 2004-2006. Geoscience Australia Record 2007/01.

Sircombe, K.N., 2002. Reconnaissance detrital zircon geochronology provenance of the Palaeoproterozoic Ashburton Formation: implications for Pilbara and Yilgarn amalgamation, 16th Australian Geological Convention Abstract, 1-5 July 2002, Adelaide, South Australia. Geological Society of Australia.

Smirnov, A. V, Evans, D.A.D., Ernst, R.E., Söderlund, U., Li, Z.-X., 2013. Trading partners: Tectonic ancestry of southern Africa and western Australia, in Archean supercratons Vaalbara and Zimgarn. Precambrian Res. 224, 11–22.

Smith, A.D., 1992. Back-arc convection model for Columbia River basalt genesis. Tectonophysics 207, 269–285.

Smithies, R., Spaggiari, C., Kirkland, C., 2015. Building the crust of the Albany-Fraser Orogen: Constraints from granite geochemistry, in: GSWA 2015 Extended Abstracts-Promoting the Prospectivity of Western Australia. Geological Survey of Western Australia, pp. 31–35.

Smithies, R.H., Champion, D.C., 1999. Late Archaean felsic alkaline igneous rocks in the Eastern Goldfields, Yilgarn Craton, Western Australia: a result of lower crustal delamination? J. Geol. Soc. London. 156, 561–576.

Smithies, R.H., Howard, H.M., Kirkland, C.L., Korhonen, F.J., Medlin, C.C., Maier, W.D., de Gromard, R.Q., Wingate, M.T.D., Quentin De Gromard, R., Wingate, M.T.D., 2015. Piggy-back supervolcanoes-long-lived, voluminous, juvenile rhyolite volcanism in mesoproterozoic central Australia. J. Petrol. 56, egv015. doi:10.1093/petrology/egv015

Sobolev, A. V., Hofmann, A.W., Kuzmin, D. V., Yaxley, G.M., Arndt, N.T., Chung, S.-L., Danyushevsky, L. V., Elliott, T., Frey, F.A., Garcia, M.O., Gurenko, A.A., Kamenetsky, V.S., Kerr, A.C., Krivolutskaya, N.A., Matvienkov, V. V., Nikogosian, I.K., Rocholl, A., Sigurdsson, I.A., Sushchevskaya, N.M., Teklay, M., 2007. The amount of recycled crust in sources of mantle-derived melts. Science 316, 412–417.

Sobolev, S. V., Sobolev, A. V., Kuzmin, D. V., Krivolutskaya, N.A., Petrunin, A.G., Arndt, N.T., Radko, V.A., Vasiliev, Y.R., 2011. Linking mantle plumes, large igneous provinces and environmental catastrophes. Nature 477, 312–316. doi:10.1038/nature10385

Sobolev, A. V, Hofmann, A.W., Sobolev, S. V, Nikogosian, I.K., 2005. An olivine-free mantle source of Hawaiian shield basalts. Nature 434, 590–597.

Söderlund, U., Hellström, F.A., Kamo, S.L., 2008. Geochronology of high-pressure mafic granulite dykes in SW Sweden: tracking the P–T–t path of metamorphism using Hf isotopes in zircon and baddeleyite. J. Metamorph. Geol. 26, 539–560.

Söderlund, U., Hofmann, A., Klausen, M.B., Olsson, J.R., Ernst, R.E., Persson, P.O., 2010. Towards a complete magmatic barcode for the Zimbabwe craton: Baddeleyite U-Pb dating of regional dolerite dyke swarms and sill complexes. Precambrian Res. 183, 388–398. doi:10.1016/j.precamres.2009.11.001

Söderlund, U., Johansson, L., 2002. A simple way to extract baddeleyite (ZrO2). Geochemistry, Geophys. Geosystems 3, 1–7. doi:10.1029/2001GC000212

Sofoulis, J., 1965. Explanatory Notes on the Widgiemooltha 1: 250,000 Geological Sheet Western Australia. Geological Survey of Western Australia Record 1965/10.

Spaggiari, C.V., Kirkland, C.L., Smithies, H.R., Wingate, M.T.D., Belousova, E.A., 2015. Transformation of an Archean craton margin during Proterozoic basin formation and magmatism: The Albany–Fraser Orogen, Western Australia. Precambrian Res. 266, 440–466. doi:10.1016/j.precamres.2015.05.036

Spaggiari, C.V., Kirkland, C.L., Smithies, R., Occhipinti, S., Wingate, M., 2014a. Geological framework of the Albany-Fraser orogen, in: Spaggiari, C. V., Tyler, I.M. (Eds.), Albany-Fraser Orogen Seismic and Magnetotelluric (MT) Workshop 2014: Extended Abstracts. Geological Survey of Western Australia, Record 2014/6. pp. 12–27.

Spaggiari, C.V., Kirkland, C.L., Smithies, R.H., Wingate, M.T.D., 2014b. Tectonic links between Proterozoic sedimentary cycles, basin formation and magmatism in the Albany-Fraser Orogen, Western Australia, Geological Survey of Western Australia Report 133.

Spaggiari, C. V, Bodorkos, S., Barquero-Molina, M., Tyler, I.M., Wingate, M.T.D., 2009. Interpreted bedrock geology of the South Yilgarn and of the South Yilgarn and Central Albany-Fraser Orogen, Western Australia, Geological Survey of Western Australia Record 2009/10.

Spaggiari, C. V, Kirkland, C.L., Pawley, M.J., Smithies, R.H., Wingate, M.T.D., Doyle, M.G., Blenkinsop, T.G., Clark, C., Oorschot, C.W., Fox, L.J., 2011. The geology of the east Albany-Fraser Orogen—a field guide, Geological Survey of Western Australia Record 2011/23.

Stacey, J.S., Kramers, J.D., 1975. Approximation of terrestrial lead isotope evolution by a two-stage model. Earth Planet. Sci. Lett. 26, 207–221.

Stampfli, G.M., Hochard, C., Vérard, C., Wilhem, C., 2013. The formation of Pangea. Tectonophysics 593, 1–19.

Standing, J.G., 2008. Terrane amalgamation in the Eastern Goldfields Superterrane, Yilgarn Craton: evidence from tectonostratigraphic studies of the Laverton Greenstone Belt. Precambrian Res. 161, 114–134.

Stark, J.C., Wang, X.-C., Denyszyn, S.W., Li, Z.-X., Rasmussen, B., Zi, J.-W., Sheppard, S., Liu, Y., 2017. Newly identified 1.89 Ga mafic dyke swarm in the Archean Yilgarn Craton, Western Australia suggests a connection with India. Precambrian Res. Press. doi:10.1016/j.precamres.2017.12.036

Stark, J.C., Wilde, S.A., Söderlund, U., Li, Z.X., Rasmussen, B., Zi, J.W., 2018. First evidence of Archean mafic dykes at 2.62 Ga in the Yilgarn Craton, Western Australia: links to cratonisation and the Zimbabwe Craton. Precambrian Res. Under Rev.

Stern, R.A., 2001. A new isotopic and trace-element standard for the ion microprobe: preliminary thermal ionization mass spectrometry (TIMS) U-Pb and electron-microprobe data, Geological Survey of Canada Report 14, Current Research 2001-F.

Stern, R.A., Amelin, Y., 2003. Assessment of errors in SIMS zircon U-Pb geochronology using a natural zircon standard and NIST SRM 610 glass. Chem. Geol. 197, 111–142. doi:10.1016/S0009-2541(02)00320-0

Stern, R.A., Bodorkos, S., Kamo, S.L., Hickman, A.H., Corfu, F., 2009. Measurement of SIMS instrumental mass fractionation of Pb isotopes during zircon dating. Geostand. Geoanalytical Res. 33, 145–168. doi:10.1111/j.1751-908X.2009.00023.x

Stracke, A., Hofmann, A.W., Hart, S.R., 2005. FOZO, HIMU, and the rest of the mantle zoo. Geochemistry, Geophys. Geosystems 6, n/a-n/a. doi:10.1029/2004GC000824

Stüwe, K., Powell, R., 1989. Metamorphic evolution of the Bunger Hills, East Antarctica: evidence for substantial post-metamorphic peak compression with minimal cooling in a Proterozoic orogenic event. J. Metamorph. Geol. 7, 449–464.

Stüwe, K., Wilson, C.J.L., 1990. Interaction between deformation and charnockite emplacement in the Bunger Hills, East Antarctica. J. Struct. Geol. 12, 767–783. doi:10.1016/0191-8141(90)90088-g

Sun, S. -s., McDonough, W.F., 1989. Chemical and isotopic systematics of oceanic basalts: implications for mantle composition and processes. Geol. Soc. London, Spec. Publ. 42, 313–345. doi:10.1144/GSL.SP.1989.042.01.19

Suzuki, S., Ishizuka, H., Kagami, H., 2008. Early to middle Proterozoic dykes in the

Mt. Riiser-Larsen area of the Napier Complex, East Antarctica: tectonic implications as deduced from geochemical studies. Geol. Soc. London, Spec. Publ. 308, 195–210.

Taylor, S.R., McLennan, S.M., 1985. The continental crust: its composition and evolution, 1st ed. Blackwell Scientific Publishers, Palo Alto, CA.

Teixeira, W., D'Agrella-Filho, M.S., Hamilton, M.A., Ernst, R.E., Girardi, V.A.V., Mazzucchelli, M., Bettencourt, J.S., 2013. U–Pb (ID-TIMS) baddeleyite ages and paleomagnetism of 1.79 and 1.59Ga tholeiitic dyke swarms, and position of the Rio de la Plata Craton within the Columbia supercontinent. Lithos 174, 157–174. doi:10.1016/j.lithos.2012.09.006

Tilton, G.R., Patterson, C., Brown, H., Inghram, M., Hayden, R., Hess, D., Larsen Jr, E., 1955. Isotopic composition and distribution of lead, uranium, and thorium in a Precambrian granite. Geol. Soc. Am. Bull. 66, 1131–1148.

Tomkins, A.G., Grundy, C., 2009. Upper Temperature Limits of Orogenic Gold Deposit Formation : Constraints from the Granulite-Hosted Griffin's Find Deposit , Yilgarn Craton. Econ. Geol. 104, 669–685.

Towie, N.J., Seet, L.H., 1995. Diamond laboratory techniques. J. Geochemical Explor. 53, 205–212.

Tucker, D.H., Boyd, D.M., 1987. Dykes of Australia detected by airborne magnetic surveys, in: Fahrig, W.F., Halls, H.C. (Eds.), Mafic Dyke Swarms. Geological Association of Canada Special Paper 34, pp. 163–172.

Tucker, N.M., Hand, M., 2016. New constraints on metamorphism in the Highjump Archipelago, East Antarctica. Antarct. Sci. 28, 487–503. doi:10.1017/S095410201600033X

Tucker, N.M., Payne, J.L., Clark, C., Hand, M., Taylor, R.J., Kylander-Clark, A.R.C., 2017. Proterozoic reworking of Archean (Yilgarn) basement in the Bunger Hills, east Antarctica. Precambrian Res. 298, 16–38.

Upton, B.G.J., Rämö, O.T., Heaman, L.M., Blichert-Toft, J., Kalsbeek, F., Barry, T.L., Jepsen, H.F., 2005. The Mesoproterozoic Zig-Zag Dal basalts and associated intrusions of eastern North Greenland: Mantle plume-lithosphere interaction. Contrib. to Mineral. Petrol. 149, 40–56. doi:10.1007/s00410-004-0634-7

Upton, P., Hobbs, B., Ord, A., Zhang, Y., Drummond, B., Archibald, N., 1997.

Thermal and deformation modelling of the Yilgarn deep seismic transect, in: Geodynamics and Ore Deposits Conference Abstracts. pp. 22–25.

Van Westrenen, W., Blundy, J.D., Wood, B.J., 2001. High field strength element/rare earth element fractionation during partial melting in the presence of garnet: Implications for identification of mantle heterogeneities. Geochemistry, Geophys. Geosystems 2. doi:10.1029/2000GC000133

Vaughan, A.P.M., Storey, B.C., 2007. A new supercontinent self-destruct mechanism: evidence from the Late Triassic–Early Jurassic. J. Geol. Soc. London. 164, 383–392.

Wang, X.-C., Li, X.-H., Li, W.-X., Li, Z.-X., Liu, Y., Yang, Y.-H., Liang, X.-R., Tu, X.-L., 2008. The Bikou basalts in the northwestern Yangtze block, South China: Remnants of 820-810 Ma continental flood basalts? Geol. Soc. Am. Bull. 120, 1478–1492. doi:10.1130/B26310.1

Wang, X.-C., Li, Z.-X., Li, J., Pisarevsky, S.A., Wingate, M.T.D., 2014. Genesis of the 1.21 Ga Marnda Moorn large igneous province by plume–lithosphere interaction. Precambrian Res. 241, 85–103. doi:10.1016/j.precamres.2013.11.008

Wang, X.-C., Li, Z.-X., Li, X.-H., Li, J., Xu, Y.-G., Li, X.-H., 2013. Identification of an ancient mantle reservoir and young recycled materials in the source region of a young mantle plume: Implications for potential linkages between plume and plate tectonics. Earth Planet. Sci. Lett. 377–378, 248–259. doi:10.1016/j.epsl.2013.07.003

Wang, X.-C., Wilde, S.A., Li, Q.-L., Yang, Y.-N., 2015. Continental flood basalts derived from the hydrous mantle transition zone. Nat. Commun. 6, 7700. doi:http://dx.doi.org/10.1038/ncomms8700

Wang, X.-C., Wilde, S.A., Xu, B., Pang, C.-J., 2016. Origin of arc-like continental basalts: Implications for deep-Earth fluid cycling and tectonic discrimination. Lithos 261, 5–45. doi:10.1016/j.lithos.2015.12.014

Wang, X.C., Li, Z.X., Li, X.H., Li, J., Liu, Y., Long, W.G., Zhou, J.B., Wang, F., 2012. Temperature, Pressure, and Composition of the Mantle Source Region of Late Cenozoic Basalts in Hainan Island, SE Asia: a Consequence of a Young Thermal Mantle Plume close to Subduction Zones? J. Petrol. 53, 177–233. doi:10.1093/petrology/egr061

Ware, B., Jourdan, F., 2018. 40 Ar/39 Ar Geochronology of Terrestrial Pyroxene. Geochim. Cosmochim. Acta 230, 112–136.

Wasserburg, G.J., Jacobsen, S.B., DePaolo, D.J., McCulloch, M.T., Wen, T., 1981. Precise determination of Sm/Nd ratios, Sm and Nd isotopic abundances in standard solutions. Geochim. Cosmochim. Acta 45, 2311–2323.

Weaver, B.L., Tarney, J., 1981. The Scourie dyke suite: Petrogenesis and geochemical nature of the Proterozoic sub-continental mantle. Contrib. to Mineral. Petrol. 78, 175–188. doi:10.1007/BF00373779

Weaver, B.L., Tarney, J., 1980. Continental crust composition and nature of the lower crust: constraints from mantle Nd-Sr isotope correlation. Nature 286, 342–346.

Wetherill, G.W., 1956. Discordant uranium-lead ages, I. Eos, Trans. Am. Geophys. Union 37, 320–326.

White, R., McKenzie, D., 1989. Magmatism at rift zones: The generation of volcanic continental margins and flood basalts. J. Geophys. Res. 94, 7685. doi:10.1029/JB094iB06p07685

Wignall, P.B., 2001. Large igneous provinces and mass extinctions. Earth-Science Rev. 53, 1–33.

Wijk, J.W. van, Huismans, R.S., Ter Voorde, M., Cloetingh, S., 2001. Melt generation at volcanic continental margins: no need for a mantle plume? Geophys. Res. Lett. 28, 3995–3998.

Wilde, S.A., 1999. Evolution of the Western Margin of Australia during the Rodinian and Gondwanan Supercontinent Cycles. Gondwana Res. 2, 481–499. doi:10.1016/S1342-937X(05)70287-2

Wilde, S.A., 1990. Geology and crustal evolution of the southwestern Yilgarn Craton, in: Third International Archaean Symposium, Perth. pp. 89–122.

Wilde, S.A., 1980. The Jimperding Metamorphic Belt in the Toodyay area and the Balingup Metamorphic Belt and associated granitic rocks in the southwestern Yilgarn Craton. Excursion Guide, in: 2nd International Archaean Symposium, Geological Society of Western Australia.

Wilde, S.A., 1976. The Saddleback Group–a newly discovered Archaean greenstone belt in the southwestern Yilgarn Block. West. Aust. Geol. Surv. Annu. Rep. 92–95.

Wilde, S.A., Low, G.H., 1978. Perth, Western Australia, 1: 250 000 Geological Series Explanatory Notes. West. Aust. Geol. Surv.

Wilde, S.A., Middleton, M.F., Evans, B.J., 1996. Terrane accretion in the southwestern Yilgarn Craton: evidence from a deep seismic crustal profile. Precambrian Res. 78, 179–196.

Wilde, S.A., Pidgeon, R.T., 2006. Nature and timing of Late Archaean arc magmatism along the western margin of the Yilgarn Craton. Geochim. Cosmochim. Acta 70, A701.

Wilde, S.A., Pidgeon, R.T., 1990. The Morangup Greenstone Belt: a further discovery of Late Archaean volcanic rocks in the southwest Yilgarn Craton, Western Australia. International Archaean Symposium, 3rd Perth 1990. Abstr. Geoconferences 205–206.

Wilde, S.A., Pidgeon, R.T., 1987. U-Pb. Geochronology, Geothermometry and Petrology of the Main Areas of Gold Mineralization in the Wheat Belt Region of Western Australia Project 30 Final Report. Western Australian Mining and Petroleum Research Institute.

Wilde, S.A., Pidgeon, R.T., 1986. Geology and geochronology of the Saddleback greenstone belt in the Archaean Yilgarn Block, southwestern Australia. Aust. J. Earth Sci. 33, 491–501.

Willbold, M., Stracke, A., 2006. Trace element composition of mantle end-members: Implications for recycling of oceanic and upper and lower continental crust. Geochemistry, Geophys. Geosystems 7, n/a-n/a. doi:10.1029/2005GC001005

Williams, G.E., Schmidt, P.W., Clark, D.A., 2004. Palaeomagnetism of iron-formation from the late Palaeoproterozoic Frere Formation, Earaheedy Basin, Western Australia: palaeogeographic and tectonic implications. Precambrian Res. 128, 367–383. doi:10.1016/j.precamres.2003.09.008

Williams, H., Hoffman, P.F., Lewry, J.F., Monger, J.W.H., Rivers, T., 1991. Anatomy of North America: thematic geologic portrayals of the continent. Tectonophysics 187, 117–134.

Williams, I.S., 1998. U-Th-Pb geochronology by ion microprobe. Rev. Econ. Geol. 7, 1–35.

Wilson, J.F., Jones, D.L., Kramers, J.D., 1987. Mafic dyke swarms in Zimbabwe, in: Fahrig, W.F., Halls, H.C. (Eds.), Mafic Dyke Swarms. Geological Association of Canada Special Paper 34, pp. 433–444.

Wingate, M.T.. D., Campbell, I.H., Compston, W., Gibson, G.M., 1998. Ion microprobe U–Pb ages for Neoproterozoic basaltic magmatism in south-central Australia and implications for the breakup of Rodinia. Precambrian Res. 87, 135–159. doi:10.1016/S0301-9268(97)00072-7

Wingate, M.T.D., 2017. Mafic dyke swarms and large igneous provinces in Western Australia get a digital makeover, in: Geological Survey of Western Australia Record 2017/2. pp. 4–8.

Wingate, M.T.D., 2007. Proterozoic mafic dykes in the Yilgarn Craton, in: Proceedings of Geoconferences (WA) Inc. Kalgoorlie 2007 Conference, Kalgoorlie, Western Australia. pp. 80–84.

Wingate, M.T.D., 2003. Age and Palaeomagnetism of Dolerite Sills Intrusions of the Southeastern Collier Basin, and the Earaheedy and Yerrida Basins, Western Australia, in: Western Australian Geological Survey Record, 2003/3. Geological Survey of Western Australia, p. 35.

Wingate, M.T.D., 2002. Age and Paleomagnetism of Dolerite Sills Intruded Into the Bangemall Supergroup on the Edmund 1: 250 000 Map Sheet, Western Australia. Geological Survey of Western Australia Record 2002/4.

Wingate, M.T.D., 1999. Ion microprobe baddeleyite and zircon ages for Late Archaean mafic dykes of the Pilbara Craton, Western Australia. Aust. J. Earth Sci. 46, 493–500. doi:10.1046/j.1440-0952.1999.00726.x

Wingate, M.T.D., 1997. Testing Precambrian continental reconstructions using ion microprobe U-Pb baddeleyite geochronology and paleomagnetism of mafic igneous rocks. Australian National University PhD Thesis.

Wingate, M.T.D., Campbell, I.H., Harris, L.B., 2000. SHRIMP baddeleyite age for the Fraser dyke swarm, southeast Yilgarn Craton, Western Australia. Aust. J. Earth Sci. 47, 309–313.

Wingate, M.T.D., Compston, W., 2000. Crystal orientation effects during ion microprobe U–Pb analysis of baddeleyite. Chem. Geol. 168, 75–97. doi:10.1016/S0009-2541(00)00184-4

Wingate, M.T.D., Evans, D.A.D., 2003. Palaeomagnetic constraints on the Proterozoic tectonic evolution of Australia. Geol. Soc. London, Spec. Publ. 206, 77–91.

Wingate, M.T.D., Morris, P.A., Pirajno, F., Pidgeon, R.T., 2005. Two large igneous provinces in Late Mesoproterozoic Australia, in: Supercontinents and Earth Evolution Symposium. Geological Society of Australia Abstracts, p. 151.

Wingate, M.T.D., Pidgeon, R.T., 2005. The Marnda Moorn LIP, a late Mesoproterozoic large igneous province in the Yilgarn craton, Western Australia. July 2005 LIP of the month [WWW Document]. (unpub). Large Igneous Prov. Comm. Int. Assoc. Volcanol. Chem. Earth's Inter. URL http://www.largeigneousprovinces.org/05jul

Wingate, M.T.D., Pirajno, F., Morris, P.A., 2004. Warakurna large igneous province: a new Mesoproterozoic large igneous province in west-central Australia. Geology 32, 105–108.

Wingate, M.T.D., Pisarevsky, S.A., Evans, D.A.D., 2002. Rodinia connections between Australia and Laurentia: no SWEAT, no AUSWUS? Terra Nov. 14, 121–128.

Winter, J.D., 2014. Principles of igneous and metamorphic petrology, Second edi. ed. Pearson Education.

Witt, W.K., Cassidy, K.F., Lu, Y.-J., Hagemann, S.G., 2018. The tectonic setting and evolution of the 2.7 Ga Kalgoorlie–Kurnalpi Rift, a world-class Archean gold province. Miner. Depos. 1–31. doi:10.1007/s00126-017-0778-9

Witt, W.K., Vanderhor, F., 1998. Diversity within a unified model for Archaean gold mineralization in the Yilgarn Craton of Western Australia: an overview of the late-orogenic, structurally-controlled gold deposits. Ore Geol. Rev. 13, 29–64. doi:10.1016/S0169-1368(97)00013-9

Worsley, T.R., Moody, J.B., Nance, R.D., 1985. Proterozoic to Recent Tectonic Tuning of Biogeochemical Cycles, in: The Carbon Cycle and Atmospheric CO2: Natural Variations Archean to Present. American Geophysical Union Monograph Series, pp. 561–572. doi:10.1029/GM032p0561

Worsley, T.R., Nance, D., Moody, J.B., 1984. Global tectonics and eustasy for the past 2 billion years. Mar. Geol. 58, 373–400. doi:10.1016/0025-3227(84)90209-3

Worsley, T.R., Nance, R.D., 1989. Carbon redox and climate control through Earth history: a speculative reconstruction. Glob. Planet. Change 1, 259–282.

Worsley, T.R., Nance, R.D., Moody, J.B., 1991. Tectonics, life, and climate for the last three billion years: a unified system?, in: Schneider, S.H., Boston, P.J. (Eds.), Scientists on Gaia. MIT Press, Cambridge, MA, pp. 200–210.

Worsley, T.R., Nance, R.D., Moody, J.B., 1986. Tectonic cycles and the history of the Earth's biogeochemical and paleoceanographic record. Paleoceanography 1, 233–263.

Worsley, T.R., Nance, R.D., Moody, J.B., 1982. Plate tectonic episodicity: a deterministic model for periodic "Pangeas." Eos, Trans. Am. Geophys. Union 65, 1104.

Wu, W.N., Schmitt, A.K., Pappalardo, L., 2015. U-Th baddeleyite geochronology and its significance to date the emplacement of silica undersaturated magmas†. Am. Mineral. 100, 2082–2090.

Xia, L.-Q., 2014. The geochemical criteria to distinguish continental basalts from arc related ones. Earth-Science Rev. 139, 195–212.

Xie, H., Kröner, A., Brandl, G., Wan, Y., 2017. Two orogenic events separated by 2.6 Ga mafic dykes in the Central Zone, Limpopo Belt, southern Africa. Precambrian Res. 289, 129–141. doi:10.1016/j.precamres.2016.11.009

Yale, L.B., Carpenter, S.J., 1998. Large igneous provinces and giant dike swarms: proxies for supercontinent cyclicity and mantle convection. Earth Planet. Sci. Lett. 163, 109–122.

Yeats, C.J., McNaughton, N.J., 1997. Significance of SHRIMP II U-Pb geochronology on lode-gold deposits of the Yilgarn craton. Aust. Geol. Surv. Organ. Rec. 41, 125–130.

Yeats, C.J., McNaughton, N.J., Groves, D.I., 1996. SHRIMP U-Pb geochronological constraints on Archean volcanic-hosted massive sulfide and lode gold mineralization at Mount Gibson, Yilgarn Craton, Western Australia. Econ. Geol. 91, 1354–1371.

Young, D.N., Zhao, J., Ellis, D.J., McCulloch, M.T., 1997. Geochemical and Sr-Nd isotopic mapping of source provinces for the Mawson charnockites, east Antarctica: implications for Proterozoic tectonics and Gondwana reconstruction. Precambrian Res. 86, 1–19. doi:10.1016/S0301-9268(97)00030-2

Young, G.M., 2013. Precambrian supercontinents, glaciations, atmospheric oxygenation, metazoan evolution and an impact that may have changed the second half of Earth history. Geosci. Front. 4, 247–261.

Zeh, A., Gerdes, A., Barton Jr, J., Klemd, R., 2010. U–Th–Pb and Lu–Hf systematics of zircon from TTG's, leucosomes, meta-anorthosites and quartzites of the Limpopo Belt (South Africa): constraints for the formation, recycling and metamorphism of Palaeoarchaean crust. Precambrian Res. 179, 50–68.

Zeh, A., Gerdes, A., Klemd, R., Barton, J.M., 2007. Archaean to proterozoic crustal evolution in the central zone of the Limpopo Belt (South Africa-Botswana): Constraints from combined U-Pb and Lu-Hf isotope analyses of zircon. J. Petrol. 48, 1605–1639. doi:10.1093/petrology/egm032

Zhang, S.H., Zhao, Y., Liu, X.C., Liu, Y.S., Hou, K.J., Li, C.F., Ye, H., 2012. U-Pb geochronology and geochemistry of the bedrocks and moraine sediments from the Windmill Islands: Implications for Proterozoic evolution of East Antarctica. Precambrian Res. 206–207, 52–71. doi:10.1016/j.precamres.2012.02.019

Zhao, G., Cawood, P.A., Wilde, S.A., Sun, M., 2002. Review of global 2.1-1.8 Ga orogens: implications for a pre-Rodinia supercontinent. Earth-Science Rev. 59, 125–162.

Zhao, G., Sun, M., Wilde, S.A., Li, S., Zhang, J., 2006. Some key issues in reconstructions of Proterozoic supercontinents. J. Asian Earth Sci. 28, 3–19.

Zhao, J., Ellis, D.J., Kilpatrick, J.A., McCulloch, M.T., 1997. Geochemical and Sr-Nd isotopic study of charnockites and related rocks in the northern Prince Charles Mountains, East Antarctica: implications for charnockite petrogenesis and proterozoic crustal evolution. Precambrian Res. 81, 37–66. doi:http://dx.doi.org/10.1016/S0301-9268(96)00022-8

Zhao, Z.-F., Dai, L.-Q., Zheng, Y.-F., 2013. Postcollisional mafic igneous rocks record crust-mantle interaction during continental deep subduction. Nat. Sci. Reports 3, 3413. doi:10.1038/srep03413

Zhong, S., Zhang, N., Li, Z.-X., Roberts, J.H., 2007. Supercontinent cycles, true polar wander, and very long-wavelength mantle convection. Earth Planet. Sci. Lett. 261, 551–564.

Zi, J.W., Gregory, C.J., Rasmussen, B., Sheppard, S., Muhling, J.R., 2017. Using monazite geochronology to test the plume model for carbonatites: The example of Gifford Creek Carbonatite Complex, Australia. Chem. Geol. 463, 50–60. doi:10.1016/j.chemgeo.2017.05.007

Zi, J.W., Rasmussen, B., Muhling, J.R., Fletcher, I.R., Thorne, A.M., Johnson, S.P., Cutten, H.N., Dunkley, D.J., Korhonen, F.J., 2015. In situ U-Pb geochronology of xenotime and monazite from the Abra polymetallic deposit in the Capricorn Orogen, Australia: Dating hydrothermal mineralization and fluid flow in a long-lived crustal structure. Precambrian Res. 260, 91–112. doi:10.1016/j.precamres.2015.01.010

Zibra, I., Clos, F., Weinberg, R.F., Peternell, M., 2017a. The ~2730 Ma onset of the Neoarchean Yilgarn Orogeny. Tectonics 36, 1787–1813. doi:10.1002/2017TC004562

Zibra, I., Korhonen, F.J., Peternell, M., Weinberg, R.F., Romano, S.S., Braga, R., De Paoli, M.C., Roberts, M., 2017b. On thrusting, regional unconformities and exhumation of high-grade greenstones in Neoarchean orogens. The case of the Waroonga Shear Zone, Yilgarn Craton. Tectonophysics 712–713, 362–395. doi:10.1016/j.tecto.2017.05.017

Zindler, A., Hart, S., 1986. Chemical geodynamics. Annu. Rev. Earth Planet. Sci. 14, 493–571.

APPENDIX A FIRST AUTHOR PUBLICATIONS

Stark, J.C., Wang, X.-C., Denyszyn, S.W., Li, Z.-X., Rasmussen, B., Zi, J.-W., Sheppard, S., Liu, Y.,. Newly identified 1.89 Ga mafic dyke swarm in the Archean Yilgarn Craton, Western Australia suggests a connection with India. Precambrian Research, In Press.
Available at http://10.1016/j.precamres.2017.12.036

Stark, J.C., Wang, X.-C., Li, Z.-X., Rasmussen, B., Sheppard, S., Xi, J.-W., Clark, C., Hand, M., Li, W.-X., **2018**. In situ U-Pb geochronology and geochemistry of a 1.13 Ga mafic dyke suite at Bunger Hills, East Antarctica: the end of the Albany-Fraser Orogeny. Precambrian Res. 310, 76–92.
Available at https://doi.org/10.1016/j.precamres.2018.02.023

Stark, J.C., Wilde, S.A., Soderlund, U., Li, Z.-X., Rasmussen, B., Zi, J.-W., First evidence of Archean mafic dykes at 2.62 Ga in the Yilgarn Craton, Western Australia: links to cratonisation and the Zimbabwe Craton. Precambrian Res. 317, 1-13
Available at https://doi.org/10.1016/j.precamres.2018.08.004

Stark, J.C., Wang, X.-C., Li, Z.-X., Denyszyn, S.W., Rasmussen, B., Zi, J.-W., Sheppard, S., 1.39 Ga mafic dyke swarm in southwestern Yilgarn Craton marks Nuna to Rodinia transition in the West Australian Craton. Precambrian Res. 316, 291-304
Available at https://doi.org/10.1016/j.precamres.2018.08.014

Statement of Authorship

Title of Paper	**Newly identified 1.89 Ga mafic dyke swarm in the Archean Yilgarn Craton, Western Australia suggests a connection with India**	
Publication Status	**Published (in press)**	Accepted for publication
	Submitted for Publication	Publication Style
Publication Details	Stark, J.C., Wang, X.-C., Denyszyn, S.W., Li, Z.-X., Rasmussen, B., Zi, J.-W., Sheppard, S., Liu, Y.,. Newly identified 1.89 Ga mafic dyke swarm in the Archean Yilgarn Craton, Western Australia suggests a connection with India. **Precambrian Research**, **In Press**. Available at http://10.1016/j.precamres.2017.12.036	

Author Contributions

By signing the Statement of Authorship, each author certifies that their stated contribution to the publication is accurate and that permission is granted for the publication to be included in the candidate's thesis.

Name of Principal Author (Candidate)	Jutta Camilla Stark		
Contribution to the Paper	Jutta Camilla Stark collected and prepared most of the samples and undertook SHRIMP dating, some baddeleyite separation for ID-TIMS dating, most of the interpretation and drafted most of the manuscript		
Overall percentage (%)	60		
Signature		Date	

Name of Co-Author	Xuan-Ce Wang		
Contribution to the Paper	Xuan-Ce Wang is a supervisor of the candidate and assisted with the interpretation of the geochemical data and drafting of the manuscript		
Overall percentage (%)	10		
Signature		Date	

Name of Co-Author	Steven Denyszyn		
Contribution to the Paper	Steve Denyszyn undertook baddeleyite separation and ID-TIMS dating		
Overall percentage (%)	5		
Signature		Date	

Name of Co-Author	Zheng-Xiang Li		
Contribution to the Paper	Zheng-Xiang Li is the principal supervisor of the candidate and assisted with the concept and drafting of the manuscript and interpretation of the results		
Overall percentage (%)	5		
Signature		Date	

Name of Co-Author	Birger Rasmussen		
Contribution to the Paper	Birger Rasmussen assisted with interpretation of the SHRIMP results and drafting of the manuscript		
Overall percentage (%)	5		
Signature		Date	

Name of Co-Author	Jian-Wei Zi		
Contribution to the Paper	Jian-Wei Zi assisted with SHRIMP sample preparation, analysis and data processing		
Overall percentage (%)	5		
Signature	Zi jianwei	Date	

Name of Co-Author	Stephen Sheppard		
Contribution to the Paper	Steve Sheppard assisted with interpretation of the results and drafting of the manuscript		
Overall percentage (%)	5		
Signature	S. Sheppard	Date	

Name of Co-Author	Yebo Liu		
Contribution to the Paper	Yebo Liu assisted with drafting of the manuscript		
Overall percentage (%)	5		
Signature	Yebo Liu	Date	

Copyright Clearance Center RightsLink®

Home | Create Account | Help

Title: Newly identified 1.89 Ga mafic dyke swarm in the Archean Yilgarn Craton, Western Australia suggests a connection with India

Author: J. Camilla Stark,Xuan-Ce Wang,Steven W. Denyszyn,Zheng-Xiang Li,Birger Rasmussen,Jian-Wei Zi,Stephen Sheppard,Yebo Liu

Publication: Precambrian Research

Publisher: Elsevier

Date: Available online 19 December 2017

LOGIN

If you're a copyright.com user, you can login to RightsLink using your copyright.com credentials.

Already **a RightsLink user** or want to learn more?

Please note that, as the author of this Elsevier article, you retain the right to include it in a thesis or dissertation, provided it is not published commercially. Permission is not required, but please ensure that you reference the journal as the original source. For more information on this and on your other retained rights, please visit: https://www.elsevier.com/about/our-business/policies/copyright#Author-rights

BACK | CLOSE WINDOW

ARTICLE IN PRESS

Precambrian Research xxx (xxxx) xxx–xxx

Contents lists available at ScienceDirect

Precambrian Research

journal homepage: www.elsevier.com/locate/precamres

Newly identified 1.89 Ga mafic dyke swarm in the Archean Yilgarn Craton, Western Australia suggests a connection with India

J. Camilla Stark[a,b,c,*], Xuan-Ce Wang[b,c], Steven W. Denyszyn[d], Zheng-Xiang Li[a,b,c], Birger Rasmussen[d], Jian-Wei Zi[b], Stephen Sheppard[b], Yebo Liu[a,b,c]

[a] Earth Dynamics Group, Curtin University, GPO Box U1987, Perth, WA 6845, Australia
[b] The Institute for Geoscience Research (TIGeR), Department of Applied Geology, Curtin University, GPO Box U1987, Perth, WA 6845, Australia
[c] Department of Applied Geology, Curtin University, GPO Box U1987, Perth, WA 6845, Australia
[d] School of Earth Sciences, University of Western Australia, Perth, WA 6009, Australia

A R T I C L E I N F O

Keywords:
Yilgarn Craton
Mafic dykes
Geochronology
U-Pb baddeleyite
Large Igneous Province
Boonadgin dykes

A B S T R A C T

The Archean Yilgarn Craton in Western Australia is intruded by numerous mafic dykes of varying orientations, which are poorly exposed but discernible in aeromagnetic maps. Previous studies have identified two craton-wide dyke swarms, the 2408 Ma Widgiemooltha and the 1210 Ma Marnda Moorn Large Igneous Provinces (LIP), as well as limited occurrences of the 1075 Ma Warakurna LIP in the northern part of the craton. We report here a newly identified NW-trending mafic dyke swarm in southwestern Yilgarn Craton dated at 1888 ± 9 Ma with ID-TIMS U-Pb method on baddeleyite from a single dyke and at 1858 ± 54 Ma, 1881 ± 37 and 1911 ± 42 Ma with *in situ* SHRIMP U-Pb on baddeleyite from three dykes. Preliminary interpretation of aeromagnetic data indicates that the dykes form a linear swarm several hundred kilometers long, truncated by the Darling Fault in the west. This newly named Boonadgin dyke swarm is synchronous with post-orogenic extension and deposition of granular iron formations in the Earaheedy basin in the Capricorn Orogen and its emplacement may be associated with far field stresses. Emplacement of the dykes may also be related to initial stages of rifting and formation of the intracratonic Barren Basin in the Albany-Fraser Orogen, where the regional extensional setting prevailed for the following 300 million years. Recent studies and new paleomagnetic evidence raise the possibility that the dykes could be part of the coeval 1890 Ma Bastar-Cuddapah LIP in India. Globally, the Boonadgin dyke swarm is synchronous with a major orogenic episode and records of intracratonic mafic magmatism on many other Precambrian cratons.

1. Introduction

Regardless of their proposed mechanism of formation (e.g., mantle plume, flux melting, passive rifting or global mantle warming), large igneous provinces (LIPs; Coffin and Eldholm, 1994), including mafic dyke swarms, appear to be intimately connected with deep-Earth dynamics and supercontinent cycles (e.g., Condie, 2004; Prokoph et al., 2004; Bleeker and Ernst, 2006; Ernst et al., 2008; Li and Zhong, 2009; Goldberg, 2010). Mafic dyke swarms act as important markers for supercontinent reconstructions (e.g., Ernst and Buchan, 1997; Buchan et al., 2001; Bleeker and Ernst, 2006; Ernst and Srivastava, 2008; Ernst et al., 2010, 2013) and as indicators of paleostress fields and pre-existing crustal weaknesses (Ernst et al., 1995; Hoek and Seitz, 1995; Halls and Zhang, 1998; Hou, 2012; Ju et al., 2013). Key to such application is the availability of high-precision geochronology for mafic dykes. Recent studies have shown that orientation alone cannot be reliably used to distinguish between different dyke generations, especially near major tectonic boundaries and craton scale structures such as continental rifts (e.g., Hanson et al., 2004; Wingate, 2007; French and Heaman, 2010; Belica et al., 2014).

Like many other Archean cratons worldwide, the Yilgarn Craton in Western Australia is intruded by many generations of dyke suites with different orientations. Currently, robust geochronology is only available for two craton-wide dyke swarms at 2408 Ma (Sofoulis, 1965; Evans, 1968; Hallberg, 1987; Doehler and Heaman, 1998; Nemchin and Pidgeon, 1998; Wingate, 1999; French et al., 2002) and at 1210 Ma (Marnda Moorn LIP; Wingate et al., 1998, 2000; Wingate, 2007), and for limited dyke occurrences at 1075 Ma (Warakurna LIP; Wingate et al., 2002, 2004) and ca. 735 Ma (Nindibillup dykes; Spaggiari et al., 2009, 2011; Wingate, 2017). The magmatic record ("barcode") for the Yilgarn Craton dyke swarms is very limited compared with other Archean cratons, such as the Superior and Kola-Karelia Cratons (Ernst and

* Corresponding author at: Earth Dynamics Group, Curtin University, GPO Box U1987, Perth, WA 6845, Australia.
E-mail address: c.stark@postgrad.curtin.edu.au (J.C. Stark).

https://doi.org/10.1016/j.precamres.2017.12.036
Received 23 September 2017; Accepted 17 December 2017

Please cite this article as: Camilla Stark, J., Precambrian Research (2017), https://doi.org/10.1016/j.precamres.2017.12.036

Bleeker, 2010; Ernst et al., 2010). The apparent absence of mafic magmatism in the Yilgarn Craton during the major global episode of juvenile magmatism and crustal growth at ca. 1890 Ma is surprising since this event is found on most other Precambrian cratons worldwide (Heaman et al., 1986, 2009; Hanson et al., 2004; French et al., 2008; Minifie et al., 2008; Buchan et al., 2010; Ernst and Bell, 2010; Söderlund et al., 2010). The lack of geochronology and paleomagnetic data from the Yilgarn Craton between ca. 1900 Ma and 1300 Ma, the proposed time interval for the supercontinent Nuna/Columbia, is especially problematic for paleographic reconstructions.

Here we report *in situ* SHRIMP and ID-TIMS U-Pb results for a previously unidentified NW-trending Paleoproterozoic mafic dyke suite in the southwestern Yilgarn Craton and discuss the tectonic setting during its emplacement. A direct record of Paleoproterozoic tectonic events in the craton margins is largely absent due to extensive overprinting by younger events, so we also evaluate evidence from remnant Proterozoic sedimentary basins, which preserve a history of past tectonic setting, crustal architecture and lithospheric stress fields. In light of previous studies suggesting India-Yilgarn connection (Mohanty, 2012, 2015) and recent paleomagnetic data (Belica et al., 2014; Liu et al., 2016, 2017) we consider the possibility that the dykes may be associated with the coeval Bastar-Cuddapah LIP in India.

2. Regional geology

The Yilgarn Craton is a ca. 900 × 1000 km Archean crustal block comprising six accreted terranes: the Southwest, Narryer, Youanmi, Kalgoorlie, Kurnalpi and Burtville terranes, the latter three forming the Eastern Goldfields Superterrane (Fig. 1). These comprise variably metamorphosed granites and volcanic and sedimentary rocks with protolith ages between ca. 3730 and 2620 Ma (Cassidy et al., 2005, 2006 and references therein) and are thought to represent a series of volcanic arcs, back arc basins and microcontinents, which amalgamated between ca. 2900 and 2700 Ma (Myers, 1993; Wilde et al., 1996). Abundant granites were emplaced between ca. 2760 Ma and 2630 Ma (Cassidy et al., 2006 and references therein) and the entire craton underwent intense metamorphism and hydrothermal activity between 2780 and 2630 Ma (Myers, 1993; Nemchin et al., 1994; Nelson et al., 1995; Wilde et al., 1996). The Southwest Terrane comprises multiply deformed ca. 3200–2800 Ma high-grade metasedimentary rocks and ca. 2720–2670 Ma meta-igneous rocks intruded by 2750–2620 Ma granites (Myers, 1993; Wilde et al., 1996; Nemchin and Pidgeon, 1997).

The Yilgarn Craton is bounded by three Proterozoic orogenic belts: the ca. 2005–570 Ma Capricorn Orogen in the north (Cawood and Tyler, 2004a; Sheppard et al., 2010a; Johnson et al., 2011), the ca. 1815–1140 Ma Albany-Fraser Orogen in the south and east (Nelson et al., 1995; Clark et al., 2000; Spaggiari et al., 2015), and the ca. 1090–525 Ma Pinjarra Orogen in the west (Myers, 1990; Wilde, 1999; Ksienzyk et al., 2012). Prolonged lateritic weathering has produced the modern denuded landscape and poor exposure of basement rocks (Anand and Paine, 2002).

Following cratonisation toward the end of the Archean, the Yilgarn Craton collided along the Capricorn Orogen with the combined Pilbara Craton-Glenburgh Terrane by 1950 Ma to form the West Australian Craton (WAC: Sheppard et al., 2004, 2010a, b; Johnson et al., 2011). Four syn- to post-orogenic sedimentary basins developed along the southern Capricorn Orogen, including the Earaheedy Basin in the east (Pirajno et al., 2009). The Earaheedy succession was thought to be post-1800 Ma in age, but new dating (Rasmussen et al., 2012; Sheppard et al., 2016) shows that the basin comprises three unconformity-bound packages at ca. 1990–1950 Ma, ca. 1890 Ma and ca. 1890–1810 Ma.

The Yilgarn Craton is intruded by a large number of dykes of

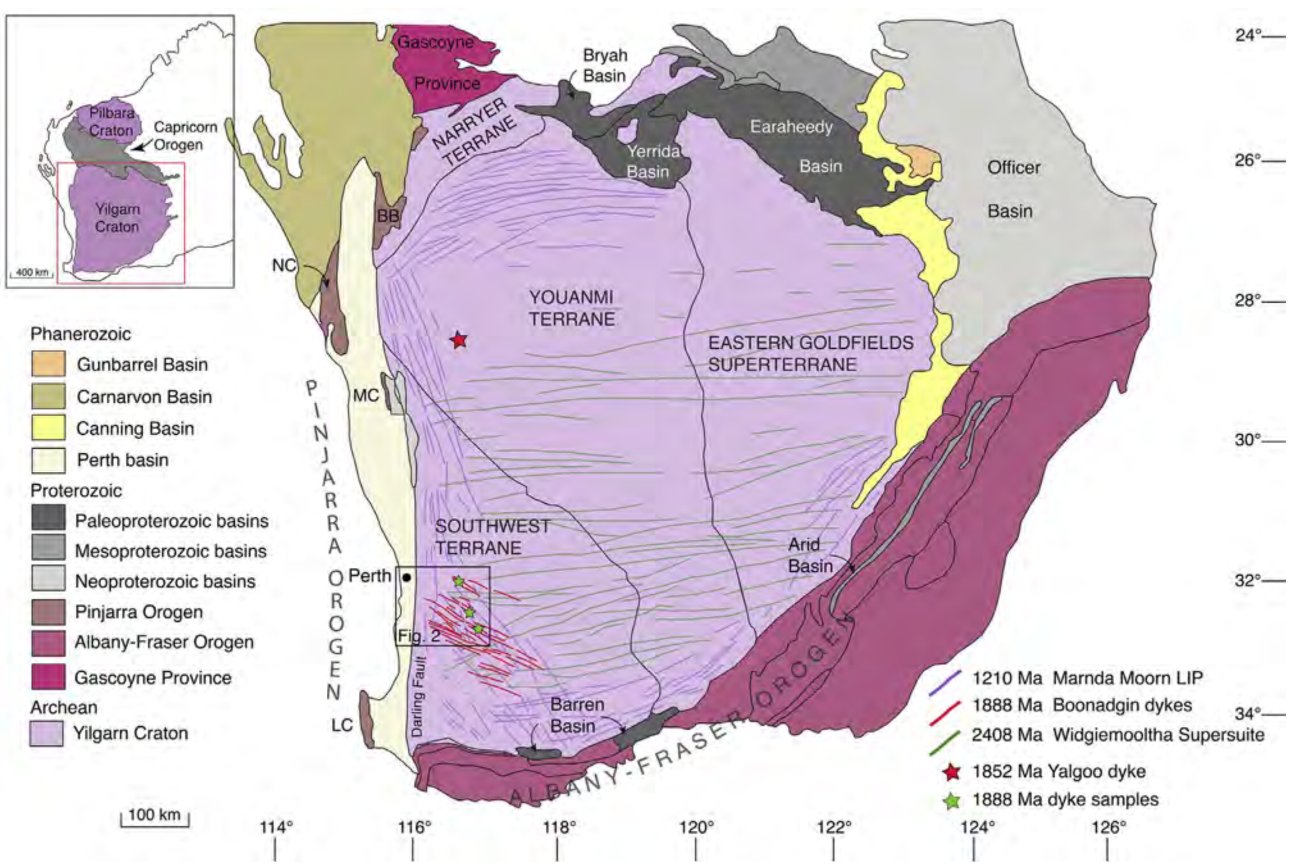

Fig. 1. Map of the Yilgarn showing major tectonic units and the Capricorn and Albany-Fraser Orogens. Inset shows the extent of the West Australian Craton (Pilbara Craton, Yilgarn Craton and Capricorn Orogen). From Geological Survey of Western Australia 1:2.5M Interpreted Bedrock Geology 2015 and 1:10M Tectonic Units 2016.

different orientations with the dyke density increasing towards the southern and western craton margins (Hallberg, 1987; Tucker and Boyd, 1987). The dykes are discernible in aeromagnetic data but difficult to sample due to deep weathering and thick regolith cover. The oldest known dykes belong to the E-W to NE-SW trending 2408 Ma Widgiemooltha Supersuite (Sofoulis, 1965; Evans, 1968; Campbell et al., 1970; Hallberg, 1987; Doehler and Heaman, 1998; Nemchin and Pidgeon, 1998; Wingate, 1999, 2007; French et al., 2002). The Widgiemooltha dykes are up to 3.2 km wide and extend up to 700 km across the craton, with the largest intrusions (Jimberlana and Binneringie) showing well developed igneous layering (Campbell et al., 1970; Lewis, 1994). The dykes exhibit dual magnetic polarity (Tucker and Boyd, 1987; Boyd and Tucker, 1990) and recent geochronology and paleomagnetic data suggest that their emplacement may have involved several pulses (Wingate, 2007; Pisarevsky et al., 2015). The second craton-wide suite is the 1210 Ma Marnda Moorn LIP which consists of several sub-swarms of different orientations intruding along the craton margins (Isles and Cooke, 1990; Evans, 1999; Wingate et al., 2000; Pidgeon and Nemchin, 2001; Pidgeon and Cook, 2003; Wingate and Pidgeon, 2005; Wingate, 2007; Claoué-Long and Hoatson, 2009). Outcrops in the southeast are limited to a single occurrence, and the extent of the dykes in the northeast is unknown due to cover rocks but one E-W oriented dioritic dyke dated at 1215 ± 11 Ma has been reported further inland (Qiu et al., 1999). Other identified dyke swarms with limited occurrences include the SW-trending dykes of the 1075 Ma Warakurna LIP in the northern Yilgarn Craton (Wingate et al., 2004), the WNW-trending ca. 735 Ma Nindibillup dykes in the central and SE Yilgarn Craton (Spaggiari et al., 2009, 2011; Wingate, 2017) and the undated (likely < 1140 Ma) NW-trending Beenong dykes in the SE Yilgarn Craton (Wingate, 2007; Spaggiari et al., 2009, 2011).

3. Samples

3.1. Field sampling

Field sampling sites were targeted using satellite imagery (Landsat/Copernicus or Astrium/CNES from Google Earth), aeromagnetic data (20–40 m cell size, Geoscience Australia magnetic grid of Australia V6 2015 base reference) and 1:250,000 geological maps from the Geological Survey of Western Australia.

Four block samples were collected from outcrops within agriculturally cleared areas where the dykes stand out as small ridges. Sample WDS09 was collected from an outcrop ca. 18 km southwest of the town of Pingelly, sample 16WDS01 and 16WDS02 ca. 29 km northwest of Pingelly and sample 16WDS06 ca. 14 km southwest of the village of Gwambygine (Fig. 2). Coordinates for sample locations are given in Table 1. Basement rocks are only exposed at the WDS09 outcrop where the dyke intrudes Archean migmatitic gneiss with a sharp chilled margin. At the 16WDS01/16WDS02 and 16WDS06 sites, geological mapping indicates that the country rocks to the dykes are mainly Archean granites. The outcrops are fresh with weathering forming a thin crust best visible along fractures.

3.2. Sample description

All samples are dolerites with intergranular ophitic to sub-ophitic texture, comprising ca. 50% plagioclase, 45% clinopyroxene, 1–2% quartz, 2–3% opaque minerals (ilmenite, magnetite and minor pyrite) and trace biotite and apatite. Sample WDS09 is relatively fresh but samples 16WDS01/02 and 16WDS06 in the northern part of the sampling area are more altered, with most clinopyroxene grains partially altered to chlorite and green amphibole. Plagioclase is affected by sericitisation but most grains still show twinning. Biotite is associated with the opaque minerals, forming corona like rims. The main U- and Th-bearing accessory minerals are baddeleyite and zirconolite, only identifiable under SEM due to their small size, typically ≤70 µm long and 20–30 µm across. Some crystals show thin zircon rims or alteration to zircon along fractures but most appear pristine.

4. U-Pb geochronology and geochemistry

4.1. SHRIMP U-Pb geochronology

Polished thin sections were scanned to identify baddeleyite, zircon and zirconolite with a Hitachi TM3030 scanning electron microscope (SEM) equipped with energy dispersive X-ray spectrometer (EDX) at Curtin University. For SHRIMP U-Pb dating, selected grains were drilled directly from the thin sections using a micro drill and mounted into epoxy disks, which were cleaned and coated with 40 nm of gold. Baddeleyite forms unaltered subhedral to euhedral equant and tabular grains and laths, some with thin zircon rims, and most are < 60 µm long and up to 20–30 µm across (Fig. 3).

Baddeleyite was analysed for U, Th and Pb using the sensitive high-resolution ion microprobe (SHRIMP II) at the John de Laeter Centre at Curtin University in Perth, Australia, following standard operating procedures after Compston et al. (1984). The SHRIMP analysis method for mounts with polished thin section plugs outlined in Rasmussen and Fletcher (2010) was modified for baddeleyite (SHRIMP operating parameters in Table 2). During each analysis session, standard zircon OG1 (Stern et al., 2009) was used to monitor instrumental mass fractionation and BR266 zircon (Stern, 2001) was used for calibrating U and Th concentration and as an accuracy standard. Phalaborwa baddeleyite (Heaman, 2009) was employed as an additional accuracy standard. Typical spot size with primary O_2^- current was 10–15 µm at 0.8–1.4 nA. Data were processed with Squid version 2.50 (Ludwig, 2009) and Isoplot version 3.76.12 (Ludwig, 2012). For common Pb correction, 1890 Ma common Pb isotopic compositions were calculated from the Stacey and Kramers (1975) two-stage terrestrial Pb isotopic evolution model. Analyses with > 1% common Pb (in ^{206}Pb) or > 10% discordance (see footnote in Table 3 for definition) are considered unreliable and were disregarded in age calculations. The assigned 1σ external Pb/U error for all analyses is 1%, except for 1.04% for 16WDS06. All weighted mean ages are given at 95% confidence level, whereas individual analyses are presented with 1σ error.

4.2. ID-TIMS U-Pb geochronology

A sample for ID-TIMS U-Pb geochronology was selected based on results from the SHRIMP dating and the highest number of identified baddeleyites in thin section. A block sample was first sawn from the field sample to remove weathering, then crushed, powdered and processed using a mineral-separation technique amended from Söderlund and Johansson (2002). Baddeleyite grains were handpicked under ethanol under a stereographic optical microscope and selected grains were cleaned with concentrated distilled HNO_3 and HCl. Due to the small size of the grains, no chemical separation methods were required.

Samples were spiked with a University of Western Australia in-house ^{205}Pb-^{235}U tracer solution, which has been calibrated against SRM981, SRM982 (for Pb), and CRM 115 (for U), as well as an externally-calibrated U-Pb solution (the JMM solution from the EarthTime consortium). This tracer is regularly checked using "synthetic zircon" solutions that yield U-Pb ages of 500 Ma and 2000 Ma, provided by D. Condon (BGS). Dissolution and equilibration of spiked single crystals was by vapour transfer of HF, using Teflon microcapsules in a Parr pressure vessel placed in a 200 °C oven for six days. The resulting residue was re-dissolved in HCl and H_3PO_4 and placed on an outgassed, zone-refined rhenium single filament with 5 µL of silicic acid gel. U–Pb isotope analyses were carried out using a Thermo Triton T1 mass spectrometer, in peak-jumping mode using a secondary electron multiplier. Uranium was measured as an oxide (UO_2). Fractionation and deadtime were monitored using SRM981 and SRM 982. Mass fractionation was 0.02 ± 0.07%/amu. Data were reduced and plotted using

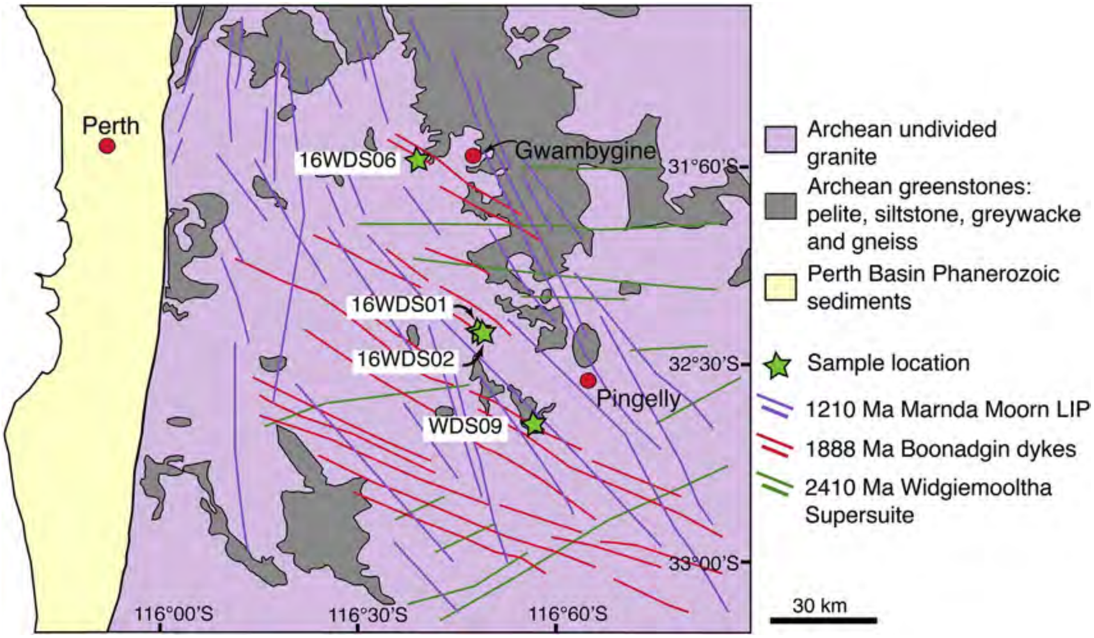

Fig. 2. Sampling locations. See Table 1 for detailed information.

Table 1
Sample locations.

Dyke ID	Dlat/Dlon	Samples	Comments
WDS09	32 39.339 S 116 57.132 E	WDS09M-N, WDS09RSA-B	NW trending dolerite dyke near West Pingelly
16WDS01	32 24.738 S 116 48.818 E	16WDS01A-D	NNW trending dolerite dyke west of Brookton, ridge
16WDS02	32 24.740 S 116 48.798 E	16WDS02A-D	NNW trending dolerite dyke west of Brookton. Same dyke as 16WDS01
16WDS06	31 59.973 S 116 39.699 E	16WDS06A-D	NW trending dyke near Talbot

Notes: Datum WGS84, Dlat = decimal latitude, Dlon = decimal longitude.

the software packages Tripoli (from CIRDLES.org) and Isoplot 4.15 (Ludwig, 2011). All uncertainties are reported at 2σ. U decay constants are from Jaffey et al. (1971). The weights of the baddeleyite crystals were calculated from measurements of photomicrographs and estimates of the third dimension. The weights are used to determine U and Pb concentrations and do not contribute to the age calculation. An uncertainty of ± 50% may be attributed to the concentration estimate.

4.3. Geochemistry

Slabs were sawn from block samples to remove weathering. After an initial crush, a small fraction of material was separated and chips with fresh fracture surfaces were handpicked under the microscope and pulverised in an agate mill for isotope analysis. Remaining material was pulverised in a low-Cr steel mill for major and trace element analysis.

Major element analysis was undertaken at Intertek Genalysis Laboratories in Perth, Western Australia using X-ray fluorescence (XRF) using the Geological Survey of Western Australia (GSWA) standard BB1 (Morris, 2007) and Genalysis laboratory internal standards SARM1 and SY-4. Trace element analysis was carried out at University of Queensland (UQ) on a Thermo XSeries 2 inductively coupled plasma mass spectrometer (ICP-MS) equipped with an ESI SC-4 DX FAST autosampler, following procedure for ICP-MS trace element analysis by Eggins et al. (1997) modified by the UQ Radiogenic Isotope Laboratory (Kamber et al., 2003). Sample solutions were diluted 4000 times and 12 ppb ^{6}Li, 6 ppb ^{61}Ni, Rh, In and Re, and 4.5 ppb ^{235}U internal spikes were added. USGS W2 was used as reference standard and crossed checked with BIR-1, BHVO-2 or other reference materials. All major element analyses have precision better than 5% and all trace element analyses have relative standard deviation (RSD) < 2%.

Rb-Sr and Sm-Nd isotope analyses were carried out at the University of Melbourne (e.g., Maas et al., 2005, 2015). Small splits (70 mg) of rock powders were spiked with ^{149}Sm-^{150}Nd and ^{85}Rb-^{84}Sr tracers, followed by dissolution at high pressure in an oven, using Krogh-type PTFE vessels with steel jackets. Sm, Nd and Sr were extracted using EICHROM Sr-, TRU- and LN-resin, and Rb was extracted using cation exchange (AG50-X8, 200–400 mesh resin). Isotopic analyses were carried out on a NU Plasma multi-collector ICP-MS coupled to a CETAC Aridus desolvation system operated in low-uptake mode. Raw data for spiked Sr and Nd fractions were corrected for instrumental mass bias by normalizing to ^{88}Sr/^{86}Sr = 8.37521 and ^{146}Nd/^{145}Nd = 2.0719425 (equivalent to ^{146}Nd/^{144}Nd = 0.7219), respectively, using the exponential law as part of an on-line iterative spike-stripping/internal normalization procedure. Sr and Nd isotope data are reported relative to SRM987 = 0.710230 and La Jolla Nd = 0.511860 and have typical in-run precisions (2sd) of ± 0.000020 (Sr) and ± 0.000012 (Nd). External precision (reproducibility, 2sd) is ± 0.000040 (Sr) and ± 0.000020 (Nd). External precisions for ^{87}Rb/^{86}Sr and ^{147}Sm/^{144}Nd obtained by isotope dilution are ± 0.5% and ± 0.2%, respectively.

5. Results

5.1. SHRIMP U-Pb geochronology

Seventeen analyses were obtained from thirteen baddeleyite grains (nine grains from WDS09, one grain from 16WDS01 and three grains from

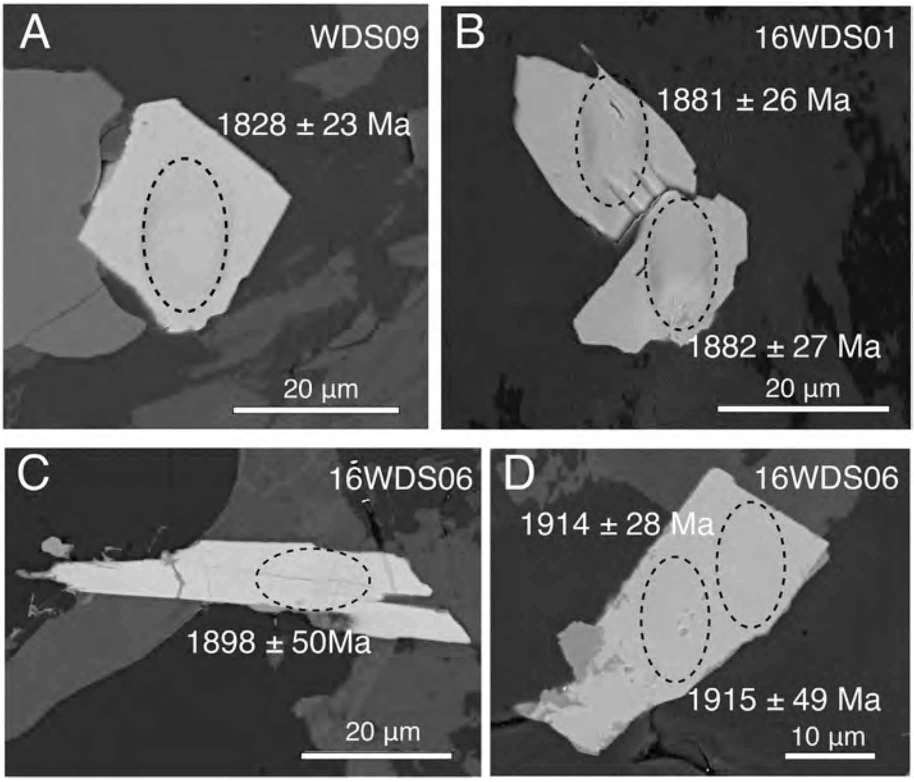

Fig. 3. SEM backscatter images showing SHRIMP baddeleyite spots and dates. (A) WDS09-2B (B) 16WDS01-372B (C) 16WDS06-405B (D) 16WDS06-406B.

Table 2
SHRIMP operating parameters.

Mount	CS16-1	CS16-6	CS16-7
Dykes analysed	WDS09, WDS09RS	16WDS01	16WDS06
Date analysed	21-Jul-16	14-Sep-16	6-Sep-16
Kohler aperture (µm)	50	50	50
Spot size (micrometres)	11	9	7
O_2^- primary current (nA)	0.9	0.6	0.2
Number of scans per analysis	8	8	8
Total number of analyses	23	32	34
Number of standard analyses	13	13	14
Pb/U external precision% (1σ)	1.00	1.00	1.00
Raster time (seconds)	120	180	180
Raster aperture (µm)	90	90	80

Notes: 1) Mass resolution for all analyses ≥5000 at 1% peak height; 2) BR266, OGC, Phalaborwa and NIST used as standards for each session; 3) Count times for each scan: ^{204}Pb, ^{206}Pb, ^{208}Pb = 10 s, ^{207}Pb = 30 s.

16WDS06) during three SHRIMP sessions (Fig. 4; detailed U-Pb data are given in Table 3). The analysed baddeleyites have low to moderate U concentrations varying from 47 to 449 ppm (median = 181 ppm) and low Th from 5 to 76 ppm, with Th/U ratios ranging from 0.02 to 0.47. Eight analyses were excluded based on their high common Pb (> 1% ^{206}Pb) and/or > 10% discordance. Sample WDS09 yielded a common Pb-corrected weighted mean ^{207}Pb/^{206}Pb date of 1858 ± 54 Ma (MSWD = 1.80, 4 analyses from 4 grains). If spot WDS09N5.29B-1, which is near-concordant (6% discordance) but contains slightly higher common Pb (1.45%) is included, the weighted mean is 1860 ± 41 Ma (MSWD = 1.4, n = 5). Two analyses on a single grain from 16WDS01 yield a ^{207}Pb/^{206}Pb weighted mean of 1881 ± 37 Ma (MSWD = 0.00075) and three analyses on 2 grains from 16WDS06 give a weighted mean of 1911 ± 42 Ma. Collectively, the 9 analyses on five baddeleyite grains from three samples give ^{207}Pb/^{206}Pb dates overlapping with each other within uncertainties; combining them yields a weighted mean of 1874 ± 25 Ma (MSWD = 1.3), which is interpreted as the best approximation of the crystallisation age of the dykes.

5.2. ID-TIMS U-Pb geochronology

Four baddeleyite crystals were analysed from sample WDS09 (Table 4, Fig. 5). Calculated weights are on the order of 0.1 µg, with low calculated U concentrations, all below 50 ppm. One grain has an apparently very low U content (3 ppm) and a concomitant low ^{206}Pb/^{204}Pb ratio of 30. This results in a relatively imprecise age determination and large analytical uncertainties for all data are the result of very low radiogenic Pb concentrations. Calculated U concentrations are unusually low for baddeleyite; this may reflect an overestimate of the grain weights, but the low Pb abundance (both radiogenic and common Pb) also implies a low initial U concentration. Th/U ratios are < 0.1, a typical value for baddeleyite. One datum is discordant but the coherence in ^{207}Pb/^{206}Pb age for all baddeleyite crystals supports our interpretation of the analyses representing a single magmatic crystallization age. The weighted-mean ^{207}Pb/^{206}Pb dates of the four single-crystal analyses is 1863 ± 50 Ma (2σ, MSWD = 0.24, n = 4), and the concordia age of the three concordant analyses is 1888.4 ± 8.8 Ma (2σ, decay-constant errors included).

5.3. Geochemistry

Due to limited age control, only three samples were available for geochemical analyses and clearly only preliminary conclusions about the geochemical characteristics of the dykes can be made based on these data. Two samples from WDS09 and one sample from 16WDS02 (same dyke as 16WDS01) were analysed for major and trace elements and for Sr and Nd isotopes. Data for the samples are presented together with major and trace element geochemistry from the 1210 Ma Marnda Moorn LIP dykes because the latter are the only known tholeiitic dyke swarm within the Yilgarn Craton with detailed studies available both in geochronology and geochemistry.

5.3.1. Major and trace elements

All samples have LOI < 1.0 wt% and display low MgO (6.18–6.73 wt%), SiO_2 (50.12–50.43 wt%), relatively high iron (FeO_{tot} = 14.10–15.09 wt%),

ARTICLE IN PRESS

Table 3
SHRIMP U-Pb data for baddeleyite from dyke samples WDS09, 16WDS01 and 16WDS6.

Spot	$f_{206\%}$	U ppm	Th ppm	Th/U	± %	Total $^{238}U/^{206}Pb$	± %	Total $^{207}Pb/^{206}Pb$	± %	$^{238}U/^{206}Pb^*$	± %	$^{207}Pb^*/^{206}Pb^*$	± %	$^{238}U/^{206}Pb^*$ Age (Ma) ± 1σ	$^{207}Pb^*/^{206}Pb^*$ Age (Ma) ± 1σ	Disc. %
WDS09N1.2B	0.40	206	5.0	0.024	1.0	3.15	1.2	0.1152	0.9	3.16	1.2	0.1117	1.3	1771 ± 19	1828 ± 23	+4
WDS09N5.38B-1	0.58	269	10.0	0.039	2.9	2.94	1.9	0.1213	0.8	2.96	1.9	0.1162	1.2	1877 ± 30	1899 ± 22	+1
WDS09RSB3.45B-1	0.72	449	76.0	0.174	7.3	2.80	1.5	0.1192	0.7	2.82	1.5	0.1129	1.3	1958 ± 25	1847 ± 23	−7
WDS09RSB1.54B-1	0.75	67	30.0	0.468	2.2	2.74	1.7	0.1196	1.5	2.76	1.7	0.1131	2.6	1994 ± 29	1849 ± 48	−9
16WDS6D.406B-1	0.08	247	23.5	0.098	1.0	2.9	1.7	0.118	1.4	2.9	1.7	0.117	1.5	1934 ± 29	1914 ± 28	−1
16WDS6D.406B-2	0.43	129	14.4	0.115	1.3	2.8	2.2	0.121	1.9	2.8	2.2	0.117	2.7	1944 ± 37	1915 ± 49	−2
16WDS6D.405B-1	0.67	251	23.9	0.098	3.9	3.0	1.8	0.122	1.7	3.1	1.8	0.116	2.8	1827 ± 29	1898 ± 50	+4
16WDS1C.372B-1	0.17	199	9.0	0.05	3.5	3.0	1.9	0.117	1.2	3.0	1.9	0.115	1.4	1870 ± 30	1881 ± 26	+1
16WDS1C.372B-2	0.07	181	6.0	0.03	2.7	2.9	1.9	0.116	1.4	2.9	1.9	0.115	1.5	1923 ± 32	1882 ± 27	−3
Excluded analyses																
WDS09N3.18B1	2.12	117	47.0	0.414	1.2	2.62	2.3	0.1379	1.8	2.67	2.3	0.1193	3.7	2050 ± 40	1946 ± 67	−6
WDS09N5.29B-1	1.45	131	8.0	0.064	3.8	3.06	2.6	0.1283	2.1	3.11	2.6	0.1156	3.3	1799 ± 42	1890 ± 60	+6
WDS09N3.21B-1	2.17	373	35.0	0.098	1.8	2.83	2.0	0.1386	0.7	2.90	2.0	0.1196	1.9	1912 ± 33	1950 ± 34	+2
WDS09N1.4B-1	0.53	97	8.0	0.082	1.1	2.57	1.6	0.1180	1.5	2.59	1.7	0.1134	2.3	2106 ± 30	1854 ± 42	−16
WDS09N1.3B-1	1.79	205	19.0	0.096	2.5	2.53	5.7	0.1401	1.4	2.58	5.7	0.1243	3.2	2113 ± 102	2019 ± 56	−5
WDS09RSB3.45B-2	3.08	178	73.0	0.425	4.2	2.28	3.9	0.1324	1.1	2.35	3.9	0.1057	3.8	2286 ± 75	1726 ± 70	−39
16WDS6D.401B-1	2.75	83	4.3	0.053	2.5	2.8	2.7	0.133	2.7	2.9	2.8	0.109	8.3	1937 ± 47	1779 ± 151	−10
16WDS6D.401B-2	2.15	47	5.9	0.129	2.3	2.3	5.9	0.124	3.7	2.3	6.0	0.105	10.1	2296 ± 116	1720 ± 185	−40

Notes: 1) f_{204} is the proportion of common Pb in ^{206}Pb, determined using the measured $^{204}Pb/^{206}Pb$ and a common Pb composition from the Stacey and Kramers (1975) model at the approximate age of the sample; 2) Disc. = 100(t$[^{207}Pb^*/^{206}Pb^*] - t[^{238}U/^{206}Pb^*]$)/t$[^{207}Pb^*/^{206}Pb^*]$.

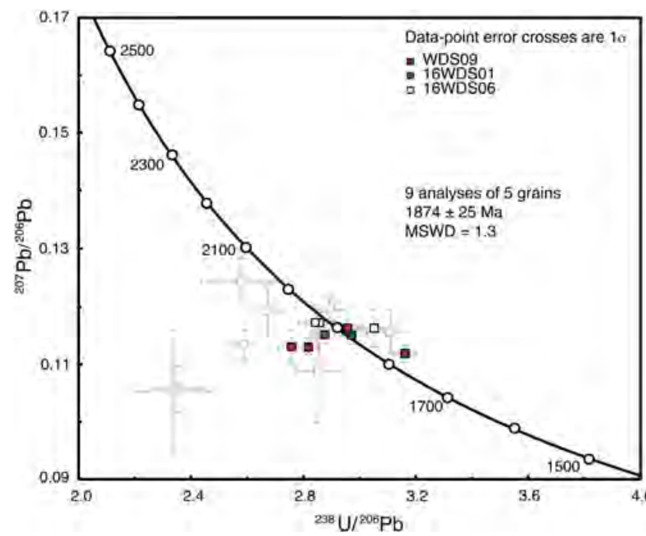

Fig. 4. Tera-Wasserburg plot of SHRIMP U-Pb baddeleyite results for samples WDS09, 16WDS01 and 16WDS06. Grey squares denote excluded data (see Section 5.1 for details).

normal to intermediate CaO (10.71–11.28 wt%) and slightly high Al_2O_3 (13.37–13.87 wt%) (Table 5). The samples have low total alkalis ($Na_2O + K_2O$ = 2.39–2.49 wt%) and high Na_2O/K_2O ratios (6.32–6.44), suggesting sodium enrichment. The Boonadgin samples are classified as sub-alkaline basalts on the TAS diagram (Fig. 6A) and belong to tholeiitic series on the AFM diagram (Fig. 6B), similar to Group 1 of the Marnda Moorn dykes (Wang et al., 2014). The chondrite normalised rare earth element (REE) distribution patterns are relatively flat (Fig. 6C) with slight enrichment of light REE (LREE), as evidenced by La_N/Yb_N = 1.48–1.57 and La_N/Sm_N = 1.18–1.26. The low Tb_N/Yb_N ratios (1.16–1.18) are similar to the average N-MORB (1.0; Sun and McDonough, 1989) and the primitive mantle-normalised trace element patterns show strong enrichment of Cs, Rb, U and Pb and a prominent negative Nb anomaly (Fig. 6D). With the exception of these fluid-mobile elements and the negative Nb anomaly, the studied samples displayed a relative flat trace element distribution patterns without significant enrichment or depletion in specific elements.

5.3.2. Nd and Sr isotopes

The same three samples were analysed for Nd and Sr isotopes (Table 5). Ratios of $^{147}Sm/^{144}Nd$ and $^{143}Nd/^{144}Nd$ are 0.1825–0.1848 and 0.512533–0.512562, respectively. The corresponding initial $\varepsilon Nd_{1.89Ga}$ values range from +1.3 to +1.6, suggesting a slightly depleted mantle component. The $^{87}Rb/^{86}Sr$ ratio ranges from 0.39999 to 0.5464, the $^{87}Sr/^{86}Sr$ ratio from 0.714588 to 0.716562, corresponding initial Sr isotopes of $(^{87}Sr/^{86}Sr)_i$ ratio varying from 0.70124 to 0.70391. The larger range of initial Sr isotope compositions is in contrast with the uniform initial Nd isotopes, and may reflect mobility of Rb. Therefore, the measured Sr isotope compositions of the studied samples may not accurately represent their primary signature.

6. Discussion

We have identified a previously unrecognized NNW-trending swarm of mafic dykes in the Yilgarn Craton, which, based on preliminary aeromagnetic interpretation, covers an area of ca. 33,000 km^2 in the southwestern part of the craton. However, until further sampling within the craton allows better delineation of the extent of the dykes, their designation as a swarm is preliminary. Emplacement of the Boonadgin dykes was synchronous with many 1890–1880 Ma LIPs worldwide, such as the Bastar-Cuddapah dykes in India (French et al., 2008; Belica et al., 2014), the Circum-Superior magmatism of the Superior Craton (Heaman et al., 1986; Halls and Heaman, 2000; Ernst and Bell, 2010), the Ghost-Mara dyke swarm of the Slave Craton (Buchan et al., 2010),

Table 4
ID-TIMS U-Pb data for baddeleyite from dyke WDS09.

Sample	wt. (μg)	U (ppm)	Pb_c (pg)	mol% Pb*	Th/U	$^{206}Pb/^{204}Pb$	$^{207}Pb/^{206}Pb$	± (%)	$^{207}Pb/^{235}U$	± (%)	$^{206}Pb/^{238}U$	± (%)	ρ	$^{206}Pb/^{238}U$ Age (Ma)	± (Ma)	$^{207}Pb/^{206}Pb$ Age (Ma)	± (Ma)
1	0.1	38	0.8	58	0.03	98	0.11340	7.20	4.6180	8.34	0.29534	1.23	0.94	1668.1	20.5	1854.7	130.1
2	0.2	3	0.4	19	0.13	30	0.11478	7.36	5.2167	10.50	0.32962	6.28	0.72	1836.5	115.4	1876.4	132.6
3	0.1	21	0.6	56	0.01	87	0.11311	3.78	5.2972	4.46	0.33966	1.05	0.71	1885.0	19.7	1850.0	68.4
4	0.2	36	0.8	59	0.07	104	0.11710	7.75	5.5091	9.03	0.34120	1.36	0.95	1892.4	25.8	1912.5	139.1

Notes: 1) All uncertainties given at 2σ; 2) ρ = error correlation coefficient of radiogenic $^{207}Pb/^{235}U$ vs. $^{206}Pb/^{238}U$; 3) Pb_c = Total common Pb including analytical blank (0.8 ± 0.3 pg per analysis); 4) Blank composition is: $^{206}Pb/^{204}Pb$ = 18.55 ± 0.63, $^{207}Pb/^{204}Pb$ = 15.50 ± 0.55, $^{208}Pb/^{204}Pb$ = 38.07 ± 1.56 (all 2σ), and a $^{206}Pb/^{204}Pb$–$^{207}Pb/^{204}Pb$ correlation of 0.9. 5) Th/U calculated from radiogenic $^{208}Pb/^{206}Pb$ and age of 1.88 Ga; 6) Sample weights are calculated from crystal dimensions and are associated with as much as 50% uncertainty (estimated); 7) Measured isotopic ratios corrected for tracer contribution and mass fractionation (0.02 ± 0.06%/amu); 8) Ratios involving ^{206}Pb are corrected for initial disequilibrium in $^{230}Th/^{238}U$ using Th/U = 4 in the crystallization environment.

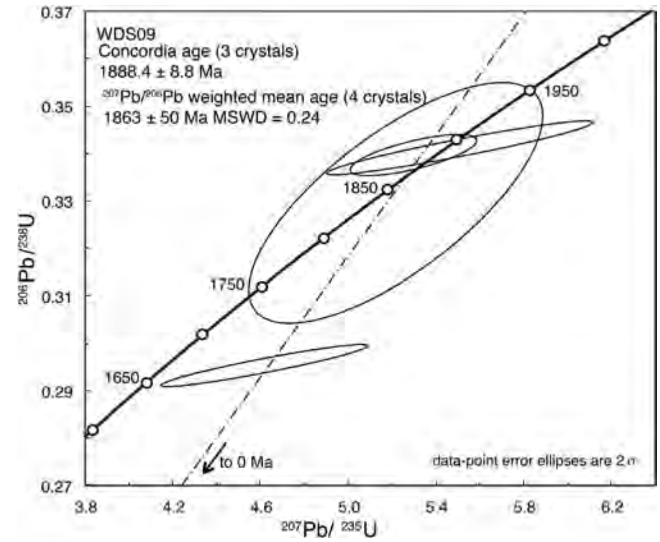

Fig. 5. Concordia plot for analysed baddeleyite ID-TIMS U-Pb results from sample WDS09.

the Uatuma dyke swarm of the Amazonian Craton (Klein et al., 2012; Antonio et al., 2017) and the Mashonaland sill province of the Zimbabwe Craton (Söderlund et al., 2010), the Soutpansperg sill province (Hanson et al., 2004) and the Black Hills dyke swarm (Olsson et al., 2016) of the Kaapvaal Craton. In the following sections, we discuss the emplacement of the dykes within the regional tectonic setting, coeval magmatism elsewhere in the region, and the implications for a recently proposed tectonic reconstruction, which raises the possibility that the dykes may be associated with the Bastar-Cuddapah LIP in India.

6.1. Coeval magmatism in Australia

No other mafic magmatism within uncertainty of the 1888 ± 9 Ma age for the Boonadgin dyke swarm is currently known in the WAC or elsewhere in Australia. However, felsic tuffs from a succession of granular iron formation (GIF) in the Frere Formation in the Earaheedy Basin have been dated at 1891 ± 8 Ma and 1885 ± 18 Ma, and linked to voluminous mantle input from an oceanic mafic source during a major global episode of mantle upwelling and crustal growth (Rasmussen et al., 2012). Evidence of synchronous magmatism elsewhere in the Capricorn Orogen is limited to a 1900 Ma zircon population peak from the Chiall Formation in the upper sequence of the Earaheedy Basin (Halilovic et al., 2004).

Ameen and Wilde (2006) reported WSW-trending mafic dykes with a zircon SHRIMP U-Pb age of 1852 ± 12 Ma from the Yalgoo greenstone belt in the Youanmi Terrane in the northwestern Yilgarn Craton (Fig. 1), ca. 360 km NNE of Perth and ca. 350 km north of sample 16WDS06. Their emplacement suggests a further episode of lithospheric extension ca. 35 Ma after the Boonadgin dykes. The WSW orientation of the Yalgoo dykes may reflect a change in the regional stress field, the influence of local crustal architecture, or a change in the position of plume centre. There is limited, but suggestive, evidence of magmatism within the Capricorn Orogen coeval with the Yalgoo dykes. The age of the Yalgoo dykes is within uncertainty of an 1842 ± 5 Ma detrital zircon population from the Leake Spring Metamorphics, a predominantly siliciclastic sequence within the northern Gascoyne Province (Sheppard et al., 2010b) and a ca. 1860 Ma detrital zircon population from turbidites in the Ashburton Basin (Sircombe, 2002).

The temporally closest mafic magmatism in the North Australian Craton (NAC) consist of the predominantly mafic volcanic rocks of the Biscay Formation in the Halls Creek Orogen in northwestern Australia, which yielded a U-Pb zircon age of 1880 ± 3 Ma (Blake et al., 1999). The Woodward Dolerite, which comprises sills intruding the succession,

Table 5
Major, trace element and isotope data for samples WDS09M, WDS09N and 16WDS02A.

	WDS09M	WDS09N	16WDS02A		WDS09M	WDS09N	16WDS02A
SiO_2	49.68	50.42	49.91	Sm (ppm)	2.43	3.13	2.90
TiO_2	1.14	1.31	1.25	Nd (ppm)	7.93	10.37	9.54
Al_2O_3	13.75	13.42	13.26	$^{143}Nd/^{144}Nd$	0.512558	0.512533	0.512562
CaO	10.65	10.71	11.19	$^{147}Sm/^{144}Nd$	0.1848	0.1825	0.1837
Fe_2O_3(tot)	14.53	15.09	14.29	$(^{143}Nd/^{144}Nd)_i$	0.510260	0.510263	0.510278
K_2O	0.32	0.34	0.32	εNd(t)	1.3	1.3	1.6
MgO	6.67	6.18	6.59	Rb (ppm)	18.13	22.04	15.39
MnO	0.23	0.24	0.23	Sr (ppm)	102.10	116.80	111.40
Na_2O	2.05	2.15	2.06	$^{87}Rb/^{86}Sr$	0.514200	0.546400	0.399900
P_2O_5	0.095	0.119	0.108	$^{87}Sr/^{86}Sr$	0.716562	0.715838	0.714588
LOI	0.69	0.03	0.54	$(^{87}Sr/^{86}Sr)_i$	0.702820	0.701240	0.703910
Total	99.81	100.01	99.75				
Mg#	51.22	48.36	51.33		BCR-2	JND-1	
Sc	45.80	46.80	47.80	$^{143}Nd/^{144}Nd$	0.512637	0.512112	
V	302.00	310.00	315.00		0.512640	0.512117	
Co	55.30	56.90	57.70		0.512623	0.512102	
Ni	87.60	121.00	87.70		0.512633		
Ga	16.40	17.40	16.60	$^{87}Sr/^{86}Sr$	0.704987		
Ge	542.00	559.00	556.00		0.705013		
Rb	17.50	22.50	18.30				
Sr	110.00	120.00	115.00				
Y	22.60	28.40	26.70				
Zr	59.00	80.50	72.40				
Nb	3.11	4.07	3.67				
Cs	0.56	1.02	0.19				
Ba	53.90	59.40	56.80				
La	4.92	6.04	5.42				
Ce	11.90	15.00	13.10				
Pr	1.75	2.20	2.00				
Nd	8.35	10.50	9.61				
Sm	2.53	3.18	2.96				
Eu	0.96	1.12	1.05				
Gd	3.27	4.09	3.80				
Tb	0.58	0.73	0.68				
Dy	3.79	4.73	4.45				
Ho	0.83	1.05	0.98				
Er	2.37	2.94	2.77				
Tm	0.35	0.45	0.42				
Yb	2.25	2.85	2.62				
Lu	0.34	0.42	0.39				
Hf	1.63	2.19	2.00				
Ta	0.21	0.28	0.25				
Pb	2.99	3.62	1.75				
Th	0.83	1.05	0.91				
U	0.30	0.38	0.30				

Notes: 1)Major elements (XRF) are given in wt% and trace elements (ICP-MS) in ppm; 2) Mg# = 100 × Mg/(Mg + Fe), Fe^{2+}/Fe_{total} = 0.85; 3) Crystallisation age t = 1890 Ma; 4) typical internal precision (2σ) is ± 0.000015 for $^{87}Sr/^{86}Sr$ and ± 0.000014 for $^{143}Nd/^{144}Nd$; 5) Recent isotope dilution analyses for USGS basalt standard BCR-2 average 6.41 ppm Sm, 28.02 ppm Nd, $^{147}Sm/^{144}Nd$ 0.1381 ± 0.0004 and $^{143}Nd/^{144}Nd$ 0.512635 ± 0.000023 (n = 6, ± 2sd); 46.5 ppm Rb, 337.6 ppm Sr, $^{87}Rb/^{86}Sr$ 0.3982 ± 0.0010, $^{87}Sr/^{86}Sr$ 0.704987 ± 0.000015 (n = 1, ± 2se). These results are consistent with TIMS and MC-ICPMS reference values. ε_{Nd} values are calculated relative to a modern chondritic mantle (CHUR) with $^{147}Sm/^{144}Nd$ = 0.1960 and $^{143}Nd/^{144}Nd$ = 0.512632 (Bouvier et al., 2008). Age-corrected initial ε_{Nd} and $^{87}Sr/^{86}Sr$ have propagated uncertainties of ± 0.5 units and ≤ ± 0.00010 (assuming an age uncertainty of ± 5 Ma), respectively. Decay constants are ^{87}Rb 1.395E^{-11}/yr and ^{147}Sm 6.54E^{-12}/yr.

has maximum and minimum ages, respectively, of ca. 1847 Ma and 1808 Ma (Blake et al., 1997) and its emplacement age is thus closer to the Yalgoo dykes. However, the Halls Creek bimodal volcanism has been associated with convergence of two cratons unrelated to the West Australian Craton, and pre-dates amalgamation of the West Australian Craton with other cratons (Bagas, 2004; Cawood and Korsch, 2008).

6.2. Tectonic and magmatic events in the WAC at ca. 1890 Ma

The Boonadgin dyke swarm was emplaced into the western margin of the WAC, about 60 million years after the WAC was assembled along the Capricorn Orogen during the Glenburgh Orogeny at 2005–1950 Ma (Sheppard et al., 2004, 2010a; Johnson et al., 2011). Following amalgamation of the WAC, the Capricorn Orogen was the site of episodic intracontinental reworking and reactivation for more than one billion years (Cawood and Tyler, 2004b; Sheppard et al., 2010a; Johnson et al., 2011). At the time the Boonadgin dykes were emplaced, the WAC was under a period of tectonic quiescence. The ca. 1891–1885 Ma felsic volcanic rocks in the Earaheedy Basin (Rasmussen et al., 2012) were emplaced during limited rifting and suggest that at least the eastern part of the Capricorn Orogen underwent lithospheric extension at this time (Sheppard et al., 2016).

Emplacement of the NW-trending Boonadgin dykes indicates regional SW-NE oriented lithospheric extension, which is consistent with direction of coeval extension within the NW-trending Earaheedy basin. In aeromagnetic images the dykes are linear, appear to have a single magnetic polarity and extend across the southwestern craton before being apparently truncated by the Darling Fault in the west and by the Albany-Fraser Orogen in the south. The orientation of the dykes is roughly parallel to the regional NW-SE tectonic grain imparted by terrane accretion during the Archean (Middleton et al., 1993; Wilde et al., 1996; Dentith and Featherstone, 2003) and suggests that they intruded along existing crustal weaknesses controlled by a regional stress field (Hou et al., 2010; Hou, 2012; Ju et al., 2013). A seismic

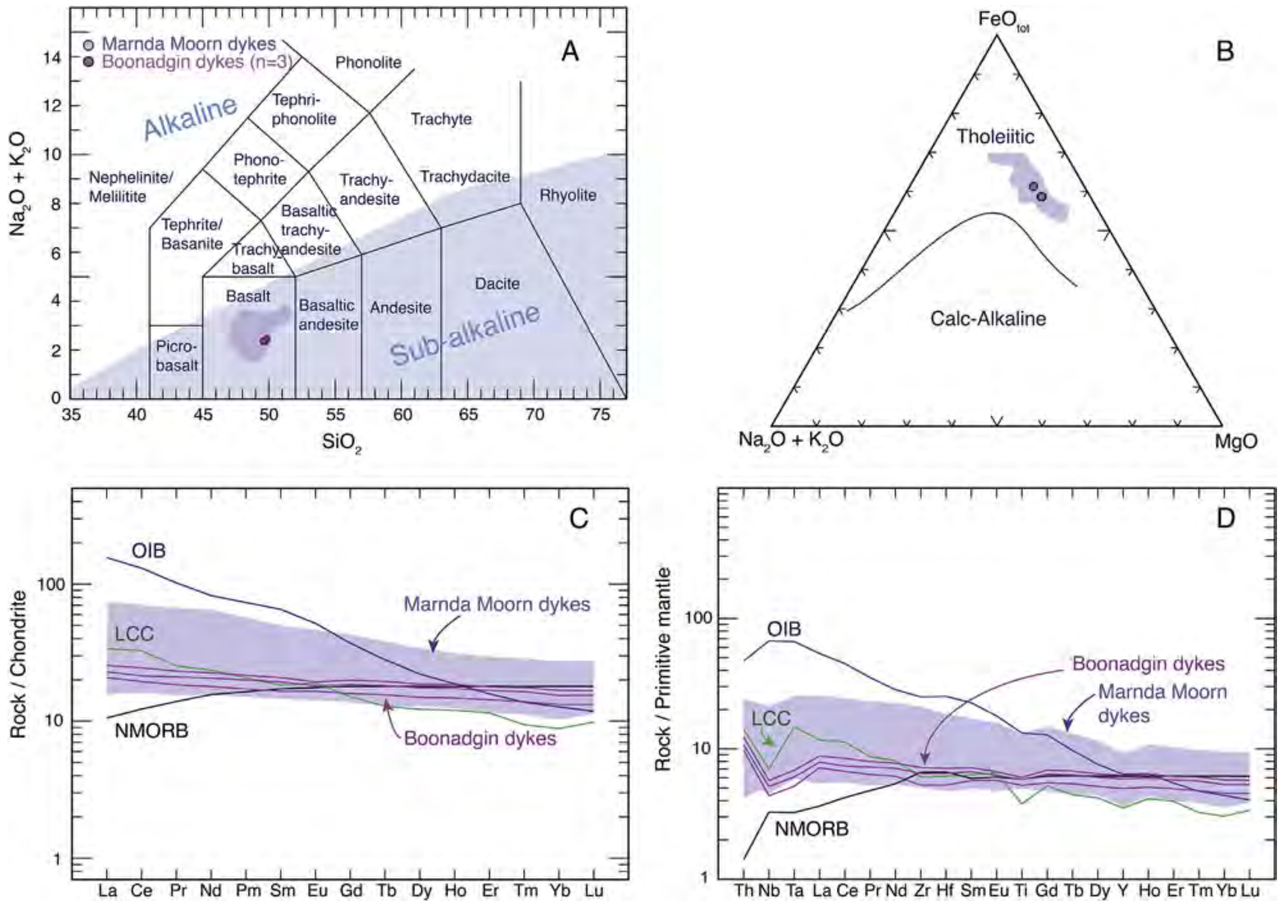

Fig. 6. (A) Total alkali-silica (TAS) plot after Le Maitre et al., 1989. Blue dots are Marnda Moorn group 1 dykes from Wang et al. (2014). (B) AFM plot after Irvine and Baragar, 1971. (C) Chondrite and (D) primitive mantle normalised multi-element plots for Boonadgin and Marnda Moorn group 1 dykes (Wang et al., 2014). LCC = lower continental crust after Rudnick and Gao (2003); OIB = ocean island basalt and NMORB = mid ocean ridge basalt after Sun and McDonough (1989). (For interpretation of the references to color in this figure legend, the reader is referred to the web version of this article.)

survey south of sample WDS09 identified a ca. 20° NE-dipping high-velocity zone, which was interpreted to represent a mafic-ultramafic body in the lower crust at ca. 30 km depth; this may be either a possible conduit for mafic magma that intruded along the suture, a zone of intrusions, or a fault-bounded terrane of possible oceanic affinity (Dentith et al., 2000; Dentith and Featherstone, 2003).

No direct Paleoproterozoic record along the western margin of Yilgarn Craton has been preserved due to younger orogenic and rifting events and it is uncertain whether it was an active plate boundary when the Boonadgin dykes were emplaced. Along the southern margin of the craton, the only known event coeval with emplacement of the Boonadgin dyke swarm could be deposition of the Stirling Range Formation in the Paleoproterozoic Barren Basin in the western Albany-Fraser Orogen. The Barren Basin comprises structural remnants of a much larger basin system deposited in an intra-continental rift or back-arc setting (Clark et al., 2000; Spaggiari et al., 2011, 2014, 2015). Formation age of the basin is unclear, but detrital zircon and monazite dating suggests that it is younger than ca. 2016 Ma and possibly formed at ca. 1895 Ma (Rasmussen and Fletcher, 2002; Rasmussen et al., 2004). Given the uncertainty of timing of early rifting in the southwest, it is difficult to link emplacement of the Boonadgin dykes with any tectonic events adjacent to the southwestern part of the craton.

6.3. Source of the Boonadgin dykes

Ratios of incompatible trace elements sensitive to source composition and partial melting effects but insensitive to crystal fractionation can be used to investigate mantle source characteristics. Zirconium can be used to evaluate mobility of major and trace elements during alteration and metamorphism (e.g., Polat et al., 2002). The Nb, Ta, Hf, Th and REE concentrations in the samples show good correlation with Zr (not shown) suggesting that these elements represent the primary composition of the dykes. The primitive mantle-normalised profile of the Boonadgin dykes (Fig. 6D; Table 5) is remarkably similar to that of the lower continental crust (LCC; Rudnick and Gao, 2003) with average ratios of Nb/La = 0.66, Th/Nb = 0.26 and Ce/Pb = 5.20 (0.63, 0.24 and 5.0, respectively for LCC). Ratios of La/Sm = 1.89 and Sm/Nd = 0.30 are near-chondritic (1.55 and 0.33, respectively; Sun and McDonough, 1989) and close to the Marnda Moorn Group 1 dykes (ca. 1.70 and 0.28, respectively). The ratio of Nb/Ta = 14.75 is much higher than the lower crust (8.33) but close to that of depleted mantle (ca. 15; Salters and Stracke, 2004) and Marnda Moorn Group 1 dykes (ca. 15; Wang et al., 2014). The ratio of Zr/Sm = 24.36 is similar to the lower crust (ca. 24) and much lower than depleted mantle (ca. 29).

The similarity of the trace element compositions of the studied samples to the average value of lower continental crust suggests the possibility of lower continental crust contamination. We conducted preliminary binary mixing modelling (Depaolo, 1981) using data from the three Boonadgin dykes samples. If the primary melt had a N-MORB-like trace element composition and $\varepsilon Nd_{1.9Ga} = +8$, incorporating 20–30% of mafic lower continental crust ($\varepsilon Nd_{1.9Ga} = -10$, estimated by Nd isotope mapping of the Yilgarn (Champion, 2013) and the method proposed by Depaolo (1981) into the primary melt can produce the observed Nd isotope and trace element compositions. The lack of prominent fractionation of HREE indicates that partial melting likely occurred within the spinel stability field (at < 70 km depth). If this is correct, the sub-continental lithospheric mantle (SCLM) beneath the margin of the Yilgarn Craton may have been largely removed or thinned. This could be attributed to lithospheric extension, consistent with basin formation along the southern margin of the craton (Section 6.2).

Another possible mechanism to produce the observed trace element compositions and slightly depleted Nd isotope signature is via melt-rock interaction with asthenospheric mantle. Because lower continental crust can founder into the convecting mantle (e.g., Gao et al., 2004), melts derived from recycled lower continental crust could interact with the ambient peridotite to form enriched pyroxenitic lithologies (Sobolev et al., 2005, 2007; Wang et al., 2014), imparting a lower continental crust signature and a slightly depleted Nd isotope signature on the resultant melts.

6.4. Was the WAC connected to other cratons at ca. 1890 Ma?

The position of WAC in Paleoproterozoic reconstruction models is highly debated partly due to the absence of robust paleomagnetic and high precision geochronological data for dyke swarms. For example, the WAC has been placed near India (Rogers and Santosh, 2002; Zhao et al., 2002; Mohanty, 2012, 2015), Kaapvaal and Zimbabwe Cratons (Zhao et al., 2002; Hou et al., 2008; Belica et al., 2014), or Siberia (Hou et al., 2008; Belica et al., 2014) in reconstructions for various Paleoproterozoic time intervals. Halls et al. (2007) used paleomagnetic data to argue that India and Australia were at high paleolatitudes but ~2000 km apart at ca. 2400–2350 Ma. Similarly, Mohanty (2012, 2015) proposed a juxtaposition of the western margin of the WAC and the eastern margin of the Bastar-Dharwar craton at ca. 2400–2300 Ma (the South India-Western Australia SIWA supercraton; Fig. 7) based on paleomagnetic data, synchronous mafic magmatism and matching dyke orientation but their relative positions by ca. 1900 Ma were unknown. Mohanty (2012, 2015) nonetheless noted that the lack of 2.0–1.8 Ga dykes in the Yilgarn Craton implies that the breakup of SIWA must have taken place during an earlier rifting event. Our discovery of the 1888 Ma Boonadgin dykes in the Yilgarn Craton makes such an early breakup unnecessary. With such a configuration at 1890 Ma, NE-SW extension and emplacement of the NW-oriented 1888 Ma Boonadgin dykes in the Yilgarn Craton is synchronous with E-W extension initiating the Cuddapah Basin and the associated 1890 Ma NW-oriented mafic dykes and ultramafic magmatism in the Dharwar Craton (Anand, 2003; French et al., 2008), as well as the emplacement of NW-oriented dykes in the Bastar Craton (French et al., 2008) as segments of a single radiating dyke swarm.

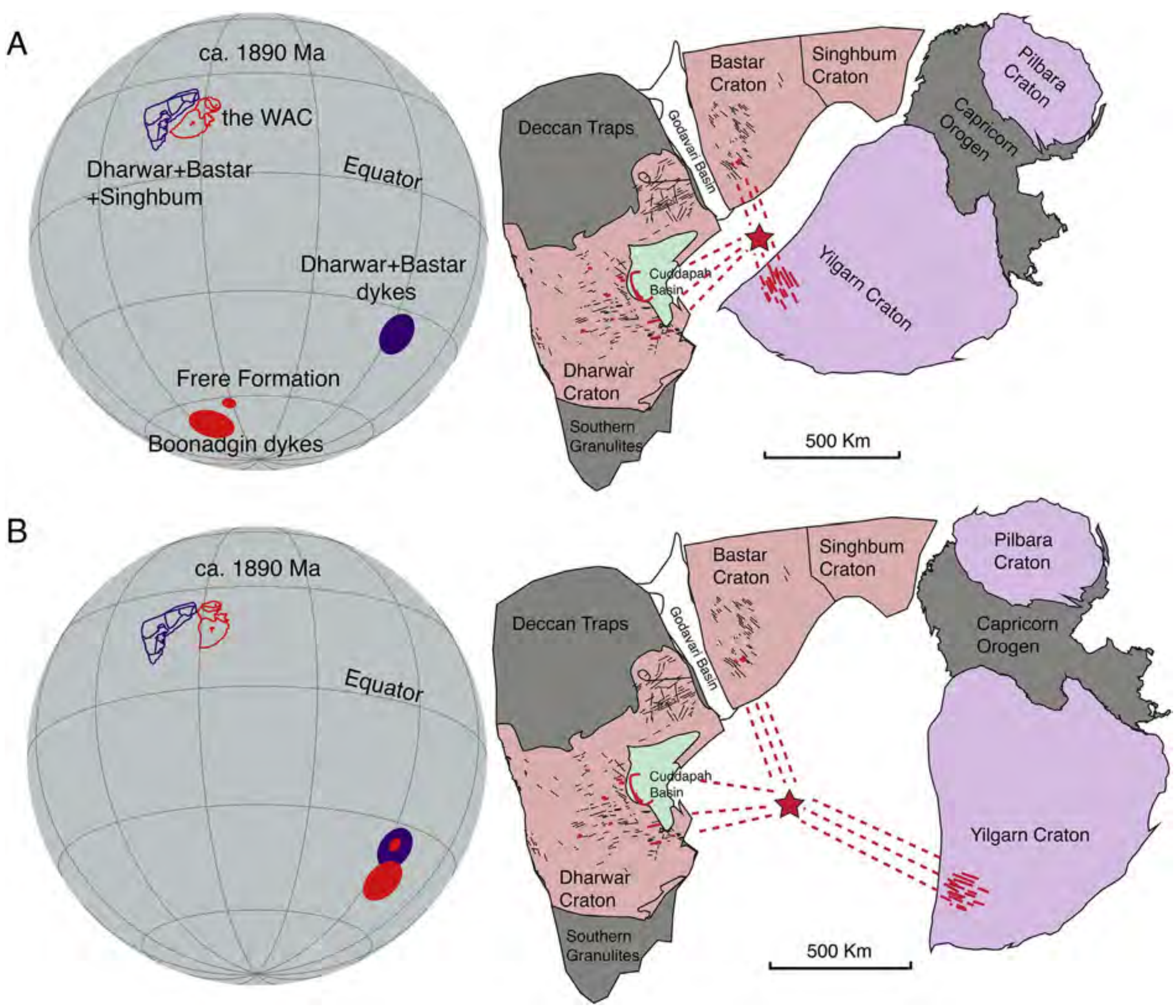

Fig. 7. Possible configurations of the WAC and Dharwar, Bastar and Singhbum cratons tested with paleomagnetic data at ca. 1890 Ma. Coeval paleopoles are plotted on the left-hand side and color coded with the respective cratons. The WAC was rotated to the Indian coordinates and more detailed reconstructions are shown on the right side. Indian dykes shown in red have been dated with U-Pb or Ar-Ar methods at 1879–1894 Ma (Chatterjee and Bhattacharji, 2001; Halls et al., 2007; French et al., 2008; Belica et al., 2014). Black undated dykes in India are modified after French et al. (2008) and Srivastava and Gautam (2015). Red star denotes possible location of a mantle plume. (A) SIWA configuration modified from ca. 2400 Ma reconstruction of Mohanty (2012); (B) Alternative configuration of Liu et al. (this issue) supported by paleomagnetic data. (For interpretation of the references to color in this figure legend, the reader is referred to the web version of this article.)

Liu et al. (this issue) obtained a high quality paleomagnetic pole from the Boonadgin dykes and used available robust paleomagnetic data to test the SIWA connection and other possible configurations. The new Boonadgin dyke pole falls close to the Frere Formation (Capricorn Orogen) pole of Williams et al. (2004), which has been considered to be 1891–1885 Ma in age (e.g., Antonio et al., 2017; Klein et al., 2016) based on zircon data from tuffs within the basal Frere Formation (Rasmussen et al., 2012). However, Williams et al. (2004) sampled the upper part of the formation, implying that the actual magnetization age for their Frere Formation pole is likely younger than 1885 Ma. Consequently, Liu et al. (this issue) suggest that the ca. 1890 Ma Boonadgin pole is coeval with the 1888–1882 Ma Dharwar-Bastar pole (Belica et al., 2014) and that the age difference between the Boonadgin and the < 1885 Ma Frere Formation poles may explain the slight difference in their positions. The Boonadgin and Dharwar-Bastar dyke poles are about 50° apart after restoration of the two continental blocks to the SIWA configuration (Fig. 7A), indicating that the SIWA fit is invalid at ca. 1890 Ma. In contrast, an alternative configuration juxtaposing the northern WAC (Pilbara) and north-eastern India (Singhbhum) is not only consistent with paleomagnetic data (Fig. 7B), but still allows the contemporaneous mafic dykes in India and the WAC to form a radiating dyke swarm. If this interpretation is correct, the 1888 Ma Boonadgin dykes in the Yilgarn Craton may be part of the Bastar-Cuddapah LIP event (French et al., 2008; Belica et al., 2014).

6.5. *Could the Boonadgin dyke swarm be part of the Bastar-Cuddapah LIP?*

Abundant, predominantly NW-SE to NNW-ESE oriented 1890–1880 Ma Bastar-Cuddapah LIP dykes intrude the Bastar and Dharwar cratons and form a radiating dyke swarm over at least 90,000 km^2 (Anand, 2003; Halls et al., 2007; French et al., 2008; Belica et al., 2014). In the southern Bastar Craton, BD2 dykes are oriented predominantly NW-SE to WNW-ESE (French et al., 2008). In the Dharwar craton, baddeleyite from the Pulivendla sill in the Cuddapah basin yielded an ID-TIMS $^{207}Pb/^{206}Pb$ age of 1885 ± 3 Ma (French et al., 2008) and paleomagnetic data suggest that dykes of this age also have NW-SE, E-W and NE-SW orientations depending on their location within the craton (Halls et al., 2007; Belica et al., 2014). The NW-trending dykes appear to be sub-parallel to the regional Archean structural grain in both the Bastar and Dharwar cratons, suggesting that they may have intruded along pre-existing faults and fabrics (Crookshank, 1963; Chatterjee and Bhattacharji, 2001). New SHRIMP U-Pb dating of felsic tuffs from the lowermost succession of the Cuddapah Basin, the Tadpatri Formation, yielded ca. 1864 Ma and ca. 1858 Ma, and mafic-ultramafic sills intruding this stratigraphic level (and higher) indicate that mafic magmatism continued until after ca. 1860 Ma (Sheppard et al., 2017). Dykes of < 1900 Ma age are present in both Bastar and Dharwar Cratons but their ages are currently either poorly constrained or unknown (Murthy, 1987; Mallikharjuna et al., 1995; Meert et al., 2010), making any comparison highly speculative.

Extensive coeval mafic magmatism and intracontinental rifting in the Dharwar Craton at ca. 1899–1885 Ma have been linked to a mantle plume beneath India or east of the Cuddapah Basin (Ernst and Srivastava, 2008; Belica et al., 2014; Mishra, 2015), or to passive rifting associated with a short lived global mantle upwelling (Anand, 2003; French et al., 2008). Two models have been proposed for formation of the Cuddapah Basin, one arguing for failed rifting (Chaudhuri et al., 2002) and another for full rifting and opening of an ocean basin (Kumar and Leelanandam, 2008; Kumar et al., 2010). Dasgupta et al. (2013) proposed that formation of the Cuddapah Basin at ca. 1890 Ma was associated with continental rifting between India and another craton. If this was the WAC, no evidence of equivalent basins is preserved on the western or southern margin of the Yilgarn Craton.

In contrast to the Boonadgin dykes, the Cuddapah sills are more enriched and contain a more significant melt component from the Archean lithosphere, with La_N/Sm_N ratios between 1.4 and 2.5, La_N/Yb_N ratios between 2.4 and 4.3 (1.18–1.26 and 1.48–1.57 for Boonadgin dykes, respectively) and $\varepsilon Nd_{1.89Ga}$ values between +1 and −10 (+1.3 to +1.6 for Boonadgin dykes) (Anand, 2003). Modelling of the Cuddapah sills suggests that they were produced by 15–20% partial melting of a lherzolitic mantle with a potential temperature of ~1500 °C, similar to ambient mantle of similar age and not necessarily indicative of a mantle plume (Anand, 2003). Current geochemical evidence is insufficient to determine whether the Boonadgin dykes and the Bastar-Cuddapah LIP are associated with the same mantle source.

Similar to the Yilgarn Craton where the Boonadgin and Yalgoo dykes are interpreted to be associated with discrete episodes of lithospheric extension, sills intruding the unconformity-bound sedimentary successions within the Cuddapah basin are coeval with episodes of lithospheric extension (Sheppard et al., 2017) In both cases, mafic magmatism appears to span 35–40 Ma (ca. 1890–1855 Ma) rather than comprising a short-lived event.

7. Conclusions

The Archean Yilgarn Craton in Western Australia is intruded by multiple generations of Precambrian mafic dykes, identified by previous studies. Until now, evidence for mafic magmatism in the Yilgarn Craton at ca. 1890 Ma has been absent, surprising since mafic magmatism of this age is found on most other Precambrian cratons worldwide. The newly named, NW-trending 1888 Ma Boonadgin dyke swarm is interpreted to extend across an area of at least 33,000 km^2 in the southwestern Yilgarn Craton. The dykes were emplaced along the southwestern margin of the Yilgarn Craton more than 50 million years after it was amalgamated with the Pilbara Craton-Glenburgh Terrane along the Capricorn Orogen to form the West Australian Craton. Intrusion of the Boonadgin dyke swarm was synchronous with minor rifting, felsic volcanism and deposition of granular iron formation in the Earaheedy Basin at the southeastern end of the Capricorn Orogen. Evidence for another pulse of mafic magmatism at ca. 1852 Ma in the northern Yilgarn Craton was also coeval with magmatism in the Capricorn Orogen, suggesting that mafic magmatism spanned at least 35 million years. Emplacement of the Boonadgin dyke swarm is contemporaneous with the Bastar-Cuddapah LIP and opening of the Cuddapah Basin on the eastern margin of India, and the ca. 1852 Ma Yalgoo dykes in northern Yilgarn may be coeval with ca. 1860 mafic magmatism in the Cuddapah basin. Moreover, existing studies and recent paleomagnetic data suggest that the Yilgarn and Bastar-Cuddapah cratons were adjacent to each other at c. 1890 Ma, raising the possibility that the Boonadgin dyke swarm may be part of a wider Bastar-Cuddapah LIP. However, Meso- to Neoproterozoic orogenic activity and Phanerozoic rifting along the western margin in the Yilgarn Craton have obliterated stratigraphic successions equivalent to the Cuddapah Basin, and poor age control of extension and initial rifting in southern Yilgarn Craton do not provide reliable geological piercing points. In contrast to proposed rifting of the Yilgarn Craton from India at ca. 2300 Ma, new evidence presented in this paper suggests that the cratons may still have been neighbours at 1890 Ma.

Acknowledgments

This work was funded by ARC Centre for Core to Crust Fluid Systems CoE Grant (CE110001017) and ARC Laureate Fellowship Grant (FL150100133) to Z.-X.L. JCS gratefully acknowledges support by Curtin University ORD Postgraduate Scholarship. We thank Cristina Talavera and Hao Gao for their invaluable support with SHRIMP U-Pb analyses at John de Laeter Centre, Curtin University. Roland Maas and Nenping Shen are thanked for their valuable assistance with geochemical analyses and Louise Heyworth for her help with sample preparation at UWA. We thank Larry Heaman and Michiel de Kock for their constructive and helpful reviews that greatly improved the manuscript.

References

Ameen, S.M.M., Wilde, S.A., 2006. Identification of 1.85 Ga mafic dykes in the Northern Yilgarn Craton: a relationship to the Columbia supercontinent? IAGR Annu. Conv. Int. Symp., 2006.
Anand, M., 2003. Early Proterozoic melt generation processes beneath the Intra-cratonic Cuddapah Basin, Southern India. J. Petrol. 44, 2139–2171. http://dx.doi.org/10.1093/petrology/egg073.
Anand, R.R., Paine, M., 2002. Regolith geology of the Yilgarn Craton, Western Australia: implications for exploration. Aust. J. Earth Sci. 49, 3–162.
Antonio, P.Y.J., D'Agrella-Filho, M.S., Trindade, R.I.F., Nédélec, A., de Oliveira, D.C., da Silva, F.F., Roverato, M., Lana, C., 2017. Turmoil before the boring billion: paleomagnetism of the 1880–1860 Ma Uatumã event in the Amazonian craton. Gondwana Res. 49, 106–129.
Bagas, L., 2004. Proterozoic evolution and tectonic setting of the northwest Paterson Orogen, Western Australia. Precambr. Res. 128, 475–496. http://dx.doi.org/10.1016/j.precamres.2003.09.011.
Belica, M.E., Piispa, E.J., Meert, J.G., Pesonen, L.J., Plado, J., Pandit, M.K., Kamenov, G.D., Celestino, M., 2014. Paleoproterozoic mafic dyke swarms from the Dharwar craton; paleomagnetic poles for India from 2.37 to 1.88 Ga and rethinking the Columbia supercontinent. Precambr. Res. 244, 100–122. http://dx.doi.org/10.1016/j.precamres.2013.12.005.
Blake, D.H., Tyler, I.M., Sheppard, S., 1997. Geology of the Ruby Plains 1:100 000 Sheet Area (4460), Western Australia. Australian Geological Survey Organisation.
Blake, D.H., Tyler, I.M., Griffin, T.J., Sheppard, S., Thorne, A.M., Warren, R.G., 1999. Geology of the Halls Creek 1:100 000 Sheet Area (4461), Western Australia. Aust. Geol. Surv. Organ., Canberra.
Bleeker, W., Ernst, R., 2006. Short-lived mantle generated magmatic events and their dyke swarms: the key unlocking Earth's paleogeographic record back to 2.6 Ga. In: Hanski, E.J., Mertanen, S., Rämö, O.T., Vuollo, J. (Eds.), Dyke Swarms—Time Markers of Crustal Evolution: Selected Papers of the Fifth International Dyke Conference in Finland, Rovaniemi, Finland, 31 July–3 August 2005 & Fourth International Dyke Conference, Kwazulu-Natal, South Africa 26–29 June 2001. CRC Press, London, pp. 3–26.
Boyd, D.M., Tucker, D.H., 1990. Australian magnetic dykes. In: Parker, A.J., Rickwood, P.C., Tucker, D.H. (Eds.), Mafic Dykes and Emplacement Mechanisms. A.A. Balkema, Rotterdam, pp. 391–399.
Bouvier, A., Vervoort, J.D., Patchett, P.J., 2008. The Lu–Hf and Sm–Nd isotopic composition of CHUR: constraints from unequilibrated chondrites and implications for the bulk composition of terrestrial planets. Earth Planet. Sci. Lett. 273, 48–57.
Buchan, K.L., Ernst, R.E., Hamilton, M.A., Mertanen, S., Pesonen, L.J., Elming, S.-Å., 2001. Rodinia: the evidence from integrated palaeomagnetism and U-Pb geochronology. Precambr. Res. 110, 9–32.
Buchan, K.L., Ernst, R.E., Bleeker, W., Davies, W., Villeneuve, M., van Breemen, O., Hamilton, M., Söderlund, U., 2010. Proterozoic magmatic events of the Slave craton, Wopmay orogen and environs. In: Geological Survey of Canada, Open File 5985. Geological Survey of Canada.
Campbell, I.H., McCall, G.J.H., Tyrwhitt, D.S., 1970. The Jimberlana Norite, Western Australia–a smaller analogue of the Great Dyke of Rhodesia. Geol. Mag. 107, 1–12.
Cassidy, K.F., Champion, D.C., Huston, D.L., 2005. Crustal evolution constraints on the metallogeny of the Yilgarn Craton. In: Mineral Deposit Research: Meeting the Global Challenge. Springer, pp. 901–904.
Cassidy, K.F., Champion, D.C., Krapez, B., Barley, M.E., Brown, S.J.A., Blewett, R.S., Groenewald, P., Tyler, I.M., 2006. A revised geological framework for the Yilgarn Craton, Western Australia. In: Geological Survey of Western Australia Record 8/2006. Geological Survey of Western Australia.
Cawood, P.A., Korsch, R.J., 2008. Assembling Australia: Proterozoic building of a continent. Precambr. Res. 166, 1–35. http://dx.doi.org/10.1016/j.precamres.2008.08.006.
Cawood, P.A., Tyler, I.M., 2004a. Assembling and reactivating the Proterozoic Capricorn Orogen: lithotectonic elements, orogenies, and significance. Precambr. Res. 128, 201–218. http://dx.doi.org/10.1016/j.precamres.2003.09.001.
Cawood, P.A., Tyler, I.M., 2004b. Assembling and reactivating the Proterozoic Capricorn Orogen: lithotectonic elements, orogenies, and significance. Precambr. Res. 128, 201–218.
Champion, D.C., 2013. Neodymium depleted mantle model age map of Australia: explanatory notes and user guide. Record 2013/44. Geosci. Aust. Rec. 209. http://dx.doi.org/10.11636/Record.2013.044.
Chatterjee, N., Bhattacharji, S., 2001. Petrology, geochemistry and tectonic settings of the mafic dikes and sills associated with the evolution of the Proterozoic Cuddapah Basin of south India. J. Earth Syst. Sci. 110, 433–453.
Chaudhuri, A.K., Saha, D., Deb, G.K., Deb, S.P., Mukherjee, M.K., Ghosh, G., 2002. The Purana basins of southern cratonic province of India-a case for Mesoproterozoic fossil rifts. Gondwana Res. 5, 23–33.
Claoué-Long, J.C., Hoatson, D.M., 2009. Guide to Using the Map of Australian Proterozoic Large Igneous Provinces. Geoscience, Australia.
Clark, D.J., Hensen, B.J., Kinny, P.D., 2000. Geochronological constraints for a two-stage history of the Albany – Fraser Orogen, Western Australia. Precambr. Res. 102, 155–183.
Coffin, M.F., Eldholm, O., 1994. Large igneous provinces: crustal structure, dimensions, and external consequences. Rev. Geophys. 32, 1–36. http://dx.doi.org/10.1029/93RG02508.
Compston, W., Williams, I.S., Meyer, C., 1984. U-Pb geochronology of zircons from lunar breccia 73217 using a sensitive high mass-resolution ion microprobe. J. Geophys. Res. 89, B525. http://dx.doi.org/10.1029/JB089iS02p0B525.
Condie, K.C., 2004. Supercontinents and superplume events: distinguishing signals in the geologic record. Phys. Earth Planet. Inter. 146, 319–332. http://dx.doi.org/10.1016/j.pepi.2003.04.002.
Crookshank, H., 1963. Geology of southern Bastar and Jeypore from the Bailadila range to the Eastern Ghats, 87th ed.
Dasgupta, S., Bose, S., Das, K., 2013. Tectonic evolution of the Eastern Ghats Belt, India. Precambr. Res. 227, 247–258. http://dx.doi.org/10.1016/j.precamres.2012.04.005.
Dentith, M.C., Featherstone, W.E., 2003. Controls on intra-plate seismicity in south-western Australia. Tectonophysics 376, 167–184. http://dx.doi.org/10.1016/j.tecto.2003.10.002.
Dentith, M.C., Dent, V.F., Drummond, B.J., 2000. Deep crustal structure in the south-western Yilgarn Craton, Western Australia. Technophysics 325, 227–255.
Depaolo, D.J., 1981. Trace element and isotopic effects of combined wallrock assimilation and fractional crystallization. Earth Planet. Sci. Lett. 53, 189–202.
Doehler, J.S., Heaman, L.M., 1998. 2.41 Ga U-Pb Baddeleyite ages for two gabbroic dykes from the Widgiemooltha swarm, Western Australia: a Yilgarn-Lewisian connection, in: America Annual Meeting in Toronto A.
Eggins, S.M., Woodhead, J.D., Kinsley, L.P.J., Mortimer, G.E., Sylvester, P., McCulloch, M.T., Hergt, J.M., Handler, M.R., 1997. A simple method for the precise determination of ≥40 trace elements in geological samples by ICPMS using enriched isotope internal standardisation. Chem. Geol. 134, 311–326.
Ernst, R.E., Bell, K., 2010. Large igneous provinces (LIPs) and carbonatites. Mineral. Petrol. 98, 55–76.
Ernst, R., Bleeker, W., 2010. Large igneous provinces (LIPs), giant dyke swarms, and mantle plumes: significance for breakup events within Canada and adjacent regions from 2.5 Ga to the present. Can. J. Earth Sci. 47, 695–739. http://dx.doi.org/10.1139/e10-025.
Ernst, R.E., Buchan, K.L., 1997. Giant radiating dyke swarms: their use in identifying pre-Mesozoic large igneous provinces and mantle plumes. In: Large Igneous Provinces: Continental, Oceanic, and Planetary Flood Volcanism. vol. 100. American Geophysical Union Monograph, pp. 297–333.
Ernst, R.E., Srivastava, R.K., 2008. India's place in the Proterozoic world: constraints from the Large Igneous Province (LIP) record. In: Srivastava, R.K., Sivaji, Ch., Chalapathi Rao, N.V. (Eds.), Geochemistry, Geophys. Geochronology Narosa Publ. House Pvt. Ltd, New Delhi, India, pp. 41–56.
Ernst, R.E., Head, J.W., Parfitt, E., Grosfils, E., Wilson, L., 1995. Giant radiating dyke swarms on Earth and Venus. Earth-Sci. Rev. 39, 1–58.
Ernst, R.E., Wingate, M.T.D., Buchan, K.L., Li, Z.X., 2008. Global record of 1600–700 Ma Large Igneous Provinces (LIPs): implications for the reconstruction of the proposed Nuna (Columbia) and Rodinia supercontinents. Precambr. Res. 160, 159–178. http://dx.doi.org/10.1016/j.precamres.2007.04.019.
Ernst, R., Srivastava, R., Bleeker, W., Hamilton, M., 2010. Precambrian Large Igneous Provinces (LIPs) and their dyke swarms: new insights from high-precision geochronology integrated with paleomagnetism and geochemistry. Precambr. Res. 183, 7–11.
Ernst, R.E., Bleeker, W., Söderlund, U., Kerr, A.C., 2013. Large Igneous Provinces and supercontinents: toward completing the plate tectonic revolution. Lithos 174, 1–14.
Evans, M.E., 1968. Magnetization of dikes: a study of the paleomagnetism of the Widgiemooltha dike suite, Western Australia. J. Geophys. Res. 73, 3261–3270.
Evans, T., 1999. Extent and Nature of the 1.2 Ga Wheatbelt Dyke Swarm, Yilgarn Craton, Western Australia (B.Sc. thesis). Univ. West. Aust., Perth.
French, J.E., Heaman, L.M., 2010. Precise U-Pb dating of Paleoproterozoic mafic dyke swarms of the Dharwar craton, India: implications for the existence of the Neoarchean supercraton Sclavia. Precambr. Res. 183, 416–441. http://dx.doi.org/10.1016/j.precamres.2010.05.003.
French, J.E., Heaman, L.M., Chacko, T., 2002. Feasibility of chemical U-Th-total Pb baddeleyite dating by electron microprobe. Chem. Geol. 188, 85–104. http://dx.doi.org/10.1016/S0009-2541(02)00074-8.
French, J.E., Heaman, L.M., Chacko, T., Srivastava, R.K., 2008. 1891–1883 Ma Southern Bastar-Cuddapah mafic igneous events, India: a newly recognized large igneous province. Precambr. Res. 160, 308–322. http://dx.doi.org/10.1016/j.precamres.2007.08.005.
Gao, S., Rudnick, R.L., Yuan, H.-L., Liu, X.-M., Liu, Y.-S., Xu, W.-L., Ling, W.-L., Ayers, J., Wang, X.-C., Wang, Q.-H., 2004. Recycling lower continental crust in the North China craton. Nature 432, 892–897.
Goldberg, A.S., 2010. Dyke swarms as indicators of major extensional events in the 1.9–1.2 Ga Columbia supercontinent. J. Geodyn. 50, 176–190.
Halilovic, J., Cawood, P.A., Jones, J.A., Pirajno, F., Nemchin, A.A., 2004. Provenance of the Earaheedy Basin: implications for assembly of the Western Australian Craton. Precambr. Res. 128, 343–366.
Hallberg, J.A., 1987. Postcratonization mafic and ultramafic dykes of the Yilgarn Block. Aust. J. Earth Sci. 34, 135–149. http://dx.doi.org/10.1080/08120098708729398.
Halls, H.C., Heaman, L.M., 2000. The paleomagnetic significance of new U-Pb age data from the Molson dyke swarm, Cauchon Lake area, Manitoba. Can. J. Earth Sci. 37, 957–966.
Halls, H.C., Zhang, B., 1998. Uplift structure of the southern Kapuskasing zone from 2.45 Ga dike swarm displacement. Geology 26, 67–70. http://dx.doi.org/10.1130/0091-7613(1998) 026<0067:USOTSK>2.3.CO;2.
Halls, H.C., Kumar, A., Srinivasan, R., Hamilton, M.A., 2007. Paleomagnetism and U-Pb geochronology of easterly trending dykes in the Dharwar craton, India: feldspar clouding, radiating dyke swarms and the position of India at 2.37 Ga. Precambr. Res. 155, 47–68. http://dx.doi.org/10.1016/j.precamres.2007.01.007.
Hanson, R.E., Gose, W.A., Crowley, J.L., Ramezani, J., Bowring, S.A., Bullen, D.S., Hall, R.P., Pancake, J.A., Mukwakwami, J., 2004. Paleoproterozoic intraplate magmatism and basin development on the Kaapvaal Craton: Age, paleomagnetism and geochemistry of ∼1.93 to ∼1.87 Ga post-Waterberg dolerites. South Afr. J. Geol. 107, 233–254.

Heaman, L.M., 2009. The application of U-Pb geochronology to mafic, ultramafic and alkaline rocks: an evaluation of three mineral standards. Chem. Geol. 261, 43–52. http://dx.doi.org/10.1016/j.chemgeo.2008.10.021.
Heaman, L.M., Machado, N., Krogh, T.E., Weber, W., 1986. Precise U-Pb zircon ages for the Molson dyke swarm and the Fox River sill: constraints for Early Proterozoic crustal evolution in northeastern Manitoba, Canada. Contrib. Miner. Petrol. 94, 82–89.
Heaman, L.M., Peck, D., Toope, K., 2009. Timing and geochemistry of 1.88 Ga Molson Igneous Events, Manitoba: insights into the formation of a craton-scale magmatic and metallogenic province. Precambr. Res. 172, 143–162.
Hoek, J.D., Seitz, H.-M., 1995. Continental mafic dyke swarms as tectonic indicators: an example from the Vestfold Hills, Antarctica. Precambr. Res. 75, 121–139.
Hou, G., 2012. Mechanism for three types of mafic dyke swarms. Geosci. Front. 3, 217–223. http://dx.doi.org/10.1016/j.gsf.2011.10.003.
Hou, G., Santosh, M., Qian, X., Lister, G.S., Li, J., 2008. Configuration of the Late Paleoproterozoic supercontinent Columbia: insights from radiating mafic dyke swarms. Gondwana Res. 14, 395–409. http://dx.doi.org/10.1016/j.gr.2008.01.010.
Hou, G., Kusky, T.M., Wang, C., Wang, Y., 2010. Mechanics of the giant radiating Mackenzie dyke swarm: a paleostress field modeling. J. Geophys. Res. Solid Earth 115. http://dx.doi.org/10.1029/2007JB005475.
Irvine, T.N.J., Baragar, W., 1971. A guide to the chemical classification of the common volcanic rocks. Can. J. Earth Sci. 8, 523–548.
Isles, D.J., Cooke, A.C., 1990. Spatial associations between post-cratonisation dykes and gold deposits in the Yilgarn Block, Western Australia. In: Parker, A.J., Rickwood, P.C., Tucker, D.H. (Eds.), Mafic Dykes and Emplacement Mechanisms. Balkema, Rotterdam, pp. 147–162.
Jaffey, A.H., Flynn, K.F., Glendenin, L.E., Bentley, W.C., Essling, A.M., 1971. Precision measurement of half-lives and specific activities of U 235 and U 238. Phys. Rev. C 4, 1889.
Johnson, S.P., Sheppard, S., Rasmussen, B., Wingate, M.T.D., Kirkland, C.L., Muhling, J.R., Fletcher, I.R., Belousova, E.A., 2011. Two collisions, two sutures: punctuated pre-1950 Ma assembly of the West Australian Craton during the Ophthalmian and Glenburgh Orogenies. Precambr. Res. 189, 239–262. http://dx.doi.org/10.1016/j.precamres.2011.07.011.
Ju, W., Hou, G., Hari, K.R., 2013. Mechanics of mafic dyke swarms in the Deccan Large Igneous Province: Palaeostress field modelling. J. Geodyn. 66, 79–91. http://dx.doi.org/10.1016/j.jog.2013.02.002.
Kamber, B.S., Greig, A., Schoenberg, R., Collerson, K.D., 2003. A refined solution to Earth's hidden niobium: implications for evolution of continental crust and mode of core formation. Precambr. Res. 126, 289–308.
Klein, E.L., Almeida, M.E., Rosa-Costa, L.T., 2012. The 1.89–1.87 Ga Uatumã Silicic Large Igneous Province, northern South America. November LIP of the Month [WWW Document]. URL http://www.largeigneousprovinces.org/12nov.
Klein, R., Pesonen, L.J., Mänttäri, I., Heinonen, J.S., 2016. A late Paleoproterozoic key pole for the Fennoscandian Shield: a paleomagnetic study of the Keuruu diabase dykes, Central Finland. Precambr. Res. 286, 379–397. http://dx.doi.org/10.1016/j.precamres.2016.10.013.
Ksienzyk, A.K., Jacobs, J., Boger, S.D., Koler, J., Sircombe, K.N., Whitehouse, M.J., 2012. U-Pb ages of metamorphic monazite and detrital zircon from the Northampton Complex: evidence of two orogenic cycles in Western Australia. Precambr. Res. 198–199, 37–50. http://dx.doi.org/10.1016/j.precamres.2011.12.011.
Kumar, K.V., Leelanandam, C., 2008. Evolution of the Eastern Ghats belt, India: a plate tectonic perspective. Geol. Soc. India 72, 720–749.
Kumar, K.V., Ernst, W.G., Leelanandam, C., Wooden, J.L., Grove, M.J., 2010. First Paleoproterozoic ophiolite from Gondwana: Geochronologic-geochemical documentation of ancient oceanic crust from Kandra, SE India. Tectonophysics 487, 22–32. http://dx.doi.org/10.1016/j.tecto.2010.03.005.
Le Maitre, R.W.B., Dudek, P., Keller, A., Lameyre, J., Le Bas, J., Sabine, M.J., Schmid, P.A., Sorensen, R., Streckeisen, H., Woolley, A., 1989. A classification of igneous rocks and glossary of terms: recommendations of the International Union of Geological Sciences, Subcommission on the Systematics of Igneous Rocks. International Union of Geological Sciences, Blackwell Scientific.
Lewis, J.D., 1994. Mafic dykes in the Williams-Wandering area, Western Australia. Geol. Surv. West Aust. Rep. 37, 37–52.
Li, Z.-X., Zhong, S., 2009. Supercontinent–superplume coupling, true polar wander and plume mobility: plate dominance in whole-mantle tectonics. Phys. Earth Planet. Inter. 176, 143–156. http://dx.doi.org/10.1016/j.pepi.2009.05.004.
Liu, Y., Li, Z.-X., Pisarevsky, S.A., Stark, J.C., 2016. Paleomagnetic investigation of mafic dykes in the southwestern Yilgarn Craton, Western Australia. In: Australian Earth Sciences Convention 2016 Abstracts. Geological Society of Australia, pp. 277.
Liu, Y., Li, Z.-X., Pisarevsky, S.A., Kirscher, U., Mitchell, R.N., Stark, J.C., 2017. Palaeomagnetism of the 1.89 Ga Boonadgin dykes of the Yilgarn Craton: possible connection with India. Precambr. Res In Review.
Ludwig, K., 2009. Squid 2.50, A User's Manual (No. 2.50.11.02.03 Rev. 03 Feb 2011). Berkeley, California, USA.
Ludwig, K.R., 2011. Isoplot/Ex, Version 4.15: A geochronological toolkit for Microsoft Excel: Geochronology Center Berkeley, v. 4.
Ludwig, K., 2012. User's Manual for Isoplot Version 3.75–4.15: A Geochronological Toolkit for Microsoft. Berkeley Geochronological Cent. Spec. Publ.
Maas, R., Kamenetsky, M.B., Sobolev, A.V., Kamenetsky, V.S., Sobolev, N.V., 2005. Sr, Nd, and Pb isotope evidence for a mantle origin of alkali chlorides and carbonates in the Udachnaya kimberlite, Siberia. Geology 33, 549–552.
Maas, R., Grew, E.S., Carson, C.J., 2015. Isotopic constraints (Pb, Rb-Sr, Sm-Nd) on the sources of early Cambrian pegmatites with Boron and Beryllium minerals in the Larsemann Hills, Prydz Bay, Antarctica. Can. Mineral. 53, 249–272.
Mallikharjuna, R.J., Bhattacharji, S., Rao, M.N., Hermes, O.D., 1995. 40Ar–39Ar ages and geochemical characteristics of dolerite dykes around the Proterozoic Cuddapah Basin, South India, in: Geological Society of India Memoir 33, pp. 307–328.
Meert, J.G., Pandit, M.K., Pradhan, V.R., Banks, J., Sirianni, R., Stroud, M., Newstead, B., Gifford, J., 2010. Precambrian crustal evolution of Peninsular India: a 3.0 billion year odyssey. J. Asian Earth Sci. 39, 483–515. http://dx.doi.org/10.1016/j.jseaes.2010.04.026.
Middleton, M.F., Wilde, S.A., Evans, B.A., Long, A., Dentith, M., 1993. A preliminary interpretation of deep seismic reflection and other geophysical data from the Darling Fault Zone, Western Australia. Explor. Geophys. 24, 711–718.
Minifie, M., Kerr, A.C., Ernst, R.E., Pearce, J.A., 2008. The origin, nature and consequences of the Circum-Superior 1880 Ma Large Igneous Province. Geochim. Cosmochim. Acta Suppl. 72, A633.
Mishra, D.C., 2015. Plume and Plate Tectonics Model for formation of some Proterozoic Basins of India along Contemporary Mobile Belts: Mahakoshal – Bijawar, Vindhyan and Cuddapah Basins. J. Geol. Soc. India 85, 525–536.
Mohanty, S., 2012. Spatio-temporal evolution of the Satpura Mountain Belt of India: a comparison with the Capricorn Orogen of Western Australia and implication for evolution of the supercontinent Columbia. Geosci. Front. 3, 241–267. http://dx.doi.org/10.1016/j.gsf.2011.10.005.
Mohanty, S., 2015. Precambrian continent assembly and dispersal events of South Indian and East Antarctic Shields. Int. Geol. Rev. 57, 1992–2027. http://dx.doi.org/10.1080/00206814.2015.1048751.
Morris, P.A., 2007. Composition of the Bunbury Basalt (BB1) and Kerba Monzogranite (KG1) geochemical reference materials, and assessing the contamination effects of mill heads, in: Geological Survey of Western Australia Record 2007/14. Geological Survey of Western Australia Record 2007/14.
Murthy, N.G.K., 1987. Mafic dyke swarms of the Indian shield. In: Mafic Dyke Swarms 34, pp. 393–400.
Myers, J.S., 1990. Pinjarra orogen. In: Geology and Mineral Resources of Western Australia. State Printing Division, pp. 264–274.
Myers, J.S., 1993. Precambrian Tectonic history of the West Australian Craton and Adjacent Orogens. Annu. Rev. Earth Planet. Sci. 21, 453–485.
Nelson, D.R., Myers, J.S., Nutman, A.P., 1995. Chronology and evolution of the Middle Proterozoic Albany-Fraser Orogen, Western Australia. Aust. J. Earth Sci. 42, 481–495. http://dx.doi.org/10.1080/08120099508728218.
Nemchin, A.A., Pidgeon, R.T., 1997. Evolution of the Darling range batholith, Yilgarn craton, western Australia: a SHRIMP zircon study. J. Petrol. 38, 625–649.
Nemchin, A.A., Pidgeon, R.T., 1998. Precise conventional and SHRIMP baddeleyite U-Pb age for the Binneringie Dyke, near Narrogin, Western Australia. Aust. J. Earth Sci. 45, 673–675.
Nemchin, A.A., Pidgeon, R.T., Wilde, S.A., 1994. Timing of Late Archaean granulite facies metamorphism in the southwestern Yilgarn Craton of Western Australia: evidence from U-Pb ages of zircons fro mafic granulites. Precambr. Res. 68, 307–321.
Olsson, J.R., Klausen, M.B., Hamilton, M.A., März, N., Söderlund, U., Roberts, R.J., 2016. Baddeleyite U-Pb ages and geochemistry of the 1875–1835 Ma Black Hills Dyke Swarm across north-eastern South Africa: part of a trans-Kalahari Craton back-arc setting? Geol. Foeren. Stockholm Foerh. 138, 183–202.
Pidgeon, R.T., Cook, T.J.F., 2003. 1214 ± 5 Ma dyke from the Darling Range, southwestern Yilgarn Craton, Western Australia. Aust. J. Earth Sci. 50, 769–773.
Pidgeon, R.T., Nemchin, A.A., 2001. 1.2 Ga Mafic dyke near York, southwestern Yilgarn Craton, Western Australia. Aust. J. Earth Sci. 48, 751–755. http://dx.doi.org/10.1046/j.1440-0952.2001.485895.x.
Pirajno, F., Hocking, R.M., Reddy, S.M., Jones, A.J., 2009. A review of the geology and geodynamic evolution of the Palaeoproterozoic Earaheedy Basin, Western Australia. Earth-Sci. Rev. 94, 39–77.
Pisarevsky, S., De Waele, B., Jones, S., Söderlund, U., Ernst, R.E., 2015. Paleomagnetism and U-Pb age of the 2.4 Ga Erayinia mafic dykes in the south-western Yilgarn, Western Australia: paleogeographic and geodynamic implications. Precambr. Res. 259, 222–231. http://dx.doi.org/10.1016/j.precamres.2014.05.023.
Polat, A., Hofmann, A.W., Rosing, M.T., 2002. Boninite-like volcanic rocks in the 3.7–3.8 Ga Isua greenstone belt, West Greenland: geochemical evidence for intra-oceanic subduction zone processes in the early earth. Chem. Geol. 184, 231–254. http://dx.doi.org/10.1016/S0009-2541(01)00363-1.
Prokoph, A., Ernst, R.E., Buchan, K.L., 2004. Time-series analysis of Large Igneous Provinces: 3500 Ma to Present. J. Geol. 112, 1–22. http://dx.doi.org/10.1086/379689.
Qiu, Y., McNaughton, N.J., Groves, D.I., Dunphy, J.M., 1999. First record of 1.2 Ga quartz dioritic magmatism in the Archaean Yilgarn Craton, Western Australia, and its significance. Aust. J. Earth Sci. 46, 421–428. http://dx.doi.org/10.1046/j.1440-0952.1999.00715.x.
Rasmussen, B., Fletcher, I.R., 2002. Indirect dating of mafic intrusions by SHRIMP U-Pb analysis of monazite in contact metamorphosed shale: an example from the Palaeoproterozoic Capricorn Orogen, Western Australia. Earth Planet. Sci. Lett. 197, 287–299. http://dx.doi.org/10.1016/S0012-821X(02)00501-0.
Rasmussen, B., Fletcher, I.R., 2010. Dating sedimentary rocks using in situ U-Pb geochronology of syneruptive zircon in ash-fall tuff & lt 1 mm thick. Geology 38, 299–302. http://dx.doi.org/10.1130/G30567.1.
Rasmussen, B., Fletcher, I.R., Bengtson, S., McNaughton, N.J., 2004. SHRIMP U-Pb dating of diagenetic xenotime in the Stirling Range Formation, Western Australia: 1.8 billion year minimum age for the Stirling biota. Precambr. Res. 133, 329–337. http://dx.doi.org/10.1016/j.precamres.2004.05.008.
Rasmussen, B., Fletcher, I.R., Bekker, A., Muhling, J.R., Gregory, C.J., Thorne, A.M., 2012. Deposition of 1.88-billion-year-old iron formations as a consequence of rapid crustal growth. Nature 484, 498–501.
Rogers, J.J.W., Santosh, M., 2002. Configuration of Columbia, a mesoproterozoic supercontinent. Gondwana Res. 5, 5–22. http://dx.doi.org/10.1016/s1342-937x(05)

70883-2.
Rudnick, R.L., Gao, S., 2003. Composition of the continental crust, in: Holland, H.D., Turekian, K.K. (Eds.), The Crust, Vol. 3. Treatise on Geochemistry. pp. 1–64.
Salters, V.J.M., Stracke, A., 2004. Composition of the depleted mantle. Geochem. Geophys. Geosyst. 5, Q05B07. http://dx.doi.org/10.1029/2003GC000597.
Sheppard, S., Occhipinti, S.A., Tyler, I.M., 2004. A 2005–1970 Ma Andean-type batholith in the southern Gascoyne Complex, Western Australia. Precambr. Res. 128, 257–277. http://dx.doi.org/10.1016/j.precamres.2003.09.003.
Sheppard, S., Bodorkos, S., Johnson, S.P., Wingate, M.T.D., Kirkland, C.L., 2010a. The Paleoproterozoic Capricorn Orogeny: intracontinental reworking not continent-continent collision. In: Geological Survey of Western Australia Report 108. Geological Survey of Western Australia.
Sheppard, S., Johnson, S.P., Wingate, M.T.D., Kirkland, C.L., Pirajno, F., 2010b. Explanatory Notes for the Gascoyne Province. Geol. Surv. West. Aust., pp. 336.
Sheppard, S., Fletcher, I.R., Rasmussen, B., Zi, J.-W., Muhling, J.R., Occhipinti, S.A., Wingate, M.T.D., Johnson, S.P., 2016. A new Paleoproterozoic tectonic history of the eastern Capricorn Orogen, Western Australia, revealed by U-Pb zircon dating of micro-tuffs. Precambr. Res. 286, 1–19. http://dx.doi.org/10.1016/j.precamres.2016.09.026.
Sheppard, S., Rasmussen, B., Zi, J.-W., Soma, V.S., Sarma, S., Mohan, M.R., Krapez, B., Wilde, S.A., McNaughton, N.J., 2017. Sedimentation and mafic magmatism in the Paleoproterozoic Cuddapah Basin, India, as a consequence of lithospheric extension. Gondwana Res. 48, 153–163. http://dx.doi.org/10.1016/j.gr.2017.04.024.
Sircombe, K.N., 2002. Reconnaissance detrital zircon geochronology provenance of the Palaeoproterozoic Ashburton Formation: implications for Pilbara and Yilgarn amalgamation. In: Australian Geological Convention Adelaide South Australia. Geological Society of Australia.
Sobolev, A.V., Hofmann, A.W., Sobolev, S.V., Nikogosian, I.K., 2005. An olivine-free mantle source of Hawaiian shield basalts. Nature 434, 590–597.
Sobolev, A.V., Hofmann, A.W., Kuzmin, D.V., Yaxley, G.M., Arndt, N.T., Chung, S.-L., Danyushevsky, L.V., Elliott, T., Frey, F.A., Garcia, M.O., Gurenko, A.A., Kamenetsky, V.S., Kerr, A.C., Krivolutskaya, N.A., Matvienkov, V.V., Nikogosian, I.K., Rocholl, A., Sigurdsson, I.A., Sushchevskaya, N.M., Teklay, M., 2007. The amount of recycled crust in sources of mantle-derived melts. Science (80-) 316, 412–417.
Söderlund, U., Johansson, L., 2002. A simple way to extract baddeleyite (ZrO_2). Geochem. Geophys. Geosyst. 3. http://dx.doi.org/10.1029/2001GC000212.
Söderlund, U., Hofmann, A., Klausen, M.B., Olsson, J.R., Ernst, R.E., Persson, P.O., 2010. Towards a complete magmatic barcode for the Zimbabwe craton: Baddeleyite U-Pb dating of regional dolerite dyke swarms and sill complexes. Precambr. Res. 183, 388–398. http://dx.doi.org/10.1016/j.precamres.2009.11.001.
Sofoulis, J., 1965. Explanatory Notes on the Widgiemooltha 1: 250,000 Geological Sheet Western Australia. Geological Survey of Western Australia.
Spaggiari, C. V, Bodorkos, S., Barquero-Molina, M., Tyler, I.M., Wingate, M.T.D., 2009. Interpreted Bedrock Geology of the South Yilgarn and of the South Yilgarn and Central Albany-Fraser Orogen, Western Australia, Record 2009/10.
Spaggiari, C.V., Kirkland, C.L., Pawley, M.J., Smithies, R.H., Wingate, M.T.D., Doyle, M.G., Blenkinsop, T.G., Clark, C., Oorschot, C.W., Fox, L.J., 2011. The Geology of the east Albany-Fraser Orogen—A Field Guide. Geol. Surv. West Aust. Rec. 2011/23 23, 97.
Spaggiari, C.V., Kirkland, C.L., Smithies, R.H., Wingate, M.T.D., 2014. Tectonic Links between Proterozoic Sedimentary Cycles, Basin Formation and Magmatism in the Albany-Fraser Orogen, Western Australia. Geological Survey of Western Australia.
Spaggiari, C.V., Kirkland, C.L., Smithies, H.R., Wingate, M.T.D., Belousova, E.A., 2015. Transformation of an Archean craton margin during Proterozoic basin formation and magmatism: the Albany-Fraser Orogen, Western Australia. Precambr. Res. 266, 440–466. http://dx.doi.org/10.1016/j.precamres.2015.05.036.
Srivastava, R.K., Gautam, G.C., 2015. Geochemistry and petrogenesis of Paleo – Mesoproterozoic mafic dyke swarms from northern Bastar craton, central India: geodynamic implications in reference to Columbia supercontinent. Gondwana Res. 28, 1061–1078.
Stacey, J.S.T., Kramers, JD, 1975. Approximation of terrestrial lead isotope evolution by a two-stage model. Earth Planet. Sci. Lett. 26, 207–221.
Stern, R.A., 2001. A New Isotopic and Trace-Element Standard for the Ion Microprobe: Preliminary Thermal Ionization Mass Spectrometry U-Pb and Electron-Microprobe Data, Geological Survey of Canada Current Research 2001-F. Geological Survey of Canada.
Stern, R.A., Bodorkos, S., Kamo, S.L., Hickman, A.H., Corfu, F., 2009. Measurement of SIMS instrumental mass fractionation of Pb isotopes during zircon dating. Geostand. Geoanal. Res. 33, 145–168. http://dx.doi.org/10.1111/j.1751-908X.2009.00023.x.
Sun, S., McDonough, W.F., 1989. Chemical and isotopic systematics of oceanic basalts: implications for mantle composition and processes. Geol. Soc. London Spec. Publ. 42, 313–345. http://dx.doi.org/10.1144/GSL.SP.1989.042.01.19.
Tucker, D.H., Boyd, D.M., 1987. Dykes of Australia detected by airborne magnetic surveys. Mafic Dyke Swarms. Geol. Assoc. Canada Spec. Pap. 34, 163–172.
Wang, X.-C., Li, Z.-X., Li, J., Pisarevsky, S.A., Wingate, M.T.D., 2014. Genesis of the 1.21 Ga Marnda Moorn large igneous province by plume–lithosphere interaction. Precambr. Res. 241, 85–103. http://dx.doi.org/10.1016/j.precamres.2013.11.008.
Wilde, S., 1999. Evolution of the Western Margin of Australia during the Rodinian and Gondwanan Supercontinent Cycles. Gondwana Res. 2, 481–499. http://dx.doi.org/10.1016/S1342-937X(05)70287-2.
Wilde, S.A., Middleton, M.F., Evans, B.J., 1996. Terrane accretion in the southwestern Yilgarn Craton: evidence from a deep seismic crustal profile. Precambr. Res. 78, 179–196.
Williams, G.E., Schmidt, P.W., Clark, D.A., 2004. Palaeomagnetism of iron-formation from the late Palaeoproterozoic Frere Formation, Earaheedy Basin, Western Australia: palaeogeographic and tectonic implications. Precambr. Res. 128, 367–383. http://dx.doi.org/10.1016/j.precamres.2003.09.008.
Wingate, M.T.D., 1999. Ion microprobe baddeleyite and zircon ages for Late Archaean mafic dykes of the Pilbara Craton, Western Australia. Aust. J. Earth Sci. 46, 493–500.
Wingate, M.T.D., 2007. Proterozoic mafic dykes in the Yilgarn Craton, in: Proceedings of Geoconferences (WA) Inc., Kalgoorlie 2007 Conference, Kalgoorlie, Western Australia, pp. 80–84.
Wingate, M.T.D., 2017. Mafic dyke swarms and large igneous provinces in Western Australia get a digital makeover. In: Geological Survey of Western Australia Record 2017/2. Geological Survey of Western Australia, pp. 4–8.
Wingate, M.T.D., Pidgeon, R.T., 2005. The Marnda Moorn LIP, a late Mesoproterozoic large igneous province in the Yilgarn craton, Western Australia. July 2005 LIP of the month [WWW Document]. URL http://www.largeigneousprovinces.org/05jul.
Wingate, M.T.D., Campbell, I.H., Compston, W., Gibson, G.M., 1998. Ion microprobe U-Pb ages for Neoproterozoic basaltic magmatism in south-central Australia and implications for the breakup of Rodinia. Precambr. Res. 87, 135–159. http://dx.doi.org/10.1016/S0301-9268(97)00072-7.
Wingate, M.T.D., Campbell, I.H., Harris, L.B., 2000. SHRIMP baddeleyite age for the Fraser dyke swarm, southeast Yilgarn Craton, Western Australia. Aust. J. Earth Sci. 47, 309–313.
Wingate, M.T.D., Pisarevsky, S.A., Evans, D.A.D., 2002. Rodinia connections between Australia and Laurentia: no SWEAT, no AUSWUS? Terra Nova 14, 121–128.
Wingate, M.T.D., Pirajno, F., Morris, P.A., 2004. Warakurna large igneous province: a new Mesoproterozoic large igneous province in west-central Australia. Geology 32, 105–108.
Zhao, G., Cawood, P.A., Wilde, S.A., Sun, M., 2002. Review of global 2.1–1.8 Ga orogens: implications for a pre-Rodinia supercontinent. Earth-Sci. Rev. 59, 125–162.

Statement of Authorship

Title of Paper	**In situ U-Pb geochronology and geochemistry of a 1.13 Ga mafic dyke suite at Bunger Hills, East Antarctica: the end of the Albany-Fraser Orogeny**	
Publication Status	**Published**	Accepted for publication
	Submitted for Publication	Publication Style
Publication Details	Stark, J.C., Wang, X.-C., Li, Z.-X., Rasmussen, B., Sheppard, S., Xi, J.-W., Clark, C., Hand, M., Li, W.-X., **2018**. In situ U-Pb geochronology and geochemistry of a 1.13 Ga mafic dyke suite at Bunger Hills, East Antarctica: the end of the Albany-Fraser Orogeny. **Precambrian Res. 310, 76–92**.	

Author Contributions

By signing the Statement of Authorship, each author certifies that their stated contribution to the publication is accurate and that permission is granted for the publication to be included in the candidate's thesis.

Name of Principal Author (Candidate)	Jutta Camilla Stark		
Contribution to the Paper	Jutta Camilla Stark prepared the samples and undertook SHRIMP dating, most of the interpretation and drafted most of the manuscript		
Overall percentage (%)	65		
Signature		Date	01/06/2018

Name of Co-Author	Xuan-Ce Wang		
Contribution to the Paper	Xuan-Ce Wang is a supervisor of the candidate and assisted with the interpretation of the geochemical data and drafting of the manuscript		
Overall percentage (%)	10		
Signature	Xuan-Ce Wang	Date	01/06/2018

Name of Co-Author	Zheng-Xiang Li		
Contribution to the Paper	Zheng-Xiang Li is the principal supervisor of the candidate and assisted with concept and drafting of the manuscript and interpretation of the results		
Overall percentage (%)	5		
Signature		Date	01/06/2018

Name of Co-Author	Birger Rasmussen		
Contribution to the Paper	Birger Rasmussen assisted with interpretation of the SHRIMP results and drafting of the manuscript		
Overall percentage (%)	5		
Signature		Date	01/06/2018

Name of Co-Author	Steve Sheppard		
Contribution to the Paper	Steve Sheppard assisted with interpretation of the results and drafting of the manuscript		
Overall percentage (%)	5		
Signature	S. Sheppard	Date	01/06/2018

Name of Co-Author	Jian-Wei Zi		
Contribution to the Paper	Jian-Wei Zi assisted with the SHRIMP dating, sample preparation and data processing		
Overall percentage (%)	5		
Signature	Zi jianwei	Date	01/06/2018

Name of Co-Author	Christopher Clark		
Contribution to the Paper	Christopher Clark collected the samples		
Overall percentage (%)	5		
Signature		Date	01/06/2018

Name of Co-Author	Martin Hand		
Contribution to the Paper	Martin Hand collected the samples		
Overall percentage (%)	5		
Signature		Date	01/06/2018

Name of Co-Author	Wu-Xian Li		
Contribution to the Paper	Wu-Xian Li assisted with the analysis of the geochemical samples		
Overall percentage (%)	5		
Signature	Wuxian Li	Date	01/06/2018

Copyright Clearance Center RightsLink®

Home | Create Account | Help

Title: In situ U-Pb geochronology and geochemistry of a 1.13 Ga mafic dyke suite at Bunger Hills, East Antarctica: The end of the Albany-Fraser Orogeny

Author: J. Camilla Stark,Xuan-Ce Wang,Zheng-Xiang Li,Birger Rasmussen,Stephen Sheppard,Jian-Wei Zi,Christopher Clark,Martin Hand,Wu-Xian Li

Publication: Precambrian Research

Publisher: Elsevier

Date: June 2018

LOGIN

If you're a copyright.com user, you can login to RightsLink using your copyright.com credentials.

Already **a RightsLink user** or want to learn more?

Please note that, as the author of this Elsevier article, you retain the right to include it in a thesis or dissertation, provided it is not published commercially. Permission is not required, but please ensure that you reference the journal as the original source. For more information on this and on your other retained rights, please visit: https://www.elsevier.com/about/our-business/policies/copyright#Author-rights

BACK | CLOSE WINDOW

Precambrian Research 310 (2018) 76–92

Contents lists available at ScienceDirect

Precambrian Research

journal homepage: www.elsevier.com/locate/precamres

In situ U-Pb geochronology and geochemistry of a 1.13 Ga mafic dyke suite at Bunger Hills, East Antarctica: The end of the Albany-Fraser Orogeny

J. Camilla Stark[a,b,c,*], Xuan-Ce Wang[b,c], Zheng-Xiang Li[a,b,c], Birger Rasmussen[d], Stephen Sheppard[c,e], Jian-Wei Zi[b,f], Christopher Clark[b,c], Martin Hand[g], Wu-Xian Li[h]

[a] Earth Dynamics Research Group, ARC Centre of Excellence for Core to Crust Fluid Systems (CCFS), Curtin University, GPO Box U1987, Perth, WA 6845, Australia
[b] The Institute for Geoscience Research (TIGeR), School of Earth and Planetary Sciences, Curtin University, GPO Box U1987, Perth, WA 6845, Australia
[c] School of Earth and Planetary Sciences, Curtin University, GPO Box U1987, Perth, WA 6845, Australia
[d] School of Earth Sciences, University of Western Australia, Perth WA 6009, Australia
[e] Prime Geological Mapping, PO Box 3014, Carlisle South, WA 6101, Australia
[f] State Key Lab of Geological Processes and Mineral Resources, China University of Geosciences, Wuhan 430074, China
[g] Department of Geology and Geophysics, School of Physical Sciences, The University of Adelaide, South Australia 5005, Australia
[h] State Key Laboratory of Isotope Geochemistry, Guangzhou Institute of Geochemistry, Chinese Academy of Sciences, Guangzhou 510640, China

A R T I C L E I N F O

Keywords:
Antarctica
Bunger Hills
Mafic dykes
Geochronology
Geochemistry
Albany-Fraser Orogeny

A B S T R A C T

Antarctica contains continental fragments of Australian, Indian and African affinities, and is one of the key elements in the reconstruction of Nuna, Rodinia and Gondwana. The Bunger Hills region in East Antarctica is widely interpreted as a remnant of the Mesoproterozoic Albany–Fraser Orogen, which formed during collision between the West Australian and Mawson cratons and is linked with the assembly of Rodinia. Previous studies have suggested that several generations of mafic dyke suites are present at Bunger Hills but an understanding of their origin and tectonic context is limited by the lack of precise age constraints. New in situ SHRIMP U-Pb zircon and baddeleyite dates of, respectively, 1134 ± 9 Ma and 1131 ± 16 Ma confirm an earlier Rb-Sr whole-rock age estimate of ca. 1140 Ma for emplacement of a major mafic dyke suite in the area. Existing and new geochemical data suggest that the source of the dyke involved an EMORB-like source reservoir that was contaminated by a lower crust-like component. The new age constraint indicates that the dykes post-date the last known phase of plutonism at Bunger Hills by ca. 20 million years and were emplaced at the end of Stage 2 of the Albany-Fraser Orogeny. In current models, post-orogenic uplift and progressive tectonic thinning of the lithosphere were associated with melting and reworking of lower and middle crust that produced abundant plutonic rocks at Bunger Hills. A major episode of mafic dyke emplacement following uplift, cooling, and plutonic activity with increasing mantle input, suggests that the dykes mark the end of a prolonged interval of thermal weakening of the lithosphere that may have been associated with continued mafic underplating during orogenic collapse. If the undated olivine gabbro dykes with similar trend, geochemistry and petrology at Windmill Islands are coeval with the ca. 1134 Ma dyke at Bunger Hills, this would suggest the presence of a major dyke swarm at least 400 km in extent. In such case, the dykes could have been emplaced laterally from a much more distant mantle source, possibly a plume, and interacted with the locally heterogeneous and variably metasomatised lithosphere.

1. Introduction

Mafic dykes are products of lithospheric extension that was sufficient to allow propagation of mantle-derived magma through rigid lithosphere. Emplacement of mafic dykes therefore acts as a proxy for paleostress fields and pre-existing crustal weaknesses (Ernst et al., 1995; Hoek and Seitz, 1995; Halls and Zhang, 1998; Hou, 2012; Ju et al., 2013). Mafic dykes are also important targets of paleomagnetic analyses for continent reconstructions (e.g., Ernst and Buchan, 1997; Buchan et al., 2001; Bleeker and Ernst, 2006; Teixeira et al., 2013) and precisely dated dyke swarms, which represent the plumbing systems of now eroded Large Igneous Provinces (LIPs) (Coffin and Eldholm, 1994), can provide a unique magmatic barcode and geological piercing points (Ernst and Buchan, 1997; Bleeker, 2004; Bleeker and Ernst, 2006; Ernst and Bleeker, 2010; Ernst et al., 2016).

Antarctica contains key elements of the supercontinents Nuna, Rodinia and Pangea that existed since ca. 2000 Ma. Some of these elements are fragments that share close affinities to the Australian,

* Corresponding author at: School of Earth and Planetary Sciences, Curtin University, GPO Box U1987, Perth, WA 6845, Australia.
E-mail address: c.stark@postgrad.curtin.edu.au (J.C. Stark).

https://doi.org/10.1016/j.precamres.2018.02.023
Received 19 November 2017; Received in revised form 24 January 2018; Accepted 25 February 2018
Available online 26 February 2018

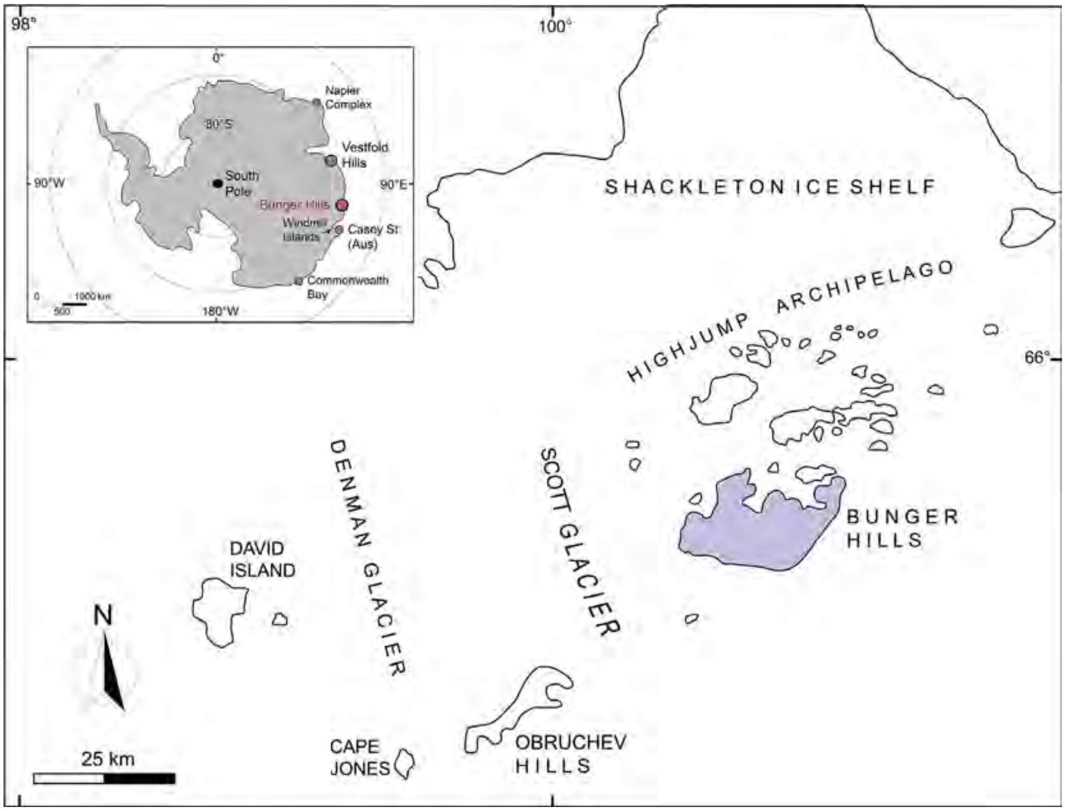

Fig. 1. Location of Bunger Hills, Highjump Archipelago and Obruchev Hills in East Antarctica. After Sheraton et al. (1990, 1995).

Indian and African continental blocks (Fitzsimons, 2000a, 2000b, 2003; Boger, 2011; Harley et al., 2013). Mafic dykes are widespread in Archean cratonic blocks in East Antarctica, being readily identifiable in the field and satellite imagery in ice-free areas. Several generations of Precambrian mafic dykes have been identified at Vestfold Hills (Collerson and Sheraton, 1986; Sheraton et al., 1987a,b; Black et al., 1991; Lanyon et al., 1993; Sheraton et al., 1993), Bunger Hills (Sheraton et al., 1990; Sheraton et al., 1993), Windmill Islands (Blight and Oliver, 1977; Post et al., 1997; Post, 2000; Zhang et al., 2012), Commonwealth Bay (Sheraton et al., 1989) and the Napier Complex (Sheraton et al., 1980; Sheraton and Black, 1982; Sheraton et al., 1987a,b; Suzuki et al., 2008). However, with the exception of the Vestfold Hills where U-Pb geochronology has permitted precise dating of five different dyke generations (Black et al., 1991; Lanyon et al., 1993), only Rb–Sr and/or Sm–Nd isotope ages are available for most dykes in Antarctica, which is problematic since these isotope systems are often disturbed by younger tectonothermal events.

The Bunger Hills, a short coastal segment outcropping in Wilkes Land in East Antarctica, have long been proposed to represent a fragment of the Mesoproterozoic Albany-Fraser Orogen in Western Australia (e.g., Sheraton et al., 1990, 1993; Black et al., 1992a,b; Fitzsimons, 2000a; Duebendorfer, 2002). The Windmill Islands, ca. 400 km east of Bunger Hills, appear to preserve a similar tectonothermal and magmatic history (Sheraton et al., 1993; Post et al., 1997; Post, 2000; Morrissey et al., 2017). Data from the Bunger Hills were first obtained during field campaigns in 1956–57 (Ravich et al., 1968) and 1986 (Sheraton et al., 1990, 1992, 1993, 1995; Stüwe and Wilson, 1990; Ding and James, 1991). In 2016, another field campaign was undertaken to study the crustal evolution at Bunger Hills (Tucker and Hand, 2016; Tucker et al., 2017) and Windmill Islands (Morrissey et al., 2017) and has led to improved tectonic models. However, current models and derived continent reconstructions have not incorporated mafic dykes in this part of Antarctica due to the imprecise age constraints for the dykes (Blight and Oliver, 1977; Sheraton et al., 1990, 1995; Post et al., 1997; Post, 2000; Zhang et al., 2012; Morrissey et al., 2017).

We present here the first baddeleyite and zircon U-Pb geochronology obtained from one of the largest and widest dykes at Bunger Hills sampled during the 2016 field campaign. We investigate the nature of the mantle source using existing and new major-trace element and isotope data, followed by a discussion on a possible tectonic setting during dyke emplacement at Bunger Hills in the wider context of the Albany–Fraser Orogen.

2. Regional geology

The Bunger Hills area forms a continuous low relief outcrop of about 300 km^2 along the coast in Wilkes Land near Shackleton Ice Shelf, approximately 400 km west of the Windmill Islands (Fig. 1). Bunger Hills forms one of three geologically distinct regions in the immediate vicinity of the Denman and Scott Glaciers; the other two areas are the Obruchev Hills between Scott and Denman Glaciers and a group of smaller outcrops west of Denman Glacier. The Highjump Archipelago extends just north-northeast from Bunger Hills and comprises a ca. 93 km-long belt of small rocky islands.

2.1. Basement lithology

The outcrop at Bunger Hills comprises predominantly granulite-facies mafic and felsic orthogneiss with subordinate paragneiss and voluminous charnockitic plutons intruded by several generations of mafic dykes (Fig. 2) (Ravich et al., 1968; Sheraton et al., 1990, 1992, 1993, 1995; Sheraton and Tingey, 1994; Tucker et al., 2017). The presence of underlying Archean basement is inferred from a ca. 2800–2700 Ma zircon population from the mafic–felsic orthogneiss (Tucker et al., 2017), which is similar to the ca. 2640 Ma tonalitic orthogneiss at Obruchev Hills ca. 30 km to the southwest (Black et al., 1992a,b). Zircon populations at ca. 1700–1500 Ma from granodioritic orthogneiss

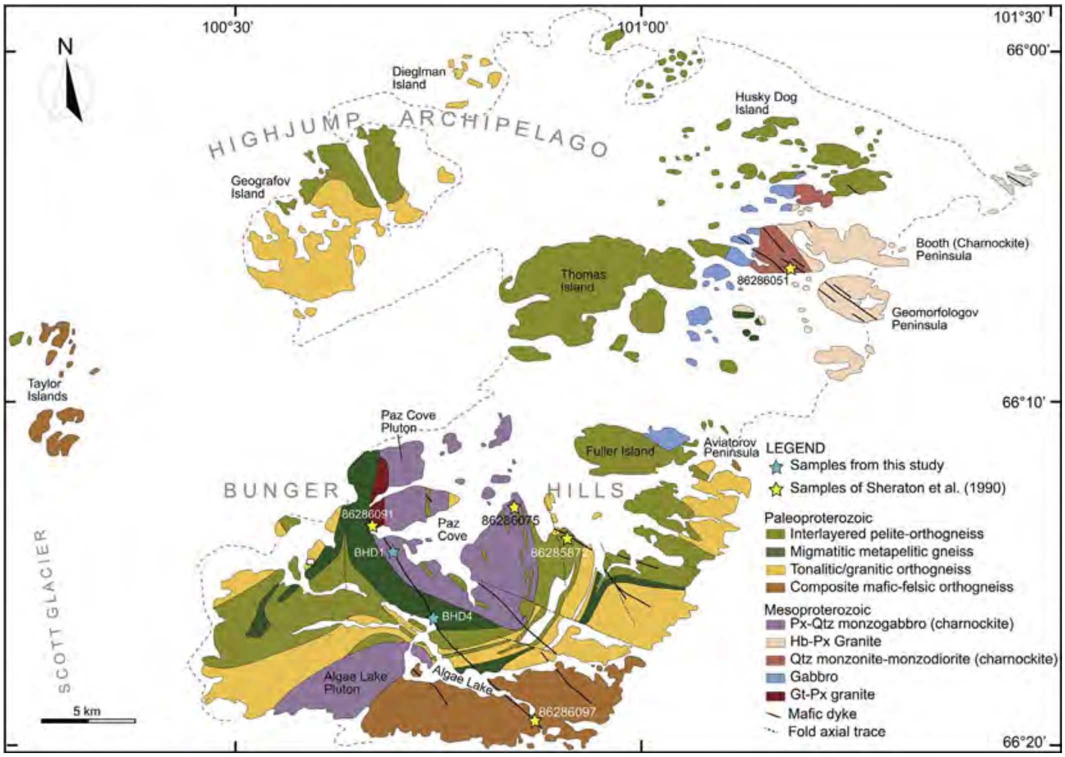

Fig. 2. Geological Map of Bunger Hills and Highjump Archipelago showing sample locations and regional geology. Modified after Sheraton and Tingey (1994) and Tucker et al. (2017). Samples in this study are from locations BHD1 and BHD4 (blue stars), the 8-digit numbers (yellow stars) denote samples of Sheraton et al. (1990). (For interpretation of the references to colour in this figure legend, the reader is referred to the web version of this article.)

(Sheraton et al., 1993, 1995), ca. 1900–1500 Ma from the extensive metapelite sequence and ca. 1734 Ma and 1666 Ma from tonalitic orthogneiss suggest that these lithologies form a Paleoproterozoic cover to Archean basement (Sheraton et al., 1992, 1993; Tucker et al., 2017).

2.2. Metamorphism and deformation

At least four metamorphic events have been identified at Bunger Hills (Stüwe and Powell, 1989; Stüwe and Wilson, 1990; Ding and James, 1991; Sheraton et al., 1993, 1995; Tucker et al., 2017). Peak granulite facies conditions of 850–900° C and 5–6 kbar were reached at 1183 ± 8 Ma in the Highjump Archipelago (Tucker and Hand, 2016), whereas conditions of 750–800 °C and 5–6 kbar at 1190 ± 15 Ma were reported at Bunger Hills proper (Sheraton et al., 1993). Recent data also indicate metamorphic zircon growth peaks at ca. 1300–1270 Ma and ca. 1250 Ma, with minor peaks at ca. 1330 Ma and 1200 Ma (Tucker et al., 2017).

Peak metamorphism at ca. 1190 Ma may have been associated with an extensional setting (Stüwe and Powell, 1989). This was followed by compressional NNW–SSE-directed deformation under granulite facies conditions by ca. 1170 Ma (Stüwe and Powell, 1989; Sheraton et al., 1992, 1993, 1995; Tucker et al., 2017), the final stage of deformation during uplift and cooling involving formation of extensive shear zones.

2.3. Plutons and mafic dykes

Three major mafic to felsic intrusive units — the Algae Lake pluton and the Paz Cove and Booth (Charnockite) Peninsula batholiths (Fig. 2) — outcrop in the Bunger Hills area. Their compositions range from subalkaline gabbro to quartz monzogabbro and they were likely emplaced at deep crustal levels (ca. 20 km) as a series of small intrusions syn- to post-peak metamorphism and deformation, between ca. 1203 Ma and 1151 Ma (Ravich et al., 1968; Sheraton et al., 1992, 1993, 1995; Tucker et al., 2017). Late-stage felsic dykes are uncommon and may be genetically related to the plutonic rocks (Sheraton et al., 1992, 1995). Several generations of mafic dyke suites have been identified at Bunger Hills (Stüwe and Powell, 1989; Sheraton et al., 1990; Stüwe and Wilson, 1990; Sheraton et al., 1993) but mafic dykes are rare west of Denman Glacier (Black et al., 1992a,b; Sheraton et al., 1995).

The oldest identifiable dykes are mafic granulites of unknown age and comprise boudinaged and deformed (proto-)olivine or quartz tholeiites within the plutons as well as mafic layers in basement gneisses. Most of the undeformed dykes cut both the basement and plutonic rocks and have a maximum age limit of ca. 1203 Ma, defined by the youngest dated pluton intruded by the dykes (Sheraton et al., 1990, 1992, 1993; Tucker et al., 2017).

The undeformed dykes comprise five compositionally distinctive groups ranging from olivine tholeiites and slightly alkaline dolerites to picrites–ankaramites (Sheraton et al., 1990, 1995). Group 1 tholeiitic dykes are < 2 m thick, relatively uncommon and found mainly in the southwestern part of Bunger Hills. Rare NW to NNW trending group 2 high-Mg dolerites have varying thicknesses whereas the most common dykes belong to groups 3 and 4, trend NW and have thicknesses up to 50 m. The youngest dykes are EW-trending alkali basalt dykes, which are generally < 1 m thick. Whole-rock Rb–Sr and Sm–Nd mineral isochron data suggest emplacement of Group 3 and 4 dykes at ca. 1140 Ma (the former group possibly slightly older) and alkali dykes at ca. 502 Ma (Sheraton et al., 1990, 1992, 1995). Group 1 dykes appear to be the oldest of the undeformed dyke suites and may be coeval with the ca. 1151 Ma Booth Peninsula monzodiorite. Mineral Rb–Sr analyses from the tholeiites and dolerites also reveal partial resetting events at ca. 907 Ma and 514 Ma. Sheraton et al. (1990) interpreted the variation in incompatible element ratios between and within the ca. 1140 Ma dyke groups (3 and 4) as lateral and vertical source heterogeneity in at least six distinctive mantle source regions. Group 1 dykes probably originated from an enriched lithospheric mantle source with an OIB-like component, whereas other dyke groups likely had at least two source components ranging from slightly depleted (Sr_i = 0.7029, εNd = +6.3) to moderately enriched (Sr_i = 0.7046–0.7053, εNd = +6.3) in composition. It was proposed that the source of group 3 and 4 dykes

Fig. 3. Sampled dyke at Algae Lake near sampling location of BHD4, looking SSW.

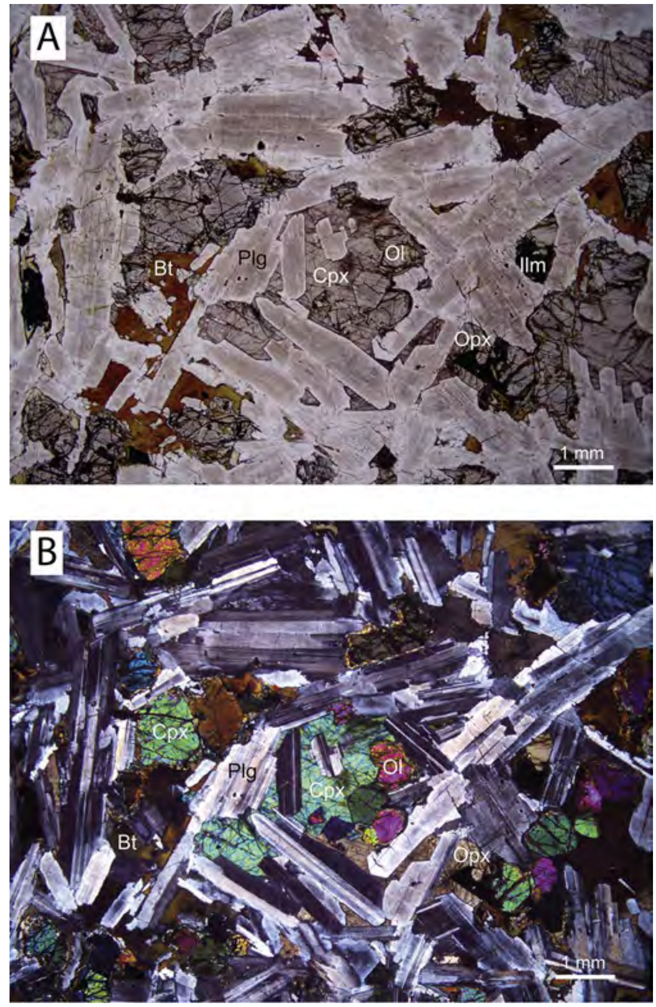

Fig. 4. Thin sections of sample BHD1-5. Note plagioclase and olivine poikilitically enclosed in clinopyroxene, biotite associated with ilmenite and abundant minute inclusions clouding the plagioclase. (A) Plane polarised light (B) Crossed polars.

consisted of a depleted mantle component and Archean or Paleoproterozoic long-term enriched lithospheric mantle containing subducted crustal materials.

3. Samples

3.1. Geochronology and geochemistry

3.1.1. Field sampling

Fourteen block samples were collected from two locations along the largest dyke on the island (Figs. 2 and 3). Seven samples were collected from each location: six samples from the mafic component for geochemistry and one sample from the associated leucocratic segregation for geochronology (Table 1).

Sample locality BHD1 is near Paz Cove where the dyke is ca. 50 m wide and intrudes the Paz Cove batholith. Chilled margins up to 10 cm wide are visible along the contact with the charnockite. Sample locality BHD4 is at the shore of Algae Lake, just south of the old Polish station Dobrowolski (Fig. 3). Here the dyke is still ca. 50 m wide and intrudes migmatitic pelitic gneiss. Samples BHD1-4, BHD1-5, and BHD1-6 (Paz Cove), and BHD4-3, BHD4-5, and BHD4-6 (Algae Lake) are gabbroic and were collected from the center of the dyke. Samples BHD1-1, BHD1-2, and BHD1-3 (Paz Cove), and BHD4-1 and BHD4-2 (Algae Lake) are doleritic and were collected closer to the edges of the dyke. Samples BHD1-7 and BHD4-7 were collected from associated leucocratic segregations. The dyke has a visible strike length of > 10 km from Algae Lake to Paz Cove and is identical to the major dyke crossing the entire Bunger Hills in a NW–SE direction that was mapped by Sheraton and Tingey (1994).

3.1.2. Sample descriptions

The dyke is an olivine gabbro with intergranular to sub-ophitic and ophitic (poikilitic) texture (Fig. 4). The gabbroic samples comprise ca. 55– 60% plagioclase, 15–25% augitic clinopyroxene, 5–10% olivine, up to 5% of orthopyroxene, 3–5% biotite, accessory opaques (ilmenite, magnetite and hematite) and apatite. Clinopyroxene is commonly poikilitic and encloses olivine and plagioclase crystals. Olivine crystals are rimmed by a thin reaction corona where in contact with plagioclase. Most plagioclase grains are strongly clouded by minute inclusions of black and brown particles (likely Fe–Ti oxides) and larger, green spherical to needle shaped grains, possibly amphiboles, and both inclusion types appear to grow preferentially, possibly along twin planes. Post-magmatic alteration appears minimal but growth of the inclusions in the plagioclase crystals may be due to emplacement and slow cooling at depth or a later thermal event (Halls and Palmer, 1990; Halls et al., 2007). Apatite forms acicular colourless needles. Brown biotite is associated with, and grows around, ilmenite, possibly due to late stage reaction with magmatic fluids common in gabbros. Leucocratic segregations comprise 75–80% plagioclase, 5–10% quartz and green amphibole, 5% brown biotite and accessory apatite, zircon and chevkinite.

No petrography was available from Sheraton et al. (1990) samples 86286091 and 86286097, which they obtained from the same dyke.

Table 1
Sampling locations. Samples were collected along strike and across the dyke.

Location	Dlat	Dlon	Easting	Northing	Zone	Samples	Comments
BHD1	66 14 43.001 S	100 42 13.312 E	576574	2651708	47D	BHD1-1 to BHD1-6 (mafic) BHD1-7 (felsic segregation)	Near Paz Cove, cross-cuts Paz Cove batholith
BHD4	66 16 36.626 S	100 45 21.554 E	578825	2648126	47D	BHD4-1 to BHD4-6 (mafic) BHD4-7 (felsic segregation)	Shore of Algae Lake, intrudes migmatitic pelitic gneiss

Notes Datum WGS84, Dlat = decimal latitude, Dlon = decimal longitude.

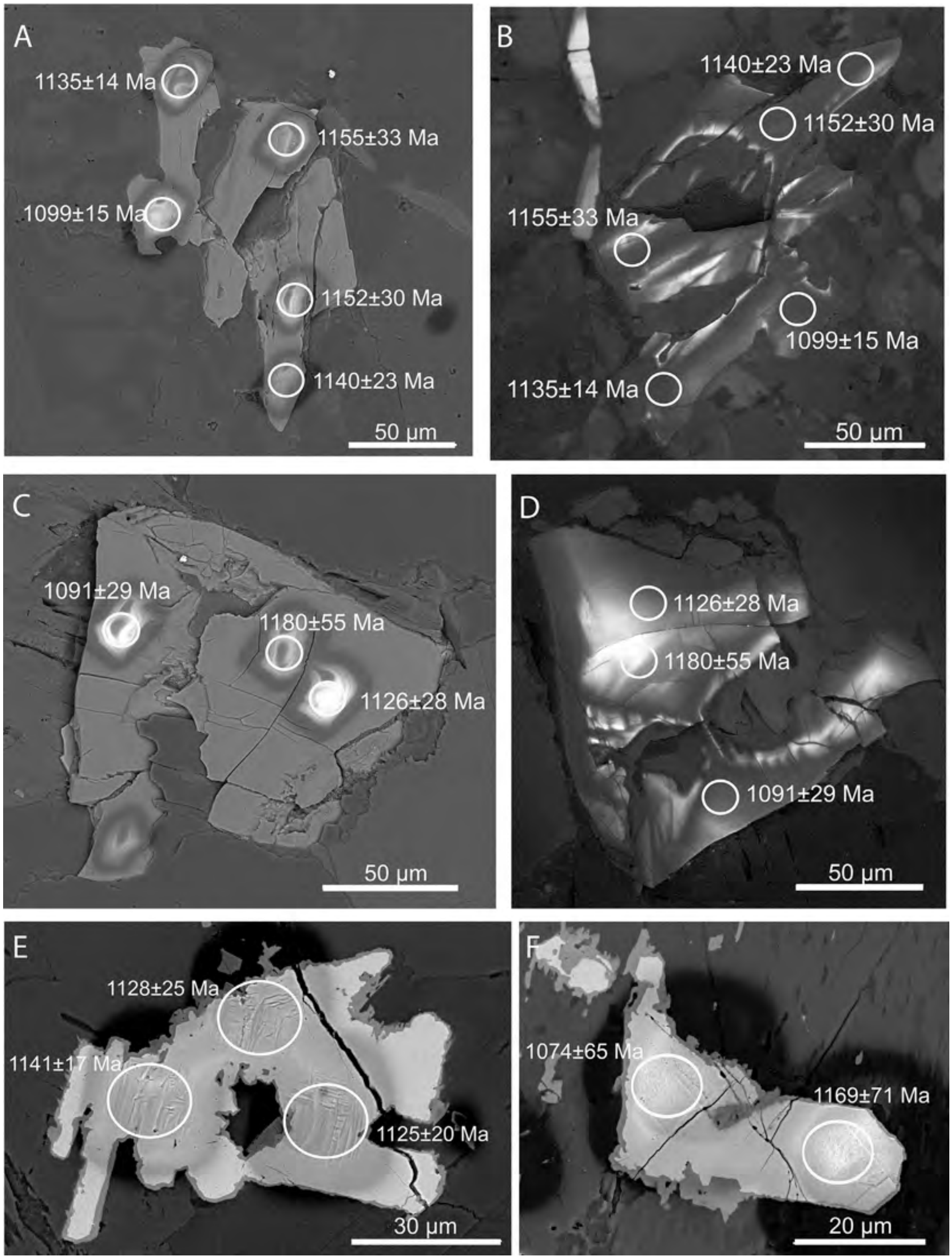

Fig. 5. SEM backscatter (BSE) and cathodoluminescence (CL) images showing SHRIMP spots and $^{207}Pb/^{206}Pb$ dates with 1**σ** error. (A) BSE and (B) CL images of zircons from BHD4-7B (note the rotation of the CL image). (C) BSE and (D) CL images of zircons from BHD4-7A. (E) and (F) SEM images of baddeleyite from BHD1-4.

However, samples from BHD1 and BHD4 are petrographically similar to samples 86286075 and 86285872 (dyke Group 4B), which Sheraton et al. (1990, 1995) collected from a NW-trending dyke east of Paz Cove. They comprise fine- to medium-grained intergranular to sub-ophitic dolerite with olivine, clinopyroxene, plagioclase and minor reddish-brown biotite associated with Fe-Ti oxides.

4. U-Pb geochronology and geochemistry

4.1. SHRIMP U-Pb geochronology

Polished thin sections were scanned for baddeleyite (ZrO_2) and zircon with a Hitachi TM3030 scanning electron microscope (SEM) equipped with energy dispersive X-ray spectrometer (EDX) at Curtin University, Perth, Australia. For SHRIMP U-Pb dating, selected grains were drilled directly from the thin sections using a micro drill and then mounted into epoxy disks, which were cleaned and coated with 40 nm of pure gold. Standards used for the SHRIMP sessions were mounted in one separate epoxy Disc and coated at the same time with the sample mounts.

In the leucocratic segregation samples from BHD1 and BHD4, zircon crystals are predominantly subhedral, prismatic to elongate ranging between 100 µm and 2 mm long, and many show thin, non-radial fractures (Fig. 5A and C). Some crystals have sharply delineated

Table 2
SHRIMP operating parameters.

Mount	CS15-5	CS15-6
Samples analysed	BHD1-7, BHD4-7	BHD1-4, BHD4-1, BHD4-5
Date analysed	25-Nov-15	20-Oct-15
Kohler aperture (μm)	70	50
Spot size (micrometres)	20	13
O2-primary current (nA)	1.3	1.5
Number of scans per analysis	6	8
Total number of analyses	27	23
Number of standard analyses	22	21
Pb/U external 1σ precision% (assigned minimum 1%)	1.0	1.0
Raster time (seconds)	120	120
Raster aperture (μm)	90	90

Notes 1) Mass resolution for all analyses ≥5000 at 1% peak height 2) BR266, OGC, Phalaborwa and NIST 611 used as standards 3) Count times for each scan for baddeleyite: ^{204}Pb, ^{206}Pb, ^{208}Pb = 10 s, ^{207}Pb = 30 s; count times for zircon: ^{204}Pb, ^{208}Pb = 10 s, ^{206}Pb = 20 s, ^{207}Pb = 30 s.

metasomatic zones but most are free from alteration. Many crystals appear skeletal or incomplete and some have quench-like textures, indicating rapid growth, consistent with their formation in a late-stage leucocratic segregation of the dyke. All crystals appear bright and unzoned under backscattered electron (BSE) microscopy and most are weakly zoned under cathodoluminescence (CL) imaging, brighter CL being associated with rims and fractures (Fig. 5B and D). Collectively, these characteristics support an igneous origin for the zircon (e.g. Corfu et al., 2003).

Baddeleyite crystals form predominantly euhedral laths between 50 and 70 μm long (Fig. 5E and F). Thin zircon rims are common but fracture-associated alteration appears insignificant.

Zircon and baddeleyite were analysed for U, Th and Pb using the sensitive high-resolution ion microprobe (SHRIMP II) at the John de Laeter Centre at Curtin University, following standard operating procedures after Compston et al. (1984). The SHRIMP analysis method for mounts with polished thin section plugs outlined in Rasmussen and Fletcher (2010) was modified for baddeleyite (SHRIMP operating parameters are given in Table 2). BR266 zircon (^{206}Pb/^{238}U age of 559 Ma, U concentration of 903 ppm; Stern, 2001) was used as a primary standard for calibrating Pb/U ratio and U concentration, and OG1 zircon with a ^{207}Pb/^{206}Pb age of 3465 Ma (Stern et al., 2009) was used to monitor the instrumental mass fractionation (IMF) in ^{207}Pb/^{206}Pb. For the baddeleyite analyses, the Phalaborwa baddeleyite (ca. 2060 Ma; Heaman, 2009) was employed as an additional standard. Typical spot size of the primary O_2^- beam was 13–20 μm with 1.3–1.5nA current.

Data were processed with Squid version 2.50 (Ludwig, 2009) and Isoplot version 3.76.12 (Ludwig, 2012). For common Pb correction, 1134 Ma common Pb isotopic compositions were calculated from the Stacey and Kramers (1975) two-stage terrestrial Pb isotopic evolution model. Analyses with > 1% common Pb (in ^{206}Pb) or > 10% discordance for baddeleyite or > 5% discordance for zircon (see footnote in Table 3 for definition of discordance) are considered unreliable and were disregarded in age calculations. All weighted mean ages are given at 95% confidence level and individual analyses are presented with 1σ error.

4.2. Geochemistry

Twelve blocks (BHD1-1 to BHD1-6 and BHD4-1 to BHD4-6) were cut from the hand specimens to remove weathered and altered parts. After initial crushing, approximately one quarter of the chips was split from each sample and the remaining material was pulverised in a chrome steel mill with quartz wash between each sample. From the quarter sample, chips with fresh fracture surfaces were picked under the microscope, washed and pulverised manually in an agate mill for isotope analysis.

Major elements were analysed at Intertek Genalysis Laboratories, Perth using X-ray fluorescence (XRF) and Genalysis laboratory internal standards SARM1 and SY-4. Trace elements were analysed with a Perkin-Elmex Sciex ELAN 6000 inductively coupled plasma mass spectrometer (ICP-MS) at Guangzhou Institute of Geochemistry, Chinese Academy of Sciences, following analytical procedures as described in Li (1997) and Liu et al. (1996). Sample powders were dissolved in high-pressure Teflon bombs using HF-HNO_3 mixture and an internal standard solution with Rh was used to monitor instrumental drift. A set of USGS standards including BHVO-2, AGV-2, GSR-3, W-2 and SARM4 were used for calibration of element concentrations. The uncertainty for major element analyses is < 5% and most trace element analyses have relative standard deviation (RSD) < 3%.

Sr, Nd and Hf isotope analyses for six samples (three samples from BHD1 and BHD4 each) were carried out at the Earth and Planetary Sciences Geoanalytical Unit at Macquarie University, Sydney (e.g., Genske et al., 2016). Whole-rock samples and USGS reference material BHVO-2 (~100 mg) were digested in Teflon beakers and loaded onto Teflon columns. Hafnium was collected with the matrix after 5.4 mL and Sr after 34.9 mL, followed by Nd. Neodymium was further separated from Sm, Ba, La, Ce using a second column and Hf was separated from the matrix using two further columns. Isotopic analyses of Sr and Nd were obtained using a Thermo Finnigan Triton thermal ionisation mass spectrometer (TIMS). Samples for Sr isotope analysis were loaded onto single rhenium filaments and analysed (1380–1430 °C, 1–11 V). Ratios were normalised to ^{86}Sr/^{88}Sr = 0.1194 to correct for mass fractionation. Samples for Nd isotope analysis were loaded onto double rhenium filaments and analysed (1200–1600 °C, 0.5–10 V). Ratios were normalised to ^{146}Nd/^{144}Nd = 0.7219 to correct for mass fractionation. Hafnium isotope analyses were obtained using a Nu Instruments multicollector (MC) ICP-MS Nu034 and ratios were normalised to ^{176}Hf/^{177}Hf = 0.7325 to correct for mass fractionation.

5. Results

5.1. SHRIMP U-Pb geochronology

Twenty-seven analyses were obtained from seven zircon crystals (four from BHD1 and three from BHD4) in one SHRIMP session (Fig. 6A, Table 3). The U and Th concentrations in most analyses are, respectively, < 500 ppm (59–1551 ppm, median 385 ppm) and < 850 ppm (40–4390 ppm, median 565 ppm). All Th/U ratios are > 0.5 (0.55–2.83, median 1.55). Seven analyses were excluded on the basis of > 5% discordance (all analyses had < 0.55% common ^{206}Pb). The remaining twenty analyses (from seven crystals) yielded a weighted mean ^{206}Pb*/^{238}U (Pb* denotes radiogenic Pb) date of 1133 ± 7 Ma (MSWD = 1.2) and a weighted mean ^{207}Pb*/^{206}Pb* date of 1134 ± 9 Ma (MSWD = 0.87).

Twenty-three analyses were obtained from eleven baddeleyite crystals (six grains from BHD1 and five grains from BHD4) in one SHRIMP session (Fig. 6B, Table 3). The U and Th concentrations range from, respectively, 56–703 ppm (median 135 ppm) and from 1 to 83 ppm (median 13 ppm). All Th/U ratios are < 0.13 (0.014–0.126, median 0.075). Twelve analyses were excluded due to > 1% common ^{206}Pb or > 10% discordance, or both. The remaining eleven analyses (from eight crystals) yielded a weighted mean ^{207}Pb*/^{206}Pb* date of 1131 ± 16 Ma (MSWD = 0.95). Only ^{207}Pb*/^{206}Pb* results are discussed here because ^{206}Pb*/^{238}U ratios measured with an ion microprobe may be significantly affected by orientation effects in baddeleyite crystals (Wingate, 1997; Wingate et al., 1998; Wingate and Compston, 2000; Schmitt et al., 2010).

The respective zircon and baddeleyite ^{207}Pb*/^{206}Pb* weighted mean dates of 1134 ± 9 Ma and 1131 ± 16 Ma are within analytical uncertainty of each other, indicating that the leucocratic segregation from

Table 3
SHRIMP U-Pb data for zircon and baddeleyite from dyke samples BHD1 and BHD4.

Spot	f_{206}%	U ppm	Th ppm	$^{232}Th/^{238}U$	± %	Total $^{238}U/^{206}Pb$	± %	Total $^{207}Pb/^{206}Pb$	± %	$^{238}U/^{206}Pb^{*}$	± %	$^{207}Pb^{*}/^{206}Pb^{*}$	± %	$^{206}Pb/^{238}U$Age (Ma)	± 1σ	$^{207}Pb/^{206}Pb$ Age (Ma)	± 1σ	Disc.%
Zircons																		
BHD1-7A.21Z-1	0.03	846	1527.07	1.86	0.54	5.16	1.3	0.07806	0.65	5.16	1.3	0.0778	0.7	1142	± 14	1142	± 14	+0
BHD1-7A.21Z-3	0.13	365	565.30	1.60	0.77	5.30	1.2	0.07786	1.00	5.31	1.2	0.0767	1.3	1112	± 13	1115	± 25	+0
BHD4-7A.104Z-1	0.00	188	102.90	0.57	0.95	5.29	1.4	0.07718	1.39	5.29	1.4	0.0772	1.4	1117	± 15	1126	± 28	+1
BHD4-7A.104Z-2	0.16	286	328.79	1.19	2.88	5.30	1.3	0.07716	1.10	5.31	1.3	0.0758	1.4	1112	± 13	1090	± 29	-2
BHD4-7A.104Z-3	–	106	96.38	0.94	0.47	5.22	1.7	0.07640	1.87	5.20	1.7	0.0793	2.8	1134	± 18	1180	± 55	+4
BHD1-7A.19Z-1	0.05	518	856.57	1.71	0.29	5.27	1.2	0.07806	0.83	5.27	1.2	0.0777	0.9	1120	± 12	1139	± 18	+2
BHD1-7A.19Z-3	–	209	281.15	1.39	0.74	5.35	1.9	0.07786	2.05	5.35	1.9	0.0783	2.1	1105	± 19	1155	± 42	+5
BHD4-7B.81Z-1	0.07	634	1429.42	2.33	0.48	5.16	1.2	0.07812	0.73	5.17	1.2	0.0775	0.8	1141	± 12	1135	± 16	-1
BHD4-7B.81Z-2	–	387	712.09	1.90	0.57	5.07	1.2	0.07877	0.97	5.07	1.2	0.0793	1.1	1161	± 13	1180	± 21	+2
BHD4-7B.81Z-3	–	510	1265.53	2.56	0.32	5.20	1.2	0.07786	0.93	5.20	1.2	0.0779	0.9	1134	± 13	1143	± 19	+1
BHD1-7B.36Z-1	0.10	550	914.92	1.72	0.82	5.27	1.6	0.07812	0.79	5.28	1.6	0.0772	1.0	1119	± 17	1127	± 19	+1
BHD4-7B.66Z-1	0.18	491	843.71	1.78	0.61	5.22	1.2	0.07923	0.87	5.23	1.2	0.0777	1.2	1129	± 12	1140	± 23	+1
BHD4-7B.66Z-2	0.54	541	832.11	1.59	1.12	5.18	1.2	0.08276	0.82	5.21	1.2	0.0782	1.5	1132	± 12	1152	± 30	+2
BHD4-7B.66Z-3	0.05	445	920.72	2.14	0.38	5.17	1.2	0.07871	1.59	5.18	1.2	0.0783	1.6	1139	± 12	1155	± 33	+1
BHD1-7B.41Z-2	0.20	987	2046.35	2.14	0.89	5.08	1.4	0.07914	0.60	5.09	1.4	0.0774	0.8	1156	± 15	1132	± 16	−2
BHD1-7B.41Z-3	–	385	390.48	1.05	0.42	5.26	1.3	0.07778	1.01	5.26	1.3	0.0781	1.1	1121	± 13	1149	± 21	+3
BHD1-7A.19Z-4	0.22	170	216.48	1.31	0.58	5.25	1.5	0.07899	1.47	5.26	1.5	0.0772	2.0	1122	± 15	1125	± 41	+0
BHD1-7B.66Z-4	0.03	701	1288.08	1.90	0.25	5.19	1.1	0.07641	0.69	5.19	1.1	0.0761	0.7	1136	± 12	1099	± 15	−4
BHD1-7B.66Z-5	0.09	971	2197.97	2.34	1.24	5.12	1.1	0.07829	0.62	5.13	1.1	0.0775	0.7	1148	± 12	1135	± 14	−1
BHD1-7B.36Z-4	0.15	305	475.12	1.61	0.60	5.12	1.3	0.07859	1.08	5.12	1.3	0.0773	1.4	1149	± 14	1129	± 28	−2
Baddeleyites																		
BHD1-4.164B-1	0.21	480	37.31	0.08	0.56	5.13	1.7	0.07959	0.92	5.14	1.7	0.0778	1.2	1146	± 18	1142	± 25	−0
BHD1-4.167B-1	0.53	92	1.28	0.01	1.92	5.15	1.4	0.08336	2.02	5.18	1.4	0.0789	3.6	1138	± 15	1169	± 71	+3
BHD1-4.167B-2	0.93	168	2.25	0.01	5.34	5.05	1.2	0.08300	1.42	5.09	1.3	0.0752	3.2	1155	± 13	1074	± 65	−8
BHD1-4.181B-1	0.04	690	61.52	0.09	0.54	5.21	1.1	0.07830	0.82	5.21	1.1	0.0779	0.9	1132	± 11	1146	± 18	+1
BHD4-1.209B-2	0.45	683	58.82	0.09	1.55	5.17	1.3	0.07805	0.96	5.19	1.3	0.0742	1.6	1136	± 14	1048	± 33	−9
BHD4-1.209B-3	0.35	703	62.16	0.09	0.70	5.17	1.4	0.08004	0.86	5.19	1.4	0.0771	1.3	1137	± 14	1123	± 27	−1
BHD4-5.115B-1	0.87	72	4.92	0.07	6.93	5.03	1.4	0.08752	1.99	5.08	1.5	0.0802	4.1	1159	± 16	1201	± 81	+4
BHD1-4.157B-1	0.11	368	28.52	0.08	0.63	5.15	1.1	0.07806	0.82	5.15	1.1	0.0772	1.0	1143	± 12	1125	± 20	−2
BHD1-4.157B-2	0.07	409	29.82	0.08	0.37	5.15	1.1	0.07840	0.77	5.15	1.1	0.0778	0.9	1143	± 11	1141	± 17	−0
BHD1-4.157B-3	0.25	388	34.33	0.09	0.40	5.30	1.6	0.07941	0.90	5.31	1.6	0.0773	1.3	1112	± 16	1128	± 25	+2
BHD4-1.205B-3	0.36	69	2.71	0.04	24.77	5.32	1.5	0.08056	2.44	5.34	1.6	0.0775	3.8	1107	± 16	1134	± 75	+3
Excluded analyses																		
Zircons																		
BHD1-7A.21Z-2	–	101	91.76	0.94	0.46	5.34	1.7	0.07832	1.76	5.31	1.7	0.0819	2.7	1111	± 18	1243	± 54	+12
BHD1-7A.19Z-2	0.15	76	50.35	0.68	1.01	5.45	1.9	0.08025	2.12	5.46	1.9	0.0790	2.7	1085	± 19	1172	± 53	+8
BHD1-7B.36Z-2	–	184	219.94	1.23	0.71	5.34	1.5	0.07920	1.44	5.33	1.5	0.0804	1.8	1108	± 15	1206	± 34	+9
BHD1-7B.36Z-3	–	222	302.89	1.41	0.29	5.17	1.4	0.08062	1.25	5.17	1.4	0.0811	1.4	1140	± 14	1223	± 27	+7
BHD1-7B.41Z-1	0.01	1551	4390.02	2.92	0.85	4.99	1.4	0.07639	0.46	4.99	1.4	0.0763	0.5	1177	± 15	1104	± 9	−7
BHD1-7A.19Z-5	–	128	131.72	1.06	0.43	5.35	1.7	0.07935	1.76	5.33	1.7	0.0820	2.5	1109	± 17	1246	± 50	+12
BHD1-7A.19Z-6	–	59	40.27	0.71	1.03	5.50	2.1	0.08099	2.45	5.47	2.2	0.0860	4.1	1082	± 21	1339	± 79	+21
Baddeleyites																		
BHD1-4.193B-1	2.30	67	1.13	0.02	2.13	5.42	3.5	0.08587	2.60	5.55	3.6	0.0668	9.8	1068	± 35	832	± 205	−31
BHD1-4.193B-2	0.45	76	1.10	0.01	2.22	5.90	2.2	0.08066	3.93	5.92	2.3	0.0769	5.4	1006	± 21	1118	± 108	+11
BHD4-1.205B-1	2.86	107	5.96	0.06	1.06	5.10	1.5	0.10447	2.04	5.25	1.6	0.0803	7.8	1123	± 17	1204	± 154	+7
BHD4-1.205B-2	6.27	81	4.54	0.06	5.98	4.70	2.6	0.12921	1.85	5.01	2.9	0.0764	12.8	1173	± 31	1107	± 256	−7
BHD1-4.179B-1	1.38	110	2.37	0.02	2.85	4.60	1.3	0.08508	2.64	4.67	1.4	0.0735	5.1	1251	± 16	1028	± 102	−24

(*continued on next page*)

Table 3 (*continued*)

Spot	f_{206}%	U ppm	Th ppm	$^{232}Th/^{238}U$	± %	Total $^{238}U/^{206}Pb$	± %	Total $^{207}Pb/^{206}Pb$	± %	$^{238}U/^{206}Pb^*$	± %	$^{207}Pb^*/^{206}Pb^*$	± %	$^{206}Pb/^{238}U$Age (Ma)	± 1σ	$^{207}Pb/^{206}Pb$ Age (Ma)	± 1σ	Disc.%
BHD1-4.179B-2	0.26	692	63.33	0.09	0.86	4.69	1.3	0.07995	0.65	4.70	1.3	0.0778	0.9	1243	± 15	1141	± 18	−10
BHD1-4.181B-2	0.27	679	83.00	0.13	3.91	4.59	2.0	0.07661	0.81	4.60	2.0	0.0744	1.2	1268	± 23	1052	± 24	-23
BHD4-1.209B-1	2.42	135	13.46	0.10	3.31	4.55	1.4	0.08223	2.95	4.66	1.5	0.0623	7.6	1253	± 17	686	± 161	−91
BHD4-5.115B-2	4.49	56	4.32	0.08	1.02	4.71	1.6	0.12511	1.89	4.93	1.8	0.0868	9.0	1190	± 20	1357	± 174	+13
BHD4-5.117B-1	0.12	343	20.19	0.06	0.79	5.62	1.4	0.08045	0.97	5.62	1.4	0.0794	1.2	1055	± 13	1183	± 23	+12
BHD4-5.125B-1	1.78	95	2.93	0.03	1.19	4.78	2.2	0.08727	2.94	4.87	2.2	0.0724	6.2	1205	± 25	996	± 127	-23
BHD4-1.209B-4	2.08	127	12.54	0.10	2.36	4.95	1.4	0.08383	1.83	5.06	1.5	0.0666	6.5	1163	± 16	826	± 135	-45

Notes 1) f_{204} is the proportion of common Pb in ^{206}Pb, determined using the measured $^{204}Pb/^{206}Pb$ and a common Pb composition from the Stacey and Kramers (1975) model at the approximate age of the sample 2) Disc. = $100(t[^{207}Pb^*/^{206}Pb^*] - t[^{238}U/^{206}Pb^*])/t[^{207}Pb^*/^{206}Pb^*]$.

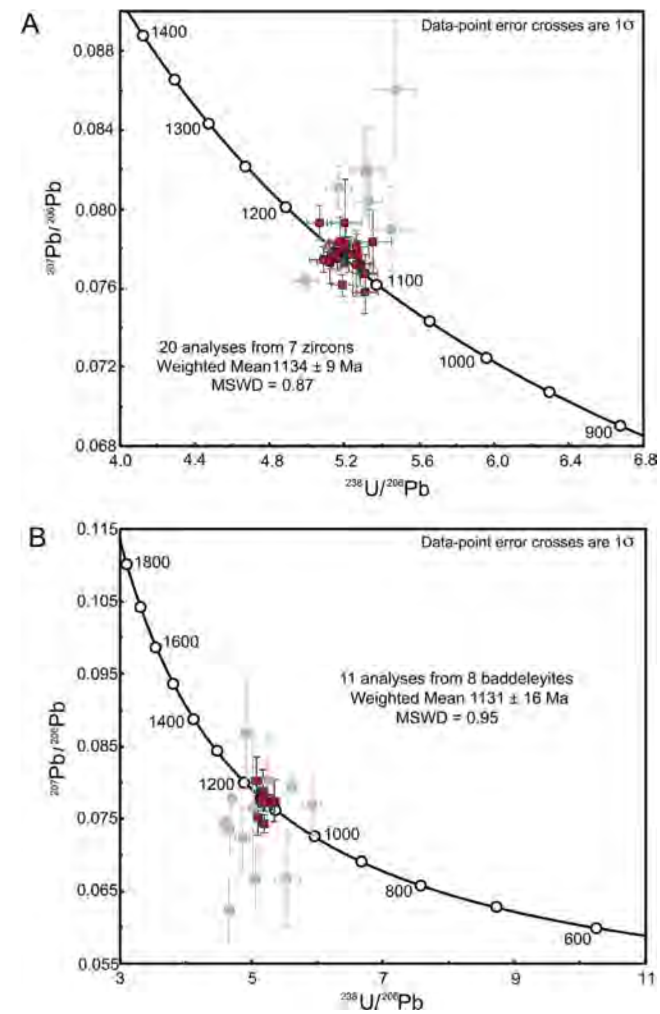

Fig. 6. Tera-Wasserburg plot of SHRIMP U-Pb results for (A) zircon and (B) baddeleyite analyses. Grey squares denote excluded data (see Section 5.1 for details).

which the zircons were sampled is part of the dyke. The more precise date of 1134 ± 9 Ma for zircons extracted from the leucocratic segregation (samples BHD1-7 and BHD4-7) is therefore considered to be the best estimate of the crystallisation age of the dyke. At BHD1, the dyke intrudes the Paz Cove charnockite, which has yielded U-Pb zircon dates of 1170 ± 4 Ma (Sheraton et al., 1992) and 1200 ± 6 Ma (Tucker et al., 2017). The pelites and orthogneisses contain zircon populations, respectively, between 1900 and 1500 Ma and between ca. 1700 and 1500 Ma, and are underlain by (unexposed) basement of Archean age (Tucker et al., 2017). These data further support the interpretation that the analysed zircons are not xenocrysts originating from the basement. The previously estimated emplacement age of ca. 1140 Ma for most of the group 3 and 4 dykes was based on Rb–Sr whole-rock and limited Sm–Nd isochron analyses by Sheraton et al. (1990) and is confirmed by our geochronology results. The most precise ages from their study were 1220 ± 80 Ma for group 3A dykes, 1120 ± 40 Ma for group 4D dykes (Sm–Nd mineral isochron) and 1160 ± 160 Ma for group 4E dykes. It is notable that the group 4D age is within uncertainty of the U-Pb ages reported here. Close agreement between the Rb-Sr (and some Sm-Nd) ages obtained from a number of NW-trending group 3 and 4 dykes by Sheraton et al. (1990) and the new U-Pb ages from the single NW-trending dyke in this study suggests that most group 3 and 4 dykes, and possibly other NW-trending dykes at Bunger Hills may be coeval and belong to the same dyke swarm.

Table 4
Major and trace element and isotope data for samples BHD1-1 to BHD1-6 and BHD4-1 to BHD4-6.

	BHD1-1	BHD1-2A	BHD1-3	BHD1-4	BHD1-5	BHD1-6	BHD4-1B	BHD4-2	BHD4-3	BHD4-4	BHD4-5	BHD4-6
SiO_2	45.81	45.51	45.76	46.99	47.05	46.69	45.36	45.49	46.44	46.38	47.20	45.51
TiO_2	3.10	3.13	3.20	1.57	1.40	1.43	2.20	2.37	1.91	1.85	1.74	3.29
Al_2O_3	15.83	15.79	15.83	17.91	17.47	17.59	17.33	16.45	18.01	17.50	19.25	16.32
CaO	8.51	8.47	8.58	8.58	8.53	7.88	7.70	7.88	8.04	7.63	8.70	9.23
$Fe_2O_{3(tot)}$	15.63	15.60	15.95	12.36	12.35	13.15	15.21	15.26	13.37	13.95	12.00	14.59
K_2O	0.90	0.89	0.89	0.76	0.67	0.78	0.65	0.70	0.67	0.69	0.66	0.63
MgO	6.13	6.16	6.16	7.92	9.28	8.90	7.59	8.20	6.96	7.65	6.42	7.08
MnO	0.21	0.21	0.22	0.16	0.17	0.17	0.18	0.19	0.15	0.18	0.15	0.19
Na_2O	3.11	3.10	3.05	2.99	2.86	3.02	3.05	3.02	3.16	3.11	3.39	2.88
P_2O_5	0.43	0.43	0.44	0.31	0.29	0.38	0.26	0.27	0.26	0.27	0.23	0.25
LOI	0.22	0.21	−0.01	−0.06	−0.14	0.03	0.40	−0.05	0.95	0.59	0.03	0.08
Total	99.66	99.29	100.08	99.55	100.07	99.99	99.53	99.83	98.97	99.21	99.74	99.97
Mg#	47.76	47.93	47.37	59.90	63.66	61.20	53.77	55.61	54.82	56.11	55.50	53.08
Sc	27.03	26.44	26.45	16.17	16.47	11.96	14.66	17.91	14.87	13.47	13.38	29.48
V	239.40	233.20	244.30	158.60	100.80	125.60	231.60	201.10	178.10	152.80	161.00	251.60
Co	57.01	55.42	57.36	59.43	63.30	65.35	67.96	68.50	70.45	69.09	55.23	60.63
Ni	93.96	90.67	94.56	189.10	213.60	220.00	167.20	169.30	191.10	181.70	147.70	145.60
Ga	21.26	20.94	21.34	18.83	17.57	18.32	18.96	18.44	18.76	18.17	19.28	19.18
Ge	3.99	3.56	3.98	3.18	2.81	3.20	3.40	3.27	3.25	3.25	2.71	3.23
Rb	18.82	17.88	17.97	17.06	14.46	17.53	12.91	13.72	12.76	13.79	11.98	12.60
Sr	293.90	289.10	293.60	317.90	305.10	306.50	309.10	303.70	333.20	320.40	365.00	292.20
Y	39.34	34.21	39.38	26.61	22.19	27.85	20.92	20.98	21.43	21.64	19.36	25.88
Zr	203.00	199.70	196.30	155.40	123.70	139.00	73.06	117.70	117.80	78.80	76.15	102.00
Nb	12.60	10.74	12.82	8.15	6.88	8.65	7.10	6.94	7.12	7.62	6.70	9.11
Cs	0.28	0.23	0.39	0.31	0.22	0.32	0.23	0.20	0.23	0.25	0.21	0.23
Ba	318.30	314.40	320.20	265.20	242.20	262.70	239.40	245.90	239.90	252.90	243.50	236.10
La	16.29	16.61	16.10	12.14	11.72	13.72	10.06	10.97	10.00	10.69	9.34	9.98
Ce	39.00	38.29	39.32	28.40	27.89	32.34	23.30	25.34	23.49	24.72	21.64	23.93
Pr	5.51	5.13	5.47	3.90	3.53	4.43	3.20	3.32	3.24	3.40	2.98	3.40
Nd	25.63	23.31	26.10	18.09	15.64	20.33	14.89	14.91	14.99	15.54	13.74	16.15
Sm	6.41	6.25	6.43	4.37	4.15	4.88	3.51	3.94	3.60	3.73	3.28	4.15
Eu	2.23	2.20	2.25	1.61	1.51	1.70	1.38	1.50	1.42	1.46	1.38	1.60
Gd	6.64	6.65	6.72	4.52	4.36	4.92	3.67	4.09	3.73	3.82	3.32	4.43
Tb	1.16	1.03	1.19	0.79	0.67	0.85	0.64	0.64	0.64	0.65	0.59	0.76
Dy	7.09	6.23	7.21	4.70	4.03	5.04	3.75	3.81	3.83	3.96	3.46	4.70
Ho	1.46	1.28	1.49	0.98	0.82	1.04	0.78	0.79	0.79	0.81	0.71	0.96
Er	3.98	3.40	4.02	2.66	2.22	2.83	2.08	2.10	2.15	2.20	1.94	2.60
Tm	0.58	0.49	0.59	0.40	0.32	0.41	0.30	0.31	0.32	0.32	0.28	0.39
Yb	3.58	3.07	3.60	2.40	2.02	2.57	1.82	1.90	1.92	1.95	1.70	2.27
Lu	0.52	0.47	0.52	0.36	0.30	0.37	0.27	0.29	0.28	0.28	0.25	0.33
Hf	5.22	4.63	5.05	3.91	2.88	3.52	1.92	2.78	2.94	2.07	1.96	2.82
Ta	0.77	0.67	0.79	0.48	0.41	0.52	0.43	0.44	0.45	0.46	0.44	0.57
Pb	4.96	4.44	5.05	4.42	3.46	4.21	4.32	3.50	3.68	3.73	3.46	3.62
Th	2.01	2.00	1.82	1.75	1.47	1.84	1.34	1.44	1.22	1.34	1.18	1.27
U	0.35	0.36	0.37	0.39	0.27	0.34	0.24	0.25	0.24	0.24	0.23	0.22

Notes 1) Major elements (XRF) are given in wt% and trace elements (ICP-MS) in ppm 2) Mg# = 100 × Mg/(Mg + Fe), Fe^{2+}/Fe_{total} = 0.85.

5.2. Geochemistry

5.2.1. Major and trace elements

The results for geochemical analyses of 12 samples, collected along strike from the same dyke, are listed in Table 4. All samples have loss on ignition (LOI) < 1 wt%, consistent with petrographic evidence for insignificant alteration. They display a wide range in MgO (6.15–9.27 wt%; Mg# = 47.37–63.66), low but near-constant SiO_2 (45.52–47.32 wt%) and relatively low CaO (7.69–9.23 wt%). They are also characterized by enrichment in FeO_{total} (12.03–15.94 wt%) and Al_2O_3 (15.82–19.30 wt%). The total alkali contents ($Na_2O + K_2O$ = 3.52–4.06 wt%) and Na_2O/K_2O ratios (3.43–5.14) are high, indicating alkali and sodium enrichment. All samples plot just outside the sub-alkaline field, in the alkaline corner of the basaltic field on the TAS diagram (Fig. 7A) (Irvine and Baragar, 1971; Le Maitre et al., 2002) and despite their alkaline character, display a tholeiitic trend on the AFM diagram (Irvine and Baragar, 1971; Fig. 7B). Modal calculations (Johannsen, 1931) indicate that all samples are hypersthene-normative with up to 5% olivine, 50–60% plagioclase, up to 5% orthoclase, 4–10% diopside, 5–16% hypersthene, up to 20% Fe–Ti oxides (ilmenite and hematite), < 1% quartz and traces of apatite, spinel and zircon. Samples from BHD4 (central part of Bunger Hills) contain more normative olivine and no quartz.

Trace element profiles on a chondrite-normalised plot show moderate enrichment of light rare earth elements (LREE) with $(La/Sm)_{CN}$ = 1.44–1.68 and $(La/Yb)_{CN}$ = 3.15–4.17 and slight fractionation of heavy rare earth elements (HREEs) with $(Sm/Yb)_{CN}$ = 1.98–2.31, $(Gd/Yb)_{CN}$ = 1.53–1.79 and $(Tb/Yb)_{CN}$ = 1.47–1.59 (Sun and McDonough, 1989, Fig. 6C). Most samples display a positive Eu anomaly (Fig. 7C, Table 4). The primitive mantle-normalised patterns show negative Nb and Ta and negative to positive Ti anomalies, elevated large ion lithophile elements (LILE) and elevated Th (Fig. 7D). Some samples also display a Zr and Hf trough. Aside from the positive Ti anomalies of the samples, the overall trace element profile of the samples is very similar to that of lower continental crust (Rudnick and Gao, 2003). BHD1 samples have higher incompatible element contents than those of BHD4 samples, and the doleritic samples (BHD1-1 to BHD1-3) are higher in most incompatible elements.

Two samples from the same dyke were collected by Sheraton et al. (1990), who classified sample 86286097 in the southeastern part of Bunger Hills as part of group 4A (Mg # = 47.5) and sample 86286091

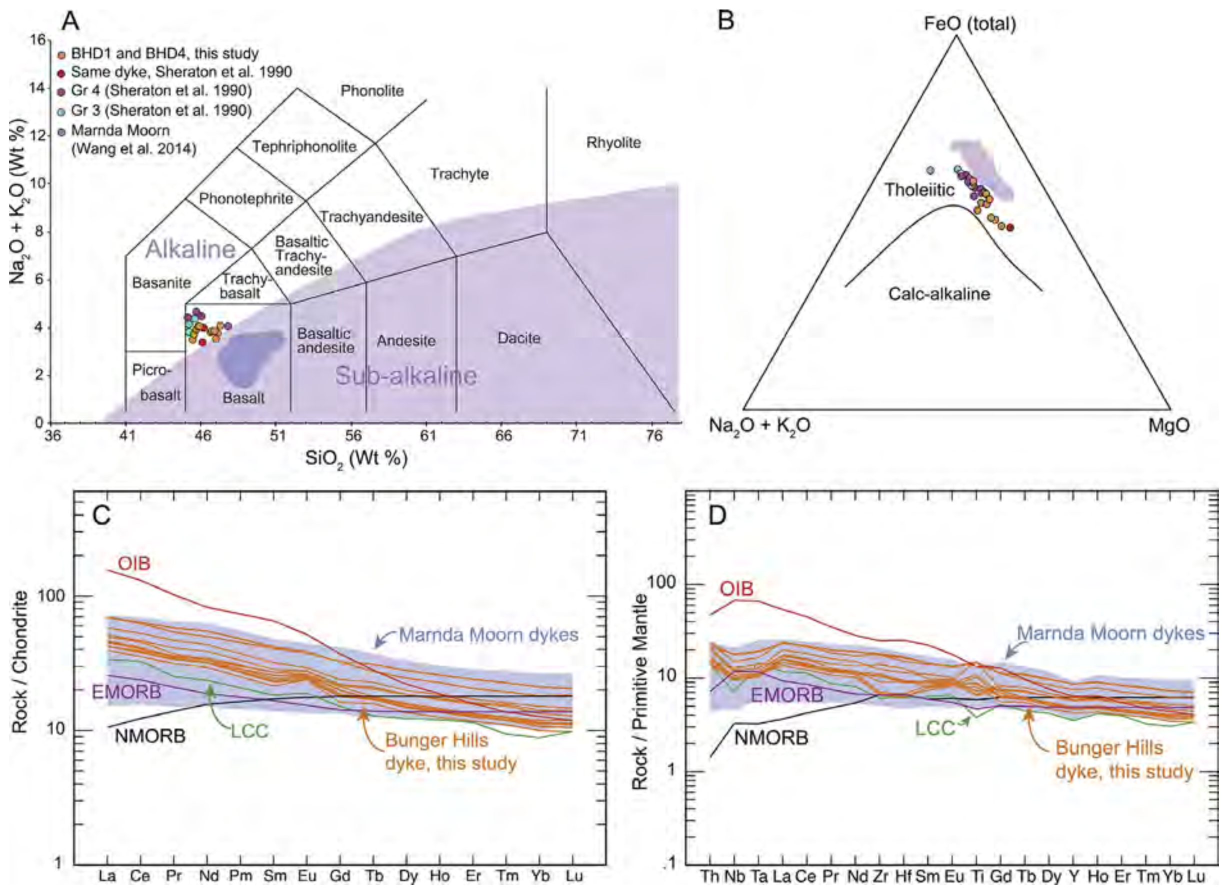

Fig. 7. (A) Total alkali-silica (TAS) plot after LeMaitre, 1989. Blue field denotes 1.21 Ga Marnda Moorn LIP dykes from Wang et al. (2014). (B) AFM plot after Irvine and Baragar (1971). (C) Chondrite and (D) primitive mantle normalised multi-element plots with blue shaded area denoting range of Marnda Moorn dykes (Wang et al., 2014). LCC = lower continental crust after Rudnick and Gao (2003); OIB = ocean island basalt, NMORB = mid ocean ridge basalt and EMORB = enriched MORB after Sun and McDonough (1989).

in the northwestern part as a less evolved variant of Group 4A. The latter has a higher Mg number of 63.33, consistent with the highest Mg number of 63.66 of the BHD1 samples nearby. Major element data in this study are consistent with compositions of samples 86286091 and 86286097 of Sheraton et al. (1990). Previous studies have shown that major element compositions and trace element ratios of a single dyke belonging to a major regional swarm (> 10 m in width) will be consistent along strike but may be different from an adjacent dyke, suggesting that each dyke represents a single magmatic pulse injected laterally from a magmatic chamber (Halls, 1986; Buchan et al., 2007; Ernst, 2014).

5.2.2. Nd and Sr isotopes

Six samples were analysed for Nd and Sr isotopes (Table 5). Measured ratios of $^{147}Sm/^{144}Nd$ and $^{143}Nd/^{144}Nd$ are, respectively, 0.1451–0.1602 and 0.5124390–0.5124560. Calculated initial ratios $^{143}Nd/^{144}Nd$ at 1134 Ma yielded 0.51125–0.51134, corresponding to $\varepsilon Nd_{1134Ma} = +1.51$ to $+3.32$, which is lower than the inferred lower estimate of $\varepsilon Nd_{DM} = +5.4$ for contemporaneous depleted mantle, calculated using the method of DePaolo (1981a,b). The $^{87}Rb/^{86}Sr$ and $^{87}Sr/^{86}Sr$ ratios are, respectively, 0.1246–0.1771 and 0.7035–0.7071, with corresponding initial ratios $(^{87}Sr/^{86}Sr)_{1134Ma}$ = 0.703625–0.7043372. These values are higher than the contemporaneous depleted mantle (ca. 0.7019; Taylor and McLennan, 1985) and compatible with those expected in lower crust, which is strongly depleted in Rb (Rudnick and Fountain, 1995; Rudnick and Gao, 2003; Hacker et al., 2015) and thus has low initial $^{87}Sr/^{86}Sr$ ratios similar to depleted mantle (Weaver and Tarney, 1980; Rollinson, 1993).

6. Discussion

6.1. Petrogenesis of the dykes

6.1.1. Fractional crystallisation

The range of Mg# (47–63) and low concentrations of compatible elements (Cr = 80.63–210.50 ppm, Ni = 88.9–220.0 ppm and MgO = 6.15–9.27 wt%) indicate that the dyke is evolved. The strong positive co-variation between Mg# and Ni ($r^2 = 0.90$) suggests olivine fractionation, consistent with presence of early (poikilitic) olivine in thin section (Fig. 4). Elevated Al_2O_3 (15.82–19.30 wt%) can be attributed to a hydrous source (e.g. Wang et al., 2016) or accumulation of plagioclase. The latter is supported by low Rb/Sr ratios (0.03–0.06) and marked positive Eu anomalies mainly in the gabbroic samples. The degree of the Eu anomaly can be estimated using $Eu/Eu* = Eu_{CN}/[(Sm_{CN}+Gd_{CN})]^{1/2}$ where Eu^* is the expected extrapolated Eu concentration (Taylor and McLennan, 1985). Magmas evolving along liquid line of descent will have $Eu/Eu^* \leq 1$, assuming that there was no initial Eu/Eu^* anomaly. All studied samples have $Eu/Eu^* > 1$ (1.04–1.28) with doleritic samples showing the smallest anomalies. The presence of positive Eu anomalies thus suggests that plagioclase is a cumulate mineral in the gabbroic samples.

The lack of correlation between Mg# and CaO ($r^2 = 0.07$) and Mg# and Sc/V ($r^2 = 0.02$) suggests that clinopyroxene fractionation may have been insignificant during magma evolution. Similarly, the presence of a strong negative covariance between Mg# and FeO_{tot} ($r^2 = 0.83$) and TiO_2 ($r^2 = 0.83$) indicates that fractionation of Fe-Ti oxides was insignificant as this would have resulted in strong depletion of these two elements.

Table 5
Isotope data for selected samples from BHD1 and BHD4.

	BHD1-3	BHD1-5	BHD1-6	BHD4-2	BHD4-4	BHD4-6
Sm (ppm)	6.428	4.145	4.879	3.935	3.734	4.148
Nd (ppm)	26.100	15.640	20.330	14.910	15.540	16.150
$^{143}Nd/^{144}Nd$	0.51245200	0.51245600	0.51242300	0.51243900	0.51242200	0.51243000
2SE	0.00000110	0.00000130	0.00000610	0.00000290	0.00000250	0.00000400
$^{147}Sm/^{144}Nd$	0.14888939	0.16021995	0.14508378	0.15954902	0.14526086	0.15527172
$(^{143}Nd/^{144}Nd)_i$	0.51134466	0.51126439	0.51134396	0.51125238	0.51134165	0.51127519
εNd(1.13 Ga)	3.32	1.75	3.30	1.51	3.26	1.96
T_{DM}(Ma)	1.64	1.97	1.61	1.99	1.62	1.87
Rb (ppm)	17.97	14.46	17.53	13.72	13.79	12.60
Sr (ppm)	293.60	305.10	306.50	303.70	320.40	292.20
$^{87}Sr/^{86}Sr$	0.70671600	0.70600000	0.70705700	0.70574500	0.70628300	0.70596200
2SE	0.00000370	0.00000250	0.00000250	0.00000250	0.00000230	0.00000360
$^{87}Rb/^{86}Sr$	0.17713193	0.13715147	0.16552773	0.13072928	0.12455414	0.12478521
$(^{87}Sr/^{86}Sr)_i$	0.70384315	0.70377558	0.70437235	0.70362474	0.70426289	0.70393814
Lu (ppm)	0.523	0.304	0.372	0.289	0.284	0.326
Hf (ppm)	5.046	2.880	3.516	2.780	2.072	2.816
$^{176}Hf/^{177}Hf$	0.28275590	0.28287650	0.28286100	0.28279270	0.28296380	0.28282200
2SE	0.00000446	0.00000498	0.00000570	0.00000380	0.00000775	0.00000847
$^{176}Lu/^{177}Hf$	0.00005729	0.00000265	0.00010676	0.00000242	0.00030381	0.00000446
$(^{176}Hf/^{177}Hf)_i$	0.28242882	0.28254339	0.28252712	0.28246464	0.28253126	0.28245667
εHf(1.13 Ga)	11.03	15.09	14.51	12.30	14.66	12.01

Notes 1) Crystallisation age t = 1134 Ma.

6.1.2. Crustal contamination

Arc-like characteristics, such as negative Nb-Ta and Zr-Hf (HFSE) anomalies and elevated LILE contents on primitive mantle-normalised plots, may be due to subduction-related metasomatic enrichment, crustal contamination, or both (e.g. Saunders et al., 1992; Puffer, 2001; Wang et al., 2016). Relative to mantle, crust has high SiO_2, La/Sm, Th/La and $^{87}Sr/^{86}Sr_i$ but low εNd_t, MgO, Sm/Nd and Nb/La. Contamination by (upper or middle) crustal material would produce positive correlations between Mg# and εNd_t, Nb/La and Sm/Nd and negative correlations between Mg# and La/Sm, Th/La and $^{87}Sr/^{86}Sr_i$ (e.g., Wang et al., 2012, 2014, 2016). Such predicted covariance is not observed in the analysed samples. Despite variations in the Mg number, the εNd_t values are nearly constant and the range of $^{87}Sr/^{86}Sr_i$ values is relatively small. In addition, ratios of La/Sm and Th/La are nearly constant and show weak positive correlation whereas ratios of Nb/La and Sm/Nd are nearly constant with a weak negative correlation. This implies that crustal contamination was not a significant process during magma evolution.

Trace element and isotope results from this study are consistent with those of Sheraton et al. (1990), who reported $^{87}Sr/^{86}Sr_i$ of 0.704 ± 0.002 for Group 4A dolerites (which includes the dyke sampled in this study) and εNd_{1140} between +2.9 and +6.3 for groups 4B, 4D and 4E, which have similar trace element profiles to group 4A. In addition, samples 86285833 from Geomorfologov Peninsula and 86286075 from the north-eastern part of Paz Cove (Group 4D and 4B dykes, respectively) have similar Sr_i (0.7044 and 0.7030, respectively) and εNd_t values (+2.9 and +3.9, respectively) as the dyke in this study. Sheraton et al. (1990) proposed that crustal contamination was significant only in Group 3A dykes and significant variability in trace element abundances and isotope compositions between dyke groups 1 to 4 was attributed to source heterogeneity.

As discussed above, crustal contamination was probably insignificant and the observed geochemical diversity likely reflects the source characteristics. As shown in Fig. 6C and D, the trace element composition of the samples is very similar to the lower continental crust (Rudnick and Gao, 2003) and the εNd_t values of the samples (+1.5 to +3.3) show slight but clear enrichment relative to the contemporary depleted mantle at 1134 Ma (+5.4; DePaolo, 1981a,b). These characteristics suggest that the source probably involved a depleted mantle type component that interacted with material that had a lower εNd_t, slightly higher (but NMORB-like) $^{87}Sr/^{86}Sr_i$ and a lower crust-like trace element composition.

6.1.3. Nature of the mantle source

Mantle source characteristics in mafic systems can be investigated using ratios of incompatible trace elements that are sensitive to source composition and partial melting processes but insensitive to crystal fractionation. Ratios of Nb/La, Nb/Ta, Th/Nb, La/Sm, La/Yb, La/Ba, Sm/Nd and Th/U in the analysed samples are near constant despite a wide range of Mg#, indicating that they behaved in an essentially incompatible manner during fractional crystallisation and likely reflect their source composition. The average ratio of Nb/La = 0.71 falls between average depleted mantle values (0.90–0.93;Sun and McDonough, 1989; Salters and Stracke, 2004) and lower crust (0.63; Rudnick and Gao, 2003) whereas the ratio of Nb/Ta = 16.23 is close to that of NMORB or enriched MORB (EMORB) (17.65/17.66; Sun and McDonough, 1989). The ratio of Th/Nb = 0.18 is close to lower crust (0.24; Rudnick and Gao, 2003) and much higher than NMORB/EMORB or OIB (0.05/0.07 and 0.08, respectively; Sun and McDonough, 1989). The average ratios of La/Sm = 2.72, Sm/Nd = 0.25 and Th/U = 5.38 are all very close to lower crustal values (2.83, 0.25 and 6.0, respectively; Rudnick and Gao, 2003). The ratio of La/Yb = 5.82 is slightly higher than the lower crust (5.33) but much higher than MORB (0.82) and much lower than typical OIB (17.13).

The composition of the source region may also be constrained by using ratios of incompatible trace elements with identical bulk partition coefficients (D) (Sims and DePaolo, 1997; Willbold and Stracke, 2006; Wang et al., 2014). In log–log plots, slopes plot near unity if the ratios of two such elements remain constant. In the studied samples, calculated slopes are near unity for Tb/Yb (log(Tb) − log(Yb) = 1.05 ± 0.02 (1se), r^2 = 1.0), Lu/Yb (log(Lu) − log(Yb) = 1.01 ± 0.02 (1se), r^2 = 0.99), Gd/Yb (log(Gd) - log(Yb) = 1.03 ± 0.07 (1se), r^2 = 0.95), Zr/Hf (log(Zr) − log(Hf) = 0.94 ± 0.04 (1se), r^2 = 0.98) and Nb/Ta (log(Nb) − log(Ta) = 0.98 ± 0.04 (1se), r^2 = 0.98). The unit slopes of correlation between Tb and Yb, Gd and Yb, and Yb and Lu indicate that the bulk partition coefficients of middle REE and HREE are identical

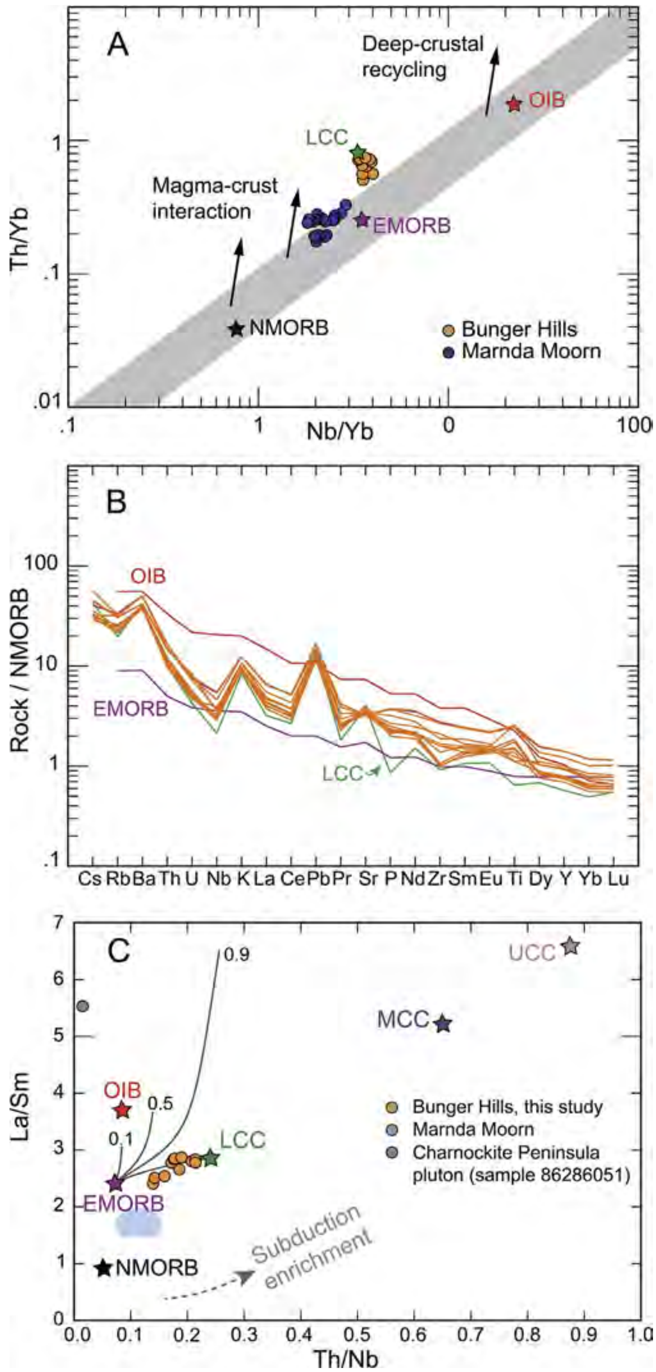

Fig. 8. Incompatible trace element plots for samples from this study and from Marnda Moorn LIP dykes (Wang et al., 2014). NMORB, EMORB and OIB data are from McDonough, 1989 and lower crust (LCC) from Rudnick and Gao (2003). MCC denotes middle continental crust and UCC upper continent crust. (A) Nb/Yb vs Th/Yb after Pearce (2008) (B) NMORB-normalised incompatible trace element profile of samples from BHD1 and BHD4 (C) Th/Nb vs La/Sm plot showing assimilation- fractional crystallisation (AFC; after DePaolo, 1981a,b) and binary mixing between EMORB of Sun and McDonough (1989) and lower crust of Rudnick and Gao (2003). Numbers denote r values. Bulk partition coefficients $D_{Th} = 0.01$, $D_{Nb} = 0.02$, $D_{La} = 0.11$ and $D_{Sm} = 0.19$ after Rollinson (1993) assuming for 5% olivine, 35% clinopyroxene, 4% orthopyroxene, 55% plagioclase and 1% magnetite.

during partial melting and magma evolution (e.g. Wang et al., 2012). Because $D_{Tb/Yb}$, $D_{Gd/Yb}$ and $D_{Yb/Lu}$ are > 1 between melt and garnet (e.g., Irving and Frey, 1978; Weaver and Tarney, 1981; Van Westrenen et al., 2001), this suggests that garnet is not the dominant phase in the residual mineral assemblage (e.g., Wang et al., 2012). However, the observed slight overall HREE depletion could be due to a phase with a more uniform K_D for HREE, such as clinopyroxene. The slope of log (Nb) versus log (La) (0.77, $r^2 = 0.74$) indicates $D_{Nb/La} < 1$, which is a typical characteristic of partial melts of peridotitic dominant source (Wang et al., 2014). However, the near-unity slopes of log (Nb)-log(Ta) and log (Zr)-log (Hf) indicate presence of rutile in the source (e.g., Foley et al., 2000; Münker et al., 2004; Wang et al., 2014) because the calculated bulk partition coefficients $D_{Zr/Hf}$ and $D_{Nb/Ta}$ for peridotitic sources are less than one ($D_{Nb/Ta} \sim 0.4$; Münker et al., 2004; Salters and Stracke, 2004; Pfänder et al., 2007; Wang et al., 2012; Zr/Hf ($D_{Zr/Hf} = 0.3$–0.4; Wang et al. 2012 and references therein). These observations support a predominantly peridotitic source composition with at least one other rutile-bearing component.

The studied samples have elevated Th/Yb ratios similar to lower continental crust (LCC), Nb/Yb ratios close to both LCC and EMORB (Fig. 8A) and, apart from elevated Th and enrichment in LILEs (Cs, Rb, K, Pb and Sr), the overall trace element distribution profiles of the samples share similarities with EMORB of Sun and McDonough (1989; Fig. 8B). All samples lie near a binary mixing line between EMORB and LCC rather than assimilation and fractional crystallisation trajectories (AFC; DePaolo, 1981a,b; Fig. 8C). Binary mixing of EMORB with a depleted mantle-like εNd_t (+5.4) and $^{87}Sr/^{86}Sr_i$ (0.7030) and 20–30% of LCC-like component ($\varepsilon Nd_t = -3.5$, same as sample 86285815 of Charnockite Peninsula pluton) would require the latter to have $^{87}Sr/^{86}Sr_i \leq 0.705$ (sample 86285815 has $^{87}Sr/^{86}Sr_i = 0.708$) to produce a reasonable mixing line between the two end member components (not shown in Fig. 8C). The above evidence is consistent with the interpretation of Sheraton et al. (1990) who on the basis of isotope data proposed that the source of group 3 and 4 dykes involved a depleted mantle component, which was probably mixed with a lithospheric component enriched in subducted crustal material and/or long-term enriched late Archean or Paleoproterozoic mantle. However, Sheraton et al. (1990) also argued that significant differences in incompatible element ratios between the various dyke groups (presumed to be of similar age) preclude simple two-component mixing, requiring a more complex source and suggesting that the source region of the dykes was both laterally and vertically heterogeneous.

6.1.4. Relationship between plutonic rocks and mafic dykes at Bunger Hills

Emplacement of the plutons at Bunger Hills pre-dates the unmetamorphosed mafic dykes by 20 myr (and possibly less), although syn-plutonic dykes have also been reported (Sheraton et al., 1990, 1992, 1995). Compositions of the plutons range from subalkaline gabbro to quartz monzogabbro with tholeiitic affinity, and have primitive mantle-like HFSE ratios and LREE and LILE enrichment (Sheraton et al., 1992). The parental magmas of the gabbroic rocks had a high $^{87}Sr/^{86}Sr_i$ (0.7091–0.7147) and low εNd_t (−9.4) composition that likely originated from a common heterogeneous, long-term LILE- and LREE-enriched, Nb-poor mantle source. Compared to the Nb/La ratios of the older plutonic rocks at Bunger Hills, the Nb/La ratio (0.81, sample 86286051) of the youngest known pluton, the 1151 ± 4 Ma Booth Peninsula batholith, is much higher and comparable to the average Nb/La ratio (0.71) of the dyke in this study. In addition, the higher εNd (−3.5) and lower $^{87}Sr/^{86}Sr_i$ (0.7082, sample 86285815) of the Booth Peninsula batholith suggest a larger contribution from asthenospheric mantle than is the case for the older plutons (Nb/La = 0.19–0.25, Paz Cove sample 86286082; $\varepsilon Nd = -9.4$ and $^{87}Sr/^{86}Sr_i = 0.71435$, Algae Lake sample 86265962, Sheraton et al., 1992). Moreover, probable syn-plutonic mafic granulite dykes with high Nb contents have been reported in the Booth Peninsula batholith (Sheraton et al., 1995).

Sheraton et al. (1992) suggested that Group 1 mafic dykes and the Charnockite Peninsula pluton could be coeval and originate from long-term (strongly) enriched lithospheric mantle with an OIB-like Nb-enriched component, whereas mafic dyke groups 3 and 4 tapped varying proportions of depleted asthenospheric mantle and only moderately enriched lithospheric mantle. Group 3 dykes have higher $^{87}Sr/^{86}Sr_i$

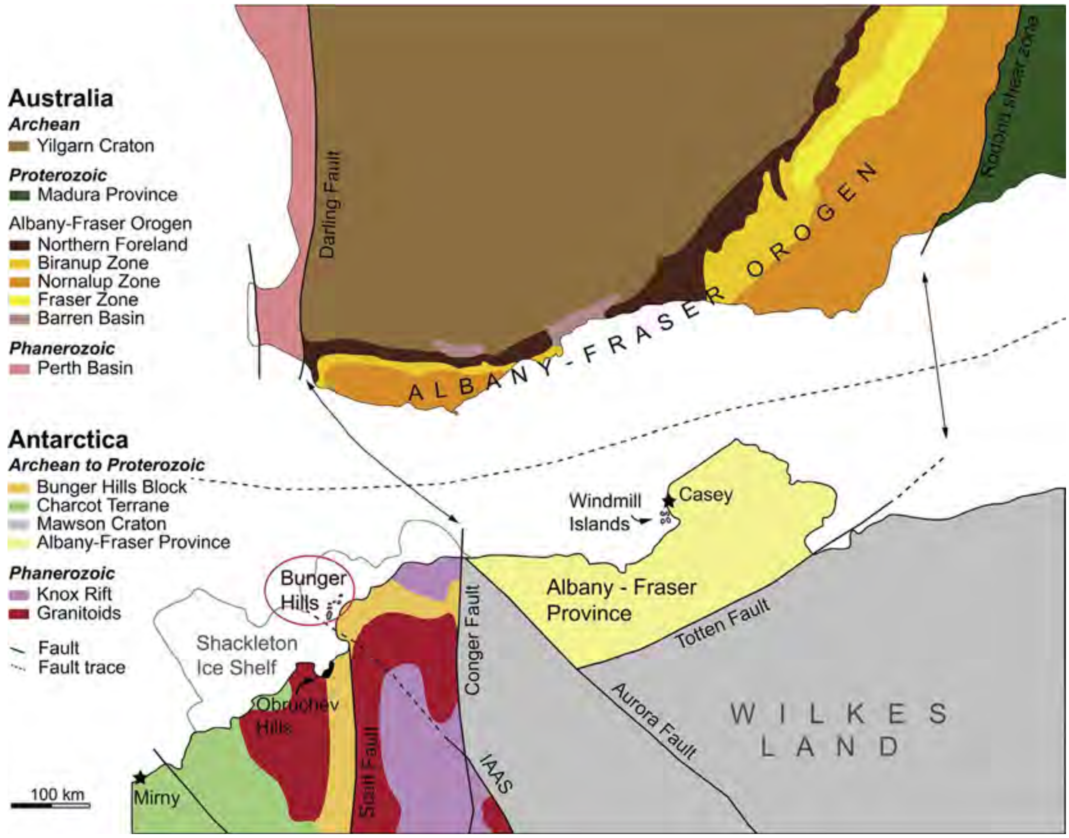

Fig. 9. Approximate reconstructed configuration of the Yilgarn Craton, Bunger Hills and Windmill Islands at ca. 1150 Ma. Modified after Tucker et al. (2017), Tucker and Hand (2016), Aitken et al. (2014, 2016), Boger (2011), Spaggiari et al. (2009) and 1:2,500,000 interpreted bedrock geology of Western Australia (Geological Survey of Western Australia, 2015). Piercing points of between the Darling–Conger and Rodona–Totten Faults are from Aitken et al. (2014, 2016).

(0.7043) than most Group 4 dykes, which results in an older apparent whole-rock Rb-Sr isochron age (1220 ± 80 Ma; Sheraton et al.,1990). If correct, this would suggest a time-progressive increase in contribution from less enriched, more depleted mantle material in the dykes, which in turn is consistent with a similar trend observed in the plutonic rocks.

6.2. *Tectonic setting of Bunger Hills at ca. 1130 Ma*

6.2.1. *Bunger Hills as part of the Albany-Fraser Orogen*

The Mesoproterozoic Albany-Fraser Orogen records two major tectonothermal events. The first stage at ca. 1340–1260 Ma was associated with the initial collision between the Western Australian and Mawson Cratons and the second at ca. 1214–1140 Ma with intracratonic reactivation and extension (Clark et al., 2000), both stages involving NW-directed compression in a transpressional setting (Myers, 1993; Nelson et al., 1995; Bodorkos and Clark, 2004). The Bunger Hills have widely been interpreted as a rifted fragment of the Albany–Fraser Orogen on the basis of similarities in lithology, structural style, kinematics, timing and degree of metamorphism (Black et al., 1992a,b; Sheraton et al., 1993, 1995; Nelson et al., 1995; Clark et al., 2000; Duebendorfer, 2002; Fitzsimons, 2003; Boger, 2011; Tucker et al., 2017) and more recently geophysical evidence (Aitken et al., 2014, 2016). The Windmill Islands, ca. 400 km east along strike of Bunger Hills, have also been proposed as an along-strike extension of the Albany–Fraser Orogen through similar arguments (Paul et al., 1995; Post et al., 1997; Zhang et al., 2012; Morrissey et al., 2017). In the recent reconstruction of Aitken et al. (2014, 2016), at ca. 1150 Ma the Bunger Hills are directly aligned with the southwestern Albany-Fraser Orogen (Fig. 9).

Tucker et al. (2017) proposed a revised model for the tectonic evolution of the Bunger Hills during the Paleo- and Mesoproterozoic, suggesting that they evolved as part of the Biranup and/or Nornalup zones of the Albany–Fraser Orogen. At ca. 1815–1650 Ma, Bunger Hills (then part of the southern margin of the Yilgarn Craton) was part of a back-arc (Biranup Zone) above a north-dipping subduction zone along the southern margin of the Yilgarn Craton (Kirkland et al., 2011; Spaggiari et al., 2015; Aitken et al., 2016). The period between ca. 1710 and 1650 Ma in the Albany-Fraser Orogen coincides with widespread magmatism, formation of a series of sedimentary basins and high-temperature metamorphism associated with the Biranup Orogeny (Kirkland et al., 2011; Spaggiari et al., 2011). Consistent with this scenario, isotope evidence suggests that recycling of an Archean basement source beneath the Bunger Hills was diluted by significant formation of new crust at ca. 1700 Ma (Tucker et al., 2017).

The ca. 1700 Ma volcaniclastic sequence at Bunger Hills described by Tucker et al. (2017) formed as part of the Biranup Zone during extension and voluminous magmatism in a back-arc setting, likely isolating the area as a basement high. The extensive metapelite sequence was deposited between ca. 1700 and 1500 Ma during uplift and erosion, possibly in a passive margin setting some distance away from the Yilgarn Craton margin (Tucker et al., 2017). After a relative period of quiescence, intense deformation and metamorphism at ca. 1330–1150 Ma followed during the two-stage Albany–Fraser Orogeny and collision of the Western Australian and Mawson cratons with peak metamorphic conditions at ca. 1200–1150 Ma associated with emplacement of voluminous isotopically evolved charnockites produced mainly by crustal reworking and varying contributions from depleted mantle. The revised model is in agreement with the interpreted location of Bunger Hills in the model of Aitken et al. (2014, 2016) and consistent with evidence for back-arc setting at Windmill Islands at ca. 1410 Ma (Morrissey et al., 2017).

6.2.2. Mesoproterozoic mafic magmatism within the Albany–Fraser Orogen

The interpreted location of Bunger Hills as part of the south-western Albany–Fraser Orogen (now Nornalup Zone) at ca. 1134 Ma suggests that dykes of this age could also be present further east within the orogen. Moreover, probable syn-plutonic mafic granulite dykes reported from the ca. 1151 Ma Booth Peninsula batholith at Bunger Hills (Sheraton et al., 1995) implies that dykes of this age may also be present elsewhere within the Albany–Fraser Orogen. Mafic dykes at Windmill Islands are undated, the only available age constraint being from a late aplite dyke dated at 1138 ± 9 Ma with zircon U-Pb (Post, 2000). Post et al. (1997, 2000) proposed that the up to 50 m-wide unmetamorphosed WNW–NW-trending olivine gabbro dykes at Windmill Islands were emplaced after peak metamorphism between ca. 1160 Ma and 1138 Ma, postdating the Ardery charnockite and the aplite dykes. Similarly to the studied dyke at Bunger Hills, the olivine gabbro dykes at Windmill Islands post-date syn- to late-tectonic charnockites and appear to have similar chemical and mineralogical characteristics (Sheraton et al., 1995). The consistencies in trend, geochemistry and petrology between dyke groups 3 and 4 at Bunger Hills, the olivine gabbro dykes at Windmill Islands and the dyke in this study suggest that these dykes could be part of the same NW trending swarm with a > 400 km lateral extent.

Mafic dykes of similar age are not known within the Albany–Fraser Orogen or elsewhere in the Yilgarn Craton. The youngest identified Gnowangerup dykes of the Marnda Moorn LIP are 1203 ± 15 Ma (Evans, 1999) and the oldest known Warakurna LIP dykes in north-western Yilgarn are 1075 ± 10 Ma (Wingate, 2003). However, undated NE-trending dykes in the Tropicana region (Spaggiari et al., 2011) and NW-trending Beenong dykes in the south-east Yilgarn Craton are visible in aeromagnetic imagery and cross-cut all structures in the orogen (Wingate, 2007; Spaggiari et al., 2009, 2011). Field evidence indicates that the NE-trending undeformed amphibolitic dykes formed after deformation had ceased but before cooling, suggesting that they are younger than ca. 1140 Ma and may have formed late in stage II of the Albany–Fraser Orogeny (Spaggiari et al., 2011). Whilst these dykes may belong to the Warakurna LIP, or another as yet unidentified event, it is equally possible that they could be part of the same magmatic event that produced the 1134 Ma mafic dykes at Bunger Hills and possibly the olivine gabbro dykes at Windmill Islands. If so, the Bunger Hills and the Windmill Islands must have cooled much more rapidly after peak metamorphism because the dykes there are unmetamorphosed. Many dykes within the Albany–Fraser Orogen that have trends similar to the Gnowangerup and Fraser dykes of the Marnda Moorn LIP have been ascribed as belonging to the Marnda Moorn suite. However, as demonstrated by evidence from other mafic dyke studies in the Yilgarn and elsewhere, it cannot always be assumed that similarly oriented dykes in a region are part of the same magmatic event (Hanson et al., 2004; Wingate, 2007; French and Heaman, 2010; Stark et al., 2017).

If the Bunger Hills and Windmill Islands areas were juxtaposed with the Albany-Fraser Orogen at the time, the NW trend of the ca. 1134 Ma dykes in both areas (assuming they are coeval) probably also reflects the regional tectonic setting of the Albany-Fraser Orogen. The structural style and kinematics between the Albany-Fraser Orogen and the Bunger Hills area have been correlated (Duebendorfer, 2002) and peak metamorphism at Bunger Hills area corresponds closely with stage 2 of the Albany Fraser Orogeny (Sheraton et al., 1993; Clark et al., 2000; Tucker and Hand, 2016; Tucker et al., 2017). The NW-trending Bunger Hills dykes were emplaced during the final phase of stage 2, which within the Albany-Fraser Orogen has been interpreted as an episode of intracratonic reactivation, metamorphism and significant extension in a NNW to NW oriented transpressional setting (Bodorkos and Clark, 2004; Kirkland et al., 2011). Moreover, the ca. 1214–1203 Ma Marnda Moorn dykes emplaced early during stage 2, have a similar WN to NNW orientation in the southwestern part of the Albany-Fraser Orogen (Wingate and Pidgeon, 2005; Wingate et al., 2005; Wingate, 2007, 2017) .

6.2.3. Tectonic setting during emplacement of the 1134 Ma mafic dykes at Bunger Hills

As discussed in Section 6.1.4, clues to the tectonic evolution leading to mafic dyke emplacement at Bunger Hills may come from the plutonic rocks in the area. Mesoproterozoic charnockites in East Antarctica have been attributed to continental collision, their formation resulting from high temperature decompression melting of dehydrated but fertile granulites in the lower crust during post-collisional exhumation and decompression (Young et al., 1997; Zhao et al., 1997; Mikhalsky et al., 2006). The presence of abundant, largely unmetamorphosed late-tectonic charnockites and clockwise P–T paths at Bunger Hills and Windmill Islands is consistent with this scenario. The ca. 1203–1151 Ma Bunger Hills charnockites are synchronous with the ca. 1200–1140 Ma Esperance Supersuite of the Albany–Fraser Orogen, the ca. 1205–1163 Ma Ardery charnockite, and the youngest known Marnda Moorn LIP dykes (the Gnowangerup suite) dated at 1203 ± 15 Ma (Evans, 1999; Post, 2000; Zhang et al., 2012; Morrissey et al., 2017). Coeval emplacement of orogen-wide plutonic rocks and the Marnda Moorn LIP dykes (Wang et al., 2014) suggests that extensive melting of lower crust and the lithospheric mantle was synchronous with emplacement of vast amounts of mafic magma along the southern, western and eastern margins of the Yilgarn Craton. Emplacement of the Marnda Moorn dykes required lithospheric extension along the entire length of the orogen (Wingate et al., 2000) and probably caused the elevated regional thermal gradient that produced metamorphic monazite growth at ca. 1205 Ma (Dawson et al., 2003). Onset of rapid uplift and cooling between 1169 Ma and 1159 Ma in the western Albany–Fraser Orogen (Scibiorski et al., 2015) coincides with ca. 1170 Ma plutonic magmatism at Bunger Hills, followed by an increase in (depleted and/or less enriched) mantle input in the Ardery charnockite at Windmill Islands by ca. 1163 Ma (Morrissey et al., 2017) and in the Booth Peninsula batholith by ca. 1151 Ma (Sheraton et al., 1992).

The source of the ca. 1203–1170 Ma Bunger Hills plutons probably involved a heterogeneous, highly enriched mantle region with contributions from the lower crust and metasomatised SCLM (Sheraton et al., 1992; Zhang et al., 2012; Morrissey et al., 2017; Tucker et al., 2017) similar to the Esperance Supersuite granites, which were derived mainly by crustal recycling (Kirkland et al., 2011; Smithies et al., 2015; Tucker et al., 2017). In contrast, the Booth Peninsula batholith and the Ardery charnockite at Windmill Islands had a distinctively less enriched source (Sheraton et al., 1992; Morrissey et al., 2017). The apparent age-progressive increase of asthenospheric mantle input in the Bunger Hills and Windmill Islands charnockites is consistent with mafic underplating associated with orogenic collapse or rapid uplift interpreted as syn-tectonic active transpression (Scibiorski et al., 2015). This uplift appears to have affected both the Bunger Hills and Windmill Islands regions and may have been long-lived, with first plutonic activity commencing by ca. 1203 Ma and continuing at least until ca. 1151 Ma. Following cooling, at the latest by 1134 Ma, the crust was brittle enough to allow emplacement of the mafic dykes.

Geochemical evidence is consistent with a depleted or slightly enriched mantle source which interacted with a component of the subcontinental lithospheric mantle (SCLM) and/or lower crust that was metasomatically enriched and hybridized by an earlier subduction event or events during the Paleoproterozoic, and possibly in the Neoarchean (Sheraton et al., 1990, 1995). At Bunger Hills, formation of orthogneisses and the mantle extraction ages of the studied dyke all fall within the ca. 1815–1650 Ma interval, which is coeval with basin formation in a back-arc setting along the southern margin of the Yilgarn Craton during active subduction. During Paleoproterozoic arc activity, the mantle wedge would have been hybridized by addition of slab-derived fluids and/or melts and later incorporated into the continental lithospheric mantle during the Biranup and Albany-Fraser orogenies. The metasomatised and highly heterogeneous (at least in part, long-term enriched) sub-arc mantle was later tapped by parent magmas to the various plutons and dykes during active tectonic uplift and cooling associated with the final stages of the Albany–Fraser Orogeny. The emplacement of the 1134 Ma mafic dyke suite could thus mark the final phase of a prolonged episode of post-orogenic uplift which was associated with continued mafic underplating, decompression melting of the SCLM and lower crust that produced the plutonic rocks and, lastly, a thinned and thermally weakened lithosphere that permitted (asthenospheric) mantle material to dominate and intrude to at least middle crustal levels.

An alternative mechanism for the formation of the dykes could involve a mantle source much further away. If the NW-trending Windmill Island dykes are coeval with the NW-trending dykes at Bunger Hills, the extent of such a dyke swarm of at least 400 km could suggest a possible plume-like mantle source, similar to the giant ca. 1270 Ma Mackenzie (e.g. Ernst and Baragar, 1992; Baragar et al., 1996; Hou et al., 2010) and the ca. 2500–2540 Ma Matachewan dyke swarms (e.g. Ernst and Bleeker, 2010; Ciborowski et al., 2015). Moreover, dyke widths more than 10 m are characteristic of regional dyke swarms that acted as plumbing systems for LIPs (e.g. Ernst and Bell, 1992; Ernst, 2014). In this scenario, the dykes could have been emplaced laterally from a distant source, interacting with the locally heterogeneous and variably metasomatised continental lithosphere. If this is the case, dykes of ca. 1134 Ma age could also be present within the Albany-Fraser Orogen.

7. Conclusions

New U-Pb geochronology for the largest NW-trending olivine gabbro dyke at Bunger Hills yields a 1134 ± 9 Ma age, which is interpreted as the crystallisation age of the dyke. The new age constraint indicates that, according to current tectonic models, the dykes were emplaced in a late- to post-orogenic extensional setting that followed the collision of the West Australian and Mawson cratons during the final stage of the Mesoproterozoic Albany-Fraser Orogeny. Post-orogenic uplift and thinning of the lithosphere was associated with at least 50 million years of episodic crustal melting and reworking that produced the abundant plutonic rocks at Bunger Hills. Geochemical evidence suggests that the source of the dyke contained at least two distinctive components: a significant proportion of material with depleted mantle-like $^{143}Nd/^{144}Nd_i$ composition and a minor lower crust-like, metasomatically enriched lithospheric contaminant. A progressive increase in mantle-derived material in the plutonic rocks suggests that lithospheric extension was accompanied by mafic underplating. Uplift, extension and continued thermal weakening of the lithosphere by 1134 Ma culminated in the emplacement of several generations of mafic dykes within a relatively short period of time, which appear to carry variable imprints of the reworked lower crust underlying Bunger Hills. The undated WNW-NW trending olivine gabbro dykes at Windmill Islands also appear to post-date syn- to late-tectonic charnockites there and similarities in trend, geochemistry and petrology with the dykes at Bunger Hills suggest that these dykes could all be part of the same NW trending swarm at least 400 km in extent. This suggests an alternative mechanism of dyke formation involving a distant mantle source, potentially a plume, with the laterally propagating magma interacting locally with the heterogeneous lithosphere.

Acknowledgments

Cristina Talavera and Hao Gao are thanked for their generous assistance with SHRIMP analyses and Ian Fitzsimons for his valuable feedback on an earlier draft. We thank Richard Ernst for his constructive and thoughtful review that greatly improved the manuscript. This work was supported by the Australian Research Council Centre of Excellence for Core to Crust Fluid Systems (CE110001017), ARC Laureate Fellowship grant to ZXL (FL150100133), ARC future fellowship grant to XCW (FT140100826), Australian Antarctic Science Project 4191 to MH and CC and Curtin University ORD postgraduate scholarship to JCS. Zircon and baddeleyite analyses were carried out on the Sensitive High Resolution Ion Micro Probe mass spectrometer (SHRIMP II) at the John de Laeter Centre, Curtin University, with the financial support of the Australian Research Council and Auscope NCRIS.

References

Aitken, A.R.A., Betts, P.G., Young, D.A., Blankenship, D.D., Roberts, J.L., Siegert, M.J., 2016. The Australo-Antarctic Columbia to Gondwana transition. Gondwana Res. 29, 136–152. http://dx.doi.org/10.1016/j.gr.2014.10.019.
Aitken, A.R.A., Young, D.A., Ferraccioli, F., Betts, P.G., Greenbaum, J.S., Richter, T.G., Roberts, J.L., Blankenship, D.D., Siegert, M.J., 2014. The subglacial geology of Wilkes Land, East Antarctica. Geophys. Res. Lett. 41, 2390–2400.
Baragar, W.R.A., Ernst, R.E., Hulbert, L., Peterson, T., 1996. Longitudinal petrochemical variation in the Mackenzie dyke swarm, northwestern Canadian Shield. J. Petrol. 37, 317–359.
Black, L.P., Harris, L.B., Delor, C.P., 1992a. Reworking of Archaean and Early Proterozoic components a progressive, Middle Proterozoic tectonothermal event in the Albany Mobile Belt, Western Australia. Precamb. Res. 59, 95–123.
Black, L.P., Kinny, P.D., Sheraton, J.W., 1991. The difficulties of dating mafic dykes: an Antarctic example. Contrib. Mineral. Petrol. 109, 183–194. http://dx.doi.org/10.1007/BF00306478.
Black, L.P., Sheraton, J.W., Tingey, R.J., McCulloch, M.T., 1992b. New U-Pb zircon ages from the Denman Glacier Area, East Antarctica, and their significance for Gondwana reconstruction. Antarct. Sci. 4, 447–460. http://dx.doi.org/10.1017/S095410209200066X.
Bleeker, W., 2004. Taking the pulse of planet Earth: a proposal for a new multi-disciplinary flagship project in Canadian solid Earth sciences. Geosci Canada 31.
Bleeker, W., Ernst, R., 2006. Short-lived mantle generated magmatic events and their dyke swarms: the key unlocking Earth's paleogeographic record back to 2.6 Ga. In: Hanski, E.J., Mertanen, S., Rämö, O.T., Vuollo, J. (Eds.), Dyke Swarms—time Markers of Crustal Evolution: Selected Papers of the Fifth International Dyke Conference in Finland, Rovaniemi, Finland, 31 July- 3 Aug 2005 & Fourth International Dyke Conference, Kwazulu-Natal, South Africa 26–29 June 2001. CRC Press, London, pp. 3–26.
Blight, D.F., Oliver, R.L., 1977. The metamorphic geology of the Windmill Islands, Antarctica: A preliminary account. J. Geol. Soc. Aust. 24, 239–262. http://dx.doi.org/10.1080/00167617708728986.
Bodorkos, S., Clark, D.J., 2004. Evolution of a crustal-scale transpressive shear zone in the Albany-Fraser Orogen, SW Australia: 1. P-T conditions of Mesoproterozoic metamorphism in the Coramup Gneiss. J. Metamorph. Geol. 22, 691–711. http://dx.doi.org/10.1111/j.1525-1314.2004.00543.x.
Boger, S.D., 2011. Antarctica—before and after Gondwana. Gondwana Res. 19, 335–371.
Buchan, K.L., Ernst, R.E., Hamilton, M.A., Mertanen, S., Pesonen, L.J., Elming, S.-Å., 2001. Rodinia: the evidence from integrated palaeomagnetism and U-Pb geochronology. Precambrian Res. 110, 9–32.
Buchan, K.L., Goutier, J., Hamilton, M.A., Ernst, R.E., Matthews, W.A., 2007. Paleomagnetism, U-Pb geochronology, and geochemistry of Lac Esprit and other dyke swarms, James Bay area, Quebec, and implications for Paleoproterozoic deformation of the Superior Province. Can. J. Earth Sci. 44, 643–664.
Ciborowski, T.J.R., Kerr, A.C., Ernst, R.E., Mcdonald, I., Minifie, M.J., Harlan, S.S., Millar, I.L., 2015. The early proterozoic Matachewan large igneous province: Geochemistry. Petrogenesis Impl. Earth Evol. 56. http://dx.doi.org/10.1093/petrology/egv038.
Clark, D.J., Hensen, B.J., Kinny, P.D., 2000. Geochronological constraints for a two-stage history of the Albany – Fraser Orogen, Western Australia. Precambr. Res. 102, 155–183.
Coffin, M.F., Eldholm, O., 1994. Large igneous provinces: crustal structure, dimensions, and external consequences. Rev. Geophys. 32, 1–36. http://dx.doi.org/10.1029/93RG02508.
Collerson, K.D., Sheraton, J.W., 1986. Age and geochemical characteristics of a mafic dyke swarm in the Archaean Vestfold Block, Antarctica: inferences about Proterozoic dyke emplacement in Gondwana. J. Petrol. 27, 853–886.
Compston, W., Williams, I.S., Meyer, C., 1984. U-Pb geochronology of zircons from lunar breccia 73217 using a sensitive high mass-resolution ion microprobe. J. Geophys. Res. 89, B525. http://dx.doi.org/10.1029/JB089iS02p0B525.
Corfu, F., Hanchar, J.M., Hoskin, P.W.O., Kinny, P., 2003. Atlas of Zircon textures. Rev. Mineral. Geochem. 53, 469–500. http://dx.doi.org/10.2113/0530469.
Dawson, G.C., Krapež, B., Fletcher, I.R., McNaughton, N.J., Rasmussen, B., 2003. 1.2 Ga thermal metamorphism in the Albany-Fraser Orogen of Western Australia: consequence of collision or regional heating by dyke swarms? J. Geol. Soc. London. 160, 29–37. http://dx.doi.org/10.1144/0166-764901-119.
DePaolo, D.J., 1981a. Neodymium isotopes in the Colorado Front Range and crust–mantle evolution in the Proterozoic. Nature 291, 193–196. http://dx.doi.org/10.1038/291193a0.
DePaolo, D.J., 1981b. Trace element and isotopic effects of combined wallrock assimilation and fractional crystallization. Earth Planet. Sci. Lett. 53, 189–202.
Ding, P., James, P.R., 1991. Structural evolution of the Bunger Hills Area of East Antarctica. Geol. Evol. Antarct. Cambridge Univ. Press, Cambridge, pp. 13–17.
Duebendorfer, E.M., 2002. Regional correlation of mesoproterozoic structures and deformational events in the Albany-Fraser orogen, Western Australia. Precambr. Res. 116, 129–154. http://dx.doi.org/10.1016/S0301-9268(02)00017-7.
Ernst, R., Bleeker, W., 2010. Large igneous provinces (LIPs), giant dyke swarms, and mantle plumes: significance for breakup events within Canada and adjacent regions from 2.5 Ga to the Present. Can. J. Earth Sci. 47, 695–739. http://dx.doi.org/10.1139/e10-025.

Ernst, R.E., 2014. Large Igneous Provinces. Cambridge University Press.
Ernst, R.E., Baragar, W.R.A., 1992. Evidence from magnetic fabric for the flow pattern of magma in the Mackenzie giant radiating dyke swarm.
Ernst, R.E., Bell, K., 1992. Petrology of the Great Abitibi Dyke, Superior Province. Canada. J. Petrol. 33, 423–469.
Ernst, R.E., Buchan, K.L., 1997. Giant radiating dyke swarms: their use in identifying pre-Mesozoic large igneous provinces and mantle plumes, in: Large Igneous Provinces: Continental, Oceanic, and Planetary Flood Volcanism. American Geophysical Union Monograph 100, pp. 297–333.
R.E. Ernst M.A. Hamilton U. Soderlund J.A. Hanes D.P. Gladkochub A.V. Okrugin T. Kolotilina A.S. Mekhonoshin W. Bleeker A.N. LeCheminant K.L. Buchan K.R. Chamberlain A.N. Didenko Long-lived connection between southern Siberia and northern Laurentia in the Proterozoic Nat. Geosci 9 2016 464 469 10.1038/ngeo2700/http://www.nature.com/ngeo/journal/v9/n6/abs/ngeo2700.html#supplementary-information
Ernst, R.E., Head, J.W., Parfitt, E., Grosfils, E., Wilson, L., 1995. Giant radiating dyke swarms on Earth and Venus. Earth-Science Rev. 39, 1–58.
Evans, T., 1999. Extent and nature of the 1.2 Ga Wheatbelt dyke swarm, Yilgarn Craton, Western Australia. B.Sc. thesis, Univ. West. Aust. Perth.
Fitzsimons, I.C.W., 2003. Proterozoic basement provinces of southern and southwestern Australia, and their correlation with Antarctica. Geol. Soc. London Spec. Publ. 206, 93–130.
Fitzsimons, I.C.W., 2000a. Grenville-age basement provinces in East Antarctica: evidence for three separate collisional orogens. Geology 28, 879–882.
Fitzsimons, I.C.W., 2000b. A review of tectonic events in the East Antarctic Shield and their implications for Gondwana and earlier supercontinents. J. African Earth Sci. 31, 3–23.
Foley, S.F., Barth, M.G., Jenner, G.A., 2000. Rutile/melt partition coefficients for trace elements and an assessment of the influence of rutile on the trace element characteristics of subduction zone magmas. Geochim. Cosmochim. Acta 64, 933–938.
French, J.E., Heaman, L.M., 2010. Precise U-Pb dating of Paleoproterozoic mafic dyke swarms of the Dharwar craton, India: Implications for the existence of the Neoarchean supercraton Sclavia. Precambrian Res. 183, 416–441. http://dx.doi.org/10.1016/j.precamres.2010.05.003.
Genske, F.S., Beier, C., Stracke, A., Turner, S.P., Pearson, N.J., Hauff, F., Schaefer, B.F., Haase, K.M., 2016. Comparing the nature of the western and eastern Azores mantle. Geochim. Cosmochim. Acta 172, 76–92. http://dx.doi.org/10.1016/j.gca.2015.08.019.
Hacker, B.R., Kelemen, P.B., Behn, M.D., 2015. Continental lower crust. Annu. Rev. Earth Planet. Sci. 43, 167–205. http://dx.doi.org/10.1146/annurev-earth-050212-124117.
Halls, H.C., 1986. Paleomagnetism, structure, and longitudinal correlation of Middle Precambrian dykes from northwestern Ontario and Minnesota. Can. J. Earth Sci. 23, 142–157.
Halls, H.C., Kumar, A., Srinivasan, R., Hamilton, M.A., 2007. Paleomagnetism and U-Pb geochronology of easterly trending dykes in the Dharwar craton, India: feldspar clouding, radiating dyke swarms and the position of India at 2.37 Ga. Precambrian Res. 155, 47–68. http://dx.doi.org/10.1016/j.precamres.2007.01.007.
Halls, H.C., Palmer, H.C., 1990. The tectonic relationship of two Early Proterozoic dyke swarms to the Kapuskasing Structural Zone: a paleomagnetic and petrographic study. Can. J. Earth Sci. 27, 87–103. http://dx.doi.org/10.1139/e90-007.
Halls, H.C., Zhang, B., 1998. Uplift structure of the southern Kapuskasing zone from 2.45 Ga dike swarm displacement. Geology 26, 67–70. http://dx.doi.org/10.1130/0091-7613(1998) 026<0067:USOTSK>2.3.CO;2.
Hanson, R.E., Gose, W.A., Crowley, J.L., Ramezani, J., Bowring, S.A., Bullen, D.S., Hall, R.P., Pancake, J.A., Mukwakwami, J., 2004. Paleoproterozoic intraplate magmatism and basin development on the Kaapvaal Craton: Age, paleomagnetism and geochemistry of ~ 1.93 to ~ 1.87 Ga post-Waterberg dolerites. South African J. Geol. 107, 233–254.
Harley, S.L., Fitzsimons, I.C.W., Zhao, Y., 2013. Antarctica and supercontinent evolution: historical perspectives, recent advances and unresolved issues. Geol. Soc. London Spec. Publ. 383, 1–34.
Heaman, L.M., 2009. The application of U-Pb geochronology to mafic, ultramafic and alkaline rocks: An evaluation of three mineral standards. Chem. Geol. 261, 43–52. http://dx.doi.org/10.1016/j.chemgeo.2008.10.021.
Hoek, J.D., Seitz, H.-M., 1995. Continental mafic dyke swarms as tectonic indicators: an example from the Vestfold Hills, Antarctica. Precambr. Res. 75, 121–139.
Hou, G., 2012. Mechanism for three types of mafic dyke swarms. Geosci. Front. 3, 217–223. http://dx.doi.org/10.1016/j.gsf.2011.10.003.
Hou, G., Kusky, T.M., Wang, C., Wang, Y., 2010. Mechanics of the giant radiating Mackenzie dyke swarm: A paleostress field modeling. J. Geophys. Res. Solid Earth 115. http://dx.doi.org/10.1029/2007JB005475.
Irvine, T.N.J., Baragar, W., 1971. A guide to the chemical classification of the common volcanic rocks. Can. J. Earth Sci. 8, 523–548.
Irving, A.J., Frey, F.A., 1978. Distribution of trace elements between garnet megacrysts and host volcanic liquids of kimberlitic to rhyolitic composition. Geochim. Cosmochim. Acta 42, 771–787.
Johannsen, A., 1931. A Descriptive Petrography of The Igneous Rocks. The University of Chicago Press, Chicago.
Ju, W., Hou, G., Hari, K.R., 2013. Mechanics of mafic dyke swarms in the Deccan Large Igneous Province: Palaeostress field modelling. J. Geodyn. 66, 79–91. http://dx.doi.org/10.1016/j.jog.2013.02.002.
Kirkland, C.L., Spaggiari, C.V., Pawley, M.J., Wingate, M.T.D., Smithies, R.H., Howard, H.M., Tyler, I.M., Belousova, E.A., Poujol, M., 2011. On the edge: U-Pb, Lu–Hf, and Sm–Nd data suggests reworking of the Yilgarn craton margin during formation of the Albany-Fraser Orogen. Precambrian Res. 187, 223–247.
Lanyon, R., Black, L.P., Seitz, H.-M., 1993. U-Pb zircon dating of mafic dykes and its application to the Proterozoic geological history of the Vestfold Hills, East Antarctica. Contrib. Mineral. Petrol. 115, 184–203.
Le Maitre, R.W., Streckeisen, A., Zanettin, B., Le Bas, M.J., Bonin, B., Bateman, P., Bellieni, G., Dudek, A., Efremova, S., Keller, J., Lameyre, J., Sabine, P.A., Schmid, R., Sørensen, H., Woolley, A.R., 2002. Igneous Rocks: A Classification and Glossary of Terms: Recommendations of the International Union of Geological Sciences Subcommission on the Systematics of Igneous Rocks, second ed. Cambridge University Press, New York.
Li, X.-H., 1997. Geochemistry of the Longsheng Ophiolite from the southern margin of Yangtze Craton, SE China. Geochem. J. 31, 323–337. http://dx.doi.org/10.2343/geochemj.31.323.
Liu, Y., Liu, H., Li, X., 1996. Simultaneous and precise determination of 40 trace elements in rock samples using ICP-MS. Geochimica 6.
Ludwig, K., 2012. User's manual for Isoplot version 3.75–4.15: a geochronological toolkit for Microsoft. Berkeley Geochronological Cent. Spec. Publ.
Ludwig, K., 2009. Squid 2.50, A User's Manual (No. 2.50.11.02.03 Rev. 03 Feb 2011). Berkeley, California, USA.
Mikhalsky, E.V., Sheraton, J.W., Hahne, K., Prince, N., Mountains, C., Coast, M., 2006. Charnockite composition in relation to the tectonic evolution of East Antarctica. Gondwana Res. 9, 379–397. http://dx.doi.org/10.1016/j.gr.2005.11.007.
Morrissey, L.J., Payne, J.L., Hand, M., Clark, C., Taylor, R., Kirkland, C.L., Kylander-Clark, A., 2017. Linking the Windmill Islands, east Antarctica and the Albany-Fraser Orogen: Insights from U-Pb zircon geochronology and Hf isotopes. Precambr. Res. 293, 131–149 10.1016/j.precamres.2017.03.005.
Münker, C., Wörner, G., Yogodzinski, G., Churikova, T., 2004. Behaviour of high field strength elements in subduction zones: constraints from Kamchatka-Aleutian arc lavas. Earth Planet. Sci. Lett. 224, 275–293. http://dx.doi.org/10.1016/j.epsl.2004.05.030.
Myers, J.S., 1993. Precambrian tectonic history of the West Australian craton and adjacent orogens. Annu. Rev. Earth Planet. Sci. 21, 453–485.
Nelson, D.R., Myers, J.S., Nutman, A.P., 1995. Chronology and evolution of the Middle Proterozoic Albany-Fraser Orogen. Western Australia. Aust. J. Earth Sci. 42, 481–495.
Paul, E., Stuwe, K., Teasdale, J., Worley, B., 1995. Structural and Metamorphic Geology of the Windmill-Islands, East Antarctica - Field Evidence for Repeated Tectonothermal Activity. Aust. J. Earth Sci. 42, 453–469. http://dx.doi.org/10.1080/08120099508728216.
Pearce, J.A., 2008. Geochemical fingerprinting of oceanic basalts with applications to ophiolite classification and the search for Archean oceanic crust. Lithos 100, 14–48. http://dx.doi.org/10.1016/j.lithos.2007.06.016.
Pfänder, J.A., Münker, C., Stracke, A., Mezger, K., 2007. Nb/Ta and Zr/Hf in ocean island basalts — Implications for crust–mantle differentiation and the fate of Niobium. Earth Planet. Sci. Lett. 254, 158–172. http://dx.doi.org/10.1016/j.epsl.2006.11.027.
Post, N.J., 2000. Unravelling Gondwana fragments: an integrated structural, isotopic and petrographic investigation of the Windmill Islands, Antarctica. University of New South Wales PhD Thesis.
Post, N.J., Hensen, B.J., Kinny, P.D., 1997. Two metamorphic episodes during a 1340–1180 Ma convergent tectonic event in the Windmill Islands, East Antarctica. Antarct. Reg. Geol. Evol. Process. Terra Antarct. Sienna 157–161.
Puffer, J.H., 2001. Contrasting high field strength element contents of continental flood basalts from plume versus reactivated-arc sources. Geology 29, 675–678. http://dx.doi.org/10.1130/0091-7613(2001) 029<0675:CHFSEC>2.0.CO.
Rasmussen, B., Fletcher, I.R., 2010. Dating sedimentary rocks using in situ U-Pb geochronology of syneruptive zircon in ash-fall tuff & lt 1 mm thick. Geology 38, 299–302. http://dx.doi.org/10.1130/G30567.1.
Ravich, M.G., Klimov, L. V, Solov'ev, D.S., 1968. The Pre-Cambrian of East Antarctica. Israel Program for Scientific Translations [available from the US Department of Commerce, Clearinghouse for Federal Scientific and Technical Information, Springfield, Va.].
Rollinson, H.R., 1993. Using geochemical data: evaluation, presentation, interpretation. Longman Scientific & Technical; Copublished in the US with J. Wiley & Sons.
Rudnick, R.L., Fountain, D.M., 1995. Nature and composition of the continental crust: A lower crustal perspective. Rev. Geophys. 33, 267. http://dx.doi.org/10.1029/95RG01302.
Rudnick, R.L., Gao, S., 2003. Composition of the continental crust, in: Holland, H.D., Turekian, K.K. (Eds.), The Crust Vol. 3. Treatise on Geochemistry. pp. 1–64.
Salters, V.J.M., Stracke, A., 2004. Composition of the depleted mantle. Geochemistry, Geophys. Geosystems 5, Q05B07. doi:10.1029/2003GC000597
Saunders, A.D.A.D., Storey, M., Kent, R.W.W., Norry, M.J., Norrry, M.J., 1992. Consequences of plume-lithosphere interactions. Geol. Soc. Spec. Publ. London 68, 41–60.
Schmitt, A.K., Chamberlain, K.R., Swapp, S.M., Harrison, T.M., 2010. In situ U-Pb dating of micro-baddeleyite by secondary ion mass spectrometry. Chem. Geol. 269, 386–395. http://dx.doi.org/10.1016/j.chemgeo.2009.10.013.
Scibiorski, E., Tohver, E., Jourdan, F., 2015. Rapid cooling and exhumation in the western part of the Mesoproterozoic Albany-Fraser Orogen, Western Australia. Precambr. Res. http://dx.doi.org/10.1016/j.precamres.2015.02.005.
Sheraton, J.W., Black, L.P., 1982. Geochemistry and geochronology of Proterozoic tholeiite dykes of East Antarctica: evidence for mantle metasomatism. Contrib. Mineral. Petrol. 78, 305–317.
Sheraton, J.W., Black, L.P., McCulloch, M.T., Oliver, R.L., 1990. Age and origin of a compositionally varied mafic dyke swarm in the Bunger Hills, East Antarctica. Chem. Geol. 85, 215–246.
Sheraton, J.W., Black, L.P., Tindle, A.G., 1992. Petrogenesis of plutonic rocks in a Proterozoic granulite-facies terrane — the Bunger Hills, East Antarctica. Chem. Geol. 97, 163–198. http://dx.doi.org/10.1016/0009-2541(92)90075-G.

Sheraton, J.W., Offe, L.A., Tingey, R.J., Ellis, D.J., 1980. Enderby land, Antarctica—an unusual Precambrian high-grade metamorphic terrain. J. Geol. Soc. Aust. 27, 1–18.

Sheraton, J.W., Oliver, R.L., Stüwe, K., 1989. Geochemistry of Proterozoic Amphibolite dykes of Commonwealth Bay, Antarctica, and possible correlations with mafic dyke swarms elsewhere in Gondwanaland. Precambr. Res. 44, 353–361. http://dx.doi.org/10.1016/0301-9268(89)90052-1.

Sheraton, J.W., Thomson, J.W., Collerson, K.D., 1987a. Mafic dyke swarms of Antarctica. Mafic Dyke Swarms 419–432.

Sheraton, J.W., Tingey, R.J., 1994. Bedrock Geology of the Bunger Hills-Denman Glacier Region, Australian Antarctic Territory. Aust. Geol. Surv. Organ. 1250 000 Map Ser.

Sheraton, J.W., Tingey, R.J., Black, L.P., Offe, L.A., Ellis, D.J., 1987b. Geology of Enderby Land and western Kemp Land. Antarctica. BMR Bull. 233, 51p.

Sheraton, J.W., Tingey, R.J., Black, L.P., Oliver, R.L., 1993. Geology of the Bunger Hills area, Antarctica: implications for Gondwana correlations. Antarct. Sci. 5, 85–102. http://dx.doi.org/10.1017/S0954102093000112.

Sheraton, J.W., Tingey, R.J., Oliver, R.L., Black, L.P., 1995. Geology of the Bunger Hills-Denman Glacier region, East Antarctica, BMR Bulletin 244. Australian Geological Survey Organisation.

Sims, K.W.W., DePaolo, D.J., 1997. Inferences about mantle magma sources from incompatible element concentration ratios in oceanic basalts. Geochim. Cosmochim. Acta 61, 765–784. http://dx.doi.org/10.1016/S0016-7037(96)00372-9.

Smithies, R., Spaggiari, C., Kirkland, C., 2015. Building the crust of the Albany-Fraser Orogen: Constraints from granite geochemistry, in: GSWA 2015 Extended Abstracts-Promoting the Prospectivity of Western Australia. Geological Survey of Western Australia, pp. 31–35.

Spaggiari, C.V., Kirkland, C.L., Smithies, H.R., Wingate, M.T.D., Belousova, E.A., 2015. Transformation of an Archean craton margin during Proterozoic basin formation and magmatism: The Albany-Fraser Orogen, Western Australia. Precamb. Res. 266, 440–466. http://dx.doi.org/10.1016/j.precamres.2015.05.036.

Spaggiari, C. V, Bodorkos, S., Barquero-Molina, M., Tyler, I.M., Wingate, M.T.D., 2009. Interpreted bedrock geology of the South Yilgarn and of the South Yilgarn and Central Albany-Fraser Orogen, Western Australia, Record 2009/10.

Spaggiari, C. V, Kirkland, C.L., Pawley, M.J., Smithies, R.H., Wingate, M.T.D., Doyle, M. G., Blenkinsop, T.G., Clark, C., Oorschot, C.W., Fox, L.J., 2011. The geology of the east Albany-Fraser Orogen—a field guide. Geol. Surv. West. Aust. Rec. 2011/23 23, 97.

Stacey, J.S.T., Kramers, J.D., 1975. Approximation of terrestrial lead isotope evolution by a two-stage model. Earth Planet. Sci. Lett. 26, 207–221.

Stark, J.C., Wang, X.-C., Denyszyn, S.W., Li, Z.-X., Rasmussen, B., Zi, J.-W., Sheppard, S., Liu, Y., 2017. Newly identified 1.89 Ga mafic dyke swarm in the Archean Yilgarn Craton, Western Australia suggests a connection with India. Precamb. Res. http://dx.doi.org/10.1016/j.precamres.2017.12.036.

Stern, R.A., 2001. A new isotopic and trace-element standard for the ion microprobe: preliminary thermal ionization mass spectrometry (TIMS) U-Pb and electron-microprobe data, Geological Survey of Canada Current Research 2001-F. Geological Survey of Canada.

Stern, R.A., Bodorkos, S., Kamo, S.L., Hickman, A.H., Corfu, F., 2009. Measurement of SIMS instrumental mass fractionation of Pb isotopes during zircon dating. Geostand. Geoanalytical Res. 33, 145–168. http://dx.doi.org/10.1111/j.1751-908X.2009.00023.x.

Stüwe, K., Powell, R., 1989. Metamorphic evolution of the Bunger Hills, East Antarctica: evidence for substantial post-metamorphic peak compression with minimal cooling in a Proterozoic orogenic event. J. Metamorph. Geol. 7, 449–464.

Stüwe, K., Wilson, C.J.L., 1990. Interaction between deformation and charnockite emplacement in the Bunger Hills, East Antarctica. J. Struct. Geol. 12, 767–783. http://dx.doi.org/10.1016/0191-8141(90)90088-g.

Sun, S.-S., McDonough, W.F., 1989. Chemical and isotopic systematics of oceanic basalts: implications for mantle composition and processes. Geol. Soc. London Spec. Publ. 42, 313–345. http://dx.doi.org/10.1144/GSL.SP.1989.042.01.19.

Suzuki, S., Ishizuka, H., Kagami, H., 2008. Early to middle Proterozoic dykes in the Mt. Riiser-Larsen area of the Napier Complex, East Antarctica: tectonic implications as deduced from geochemical studies. Geol. Soc. London Spec. Publ. 308, 195–210.

Taylor, S.R., McLennan, S.M., 1985. The Continental Crust: Its Composition and Evolution, first ed. Blackwell Scientific Publishers, Palo Alto, CA.

Teixeira, W., D'Agrella-Filho, M.S., Hamilton, M.A., Ernst, R.E., Girardi, V.A.V., Mazzucchelli, M., Bettencourt, J.S., 2013. U-Pb (ID-TIMS) baddeleyite ages and paleomagnetism of 1.79 and 1.59Ga tholeiitic dyke swarms, and position of the Rio de la Plata Craton within the Columbia supercontinent. Lithos 174, 157–174. http://dx.doi.org/10.1016/j.lithos.2012.09.006.

Tucker, N.M., Hand, M., 2016. New constraints on metamorphism in the Highjump Archipelago, East Antarctica. Antarct. Sci. 28, 487–503. http://dx.doi.org/10.1017/S095410201600033X.

Tucker, N.M., Payne, J.L., Clark, C., Hand, M., Taylor, R.J., Kylander-Clark, A.R.C., 2017. Proterozoic reworking of Archean (Yilgarn) basement in the Bunger Hills, east Antarctica. Precamb. Res. 298, 16–38.

Van Westrenen, W., Blundy, J.D., Wood, B.J., 2001. High field strength element/rare earth element fractionation during partial melting in the presence of garnet: Implications for identification of mantle heterogeneities. Geochemistry, Geophys. Geosystems 2. doi:10.1029/2000GC000133.

Wang, X.-C., Li, Z.-X., Li, J., Pisarevsky, S.A., Wingate, M.T.D., 2014. Genesis of the 1.21 Ga Marnda Moorn large igneous province by plume–lithosphere interaction. Precamb. Res. 241, 85–103. http://dx.doi.org/10.1016/j.precamres.2013.11.008.

Wang, X.-C., Wilde, S.A., Xu, B., Pang, C.-J., 2016. Origin of arc-like continental basalts: Implications for deep-Earth fluid cycling and tectonic discrimination. Lithos. http://dx.doi.org/10.1016/j.lithos.2015.12.014.

Wang, X.C., Li, Z.X., Li, X.H., Li, J., Liu, Y., Long, W.G., Zhou, J.B., Wang, F., 2012. Temperature, Pressure, and Composition of the Mantle Source Region of Late Cenozoic Basalts in Hainan Island, SE Asia: a Consequence of a Young Thermal Mantle Plume close to Subduction Zones? J. Petrol. 53, 177–233. http://dx.doi.org/10.1093/petrology/egr061.

Weaver, B.L., Tarney, J., 1981. The Scourie dyke suite: Petrogenesis and geochemical nature of the Proterozoic sub-continental mantle. Contrib. Mineral. Petrol. 78, 175–188. http://dx.doi.org/10.1007/BF00373779.

Weaver, B.L., Tarney, J., 1980. Continental crust composition and nature of the lower crust: constraints from mantle Nd-Sr isotope correlation. Nature 286, 342–346.

Willbold, M., Stracke, A., 2006. Trace element composition of mantle end-members: Implications for recycling of oceanic and upper and lower continental crust. Geochemistry, Geophys. Geosystems 7, n/a-n/a. doi:10.1029/2005GC001005.

Wingate, M.T.D., Campbell, I.H., Compston, W., Gibson, G.M., 1998. Ion microprobe U-Pb ages for Neoproterozoic basaltic magmatism in south-central Australia and implications for the breakup of Rodinia. Precamb. Res. 87, 135–159. http://dx.doi.org/10.1016/S0301-9268(97)00072-7.

Wingate, M.T.D., 2017. Mafic dyke swarms and large igneous provinces in Western Australia get a digital makeover, in: Geological Survey of Western Australia Record 2017/2. Geological Survey of Western Australia, pp. 4–8.

Wingate, M.T.D., 2007. Proterozoic mafic dykes in the Yilgarn Craton, in: Proceedings of Geoconferences (WA) Inc. Kalgoorlie 2007 Conference, Kalgoorlie, Western Australia. pp. 80–84.

Wingate, M.T.D., 2003. Age and Palaeomagnetism of Dolerite Sills Intrusions of the Southeastern Collier Basin, and the Earaheedy and Yerrida Basins, Western Australia, in: Western Australian Geological Survey Record, 2003/3. Geological Survey of Western Australia, p. 35.

Wingate, M.T.D., 1997. Testing Precambrian continental reconstructions using ion microprobe U-Pb baddeleyite geochronology and paleomagnetism of mafic igneous rocks. Australian National University.

Wingate, M.T.D., Campbell, I.H., Harris, L.B., 2000. SHRIMP baddeleyite age for the Fraser dyke swarm, southeast Yilgarn Craton. Western Australia. Aust. J. Earth Sci. 47, 309–313.

Wingate, M.T.D., Compston, W., 2000. Crystal orientation effects during ion microprobe U-Pb analysis of baddeleyite. Chem. Geol. 168, 75–97. http://dx.doi.org/10.1016/S0009-2541(00)00184-4.

Wingate, M.T.D., Morris, P.A., Pirajno, F., Pidgeon, R.T., 2005. Two large igneous provinces in Late Mesoproterozoic Australia, in: Supercontinents and Earth Evolution Symposium. Geological Society of Australia Abstracts, p. 151.

Wingate, M.T.D., Pidgeon, R.T., 2005. The Marnda Moorn LIP, a late Mesoproterozoic large igneous province in the Yilgarn craton, Western Australia. July 2005 LIP of the month [WWW Document]. (unpub). Large Igneous Prov. Comm. Int. Assoc. Volcanol. Chem. Earth's Inter. URL http://www.largeigneousprovinces.org/05jul

Young, D.N., Zhao, J., Ellis, D.J., McCulloch, M.T., 1997. Geochemical and Sr-Nd isotopic mapping of source provinces for the Mawson charnockites, east Antarctica: implications for Proterozoic tectonics and Gondwana reconstruction. Precamb. Res. 86, 1–19. http://dx.doi.org/10.1016/S0301-9268(97)00030-2.

Zhang, S.H., Zhao, Y., Liu, X.C., Liu, Y.S., Hou, K.J., Li, C.F., Ye, H., 2012. U-Pb geochronology and geochemistry of the bedrocks and moraine sediments from the Windmill Islands: Implications for Proterozoic evolution of East Antarctica. Precamb. Res. 206–207, 52–71. http://dx.doi.org/10.1016/j.precamres.2012.02.019.

Zhao, J., Ellis, D.J., Kilpatrick, J.A., McCulloch, M.T., 1997. Geochemical and Sr-Nd isotopic study of charnockites and related rocks in the northern Prince Charles Mountains, East Antarctica: implications for charnockite petrogenesis and proterozoic crustal evolution. Precamb. Res. 81, 37–66. http://dx.doi.org/10.1016/S0301-9268(96)00022-8.

Statement of Authorship

Title of Paper	**First evidence of Archean mafic dykes at 2.62 Ga in the Yilgarn Craton, Western Australia: links to cratonisation and the Zimbabwe Craton**	
Publication Status	**Published**	Accepted for publication
	Submitted for publication	Publication Style
Publication Details	Stark, J.C., Wilde, S.A., Söderlund, U., Li, Z.-X., Rasmussen, B., Zi, J.-W., 2018. First evidence of Archean mafic dykes at 2.62 Ga in the Yilgarn Craton, Western Australia: links to cratonisation and the Zimbabwe Craton. Precambrian Res. 317, 1–13.	

Author Contributions

By signing the Statement of Authorship, each author certifies that their stated contribution to the publication is accurate and that permission is granted for the publication to be included in the candidate's thesis.

Name of Principal Author (Candidate)	Jutta Camilla Stark		
Contribution to the Paper	Jutta Camilla Stark collected the samples, undertook SHRIMP dating and most of the interpretation and drafted the manuscript		
Overall percentage (%)	65		
Signature		Date	01/06/2018

Name of Co-Author	Simon Wilde		
Contribution to the Paper	Simon Wilde assisted with the concept and drafting of the manuscript and with the interpretation of the results		
Overall percentage (%)	10		
Signature		Date	01/06/2018

Name of Co-Author	Ulf Söderlund		
Contribution to the Paper	Ulf Söderlund undertook baddeleyite separation and ID-TIMS dating		
Overall percentage (%)	10		
Signature		Date	01/06/2018

Name of Co-Author	Zheng-Xiang Li		
Contribution to the Paper	Zheng-Xiang Li is the principal supervisor of the candidate and assisted with the concept, drafting of the manuscript and interpretation of the results		
Overall percentage (%)	5		
Signature		Date	01/06/2018

Name of Co-Author	Birger Rasmussen		
Contribution to the Paper	Birger Rasmussen assisted with the SHRIMP U-Pb geochronology and interpretation of the results		
Overall percentage (%)	5		
Signature		Date	01/06/2018

Name of Co-Author	Jian-Wei Zi		
Contribution to the Paper	Jian-Wei Zi assisted with the SHRIMP dating, sample preparation and data processing		
Overall percentage (%)	5		
Signature	Zi jianwei	Date	01/06/2018

Copyright Clearance Center RightsLink®

Home | Create Account | Help

Title: First evidence of Archean mafic dykes at 2.62 Ga in the Yilgarn Craton, Western Australia: Links to cratonisation and the Zimbabwe Craton

Author: J. Camilla Stark,Simon A. Wilde,Ulf Söderlund,Zheng-Xiang Li,Birger Rasmussen,Jian-Wei Zi

Publication: Precambrian Research

Publisher: Elsevier

Date: October 2018

LOGIN

If you're a copyright.com user, you can login to RightsLink using your copyright.com credentials.
Already **a RightsLink user** or want to learn more?

Please note that, as the author of this Elsevier article, you retain the right to include it in a thesis or dissertation, provided it is not published commercially. Permission is not required, but please ensure that you reference the journal as the original source. For more information on this and on your other retained rights, please visit: https://www.elsevier.com/about/our-business/policies/copyright#Author-rights

BACK | CLOSE WINDOW

Precambrian Research 317 (2018) 1–13

Contents lists available at ScienceDirect

Precambrian Research

journal homepage: www.elsevier.com/locate/precamres

First evidence of Archean mafic dykes at 2.62 Ga in the Yilgarn Craton, Western Australia: Links to cratonisation and the Zimbabwe Craton

J. Camilla Stark[a,b,*], Simon A. Wilde[b], Ulf Söderlund[c,d], Zheng-Xiang Li[a,b], Birger Rasmussen[e], Jian-Wei Zi[b,f]

[a] Earth Dynamics Group, Curtin University, GPO Box U1987, Perth, WA 6845, Australia
[b] The Institute for Geoscience Research (TIGeR), School of Earth and Planetary Sciences, Curtin University, GPO Box U1987, Perth, WA 6845, Australia
[c] Department of Geology, Lund University, Sölvegatan 12, SE-223 62 Lund, Sweden
[d] Department of Geosciences, Swedish Museum of Natural History, Box 50 007, SE-104 05 Stockholm, Sweden
[e] School of Earth Sciences, The University of Western Australia, Perth, WA 6009, Australia
[f] State Key Lab of Geological Processes and Mineral Resources, China University of Geosciences, Wuhan 430074, China

ARTICLE INFO

Keywords:
Yilgarn Craton
Zimbabwe Craton
Mafic dykes
Geochronology
U-Pb baddeleyite
Yandinilling dyke swarm

ABSTRACT

The Archean Yilgarn Craton in Western Australia hosts at least five generations of Proterozoic mafic dykes, the oldest previously identified dykes belonging to the ca. 2408–2401 Ma Widgiemooltha Supersuite. We report here the first known Archean mafic dyke dated at 2615 ± 6 Ma by the ID-TIMS U-Pb method on baddeleyite and at 2610 ± 25 Ma using *in situ* SHRIMP U-Pb dating of baddeleyite. Aeromagnetic data suggest that the dyke is part of a series of NE-trending intrusions that potentially extend hundreds of kilometres in the southwestern part of the craton, here named the Yandinilling dyke swarm. Mafic magmatism at 2615 Ma was possibly related to delamination of the lower crust during the final stages of assembly and cratonisation, and was coeval with the formation of late-stage gold deposit at Boddington. Paleogeographic reconstructions suggest that the Yilgarn and Zimbabwe cratons may have been neighbours from ca. 2690 Ma to 2401 Ma and if the Zimbabwe and Kaapvaal cratons amalgamated at 2660–2610 Ma, the 2615 Ma mafic magmatism in the southwestern Yilgarn Craton may be associated with the same tectonic event that produced the ca. 2607–2604 Ma Stockford dykes in the Central Zone of the Limpopo Belt. Paleomagnetic evidence and a similar tectonothermal evolution, including coeval low-pressure high-temperature metamorphism, voluminous magmatism, and emplacement of mafic dykes, support a configuration where the northern part of the Zimbabwe Craton was adjacent to the western margin of the Yilgarn Craton during the Neoarchean. Worldwide, reliably dated mafic dykes of this age have so far been reported from the Yilgarn Craton, the Limpopo Belt and the São Francisco Craton.

1. Introduction

Mafic dyke swarms are important markers for supercontinent reconstructions and mantle plumes (e.g., Ernst and Buchan, 1997; Buchan et al., 2001; Bleeker and Ernst, 2006; Ernst and Srivastava, 2008; Ernst et al., 2010, 2013) and act as indicators of local tectonic setting, including paleostress fields and pre-existing crustal weaknesses (Ernst et al., 1995; Hoek and Seitz, 1995; Halls and Zhang, 1998; Hou, 2012; Ju et al., 2013). Throughout the geological evolution of the Earth, mafic dykes have been associated with processes causing intracratonic extension of the crust, such as subduction (back-arc extension), post-orogenic collapse, plumes and rifting during supercontinent breakup. However, mafic dykes may also be linked with early cratonisation history soon after amalgamation and stabilization of crustal blocks. A recent example is reported from the North China Craton, where emplacement of ca. 2516–2504 Ma dykes signifies the presence of a deep subcontinental lithosphere and constrains the time of final cratonisation during the Neoarchean (Li et al., 2010).

The Archean Yilgarn Craton of Western Australia hosts at least five generations of Proterozoic mafic dykes, including the 2408–2401 Ma Widgiemooltha Supersuite (Sofoulis, 1965; Evans, 1968; Hallberg, 1987; Doehler and Heaman, 1998; Nemchin and Pidgeon, 1998; Wingate, 1999; French et al., 2002; Pisarevsky et al., 2015), the 1888 Ma Boonadgin dykes (Stark et al., 2017), the 1210 Ma Marnda Moorn Large Igneous Province (LIP; Wingate et al., 1998, 2000; Wingate, 2007), and limited occurrences of the 1075 Ma Warakurna LIP dykes (Wingate et al., 2002, 2004) and the 735 Ma Nindibillup dykes (Spaggiari et al., 2009, 2011; Wingate, 2017). The Widgiemooltha

* Corresponding author at: Earth Dynamics Group, Curtin University, GPO Box U1987, Perth, WA 6845, Australia.
E-mail address: c.stark@postgrad.curtin.edu.au (J.C. Stark).

https://doi.org/10.1016/j.precamres.2018.08.004
Received 9 March 2018; Received in revised form 28 May 2018; Accepted 20 August 2018
Available online 24 August 2018
0301-9268/

Supersuite has been linked with a mantle plume and rifting of an Archean supercraton (Heaman, 1997; Halls et al., 2007; Mohanty, 2015), the Boonadgin dykes with post-orogenic far-field extension or a mantle plume (Stark et al., 2017) and the Marnda Moorn and Warakurna LIPs also with mantle plumes (Wingate et al., 2004; Wang et al., 2014). We present here *in situ* SHRIMP and ID-TIMS U-Pb results for the first known Archean mafic dyke within the Yilgarn Craton, emplaced during the final stages of cratonisation and marking one of the earliest tectonothermal events affecting the stabilized craton. We discuss the tectonic setting, timing of emplacement and the possible association of the mafic dykes with post-orogenic processes during final stages of cratonisation. We also consider evidence from paleogeographic reconstructions and coeval tectonothermal events that may link the evolution of the Yilgarn and Zimbabwe cratons during the Neoarchean.

2. Regional geology

2.1. The Yilgarn Craton

The Archean Yilgarn Craton of Western Australia is a ca. 900 × 1000 km granite-greenstone crustal block, which is divided into the South West, Narryer, Youanmi, Kalgoorlie, Kurnalpi and Burtville terranes, the latter three forming the Eastern Goldfields Superterrane (Fig. 1) (Cassidy et al., 2006). The craton is bounded by three Proterozoic orogenic belts: the ca. 2005–570 Ma Capricorn Orogen in the north (Cawood and Tyler, 2004; Sheppard et al., 2010; Johnson et al., 2011), the ca. 1815–1140 Ma Albany-Fraser Orogen in the south and east (Nelson et al., 1995; Clark et al., 2000; Spaggiari et al., 2015), and the ca. 1600–525 Ma Pinjarra Orogen in the west (Myers, 1990; Wilde, 1999; Ksienzyk et al., 2012). Most of the terranes formed between ca. 3050 and 2550 Ma and whereas the South West and Narryer Terranes in the west comprise high-grade supracrustal rocks, granitic gneisses and granites, the Youanmi and Eastern Goldfields Terranes in the east are dominated by greenstone belts separated by granites and granitic gneisses (Fig. 2) (e.g., Gee et al., 1981; Pidgeon and Wilde, 1990; Myers, 1993; Wilde et al., 1996; Nelson, 1997; Cassidy et al., 2002; Barley et al., 2003). Recent Sm-Nd isotopic mapping suggests the presence of an older western proto-craton comprising the Narryer, South West and Youanmi Terranes and a younger (more juvenile) eastern part, which comprises the Eastern Goldfields Superterrane (e.g. Champion and Cassidy, 2007; Mole et al., 2015; Witt et al., 2018).

Amalgamation of the Yilgarn Craton involved repeated collisions during a Neoarchean orogeny between ca. 2730 and 2625 Ma (Myers, 1993, 1995; Barley et al., 2003; Blewett and Hitchman, 2006; Korsch et al., 2011; Zibra et al., 2017a; Witt et al., 2018) with development of a stable cratonic lithosphere by ca. 2660 Ma (Zibra et al., 2017b). The Youanmi Terrane is considered to be the isotopically oldest nucleus of the Yilgarn Craton onto which other terranes accreted (Cassidy et al., 2002, 2006; Champion and Cassidy, 2008; Champion, 2013), with collisions between the Youanmi and Narryer terranes sometime between ca. 2780 and 2630 Ma (Myers, 1993, 1995; Nutman et al., 1993; Cassidy et al., 2002), the Youanmi and Kalgoorlie Terranes between ca. 2678 and 2658 Ma (Standing, 2008; Czarnota et al., 2010) and the Youanmi and the South West Terranes between ca. 2652 and 2625 Ma (Wilde and Pidgeon, 1987; Nemchin et al., 1994; Qiu et al., 1997a; Qiu and Groves, 1999; McFarlane, 2010). Cratonisation was accompanied by widespread granitic magmatism between ca. 2690 Ma and 2625 Ma (Compston et al., 1986; Wilde and Pidgeon, 1986; Champion and

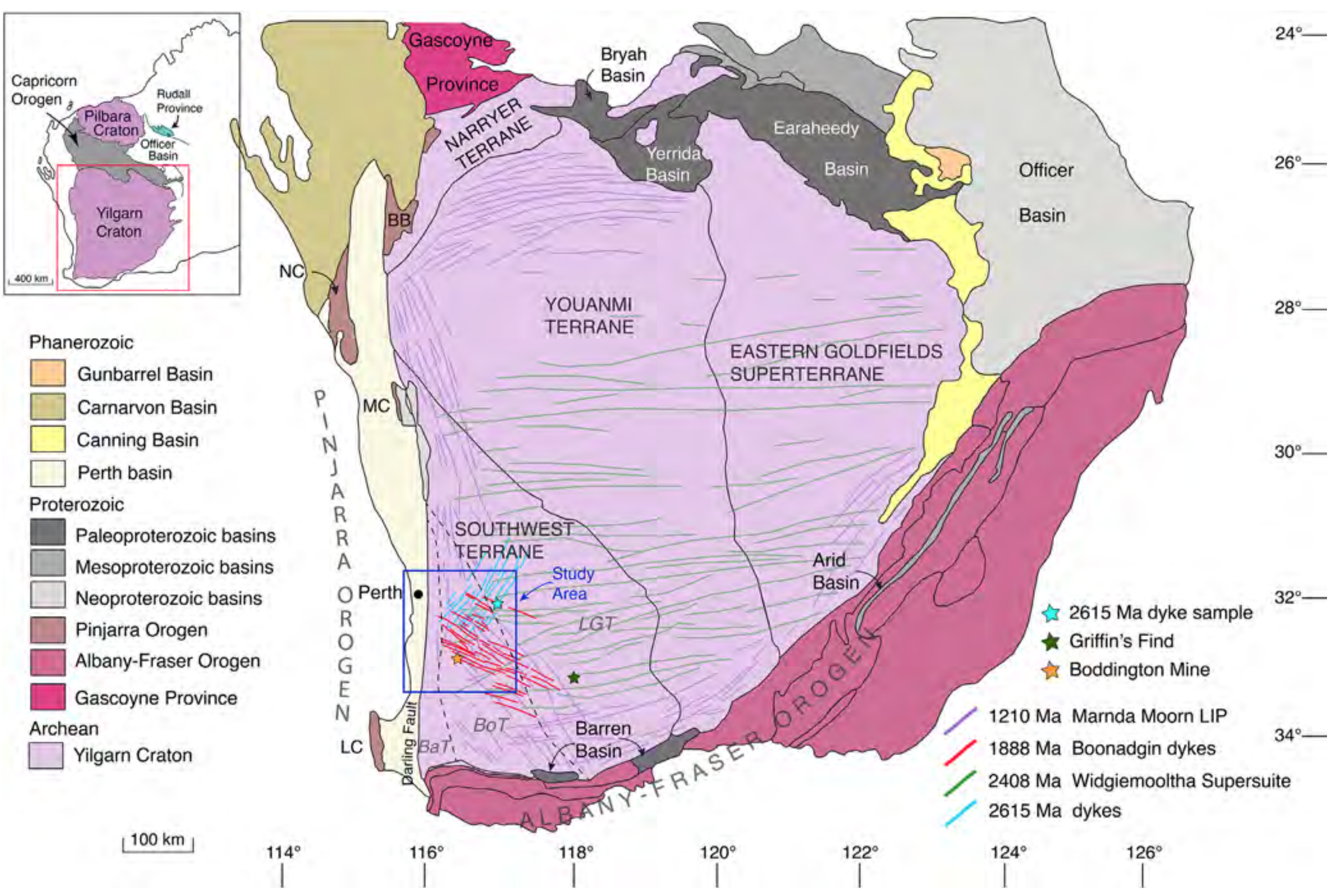

Fig. 1. Map of the Yilgarn Craton showing major tectonic units. Inset shows the extent of the West Australian Craton (Pilbara Craton, Yilgarn Craton and Capricorn Orogen). From Geological Survey of Western Australia 1:2.5 M Interpreted Bedrock Geology 2015 and 1:10 M Tectonic Units 2016. Dashed lines are terrane boundaries within the southwestern Yilgarn Craton after Wilde et al. (1996): BaT = Balingup Terrane, BoT = Boddington Terrane and LGT = Lake Grace Terrane.

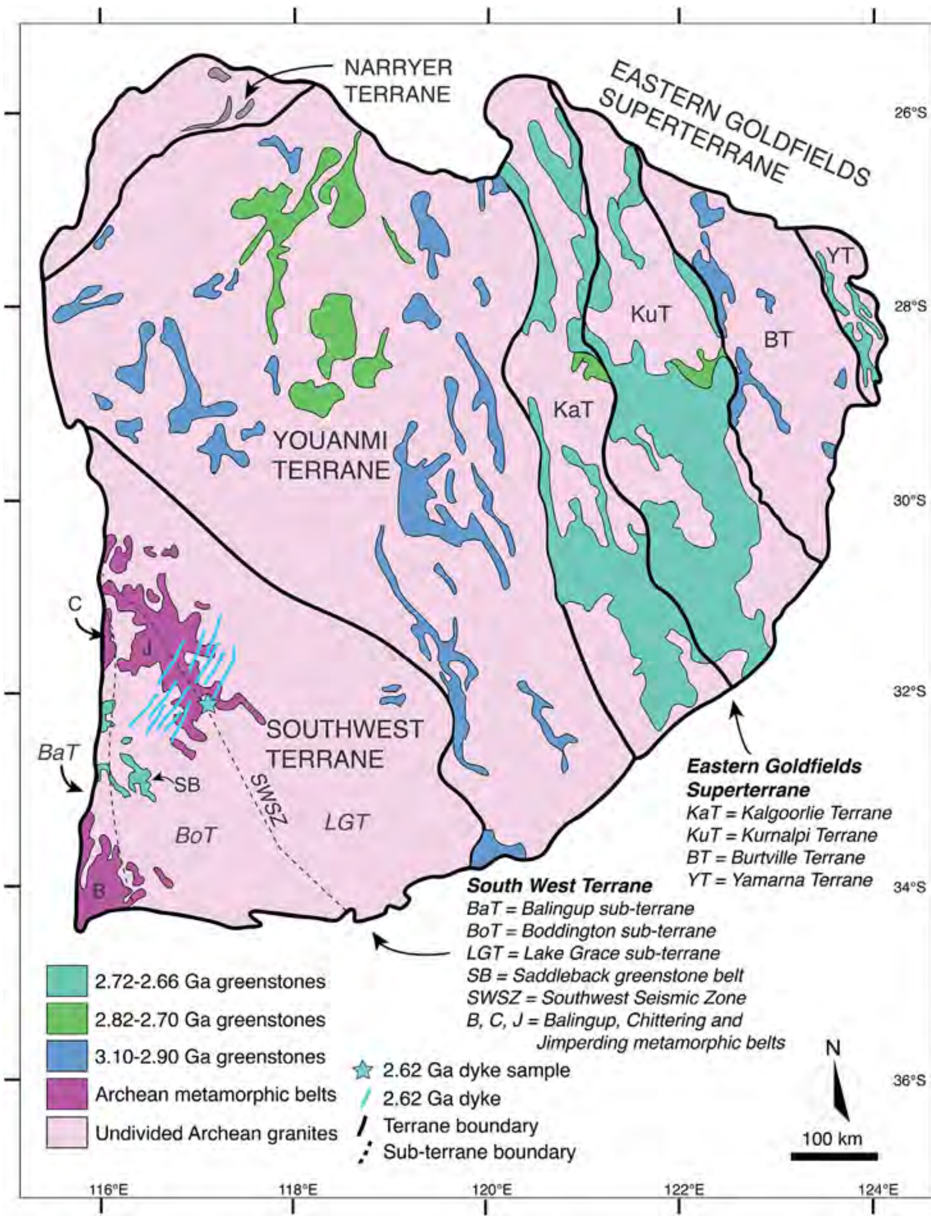

Fig. 2. Map of the Yilgarn Craton showing terrane and sub-terrane boundaries and greenstone belt and granite distributions. Modified after Witt et al. (2018). South West Terrane sub-terranes are from Wilde et al. (1996) and the boundary with the Youanmi Terrane is after Cassidy et al. (2006).

Sheraton, 1997; Nemchin and Pidgeon, 1997; Qiu et al., 1997a,b; Smithies and Champion, 1999; Cassidy et al., 2002; Mole et al., 2012). Extensive gold mineralisation was associated with the late stages of cratonisation (Kent et al., 1996; McNaughton and Groves, 1996; Yeats et al., 1996; Allibone et al., 1998; Witt and Vanderhor, 1998; Qiu and Groves, 1999; Blewett et al., 2010).

2.2. The South West Terrane

Following the model of Wilde et al. (1996), the South West Terrane is divided (from west to east) into the Balingup, Boddington and Lake Grace sub-terranes (Figs. 1 and 2) based on U-Pb geochronology, deep crustal seismic data and re-evaluation of regional geology. It should be noted that Mole et al. (2012) proposed that the eastern part of the South West terrane could be part of the Youanmi Terrane crust on the basis of zircon U-Pb geochronology and spatial occurrence of granite pulses.

The Balingup Terrane comprises ca. 3070–2830 Ma amphibolite facies supracrustal rocks of the Balingup and Chittering metamorphic belts (Fig. 2), interpreted as sedimentation at an evolving continental margin (Wilde, 1980, 1990; Gee et al., 1981; Fletcher et al., 1985). Granitoids emplaced in the central and northern part of the terrane include the ca. 2677–2626 Ma Darling Range batholith (Wilde and Low, 1978; Nieuwland and Compston, 1981; Nemchin and Pidgeon, 1997) and the ca. 2612 Ma Logue Brook Granite, although the latter may represent a recrystallisation age (Compston et al., 1986; Nemchin and Pidgeon, 1997).

The Boddington Terrane is separated from the Balingup Terrane by a ca. 2 km-wide shear zone and consists predominantly of granitoids of the Darling Range batholith, which enclose the greenschist facies Saddleback and Morangup greenstone belts and parts of the Jimperding metamorphic belt (Fig. 2) (Wilde and Low, 1978; Wilde, 1980, 1990; Wilde et al., 1996). The ca. 3177–3100 Ma amphibolite facies Jimperding metamorphic belt consists of supracrustal rocks (Gee et al., 1981; Wilde, 1990) whereas the ca. 2714–2660 Ma Saddleback greenstone belt (Wilde, 1976; Wilde and Pidgeon, 1986; Pidgeon and Wilde, 1990; Allibone et al., 1998) within the Boddington domain has been

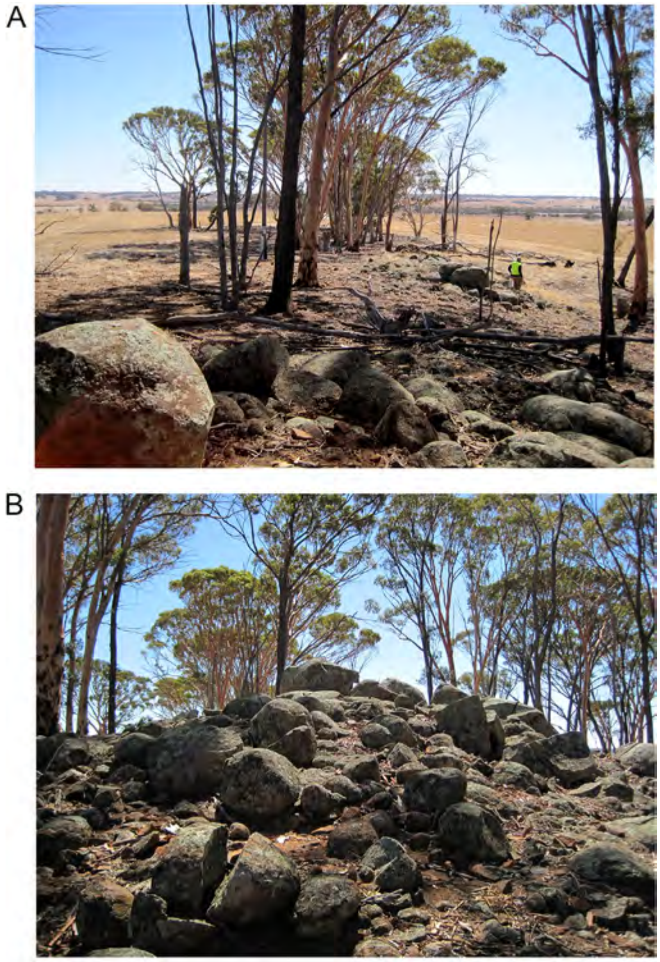

Fig. 3. Field photos of the dyke at the sample location (sample 16WDS13) (A) looking NE and (B) looking north. The dyke forms a wide NE-trending ridge, which extends along strike as a series of similar discontinuous ridges.

interpreted as a remnant oceanic island or continental margin arc (Wilde et al., 1996; Korsch et al., 2011) and hosts the ca. 2675–2611 Ma Boddington Cu-Au deposit (e.g. Roth et al., 1990, 1991; Allibone et al., 1998). The greenschist facies Morangup greenstone belt in the northern part of the terrane is considered to be coeval with the Saddleback belt and comprises rocks with similar arc-type geochemical signatures (Wilde, 1990; Wilde and Pidgeon, 1990).

The transition to the Lake Grace Terrane is marked by a change in structural style and increasing metamorphic grade (Wilde and Low, 1978; Wilde et al., 1996) across a major crustal discontinuity marked by the South West Seismic Zone (Fig. 2) (Doyle, 1971; Dentith et al., 2000; Dentith and Featherstone, 2003). The terrane comprises deformed granitoids, felsic gneisses, several greenstone belt remnants and the eastern apart of the Jimperding metamorphic belt, all metamorphosed under low-pressure granulite facies conditions (Gee et al., 1981; Wilde, 1990; Wilde et al., 1996). Estimates of timing of peak metamorphism range between ca. 2649 and 2625 Ma (Wilde and Pidgeon, 1987; Nemchin et al., 1994; Qiu et al., 1997b; McFarlane, 2010) and lower amphibolite facies conditions may have been reached at ca. 2645 Ma (McFarlane, 2010). Griffin's Find, a small gold deposit ca. 175 km ESE of Boddington (Fig. 1), records peak metamorphic conditions with temperatures of 820–870 °C and at least 5.5 kbar (Tomkins and Grundy, 2009). Charnockites emplaced at ca. 2627 Ma have been interpreted as emplaced during syn-peak metamorphism (Wilde and Pidgeon, 1987; Wilde et al., 1996), although younger ca. 2587 Ma granitoids are also present (Wilde and Pidgeon, 1987).

2.3. Mafic dykes

The Yilgarn Craton hosts numerous dyke suites of different orientations and dyke density that increase towards the southern and western craton margins (Hallberg, 1987; Tucker and Boyd, 1987). The dykes are clearly discernible in aeromagnetic data but deep weathering and thick regolith cover make sampling difficult. The largest dykes belong to the E-W to NE-SW trending 2418–2408 Ma Widgiemooltha Supersuite (Sofoulis, 1965; Evans, 1968; Campbell et al., 1970; Hallberg, 1987; Doehler and Heaman, 1998; Nemchin and Pidgeon, 1998; Wingate, 1999, 2007; French et al., 2002), which includes the 2401 ± 1 Ma Eraynia dykes in the eastern part of the craton (Pisarevsky et al., 2015). The Widgiemooltha dykes are up to 3.2 km wide and extend up to 700 km across the craton, with the largest intrusions (Jimberlana and Binneringie) showing well-developed igneous layering (Campbell et al., 1970; Lewis, 1994). The most extensive dyke swarm in the craton is the 1210 Ma Marnda Moorn LIP which consists of several sub-swarms of different orientations intruding along the craton margins (Isles and Cooke, 1990; Evans, 1999; Wingate et al., 2000; Pidgeon and Nemchin, 2001; Pidgeon and Cook, 2003; Wingate and Pidgeon, 2005; Wingate, 2007; Claoué-Long et al., 2009). Outcrops in the southeast are limited to a single occurrence, and the extent of the dykes in the northeast is unknown due to cover rocks, although one E-W oriented dioritic dyke dated at 1215 ± 11 Ma has been reported further inland (Qiu et al., 1999). Recently, a NW-trending 1888 Ma dyke swarm of unknown extent has been identified in the southwestern Yilgarn Craton and may be part of the Bastar-Cuddapah LIP of India (Stark et al., 2017; Shellnutt et al., 2018). Other known dyke swarms with limited occurrences include the SW-trending dykes of the 1075 Ma Warakurna LIP in the northern Yilgarn Craton (Wingate et al., 2004), the WNW-trending ca. 735 Ma Nindibillup dykes in the central and SE Yilgarn Craton (Spaggiari et al., 2009, 2011; Wingate, 2017), the NNE-trending ca. 750 Ma Northampton dykes in the far west (Embleton and Schmidt, 1985) and the undated (likely < 1140 Ma) NW-trending Beenong dykes in the southeastern Yilgarn Craton (Wingate, 2007; Spaggiari et al., 2009, 2011).

3. Samples

3.1. Field sampling

The field sampling area was selected using satellite imagery (Landsat/Copernicus or Astrium/CNES from Google Earth) and 1:250 000 geological maps from the Geological Survey of Western Australia (GSWA). The Corrigin map sheet (GSWA Corrigin 1:250,000 geological map, SI 50-3, 1985) shows several NE-trending mapped dykes in the area and the aeromagnetic data roughly coincides with some of these. Sample 16WDS13 (32 06.588 S, 117 09.072 E) was collected from a small ridge within an agriculturally cleared area adjacent to the main road (Fig. 3), ca. 21 km east of the town of Beverley and is interpreted to be representative the NE-trending dykes in the area. Basement rocks are not exposed at the outcrop but geological mapping indicates that the dyke intrudes Archean metagranite at this location. The outcrop at the sample location is fresh and shows minor surficial weathering.

3.2. Sample description

Petrography indicates that the dyke is a fresh dolerite with intergranular ophitic to sub-ophitic texture, comprising ca. 45–50% plagioclase, 35–40% pyroxene, up to 5% ilmenite and magnetite, 1–2% sulfides (mainly pyrite and chalcopyrite) and < 1% chlorite, quartz and apatite (Fig. 4). Plagioclase is slightly affected by sericitisation and most pyroxene grains have been altered to a variable degree. The main U- and Th-bearing accessory mineral is baddeleyite, only identifiable using an SEM due to small crystal size (typically ≤70 μm long and 20–30 μm wide). Rare zirconolite crystals are also present and form

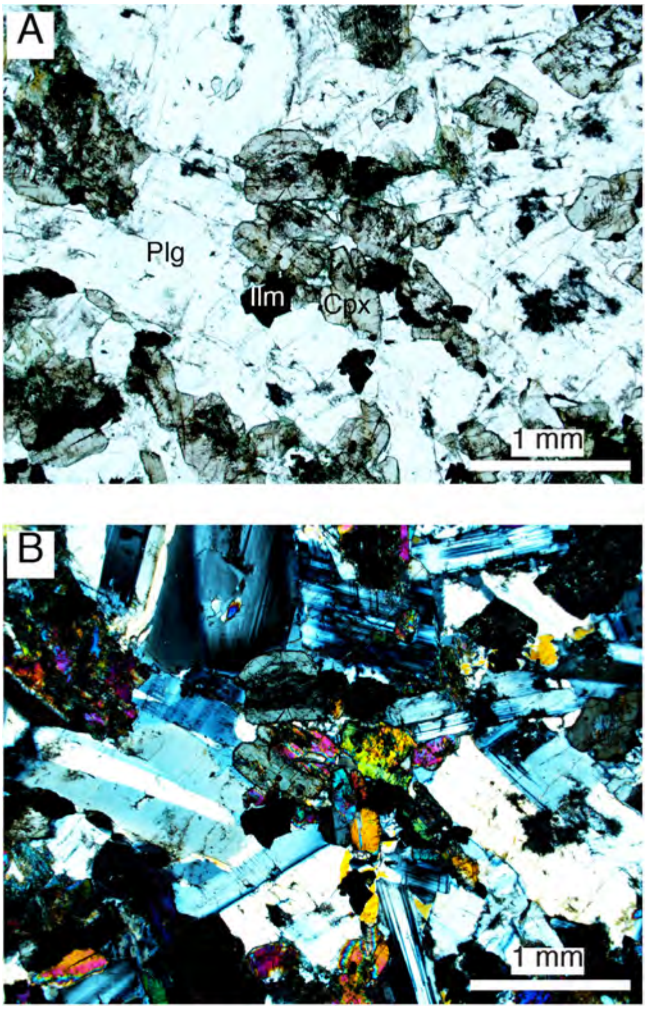

Fig. 4. Plane (A) and crossed polar (B) photomicrographs of sample 16WDS13E.

euhedral to subhedral prisms and laths up to 60 µm long and 10 µm wide.

4. U-Pb geochronology

4.1. SHRIMP U-Pb geochronology

Polished thin sections were scanned to identify baddeleyite, zircon and zirconolite with a Hitachi TM3030 scanning electron microscope (SEM) equipped with energy dispersive X-ray spectrometer (EDX) at Curtin University. For SHRIMP (Sensitive High Resolution Ion Microprobe) U-Pb dating, selected grains were drilled directly from the thin sections using a micro drill and mounted into epoxy disks, which were cleaned and coated with 40 nm of gold. Baddeleyite in thin sections forms subhedral to euhedral equant, prismatic and tabular grains and laths, some with thin zircon rims, and most are < 70 µm long and up to 30 µm across. Only one crystal with suitable dimensions for SHRIMP dating was identified, closely associated with quartz (Fig. 5).

Baddeleyite was analysed for U, Th and Pb using the SHRIMP II at the John de Laeter Centre at Curtin University in Perth, Australia, following standard operating procedures after Williams (1998). The SHRIMP analysis method for mounts with polished thin section plugs, as outlined in Rasmussen and Fletcher (2010), was modified for baddeleyite. Mass resolution for all analyses was ≥ 5000. During the session, 19 baddeleyite and 13 standard analyses were undertaken, with standard zircon OG1 (Stern et al., 2009) employed for monitoring of

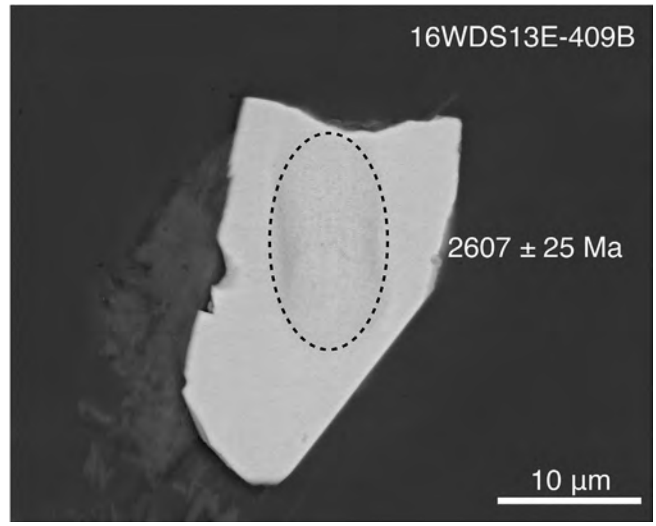

Fig. 5. SEM backscatter image showing SHRIMP spot on baddeleyite crystal 16WDS13E-409B.

instrumental mass fractionation and BR266 zircon (Stern, 2001) for calibration of U and Th concentration and as an accuracy standard. Phalaborwa baddeleyite (Heaman, 2009) and NIST were analysed as additional standards. Spot size was ca. 11 µm with primary O_2^- current at 0.5 nA and count times 10 s for ^{204}Pb, ^{206}Pb, ^{208}Pb and 30 s for ^{207}Pb. Data were processed with Squid version 2.50 (Ludwig, 2009) and Isoplot version 3.76.12 (Ludwig, 2012). For common Pb correction, common Pb isotopic composition was calculated from the Stacey and Kramers (1975) two-stage terrestrial Pb isotopic evolution model. The assigned 1σ external Pb/U error is 1% and analysis is given with 1σ error.

4.2. ID-TIMS U-Pb geochronology

One block was sawn from the field bulk rock sample 16WDS13E to remove weathering and approximately 40 baddeleyite grains were separated using the technique of Söderlund and Johansson (2002). The best-quality baddeleyite grains were split into three fractions of 5–6 grains each and thereafter transferred into Teflon© capsules. The grains were carefully washed in several steps using ultrapure 3 M HNO_3. A small amount of a ^{205}Pb-$^{233\text{-}236}$U tracer solution and 10 drops of concentrated HF and HNO_3 (in proportion 10:1) were added to the Teflon© capsules. The capsules were inserted into steel jackets and placed in an oven at 200 °C for 3 days. After being dried down on a hotplate, 1 drop of 0.25 M H_3PO_4 was added to each capsule along with 10 drops of 6.2 M ultra-pure HCl. The capsules were dried again on a hotplate at 100 °C. Each sample was re-dissolved in 2 µl of silica gel and then loaded on an out-gassed, single Re filament.

The intensities of U and Pb isotopes were measured on a Finnigan Triton thermal ionization multi-collector mass spectrometer at the Swedish Museum of Natural History in Stockholm. The mass spectrometer is equipped with Faraday cups and an ETP Secondary Electron Multiplier. Lead was analysed at filament temperatures of 1210–1240 °C, while the intensities of ^{233}U, ^{236}U and ^{238}U were recorded subsequently at filament temperatures exceeding 1320 °C. The initial Pb composition was taken from Stacey and Kramers (1975), and the ^{238}U and ^{235}U decay constants are from Jaffey et al. (1971). Procedural blank level was 0.6 pg for Pb and 0.06 pg for U.

Table 1
SHRIMP U-Pb data for baddeleyite from dyke sample 16WDS13E.

Spot	f_{206} %	U ppm	Th ppm	Th/U	± %	Total $^{238}U/^{206}Pb$	± %	Total $^{207}Pb/^{206}Pb$	± %	$^{238}U/^{206}Pb^*$	± %	$^{207}Pb^*/^{206}Pb^*$	± %	$^{206}Pb^*/^{238}U$ Age (Ma) ± 1σ		$^{207}Pb^*/^{206}Pb^*$ Age (Ma) ± 1σ		Disc. %
16WDS13E.409B-1	0.22	89	2	0.02	2.3	1.80	1.90	0.177	1.3	1.8	1.9	0.175	1.5	2819	± 43	2607	± 25	−10

Notes 1) f_{204} is the proportion of common Pb in ^{206}Pb, determined using the measured $^{204}Pb/^{206}Pb$ and the common Pb composition from the Stacey and Kramers (1975) model at the approximate age of the sample 2)
Disc. = $100(t[^{207}Pb^*/^{206}Pb^*] - t[^{238}U/^{206}Pb^*/])/t[^{207}Pb^*/^{206}Pb^*]$.

5. Results

5.1. SHRIMP U-Pb geochronology

As part of preliminary reconnaissance SHRIMP dating of several dykes sampled in the area, one analysis (Table 1) was obtained from one baddeleyite grain during the SHRIMP session (Fig. 5). The analysed baddeleyite crystal had U and Th concentrations of 59.7 ppm and 1.4 ppm, respectively, and yielded a common Pb-corrected $^{207}Pb/^{206}Pb$ date of 2607 ± 25 Ma (1σ), which is interpreted as indicative of the crystallisation age of the dyke. Based on this preliminary result, TIMS U-Pb analysis was carried out on baddeleyite from the same sample. It should be noted that despite only having one analysis available, the decision to proceed with TIMS dating was based on the initial identification of a potentially new dyke age from SHRIMP dating.

5.2. ID-TIMS U-Pb geochronology

U-Pb data for the samples is presented in Table 2 and the calculated isotopic ages are shown in the concordia diagram in Fig. 6. One fraction of five grains and two fractions of six grains yielded slightly discordant common Pb-corrected $^{207}Pb/^{206}Pb$ dates of 2615.7 ± 2.9 Ma, 2616.7 ± 3.1 Ma and 2611.3 ± 3.3 Ma, respectively, giving a weighted mean $^{207}Pb/^{206}Pb$ date of 2615 ± 6 Ma (MSWD = 2.8). Forced regression through 0 Ma yields an upper intercept date of 2615 ± 3 Ma. However, despite higher uncertainty, the weighted mean $^{207}Pb/^{206}Pb$ date is preferred due to slight discordance of the analyses. Thus, the $^{207}Pb/^{206}Pb$ age is interpreted as the best, though conservative, emplacement age of the mafic dyke.

6. Discussion

We have identified the oldest known mafic dyke within the Yilgarn Craton, here informally named as the Yandinilling dyke. The extent of dykes of this age within the craton is currently unknown but aeromagnetic data (Geological Survey of Western Australia magnetic anomaly grids with 20–40 m cell size, Geoscience Australia magnetic grid of Australia V6 2015 base reference) show that linear NE-trending features interpreted as dykes extend at least 150 km northeast from Boddington and across the Boddington and Lake Grace terrane boundary. The dyke dated in this study lies on one of these features, suggesting it is part of a much longer intrusion that may belong to a major dyke swarm. The temporally closest known mafic magmatic event within the Yilgarn Craton produced the ca. 2410 Ma Widgiemooltha Supersuite (Sofoulis, 1965; Evans, 1968; Campbell et al., 1970; Hallberg, 1987; Doehler and Heaman, 1998; Nemchin and Pidgeon, 1998; Wingate, 1999, 2007; French et al., 2002). The E- to ENE-trending Widgiemooltha dykes traverse nearly the entire width of the craton approximately orthogonally to the regional structural grain, similar to the ca. 2480–2450 Ma Matachewan and Hearst dykes in North America (Heaman, 1997). Worldwide, mafic dykes of similar age to the Yandinilling dyke are found in the São Francisco Craton in Brazil, dated at 2624 ± 7 Ma (Oliveira et al., 2013), and in the high-grade Limpopo Belt between the Zimbabwe and Kaapvaal cratons in of southern Africa, where deformed dykes have been dated at 2559 ± 4 Ma, 2607 ± 5 Ma and 2604 ± 6 Ma (Xie et al., 2017). Evidence for a possible connection between the Yilgarn and Zimbabwe cratons is discussed in the following sections.

6.1. Assembly of the South West Terrane

Amalgamation of the South West Terrane is considered to have involved subduction in the west and continental collision in the east. The ca. 2715–2675 Ma Saddleback greenstone belt has been interpreted as an island or continental arc (Wilde, 1990; Wilde et al., 1996; Korsch et al., 2011). Subduction of the Balingup Terrane beneath the

Table 2
ID-TIMS U-Pb data for baddeleyite from dyke sample 16WDS13E.

Analysis no. (number of grains)	U/Th	Pb_c/Pb_{tot}[1]	$^{206}Pb/^{204}Pb$	$^{207}Pb/^{235}U$	± 2 s % err	$^{206}Pb/^{238}U$	± 2s % err	$^{207}Pb/^{235}U$	± 2 s	$^{206}Pb/^{238}Pb$	± 2 s	$^{207}Pb/^{206}Pb$	± 2 s	Concordance
			Raw[2]	[Corr][3]				[Age, Ma]						
Bd-1 (5 grains)	6.3	0.045	1280.3	12.0130	0.55	0.49498	0.54	2605.4	5.2	2592.2	11.4	2615.7	2.9	0.991
Bd-2 (6 grains)	6.0	0.039	1555.0	11.8670	0.65	0.48887	0.64	2594.0	6.1	2565.8	13.5	2616.1	3.1	0.981
Bd-3 (6 grains)	7.5	0.056	1062.7	12.005	0.74	0.49599	0.73	2604.8	6.9	2596.6	15.6	2611.3	3.3	0.994

Initial common Pb corrected with isotopic compositions from the model of Stacey and Kramers (1975) at the age of the sample.
[1] Pb_c = common Pb; Pb_{tot} = total Pb (radiogenic + blank + initial).
[2] Measured ratio, corrected for fractionation and spike.
[3] Isotopic ratios corrected for fractionation (0.1% per amu for Pb), spike contribution, blank (0.6 pg Pb and 0.06 pg U), and initial common Pb.

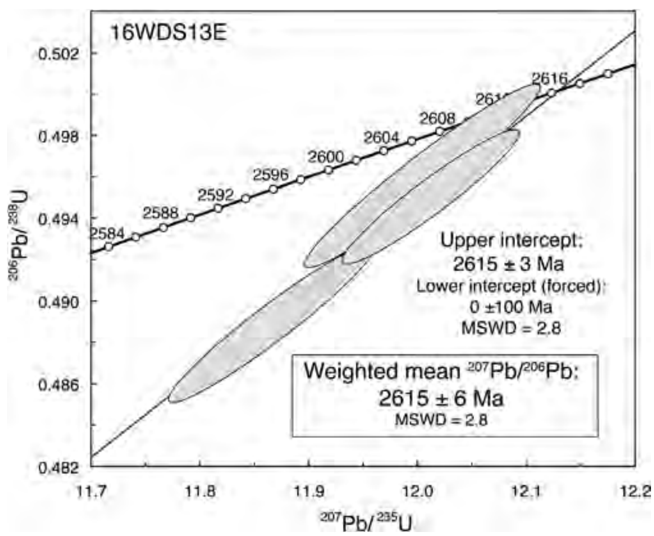

Fig. 6. Concordia plot for analysed baddeleyite ID-TIMS U-Pb results from sample 16WDS13E.

Boddington Terrane between ca. 2714 Ma and 2969 Ma (Korsch et al., 2011) and collision between ca. 2696 and 2675 Ma is constrained by calc-alkaline magmatism and granitic intrusions within the Saddleback Group (Allibone et al., 1998; Cassidy et al., 1998; Wilde and Pidgeon, 2006). Following their amalgamation, the Lake Grace Terrane was subducted under the newly formed Balingup-Boddington Terrane producing the pyroclastic and intrusive rocks of the upper Saddleback Group at ca. 2675–2650 Ma (Wilde and Pidgeon, 1986; Allibone et al., 1998; Zhao et al., 2006). Collision and final formation of the South West Terrane along a suture now marked by the South West Seismic Zone (Doyle, 1971; Middleton et al., 1993; Wilde et al., 1996; Dentith et al., 2000) is uncertain but probably took place sometime between ca. 2649 and 2625 Ma, constrained by low-pressure amphibolite to granulite facies metamorphism at ca. 2649–2640 Ma (Nemchin et al., 1994; McFarlane, 2010), emplacement of charnockites at ca. 2627 Ma (Wilde and Pidgeon, 1987; Wilde et al., 1996) and monazite and zircon growth at ca. 2625 Ma (McFarlane, 2010) in the eastern Lake Grace Terrane.

6.2. Mechanism and timing of 2615 Ma mafic magmatism: post-orogenic lithospheric delamination beneath the Yilgarn Craton?

The nature of widespread granitic magmatism during the amalgamation of the Yilgarn Craton provides evidence for significant changes in tectonic setting during the Neoarchean. The ca. 2690–2650 Ma high-Ca granites (Champion and Sheraton, 1997) were associated with orogenic thickening of the crust and partial melting of an isotopically young, deep source of basaltic composition, whereas the ca. 2650–2625 Ma low-Ca granites were emplaced craton-wide and involved partial melting of a shallow, isotopically older tonalitic source (Champion and Sheraton, 1997; Qiu and Groves, 1999; Cassidy et al., 2002; Mole et al., 2012). Smithies and Champion (1999) proposed that emplacement of the low-Ca granites and syenites in the Eastern Goldfields (Fig. 1) at ca. 2650–2630 Ma was a result of delamination or convective thinning of dense eclogitic lower crust ca. 10–15 m.y. after a major partial melting event. Cassidy et al. (2002) argued that the craton-wide extent of low-Ca magmatism at ca. 2650–2630 Ma indicates that the entire craton was undergoing extension or post-orogenic attenuation at this time, possibly associated with the end of a major compressional event in the Eastern Goldfields, as originally proposed by Smithies and Champion (1999). Geophysical investigations of the deep crustal architecture beneath the Eastern Goldfields Superterrane (Fig. 2) are also consistent with delamination of the lower lithosphere (Nelson, 1992), including ca. 40 km thick crust underlain by a flat, east-dipping Moho and a high-velocity layer at 100–200 km (Blewett et al., 2010). Delamination of the lower lithosphere can occur through thermal, compositional or phase changes, which render it gravitationally unstable (denser than the underlying material) and viscous enough to allow flow (Schott and Schmeling, 1998; Elkins Tanton and Hager, 2000; Elkins-Tanton, 2005). Smithies and Champion (1999) advocate a model where the delamination (or convective thinning) was a direct result of partial melting and eclogitic restite formation in the lower crust due to orogenic thickening. The timing of the proposed delamination ca. 10–15 m.y. after the partial melting event, the consequent A-type syenitic and widespread low-Ca granitic magmatism and high-temperature metamorphism fit well with this scenario. An alternative mechanism could be the arrival of a mantle plume, which would cause the thickened lithospheric root to become less viscous and thermally unstable. Other workers have proposed that a mantle plume event at ca. 2700 Ma was responsible for komatiitic and felsic magmatism and a diachronous regional metamorphic peak at ca. 2690–2630 Ma (Campbell and Hill, 1988; Upton et al., 1997) but this model is not favoured by Smithies and Champion (1999) because it would be difficult to explain the timing and duration of the felsic alkaline and low-Ca granitic magmatism and the craton-wide E-W shortening at ca. 2690–2650 Ma.

In the western Yilgarn Craton, low-pressure granulite facies metamorphism at ca. 2649–2625 Ma, emplacement of charnockites at ca. 2652–2627 Ma within the Lake Grace Terrane (Wilde and Pidgeon, 1987; Nemchin et al., 1994; McFarlane, 2010) and the emplacement of the Darling Range batholith at ca. 2648–2626 Ma within the Boddington and Balingup Terranes (Nemchin and Pidgeon, 1997) are also consistent with the delamination model. Granites of ca. 2612 Ma age near the western margin of the South West Terrane have isotopic compositions of $\varepsilon Nd_{(2612)} = -2.9$ and $\varepsilon Nd_{(2612)} = 0$, respectively, suggesting that their source involved significant mixing of younger mantle-derived crust with older crust (Compston et al., 1986) or that the granitic magmas could have originated from partial melting of recently crystallised mafic rocks in the lower crust (e.g. Smithies et al., 2015). Qiu and Groves (1999) suggested that the geochemical characteristics of the ca. 2640–2630 Ma granites, the presence of igneous

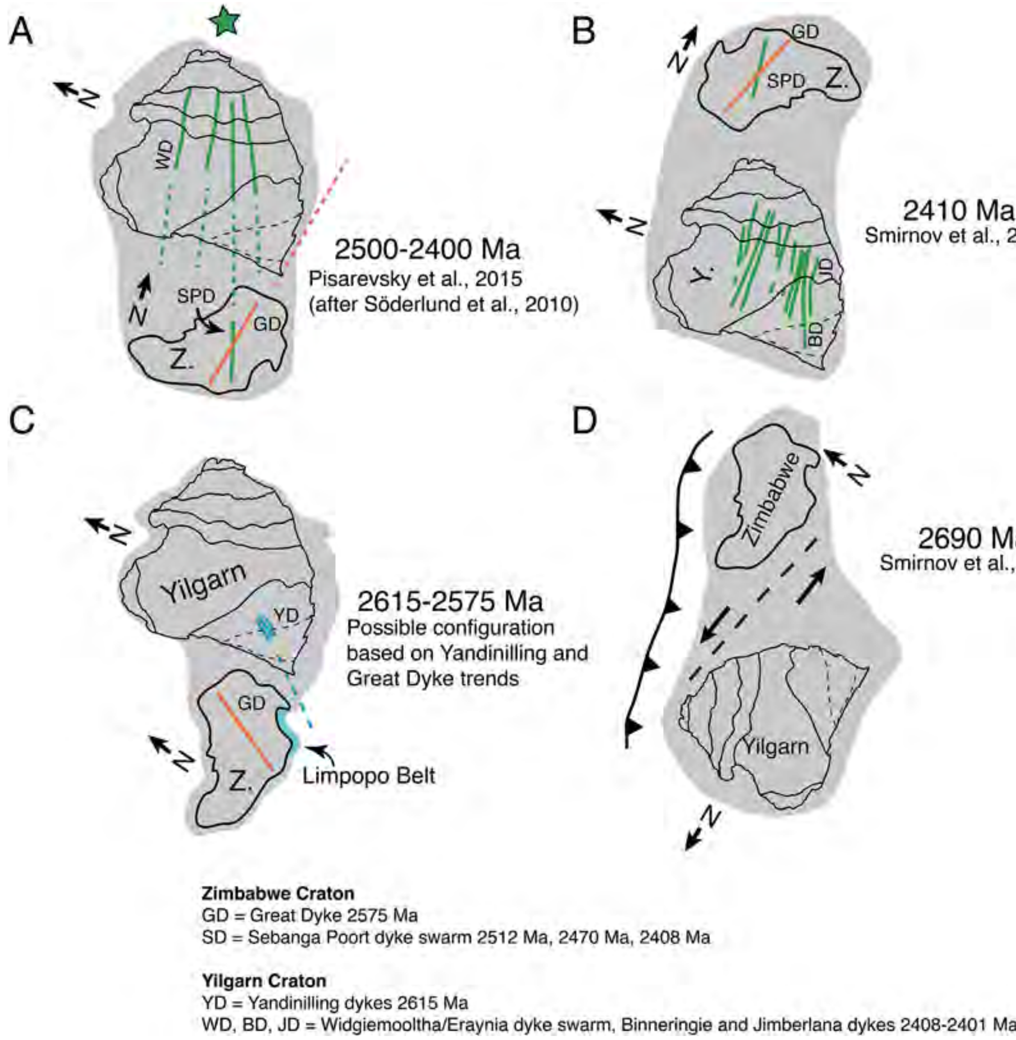

Fig. 7. Paleogeographic reconstructions of the Yilgarn and Zimbabwe cratons. (A) Superia configuration after Söderlund et al. (2010) and Pisarevsky et al. (2015) at ca. 2500–2400 Ma. Only the Yilgarn and Zimbabwe cratons are shown. (B) Reconstruction of Smirnov et al. (2013) at ca. 2410 Ma, (C) Relative orientations of the Yilgarn and Zimbabwe cratons rotated from (A) to an approximate alignment of the 2615 Ma Yandinilling swarm with the 2575 Ma Great Dyke. and (D) reconstruction of Smirnov et al. (2013) at ca. 2690 Ma. Yilgarn Craton: green = Widgiemooltha/Eraynia dykes, BD = Binneringie Dyke and JD = Jimberlana Dyke (both part of the Widgiemooltha swarm), blue = Yandinilling swarm, green star = possible mantle plume location. Zimbabwe Craton: GD (orange) = the Great Dyke, SPD (green) = the Sebanga Poort Dyke, SD = Sebanga dykes. (For interpretation of the references to colour in this figure legend, the reader is referred to the web version of this article.)

charnockites, and coeval widespread intrusion of other granitoids in the southern Lake Grace and Youanmi terranes collectively suggest massive melting of lower crust at high temperatures at ca. 2640–2630 Ma. They attributed the sudden significant increase in geothermal gradient over < 10 m.y. and the lower partial melting pressures of the younger granites (indicating thinner crust) to lithospheric delamination during a late orogenic stage and suggested that the lack of known significant mafic intrusions of this age probably indicated partial, instead of complete, removal of the lower crust.

Collectively, these data and the newly discovered mafic magmatism in the South West Terrane are consistent with the presence of hot mantle material impinging on a thinned crust beneath most of the Yilgarn Craton, if not the entire Yilgarn Craton, between ca. 2652 Ma and 2615 Ma. Several lines of evidence suggest possible thermal effects that were associated with intrusion of the 2615 Ma mafic dykes, similar to the effects the Marnda Moorn LIP dykes in the middle Proterozoic Albany-Fraser Orogen (Dawson et al., 2003). Nemchin and Pidgeon (1997) reported extensive recrystallisation of zircon rims at 2628–2616 Ma and growth of titanite at ca. 2615 Ma within the Darling Range batholith. The 2615 ± 3 Ma titanite and the 2616 ± 21 Ma zircon recrystallisation ages are within uncertainty of the 2615 ± 6 Ma mafic dyke age reported here and strongly suggest that they are related. Moreover, zircons from a ca. 2612 Ma granite ca. 130 km southwest of the 2615 Ma dyke, yield dates of 2612 ± 5 Ma and 2613 ± 5 Ma, which could represent either the timing of recrystallisation or the emplacement (Nemchin and Pidgeon, 1997). Other coeval magmatism includes a felsic intrusive at ca. 2611 Ma within the Saddleback greenstone belt (Allibone et al., 1998) and a monzogranite dyke and a granodiorite at 2610 ± 6 Ma and 2610 ± 8 Ma, respectively, in the southern Boddington Terrane (Sircombe, 2007). The NE-SW trend of the Yandinilling dyke suggests NW-SE oriented regional extension, which is consistent with the inferred NE-SW oriented contraction and strike-slip movement in the eastern part of the craton, constrained by syn-kinematic emplacement of low-Ca granites at 2637 ± 7 Ma (Dunphy et al., 2003).

6.3. Timing of mafic magmatism and gold mineralisation

Craton-wide (> 400,000 km^2) gold mineralisation at ca. 2640–2630 Ma was associated with a major tectonothermal event

(Groves, 1993; Kent et al., 1996; Yeats and McNaughton, 1997; Qiu and Groves, 1999 and references therein) involving a deep crustal fluid source (McNaughton and Groves, 1996; Qiu and Groves, 1999), which Qiu and Groves (1999) argued was driven by lithospheric delamination. The mafic magmatism dated at 2615 ± 6 Ma in the South West Terrane thus post-dates the main mineralisation event but may have been synchronous with formation of late-stage gold deposits. Gold mineralisation at Boddington may also have been synchronous with the ca. 2611 Ma felsic intrusives and movement along brittle shear zones (Allibone et al., 1998).

6.4. The Neoarchean tectonic and paleogeographic setting of the Yilgarn Craton: links to the Zimbabwe Craton

Using coeval mafic dyke swarms as a magmatic barcode (Bleeker and Ernst, 2006) between the Zimbabwe and Yilgarn cratons, Söderlund et al. (2010) proposed that both could have been part of the ca. 2510–2100 Ma Superia supercraton (Bleeker and Ernst, 2006; Ernst and Bleeker, 2010). Paleomagnetic data from the E- to ENE-trending ca. 2408 Ma Widgiemooltha and ca. 2401 Ma Erayinia dykes (Sofoulis, 1965; Evans, 1968; Campbell et al., 1970; Hallberg, 1987; Doehler and Heaman, 1998; Nemchin and Pidgeon, 1998; Wingate, 1999, 2007; French et al., 2002; Pisarevsky et al., 2015) and the NNW-trending ca. 2408 Ma Sebanga dyke swarm (Wilson et al., 1987; Mushayandebvu et al., 1995; Söderlund et al., 2010) permit a possible configuration where the western Yilgarn Craton is attached to the northern Zimbabwe Craton and the Sebanga dyke swarm could be a continuation of the Widgiemooltha/Erayinia dyke swarm (Fig. 7A) (Pisarevsky et al., 2015). The Yandinilling dyke swarm is older than the 2575 Ma Great Dyke (Oberthür et al., 2002) and the Umvimeela satellite dyke (Söderlund et al., 2010), which are currently the oldest known mafic dykes with robust geochronology in the Zimbabwe Craton. However, the Sebanga dyke swarm includes two dyke generations at ca. 2512 Ma and 2470 Ma, both considered to be part of the same swarm (Söderlund et al., 2010). This suggests that if the Yilgarn and the Zimbabwe cratons were neighbours, yet to be identified mafic magmatism of these ages could be present in the Yilgarn Craton. If the configuration of Söderlund et al. (2010) and Pisarevsky et al. (2015) at ca. 2400 Ma is accepted and the Yandinilling dyke and the Umvimeela/Great Dyke are considered as part of the same swarm (despite their up to 40 m.y. age difference), the barcode between the two cratons does not match unless one of the cratons rotated significantly between ca. 2575 Ma and 2512 Ma (or their respective regional stress fields were very different) (Fig. 7C). If the Yilgarn and Zimbabwe cratons were adjacent to each other between 2615 Ma and 2408 Ma, continuous but episodic mafic magmatism on these cratons lasting for more than 200 m.y. suggests that at least some of the dyke swarms could be associated with processes other than a mantle plume, or that several plumes were involved.

In contrast to the reconstructions of Söderlund et al. (2010), Smirnov et al. (2013) proposed that at ca. 2410 Ma, the eastern margin of the Yilgarn Craton was adjacent to the southern margin of the Zimbabwe Craton, forming the Zimgarn supercraton and aligning the Sebanga swarm approximately parallel to the Widgiemooltha dykes (Fig. 7B). Whilst noting that the paleomagnetic data used for such a reconstruction were limited, these authors preferred the position of the Zimbabwe Craton north of the Yilgarn Craton because the juvenile eastern margin of the Yilgarn Craton was a better match with the progressive west to east cratonisation of the Zimbabwe Craton, and because offsets on major terrane-bounding shear zones in the eastern Yilgarn Craton could be restored to a feasible proto-Zimgarn configuration at ca. 2690 Ma (Fig. 7D). In the ca. 2690 Ma configuration, Smirnov et al. (2013) aligned the southeastern margin of the Yilgarn Craton directly with the southwestern margin of the Zimbabwe Craton. Pisarevsky et al. (2015) noted that if the Zimgarn model of Smirnov et al. (2013) at ca. 2400 Ma is accepted, then paleomagnetic constraints imply that the Zimbabwe and Yilgarn cratons were not part of Superia. This does not preclude the Smirnov et al. (2013) configuration, but there is currently no evidence of mafic dykes or sills older than 2401 Ma in the eastern Yilgarn Craton.

Xie et al. (2017) recently obtained 2607 ± 5 Ma and 2604 ± 6 Ma SHRIMP U-Pb zircon ages for tholeiitic Stockford dykes within the Central Zone of the Limpopo Belt, which separates the Archean Kaapvaal and Zimbabwe cratons in South Africa. The Stockford dykes were deformed and metamorphosed under granulite facies conditions at ca. 2014–2005 Ma (Xie et al., 2017) and intrude the Paleoarchean Sand River Gneiss, which records high-grade metamorphic events at ca. 2640 Ma and ca. 2025 Ma (Zeh et al., 2007, 2010; Gerdes and Zeh, 2009). The timing of the amalgamation of the Central Zone to the Zimbabwe Craton is uncertain, but is thought to have occurred during the collision and amalgamation between the Kaapvaal and Zimbabwe cratons at ca. 2660–2610 Ma (Burke et al., 1986; Kramers et al., 2011; Xie et al., 2017; Brandt et al., 2018) or at ca. 2020 Ma (e.g. Holzer et al., 1998; Söderlund et al., 2010). If the Zimbabwe and Kaapvaal Cratons amalgamated at this time, the 2615 Ma mafic magmatism in the southwestern Yilgarn Craton may be associated with the same tectonic event that produced the ca. 2607–2604 Ma Stockford dykes in the Central Zone of the Limpopo Belt. The South West Terrane and the Central Zone share a similar tectonothermal evolution in an orogenic setting that involved contemporaneous low-pressure granulite facies metamorphism associated with voluminous felsic magmatism, closely followed by mafic magmatism. Voluminous magmatism in the Central Zone at ca. 2650–2610 Ma includes the 2612 ± 7 Ma Bulai pluton and the 2613 ± 7 Ma Zanzibar gneiss (Zeh et al., 2007; Millonig et al., 2008), which are coeval with the ca. 2612–2611 Ma Logue Brook Granite (Compston et al., 1986; Nemchin and Pidgeon, 1997) and ca. 2611–2610 felsic magmatism elsewhere within the South West Terrane (Allibone et al., 1998; Sircombe, 2007). Moreover, a low-pressure high-grade tectonothermal event at ca. 2650–2644 Ma in the Central Zone of the Zimbabwe Craton (Holzer et al., 1998; Zeh et al., 2007, 2010; Millonig et al., 2008), possibly linked to magmatic underplating (e.g. Holzer et al., 1998), is coeval with the ca. 2650 Ma low-pressure granulite facies metamorphism in the Lake Grace Terrane and the timing of proposed lithospheric delamination beneath the Yilgarn Craton (Section 6.2). Furthermore, Brandt et al. (2018) propose that the UHT metamorphic event in the Central Zone at ca. 2660–2610 was likely due to lithospheric delamination and Kröner et al. (1999), Kamber and Biino (1995) and Berger et al. (1995) favoured a lithospheric delamination (or mantle plume) model for the ca.2700–2600 Ma high-grade event in the Northern Marginal Zone. Similar to the Yandinilling swarm reported here, Xie et al. (2017) argued that the Stockford dykes may have formed in a post-collisional extensional environment during orogenic collapse, which they consider to represent the Neoarchean amalgamation of the Zimbabwe and Kaapvaal cratons. Alternatively, an upwelling mantle plume could explain the wide extent of magmatic underplating and low-pressure high-temperature metamorphism followed by the emplacement of mafic dykes. Such an event would be expected to show up as mafic magmatism in other nearby crustal blocks but reliably dated mafic dykes of ca. 2620–2600 Ma age are currently not known from other cratons. If the Zimbabwe and Kaapvaal cratons amalgamated at ca. 2660–2610 Ma, the Smirnov et al. (2013) reconstruction at ca. 2410 Ma (Fig. 7B) would not be feasible and would require adjustment to accommodate the consolidated Zimbabwe-Kaapvaal Craton. This also raises the possibility that ca. 2615 Ma mafic magmatism coeval with the Yandinilling dyke may be present in the Kaapvaal Craton (Fig. 7C).

7. Conclusions

We have identified the oldest known mafic dyke in the Yilgarn Craton of Western Australia, dated at 2615 ± 6 Ma by ID-TIMS on baddeleyite and at 2610 ± 25 Ma utilizing *in situ* SHRIMP U-Pb dating of baddeleyite. Aeromagnetic data suggest that the dyke is part of a series of NE-trending intrusions, here named the Yandinilling dyke swarm, that extend hundreds of kilometers within the southwestern part of the craton. The 2615 Ma mafic magmatism postdates the ca. 2650–2630 Ma craton-wide emplacement of low-Ca granites that have been linked with post-orogenic collapse and delamination of the lower crust beneath the Yilgarn Craton. The Yandinilling swarm also postdates the ca. 2640–2630 Ma craton-wide gold mineralisation event, but may be coeval with some late-stage gold mineralisation at Kambalda and Boddington. Paleogeographic reconstructions suggest that the Yilgarn and Zimbabwe cratons may have been neighbours between ca. 2690 Ma and 2401 Ma. If the Zimbabwe and Kaapvaal Cratons amalgamated at ca. 2660–2610 Ma, the 2615 Ma mafic magmatism in the southwestern Yilgarn Craton may be associated with the same tectonic event that produced the ca. 2607–2604 Ma Stockford dykes in the Central Zone of the Limpopo Belt. Paleomagnetic evidence, coeval granitic magmatism, high-grade metamorphism, and emplacement of mafic dykes support a configuration where the northern part of the Zimbabwe Craton may have been adjacent to the western margin of the Yilgarn Craton during the Neoarchean. Worldwide, reliably dated mafic dykes of this age have so far been reported from the Yilgarn Craton, the Limpopo Belt and the São Francisco Craton.

Acknowledgments

This work was funded by the Australian Research Council (ARC) Centre of Excellence for Core to Crust Fluid Systems Grant (CE110001017) and the ARC Laureate Fellowship (FL150100133) to Z.-X.L. JCS acknowledges support from a Curtin University Postgraduate Scholarship. We thank Gregory Shellnutt and Timothy Kusky for helpful and constructive reviews that greatly improved the manuscript. We also thank Cristina Talavera and Hao Gao for their generous support with SHRIMP analyses and Stephen Sheppard is thanked for helpful discussion and feedback on a previous version of the manuscript. Baddeleyite analyses were carried out on the Sensitive High Resolution Ion Micro Probe mass spectrometer (SHRIMP II) at the John de Laeter Centre, Curtin University, with the financial support of the Australian Research Council and Auscope NCRI. BSE imaging was undertaken at the Australian Microscopy and Microanalysis Research Facility at the Centre for Microscopy, Characterisation and Analysis (CMCA) at the University of Western Australia. This is a contribution to IGCP project 648.

References

Allibone, A.H., Windh, J., Etheridge, M.A., Burton, D., Anderson, G., Edwards, P.W., Miller, A., Graves, C., Fanning, C.M., Wysoczanski, R., 1998. Timing relationships and structural controls on the location of Au-Cu mineralization at the Boddington gold mine, Western Australia. Econ. Geol. 93, 245–270.

Barley, M.E., Brown, S.J.A., Cas, R.A.F., Cassidy, K.F., Champion, D.C., Gardoll, S.J., Krapež, B., 2003. An integrated geological and metallogenic framework for the eastern Yilgarn Craton: developing geodynamic models of highly mineralised Archaean granite–greenstone terranes. AMIRA Project P624.

Berger, M., Kramers, J.D., Nägler, T., 1995. Geochemistry and geochronology of charnoenderbites in the northern marginal zone of the Limpopo Belt, Southern Africa, and genetic models. Schweizerische Mineral. Petrogr. Mitteilungen 75, 17–42.

Bleeker, W., Ernst, R., 2006. Short-lived mantle generated magmatic events and their dyke swarms: the key unlocking Earth's paleogeographic record back to 2.6 Ga. In: Hanski, E.J., Mertanen, S., Rämö, O.T., Vuollo, J. (Eds.), Dyke Swarms—time Markers of Crustal Evolution: Selected Papers of the Fifth International Dyke Conference in Finland, Rovaniemi, Finland, 31 July–3 Aug 2005 & Fourth International Dyke Conference, Kwazulu-Natal, South Africa 26–29 June 2001. CRC Press, London, pp. 3–26.

Blewett, R.S., Hitchman, A.P., 2006. 3D Geological Models of the Eastern Yilgarn Craton: Final Report pmd* CRC Y2 Project September 2001–December 2004. Geoscience Australia Record 2006/05.

Blewett, R.S., Henson, P.A., Roy, I.G., Champion, D.C., Cassidy, K.F., 2010. Scale-integrated architecture of a world-class gold mineral system: The Archaean eastern Yilgarn Craton, Western Australia. Precambrian Res. 183, 230–250 10.1016/j.precamres.2010.06.004.

Brandt, S., Klemd, R., Li, Q., Kröner, A., Brandl, G., Fischer, A., Bobek, P., Zhou, T., 2018. Pressure-temperature evolution during two granulite-facies metamorphic events (2.62 and 2.02 Ga) in rocks from the Central Zone of the Limpopo Belt, South Africa (in press). Precambrian Res. https://doi.org/10.1016/j.precamres.2018.03.002.

Buchan, K.L., Ernst, R.E., Hamilton, M.A., Mertanen, S., Pesonen, L.J., Elming, S.-Å., 2001. Rodinia: the evidence from integrated palaeomagnetism and U-Pb geochronology. Precambrian Res. 110, 9–32.

Burke, K., Kidd, W.S.F., Kusky, T.M., 1986. Archean foreland basin tectonics in the Witwatersrand, South Africa. Tectonics 5, 439–456.

Campbell, I.H., Hill, R.I., 1988. A two-stage model for the formation of the granite-greenstone terrains of the Kalgoorlie-Norseman area, Western Australia. Earth Planet. Sci. Lett. 90, 11–25.

Campbell, I.H., McCall, G.J.H., Tyrwhitt, D.S., 1970. The Jimberlana Norite, Western Australia–a smaller analogue of the Great Dyke of Rhodesia. Geol. Mag. 107, 1–12.

Cassidy, K.F., Champion, D.C., Wyborn, L.A.I., 1998. A Geochemical Study of Granitoids of the Boddington Gold Mine: Final Report to SRK (Australasia) Ltd. Australian Geological Survey Organisation.

Cassidy, K.F., Champion, D.C., McNaughton, N.J., Fletcher, I.R., Whitaker, A.J., Bastrakova, I.V, Budd, A.R., 2002. Characterisation and metallogenic significance of Archaean granitoids of the Yilgarn Craton, Western Australia, Minerals and Energy Research Institute of Western Australia (MERIWA) Report P482.

Cassidy, K.F., Champion, D.C., Krapez, B., Barley, M.E., Brown, S.J.A., Blewett, R.S., Groenewald, Pb., Tyler, I.M., 2006. A revised geological framework for the Yilgarn Craton, Western Australia. In: Geological Survey of Western Australia Record 8/2006. Geological Survey of Western Australia.

Cawood, P.A., Tyler, I.M., 2004. Assembling and reactivating the Proterozoic Capricorn Orogen: lithotectonic elements, orogenies, and significance. Precambrian Res. 128, 201–218. https://doi.org/10.1016/j.precamres.2003.09.001.

Champion, D.C., 2013. Neodymium depleted mantle model age map of Australia: explanatory notes and user guide. Geosci. Aust. Rec. 2013 (44), 209. https://doi.org/10.11636/Record.2013.044.

Champion, D.C., Cassidy, K.F., 2007. An overview of the Yilgarn Craton and its crustal evolution. Geosci. Aust. Rec. 8–13.

Champion, D.C., Cassidy, K.F., 2008. Geodynamics: Using geochemistry and isotopic signatures of granites to aid mineral systems studies: An example from the Yilgarn craton. Geosci. Aust. Rec. 9, 7–16.

Champion, D.C., Sheraton, J.W., 1997. Geochemistry and Nd isotope systematics of Archaean granites of the Eastern Goldfields, Yilgarn Craton, Australia: implications for crustal growth processes. Precambrian Res. 83, 109–132.

Claoué-Long, J.C., Hoatson, D.M., Australia, G., 2009. Guide to using the Map of Australian Proterozoic Large Igneous Provinces. Geoscience Australia.

Clark, D.J., Hensen, B.J., Kinny, P.D., 2000. Geochronological constraints for a two-stage history of the Albany – Fraser Orogen, Western Australia. Precambrian Res. 102, 155–183.

Compston, W., Williams, I.S., McCulloch, M.T., 1986. Contrasting zircon U-Pb and model Sm-Nd ages for the Archaean Logue Brook Granite. Aust. J. Earth Sci. 33, 193–200. https://doi.org/10.1080/08120098608729359.

Czarnota, K., Champion, D.C., Goscombe, B., Blewett, R.S., Cassidy, K.F., Henson, P.A., Groenewald, P.B., 2010. Geodynamics of the eastern Yilgarn Craton. Precambrian Res. 183, 175–202. https://doi.org/10.1016/j.precamres.2010.08.004.

Dawson, G.C., Krapež, B., Fletcher, I.R., McNaughton, N.J., Rasmussen, B., 2003. 1.2 Ga thermal metamorphism in the Albany-Fraser Orogen of Western Australia: consequence of collision or regional heating by dyke swarms? J. Geol. Soc. Lond. 160, 29–37. https://doi.org/10.1144/0166-764901-119.

Dentith, M.C., Featherstone, W.E., 2003. Controls on intra-plate seismicity in southwestern Australia. Tectonophysics 376, 167–184. https://doi.org/10.1016/j.tecto.2003.10.002.

Dentith, M.C., Dent, V.F., Drummond, B.J., 2000. Deep crustal structure in the southwestern Yilgarn Craton, Western Australia. Tectonophysics 325, 227–255.

Doehler, J.S., Heaman, L.M., 1998. 2.41 Ga U–Pb Baddeleyite ages for two gabbroic dykes from the Widgiemooltha swarm, Western Australia: a Yilgarn–Lewisian connection. In: Geological Society of America 1998 Annual Meeting, Abstracts with Programs. Geological Society of America, pp. 291–292.

Doyle, H.A., 1971. Seismicity and structure in Australia. Bull. R. Soc. New Zeal. 9, 149–152.

Dunphy, J.M., Fletcher, I.R., Cassidy, K.F., Champion, D.C., 2003. Compilation of SHRIMP U-Pb geochronological data, Yilgarn Craton, Western Australia, 2001–2002. Geosci. Aust. Rec. 15, 139.

Elkins Tanton, L.T., Hager, B.H., 2000. Melt intrusion as a trigger for lithospheric foundering and the eruption of the Siberian flood basalts. Geophys. Res. Lett. 27, 3937–3940.

Elkins-Tanton, L.T., 2005. Continental magmatism caused by lithospheric delamination. Geol. Soc. Am. Spec. Pap. 80301, 449–461. https://doi.org/10.1130/2005.2388(27).

Embleton, B.J.J., Schmidt, P.W., 1985. Age and significance of magnetizations in dolerite dykes from the Northampton Block, Western Australia. Aust. J. Earth Sci. 32, 279–286.

Ernst, R.E., Buchan, K.L., 1997. Giant radiating dyke swarms: their use in identifying pre-Mesozoic large igneous provinces and mantle plumes, in: Large Igneous Provinces: Continental, Oceanic, and Planetary Flood Volcanism. American Geophysical Union Monograph 100, pp. 297–333.

Ernst, R., Bleeker, W., 2010. Large igneous provinces (LIPs), giant dyke swarms, and mantle plumes: significance for breakup events within Canada and adjacent regions from 2.5 Ga to the Present. Can. J. Earth Sci. 47, 695–739. https://doi.org/10.1139/e10-025.

Ernst, R.E., Head, J.W., Parfitt, E., Grosfils, E., Wilson, L., 1995. Giant radiating dyke swarms on Earth and Venus. Earth-Sci. Rev. 39, 1–58.

Ernst, R.E., Srivastava, R.K., 2008. India's place in the Proterozoic world: constraints from the Large Igneous Province (LIP) record. Indian dykes. In: Srivastava, R.K., Sivaji, Ch., Chalapathi Rao, N.V. (Eds.), Geochemistry, Geophys. Geochronology. Narosa

Publ. House Pvt. Ltd, New Delhi, India, pp. 41–56.
Ernst, R.E., Bleeker, W., Söderlund, U., Kerr, A.C., 2013. Large Igneous Provinces and supercontinents: toward completing the plate tectonic revolution. Lithos 174, 1–14.
Ernst, R., Srivastava, R., Bleeker, W., Hamilton, M., 2010. Precambrian Large Igneous Provinces (LIPs) and their dyke swarms: New insights from high-precision geochronology integrated with paleomagnetism and geochemistry. Precambrian Res. 183, vii–xi.
Evans, M.E., 1968. Magnetization of dikes: a study of the paleomagnetism of the Widgiemooltha dike suite, Western Australia. J. Geophys. Res. 73, 3261–3270.
Evans, T., 1999. Extent and nature of the 1.2 Ga Wheatbelt dyke swarm, Yilgarn Craton, Western Australia (B.Sc. thesis). Univ. West. Aust, Perth.
Fletcher, I.R., Wilde, S.A., Rosman, K.J., 1985. Sm-Nd model ages across the margins of the Archaean Yilgarn block, Western Australia — III. The western margin. Aust. J. Earth Sci. 32, 73–82. https://doi.org/10.1080/08120098508729314.
French, J.E., Heaman, L.M., Chacko, T., 2002. Feasibility of chemical U-Th-total Pb baddeleyite dating by electron microprobe. Chem. Geol. 188, 85–104. https://doi.org/10.1016/S0009-2541(02)00074-8.
Gee, R.D., Baxter, J.L., Wilde, S.A., Williams, I.R., 1981. Crustal development in the Archaean Yilgarn Block, Western Australia. Spec. Publ. Geol. Soc. Aust 7, 43–56.
Gerdes, A., Zeh, A., 2009. Zircon formation versus zircon alteration – new insights from combined U-Pb and Lu-Hf in-situ LA-ICP-MS analyses, and consequences for the interpretation of Archean zircon from the Central Zone of the Limpopo Belt. Chem. Geol. 261, 230–243. https://doi.org/10.1016/j.chemgeo.2008.03.005.
Groves, D.I., 1993. The crustal continuum model for late-Archaean lode-gold deposits of the Yilgarn Block, Western Australia. Miner. Depos. 28, 366–374.
Hallberg, J.A., 1987. Postcratonization mafic and ultramafic dykes of the Yilgarn Block. Aust. J. Earth Sci. 34, 135–149. https://doi.org/10.1080/08120098708729398.
Halls, H.C., Kumar, A., Srinivasan, R., Hamilton, M.A., 2007. Paleomagnetism and U-Pb geochronology of easterly trending dykes in the Dharwar craton, India: feldspar clouding, radiating dyke swarms and the position of India at 2.37 Ga. Precambrian Res. 155, 47–68. https://doi.org/10.1016/j.precamres.2007.01.007.
Halls, H.C., Zhang, B., 1998. Uplift structure of the southern Kapuskasing zone from 2.45 Ga dike swarm displacement. Geology 26, 67–70. https://doi.org/10.1130/0091-7613(1998) 026<0067:USOTSK>2.3.CO;2.
Heaman, L.M., 1997. Global mafic magmatism at 2.45 Ga: Remnants of an ancient large igneous province? Geology 25, 299–302.
Heaman, L.M., 2009. The application of U-Pb geochronology to mafic, ultramafic and alkaline rocks: an evaluation of three mineral standards. Chem. Geol. 261, 43–52. https://doi.org/10.1016/j.chemgeo.2008.10.021.
Hoek, J.D., Seitz, H.-M., 1995. Continental mafic dyke swarms as tectonic indicators: an example from the Vestfold Hills, Antarctica. Precambrian Res. 75, 121–139.
Holzer, L., Frei, R., Barton, J.M., Kramers, J.D., 1998. Unraveling the record of successive high grade events in the Central Zone of the Limpopo Belt using Pb single phase dating of metamorphic minerals. Precambrian Res. 87, 87–115. https://doi.org/10.1016/S0301-9268(97)00058-2.
Hou, G., 2012. Mechanism for three types of mafic dyke swarms. Geosci. Front. 3, 217–223. https://doi.org/10.1016/j.gsf.2011.10.003.
Isles, D.J., Cooke, A.C., 1990. Spatial associations between post-cratonisation dykes and gold deposits in the Yilgarn Block, Western Australia. In: Parker, A.J., Rickwood, P.C., Tucker, D.H. (Eds.), Mafic dykes and emplacement mechanisms. Balkema, Rotterdam, pp. 147–162.
Jaffey, A.H., Flynn, K.F., Glendenin, L.E., Bentley, W.C.T., Essling, A.M., 1971. Precision measurement of half-lives and specific activities of U 235 and U 238. Phys. Rev. C 4, 1889.
Johnson, S.P., Sheppard, S., Rasmussen, B., Wingate, M.T.D., Kirkland, C.L., Muhling, J.R., Fletcher, I.R., Belousova, E.A., 2011. Two collisions, two sutures: punctuated pre-1950Ma assembly of the West Australian Craton during the Ophthalmian and Glenburgh Orogenies. Precambrian Res. 189, 239–262. https://doi.org/10.1016/j.precamres.2011.07.011.
Ju, W., Hou, G., Hari, K.R., 2013. Mechanics of mafic dyke swarms in the Deccan Large Igneous Province: palaeostress field modelling. J. Geodyn. 66, 79–91. https://doi.org/10.1016/j.jog.2013.02.002.
Kamber, B.S., Biino, G.G., 1995. The evolution of high T-low P granulites in the Northern Marginal Zone sensu stricto, Limpopo Belt, Zimbabwe-the case for petrography. Schweizerische Mineral. Petrogr. Mitteilungen 75, 427–454.
Kent, A.J.R., Cassidy, K.F., Fanning, M.C., 1996. Archean gold mineralisation synchronous with the final stages of cratonization, Yilgarn Craton, Western Australia. Geology 96, 879–882. https://doi.org/10.1130/0091-7613(1996) 024<0879.
Korsch, R.J., Kositcin, N., Champion, D.C., 2011. Australian island arcs through time: Geodynamic implications for the Archean and Proterozoic. Gondwana Res. 19, 716–734. https://doi.org/10.1016/j.gr.2010.11.018.
Kramers, J.D., McCourt, S., Roering, C., Smit, C.A., Van Reenen, D.D., 2011. Tectonic models proposed for the Limpopo Complex: mutual compatibilities and constraints. Geol. Soc. Am. Mem. 207, 311–324.
Kröner, A., Jaeckel, P., Brandl, G., Nemchin, A.A., Pidgeon, R.T., 1999. Single zircon ages for granitoid gneisses in the Central Zone of the Limpopo Belt, Southern Africa and geodynamic significance. Precambrian Res. 93, 299–337. https://doi.org/10.1016/S0301-9268(98)00102-8.
Ksienzyk, A.K., Jacobs, J., Boger, S.D., Kosler, J., Sircombe, K.N., Whitehouse, M.J., 2012. U-Pb ages of metamorphic monazite and detrital zircon from the Northampton Complex: evidence of two orogenic cycles in Western Australia. Precambrian Res. 198–199, 37–50. https://doi.org/10.1016/j.precamres.2011.12.011.
Lewis, J.D., 1994. Mafic dykes in the Williams-Wandering area, Western Australia. Geol. Surv. West. Aust. Rep. 37, 37–52.
Li, T., Zhai, M., Peng, P., Chen, L., Guo, J., 2010. Ca. 2.5 billion year old coeval ultramafic-mafic and syenitic dykes in Eastern Hebei: Implications for cratonization of the North China Craton. Precambrian Res. 180, 143–155. https://doi.org/10.1016/j.precamres.2010.04.001.
Ludwig, K., 2009. Squid 2.50, A User's Manual (No. 2.50.11.02.03 Rev. 03 Feb 2011). Berkeley, California, USA.
Ludwig, K., 2012. User's manual for Isoplot version 3.75–4.15: a geochronological toolkit for Microsoft. Berkeley Geochronological Cent. Spec. Publ.
McFarlane, C.R.M., 2010. Geodynamic constraints on mineralization and metamorphism at the Griffin's Find gold deposit, Western Australia, from calibrated Tt trajectories. GeoCanada 2010, Calgary May 10–14. Canadian Society of Petroleum Geoscientists, Calgary.
McNaughton, N.J., Groves, D.I., 1996. A review of Pb-isotope constraints on the genesis of lode-gold deposits in the Yilgarn Craton, Western Australia. J. R. Soc. West. Aust. 79, 123–129.
Middleton, M.F., Wilde, S.A., Evans, B.A., Long, A., Dentith, M., 1993. A preliminary interpretation of deep seismic reflection and other geophysical data from the Darling Fault Zone, Western Australia. Explor. Geophys. 24, 711–718.
Millonig, L., Zeh, A., Gerdes, A., Klemd, R., 2008. Neoarchaean high-grade metamorphism in the Central Zone of the Limpopo Belt (South Africa): combined petrological and geochronological evidence from the Bulai pluton. Lithos 103, 333–351. https://doi.org/10.1016/j.lithos.2007.10.001.
Mohanty, S., 2015. Precambrian continent assembly and dispersal events of South Indian and East Antarctic Shields. Int. Geol. Rev. 57, 1992–2027. https://doi.org/10.1080/00206814.2015.1048751.
Mole, D.R., Fiorentini, M.L., Thebaud, N., McCuaig, T.C., Cassidy, K.F., Kirkland, C.L., Wingate, M.T.D., Romano, S.S., Doublier, M.P., Belousova, E.A., 2012. Spatio-temporal constraints on lithospheric development in the southwest–central Yilgarn Craton, Western Australia. Aust. J. Earth Sci. 59, 625–656. https://doi.org/10.1080/08120099.2012.691213.
Mole, D.R., Fiorentini, M.L., Cassidy, K.F., Kirkland, C.L., Thebaud, N., McCuaig, T.C., Doublier, M.P., Duuring, P., Romano, S.S., Maas, R., Belousova, E.A., Barnes, S.J., Miller, J., 2015. Crustal evolution, intra-cratonic architecture and the metallogeny of an Archaean craton. Geol. Soc. London Spec. Publ. 393, 23–80. https://doi.org/10.1144/SP393.8.
Mushayandebvu, M.F., Jones, D.L., Briden, J.C., Baer, G., Heimann, A., 1995. Palaeomagnetic and geochronological results from Proterozoic mafic intrusions in southern Zimbabwe. In: Physics and Chemistry of Dykes. Balkema Rotterdam, pp. 293–303.
Myers, J.S., 1993. Precambrian tectonic history of the West Australian Craton and adjacent orogens. Annu. Rev. Earth Planet. Sci. 21, 453–485.
Myers, J.S., 1995. The generation and assembly of an Archaean supercontinent: evidence from the Yilgarn craton, Western Australia. Geol. Soc. London Spec. Publ. 95, 143–154.
Myers, J.S., 1990. Pinjarra orogen. In: Geology and Mineral Resources of Western Australia. State Printing Division, pp. 264–274.
Nelson, K.D., 1992. Are crustal thickness variations in old mountain belts like the Appalachians a consequence of lithospheric delamination? Geology 20, 498–502.
Nelson, D.R., 1997. Evolution of the Archaean granite-greenstone terranes of the Eastern Goldfields, Western Australia: SHRIMP U-Pb zircon constraints. Precambrian Res. 83, 57–81. https://doi.org/10.1016/S0301-9268(97)00005-3.
Nelson, D.R., Myers, J.S., Nutman, A.P., 1995. Chronology and evolution of the Middle Proterozoic Albany-Fraser Orogen. Western Australia. Aust. J. Earth Sci. 42, 481–495. https://doi.org/10.1080/08120099508728218.
Nemchin, A.A., Pidgeon, R.T., 1997. Evolution of the Darling Range batholith, Yilgarn Craton, Western Australia: a SHRIMP zircon study. J. Petrol. 38, 625–649.
Nemchin, A.A., Pidgeon, R.T., 1998. Precise conventional and SHRIMP baddeleyite U-Pb age for the Binneringie Dyke, near Narrogin, Western Australia. Aust. J. Earth Sci. 45, 673–675.
Nemchin, A.A., Pidgeon, R.T., Wilde, S.A., 1994. Timing of Late Archaean granulite facies metamorphism in the southwestern Yilgarn Craton of Western Australia: evidence from U-Pb ages of zircons fro mafic granulites. Precambrian Res. 68, 307–321.
Nieuwland, D.A., Compston, W., 1981. Crustal evolution in the Yilgarn block near Perth, Western Australia. In: Archean Geology, Second International Symposium (Perth 1980): Geological Society of Australia, Special Publication. pp. 159–171.
Nutman, A.P., Bennett, V.C., Kinny, P.D., Price, R., 1993. Large-scale crustal structure of the Northwestern Yilgarn Craton, western Australia: Evidence from Nd isotopic data and zircon geochronology. Tectonics 12, 971–981. https://doi.org/10.1029/93TC00377.
Oberthür, T., Davis, D.W., Blenkinsop, T.G., Höhndorf, A., 2002. Precise U-Pb mineral ages, Rb–Sr and Sm–Nd systematics for the Great Dyke, Zimbabwe—constraints on late Archean events in the Zimbabwe craton and Limpopo belt. Precambrian Res. 113, 293–305.
Oliveira, E.P., Silveira, E.M., Söderlund, U., Ernst, R.E., 2013. U-Pb ages and geochemistry of mafic dyke swarms from the Uauá Block, São Francisco Craton, Brazil: LIPs remnants relevant for Late Archaean break-up of a supercraton. Lithos 174, 308–322. https://doi.org/10.1016/j.lithos.2012.05.025.
Pidgeon, R.T., Cook, T.J.F., 2003. 1214 ± 5 Ma dyke from the Darling Range, southwestern Yilgarn Craton, Western Australia. Aust. J. Earth Sci. 50, 769–773.
Pidgeon, R.T., Nemchin, A.A., 2001. 1.2 Ga Mafic dyke near York, southwestern Yilgarn Craton, Western Australia. Aust. J. Earth Sci. 48, 751–755. https://doi.org/10.1046/j.1440-0952.2001.485895.x.
Pidgeon, R.T., Wilde, S.A., 1990. The distribution of 3.0 Ga and 2.7 Ga volcanic episodes in the Yilgarn Craton of Western Australia. Precambrian Res. 48, 309–325.
Pisarevsky, S.A., De Waele, B., Jones, S., Söderlund, U., Ernst, R.E., 2015. Paleomagnetism and U-Pb age of the 2.4 Ga Erayinia mafic dykes in the south-western Yilgarn, Western Australia: paleogeographic and geodynamic implications. Precambrian Res. 259, 222–231. https://doi.org/10.1016/j.precamres.2014.05.023.

Qiu, Y., Groves, D.I., 1999. Late Archean collision and delamination in the Southwest Yilgarn Craton; the driving force for Archean orogenic lode gold mineralization? Econ. Geol. 94, 115–122.

Qiu, Y., McNaughton, N.J., Groves, D., Dalstra, H.J., 1997b. Shrimp U-Pb in zircon and lead-isotope constraints on the timing and source of an Archaean granulite-hosted lode-gold deposit at Griffin's Find, Yilgarn craton, Western Australia. Chron. Rech. Min. 91–104.

Qiu, Y., Groves, D.I., McNaughton, N.J., 1997a. Deep-seated granitoids: implications for Late Archaean subduction-collision-lithospheric delamination and gold mineralization in the Yilgarn Craton. Aust. Geol. Surv. Organ. Rec. 41, 65–69.

Qiu, Y., McNaughton, N.J., Groves, D.I., Dunphy, J.M., 1999. First record of 1.2 Ga quartz dioritic magmatism in the Archaean Yilgarn Craton, Western Australia, and its significance. Aust. J. Earth Sci. 46, 421–428. https://doi.org/10.1046/j.1440-0952.1999.00715.x.

Rasmussen, B., Fletcher, I.R., 2010. Dating sedimentary rocks using in situ U-Pb geochronology of syneruptive zircon in ash-fall tuff & lt 1 mm thick. Geology 38, 299–302. https://doi.org/10.1130/G30567.1.

Roth, E., Bennett, J.M., Symons, P.M., 1990. Boddington and Black Flag: anomalous Archaean gold deposits. Geol. Dep. Univ. Extension. Univ. West. Aust. Publ. 20, 189–194.

Roth, E., Groves, D., Anderson, G., Daley, L., Staley, R., 1991. Primary mineralization at the Boddington gold mine, Western Australia: An Archean porphyry Cu-Au-Mo deposit, in: Brazil Gold. pp. 481–488.

Schott, B., Schmeling, H., 1998. Delamination and detachment of a lithospheric root. Tectonophysics 296, 225–247.

Shellnutt, J.G., Hari, K.R., Liao, A.C.-Y., Denyszyn, S.W., Vishwakarma, N., 2018. A 1.88 Ga giant radiating mafic dyke swarm across Southern India and Western Australia. Precambrian Res. 308, 58–74.

Sheppard, S., Bodorkos, S., Johnson, S.P., Wingate, M.T.D., Kirkland, C.L., 2010. The Paleoproterozoic Capricorn Orogeny: intracontinental reworking not continent–continent collision, Geological Survey of Western Australia Report 108. Geological Survey of Western Australia.

Sircombe, K.N., 2007. Compilation of SHRIMP U-Pb geochronological data, Yilgarn Craton, Western Australia, 2004–2006. Geoscience Australia.

Smirnov, A.V., Evans, D.A.D., Ernst, R.E., Söderlund, U., Li, Z.-X., 2013. Trading partners: tectonic ancestry of southern Africa and western Australia, in Archean supercratons Vaalbara and Zimgarn. Precambrian Res. 224, 11–22.

Smithies, R.H., Champion, D.C., 1999. Late Archaean felsic alkaline igneous rocks in the Eastern Goldfields, Yilgarn Craton, Western Australia: a result of lower crustal delamination? J. Geol. Soc. London. 156, 561–576.

Smithies, R.H., Howard, H.M., Kirkland, C.L., Korhonen, F.J., Medlin, C.C., Maier, W.D., de Gromard, R.Q., Wingate, M.T.D., Quentin De Gromard, R., Wingate, M.T.D., 2015. Piggy-back supervolcanoes-long-lived, voluminous, juvenile rhyolite volcanism in mesoproterozoic central Australia. J. Petrol. 56, egv015. https://doi.org/10.1093/petrology/egv015.

Söderlund, U., Hofmann, A., Klausen, M.B., Olsson, J.R., Ernst, R.E., Persson, P.O., 2010. Towards a complete magmatic barcode for the Zimbabwe craton: Baddeleyite U-Pb dating of regional dolerite dyke swarms and sill complexes. Precambrian Res. 183, 388–398. https://doi.org/10.1016/j.precamres.2009.11.001.

Söderlund, U., Johansson, L., 2002. A simple way to extract baddeleyite (ZrO_2). Geochem. Geophys. Geosyst. 3. https://doi.org/10.1029/2001GC000212.

Sofoulis, J., 1965. Explanatory Notes on the Widgiemooltha 1: 250,000 Geological Sheet Western Australia. Geological Survey of Western Australia.

Spaggiari, C. V, Bodorkos, S., Barquero-Molina, M., Tyler, I.M., Wingate, M.T.D., 2009. Interpreted bedrock geology of the South Yilgarn and of the South Yilgarn and Central Albany-Fraser Orogen, Western Australia, Geological Survey of Western Australia Record 2009/10.

Spaggiari, C. V, Kirkland, C.L., Pawley, M.J., Smithies, R.H., Wingate, M.T.D., Doyle, M. G., Blenkinsop, T.G., Clark, C., Oorschot, C.W., Fox, L.J., 2011. The geology of the east Albany-Fraser Orogen—a field guide, Geological Survey of Western Australia Record 2011/23.

Spaggiari, C.V., Kirkland, C.L., Smithies, H.R., Wingate, M.T.D., Belousova, E.A., 2015. Transformation of an Archean craton margin during Proterozoic basin formation and magmatism: the Albany-Fraser Orogen, Western Australia. Precambrian Res. 266, 440–466. https://doi.org/10.1016/j.precamres.2015.05.036.

Stacey, J.S., Kramers, J.D., 1975. Approximation of terrestrial lead isotope evolution by a two-stage model. Earth Planet. Sci. Lett. 26, 207–221.

Standing, J.G., 2008. Terrane amalgamation in the Eastern Goldfields Superterrane, Yilgarn Craton: evidence from tectonostratigraphic studies of the Laverton Greenstone Belt. Precambrian Res. 161, 114–134.

Stark, J.C., Wang, X.-C., Denyszyn, S.W., Li, Z.-X., Rasmussen, B., Zi, J.-W., Sheppard, S., Liu, Y., 2017. Newly identified 1.89 Ga mafic dyke swarm in the Archean Yilgarn Craton, Western Australia suggests a connection with India (in press). Precambrian Res. https://doi.org/10.1016/j.precamres.2017.12.036.

Stern, R.A., Bodorkos, S., Kamo, S.L., Hickman, A.H., Corfu, F., 2009. Measurement of SIMS instrumental mass fractionation of Pb isotopes during zircon dating. Geostand. Geoanal. Res. 33, 145–168. https://doi.org/10.1111/j.1751-908X.2009.00023.x.

Stern, R.A., 2001. A new isotopic and trace-element standard for the ion microprobe: preliminary thermal ionization mass spectrometry (TIMS) U-Pb and electron-microprobe data, Geological Survey of Canada Current Research 2001-F.

Tomkins, A.G., Grundy, C., 2009. Upper temperature limits of orogenic gold deposit formation: constraints from the granulite-hosted Griffin's Find Deposit, Yilgarn Craton. Econ. Geol. 104, 669–685.

Tucker, D.H., Boyd, D.M., 1987. Dykes of Australia detected by airborne magnetic surveys. In: Fahrig, W.F., Halls, H.C. (Eds.), Mafic Dyke Swarms. Geological Association of Canada, pp. 163–172.

Upton, P., Hobbs, B., Ord, A., Zhang, Y., Drummond, B., Archibald, N., 1997. Thermal and deformation modelling of the Yilgarn deep seismic transect. Geodyn. Ore Dep. Conf. Abst. 22–25.

Wang, X.-C., Li, Z.-X., Li, J., Pisarevsky, S.A., Wingate, M.T.D., 2014. Genesis of the 1.21 Ga Marnda Moorn large igneous province by plume–lithosphere interaction. Precambrian Res. 241, 85–103. https://doi.org/10.1016/j.precamres.2013.11.008.

Wilde, S.A., 1976. The Saddleback Group–a newly discovered Archaean greenstone belt in the southwestern Yilgarn Block. West. Aust. Geol. Surv. Annu. Rep. 92–95.

Wilde, S.A., 1999. Evolution of the Western Margin of Australia during the Rodinian and Gondwanan Supercontinent Cycles. Gondwana Res. 2, 481–499. https://doi.org/10.1016/S1342-937X(05)70287-2.

Wilde, S.A., Pidgeon, R.T., 1987. U-Pb. Geochronology, Geothermometry and Petrology of the Main Areas of Gold Mineralization in the Wheat Belt Region of Western Australia Project 30 Final Report. Western Australian Mining and Petroleum Research Institute.

Wilde, S.A., Pidgeon, R.T., 1990. The Morangup Greenstone Belt: a further discovery of Late Archaean volcanic rocks in the southwest Yilgarn Craton, Western Australia. International Archaean Symposium, 3rd Perth 1990. Abstr. Geoconferences 205–206.

Wilde, S.A., Low, G.H., 1978. Perth, Western Australia, 1:250,000 geological series explanatory notes. West. Aust. Geol Surv.

Wilde, S.A., Pidgeon, R.T., 1986. Geology and geochronology of the Saddleback greenstone belt in the Archaean Yilgarn Block, southwestern Australia. Aust. J. Earth Sci. 33, 491–501.

Wilde, S.A., Middleton, M.F., Evans, B.J., 1996. Terrane accretion in the southwestern Yilgarn Craton: evidence from a deep seismic crustal profile. Precambrian Res. 78, 179–196.

Wilde, S.A., Pidgeon, R.T., 2006. Nature and timing of Late Archaean arc magmatism along the western margin of the Yilgarn Craton. Geochim. Cosmochim. Acta 70, A701.

Wilde, S.A., 1980. The Jimperding Metamorphic Belt in the Toodyay area and the Balingup Metamorphic Belt and associated granitic rocks in the southwestern Yilgarn Craton. Excursion Guide, In: 2nd International Archaean Symposium, Geological Society of Western Australia.

Wilde, S.A., 1990. Geology and crustal evolution of the southwestern Yilgarn Craton. In: Third International Archaean Symposium, Perth. pp. 89–122.

Williams, I.S., 1998. U-Th-Pb geochronology by ion microprobe. Rev. Econ. Geol. 7, 1–35.

Wilson, J.F., Jones, D.L., Kramers, J.D., 1987. Mafic dyke swarms in Zimbabwe. In: Fahrig, W.F., Halls, H.C. (Eds.), Mafic Dyke Swarms. Geological Association of Canada, pp. 433–444.

Wingate, M.T.D., 1999. Ion microprobe baddeleyite and zircon ages for Late Archaean mafic dykes of the Pilbara Craton, Western Australia. Aust. J. Earth Sci. 46, 493–500. https://doi.org/10.1046/j.1440-0952.1999.00726.x.

Wingate, M.T.D., Pidgeon, R.T., 2005. The Marnda Moorn LIP, a late Mesoproterozoic large igneous province in the Yilgarn craton, Western Australia. July 2005 LIP of the month [WWW Document]. (unpub). Large Igneous Prov. Comm. Int. Assoc. Volcanol. Chem. Earth's Inter. URL http://www.largeigneousprovinces.org/05jul.

Wingate, M.T.D., Campbell, I.H., Compston, W., Gibson, G.M., 1998. Ion microprobe U-Pb ages for Neoproterozoic basaltic magmatism in south-central Australia and implications for the breakup of Rodinia. Precambrian Res. 87, 135–159. https://doi.org/10.1016/S0301-9268(97)00072-7.

Wingate, M.T.D., Campbell, I.H., Harris, L.B., 2000. SHRIMP baddeleyite age for the Fraser dyke swarm, southeast Yilgarn Craton, Western Australia. Aust. J. Earth Sci. 47, 309–313.

Wingate, M.T.D., Pisarevsky, S.A., Evans, D.A.D., 2002. Rodinia connections between Australia and Laurentia: no SWEAT, no AUSWUS? Terra Nov. 14, 121–128.

Wingate, M.T.D., Pirajno, F., Morris, P.A., 2004. Warakurna large igneous province: a new Mesoproterozoic large igneous province in west-central Australia. Geology 32, 105–108.

Wingate, M.T.D., 2007. Proterozoic mafic dykes in the Yilgarn Craton. In: Proceedings of Geoconferences (WA) Inc. Kalgoorlie 2007 Conference, Kalgoorlie, Western Australia. pp. 80–84.

Wingate, M.T.D., 2017. Mafic dyke swarms and large igneous provinces in Western Australia get a digital makeover. In: Geological Survey of Western Australia Record 2017/2. pp. 4–8.

Witt, W.K., Vanderhor, F., 1998. Diversity within a unified model for Archaean gold mineralization in the Yilgarn Craton of Western Australia: an overview of the late-orogenic, structurally-controlled gold deposits. Ore Geol. Rev. 13, 29–64. https://doi.org/10.1016/S0169-1368(97)00013-9.

Witt, W.K., Cassidy, K.F., Lu, Y.-J., Hagemann, S.G., 2018. The tectonic setting and evolution of the 2.7 Ga Kalgoorlie–Kurnalpi Rift, a world-class Archean gold province. Miner. Depos. https://doi.org/10.1007/s00126-017-0778-9.

Xie, H., Kröner, A., Brandl, G., Wan, Y., 2017. Two orogenic events separated by 2.6 Ga mafic dykes in the Central Zone, Limpopo Belt, southern Africa. Precambrian Res. 289, 129–141. https://doi.org/10.1016/j.precamres.2016.11.009.

Yeats, C.J., McNaughton, N.J., 1997. Significance of SHRIMP II U-Pb geochronology on lode-gold deposits of the Yilgarn craton. Aust. Geol. Surv. Organ. Rec. 41, 125–130.

Yeats, C.J., McNaughton, N.J., Groves, D.I., 1996. SHRIMP U-Pb geochronological constraints on Archean volcanic-hosted massive sulfide and lode gold mineralization at Mount Gibson, Yilgarn Craton, Western Australia. Econ. Geol. 91, 1354–1371.

Zeh, A., Gerdes, A., Klemd, R., Barton, J.M., 2007. Archaean to proterozoic crustal evolution in the central zone of the Limpopo Belt (South Africa-Botswana): constraints from combined U-Pb and Lu-Hf isotope analyses of zircon. J. Petrol. https://doi.org/10.1093/petrology/egm032.

Zeh, A., Gerdes, A., Barton Jr, J., Klemd, R., 2010. U–Th–Pb and Lu–Hf systematics of zircon from TTG's, leucosomes, meta-anorthosites and quartzites of the Limpopo Belt (South Africa): constraints for the formation, recycling and metamorphism of

Palaeoarchaean crust. Precambrian Res. 179, 50–68.
Zhao, G., Sun, M., Wilde, S.A., Li, S., Zhang, J., 2006. Some key issues in reconstructions of Proterozoic supercontinents. J. Asian Earth Sci. 28, 3–19.
Zibra, I., Clos, F., Weinberg, R.F., Peternell, M., 2017a. The ∼2730 Ma onset of the Neoarchean Yilgarn Orogeny. Tectonics 36, 1787–1813. https://doi.org/10.1002/2017TC004562.
Zibra, I., Korhonen, F.J., Peternell, M., Weinberg, R.F., Romano, S.S., Braga, R., De Paoli, M.C., Roberts, M., 2017b. On thrusting, regional unconformities and exhumation of high-grade greenstones in Neoarchean orogens. The case of the Waroonga Shear Zone, Yilgarn Craton. Tectonophysics 712–713, 362–395. https://doi.org/10.1016/j.tecto.2017.05.017.

Statement of Authorship

Title of Paper	**1.39 Ga mafic dyke swarm in southwestern Yilgarn Craton marks Nuna to Rodinia transition in the West Australian Craton**	
Publication Status	**Published**	Accepted for publication
	Submitted for Publication	Publication Style
Publication Details	Stark, J.C., Wang, X.-C., Li, Z.-X., Denyszyn, S.W., Rasmussen, B., Zi, J.-W., Sheppard, S., 2018. 1.39 Ga mafic dyke swarm in southwestern Yilgarn Craton marks Nuna to Rodinia transition in the West Australian Craton. Precambrian Res. 316, 291–304.	

Author Contributions

By signing the Statement of Authorship, each author certifies that their stated contribution to the publication is accurate and that permission is granted for the publication to be included in the candidate's thesis.

Name of Principal Author (Candidate)	Jutta Camilla Stark		
Contribution to the Paper	Jutta Camilla Stark collected and prepared most of the samples and undertook SHRIMP dating, some baddeleyite separation for ID-TIMS dating, most of the interpretation and drafted most of the manuscript		
Overall percentage (%)	60		
Signature		Date	01/06/2018

Name of Co-Author	Xuan-Ce Wang		
Contribution to the Paper	Xuan-Ce Wang is a supervisor of the candidate and assisted with the interpretation of the geochemical data and drafting of the manuscript		
Overall percentage (%)	10		
Signature		Date	01/06/2018

Name of Co-Author	Steven Denyszyn		
Contribution to the Paper	Steve Denyszyn undertook baddeleyite separation and ID-TIMS dating		
Overall percentage (%)	5		
Signature		Date	01/06/2018

Name of Co-Author	Zheng-Xiang Li		
Contribution to the Paper	Zheng-Xiang Li is the principal supervisor of the candidate and assisted with the concept and drafting of the manuscript and interpretation of the results		
Overall percentage (%)	5		
Signature		Date	01/06/2018

Name of Co-Author	Birger Rasmussen		
Contribution to the Paper	Birger Rasmussen assisted with interpretation of the SHRIMP results and drafting of the manuscript		
Overall percentage (%)	5		
Signature		Date	01/06/2018

Name of Co-Author	Jian-Wei Zi		
Contribution to the Paper	Jian-Wei Zi assisted with SHRIMP sample preparation, analysis and data processing		
Overall percentage (%)	5		
Signature		Date	01/06/2018

Copyright Clearance Center RightsLink®

Home | Create Account | Help

Title: 1.39 Ga mafic dyke swarm in southwestern Yilgarn Craton marks Nuna to Rodinia transition in the West Australian Craton

Author: J. Camilla Stark,Xuan-Ce Wang,Zheng-Xiang Li,Steven W. Denyszyn,Birger Rasmussen,Jian-Wei Zi

Publication: Precambrian Research

Publisher: Elsevier

Date: October 2018

LOGIN

If you're a copyright.com user, you can login to RightsLink using your copyright.com credentials.
Already **a RightsLink user** or want to learn more?

Please note that, as the author of this Elsevier article, you retain the right to include it in a thesis or dissertation, provided it is not published commercially. Permission is not required, but please ensure that you reference the journal as the original source. For more information on this and on your other retained rights, please visit: https://www.elsevier.com/about/our-business/policies/copyright#Author-rights

BACK | CLOSE WINDOW

Precambrian Research 316 (2018) 291–304

Contents lists available at ScienceDirect

Precambrian Research

journal homepage: www.elsevier.com/locate/precamres

1.39 Ga mafic dyke swarm in southwestern Yilgarn Craton marks Nuna to Rodinia transition in the West Australian Craton

J. Camilla Stark[a,b,c,*], Xuan-Ce Wang[b,c], Zheng-Xiang Li[a,b,c], Steven W. Denyszyn[d], Birger Rasmussen[d], Jian-Wei Zi[b,e]

[a] Earth Dynamics Group, ARC Centre of Excellence for Core to Crust Fluid Systems (CCFS), Curtin University, GPO Box U1987, Perth, WA 6845, Australia
[b] The Institute for Geoscience Research (TIGeR), School of Earth and Planetary Sciences, Curtin University, GPO Box U1987, Perth, WA 6845, Australia
[c] School of Earth and Planetary Sciences, Curtin University, GPO Box U1987, Perth, WA 6845, Australia
[d] School of Earth Sciences, University of Western Australia, Perth WA 6009, Australia
[e] State Key Lab of Geological Processes and Mineral Resources, China University of Geosciences, Wuhan 430074, China

ARTICLE INFO

Keywords:
Yilgarn Craton
Mafic dykes
Geochronology
U-Pb baddeleyite
Large Igneous Province
Biberkine dykes

ABSTRACT

The Archean Yilgarn Craton in Western Australia hosts at least five generations of mafic dykes ranging from Archean to Neoproterozoic in age, including the craton-wide ca. 2408 Ma Widgiemooltha and the 1210 Ma Marnda Moorn Large Igneous Provinces (LIP), the 1888 Ma Boonadgin dykes in the southwest and the 1075 Ma Warakurna LIP in the northern part of the craton. We report here a newly identified NNW-trending mafic dyke swarm, here named the Biberkine dyke swarm, in the southwestern Yilgarn Craton dated at 1390 ± 3 Ma by ID-TIMS U-Pb geochronology of baddeleyite. The regional extent of the dyke swarm is uncertain but aeromagnetic data suggest that the dykes are part of a linear swarm several hundred kilometers long, truncated by the Mesoproterozoic Albany-Fraser Orogen to the south. Geochemical data indicate that the dykes have tholeiitic compositions with a significant contribution from metasomatically enriched subcontinental lithospheric mantle and/or lower continental crust. Paleogeographic reconstructions suggest that a prolonged tectonic quiescence in the Yilgarn Craton from ca. 1600 Ma was interrupted by renewed subduction along the southern and south-eastern margin at ca. 1400 Ma, reflecting a transition from Nuna to Rodinia configuration. The 1390 Ma Biberkine dykes may be a direct consequence of this transition and mark the change from a passive to active tectonic setting, which culminated in the Albany-Fraser Orogeny at ca. 1330 Ma. The Biberkine dykes are coeval with a number of other mafic dyke swarms worldwide and provide an important target for paleomagnetic studies.

1. Introduction

Mafic dyke swarms act as important markers for supercontinent reconstructions (e.g. Ernst and Buchan, 1997; Buchan et al., 2001; Bleeker and Ernst, 2006; Ernst and Srivastava, 2008; Ernst et al., 2010, 2013) and as indicators of paleostress fields and pre-existing crustal weaknesses (Ernst et al., 1995; Hoek and Seitz, 1995; Halls and Zhang, 1998; Hou, 2012; Ju et al., 2013). They appear to be intimately connected with deep-Earth dynamics and supercontinent cycles (e.g. Condie, 2004; Prokoph et al., 2004; Bleeker and Ernst, 2006; Ernst et al., 2008; Li and Zhong, 2009; Goldberg, 2010) and their presence acts as a tectonic fingerprint of intracratonic crustal extension associated with processes such as subduction (back-arc extension), mantle plumes and rifting during supercontinent breakup.

The Archean Yilgarn Craton in Western Australia shared a large part of its tectonic evolution with Antarctica during the Mesoproterozoic and is thus an important component in reconstructions for the Nuna and Rodinia supercontinents (Dalziel, 1991; Meert, 2002; Rogers and Santosh, 2002; Wingate et al., 2002; Li et al., 2008; Nance et al., 2014; Pisarevsky et al., 2014; Meert and Santosh, 2017). The transition from Nuna to Rodinia likely occurred after ca. 1400 Ma (Li et al., 2008; Evans and Mitchell, 2011; Pisarevsky et al., 2014; Aitken et al., 2016), after an interval of apparent tectonic quiescence in the Yilgarn Craton since ca. 1600 Ma. Here we report the discovery of a Mesoproterozoic (1390 Ma) NNW-trending mafic dyke swarm in the southwestern Yilgarn Craton, identified by U-Pb geochronology using a combination of *in situ* SHRIMP and ID-TIMS methodologies. We also present results from a preliminary geochemical analysis and discuss the tectonic setting

* Corresponding author at: Earth Dynamics Group, ARC Centre of Excellence for Core to Crust Fluid Systems (CCFS), Curtin University, GPO Box U1987, Perth, WA 6845, Australia.
E-mail address: c.stark@postgrad.curtin.edu.au (J.C. Stark).

https://doi.org/10.1016/j.precamres.2018.08.014
Received 11 May 2018; Received in revised form 8 August 2018; Accepted 21 August 2018
Available online 23 August 2018
0301-9268/

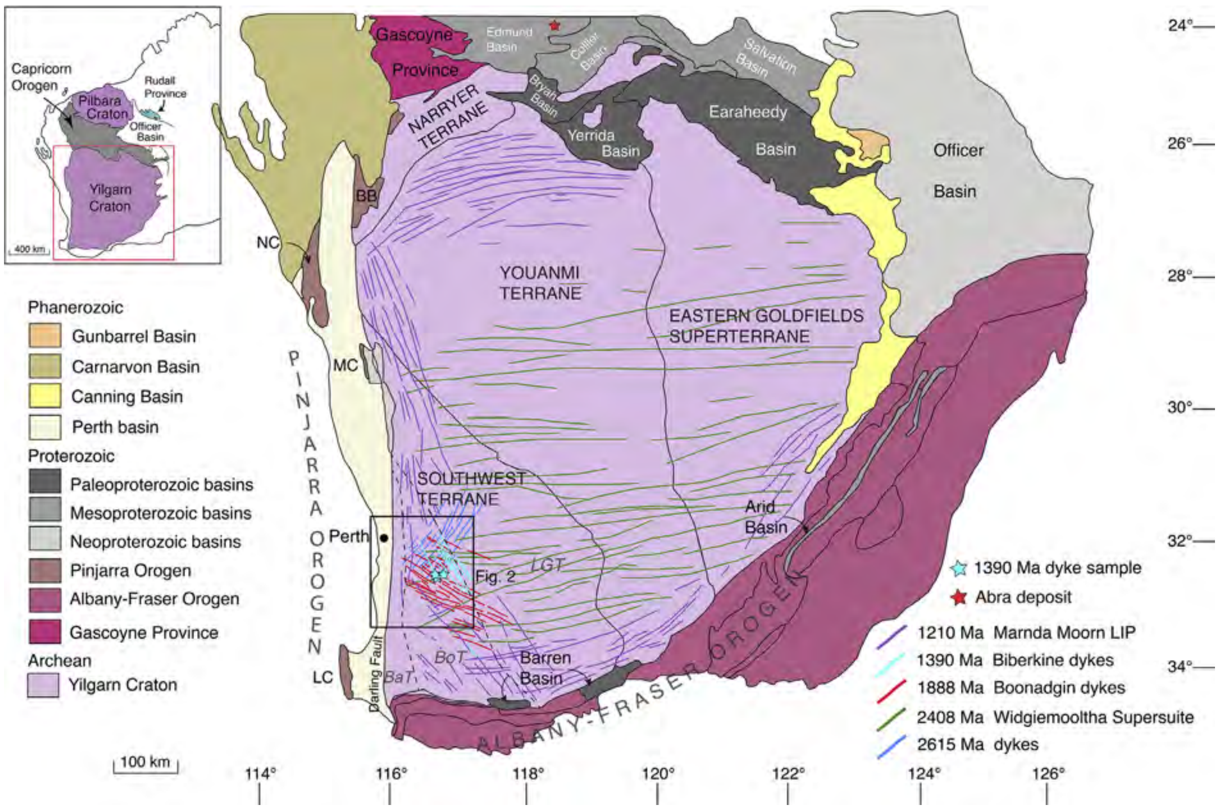

Fig. 1. Map of the Yilgarn Craton showing major tectonic units and the Capricorn and Albany-Fraser orogens. Inset shows the extent of the West Australian Craton (Pilbara Craton, Yilgarn Craton and Capricorn Orogen). From Geological Survey of Western Australia 1:2.5 M Interpreted Bedrock Geology 2015 and 1:10 M Tectonic Units 2016.

during emplacement of the dykes and implications for regional tectonic models.

2. Regional geology

The Yilgarn Craton is a ca. 900 × 1000 km Archean crustal block comprising six accreted terranes: the Southwest, Narryer, Youanmi, Kalgoorlie, Kurnalpi and Burtville terranes, the latter three forming the Eastern Goldfields Superterrane (Fig. 1). These comprise variably metamorphosed granites and volcanic and sedimentary rocks with protolith ages between ca. 3730 and 2620 Ma (Cassidy et al., 2005, 2006 and references therein) and are thought to represent a series of volcanic arcs and back- arc basins, which amalgamated during a Neoarchean orogeny between ca. 2730 and 2625 Ma (Myers, 1993, 1995; Wilde et al., 1996; Barley et al., 2003; Blewett and Hitchman, 2006; Korsch et al., 2011; Witt et al., 2018). Abundant granites were emplaced between ca. 2760 Ma and 2630 Ma (Cassidy et al., 2006 and references therein) and the entire craton underwent intense metamorphism and hydrothermal activity between 2780 and 2630 Ma (Myers, 1993; Nemchin et al., 1994; Nelson et al., 1995; Wilde et al., 1996). The Southwest Terrane comprises multiply deformed ca. 3200–2800 Ma high-grade metasedimentary rocks and ca. 2720–2670 Ma *meta*-igneous rocks intruded by 2750–2620 Ma granites (Myers, 1993; Wilde et al., 1996; Nemchin and Pidgeon, 1997).

The Yilgarn Craton is bounded by three Proterozoic orogenic belts: the ca. 2005–570 Ma Capricorn Orogen in the north (Cawood and Tyler, 2004; Sheppard et al., 2010a; Johnson et al., 2011), the ca. 1815–1140 Ma Albany-Fraser Orogen in the south and east (Nelson et al., 1995; Clark et al., 2000; Spaggiari et al., 2015), and the ca. 1090–525 Ma Pinjarra Orogen in the west (Myers, 1990; Wilde, 1999; Ksienzyk et al., 2012). Following cratonisation toward the end of the Archean, the Yilgarn Craton collided along the Capricorn Orogen with the combined Pilbara Craton-Glenburgh Terrane by 1950 Ma to form the West Australian Craton (WAC) (Sheppard et al., 2004, 2010; Johnson et al., 2011). Prolonged lateritic weathering has produced the modern denuded landscape and poor exposure of basement rocks (Anand and Paine, 2002).

The Yilgarn Craton hosts a large number of mafic dykes of different orientations with the dyke density increasing towards the southern and western craton margins (Hallberg, 1987; Tucker and Boyd, 1987). The dykes are discernible in aeromagnetic data but outcrops are difficult to identify and sample due to deep weathering and thick regolith cover. The oldest known mafic dyke in the Yilgarn Craton is the NE-trending ca. 2620 Ma Yandinilling dyke, which has been dated from one outcrop 120 km east of Perth but is probably part of a large dyke swarm that extends at least across the South West Terrane (Stark et al., 2018). The oldest mafic dykes with craton-wide extent belong to the E- to NE-trending 2418–2408 Ma Widgiemooltha dyke swarm (Sofoulis, 1965; Evans, 1968; Campbell et al., 1970; Hallberg, 1987; Doehler and Heaman, 1998; Nemchin and Pidgeon, 1998; Wingate, 1999, 2007; French et al., 2002; Pisarevsky et al., 2015). The Widgiemooltha dykes are up to 3.2 km wide and extend up to 700 km across the craton, with the largest intrusions (Jimberlana and Binneringie) showing well-developed igneous layering (Campbell et al., 1970; Lewis, 1994). The dykes exhibit dual magnetic polarity (Tucker and Boyd, 1987; Boyd and Tucker, 1990) and recent geochronology and paleomagnetic data suggest that their emplacement may have involved several pulses (Wingate, 2007; Smirnov et al., 2013; Pisarevsky et al., 2015). The second craton-wide suite is the 1210 Ma Marnda Moorn LIP, which consists of several sub-swarms of different orientations intruding along the craton margins (Isles and Cooke, 1990; Evans, 1999; Wingate et al., 2000; Pidgeon and Nemchin, 2001; Pidgeon and Cook, 2003; Rasmussen and Fletcher, 2004; Wingate and Pidgeon, 2005; Wingate, 2007; Claoué-Long and Hoatson, 2009). Outcrops in the southeast are limited to a single occurrence, and the extent of the dykes in the northeast is unknown due to cover rocks but one E-trending dioritic dyke dated at 1215 ± 11 Ma has been reported further inland (Qiu et al., 1999). Other identified dyke swarms include the NW-trending ca. 1888 Ma Boonadgin dyke swarm in the southwest (Stark et al., in press), the SW-trending dykes of the 1075 Ma Warakurna LIP in the northern Yilgarn Craton (Wingate et al., 2004), the WNW-trending ca. 735 Ma Nindibillup dykes in the central and southeast Yilgarn Craton (Spaggiari et al., 2009, 2011; Wingate, 2017) and the undated (likely < 1140 Ma) NW-trending Beenong dykes in the southeast Yilgarn Craton (Wingate, 2007; Spaggiari et al., 2009, 2011).

3. Samples

3.1. Field sampling

Field sampling sites were targeted using satellite imagery (Landsat/Copernicus or Astrium/CNES from Google Earth), aeromagnetic data (20–40 m cell size, Geoscience Australia magnetic grid of Australia V6 2015 base reference) and 1:250 000 geological maps from the Geological Survey of Western Australia.

Three block samples were collected from outcrops SW to WSW of the town of Pingelly from outcrops within agriculturally cleared areas near accessible roads (Fig. 2, Table 1). Basement rocks are not exposed at any of the sampling sites but geological mapping indicates that the country rocks to the dykes are Archean granites (Baxter et al., 1980). Dykes form gentle ridges often associated with large trees, where farming is difficult due to concentrations of large boulders of dolerite (Fig. 3). Due to the lack of exposed contacts, the widths of the dykes are unknown, however at WDS10 the dyke is probably > 60 m wide, based on the extents of partially exposed rock. All outcrops appear relatively fresh and weathering forms a light red-brown crust of varying thickness that is best visible along fractures (Fig. 3).

3.2. Sample description

All samples are dolerites with intergranular ophitic to sub-ophitic texture, comprising 45–50% plagioclase, 25–35% pyroxene, up to 10% quartz and 10–15% opaque minerals (magnetite and ilmenite) and trace apatite. The samples are relatively fresh apart from uralitic alteration of pyroxene and variable but relatively minor sericitisation of plagioclase (Fig. 4). Most clinopyroxene grains have been affected by alteration, ranging in intensity from the growth of brown amphibole near grain boundaries to pervasive alteration of the entire grain into a mixture of brown and green amphibole. Plagioclase preserves original twinning and some zoned grains exhibit weak alteration along fractures. Abundant opaque minerals appear as subhedral to euhedral grains in the groundmass but also as extremely fine-grained masses within altered pyroxene and along grain boundaries.

Table 1
Sample locations *Notes* Datum WGS84, Dlat = DDM latitude, Dlon = DDM longitude.

Dyke ID	Dlat / Dlon	Samples	Comments
WDS10	32 34.842 S 116 55.046 E	WDS10C	NNW trending dyke on the east side of York-Williams Road
WDS14	32 35.232 S 116 46.656 E	WDS14B	NNW trending dyke, intersection of Potts Road and North Wandering Road
15WDS16	32 40.065 S 116 48.723 E	15WDS16B2	NNW trending dolerite dyke off Wandering-Pingelly Road

4. U-Pb geochronology and geochemistry methodologies

4.1. SHRIMP U-Pb geochronology

Polished thin sections were scanned to identify baddeleyite, zircon and zirconolite with a Hitachi TM3030 scanning electron microscope (SEM) equipped with energy dispersive X-ray spectrometer (EDX) at Curtin University. For SHRIMP U-Pb dating, selected grains were drilled directly from the thin sections using a micro drill and mounted into epoxy disks, which were cleaned and coated with 40 nm of gold. Baddeleyite forms mostly unaltered, subhedral to euhedral equant and tabular grains, some with thin zircon rims. Most baddeleyite grains are up to 100 µm long and up to 30 µm across (Fig. 5).

Baddeleyite was analysed for U, Th and Pb using the sensitive high-resolution ion microprobe (SHRIMP II) at the John de Laeter Centre at Curtin University in Perth, Australia, following standard operating procedures after Williams (1998). The SHRIMP analysis method for mounts with polished thin section plugs outlined in Rasmussen and Fletcher (2010) was modified for baddeleyite (SHRIMP operating parameters in Table 2). During each analytical session, standard zircon OG1 (Stern et al., 2009) was used to monitor instrumental mass fractionation and BR266 zircon (Stern, 2001) was used for calibrating U and Th concentration and as an accuracy standard. Phalaborwa baddeleyite (Heaman, 2009) was employed as an additional accuracy standard. Typical spot size with primary O_2^- current was 10–15 µm at

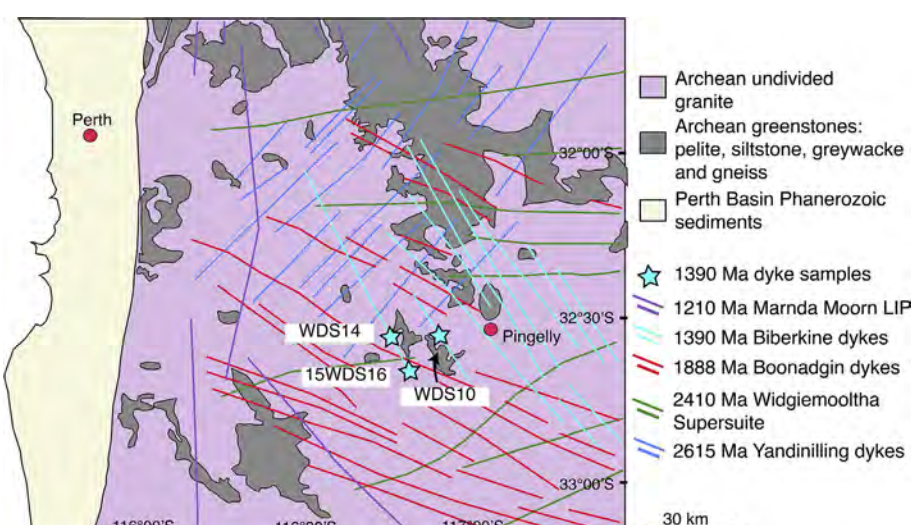

Fig. 2. Sample localities. See Table 1 for detailed information.

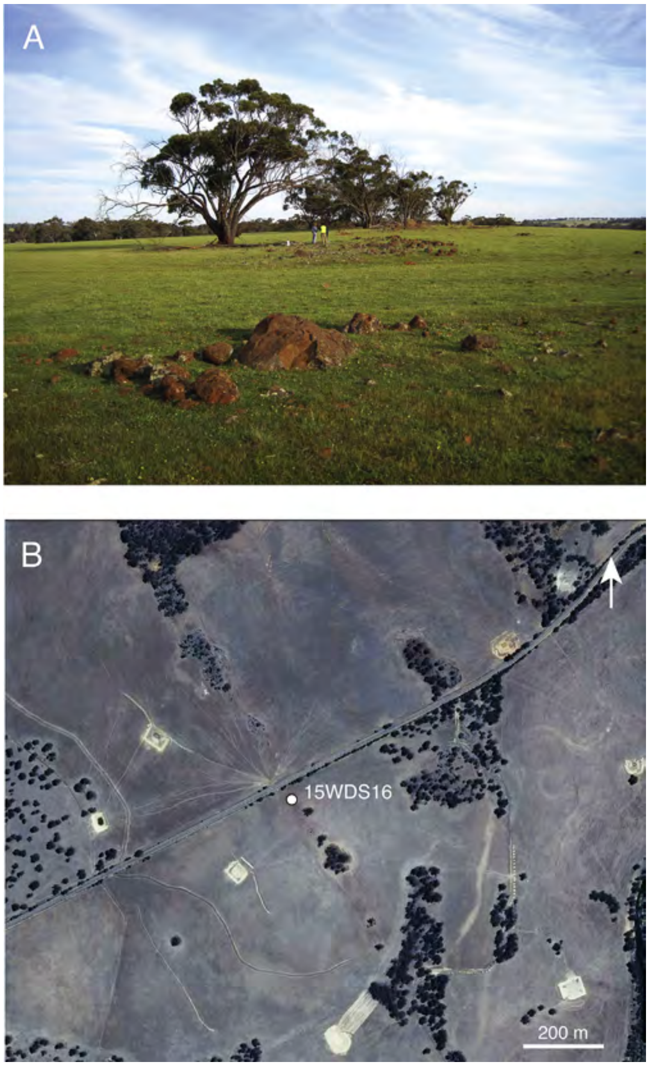

Fig. 3. (A) 15WDS16 sample location, looking SSE. (B) Satellite image showing the location of sample 15WDS16. Note the faint but visible NNW trending trace of the dyke, associated with clusters of trees.

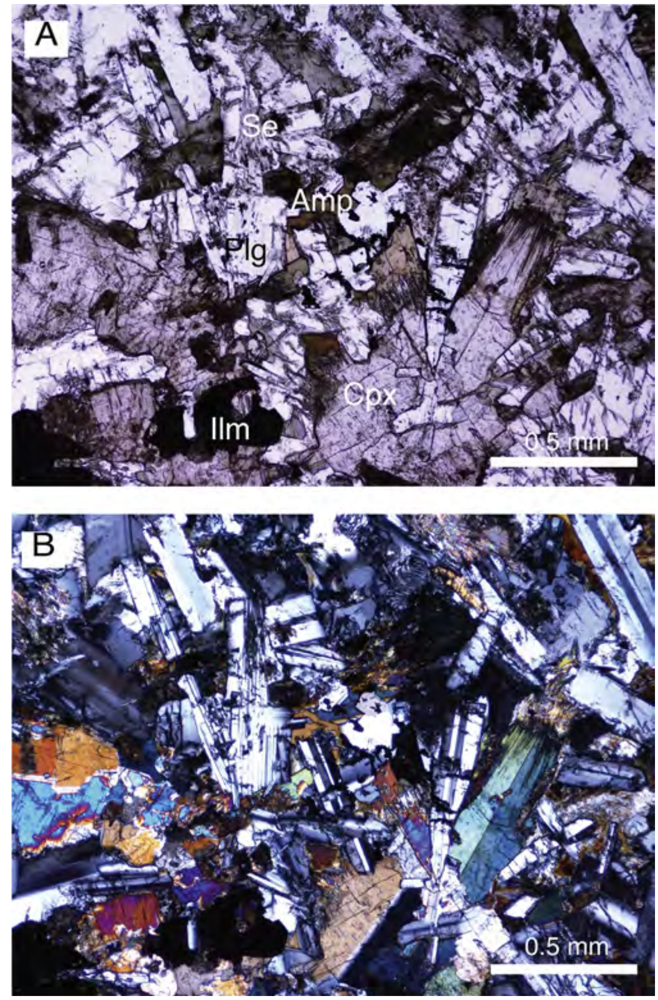

Fig. 4. Photomicrograph of sample WDS10C. (A) Plane polarised light (PPL) image showing subophitic growth of plagioclase within clinopyroxene in the lower right quadrant and the growth of brown and green amphibole near and within intercumulus grain boundaries. (B) Cross-polarized light (XPL) image showing twinning in the poikilitic clinopyroxene in the lower right quadrant. Plg = plagioclase, Cpx = clinopyroxene, Amp = amphibole, Se = sericite, Ilm = ilmenite. (For interpretation of the references to colour in this figure legend, the reader is referred to the web version of this article.)

0.1–0.2nA. Data were processed with Squid version 2.50 (Ludwig, 2009) and Isoplot version 3.76.12 (Ludwig, 2012). For common Pb correction, 1390 Ma common Pb isotopic compositions were calculated from the Stacey and Kramers (1975) two-stage terrestrial Pb isotopic evolution model. Analyses with > 1% common Pb (in ^{206}Pb) or > 10% discordance (see footnote in Table 3 for definition) are considered unreliable and were disregarded in age calculations. The assigned 1σ external Pb/U error for all analyses is 1%. All weighted mean ages are given at 95% confidence level, except 15WDS16 where 2σ internal error is used. All individual analyses are presented with 1σ error.

4.2. ID-TIMS U-Pb geochronology

A sample for ID-TIMS U-Pb geochronology was selected based on results from the SHRIMP dating and the highest number of identified baddeleyite crystals in thin section. A block sample was first sawn from the field sample to remove weathering, then crushed, powdered and processed using a mineral-separation technique modified after Söderlund and Johansson (2002). Baddeleyite grains were hand picked under ethanol under a stereographic optical microscope and selected grains were cleaned with concentrated distilled HNO_3 and HCl. Due to the small size of the separated fractions, no chemical separation methods were required.

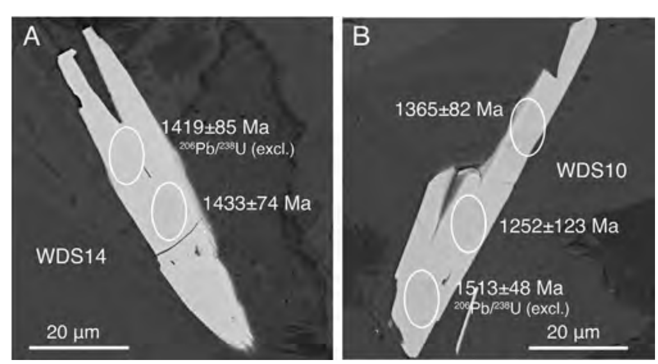

Fig. 5. Back-scattered electron (BSE) images showing SHRIMP analytical spots and corresponding Pb/Pb dates for baddeleyite. (A) WDS14 spots WDS14B1.109B-1 (lower) and WDS14B1.109B-2 (upper) (B) WDS10 spots WDS10C4.177B-1 (lower), WDS10C4.177B-2 (middle) and WDS10C4.177B-3 (upper). Note the excluded spots shown with more precise ^{206}Pb/^{238}U dates despite known crystal orientation effects in baddeleyite (discussed in section 5.1).

Table 2
SHRIMP operating parameters *Notes* **1)** Mass resolution for all analyses ≥ 5000 at 1% peak height **2)** BR266, OGC, Phalaborwa and NIST used as standards for each session **3)** Count times for each scan: ^{204}Pb, ^{206}Pb, ^{208}Pb = 10 s, ^{207}Pb = 30 s.

Mount	CS16-2	CS16-4
Dykes analysed	WDS10, WDS14	15WDS16
Date analysed	21-Jul-16	19-Aug-16
Kohler aperture (µm)	30	30
Spot size (micrometres)	8	10
O2– primary current (nA)	0.1–0.2	0.2
Number of scans per analysis	8	8
Total number of analyses in session	41	42
Number of standard analyses in session	24	26
Pb/U external precision % (1σ)	1.00	1.00
Raster time (seconds)	120	120
Raster aperture (µm)	80	80

Samples were spiked with a University of Western Australia in-house ^{205}Pb-^{235}U tracer solution, which has been calibrated against SRM981, SRM982 (for Pb), and CRM 115 (for U), as well as an externally-calibrated U-Pb solution (the JMM solution from the EarthTime consortium). This tracer is regularly checked using "synthetic zircon" solutions that yield U-Pb ages of 500 Ma and 2000 Ma, provided by D. Condon (British Geological Survey). Dissolution and equilibration of spiked single crystals was by vapour transfer of HF, using Teflon microcapsules in a Parr pressure vessel placed in a 200 °C oven for six days. The resulting residue was re-dissolved in HCl and H_3PO_4 and placed on an outgassed, zone-refined rhenium single filament with 5 µL of silicic acid gel. U–Pb isotope analyses were carried out using a Thermo Triton T1 mass spectrometer, in peak-jumping mode using a secondary electron multiplier. Uranium was measured as an oxide (UO_2). Fractionation and deadtime were monitored using SRM981 and SRM 982. Mass fractionation was 0.02 ± 0.06%/amu. Data were reduced and plotted using the software packages Tripoli (from CIRDLES.org) and Isoplot 4.15 (Ludwig, 2011). All uncertainties are reported at 2σ. U decay constants are from Jaffey et al. (1971). The weights of the baddeleyite crystals were calculated from measurements of photomicrographs and estimates of the third dimension. The weights are used to determine U and Pb concentrations and do not contribute to the age calculation. An uncertainty of ± 50% may be attributed to the concentration estimate.

4.3. Geochemistry

Slabs were sawn from block samples to remove weathering. After an initial crush, a small fraction of material was separated and chips with fresh fracture surfaces were hand picked under the microscope and pulverised in an agate mill for isotope analysis. Remaining material was pulverised in a low-Cr steel mill for major and trace element analysis.

Major element analysis was undertaken at Intertek Genalysis Laboratories in Perth, Western Australia using X-ray fluorescence (XRF) using the Geological Survey of Western Australia (GSWA) standard BB1 (Morris, 2007) and Genalysis laboratory internal standards SARM1 and SY-4. Trace element analysis was carried out at University of Queensland (UQ) on a Thermo XSeries 2 inductively coupled plasma mass spectrometer (ICP-MS) equipped with an ESI SC-4 DX FAST autosampler, following procedure for ICP-MS trace element analysis by Eggins et al. (1997) modified by the UQ Radiogenic Isotope Laboratory (Kamber et al., 2003). Sample solutions were diluted 4,000 times, and 12 ppb ^{6}Li, 6 ppb ^{61}Ni, Rh, In and Re, and 4.5 ppb ^{235}U internal spikes were added. USGS W2 was used as reference standard and crossed checked with BIR-1, BHVO-2 or other reference materials. All major element analyses have precision better than 5% and all trace element analyses have relative standard deviation (RSD) < 2%.

Rb-Sr and Sm-Nd isotope analyses were carried out at the University of Melbourne (e.g. Maas et al., 2005, 2015). Small splits (70 mg) of rock powders were spiked with ^{149}Sm-^{150}Nd and ^{85}Rb-^{84}Sr tracers, followed by dissolution at high pressure in an oven, using Krogh-type PTFE vessels with steel jackets. Sm, Nd and Sr were extracted using EICHROM Sr-, TRU- and LN-resin, and Rb was extracted using cation exchange (AG50-X8, 200–400 mesh resin). Isotopic analyses were carried out on a NU Plasma multi-collector ICP-MS coupled to a CETAC Aridus desolvation system operated in low-uptake mode. Raw data for spiked Sr and Nd fractions were corrected for instrumental mass bias by normalizing to ^{88}Sr/^{86}Sr = 8.37521 and ^{146}Nd/^{145}Nd = 2.0719425 (equivalent to ^{146}Nd/^{144}Nd = 0.7219), respectively, using the exponential law as part of an on-line iterative spike-stripping/internal normalization procedure. Sr and Nd isotope data are reported relative to SRM987 = 0.710230 and La Jolla Nd = 0.511860 and have typical in-run precisions (2sd) of ± 0.000020 (Sr) and ± 0.000012 (Nd). External precision (reproducibility, 2sd) is ± 0.000040 (Sr) and ± 0.000020 (Nd). External precisions for ^{87}Rb/^{86}Sr and ^{147}Sm/^{144}Nd obtained by isotope dilution are ± 0.5% and ± 0.2%, respectively.

5. Results

5.1. SHRIMP U-Pb geochronology

Twenty-three analyses were obtained from 13 baddeleyite crystals (4 grains from WDS10, 5 grains from WDS14 and 4 grains from 15WDS16) during two SHRIMP sessions (Fig. 6; detailed U-Pb data are given in Table 3). The analysed baddeleyite crystals have low to moderate U concentrations varying from 40 to 330 ppm (median = 163 ppm) and low Th concentrations ranging from 1 to 89 ppm, with Th/U ratios ranging from 0.23 to 0.28. Fourteen analyses were excluded based on their high common Pb (> 1.58% ^{206}Pb) and/or > 18% discordance. The small size and narrow shape of the baddeleyite crystals made it difficult to place the ion beam without overlapping onto adjacent minerals (e.g. Fig. 5B). Crystal orientation dependent Pb/U fractionation effects in baddeleyite during secondary ion mass spectrometry (SIMS) can lead to biased ^{206}Pb/^{238}U ages but this is not necessarily the case for all crystals (e.g. Wingate and Compston, 2000; Schmitt et al., 2010), and in some instances, the ^{204}Pb-corrected ^{206}Pb/^{238}U dates were more precise than the ^{204}Pb-corrected ^{207}Pb/^{206}Pb dates (Table 3). Four analyses from three grains from sample WDS10 yielded a common Pb-corrected ^{207}Pb/^{206}Pb weighted mean of 1442 ± 250 Ma (MSWD = 3.3), four analyses from two grains from 15WDS16 gave a common Pb-corrected ^{207}Pb/^{206}Pb weighted mean of 1470 ± 58 Ma (MSWD = 2.11, 2σ internal error) and one analysis from one grain from WDS14 gave 1433 ± 74 Ma. Despite the low precision of the individual analyses, we consider the age difference between the dykes insignificant relative to the analytical uncertainty. Combining all valid analyses from WDS10, WDS14 and 15WDS16 yields a ^{207}Pb/^{206}Pb weighted mean age of 1458 ± 76 Ma (MSWD = 2.09; n = 9, six grains).

5.2. ID-TIMS U-Pb geochronology

Four baddeleyite crystals were analyzed from sample WDS10 (Table 4, Fig. 7). Calculated weights are on the order of 0.1 µg, with low calculated U concentrations between 21 ppm and 80 ppm. Calculated U concentrations are unusually low for baddeleyite and this may reflect an overestimate of the grain weights, but the low Pb abundance (both radiogenic and common Pb) also implies a low initial U concentration. Th/U ratios are < 0.1, a typical value for baddeleyite. Coherence in age of all measured baddeleyite crystals supports our interpretation of the analyses representing a single magmatic crystallization age. The weighted mean ^{207}Pb/^{206}Pb age of the four concordant single-crystal analyses is 1389 ± 14 Ma (2σ, n = 4, MSWD = 0.57) and the weighted mean ^{206}Pb/^{238}U age of these analyses is 1389.9 ± 3.0 Ma (2σ, n = 4, MSWD = 1.4). This precise 1390 ± 3 Ma age is within the uncertainty

Table 3
SHRIMP U-Pb data for baddeleyite from dyke samples WDS10, WDS14 and 15WDS16. Note common Pb and discordance thresholds of 1.58% and 18%, respectively, for accepted analyses.

Spot	f_{206} %	U ppm	Th ppm	Th/U	± %	Total $^{238}U/^{206}Pb$	± %	Total $^{207}Pb/^{206}Pb$	± %	$^{238}U/^{206}Pb^{*}$	± %	$^{207}Pb^{*}/^{206}Pb$	± %	$^{206}Pb^{*}/^{238}U$ Age (Ma)	± 1σ	$^{207}Pb^{*}/^{206}Pb^{*}$ Age (Ma)	± 1σ	Disc. %
WDS10C1.11B-1	0.25	246	21.5	0.090	5.8	3.64	2.3	0.101	2.7	3.65	2.3	0.098	3.5	1563	± 32	1595	± 66	+2
WDS10C2.44B-1	0.83	256	37.4	0.151	1.3	4.19	2.1	0.093	2.5	4.22	2.2	0.086	4.9	1371	± 27	1336	± 96	−3
WDS10C4.177B-2	1.04	151	7.3	0.050	5.1	4.02	2.9	0.091	2.8	4.06	2.9	0.082	6.3	1418	± 37	1252	± 123	−15
WDS10C4.177B-3	0.60	203	10.0	0.051	2.5	3.56	2.5	0.092	2.4	3.58	2.5	0.087	4.3	1588	± 35	1365	± 82	−18
WDS14B1.109B-1	0.26	181	13.6	0.078	1.9	3.84	2.3	0.093	2.9	3.85	2.3	0.090	3.9	1489	± 30	1433	± 74	−4
15WDS16B2R.258B-1	1.35	53	1.2	0.023	5.0	3.85	3.1	0.108	3.5	3.91	3.2	0.096	8.1	1470	± 42	1557	± 152	+6
15WDS16B2R.258B-2	0.18	231	11.5	0.052	1.5	3.78	1.7	0.097	1.7	3.78	1.7	0.095	2.1	1512	± 22	1527	± 39	+1
15WDS16B1.248B-1	1.58	308	52.0	0.175	2.9	4.08	2.6	0.103	1.2	4.14	2.6	0.089	3.6	1394	± 33	1407	± 68	+1
15WDS16B1.248B-2	1.21	330	88.9	0.279	1.9	3.79	1.5	0.098	1.9	3.84	1.5	0.087	3.1	1493	± 20	1365	± 61	−10
Excluded analyses																		
WDS10C1.10B-1	3.20	119	9.3	0.081	5.2	3.88	2.9	0.099	3.7	4.01	3.1	0.072	14.5	1435	± 40	995	± 294	−49
WDS10C1.10B-2	9.72	155	20.8	0.139	9.0	2.58	13.2	0.140	3.4	2.85	13.5	0.060	34.7	1936	± 225	615	± 749	−250
WDS10C4.177B-1	1.31	175	8.9	0.053	3.9	3.73	3.5	0.092	2.5	3.78	3.5	0.081	6.4	1513	± 48	1211	± 126	−28
WDS14B2.187B-1	6.23	114	6.9	0.063	2.9	3.84	4.7	0.120	3.5	4.09	5.1	0.068	24.4	1409	± 64	870	± 505	−69
WDS14B2.187B-2	3.03	222	18.1	0.084	2.0	3.37	4.1	0.097	2.7	3.47	4.2	0.072	11.6	1631	± 61	988	± 235	−74
WDS14B3.191B-1	3.81	314	50.1	0.165	2.8	3.89	5.6	0.100	2.5	4.04	5.7	0.068	12.3	1426	± 73	882	± 254	−69
WDS14B1.109B-2	–	163	12.0	0.076	2.6	4.08	6.7	0.102	5.0	4.06	6.7	0.106	5.8	1419	± 85	1724	± 107	+20
WDS14B2.184B-1	5.88	81	5.8	0.074	2.9	3.99	3.4	0.103	5.2	4.24	3.8	0.055	27.4	1366	± 47	427	± 610	−245
WDS14B3.192B-1	24.75	47	5.2	0.116	3.9	3.66	8.1	0.169	5.8	4.87	11.6	0.080	40.6	1204	± 127	1196	± 801	−1
WDS14B3.192B-2	8.42	40	2.3	0.059	5.4	4.35	5.2	0.085	11.3	4.75	7.0	0.016	239.4	1231	± 78			
15WDS16B2R.266B-1	2.24	68	6.0	0.092	2.3	4.11	2.7	0.104	3.2	4.20	2.8	0.085	10.2	1376	± 35	1320	± 197	−5
15WDS16B2R.266B-2	6.53	94	6.7	0.073	4.6	3.72	4.4	0.134	2.8	3.98	4.7	0.079	17.9	1445	± 61	1170	± 355	−26
15WDS16B2R.266B-3	2.56	71	6.2	0.091	2.1	3.83	2.7	0.102	3.1	3.93	2.9	0.081	11.2	1460	± 37	1215	± 220	–22
15WDS16B1.246B-1	4.26	297	29.4	0.102	1.3	3.52	1.8	0.127	4.8	3.68	2.0	0.090	10.7	1551	± 27	1436	± 204	−9

Notes 1) f_{204} is the proportion of common Pb in ^{206}Pb, determined using the measured $^{204}Pb/^{206}Pb$ and a common Pb composition from the Stacey and Kramers (1975) model at the approximate age of the sample 2) Disc. = $100(t[^{207}Pb^{*}/^{206}Pb^{*}] - t[^{238}U/^{206}Pb^{*}/])/t[^{207}Pb^{*}/^{206}Pb^{*}]$

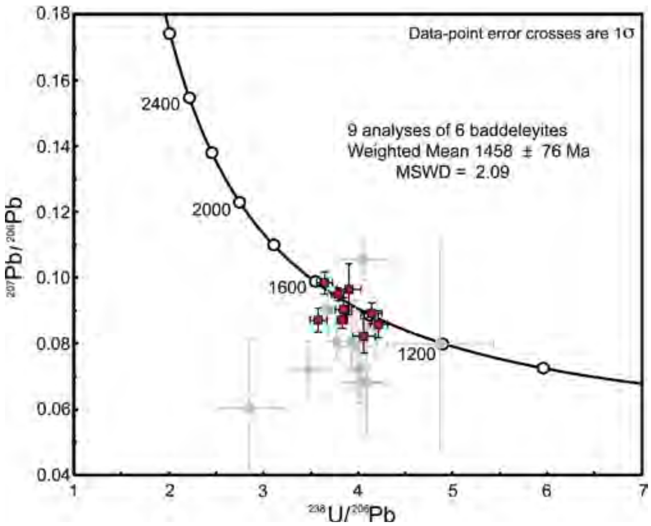

Fig. 6. Tera-Wasserburg plot of SHRIMP U-Pb baddeleyite results for samples WDS10, WDS14 and 15WDS16. Grey squares denote excluded data (see section 5.1 and Table 3 for details).

of our baddeleyite SHRIMP U-Pb $^{207}Pb/^{206}Pb$ date of 1458 ± 76 Ma, and is therefore considered as the best estimate of the crystallisation age of the sampled dykes.

5.3. Geochemistry

Due to limited age control, only four samples from three dykes were available for geochemical analyses. Consequently, only preliminary conclusions about the geochemical characteristics of the dykes can be made. Two samples from WDS10, one sample from WDS14 and one sample from 15WDS16 were analysed for major and trace elements and for Sr and Nd isotopes. Data for the samples are presented together with major and trace element geochemistry from the 1210 Ma Marnda Moorn and the 1888 Ma Boonadgin dykes.

5.3.1. Major and trace elements

Three samples have LOI < 1.0 wt% and one (15WDS16A) has LOI of 1.63%. All samples display low MgO (5.99–6.90 wt%), moderate SiO_2 (49.02–50.84 wt%), FeO_{tot} (12.92–14.55 wt%) and CaO (9.55–10.48 wt%), and moderate to high Al_2O_3 (13.31–14.29 wt%) (Table 5). All samples have moderate total alkalis ($Na_2O + K_2O$ = 2.79–3.08 wt%) and Na_2O/K_2O ratios (2.54–3.81). The sampled dykes are classified as sub-alkaline basalts on the TAS diagram (Fig. 8A, Irvine and Baragar, 1971; Le Maitre et al., 1989) and belong to the tholeiitic series on the AFM diagram (Fig. 8B, Irvine and Baragar, 1971), similar to Group 1 of the ca. 1210 Ma Marnda Moorn LIP (Wang et al., 2014) and the ca. 1888 Ma Boonadgin dykes (Stark et al., in press). The chondrite-normalised rare earth element patterns (Fig. 8C) shows moderate enrichment of light REE (LREE) with La_N/Yb_N = 4.50 to 4.80 and La_N/Sm_N = 2.40 to 2.51, whereas the heavy REE (HREE) profiles are flat, with low Tb_N/Yb_N ratios (1.32 to 1.37) slightly higher than the average values of N-MORB and E-MORB (1.0; Sun and McDonough, 1989). The primitive mantle-normalised trace element patterns show depletion of high field strength elements (HFSE) with prominent negative Nb-Ta and slightly negative Zr-Hf and Ti anomalies (Fig. 8D) and enrichment in Cs, Rb and Ba (large ion lithophile elements LILEs, not shown).

5.3.2. Nd and Sr isotopes

All four samples were analysed for Nd and Sr isotopes (Table 5). Ratios of $^{147}Sm/^{144}Nd$ and $^{143}Nd/^{144}Nd$ are 0.1355–0.1380 and 0.511845–0.511877, respectively. The corresponding initial

Table 4
ID-TIMS U-Pb data for baddeleyite from dyke WDS10 *Notes* **1)** All uncertainties given at 2σ **2)** ρ = error correlation coefficient of radiogenic $^{207}Pb/^{235}U$ vs. $^{206}Pb/^{238}U$ **3)** Pb_c = Total common Pb including analytical blank (0.8 ± 0.3 pg per analysis) **4)** Blank composition is: $^{206}Pb/^{204}Pb$ = 18.55 ± 0.63, $^{207}Pb/^{204}Pb$ = 15.50 ± 0.55, $^{208}Pb/^{204}Pb$ = 38.07 ± 1.56 (all 2σ), and a $^{206}Pb/^{204}Pb$ – $^{207}Pb/^{204}Pb$ correlation of 0.9. **5)** Th/U calculated from radiogenic $^{208}Pb/^{206}Pb$ age **6)** Sample weights are calculated from crystal dimensions and are associated with as much as 50% uncertainty (estimated) **7)** Measured isotopic ratios corrected for tracer contribution and mass fractionation (0.02 ± 0.06%/amu), and **8)** Ratios involving ^{206}Pb are corrected for initial disequilibrium in $^{230}Th/^{238}U$ using Th/U = 4 in the crystallization environment.

Sample	wt. (μg)	U (ppm)	Pb_c (pg)	mol% Pb*	Th U	^{206}Pb ^{204}Pb	^{207}Pb ^{206}Pb	± (%)	^{207}Pb ^{235}U	± (%)	^{206}Pb ^{238}U	± (%)	ρ	$^{206}Pb/^{238}U$ Age (Ma)	± (Ma)	$^{207}Pb/^{206}Pb$ Age (Ma)	± (Ma)
1	0.3	80	1.6	53	0.04	90	0.08821	1.26	2.9233	1.42	0.24036	0.28	.65	1388.5	3.8	1387.0	24.2
2	0.1	21	1.9	20	0.02	35	0.08842	3.75	2.9635	4.24	0.24305	0.98	.59	1402.5	13.8	1391.7	71.9
3	0.1	44	0.8	54	0.01	88	0.08801	1.07	2.9199	1.26	0.24062	0.44	.57	1389.9	6.1	1382.7	20.6
4	0.3	25	0.9	39	0.03	56	0.08907	1.52	2.9620	1.84	0.24118	0.76	.59	1392.8	10.5	1405.6	29.1

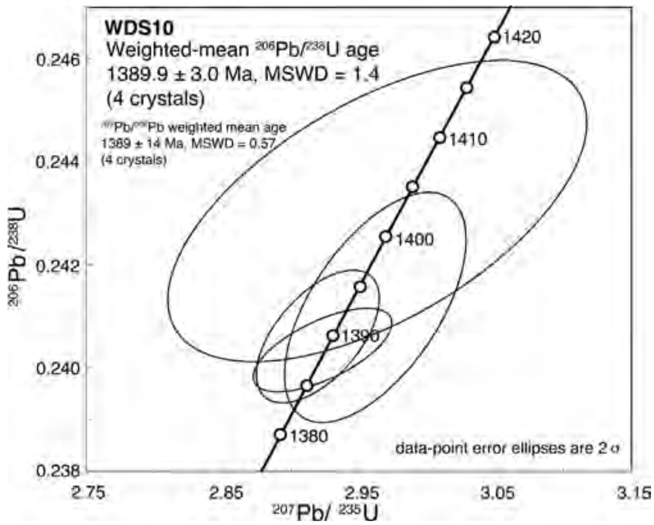

Fig. 7. Concordia plot for analysed baddeleyite ID-TIMS U-Pb results from sample WDS10.

εNd_{1389Ma}values range from −4.4 to −4.5, which are much lower than the inferred lower estimate of εNd_{DM} = +4.8 for the contemporaneous depleted mantle (calculated using the method of DePaolo, 1981), suggesting involvement of an enriched reservoir (crustal component or enriched subcontinent lithospheric mantle). The $^{87}Rb/^{86}Sr$ ratio ranges from 0.2398 to 0.8046 and the $^{87}Sr/^{86}Sr$ ratio from 0.710143 to 0.726251, the corresponding initial ratios $(^{87}Sr/^{86}Sr)_{1390\ Ma}$ varying from 0.70497 to 0.71050. The latter are significantly higher than 0.7017 estimated for contemporaneous mantle (calculated using $^{87}Rb/^{86}Sr = 0.046$ and $^{87}Sr/^{86}Sr = 0.7026$ for modern depleted mantle; Taylor and McLennan, 1985) and also suggest involvement of an enriched reservoir or an effect of alteration of the Rb-Sr isotope system. In contrast with the uniform initial Nd isotopes, the wide range of initial Sr isotope compositions and positive correlation between LOI and the initial $^{87}Sr/^{86}Sr$ ratios (not shown) suggest mobility of Rb during alteration, leading to disturbance of the Rb-Sr isotope system. Consequently, Sr isotope data are excluded from the following discussion.

6. Discussion

We have identified a previously unknown Mesoproterozoic NNW-trending mafic dyke swarm in the southwestern Yilgarn Craton, here named the Biberkine dykes. Aeromagnetic data suggest that the dyke swarm extends several hundred kilometers across the South West Terrane, truncated by the Albany-Fraser Orogen in the south and the Darling Fault in the west (Fig. 1). However, until further sampling within the craton allows a better delineation of the extent of the dykes, their designation as a swarm is preliminary.

The Biberkine dykes are coeval with several mafic magmatic events worldwide (Ernst et al., 2008), such as the ca. 1386–1380 Ma Hart River dykes (Abbott, 1997) and the ca. 1379 Ma Salmon River Arch sills (Doughty and Chamberlain, 1996) in North America, the ca. 1384 Ma Chieress dykes in Siberia (Okrugin et al., 1990; Ernst et al., 2000), the ca. 1380 Ma dykes at Vestfold Hills in East Antarctica (Lanyon et al., 1993), the ca. 1382 Ma Zig Zag Dal Formation in Greenland (Upton et al., 2005), the giant Lake Victoria dyke swarm in east Africa (Mäkitie et al., 2014) and the ca. 1385 Ma Mashak igneous event (Ronkin et al., 2005; Ernst et al., 2006). No other mafic magmatism within uncertainty of the 1390 ± 3 Ma age for the Biberkine dykes is currently known in the WAC or elsewhere in Australia and the temporally closest magmatic events within the WAC are the ca. 1360 Ma Gifford Creek carbonatite in the Edmund Basin of the Capricorn Orogen (Zi et al., 2017) and the ca. 1465 Ma mafic sills of the Narimbunna dolerite (Wingate, 2002; Morris and Pirajno, 2005; Sheppard et al., 2010b).

6.1. Nature of the mantle source of the Biberkine dykes

Zirconium can be used to evaluate mobility of major and trace elements during alteration and metamorphism (e.g. Polat et al., 2002; Wang et al., 2008, 2014). The Nb, Ta, Hf, Th and REE concentrations in the samples display good correlation with Zr (not shown) indicating that these elements have been unaffected by post-magmatic processes and reflect the primary composition of the magma. The Biberkine dykes display arc-like geochemical characteristics, including depletion of HFSE, unradiogenic initial Nd isotopes and enrichment of LILE and radiogenic Sr isotopes, which may have been imparted either by crustal contamination or inherited from heterogeneous metasomatically enriched source region, or both (Hawkesworth et al., 1990; Hawkesworth, 1993; Puffer, 2001; Zhao et al., 2013; Wang et al., 2016). Crustal contamination during magma ascent would produce synchronous changes between major and trace elements and radiogenic isotope compositions (Brandon et al., 1993; Hawkesworth et al., 1995; Wang et al., 2008, 2014). Relative to rocks sourced from asthenospheric mantle, crustal material is characterised by high La/Sm and Th/La and low Sm/Nd, Nb/La and εNd, and crustal contamination during magma ascent would therefore produce negative and positive correlations, respectively, with Mg# (e.g. Wang et al., 2008, 2014). No such correlations are evident in the data or in the Sm/Nd and Nb/La ratios. The nearly constant initial $\varepsilon Nd_{(t)}$ values, near uniform SiO_2 contents (49.02–50.84 wt%) and incompatible trace element ratios (Sm/Nd = 0.23 and La/Sm = 3.9–3.7) with a large range of Mg# values (49–55) do not support significant crustal contamination in the generation of these dykes. This is supported further by primitive mantle–like trace element ratios of Nb/Ta (16.3–16.5), Zr/Hf (39.1–40.0) and Zr/Sm (26.2–28.9) of the dykes (primitive mantle: Nb/Ta = 17.39, Zr/Hf = 36.25 and Zr/Sm = 25.23; Sun and McDonough, 1989), which are also similar to typical asthenospheric mantle-derived melts, such as MORB (Sun and McDonough, 1989). Although significant crustal contamination appears unlikely, the dykes display arc-like trace element signatures such as depletion of HFSE and enrichment of LILE. These characteristics may be attributed to Earth deep volatile cycling (e.g. Wang et al., 2016) or partial melting of SCLM enriched by previous subduction processes or recycled components (Wang et al., 2008, 2014). On the basis of the above evidence and the unradiogenic initial Nd isotopes, we prefer an interpretation where the predominant source of the dykes is an enriched SCLM. Geochemical analysis of a much larger number of samples across the dyke swarm is required to further constrain the nature of the source of the Biberkine dykes.

The flat HREE profiles of the 1390 Ma Biberkine, 1888 Ma Boonadgin and 1210 Ma Marnda Moorn dykes indicate that partial melting likely occurred within the spinel stability field (at < 75 km depth), suggesting that the SCLM at least beneath and near the margin of the Yilgarn Craton may have been largely removed or thinned sometime before 1888 Ma. Smithies and Champion (1999) argued for a craton-wide delamination of the lower crust at ca. 2650 Ma during the final stages of cratonisation and seismic data from eastern Yilgarn Craton supports presence of a delaminated lower crustal layer that foundered in the upper mantle (Blewett et al., 2010). Moreover, evidence for a mafic–ultramafic layer in the lower crust beneath the southwestern Yilgarn Craton may be related to underplating during crustal extension (Dentith et al., 2000). The Biberkine and Boonadgin dykes, although separated by ca. 500 m.y. in age, were emplaced through the same SCLM because they were sampled in areas where they outcrop close to each other (Fig. 2). Whereas the Boonadgin dykes have similar primitive mantle-normalised profiles and LCC-like trace element ratios, they have significantly higher $\varepsilon Nd_{(t)}$ values of +1.3 to +1.6 (Stark et al., in press) than the Biberkine dykes, suggesting that their source involved a higher proportion of depleted mantle with less

Table 5
Major, trace element and isotope data for the samples *Notes* **1)** Major elements (XRF) are given in wt % and trace elements (ICP-MS) in ppm **2)** Mg# = 100 × Mg/(Mg + Fe), Fe^{2+}/Fe_{total} = 0.85 **3)** Crystallisation age t = 1390 Ma **4)** typical internal precision (2σ) is ± 0.000015 for $^{87}Sr/^{86}Sr$ and ± 0.000014 for $^{143}Nd/^{144}Nd$ **5)** Recent isotope dilution analyses for USGS basalt standard BCR-2 average 6.41 ppm Sm, 28.02 ppm Nd, $^{147}Sm/^{144}Nd$ 0.1381 ± 0.0004 and $^{143}Nd/^{144}Nd$ 0.512635 ± 0.000023 (n = 6, ± 2sd); 46.5 ppm Rb, 337.6 ppm Sr, $^{87}Rb/^{86}Sr$ 0.3982 ± 0.0010, $^{87}Sr/^{86}Sr$ 0.704987 ± 0.000015 (n = 1, ± 2se). These results are consistent with TIMS and MC-ICPMS reference values. ε_{Nd} values are calculated relative to a modern chondritic mantle (CHUR) with $^{147}Sm/^{144}Nd$ = 0.1960 and $^{143}Nd/^{144}Nd$ = 0.512632 (Bouvier et al., 2008). Age-corrected initial ε_{Nd} and $^{87}Sr/^{86}Sr$ have propagated uncertainties of ± 0.5 units and ≤ ± 0.00010 (assuming an age uncertainty of ± 5 Ma), respectively. Decay constants are ^{87}Rb 1.395E^{-11}/yr and ^{147}Sm 6.54E^{-12}/yr.

	WDS10D	WDS10E	WDS14B	15WDS16A
SiO_2	50.61	50.63	50.84	49.02
TiO_2	1.63	1.64	1.38	1.51
Al_2O_3	13.65	13.65	14.29	13.31
CaO	10.1	9.9	10.48	9.55
$Fe_2O_{3(tot)}$	14.36	14.47	12.92	14.55
K_2O	0.68	0.85	0.58	0.73
MgO	5.99	6.01	6.79	6.9
MnO	0.21	0.22	0.21	0.24
Na_2O	2.16	2.16	2.21	2.35
P_2O_5	0.185	0.186	0.152	0.161
LOI	0.46	0.39	0.3	1.63
Total	100.04	100.11	100.15	99.96
Mg#	49.30	49.19	55.06	52.50
Sc	41.2	41.2	40.4	41
V	337	335	296	306
Co	50.5	50.9	48.6	50.4
Ni	55	57.2	69.4	65.8
Ga	18.2	18.5	17.5	17.2
Ge	533	529	529	522
Rb	27.9	37.2	19.8	43.1
Sr	193	203	236	188
Y	28	28.5	22.7	23.4
Zr	127	131	103	97.1
Nb	10.7	11.1	9.27	9.37
Cs	1.83	1.7	1.38	1.83
Ba	212	227	209	165
La	16.9	17.5	14.4	13.8
Ce	36.5	37.7	31.1	29.7
Pr	4.64	4.78	3.94	3.81
Nd	19.1	19.6	16.2	15.9
Sm	4.4	4.52	3.7	3.71
Eu	1.43	1.48	1.28	1.3
Gd	4.71	4.8	3.89	4.01
Tb	0.782	0.8	0.641	0.661
Dy	4.83	4.89	3.95	4.12
Ho	1.03	1.04	0.829	0.866
Er	2.85	2.91	2.3	2.38
Tm	0.426	0.431	0.342	0.354
Yb	2.69	2.72	2.15	2.2
Lu	0.398	0.401	0.319	0.325
Hf	3.25	3.34	2.63	2.43
Ta	0.658	0.682	0.565	0.567
Pb	4.61	3.34	3.44	3.69
Th	2.24	2.32	1.81	1.68
U	0.461	0.484	0.377	0.365

ID-TIMS	WDS10D	WDS10E	WDS14B	15WDS16A
Sm (ppm)	4.29	4.33	3.62	3.51
Nd (ppm)	18.86	19.07	16.12	15.34
$^{143}Nd/^{144}Nd$	0.511868	0.511864	0.511845	0.511877
$^{147}Sm/^{144}Nd$	0.1375	0.1372	0.1355	0.138
$(^{143}Nd/^{144}Nd)_i$	0.510612	0.510611	0.510607	0.510616
εNd(t)	−4.5	−4.5	−4.6	−4.4
Rb (ppm)	27.55	35.78	19.02	49.05
Sr (ppm)	189.8	189.8	229.5	176.7
$^{87}Rb/^{86}Sr$	0.4201	0.4201	0.2398	0.8046
$^{87}Sr/^{86}Sr$	0.713193	0.713193	0.710143	0.726251
$(^{87}Sr/^{86}Sr)_i$	0.70496648	0.70497	0.70545	0.7105

ID-TIMS	BCR-2	JND-1
$^{143}Nd/^{144}Nd$	0.512637	0.512112
	0.512640	0.512117
	0.512623	0.512102
	0.512633	
$^{87}Sr/^{86}Sr$	0.704987	
	0.705013	

contribution from the enriched component. The enriched LREE, LILE and isotopic compositions of both the Biberkine and the Boonadgin dykes could have been produced either via mixing of lower crust and depleted asthenospheric mantle, or through interaction between asthenospheric mantle and metasomatically enriched regions within the SCLM (and possibly the lower crust) that formed during earlier subduction events.

6.2. Tectonic setting of the WAC at 1390 Ma

The interval between ca. 1600–1350 Ma is considered a period of relative tectonic quiescence in the West Australian Craton, characterised by the formation of extensive basins in a passive margin setting along the southern and southeastern margins of the craton (Spaggiari et al., 2015). Aitken et al. (2016) argued that reorganization of Nuna to Rodinia occurred between ca. 1500 Ma and 1300 Ma and involved relative motion and rotation between the South Australian/Mawson cratons and the West and North Australian cratons. They suggested that this adjustment was responsible for the renewed subduction along the southern and southeastern margins of the craton. If this model is correct, and the subduction was west dipping, the Biberkine dykes may be a direct consequence of the plate movement during this transition. Alternatively, regional dyke swarms may be associated with laterally injected magma propagating from a distal plume (Baragar et al., 1996; Ernst and Buchan, 1997, 2001). If this were the case, the trace element profiles of the Biberkine dykes could reflect compositional variation in the SCLM and the lower crust at a much greater distance.

Paleogeographic reconstructions at ca. 1400 Ma suggest that the southern and southeastern margins of the West Australian Craton were in a back-arc setting, converging with the northwestern margin of the Mawson Craton (Fig. 9) (Boger, 2011; Kirkland et al., 2011; Spaggiari et al., 2011, 2014, 2015; Aitken et al., 2014, 2016). This NW-SE movement led to Albany-Fraser Orogeny stage 1 at ca. 1345 Ma with

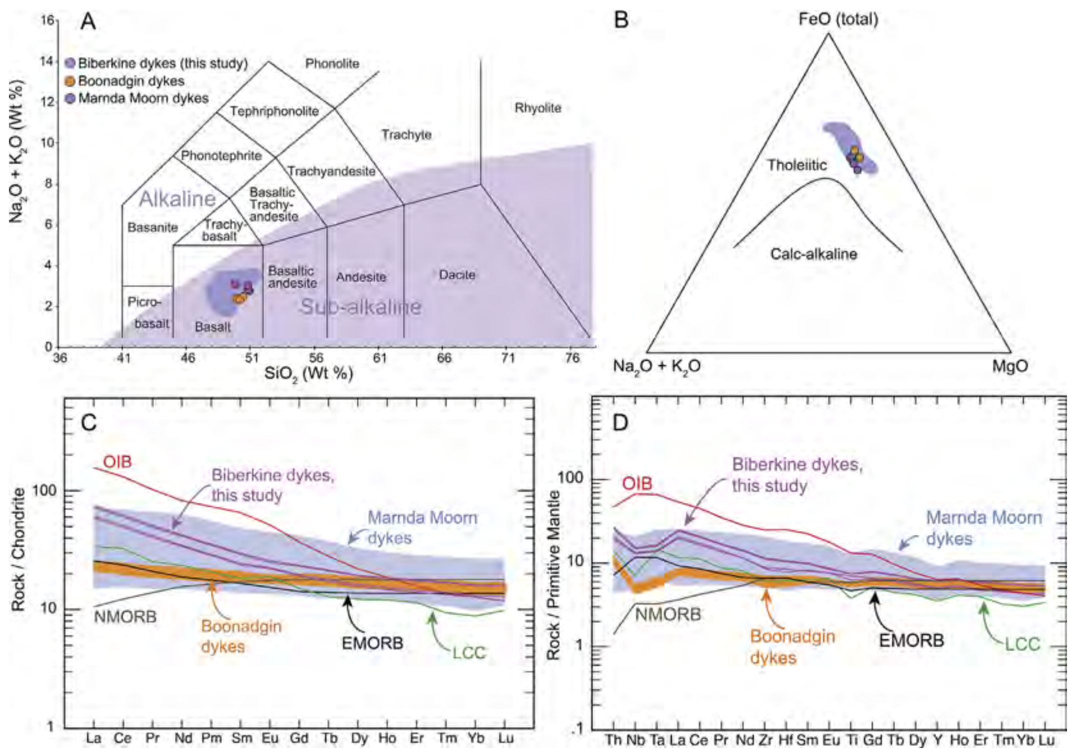

Fig. 8. (A) Total alkali-silica (TAS) plot after LeMaitre (1989) with alkaline-sub-alkaline boundary after Irvine and Baragar (1971). Orange dots denote ca. 1888 Ma Boonadgin dykes from Stark et al. (in press) and blue field the ca. 1210 Ma Marnda Moorn group 1 dykes from Wang et al. (2014). (B) AFM plot after Irvine and Baragar (1971). (C) Chondrite and (D) primitive mantle normalised multi- element plots for Biberkine, Boonadgin and Marnda Moorn group 1 dykes. LCC = lower continental crust after Rudnick and Gao (2003); OIB = ocean island basalt, NMORB = mid ocean ridge basalt and EMORB = enriched MORB after Sun and McDonough (1989). (For interpretation of the references to colour in this figure legend, the reader is referred to the web version of this article.)

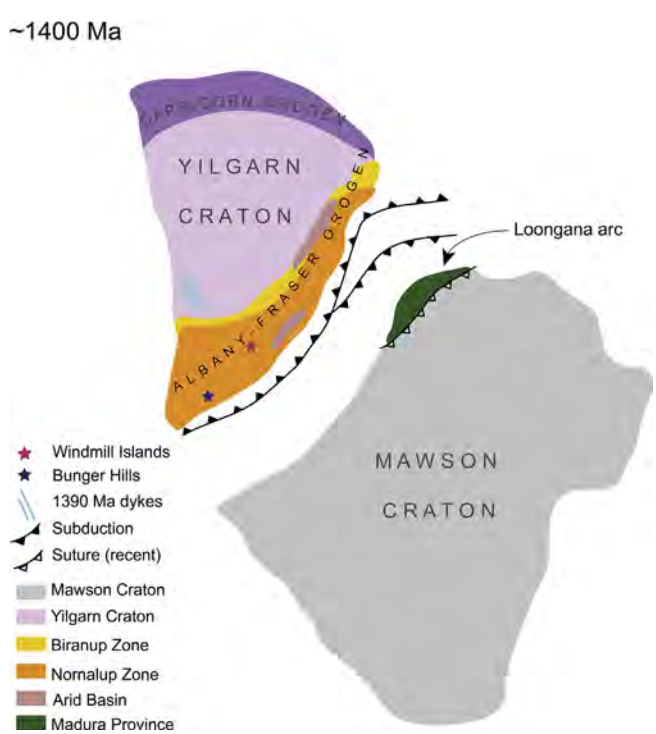

Fig. 9. . Simplified paleogeographic reconstruction of the Yilgarn and Mawson cratons at ca. 1400 Ma. Modified after Aitken et al. (2016), only the Yilgarn Craton and Capricorn Orogen of the WAC and the northern part of the Mawson Craton are shown. Note stars denoting the inferred original locations of Bunger Hills and Windmill Islands (based on interpretations of Tucker et al., 2017; Morrissey et al., 2017, respectively). See Fig. 10 for details.

continent–continent collision inferred at ca. 1310–1290 Ma (Clark et al., 2000; Bodorkos and Clark, 2004a, 2004b; Aitken et al., 2016), although some workers suggest that this represents a west-directed soft collision at ca. 1310 Ma involving accretion of the oceanic Loongana arc (Madura Province; Figs. 9 and 10) to the southeastern margin of the West Australian Craton (Spaggiari et al., 2015). Aitken et al. (2016) argue that after predominantly east-dipping subduction and clockwise rotation of the Mawson Craton until ca. 1400 Ma, a switch in polarity to west-dipping subduction beneath the West Australian Craton ended in hard collision at ca. 1290 Ma. Further evidence for a change in tectonic setting from passive to a convergent margin is recorded in the Arid Basin in eastern Albany-Fraser Orogen (Figs. 9 and 10), where detritus previously sourced predominantly from the Yilgarn Craton became dominated by input from the approaching Loongana arc at ca. 1425 Ma (Spaggiari et al., 2014, 2015).

It is difficult to link the 1390 Ma mafic magmatism in the southwestern Yilgarn Craton directly with known contemporaneous tectonic or magmatic events within the West Australian Craton because there is limited evidence for tectonic activity between ca. 1400 Ma and 1345 Ma (Aitken et al., 2016). However, a small ca. 1388 Ma detrital zircon population in the Fraser Complex in southeastern Albany-Fraser Orogen suggests coeval active magmatism (Clark et al., 1999; Spaggiari et al., 2009). Furthermore, ca. 1390–1370 Ma inherited and detrital zircon populations have been identified at the Windmill Islands and zircon rim growth at ca. 1397–1368 Ma at Bunger Hills in East Antarctica, both of which have been interpreted as part of the Albany-Fraser Orogen during the Mesoproterozoic (Figs. 9 and 10) (Zhang et al., 2012; Morrissey et al., 2017; Tucker et al., 2017). At ca. 1410 Ma, the Arid Basin (ca. 1600–1305 Ma, Figs. 9 and 10) likely formed in a passive margin setting with east-dipping subduction of the Yilgarn Craton crust beneath the Loongana oceanic arc (Spaggiari et al., 2011, 2014, 2015) or as a back-arc basin with west-dipping subduction of the approaching Loongana arc from the east beneath the Yilgarn Craton

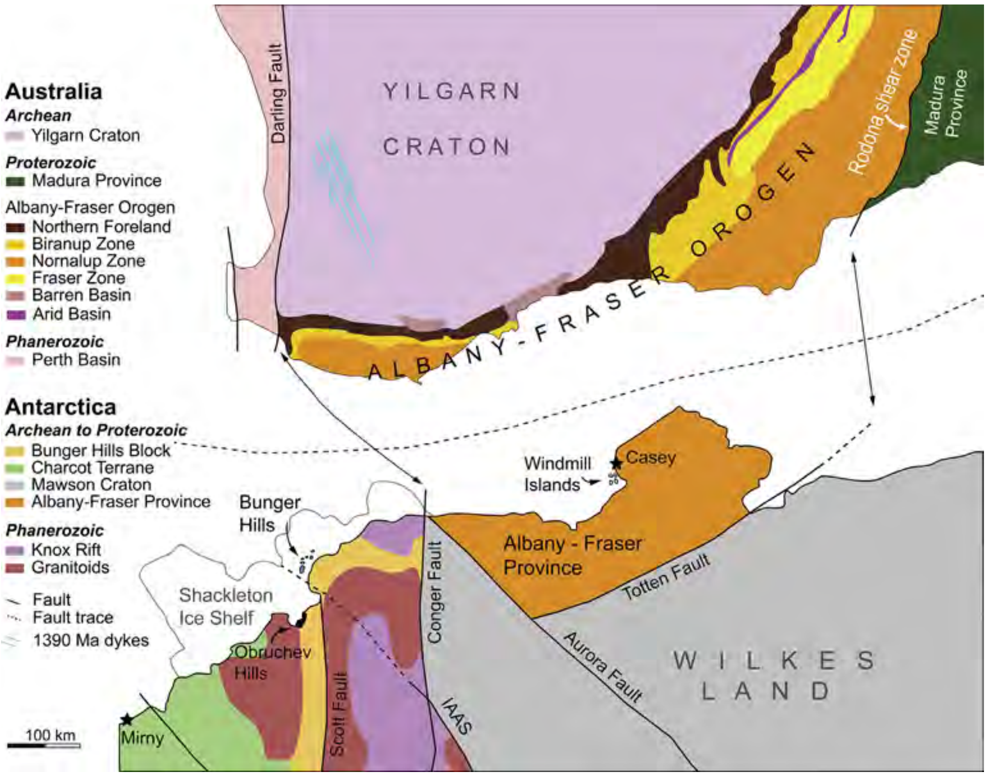

Fig. 10. Possible configuration of the Yilgarn and Mawson cratons during the Mesoproterozoic showing common tectonic elements between the Yilgarn Craton, Bunger Hills and Windmill Islands. Modified after Aitken et al. (2016), Tucker et al. (2017) and Tucker and Hand (2016) and interpreted bedrock geology of Western Australia (Geological Survey of Western Australia, 2015). Piercing points of between the Darling–Conger and Rodona–Totten Faults are from Aitken et al. (2014, 2016).

(Morrissey et al., 2017). The ca. 1415–1400 Ma magmatism in the Madura Province (Figs. 9 and 10) has also been interpreted as evidence for subduction (Kirkland et al., 2013; Spaggiari et al., 2014; Aitken et al., 2016). Collectively, this evidence suggests the presence of an active subduction zone and NW-directed convergence along the southeastern (and possibly southern) margin of the Yilgarn Craton at ca. 1410–1310 Ma. If the Biberkine dykes are associated with subduction (back-arc extension), this implies presence of a west dipping subduction zone as suggested by Morrissey et al. (2017) and Aitken et al. (2016). Alternatively, if the dykes intruded through lateral propagation of magma from a distal source, their emplacement could be due to intracontinental rifting and lithospheric extension associated with a mantle plume.

The Capricorn Orogen north of the Yilgarn Craton (Fig. 1) formed during assembly of the West Australian Craton during the Glenburgh Orogeny at 2005–1950 Ma and was subjected to repeated episodic intracontinental reworking and reactivation over the following billion years (Cawood and Tyler, 2004; Sheppard et al., 2004, 2010a; Johnson et al., 2011). Hydrothermal monazite in the Abra polymetallic deposit in the Edmund Basin (Fig. 1) records a tectonothermal event at 1375 ± 14 Ma, possibly a regional-scale episode of intracontinental reworking (Zi et al., 2015). The ca. 1360 Ma Gifford Creek carbonatite complex, also in the Edmund Basin, occurs within a major crustal suture, and may have formed in response to reactivation of this suture during far field stresses associated with plate reorganization (Zi et al., 2017). The ca. 1888 Ma Boonadgin dyke swarm in the southwestern Yilgarn Craton has also been linked with possible far-field tectonic stresses and lithospheric extension in the eastern Capricorn Orogen (Stark et al., in press), where coeval felsic volcanic rocks were emplaced during limited rifting at ca. 1891–1885 Ma (Rasmussen et al., 2012; Sheppard et al., 2016). Emplacement of the NNW-trending Biberkine dykes indicates regional SSW-NNE oriented lithospheric extension, which is consistent with interpreted NW-trending convergence and subduction along the southeastern craton margin. The orientation of the dykes is roughly parallel to the regional NW-SE tectonic grain imparted by terrane accretion during the Archean (Middleton et al., 1993; Wilde et al., 1996; Dentith and Featherstone, 2003) and suggests that, like the NW-trending 1888 Ma Boonadgin dyke swarm (Stark et al., in press), they intruded along existing crustal weaknesses controlled by a regional stress field (Hou et al., 2010; Hou, 2012; Ju et al., 2013). This may be supported by the presence of a high-velocity zone at ca. 30 km depth south of sample 15WDS16, interpreted as a mafic–ultramafic body in the lower crust that could represent a conduit for mafic magma that intruded along the suture (Dentith et al., 2000; Dentith and Featherstone, 2003).

7. Conclusions

Newly discovered NNW-trending ca. 1390 Ma mafic dykes, here named the Biberkine dykes, have been identified in the southwestern Yilgarn Craton in Western Australia using *in situ* SHRIMP and ID-TIMS U-Pb methods. The extent of the dyke swarm is unknown but in aeromagnetic data they appear to extend several hundred kilometres across the South West Terrane. The Biberkine dykes are coeval with a number of other mafic dyke swarms worldwide and thus provide an important target for paleomagnetic studies. Preliminary geochemical analysis indicates that the dykes have tholeiitic compositions with a significant contribution from metasomatically enriched subcontinental lithosphere and/or lower crust. Current models for the Yilgarn Craton infer a tectonically quiescent period between ca. 1600 Ma and 1345 Ma but indirect evidence from the Albany-Fraser Orogen and from Windmill Islands and Bunger Hills in East Antarctica support renewed subduction along the southeastern and possibly southern margin of the craton by ca. 1410 Ma. Paleogeographic reconstructions suggest that this was a result of relative motion and rotation between the West Australian, South Australian and Mawson cratons and represents transition from Nuna to Rodinia configuration for the three cratons. The 1390 Ma Biberkine dykes are likely a direct consequence of this transition and mark the change from passive to active tectonic setting, which culminated in the Albany-Fraser Orogeny at ca. 1330 Ma.

Acknowledgments

This work was funded by Australian Research Council (ARC) Centre for Core to Crust Fluid Systems CoE Grant (CE110001017) and ARC Laureate Fellowship Grant (FL150100133) to Z.-X.L. JCS was supported by Curtin University Postgraduate Scholarship. We thank Richard Ernst and Ulf Söderlund for their thoughtful and constructive reviews. Cristina Talavera and Hao Gao are thanked for their support with SHRIMP U-Pb analyses at John de Laeter Centre, Curtin University. We also thank Roland Maas and Nenping Shen for their valuable assistance with geochemical analyses and Louise Heyworth for her help with sample preparation at the University of Western Australia (UWA). BSE imaging was undertaken at the Australian Microscopy and Microanalysis Research Facility at the Centre for Microscopy, Characterisation and Analysis (CMCA) at UWA. This is a contribution to IGCP project 648.

References

Abbott, G., 1997. Geology of the Upper Hart River Area, Eastern Ogilvie Mountains, Yukon Territory (9116A/10, 116A/11) Bulletin 9. Indian and Northern Affairs Canada, Exploration and Geological Services Division.

Aitken, A.R.A., Betts, P.G., Young, D.A., Blankenship, D.D., Roberts, J.L., Siegert, M.J., 2016. The Australo-Antarctic Columbia to Gondwana transition. Gondwana Res. 29, 136–152. https://doi.org/10.1016/j.gr.2014.10.019.

Aitken, A.R.A., Young, D.A., Ferraccioli, F., Betts, P.G., Greenbaum, J.S., Richter, T.G., Roberts, J.L., Blankenship, D.D., Siegert, M.J., 2014. The subglacial geology of Wilkes Land, East Antarctica. Geophys. Res. Lett. 41, 2390–2400.

Anand, R.R., Paine, M., 2002. Regolith geology of the Yilgarn Craton, Western Australia: implications for exploration. Aust. J. Earth Sci. 49, 3–162.

Baragar, W.R.A., Ernst, R.E., Hulbert, L., Peterson, T., 1996. Longitudinal petrochemical variation in the Mackenzie dyke swarm, northwestern Canadian Shield. J. Petrol. 37, 317–359.

Barley, M.E., Brown, S.J.A., Cas, R.A.F., Cassidy, K.F., Champion, D.C., Gardoll, S.J., Krapež, B., 2003. An integrated geological and metallogenic framework for the eastern Yilgarn Craton: developing geodynamic models of highly mineralised Archaean granite–greenstone terranes. AMIRA Project P624.

Baxter, J.L., Lipple, S.L., Playford, P.E., Low, G.H., Lowry, D.C., 1980. Pinjarra, WA Sheet SI 50-2, 1:250 000 Geological Series Maps.

Bleeker, W., Ernst, R., 2006. Short-lived mantle generated magmatic events and their dyke swarms: the key unlocking Earth's paleogeographic record back to 2.6 Ga. In: Hanski, E.J., Mertanen, S., Rämö, O.T., Vuollo, J. (Eds.), Dyke Swarms—time Markers of Crustal Evolution: Selected Papers of the Fifth International Dyke Conference in Finland, Rovaniemi, Finland, 31 July–3 Aug 2005 & Fourth International Dyke Conference, Kwazulu-Natal, South Africa 26–29 June 2001. CRC Press, London, pp. 3–26.

Blewett, R.S., Henson, P.A., Roy, I.G., Champion, D.C., Cassidy, K.F., 2010. Scale-integrated architecture of a world-class gold mineral system: The Archaean eastern Yilgarn Craton, Western Australia. Precambr. Res. 183, 230–250. https://doi.org/10.1016/j.precamres.2010.06.004.

Blewett, R.S., Hitchman, A.P., 2006. 3D Geological Models of the Eastern Yilgarn Craton: Final Report pmd* CRC Y2 Project September 2001–December 2004. Geoscience Australia Record 2006/05.

Bodorkos, S., Clark, D.J., 2004a. Evolution of a crustal-scale transpressive shear zone in the Albany-Fraser Orogen, SW Australia: 2. Tectonic history of the Coramup Gneiss and a kinematic framework for Mesoproterozoic collision of the West Australian and Mawson cratons. J. Metamorph. Geol. 22, 713–731. https://doi.org/10.1111/j.1525-1314.2004.00544.x.

Bodorkos, S., Clark, D.J., 2004b. Evolution of a crustal-scale transpressive shear zone in the Albany-Fraser Orogen, SW Australia: 1. P-T conditions of Mesoproterozoic metamorphism in the Coramup Gneiss. J. Metamorph. Geol. 22, 691–711. https://doi.org/10.1111/j.1525-1314.2004.00543.x.

Boger, S.D., 2011. Antarctica—before and after Gondwana. Gondwana Res. 19, 335–371.

Bouvier, A., Vervoort, J.D., Patchett, P.J., 2008. The Lu–Hf and Sm–Nd isotopic composition of CHUR: Constraints from unequilibrated chondrites and implications for the bulk composition of terrestrial planets. Earth Planet. Sci. Lett. 273, 48–57.

Boyd, D.M., Tucker, D.H., 1990. Australian magnetic dykes. In: Parker, A.J., Rickwood, P.C., Tucker, D.H. (Eds.), Mafic Dykes and Emplacement Mechanisms. A.A.Balkema, Rotterdam, pp. 391–399.

Brandon, A.D., Hooper, P.R., Goles, G.G., Lambert, R.S.J., 1993. Evaluating crustal contamination in continental basalts: the isotopic composition of the Picture Gorge Basalt of the Columbia River Basalt Group. Contrib. Mineral. Petrol. 114, 452–464. https://doi.org/10.1007/BF00321750.

Buchan, K.L., Ernst, R.E., Hamilton, M.A., Mertanen, S., Pesonen, L.J., Elming, S.-Å., 2001. Rodinia: the evidence from integrated palaeomagnetism and U-Pb geochronology. Precambr. Res. 110, 9–32.

Campbell, I.H., McCall, G.J.H., Tyrwhitt, D.S., 1970. The Jimberlana Norite, Western Australia–a smaller analogue of the Great Dyke of Rhodesia. Geol. Mag. 107, 1–12.

Cassidy, K.F., Champion, D.C., Huston, D.L., 2005. Crustal evolution constraints on the metallogeny of the Yilgarn Craton. In: Mineral Deposit. Springer, Berlin, pp. 901–904.

Cassidy, K.F., Champion, D.C., Krapez, B., Barley, M.E., Brown, S.J.A., Blewett, R.S., Groenewald, Pb., Tyler, I.M., 2006. A revised geological framework for the Yilgarn Craton, Western Australia, in: Geological Survey of Western Australia Record 8/2006. Geological Survey of Western Australia.

Cawood, P.A., Tyler, I.M., 2004. Assembling and reactivating the Proterozoic Capricorn Orogen: lithotectonic elements, orogenies, and significance. Precambr. Res. 128, 201–218. https://doi.org/10.1016/j.precamres.2003.09.001.

Claoué-Long, J.C., Hoatson, D.M., 2009. Guide to using the map of Australian Proterozoic large igneous provinces. Geoscience Australia.

Clark, D.J., Hensen, B.J., Kinny, P.D., 2000. Geochronological constraints for a two-stage history of the Albany – Fraser Orogen, Western Australia. Precambr. Res. 102, 155–183.

Clark, D.J., Kinny, P.D., Post, N.J., 1999. Relationships between magmatism, metamorphism and deformation in the Fraser Complex, Western Australia: constraints from new SHRIMP U-Pb zircon geochronology. Aust. J. Earth Sci. 46, 923–932.

Condie, K.C., 2004. Supercontinents and superplume events: distinguishing signals in the geologic record. Phys. Earth Planet. Inter. 146, 319–332. https://doi.org/10.1016/j.pepi.2003.04.002.

Dalziel, I.W.D., 1991. Pacific margins of Laurentia and East Antarctica-Australia as a conjugate rift pair: evidence and implications for an Eocambrian supercontinent. Geology 19, 598–601.

Dentith, M.C., Dent, V.F., Drummond, B.J., 2000. Deep crustal structure in the southwestern Yilgarn Craton, Western Australia. Tectonophysics 325, 227–255.

Dentith, M.C., Featherstone, W.E., 2003. Controls on intra-plate seismicity in southwestern Australia. Tectonophysics 376, 167–184. https://doi.org/10.1016/j.tecto.2003.10.002.

DePaolo, D.J., 1981. Neodymium isotopes in the Colorado Front Range and crust–mantle evolution in the Proterozoic. Nature 291, 193–196. https://doi.org/10.1038/291193a0.

Doehler, J.S., Heaman, L.M., 1998. 2.41 Ga U–Pb Baddeleyite ages for two gabbroic dykes from the Widgiemooltha swarm, Western Australia: a Yilgarn–Lewisian connection, in: Geological Society of America 1998 Annual Meeting, Abstracts with Programs. Geological Society of America, pp. 291–292.

Doughty, P.T., Chamberlain, K.R., 1996. Salmon River Arch revisited: New evidence for 1370 Ma rifting near the end of deposition in the Middle Proterozoic Belt basin. Can. J. Earth Sci. 33, 1037–1052.

Eggins, S.M., Woodhead, J.D., Kinsley, L.P.J., Mortimer, G.E., Sylvester, P., McCulloch, M.T., Hergt, J.M., Handler, M.R., 1997. A simple method for the precise determination of ≥40 trace elements in geological samples by ICPMS using enriched isotope internal standardisation. Chem. Geol. 134, 311–326.

Ernst, R., Srivastava, R., Bleeker, W., Hamilton, M., 2010. Precambrian Large Igneous Provinces (LIPs) and their dyke swarms: new insights from high-precision geochronology integrated with paleomagnetism and geochemistry. Precambr. Res. 183, vii–xi.

Ernst, R.E., Bleeker, W., Söderlund, U., Kerr, A.C., 2013. Large Igneous Provinces and supercontinents: toward completing the plate tectonic revolution. Lithos 174, 1–14.

Ernst, R.E., Buchan, K.L., 2001. Large mafic magmatic events through time and links to mantle-plume heads. Geological Society of America Special Paper, pp. 483–576.

Ernst, R.E., Buchan, K.L., 1997. Giant radiating dyke swarms: their use in identifying pre-Mesozoic large igneous provinces and mantle plumes. In: Large Igneous Provinces: Continental, Oceanic, and Planetary Flood Volcanism. American Geophysical Union Monograph, pp. 297–333.

Ernst, R.E., Buchan, K.L., Hamilton, M.A., Okrugin, A.V., Tomshin, M.D., 2000. Integrated paleomagnetism and U-Pb geochronology of mafic dikes of the eastern Anabar Shield region, Siberia: Implications for Mesoproterozoic paleolatitude of Siberia and comparison with Laurentia. J. Geol. 108, 381–401.

Ernst, R.E., Head, J.W., Parfitt, E., Grosfils, E., Wilson, L., 1995. Giant radiating dyke swarms on Earth and Venus. Earth-Sci. Rev. 39, 1–58.

Ernst, R.E., Pease, V., Puchkov, V.N., Kozlov, V.I., Sergeeva, N.D., Hamilton, M., 2006. Geochemical characterization of Precambrian magmatic suites of the Southeastern margin of the East European Craton, Southern Urals. Russia. Geol. Sb. 119–161.

Ernst, R.E., Srivastava, R.K., 2008. India's place in the Proterozoic world: constraints from the Large Igneous Province (LIP) record. Indian dykes. Ed. by RK Srivastava, Ch. Sivaji, NV Chalapathi Rao. Geochemistry, Geophys. Geochronology, Narosa Publ. House Pvt. Ltd, New Delhi, India 41–56.

Ernst, R.E., Wingate, M.T.D., Buchan, K.L., Li, Z.X., 2008. Global record of 1600–700Ma Large Igneous Provinces (LIPs): Implications for the reconstruction of the proposed Nuna (Columbia) and Rodinia supercontinents. Precambr. Res. 160, 159–178. https://doi.org/10.1016/j.precamres.2007.04.019.

Evans, D.A.D., Mitchell, R.N., 2011. Assembly and breakup of the core of Paleoproterozoic-Mesoproterozoic supercontinent Nuna. Geology 39, 443–446.

Evans, M.E., 1968. Magnetization of dikes: a study of the paleomagnetism of the Widgiemooltha dike suite, Western Australia. J. Geophys. Res. 73, 3261–3270.

T. Evans Evans, T., 1999. Extent and nature of the 1.2 Ga Wheatbelt dyke swarm, Yilgarn Craton, Western Australia. B.Sc. thesis, Univ. West. Aust. Perth.

French, J.E., Heaman, L.M., Chacko, T., 2002. Feasibility of chemical U-Th-total Pb baddeleyite dating by electron microprobe. Chem. Geol. 188, 85–104. https://doi.org/10.1016/S0009-2541(02)00074-8.

Goldberg, A.S., 2010. Dyke swarms as indicators of major extensional events in the 1.9–1.2 Ga Columbia supercontinent. J. Geodyn. 50, 176–190.

Hallberg, J.A., 1987. Postcratonization mafic and ultramafic dykes of the Yilgarn Block. Aust. J. Earth Sci. 34, 135–149. https://doi.org/10.1080/08120098708729398.

Halls, H.C., Zhang, B., 1998. Uplift structure of the southern Kapuskasing zone from 2.45 Ga dike swarm displacement. Geology 26, 67–70. https://doi.org/10.1130/0091-7613(1998) 026<0067:USOTSK>2.3.CO;2.

Hawkesworth, C., 1993. Mantle and Slab Contribution in Arc Magmas. Annu. Rev. Earth

Planet. Sci. 21, 175–204. https://doi.org/10.1146/annurev.earth.21.1.175.
Hawkesworth, C.J., Kempton, P.D., Rogers, N.W., Ellam, R.M., van Calsteren, P.W., 1990. Continental mantle lithosphere, and shallow level enrichment processes in the Earth's mantle. Earth Planet. Sci. Lett. 96, 256–268.
Hawkesworth, C.J., Lightfoot, P.C., Fedorenko, V.A., Blake, S., Naldrett, A.J., Doherty, W., Gorbachev, N.S., 1995. Magma differentiation and mineralisation in the Siberian continental flood basalts. LITHOS 34, 61–88. https://doi.org/10.1016/0024-4937(95)90011-X.
Heaman, L.M., 2009. The application of U-Pb geochronology to mafic, ultramafic and alkaline rocks: an evaluation of three mineral standards. Chem. Geol. 261, 43–52. https://doi.org/10.1016/j.chemgeo.2008.10.021.
Hoek, J.D., Seitz, H.-M., 1995. Continental mafic dyke swarms as tectonic indicators: an example from the Vestfold Hills, Antarctica. Precambr. Res. 75, 121–139.
Hou, G., 2012. Mechanism for three types of mafic dyke swarms. Geosci. Front. 3, 217–223. https://doi.org/10.1016/j.gsf.2011.10.003.
Hou, G., Kusky, T.M., Wang, C., Wang, Y., 2010. Mechanics of the giant radiating Mackenzie dyke swarm: a paleostress field modeling. J. Geophys. Res. Solid Earth 115. https://doi.org/10.1029/2007JB005475.
Irvine, T.N.J., Baragar, W., 1971. A guide to the chemical classification of the common volcanic rocks. Can. J. Earth Sci. 8, 523–548.
Isles, D.J., Cooke, A.C., 1990. Spatial associations between post-cratonisation dykes and gold deposits in the Yilgarn Block, Western Australia. In: Parker, A.J., Rickwood, P.C., Tucker, D.H. (Eds.), Mafic Dykes and Emplacement Mechanisms. Balkema, Rotterdam, pp. 147–162.
Jaffey, A.H., Flynn, K.F., Glendenin, L.E., Bentley, W.C.t., Essling, A.M., 1971. Precision measurement of half-lives and specific activities of U 235 and U 238. Phys. Rev. C 4 1889.
Johnson, S.P., Sheppard, S., Rasmussen, B., Wingate, M.T.D., Kirkland, C.L., Muhling, J.R., Fletcher, I.R., Belousova, E.A., 2011. Two collisions, two sutures: Punctuated pre-1950Ma assembly of the West Australian Craton during the Ophthalmian and Glenburgh Orogenies. Precambr. Res. 189, 239–262. https://doi.org/10.1016/j.precamres.2011.07.011.
Ju, W., Hou, G., Hari, K.R., 2013. Mechanics of mafic dyke swarms in the Deccan Large Igneous Province: Palaeostress field modelling. J. Geodyn. 66, 79–91. https://doi.org/10.1016/j.jog.2013.02.002.
Kamber, B.S., Greig, A., Schoenberg, R., Collerson, K.D., 2003. A refined solution to Earth's hidden niobium: implications for evolution of continental crust and mode of core formation. Precambr. Res. 126, 289–308.
Kirkland, C.L., Smithies, R.H., Woodhouse, A.J., Howard, H.M., Wingate, M.T.D., Belousova, E.A., Cliff, J.B., Murphy, R.C., Spaggiari, C.V., 2013. Constraints and deception in the isotopic record; the crustal evolution of the west Musgrave Province, central Australia. Gondwana Res. 23, 759–781.
Kirkland, C.L., Spaggiari, C.V., Pawley, M.J., Wingate, M.T.D., Smithies, R.H., Howard, H.M., Tyler, I.M., Belousova, E.A., Poujol, M., 2011. On the edge: U-Pb, Lu–Hf, and Sm–Nd data suggests reworking of the Yilgarn craton margin during formation of the Albany-Fraser Orogen. Precambr. Res. 187, 223–247.
Korsch, R.J., Kositcin, N., Champion, D.C., 2011. Australian island arcs through time: geodynamic implications for the Archean and Proterozoic. Gondwana Res. 19, 716–734. https://doi.org/10.1016/j.gr.2010.11.018.
Ksienzyk, A.K., Jacobs, J., Boger, S.D., Kosler, J., Sircombe, K.N., Whitehouse, M.J., 2012. U-Pb ages of metamorphic monazite and detrital zircon from the Northampton Complex: evidence of two orogenic cycles in Western Australia. Precambr. Res. 198–199, 37–50. https://doi.org/10.1016/j.precamres.2011.12.011.
Lanyon, R., Black, L.P., Seitz, H.-M., 1993. U-Pb zircon dating of mafic dykes and its application to the Proterozoic geological history of the Vestfold Hills, East Antarctica. Contrib. Mineral. Petrol. 115, 184–203.
Le Maitre, R.W.B., Dudek, P., Keller, A., Lameyre, J., Le Bas, J., Sabine, M.J., Schmid, P.A., Sorensen, R., Streckeisen, H., Woolley, A., 1989. A classification of igneous rocks and glossary of terms: Recommendations of the International Union of Geological Sciences, Subcommission on the Systematics of Igneous Rocks International Union of Geological Sciences. Blackwell Scientific.
Lewis, J.D., 1994. Mafic dykes in the Williams-Wandering area, Western Australia. Geol. Surv. West. Aust. Rep. 37, 37–52.
Li, Z.-X., Zhong, S., 2009. Supercontinent–superplume coupling, true polar wander and plume mobility: plate dominance in whole-mantle tectonics. Phys. Earth Planet. Inter. 176, 143–156. https://doi.org/10.1016/j.pepi.2009.05.004.
Li, Z.X., Bogdanova, S.V., Collins, A.S., Davidson, A., De Waele, B., Ernst, R.E., Fitzsimons, I.C.W., Fuck, R.A., Gladkochub, D.P., Jacobs, J., Karlstrom, K.E., Lu, S., Natapov, L.M., Pease, V., Pisarevsky, S.A., Thrane, K., Vernikovsky, V., 2008. Assembly, configuration, and break-up history of Rodinia: a synthesis. Precambr. Res. 160, 179–210. https://doi.org/10.1016/j.precamres.2007.04.021.
Ludwig, K.R., 2011. Isoplot/Ex, Version 4.15: A geochronological toolkit for Microsoft Excel: Geochronology Center Berkeley, v. 4.
Ludwig, K., 2012. User's manual for Isoplot version 3.75–4.15: a geochronological toolkit for Microsoft. Berkeley Geochronological Cent. Spec. Publ.
Ludwig, K., 2009. Squid 2.50, A User's Manual (No. 2.50.11.02.03 Rev. 03 Feb 2011). Berkeley, California, USA.
Maas, R., Grew, E.S., Carson, C.J., 2015. Isotopic constraints (Pb, Rb-Sr, Sm-Nd) on the sources of early Cambrian pegmatites with Boron and Beryllium minerals in the Larsemann Hills, Prydz Bay. Antarctica. Can. Mineral. 53, 249–272.
Maas, R., Kamenetsky, M.B., Sobolev, A.V., Kamenetsky, V.S., Sobolev, N.V., 2005. Sr, Nd, and Pb isotope evidence for a mantle origin of alkali chlorides and carbonates in the Udachnaya kimberlite, Siberia. Geology 33, 549–552.
Mäkitie, H., Data, G., Isabirye, E., Mänttäri, I., Huhma, H., Klausen, M.B., Pakkanen, L., Virransalo, P., 2014. Petrology, geochronology and emplacement model of the giant 1.37 Ga arcuate Lake Victoria Dyke Swarm on the margin of a large igneous province in eastern Africa. J. African Earth Sci. 97, 273–296.
Meert, J.G., 2002. Paleomagnetic evidence for a Paleo-Mesoproterozoic supercontinent Columbia. Gondwana Res. 5, 207–215.
Meert, J.G., Santosh, M., 2017. The Columbia supercontinent revisited. Gondwana Res. 50, 67–83. https://doi.org/10.1016/j.gr.2017.04.011.
Middleton, M.F., Wilde, S.A., Evans, B.A., Long, A., Dentith, M., 1993. A preliminary interpretation of deep seismic reflection and other geophysical data from the Darling Fault Zone, Western Australia. Explor. Geophys. 24, 711–718.
Morris, P.A., 2007. Composition of the Bunbury Basalt (BB1) and Kerba Monzogranite (KG1) geochemical reference materials, and assessing the contamination effects of mill heads, in: Geological Survey of Western Australia Record 2007/14. Geological Survey of Western Australia Record 2007/14.
Morris, P.A., Pirajno, F., 2005. Mesoproterozoic sill complexes in the Bangemall Supergroup, Western Australia: geology, geochemistry and mineralization potential. Geological Survey of Western Australia Report 99.
Morrissey, L.J., Payne, J.L., Hand, M., Clark, C., Taylor, R., Kirkland, C.L., Kylander-Clark, A., 2017. Linking the Windmill Islands, east Antarctica and the Albany-Fraser Orogen: insights from U-Pb zircon geochronology and Hf isotopes. Precambr. Res. 293, 131–149. https://doi.org/10.1016/j.precamres.2017.03.005.
Myers, J.S., 1995. The generation and assembly of an Archaean supercontinent: evidence from the Yilgarn craton, Western Australia. Geol. Soc. London Spec. Publ., pp. 143–154.
Myers, J.S., 1993. Precambrian tectonic history of the west australian craton and adjacent orogens. Annu. Rev. Earth Planet. Sci. 21, 453–485.
Myers, J.S., 1990. Pinjarra orogen, in: Geology and Mineral Resources of Western Australia. State Printing Division, pp. 264–274.
Nance, R.D., Murphy, J.B., Santosh, M., 2014. The supercontinent cycle: a retrospective essay. Gondwana Res. 25, 4–29. https://doi.org/10.1016/j.gr.2012.12.026.
Nelson, D.R., Myers, J.S., Nutman, A.P., 1995. Chronology and evolution of the Middle Proterozoic Albany-Fraser Orogen, Western Australia. Aust. J. Earth Sci. 42, 481–495. https://doi.org/10.1080/08120099508728218.
Nemchin, A.A., Pidgeon, R.T., 1998. Precise conventional and SHRIMP baddeleyite U-Pb age for the Binneringie Dyke, near Narrogin, Western Australia. Aust. J. Earth Sci. 45, 673–675.
Nemchin, A.A., Pidgeon, R.T., 1997. Evolution of the Darling Range batholith, Yilgarn Craton, Western Australia: a SHRIMP zircon study. J. Petrol. 38, 625–649.
Nemchin, A.A., Pidgeon, R.T., Wilde, S.A., 1994. Timing of Late Archaean granulite facies metamorphism in the southwestern Yilgarn Craton of Western Australia: evidence from U-Pb ages of zircons fro mafic granulites. Precambr. Res. 68, 307–321.
Okrugin, A.V., Oleinikov, B.V., Savvinov, V.T., Tomshin, M.D., 1990. Late Precambrian dyke swarms of the Anabar massif, Siberian platform, USSR. In: Mafic Dykes and Emplacement Mechanisms. Balkema, Rotterdam, pp. 529–533.
Pidgeon, R.T., Cook, T.J.F., 2003. 1214 ± 5 Ma dyke from the Darling Range, south-western Yilgarn Craton, Western Australia. Aust. J. Earth Sci. 50, 769–773.
Pidgeon, R.T., Nemchin, A.A., 2001. 1.2 Ga Mafic dyke near York, southwestern Yilgarn Craton, Western Australia. Aust. J. Earth Sci. 48, 751–755. https://doi.org/10.1046/j.1440-0952.2001.485895.x.
Pisarevsky, S.A., Elming, S.-Å., Pesonen, L.J., Li, Z.-X., 2014. Mesoproterozoic paleogeography: supercontinent and beyond. Precambr. Res. 244, 207–225. https://doi.org/10.1016/j.precamres.2013.05.014.
Pisarevsky, S., De Waele, B., Jones, S., Söderlund, U., Ernst, R.E., 2015. Paleomagnetism and U-Pb age of the 2.4Ga Erayinia mafic dykes in the south-western Yilgarn, Western Australia: paleogeographic and geodynamic implications. Precambr. Res. 259, 222–231. https://doi.org/10.1016/j.precamres.2014.05.023.
Polat, a., Hofmann, a.W., Rosing, M.T., 2002. Boninite-like volcanic rocks in the 3.7-3.8 Ga isua greenstone belt, West Greenland: Geochemical evidence for intra-oceanic subduction zone processes in the early earth. Chem. Geol. 184, 231–254. https://doi.org/10.1016/S0009-2541(01)00363-1.
Prokoph, A., Ernst, R.E., Buchan, K.L., 2004. Time-Series Analysis of Large Igneous Provinces: 3500 Ma to Present. J. Geol. 112, 1–22. https://doi.org/10.1086/379689.
Puffer, J.H., 2001. Contrasting high field strength element contents of continental flood basalts from plume versus reactivated-arc sources. Geology 29, 675–678.
Qiu, Y., McNaughton, N.J., Groves, D.I., Dunphy, J.M., 1999. First record of 1.2 Ga quartz dioritic magmatism in the Archaean Yilgarn Craton, Western Australia, and its significance. Aust. J. Earth Sci. 46, 421–428. https://doi.org/10.1046/j.1440-0952.1999.00715.x.
Rasmussen, B., Fletcher, I.R., 2010. Dating sedimentary rocks using in situ U-Pb geochronology of syneruptive zircon in ash-fall tuff & lt 1 mm thick. Geology 38, 299–302. https://doi.org/10.1130/G30567.1.
Rasmussen, B., Fletcher, I.R., 2004. Zirconolite: a new U-Pb chronometer for mafic igneous rocks. Geology 32, 785–788.
Rasmussen, B., Fletcher, I.R., Bekker, A., Muhling, J.R., Gregory, C.J., Thorne, A.M., 2012. Deposition of 1.88-billion-year-old iron formations as a consequence of rapid crustal growth. Nature 484, 498–501.
Rogers, J.J.W., Santosh, M., 2002. Configuration of Columbia, a mesoproterozoic supercontinent. Gondwana Res. 5, 5–22. https://doi.org/10.1016/s1342-937x(05)70883-2.
Ronkin, Y.L., Maslov, A.V., Matukov, D.I., Lepikhina, O.P., Popova, O.Y., 2005. The Mashak riftogenic event of the Riphean type region (southern Urals): new isotopic-geochronological framework. Struct. Geodyn. Mineral. Process. Lithosphere. Geoprint, Syktyvkar 305–307.
Rudnick, R.L., Gao, S., 2003. Composition of the continental crust. In: Holland, H.D., Turekian, K.K. (Eds.), The Crust Vol. 3. Treatise on Geochemistry, pp. 1–64.
Schmitt, A.K., Chamberlain, K.R., Swapp, S.M., Harrison, T.M., 2010. In situ U-Pb dating of micro-baddeleyite by secondary ion mass spectrometry. Chem. Geol. 269, 386–395. https://doi.org/10.1016/j.chemgeo.2009.10.013.

Sheppard, S., Bodorkos, S., Johnson, S.P., Wingate, M.T.D., Kirkland, C.L., 2010a. The Paleoproterozoic Capricorn Orogeny: intracontinental reworking not continent–continent collision, Geological Survey of Western Australia Report 108. Geological Survey of Western Australia.
Sheppard, S., Fletcher, I.R., Rasmussen, B., Zi, J.-W., Muhling, J.R., Occhipinti, S.A., Wingate, M.T.D., Johnson, S.P., 2016. A new Paleoproterozoic tectonic history of the eastern Capricorn Orogen, Western Australia, revealed by U-Pb zircon dating of micro-tuffs. Precambr. Res. 286, 1–19. https://doi.org/10.1016/j.precamres.2016.09.026.
Sheppard, S., Johnson, S.P., Wingate, M.T.D., Kirkland, C.L., Pirajno, F., 2010. Explanatory notes for the Gascoyne Province, Geological Survey of Western Australia Report 336.
Sheppard, S., Occhipinti, S.A.A., Tyler, I.M.M., 2004. A 2005–1970 Ma Andean-type batholith in the southern Gascoyne Complex, Western Australia. Precambr. Res. 128, 257–277. https://doi.org/10.1016/j.precamres.2003.09.003.
Smirnov, A.V., Evans, D.A.D., Ernst, R.E., Söderlund, U., Li, Z.-X., 2013. Trading partners: Tectonic ancestry of southern Africa and western Australia, in Archean supercratons Vaalbara and Zimgarn. Precambr. Res. 224, 11–22.
Smithies, R.H., Champion, D.C., 1999. Late Archaean felsic alkaline igneous rocks in the Eastern Goldfields, Yilgarn Craton, Western Australia: a result of lower crustal delamination? J. Geol. Soc. London. 156, 561–576.
Söderlund, U., Johansson, L., 2002. A simple way to extract baddeleyite (ZrO_2). Geochemistry. Geophys. Geosyst. 3. https://doi.org/10.1029/2001GC000212.
Sofoulis, J., 1965. Explanatory Notes on the Widgiemooltha 1: 250,000 Geological Sheet Western Australia. Geological Survey of Western Australia.
Spaggiari, C.V., Kirkland, C.L., Smithies, H.R., Wingate, M.T.D., Belousova, E.A., 2015. Transformation of an Archean craton margin during Proterozoic basin formation and magmatism: The Albany-Fraser Orogen, Western Australia. Precambr. Res. 266, 440–466. https://doi.org/10.1016/j.precamres.2015.05.036.
Spaggiari, C.V., Kirkland, C.L., Smithies, R.H., Wingate, M.T.D., 2014. Tectonic links between proterozoic sedimentary cycles, basin formation and magmatism in the Albany-Fraser Orogen, Western Australia, Geological Survey of Western Australia Report 133.
Spaggiari, C. V, Bodorkos, S., Barquero-Molina, M., Tyler, I.M., Wingate, M.T.D., 2009. Interpreted bedrock geology of the South Yilgarn and of the South Yilgarn and Central Albany-Fraser Orogen, Western Australia, Geological Survey of Western Australia Record 2009/10.
Spaggiari, C. V, Kirkland, C.L., Pawley, M.J., Smithies, R.H., Wingate, M.T.D., Doyle, M. G., Blenkinsop, T.G., Clark, C., Oorschot, C.W., Fox, L.J., 2011. The geology of the east Albany-Fraser Orogen—a field guide, Geological Survey of Western Australia Record 2011/23.
Stacey, J.S., Kramers, J.D., 1975. Approximation of terrestrial lead isotope evolution by a two-stage model. Earth Planet. Sci. Lett. 26, 207–221.
Stark, J.C., Wang, X.-C., Denyszyn, S.W., Li, Z.-X., Rasmussen, B., Zi, J.-W., Sheppard, S., Liu, Y., 2017. Newly identified 1.89 Ga mafic dyke swarm in the Archean Yilgarn Craton, Western Australia suggests a connection with India. Precambr. Res. Press. https://doi.org/10.1016/j.precamres.2017.12.036.
Stark, J.C., Wilde, S.A., Söderlund, U., Li, Z.X., Rasmussen, B., Zi, J.W., 2018. First evidence of Archean mafic dykes at 2.62 Ga in the Yilgarn Craton, Western Australia: links to cratonisation and the Zimbabwe Craton. Precambr. Res. Under Rev.
Stern, R.A., 2001. A new isotopic and trace-element standard for the ion microprobe: preliminary thermal ionization mass spectrometry (TIMS) U-Pb and electron-microprobe data, Geological Survey of Canada Current Research 2001-F.
Stern, R.A., Bodorkos, S., Kamo, S.L., Hickman, A.H., Corfu, F., 2009. Measurement of SIMS instrumental mass fractionation of Pb isotopes during zircon dating. Geostand. Geoanalytical Res. 33, 145–168. https://doi.org/10.1111/j.1751-908X.2009.00023.x.
Sun, S-.S., McDonough, W.F., 1989. Chemical and isotopic systematics of oceanic basalts: implications for mantle composition and processes. Geol. Soc. London Spec. Publ., pp. 313–345. https://doi.org/10.1144/GSL.SP.1989.042.01.19.
Taylor, S.R., McLennan, S.M., 1985. The continental crust: its composition and evolution, 1st ed. Blackwell Scientific Publishers, Palo Alto, CA.
Tucker, D.H., Boyd, D.M., 1987. Dykes of Australia detected by airborne magnetic surveys. In: Fahrig, W.F., Halls, H.C. (Eds.), Mafic Dyke Swarms. Geological Association of Canada pp. 163–172.
Tucker, N.M., Hand, M., 2016. New constraints on metamorphism in the Highjump Archipelago, East Antarctica. Antarct. Sci. 28, 487–503.
Tucker, N.M., Payne, J.L., Clark, C., Hand, M., Taylor, R.J., Kylander-Clark, A.R.C., 2017. Proterozoic reworking of Archean (Yilgarn) basement in the Bunger Hills, east Antarctica. Precambr. Res. 298, 16–38.
Upton, B.G.J., Rämö, O.T., Heaman, L.M., Blichert-Toft, J., Kalsbeek, F., Barry, T.L., Jepsen, H.F., 2005. The Mesoproterozoic Zig-Zag Dal basalts and associated intrusions of eastern North Greenland: Mantle plume-lithosphere interaction. Contrib. Mineral. Petrol. 149, 40–56. https://doi.org/10.1007/s00410-004-0634-7.
Wang, X.-C., Li, X.-H., Li, W.-X., Li, Z.-X., Liu, Y., Yang, Y.-H., Liang, X.-R., Tu, X.-L., 2008. The Bikou basalts in the northwestern Yangtze block, South China: remnants of 820–810 Ma continental flood basalts? Geol. Soc. Am. Bull. 120, 1478–1492. https://doi.org/10.1130/B26310.1.
Wang, X.-C., Li, Z.-X., Li, J., Pisarevsky, S.A., Wingate, M.T.D., 2014. Genesis of the 1.21 Ga Marnda Moorn large igneous province by plume–lithosphere interaction. Precambr. Res. 241, 85–103. https://doi.org/10.1016/j.precamres.2013.11.008.
Wang, X.-C., Wilde, S.A., Xu, B., Pang, C.-J., 2016. Origin of arc-like continental basalts: Implications for deep-earth fluid cycling and tectonic discrimination. Lithos 261, 5–45. https://doi.org/10.1016/j.lithos.2015.12.014.
Wilde, S.A., 1999. Evolution of the Western Margin of Australia during the Rodinian and Gondwanan Supercontinent Cycles. Gondwana Res. 2, 481–499. https://doi.org/10.1016/S1342-937X(05)70287-2.
Wilde, S.A., Middleton, M.F., Evans, B.J., 1996. Terrane accretion in the southwestern Yilgarn Craton: evidence from a deep seismic crustal profile. Precambr. Res. 78, 179–196.
Williams, I.S., 1998. U-Th-Pb geochronology by ion microprobe. Rev. Econ. Geol. 7, 1–35.
Wingate, M.T.D., 2017. Mafic dyke swarms and large igneous provinces in Western Australia get a digital makeover, in: Geological Survey of Western Australia Record 2017/2. pp. 4–8.
Wingate, M.T.D., 2007. Proterozoic mafic dykes in the Yilgarn Craton, in: Proceedings of Geoconferences (WA) Inc. Kalgoorlie 2007 Conference, Kalgoorlie, Western Australia. pp. 80–84.
Wingate, M.T.D., 2002. Age and Paleomagnetism of Dolerite Sills Intruded Into the Bangemall Supergroup on the Edmund 1: 250 000 Map Sheet, Western Australia. Geological Survey of Western Australia.
Wingate, M.T.D., 1999. Ion microprobe baddeleyite and zircon ages for Late Archaean mafic dykes of the Pilbara Craton, Western Australia. Aust. J. Earth Sci. 46, 493–500. https://doi.org/10.1046/j.1440-0952.1999.00726.x.
Wingate, M.T.D., Campbell, I.H., Harris, L.B., 2000. SHRIMP baddeleyite age for the Fraser dyke swarm, southeast Yilgarn Craton, Western Australia. Aust. J. Earth Sci. 47, 309–313.
Wingate, M.T.D., Compston, W., 2000. Crystal orientation effects during ion microprobe U-Pb analysis of baddeleyite. Chem. Geol. 168, 75–97. https://doi.org/10.1016/S0009-2541(00)00184-4.
Wingate, M.T.D., Pidgeon, R.T., 2005. The Marnda Moorn LIP, a late Mesoproterozoic large igneous province in the Yilgarn craton, Western Australia. July 2005 LIP of the month [WWW Document]. (unpub). Large Igneous Prov. Comm. Int. Assoc. Volcanol. Chem. Earth's Inter. URL http://www.largeigneousprovinces.org/05jul.
Wingate, M.T.D., Pirajno, F., Morris, P.A., 2004. Warakurna large igneous province: a new Mesoproterozoic large igneous province in west-central Australia. Geology 32, 105–108.
Wingate, M.T.D., Pisarevsky, S.A., Evans, D.A.D., 2002. Rodinia connections between Australia and Laurentia: no SWEAT, no AUSWUS? Terra Nov. 14, 121–128.
Witt, W.K., Cassidy, K.F., Lu, Y.-J., Hagemann, S.G., 2018. The tectonic setting and evolution of the 2.7 Ga Kalgoorlie–Kurnalpi Rift, a world-class Archean gold province. Miner. Depos. https://doi.org/10.1007/s00126-017-0778-9.
Zhang, S.H., Zhao, Y., Liu, X.C., Liu, Y.S., Hou, K.J., Li, C.F., Ye, H., 2012. U-Pb geochronology and geochemistry of the bedrocks and moraine sediments from the Windmill Islands: implications for Proterozoic evolution of East Antarctica. Precambr. Res. 206–207, 52–71. https://doi.org/10.1016/j.precamres.2012.02.019.
Zhao, Z.-F., Dai, L.-Q., Zheng, Y.-F., 2013. Postcollisional mafic igneous rocks record crust-mantle interaction during continental deep subduction. Nat. Sci. Reports 3, 3413. https://doi.org/10.1038/srep03413.
Zi, J.W., Gregory, C.J., Rasmussen, B., Sheppard, S., Muhling, J.R., 2017. Using monazite geochronology to test the plume model for carbonatites: the example of Gifford Creek Carbonatite Complex. Australia. Chem. Geol. 463, 50–60. https://doi.org/10.1016/j.chemgeo.2017.05.007.
Zi, J.W., Rasmussen, B., Muhling, J.R., Fletcher, I.R., Thorne, A.M., Johnson, S.P., Cutten, H.N., Dunkley, D.J., Korhonen, F.J., 2015. In situ U-Pb geochronology of xenotime and monazite from the Abra polymetallic deposit in the Capricorn Orogen, Australia: Dating hydrothermal mineralization and fluid flow in a long-lived crustal structure. Precambr. Res. 260, 91–112. https://doi.org/10.1016/j.precamres.2015.01.010.

APPENDIX B SUPPLEMENTARY MAJOR AND TRACE ELEMENT DATA FOR CHAPTERS 4-7

All major elements units are wt %

Sample	Intertek batch	Cr[2]O[3]	Al[2]O[3]	CaO	Fe[2]O[3]	K[2]O	MgO	MnO	Na[2]O	P[2]O[5]	SiO[2]	TiO[2]	LOI	Total
WDS09M	194_4_1511232	0.019	13.75	10.65	14.53	0.32	6.67	0.23	2.05	0.095	49.68	1.14	0.69	99.12
WDS09N	194_4_1511232	0.014	13.42	10.71	15.09	0.34	6.18	0.24	2.15	0.119	50.42	1.31	0.03	99.98
WDS10D	194_4_1511232	0.027	13.65	10.1	14.36	0.68	5.99	0.21	2.16	0.185	50.61	1.63	0.46	99.58
WDS10E	194_4_1511232	0.017	13.65	9.9	14.47	0.85	6.01	0.22	2.16	0.186	50.63	1.64	0.39	99.72
WDS14B	194_4_1511232	0.029	14.29	10.48	12.92	0.58	6.79	0.21	2.21	0.152	50.84	1.38	0.3	99.85
WDS14D	194_4_1511232	0.039	13.96	10.53	12.76	0.67	6.89	0.21	2.18	0.157	50.41	1.4	0.65	99.17
15WDS16A	194_4_1611361	0.03	13.31	9.55	14.55	0.73	6.9	0.24	2.35	0.161	49.02	1.51	1.63	98.32
16WDS02A	194_4_1515579	0.02	13.26	11.19	14.29	0.32	6.59	0.23	2.06	0.108	49.91	1.25	0.54	99.21
BHD1-1	194_4_1515579	0.014	15.83	8.51	15.63	0.9	6.13	0.21	3.11	0.429	45.81	3.1	0.22	99.66
BHD1-2A	194_4_1515579	0.015	15.79	8.47	15.6	0.89	6.16	0.21	3.1	0.431	45.51	3.13	0.21	99.29
BHD1-2B	194_4_1515579	0.014	15.87	8.51	15.66	0.88	6.18	0.22	3.1	0.44	45.6	3.17	0.09	99.63
BHD1-3	194_4_1515579	0.013	15.83	8.58	15.95	0.89	6.16	0.22	3.05	0.438	45.76	3.2	-0.01	100.08
BHD1-4	194_4_1515579	0.022	17.91	8.58	12.36	0.76	7.92	0.16	2.99	0.312	46.99	1.57	-0.06	99.55
BHD1-5	194_4_1515579	0.022	17.47	8.53	12.35	0.67	9.28	0.17	2.86	0.293	47.05	1.4	-0.14	100.07
BHD1-6	194_4_1515579	0.026	17.59	7.88	13.15	0.78	8.9	0.17	3.02	0.375	46.69	1.43	0.03	99.99
BHD4-1A	194_4_1515579	0.02	17.38	8.03	14.52	0.68	7.72	0.18	3.11	0.264	45.98	2.17	-0.09	100.03
BHD4-1B	194_4_1515579	0.027	17.33	7.7	15.21	0.65	7.59	0.18	3.05	0.258	45.36	2.2	0.4	99.53
BHD4-2	194_4_1515579	0.026	16.45	7.88	15.26	0.7	8.2	0.19	3.02	0.269	45.49	2.37	-0.05	99.83
BHD4-3	194_4_1515579	0.033	18.01	8.04	13.37	0.67	6.96	0.15	3.16	0.259	46.44	1.91	0.95	98.97
BHD4-4	194_4_1515579	0.021	17.50	7.63	13.95	0.69	7.65	0.18	3.11	0.272	46.38	1.85	0.59	99.21
BHD4-5	194_4_1515579	0.026	19.25	8.7	12	0.66	6.42	0.15	3.39	0.232	47.2	1.74	0.03	99.74
BHD4-6	194_4_1515579	0.02	16.32	9.23	14.59	0.63	7.08	0.19	2.88	0.249	45.51	3.29	0.08	99.97

All trace elements units are ppm

Sample	Laboratory	Ba	Be	Bi	Cd	Ce	Co	Cr	Cs	Cu	Dy	Er	Eu	Ga	Gd	Ge
WDS09M	UQ	53.90	0.50	0.03	0.05	11.90	55.30	116.00	0.56	105.00	3.79	2.37	0.96	16.40	3.27	542.00
WDS09N	UQ	59.40	0.66	0.03	0.06	15.00	56.90	164.00	1.02	168.00	4.73	2.94	1.12	17.40	4.09	559.00
WDS10D	UQ	212.00	0.99	0.03	0.07	36.50	50.50	104.00	1.83	88.00	4.83	2.85	1.43	18.20	4.71	533.00
WDS10E	UQ	227.00	1.04	0.03	0.09	37.70	50.90	117.00	1.70	92.80	4.89	2.91	1.48	18.50	4.80	529.00
WDS14B	UQ	209.00	0.79	0.02	0.07	31.10	48.60	195.00	1.38	90.70	3.95	2.30	1.28	17.50	3.89	529.00
WDS14D	UQ	85.80	0.72	0.04	0.07	20.40	45.10	128.00	0.60	133.00	3.72	2.20	1.04	16.20	3.50	503.00
15WDS16A	UQ	165.00	0.76	0.04	0.09	29.70	50.40	185.00	1.83	98.80	4.12	2.38	1.30	17.20	4.01	522.00
16WDS02A	UQ	56.80	0.55	0.04	0.05	13.10	57.70	149.00	0.19	133.00	4.45	2.77	1.05	16.60	3.80	556.00
BHD1-1	Guangzhou	318.3				39	57.01	115.7	0.283	43.9	7.085	3.979	2.23	21.26	6.644	3.987
BHD1-2A	Guangzhou	314.4				38.29	55.42	100.3	0.225	43.72	6.226	3.398	2.197	20.94	6.648	3.557
BHD1-2B	194_4_1515579	307.2	1.13	0.04	0.1	37.5	53.7	88.1	0.3	36.4	6.7	4	2.1	19.6	7.2	0.72
BHD1-3	Guangzhou	320.2				39.32	57.36	105.5	0.394	46.35	7.207	4.016	2.245	21.34	6.72	3.977
BHD1-4	Guangzhou	265.2				28.4	59.43	143.3	0.313	53.81	4.7	2.657	1.609	18.83	4.521	3.177
BHD1-5	Guangzhou	242.2				27.89	63.3	147	0.215	27.55	4.03	2.218	1.514	17.57	4.357	2.808
BHD1-6	Guangzhou	262.7				32.34	65.35	181.9	0.317	30.9	5.041	2.833	1.697	18.32	4.919	3.198
BHD4-1A	194_4_1515579	240.8	0.8	0.03	0.1	25.9	61.4	132.4	0.4	55.3	4	2.4	1.4	19.6	4.1	0.65
BHD4-1B	Guangzhou	239.4				23.3	67.96	103.5	0.227	60.58	3.754	2.078	1.378	18.96	3.671	3.399
BHD4-2	Guangzhou	245.9				25.34	68.5	173.4	0.202	45.56	3.808	2.101	1.495	18.44	4.093	3.265
BHD4-3	Guangzhou	239.9				23.49	70.45	210.5	0.234	39.53	3.832	2.148	1.422	18.76	3.726	3.246
BHD4-4	Guangzhou	252.9				24.72	69.09	82.25	0.25	37.04	3.959	2.2	1.464	18.17	3.824	3.246
BHD4-5	Guangzhou	243.5				21.64	55.23	130	0.214	38.75	3.461	1.941	1.381	19.28	3.324	2.706
BHD4-6	Guangzhou	236.1				23.93	60.63	80.63	0.231	61.59	4.698	2.6	1.597	19.18	4.434	3.226

Sample	Laboratory	Hf	Ho	La	Li	Lu	Mo	Nb	Nd	Ni	Pb	Pr	Rb	Sb	Sc	Sm
WDS09M	UQ	1.63	0.83	4.92	9.94	0.34	0.49	3.11	8.35	87.60	2.99	1.75	17.50	0.02	45.80	2.53
WDS09N	UQ	2.19	1.05	6.04	8.65	0.42	1.55	4.07	10.50	121.00	3.62	2.20	22.50	0.03	46.80	3.18
WDS10D	UQ	3.25	1.03	16.90	14.30	0.40	0.72	10.70	19.10	55.00	4.61	4.64	27.90	0.04	41.20	4.40
WDS10E	UQ	3.34	1.04	17.50	13.10	0.40	0.80	11.10	19.60	57.20	3.34	4.78	37.20	0.03	41.20	4.52
WDS14B	UQ	2.63	0.83	14.40	8.67	0.32	0.65	9.27	16.20	69.40	3.44	3.94	19.80	0.02	40.40	3.70
WDS14D	UQ	2.16	0.79	8.97	12.30	0.31	0.67	5.72	11.80	82.60	3.27	2.74	9.27	0.07	41.40	3.08
15WDS16A	UQ	2.43	0.87	13.80	25.80	0.33	0.48	9.37	15.90	65.80	3.69	3.81	43.10	0.04	41.00	3.71
16WDS02A	UQ	2.00	0.98	5.42	9.34	0.39	0.26	3.67	9.61	87.70	1.75	2.00	18.30	0.03	47.80	2.96
BHD1-1	Guangzhou	5.22	1.462	16.29		0.52		12.6	25.63	93.96	4.961	5.506	18.82		27.03	6.408
BHD1-2A	Guangzhou	4.631	1.284	16.61		0.465		10.74	23.31	90.67	4.442	5.127	17.88		26.44	6.25
BHD1-2B	194_4_1515579	4.7	1.3	15.9	6.6	0.5	0.9	10.6	24	88.9	5.2	5.2	17.4		23.93	5.2
BHD1-3	Guangzhou	5.046	1.492	16.1		0.523		12.82	26.1	94.56	5.053	5.472	17.97		26.45	6.428
BHD1-4	Guangzhou	3.909	0.981	12.14		0.355		8.145	18.09	189.1	4.419	3.902	17.06		16.17	4.367
BHD1-5	Guangzhou	2.88	0.824	11.72		0.304		6.883	15.64	213.6	3.456	3.528	14.46		16.47	4.145
BHD1-6	Guangzhou	3.516	1.043	13.72		0.372		8.649	20.33	220	4.211	4.434	17.53		11.96	4.879
BHD4-1A	194_4_1515579	2.5	0.8	11	7.3	0.3	0.5	6.4	14.2	148.4	4	3.4	11.9		15.38	3.4
BHD4-1B	Guangzhou	1.924	0.775	10.06		0.267		7.095	14.89	167.2	4.324	3.2	12.91		14.66	3.514
BHD4-2	Guangzhou	2.78	0.789	10.97		0.289		6.937	14.91	169.3	3.499	3.321	13.72		17.91	3.935
BHD4-3	Guangzhou	2.937	0.793	10		0.28		7.119	14.99	191.1	3.683	3.241	12.76		14.87	3.598
BHD4-4	Guangzhou	2.072	0.812	10.69		0.284		7.616	15.54	181.7	3.733	3.397	13.79		13.47	3.734
BHD4-5	Guangzhou	1.956	0.709	9.344		0.249		6.701	13.74	147.7	3.455	2.981	11.98		13.38	3.279
BHD4-6	Guangzhou	2.816	0.958	9.983		0.326		9.105	16.15	145.6	3.618	3.397	12.6		29.48	4.148

Sample	Laboratory	Sr	Ta	Tb	Th	Tl	Tm	U	V	W	Y	Yb	Zn	Zr	BaO
WDS09M	UQ	110.00	0.21	0.58	0.83	0.07	0.35	0.30	302.00	0.20	22.60	2.25	85.20	59.00	0.01
WDS09N	UQ	120.00	0.28	0.73	1.05	0.12	0.45	0.38	310.00	0.35	28.40	2.85	96.40	80.50	0.01
WDS10D	UQ	193.00	0.66	0.78	2.24	0.16	0.43	0.46	337.00	0.35	28.00	2.69	104.00	127.00	0.02
WDS10E	UQ	203.00	0.68	0.80	2.32	0.19	0.43	0.48	335.00	0.37	28.50	2.72	107.00	131.00	0.02
WDS14B	UQ	236.00	0.57	0.64	1.81	0.10	0.34	0.38	296.00	0.32	22.70	2.15	89.10	103.00	0.02
WDS14D	UQ	149.00	0.37	0.59	2.27	0.05	0.33	0.64	308.00	0.36	21.60	2.08	80.20	81.10	0.02
15WDS16A	UQ	188.00	0.57	0.66	1.68	0.20	0.35	0.37	306.00	0.25	23.40	2.20	128.00	97.10	0.02
16WDS02A	UQ	115.00	0.25	0.68	0.91	0.08	0.42	0.30	315.00	0.15	26.70	2.62	72.50	72.40	
BHD1-1	Guangzhou	293.9	0.771	1.16	2.01		0.576	0.352	239.4		39.34	3.581	140	203	0.04
BHD1-2A	Guangzhou	289.1	0.671	1.027	1.995		0.493	0.359	233.2		34.21	3.071	138.1	199.7	0.03
BHD1-2B	194_4_1515579	280.5	0.8	1.2	1.9	0.1	0.5	0.3	230		34.5	3.3	125	180	0.04
BHD1-3	Guangzhou	293.6	0.788	1.189	1.823		0.587	0.368	244.3		39.38	3.601	147.1	196.3	0.04
BHD1-4	Guangzhou	317.9	0.482	0.787	1.745		0.398	0.392	158.6		26.61	2.403	112.6	155.4	0.03
BHD1-5	Guangzhou	305.1	0.414	0.666	1.465		0.321	0.266	100.8		22.19	2.015	95.26	123.7	0.03
BHD1-6	Guangzhou	306.5	0.518	0.853	1.842		0.41	0.342	125.6		27.85	2.571	102.1	139	0.03
BHD4-1A	194_4_1515579	306.5	0.5	0.6	1.4	0.04	0.4	0.3	202		20.7	2	116	113	0.03
BHD4-1B	Guangzhou	309.1	0.43	0.637	1.339		0.304	0.243	231.6		20.92	1.819	121.7	73.06	0.03
BHD4-2	Guangzhou	303.7	0.444	0.637	1.438		0.306	0.251	201.1		20.98	1.896	117.9	117.7	0.03
BHD4-3	Guangzhou	333.2	0.446	0.638	1.223		0.317	0.239	178.1		21.43	1.922	130.1	117.8	0.03
BHD4-4	Guangzhou	320.4	0.458	0.651	1.342		0.318	0.239	152.8		21.64	1.947	108.6	78.8	0.03
BHD4-5	Guangzhou	365	0.442	0.591	1.176		0.281	0.227	161		19.36	1.7	94.98	76.15	0.03
BHD4-6	Guangzhou	292.2	0.568	0.763	1.269		0.387	0.217	251.6		25.88	2.274	123.8	102	0.03

APPENDIX C SUPPLEMENTARY SHRIMP DATA FOR CHAPTERS 4-7

Supplementary SHRIMP U-Pb data for Chapter 4 - 2.62 Ga Yandinilling dykes

Mount CS16-6 Spot	204Pb /206Pb	±%	207Pb /206Pb	±%	208Pb /206Pb	±%	206Pb /238U	±%	% $206Pb_c$	ppm U	ppm Th	4-corr ppm 206Pb*	4-corr ppm 208Pb*	232Th /238U	±%	(1) 206Pb /238U Age	
16WDS13E.409B-1	1.2E-4	71	0.177	1.3	0.01	12.6	0.49	2.1	0.22	89	2	42	0.2	0.02	2.3	2819	±43
PHAL.2-2	4.7E-4	35	0.126	1.5	0.00	20.4	0.26	3.1	0.83	158	2	50	-0.7	0.01	2.3	2027	±38
PHAL.2-1	1.6E-4	58	0.125	1.4	0.00	16.1	0.26	2.3	0.29	186	2	60	-0.1	0.01	2.3	2060	±27
PHAL.1-1	-2.2E-4	71	0.128	2.0	0.01	21.2	0.19	1.3	--	120	1	38	0.6	0.01	3.1	2021	±41
PHAL.1-2	---	---	0.132	2.4	0.01	18.1	0.20	1.6	0.00	92	1	28	0.3	0.01	6.3	1941	±33
PHAL.1-3	-1.6E-4	100	0.135	2.4	0.01	18.8	0.19	3.0	--	91	1	28	0.5	0.02	3.3	1953	±34
OGC.2-2	4.0E-5	71	0.294	1.3	0.22	3.1	1.47	3.4	0.07	120	99	70	15.2	0.86	2.8	3334	±89
OGC.1-5	4.7E-5	50	0.298	1.0	0.22	1.1	1.24	3.8	0.08	207	160	120	27.0	0.80	1.1	3324	±37
OGC.1-2	5.1E-5	71	0.300	0.7	0.15	3.5	1.31	2.0	0.09	93	52	54	8.2	0.58	0.6	3331	±47
OGC.1-1	----	---	0.300	0.6	0.14	1.8	1.34	2.8	--	107	54	63	8.6	0.53	0.5	3354	±43
OGC.1-3	1.2E-4	33	0.301	1.2	0.12	2.6	1.24	4.4	0.21	211	99	122	14.7	0.49	1.2	3322	±38
OGC.2-1	3.7E-5	58	0.301	1.6	0.24	2.2	1.38	3.7	0.07	206	192	127	31.2	0.96	0.4	3490	±101
OGC.2-3	1.3E-4	50	0.302	0.8	0.16	2.2	1.29	3.8	0.23	78	43	44	6.8	0.58	0.6	3267	±50
OGC.1-4	-3.6E-5	71	0.301	1.1	0.14	1.7	1.28	3.9	--	140	71	83	11.5	0.52	0.8	3386	±43

Supplementary SHRIMP U-Pb data for Chapter 4 - 2.62 Ga Yandinilling dykes, mount CS16-6

Mount CS16-6 Spot	(2) 206Pb /238U Age		(1) 207Pb /206Pb Age		% Dis-cor-dant	7corr 208Pb* /232Th	±%	(1) 238U /206Pb*	±%	(1) 207Pb* /206Pb*	±%	(1) 207Pb* /235U	±%	(1) 206Pb* /238U	±%	err corr
16WDS13E.409B-1	2968	±89	2607	±25	-10	3.315	34.7	1.8	1.9	0.175	1.5	13.2	2.4	0.549	1.9	0.8
PHAL.2-2	2041	±46	1950	±44	-5	0.102	304.9	2.7	2.2	0.120	2.4	6.1	3.3	0.369	2.2	0.7
PHAL.2-1	2071	±32	2001	±31	-3	0.384	72.5	2.7	1.5	0.123	1.8	6.4	2.3	0.376	1.5	0.6
PHAL.1-1	2003	±49	2115	±44	+5	-0.233	-173.8	2.7	2.4	0.131	2.5	6.7	3.5	0.368	2.4	0.7
PHAL.1-2	1906	±39	2131	±42	+10	-0.863		2.8	2.0	0.132	2.4	6.4	3.1	0.351	2.0	0.6
PHAL.1-3	1907	±40	2194	±49	+13	-0.929		2.8	2.0	0.137	2.8	6.7	3.5	0.354	2.0	0.6
OGC.2-2	3100	±201	3435	±21	+4	0.024	446.4	1.5	3.4	0.293	1.3	27.4	3.7	0.677	3.4	0.9
OGC.1-5	3044	±79	3455	±16	+5	0.000		1.5	1.4	0.297	1.0	27.6	1.8	0.675	1.4	0.8
OGC.1-2	3033	±96	3468	±12	+5	-0.099	-54.7	1.5	1.8	0.300	0.8	27.9	2.0	0.676	1.8	0.9
OGC.1-1	3081	±94	3468	±10	+4	-0.104	-58.9	1.5	1.6	0.300	0.6	28.2	1.8	0.683	1.6	0.9
OGC.1-3	3016	±79	3469	±19	+5	-0.172	-32.7	1.5	1.5	0.300	1.2	27.9	1.9	0.674	1.5	0.8
OGC.2-1			3472	±25	-1			1.4	3.8	0.300	1.6	29.8	4.1	0.718	3.8	0.9
OGC.2-3	2908	±86	3475	±13	+8	-0.152	-27.2	1.5	2.0	0.301	0.9	27.4	2.1	0.660	2.0	0.9
OGC.1-4	3136	±106	3477	±17	+3	-0.078	-102.6	1.4	1.6	0.301	1.1	28.7	1.9	0.691	1.6	0.8

Errors are 1-sigma; Pb_c and Pb^* indicate the common and radiogenic portions, respectively.
Error in Standard calibration was 0.33% (not included in above errors but required when comparing data from different mounts).

(1) Common Pb corrected using measured ^{204}Pb.

(2) Common Pb corrected by assuming $^{206}Pb/^{238}U$-$^{207}Pb/^{235}U$ age-concordance

Supplementary SHRIMP U-Pb data for Chapter 5 - 1.89 Ga Boonadgin dykes, mount CS16-1

Mount CS16-1 Spot	204Pb /206Pb	±%	207Pb /206Pb	±%	208Pb /206Pb	±%	206Pb /238U	±%	% 206Pbc	ppm U	ppm Th	4-corr ppm 206Pb*	4-corr ppm 208Pb*	232Th /238U	±%	(1) 206Pb /238U Age	
WDS09N1.2B	2.60E-04	28	0.1152	0.9	0.009	4.8	0.356	1.7	0.4	206	5	56	0	0.024	1	1771	±19
WDS09N3.18B1	1.40E-03	19	0.1379	1.8	0.211	2.6	0.428	1.8	2.12	117	47	38	6.3	0.414	1.2	2050	±40
WDS09N5.29B-1	9.40E-04	21	0.1283	2.1	0.062	6.1	0.266	2.2	1.45	131	8	36	1.1	0.064	3.8	1799	±42
WDS09N5.38B-1	3.80E-04	21	0.1213	0.8	0.031	5.4	0.332	2.8	0.58	269	10	78	1.4	0.039	2.9	1877	±30
WDS09N3.21B-1	1.40E-03	10	0.1386	0.7	0.096	2.5	0.418	1.6	2.17	373	35	111	5.3	0.098	1.8	1912	±33
WDS09N1.4B-1	3.40E-04	41	0.118	1.5	0.056	3.4	0.363	2.1	0.53	97	8	32	1.4	0.082	1.1	2106	±30
WDS09RSB3.45B-1	4.60E-04	18	0.1192	0.7	0.08	2.4	0.318	1.8	0.72	449	76	137	8.9	0.174	7.3	1958	±25
WDS09RSB1.54B-1	4.90E-04	35	0.1196	1.5	0.174	2.1	0.397	1.1	0.75	67	30	21	3.3	0.468	2.2	1994	±29
WDS09N1.3B-1	1.20E-03	21	0.1401	1.4	0.115	2.4	0.272	4.1	1.79	205	19	68	5.2	0.096	2.5	2113	±102
WDS09RSB3.45B-2	2.00E-03	13	0.1324	1.1	0.21	4.8	0.558	4.4	3.08	178	73	65	9.5	0.425	4.2	2286	±75
PHAL.1-1	3.70E-04	38	0.1287	1.4	0.006	10.1	0.268	1.8	0.55	112	2	30	-0.2	0.015	2	1779	±40
PHAL.1-2	3.00E-04	45	0.126	1.5	0.007	10	0.277	1	0.46	93	1	26	-0.1	0.014	2.3	1824	±25
PHAL.2-1	-1.20E-04	71	0.1273	1.5	0.009	9	0.243	1.6	--	108	2	33	0.4	0.015	2.2	1965	±40
PHAL.2-2	5.90E-05	100	0.1288	2.4	0.006	10.8	0.234	1	0.09	116	2	36	0.1	0.014	2.1	1963	±25
PHAL.1-3	-5.40E-05	100	0.1263	1.4	0.008	9.1	0.27	1	--	113	2	31	0.3	0.014	2.1	1803	±32
PHAL.2-3	-1.30E-04	71	0.1294	1.5	0.007	10.6	0.256	1.6	--	100	1	31	0.3	0.014	2.3	1986	±27
PHAL.2-4	5.70E-04	35	0.1278	1.6	0.007	10.5	0.24	1.8	0.86	102	1	31	-0.4	0.014	2.4	1934	±27
OGC.1-1	9.80E-05	33	0.3001	0.5	0.232	1.8	0.984	3.1	0.12	214	188	126	29	0.911	0.9	3362	±49
OGC.2-1	5.30E-05	50	0.2981	0.9	0.15	1.5	1.452	0.7	0.06	105	59	62	9.2	0.582	0.4	3347	±54
OGC.2-2	2.40E-05	58	0.298	0.4	0.146	0.8	1.234	3.4	0.03	233	129	138	20.2	0.574	0.6	3372	±42
OGC.1-2	1.60E-05	100	0.2982	0.6	0.246	1.5	0.874	3.7	0.02	222	213	127	31.3	0.991	0.8	3276	±67
OGC.2-3	8.10E-06	100	0.2968	0.7	0.136	1.6	1.366	2	0.01	175	89	103	14.1	0.528	0.5	3372	±62
OGC.1-3	-1.40E-05	100	0.2984	0.6	0.276	0.8	0.902	2.2	--	247	263	148	41.3	1.101	1.1	3418	±67

Supplementary SHRIMP U-Pb data for Chapter 5 - 1.89 Ga Boonadgin dykes, mount CS16-1

Mount CS16-1 Spot	(2) 206Pb /238U Age		(1) 207Pb /206Pb Age		% Dis-cor-dant	7corr 208Pb* /232Th	±%	(1) 238U /206Pb*	±%	(1) 207Pb* /206Pb*	±%	(1) 207Pb* /235U	±%	(1) 206Pb* /238U	±%	err corr
WDS09N1.2B	1764	±21	1828	±23	4	-0.13	-46.8	3.16	1.2	0.1117	1.3	4.87	1.8	0.316	1.2	0.7
WDS09N3.18B1	2067	±47	1946	±67	-6	0.17	7.5	2.67	2.3	0.1193	3.7	6.16	4.4	0.374	2.3	0.5
WDS09N5.29B-1	1787	±46	1890	±60	6	0.06	88.4	3.11	2.6	0.1156	3.3	5.13	4.3	0.322	2.6	0.6
WDS09N5.38B-1	1874	±34	1899	±22	1	0.12	47.8	2.96	1.9	0.1162	1.2	5.42	2.2	0.338	1.9	0.8
WDS09N3.21B-1	1906	±37	1950	±34	2	0.14	18.2	2.9	2	0.1196	1.9	5.69	2.7	0.345	2	0.7
WDS09N1.4B-1	2149	±36	1854	±42	-16	0.46	10.5	2.59	1.7	0.1134	2.3	6.04	2.8	0.386	1.7	0.6
WDS09RSB3.45B-1	1974	±29	1847	±23	-7	0.18	10.3	2.82	1.5	0.1129	1.3	5.53	2	0.355	1.5	0.8
WDS09RSB1.54B-1	2016	±34	1849	±48	-9	0.14	5.7	2.76	1.7	0.1131	2.6	5.65	3.1	0.362	1.7	0.5
WDS09N1.3B-1	2129	±122	2019	±56	-5	0.39	27.7	2.58	5.7	0.1243	3.2	6.65	6.5	0.388	5.7	0.9
WDS09RSB3.45B-2	2401	±100	1726	±70	-39	0.28	12.6	2.35	3.9	0.1057	3.8	6.2	5.4	0.426	3.9	0.7
PHAL.1-1	1749	±44	2013	±37	13			3.15	2.6	0.1239	2.1	5.43	3.3	0.318	2.6	0.8
PHAL.1-2	1803	±28	1985	±39	9	-0.79	-32.2	3.06	1.6	0.122	2.2	5.5	2.7	0.327	1.6	0.6
PHAL.2-1	1947	±45	2083	±31	7	-0.28	-82.5	2.81	2.3	0.1289	1.7	6.33	2.9	0.356	2.3	0.8
PHAL.2-2	1946	±29	2071	±43	6	-0.46	-70.1	2.81	1.5	0.128	2.5	6.28	2.9	0.356	1.5	0.5
PHAL.1-3	1770	±35	2057	±27	14	-0.88		3.1	2	0.127	1.5	5.65	2.5	0.323	2	0.8
PHAL.2-3	1966	±31	2112	±31	7	-0.41	-55	2.77	1.6	0.1311	1.8	6.52	2.3	0.361	1.6	0.7
PHAL.2-4	1930	±30	1959	±51	1	-0.45	-52.1	2.86	1.6	0.1202	2.8	5.8	3.3	0.35	1.6	0.5
OGC.1-1	3246	±90	3466	±8	4	0.08	43.2	1.46	1.9	0.2991	0.5	28.24	1.9	0.685	1.9	1
OGC.2-1	3226	±99	3458	±13	4	0.03	206.6	1.47	2.1	0.2976	0.9	27.92	2.3	0.681	2.1	0.9
OGC.2-2	3271	±80	3459	±7	3	0.05	100.2	1.46	1.6	0.2978	0.4	28.21	1.7	0.687	1.6	1
OGC.1-2	3103	±107	3460	±9	7	0.04	73.4	1.51	2.6	0.298	0.6	27.21	2.7	0.662	2.6	1
OGC.2-3	3278	±119	3453	±12	3	0.05	168.1	1.46	2.4	0.2967	0.7	28.12	2.5	0.687	2.4	1
OGC.1-3	3360	±143	3463	±9	2	0.14	43.5	1.43	2.5	0.2985	0.6	28.79	2.6	0.699	2.5	1

Supplementary SHRIMP U-Pb data for Chapter 5 - 1.89 Ga Boonadgin dykes, mount CS16-6

Mount CS16-6 Spot	204Pb /206Pb	±%	207Pb /206Pb	±%	208Pb /206Pb	±%	206Pb /238U	±%	% 206Pbc	ppm U	ppm Th	4-corr ppm 206Pb*	4-corr ppm 208Pb*	232Th /238U	±%	(1) 206Pb /238U Age	
16WDS1C.372B-1	1.10E-04	58	0.117	1.2	0.02	6.5	0.32	1.2	0.17	199	9	57	0.9	0.05	3.5	1870	±30
16WDS1C.372B-2	4.80E-05	100	0.116	1.4	0.02	8.1	0.3	2.1	0.07	181	6	54	0.8	0.03	2.7	1923	±32
OGC.1-1	----	---	0.3	0.6	0.14	1.8	1.34	2.8	--	107	54	63	8.6	0.53	0.5	3354	±43
OGC.1-2	5.10E-05	71	0.3	0.7	0.15	3.5	1.31	2	0.06	93	52	54	8.3	0.58	0.6	3332	±47
OGC.2-1	3.70E-05	58	0.301	1.6	0.24	2.2	1.38	3.7	0.04	206	192	127	31.3	0.96	0.4	3491	±101
OGC.1-3	1.20E-04	33	0.301	1.2	0.12	2.6	1.24	4.4	0.14	211	99	122	14.8	0.49	1.2	3324	±38
OGC.2-2	4.00E-05	71	0.294	1.3	0.22	3.1	1.47	3.4	0.05	120	99	70	15.2	0.86	2.8	3335	±89
OGC.2-3	1.30E-04	50	0.302	0.8	0.16	2.2	1.29	3.8	0.15	78	43	44	6.9	0.58	0.6	3269	±50
OGC.1-4	-3.60E-05	71	0.301	1.1	0.14	1.7	1.28	3.9	--	140	71	83	11.5	0.52	0.8	3385	±43
OGC.1-5	4.70E-05	50	0.298	1	0.22	1.1	1.24	3.8	0.06	207	160	120	27	0.8	1.1	3325	±37
PHAL.1-1	-2.20E-04	71	0.128	2	0.01	21.2	0.19	1.3	--	120	1	38	0.5	0.01	3.1	2020	±41
PHAL.1-2	---	---	0.132	2.4	0.01	18.1	0.2	1.6	0	92	1	28	0.3	0.01	6.3	1941	±33
PHAL.1-3	-1.60E-04	100	0.135	2.4	0.01	18.8	0.19	3	--	91	1	28	0.5	0.02	3.3	1952	±34
PHAL.2-1	1.60E-04	58	0.125	1.4	0	16.1	0.26	2.3	0.24	186	2	60	0	0.01	2.3	2060	±26
PHAL.2-2	4.70E-04	35	0.126	1.5	0	20.4	0.26	3.1	0.71	158	2	50	-0.7	0.01	2.3	2029	±38

Supplementary SHRIMP U-Pb data for Chapter 5 - 1.89 Ga Boonadgin dykes, mount CS16-6

Mount CS16-6 Spot	(2) 206Pb /238U Age		(1) 207Pb /206Pb Age		% Dis-cor-dant	7corr 208Pb* /232Th	±%	(1) 238U /206Pb*	±%	(1) 207Pb* /206Pb*	±%	(1) 207Pb* /235U	±%	(1) 206Pb* /238U	±%	err corr
16WDS1C.372B-1	1869	±34	1881	±26	1	0.093	53.6	3	1.9	0.115	1.4	5.3	2.4	0.337	1.9	0.8
16WDS1C.372B-2	1928	±37	1882	±27	-3	0.233	36.2	2.9	1.9	0.115	1.5	5.5	2.5	0.347	1.9	0.8
OGC.1-1	3228	±78	3468	±10	4	0.009	582.7	1.5	1.6	0.3	0.6	28.2	1.8	0.683	1.6	0.9
OGC.1-2	3188	±83	3468	±12	5	0.005	996.3	1.5	1.8	0.3	0.8	28	2	0.677	1.8	0.9
OGC.2-1	3522	±293	3472	±25	-1	0.205		1.4	3.8	0.3	1.6	29.8	4.1	0.719	3.8	0.9
OGC.1-3	3175	±67	3469	±19	5	-0.046	-107.6	1.5	1.5	0.3	1.2	27.9	1.9	0.675	1.5	0.8
OGC.2-2	3227	±163	3435	±21	4	0.085	86.5	1.5	3.4	0.293	1.3	27.4	3.7	0.677	3.4	0.9
OGC.2-3	3080	±79	3475	±13	8	-0.048	-84.8	1.5	2	0.301	0.9	27.4	2.1	0.66	2	0.9
OGC.1-4	3277	±83	3477	±17	3	0.036	171.5	1.4	1.6	0.301	1.1	28.7	1.9	0.691	1.6	0.8
OGC.1-5	3191	±66	3455	±16	5	0.072	40.7	1.5	1.4	0.297	1	27.7	1.8	0.675	1.4	0.8
PHAL.1-1	2005	±48	2115	±44	5	-0.19	-189.5	2.7	2.4	0.131	2.5	6.7	3.5	0.368	2.4	0.7
PHAL.1-2	1912	±38	2131	±42	10	-0.757	-104.1	2.8	2	0.132	2.4	6.4	3.1	0.351	2	0.6
PHAL.1-3	1915	±39	2194	±49	13	-0.81		2.8	2	0.137	2.8	6.7	3.5	0.354	2	0.6
PHAL.2-1	2070	±31	2001	±31	-3	0.36	69.6	2.7	1.5	0.123	1.8	6.4	2.3	0.377	1.5	0.6
PHAL.2-2	2041	±44	1950	±44	-5	0.101	277.2	2.7	2.2	0.12	2.4	6.1	3.3	0.37	2.2	0.7

Supplementary SHRIMP U-Pb data for Chapter 5 - 1.89 Ga Boonadgin dykes, mount CS16-7

Mount CS16-7 Spot	204Pb /206Pb	±%	207Pb /206Pb	±%	208Pb /206Pb	±%	206Pb /238U	±%	% 206Pbc	ppm U	ppm Th	4-corr ppm 206Pb*	4-corr ppm 208Pb*	232Th /238U	±%	(1) 206Pb /238U Age	
16WDS6D.406B-1	5.10E-05	100	0.118	1.4	0.034	6	0.557	1.1	0.08	247	23.5	74	2.41	0.098	1	1934	±29
16WDS6D.406B-2	2.80E-04	58	0.121	1.9	0.044	7	0.549	2.4	0.43	129	14.4	39	1.35	0.115	1.3	1944	±37
16WDS6D.405B-1	4.40E-04	41	0.122	1.7	0.058	5	0.402	1.9	0.67	251	23.9	71	3.1	0.098	3.9	1827	±29
16WDS6D.401B-1	1.80E-03	33	0.133	2.7	0.058	9	0.39	3.9	2.75	83	4.3	25	-0.11	0.053	2.5	1937	±47
16WDS6D.401B-2	1.40E-03	50	0.124	3.7	0.098	9	0.392	2.5	2.15	47	5.9	17	0.89	0.129	2.3	2296	±116
OGC.1-1	2.30E-04	38	0.297	1.4	0.129	2	1.578	1.2	0.27	157	69.7	83	10.24	0.458	0.7	3094	±51
OGC.2-1	3.90E-05	100	0.308	0.9	0.207	2	1.59	1.3	0.05	136	102.6	81	16.88	0.78	1.5	3401	±60
OGC.1-2	1.10E-04	71	0.303	1.1	0.165	3	1.618	2.4	0.13	98	60.3	56	9.16	0.634	0.9	3281	±67
OGC.2-2	5.10E-05	71	0.299	0.7	0.228	2	1.586	1.1	0.06	212	179.6	123	28.23	0.877	0.5	3341	±50
OGC.1-3	---	---	0.306	0.9	0.193	2	1.639	1.3	0	138	98.3	82	15.95	0.738	0.7	3397	±58
OGC.2-3	5.60E-05	71	0.297	0.8	0.248	2	1.654	1.1	0.07	178	166.1	111	27.55	0.967	0.6	3516	±54
OGC.3-1	-3.50E-05	100	0.297	0.9	0.191	2	1.53	1.2	--	160	114.5	98	19.04	0.738	0.7	3476	±57
OGC.1-4	1.60E-04	50	0.295	0.9	0.077	3	1.389	2.2	0.19	143	31.4	84	6.16	0.227	1	3362	±95
PHAL.1-1	---	100	0.12	3	0.008	24	0.323	2	0	77	1	24	0.21	0.013	5	2011	±47
PHAL.2-1	1.60E-04	100	0.125	2.6	0.007	22	0.321	4	0.25	109	1.6	34	0.05	0.015	3.9	1977	±40
PHAL.1-2	2.40E-04	100	0.127	3	0.012	20	0.306	3.2	0.36	82	1.1	25	0.08	0.014	4.7	1986	±47
PHAL.2-2	1.70E-04	100	0.128	2.5	0.006	23	0.313	3.6	0.26	111	1.2	36	0.02	0.012	4.5	2062	±61
PHAL.1-3	-5.10E-04	71	0.119	3.2	0.009	24	0.287	3.4	--	81	1.2	25	0.68	0.015	4.8	2006	±49
PHAL.2-3	-3.50E-04	71	0.121	4.2	0.006	24	0.314	5.4	--	105	1.3	33	0.6	0.013	4.3	2041	±42

Supplementary SHRIMP U-Pb data for Chapter 5 - 1.89 Ga Boonadgin dykes, mount CS16-7

Mount CS16-7 Spot	(2) 206Pb /238U Age		(1) 207Pb /206Pb Age		% Dis-cor-dant	7corr 208Pb* /232Th	±%	(1) 238U /206Pb*	±%	(1) 207Pb* /206Pb*	±%	(1) 207Pb* /235U	±%	(1) 206Pb* /238U	±%	err corr
16WDS6D.406B-1	1936	±33	1914	±28	-1	0.128	22	2.9	1.7	0.117	1.5	5.7	2.3	0.35	1.7	0.7
16WDS6D.406B-2	1948	±42	1915	±49	-2	0.123	27	2.8	2.2	0.117	2.7	5.7	3.5	0.35	2.2	0.6
16WDS6D.405B-1	1818	±32	1898	±50	4	0.102	28	3.1	1.8	0.116	2.8	5.2	3.3	0.33	1.8	0.6
16WDS6D.401B-1	1959	±52	1779	±151	-10	0.169	60	2.9	2.8	0.109	8.3	5.3	8.8	0.35	2.8	0.3
16WDS6D.401B-2	2415	±154	1720	±185	-40	0.634	27	2.3	6	0.105	10.1	6.2	11.7	0.43	6	0.5
OGC.1-1	2851	±70	3445	±23	13	-0.188	-21	1.6	2.1	0.295	1.5	25.1	2.6	0.62	2.1	0.8
OGC.2-1	3270	±113	3508	±14	4	0.065	86	1.4	2.3	0.307	0.9	29.5	2.4	0.69	2.3	0.9
OGC.1-2	3096	±108	3477	±18	7	-0.031	-168	1.5	2.6	0.301	1.1	27.6	2.8	0.66	2.6	0.9
OGC.2-2	3209	±88	3465	±12	5	0.07	50	1.5	1.9	0.299	0.8	28	2	0.68	1.9	0.9
OGC.1-3	3273	±111	3499	±14	4	0.063	94	1.4	2.2	0.306	0.9	29.2	2.4	0.69	2.2	0.9
OGC.2-3	3655	±232	3451	±12	-2	0.29		1.4	2	0.296	0.8	29.6	2.1	0.73	2	0.9
OGC.3-1	3510	±160	3456	±14	-1	0.218	66	1.4	2.1	0.297	0.9	29.3	2.3	0.71	2.1	0.9
OGC.1-4	3279	±183	3436	±15	3	-0.038	-806	1.5	3.6	0.293	1	27.7	3.7	0.68	3.6	1
PHAL.1-1	2020	±55	1954	±54	-3	0.558	81	2.7	2.7	0.12	3	6.1	4.1	0.37	2.7	0.7
PHAL.2-1	1973	±46	2002	±56	1	-0.092	-350	2.8	2.4	0.123	3.2	6.1	3.9	0.36	2.4	0.6
PHAL.1-2	1982	±54	2011	±71	1	-0.052	-790	2.8	2.8	0.124	4	6.2	4.9	0.36	2.8	0.6
PHAL.2-2	2064	±72	2046	±56	-1	0.13	417	2.7	3.5	0.126	3.2	6.6	4.7	0.38	3.5	0.7
PHAL.1-3	2000	±56	2045	±86	2	0.433	92	2.7	2.8	0.126	4.9	6.4	5.6	0.37	2.8	0.5
PHAL.2-3	2042	±50	2032	±85	-1	0.554	106	2.7	2.4	0.125	4.8	6.4	5.4	0.37	2.4	0.4

Supplementary SHRIMP U-Pb data for Chapter 5 - 1.89 Ga Boonadgin dykes

Mount CS16-1

Errors are 1-sigma; Pbc and Pb* indicate the common and radiogenic portions, respectively.
Error in Standard calibration was 0.49% (not included in above errors but required when comparing data from different mounts).
(1) Common Pb corrected using measured ^{204}Pb.
(2) Common Pb corrected by assuming ^{206}Pb/^{238}U-^{207}Pb/^{235}U age-concordance

Mount CS16-6

Errors are 1-sigma; Pbc and Pb* indicate the common and radiogenic portions, respectively.
Error in Standard calibration was 0.33% (not included in above errors but required when comparing data from different mounts).
(1) Common Pb corrected using measured ^{204}Pb.
(2) Common Pb corrected by assuming ^{206}Pb/^{238}U-^{207}Pb/^{235}U age-concordance

Mount CS16-7

Errors are 1-sigma; Pbc and Pb* indicate the common and radiogenic portions, respectively.
Error in Standard calibration was 0.47% (not included in above errors but required when comparing data from different mounts).
(1) Common Pb corrected using measured ^{204}Pb.
(2) Common Pb corrected by assuming ^{206}Pb/^{238}U-^{207}Pb/^{235}U age-concordance

Supplementary SHRIMP U-Pb data for Chapter 6 - 1.39 Ga Biberkine dykes, mount CS16-2

Mount CS16-2 Spot	204Pb /206Pb	± %	207Pb /206Pb	±%	208Pb /206Pb	±%	206Pb /238U	±%	% 206Pbc	ppm U	ppm Th	4-corr ppm 206Pb*	4-corr ppm 208Pb*	232Th /238U	± %	(1) 206Pb /238U Age	
WDS14B1.109B-1	1.60E-04	100	0.093	2.9	0.028	8.4	0.236	3.4	0.26	181	13.6	40	0.9	0.078	1.9	1489	±30
WDS10C1.10B-1	1.90E-03	35	0.099	3.7	0.042	9	0.212	2.3	3.2	119	9.3	25	-0.7	0.081	5.2	1435	±40
WDS14B2.187B-1	3.60E-03	29	0.12	3.5	0.066	7.5	0.241	2.5	6.23	114	6.9	24	-1.7	0.063	2.9	1409	±64
WDS14B2.187B-2	1.80E-03	30	0.097	2.7	0.058	9.3	0.279	3.4	3.03	222	18.1	55	-0.4	0.084	2	1631	±61
WDS14B3.191B-1	2.20E-03	24	0.1	2.5	0.081	6.7	0.198	2.5	3.81	314	50.1	67	0	0.165	2.8	1426	±73
WDS10C1.10B-2	5.50E-03	23	0.14	3.4	0.181	10.5	0.388	11.5	9.72	155	20.8	47	-1.3	0.139	9	1936	±225
WDS14B1.109B-2	-2.50E-04	100	0.102	5	0.026	11.5	0.276	5.5	--	163	12	34	1.2	0.076	2.6	1419	±85
WDS10C4.177B-1	7.80E-04	41	0.092	2.5	0.02	8.6	0.416	3.2	1.31	175	8.9	40	-0.3	0.053	3.9	1513	±48
WDS10C4.177B-2	6.30E-04	50	0.091	2.8	0.021	9.1	0.403	4	1.04	151	7.3	32	-0.1	0.05	5.1	1418	±37
WDS10C4.177B-3	3.70E-04	58	0.092	2.4	0.022	11.5	0.451	3.2	0.6	203	10	49	0.5	0.051	2.5	1588	±35
WDS10C2.44B-1	5.00E-04	50	0.093	2.5	0.061	8.6	0.283	2.8	0.83	256	37.4	52	2.3	0.151	1.3	1371	±27
WDS14B2.184B-1	3.30E-03	28	0.103	5.2	0.032	9.7	0.429	2.6	5.88	81	5.8	16	-1.6	0.074	2.9	1366	±47
WDS10C1.11B-1	1.60E-04	100	0.101	2.7	0.061	9.9	0.273	1.8	0.25	246	21.5	58	3.2	0.09	5.8	1563	±32
WDS11A1.199B-1	7.10E-03	38	0.115	7.1	0.1	17.9	0.267	4.8	13.33	45	1.9	7	-1.5	0.044	6.5	1131	±84
WDS11A2.173B-1	3.20E-03	71	0.127	8	0.153	11.8	0.334	6.5	5.25	41	4.5	8	0.3	0.115	5.5	1278	±101
WDS14B3.192B-1	1.50E-02	25	0.169	5.8	0.193	17	0.234	8.1	24.75	47	5.2	8	-3.8	0.116	3.9	1204	±127
WDS14B3.192B-2	4.50E-03	50	0.085	11.	0.021	23.	0.195	4.5	8.42	40	2.3	7	-1.2	0.059	5.4	1231	±78

3 2

Supplementary SHRIMP U-Pb data for Chapter 6 - 1.39 Ga Biberkine dykes, mount CS16-2

Mount CS16-2 Spot	(2) 206Pb /238U Age		(1) 207Pb /206Pb Age		% Dis-cor-dant	7corr 208Pb* /232Th	±%	(1) 238U /206Pb*	±%	(1) 207Pb* /206Pb*	±%	(1) 207Pb* /235U	±%	(1) 206Pb* /238U	±%	err corr
WDS14B1.109B-1	1494	±33	1433	±74	-4	0.1	31	3.85	2.3	0.09	3.9	3.2	4.5	0.26	2.3	0.5
WDS10C1.10B-1	1466	±42	995	±294	-49	0.07	53	4.01	3.1	0.072	14.5	2.5	14.8	0.249	3.1	0.2
WDS14B2.187B-1	1445	±66	870	±505	-69	-0.04	-144	4.09	5.1	0.068	24.4	2.3	24.9	0.244	5.1	0.2
WDS14B2.187B-2	1687	±68	988	±235	-74	0.26	21	3.47	4.2	0.072	11.6	2.9	12.3	0.288	4.2	0.3
WDS14B3.191B-1	1462	±80	882	±254	-69	0.09	23	4.04	5.7	0.068	12.3	2.3	13.6	0.247	5.7	0.4
WDS10C1.10B-2	2088	±286	615	±749	-250	0.42	48	2.85	13.5	0.06	34.7	2.9	37.2	0.35	13.5	0.4
WDS14B1.109B-2	1394	±90	1724	±107	20	-0.03	-229	4.06	6.7	0.106	5.8	3.6	8.9	0.246	6.7	0.8
WDS10C4.177B-1	1537	±52	1211	±126	-28	0.15	34	3.78	3.5	0.081	6.4	2.9	7.3	0.265	3.5	0.5
WDS10C4.177B-2	1430	±40	1252	±123	-15	0.09	47	4.06	2.9	0.082	6.3	2.8	6.9	0.246	2.9	0.4
WDS10C4.177B-3	1607	±39	1365	±82	-18	0.22	25	3.58	2.5	0.087	4.3	3.4	4.9	0.279	2.5	0.5
WDS10C2.44B-1	1373	±29	1336	±96	-3	0.07	18	4.22	2.2	0.086	4.9	2.8	5.4	0.237	2.2	0.4
WDS14B2.184B-1	1420	±48	427	±610	-245	-0.01	-490	4.24	3.8	0.055	27.4	1.8	27.6	0.236	3.8	0.1
WDS10C1.11B-1	1560	±35	1595	±66	2	0.15	21	3.65	2.3	0.098	3.5	3.7	4.2	0.274	2.3	0.6
WDS11A1.199B-1	1237	±69				0.05	309	5.21	8.1	0.004	1317.8	0.1	1317.8	0.192	8.1	0
WDS11A2.173B-1	1279	±97	1250	±832	-2	0.08	80	4.56	8.7	0.082	42.5	2.5	43.4	0.219	8.7	0.2
WDS14B3.192B-1	1424	±113	1196	±801	-1	-0.03	-328	4.87	11.6	0.08	40.6	2.3	42.3	0.205	11.6	0.3
WDS14B3.192B-2	1334	±70				0.09	141	4.75	7	0.016	239.4	0.5	239.5	0.21	7	0

Supplementary SHRIMP U-Pb data for Chapter 6 - 1.39 Ga Biberkine dykes, mount CS16-2

Mount CS16-2 Spot	204Pb /206Pb	±%	207Pb /206Pb	±%	208Pb /206Pb	±%	206Pb /238U	±%	% 206Pbc	ppm U	ppm Th	4-corr ppm 206Pb*	4-corr ppm 208Pb*	232Th /238U	±%	(1) 206Pb /238U Age	
OGC.1-1	1.90E-04	71	0.296	2.8	0.249	5.4	0.707	7.3	0.22	252	254.9	161	39.5	1.046	1	3581	±194
OGC.2-1	5.10E-05	100	0.303	1.1	0.119	2.3	0.781	2.2	0.06	345	161.6	195	23	0.484	0.9	3257	±57
OGC.3-1	3.10E-05	100	0.301	2.1	0.127	4	1.491	3.4	0.04	219	100.8	127	16.1	0.476	0.8	3330	±96
OGC.2-2	----	---	0.305	1.1	0.136	2.2	0.829	1.5	--	294	154.8	164	22.5	0.545	0.9	3223	±58
OGC.1-2	1.70E-04	71	0.303	2.3	0.235	4.2	0.713	4.2	0.2	407	363.8	255	59.2	0.923	4.2	3534	±190
OGC.2-3	7.90E-05	100	0.301	1.3	0.15	2.6	0.975	1.9	0.09	248	136	155	23.1	0.568	1.1	3525	±79
OGC.1-3	-1.60E-04	71	0.304	1.3	0.125	2.8	0.75	3	--	312	152.7	184	24.1	0.505	1.1	3367	±72
OGC.2-4	----	---	0.305	1.1	0.252	2.9	0.882	1.6	--	311	294.3	173	44.1	0.977	1.2	3217	±63
PHAL.1-1	3.70E-04	71	0.13	4.2	0.012	19	0.12	7.5	1.33	247	3.7	76	-1.4	0.016	5.4	1977	±53
PHAL.2-1	4.00E-04	71	0.134	5.2	0.008	18.1	0.302	3.7	0.6	105	1.5	30	-0.2	0.015	5.5	1829	±44
PHAL.3-1	4.40E-04	100	0.137	4.2	0.007	24.3	0.177	5.1	0.65	114	1.6	33	-0.3	0.015	7.1	1873	±55
PHAL.2-2	1.10E-03	50	0.134	3.2	0.006	20.5	0.289	2.4	1.64	102	1.3	28	-0.9	0.013	5.8	1768	±50
PHAL.3-2	1.60E-03	58	0.122	4.7	0.008	26.8	0.189	7.6	2.58	95	1.6	28	-1.5	0.017	3.1	1922	±71
PHAL.4-1	3.30E-04	58	0.126	3.3	0.007	19.7	0.413	4.7	1.29	77	1.3	28	-0.6	0.018	5.7	2273	±71
PHAL.2-3	2.90E-04	100	0.128	3.3	0.008	19.3	0.282	2.7	0.44	104	1.2	29	-0.1	0.012	7.3	1837	±53
PHAL.3-3	1.60E-03	58	0.126	4.8	0.01	22.5	0.191	5.2	2.47	113	1.1	33	-1.5	0.01	9.7	1873	±66

Supplementary SHRIMP U-Pb data for Chapter 6 - 1.39 Ga Biberkine dykes, mount CS16-2

Mount CS16-2 Spot	(2) 206Pb /238U Age		(1) 207Pb /206Pb Age		% Dis-cor-dant	7corr 208Pb* /232Th	±%	(1) 238U /206Pb*	±%	(1) 207Pb* /206Pb*	±%	(1) 207Pb* /235U	±%	(1) 206Pb* /238U	±%	err corr
OGC.1-1	0	±264	3440	±45	-5			1.35	7	0.294	2.9	30.1	7.6	0.743	7	0.9
OGC.2-1	3054	±88	3483	±17	8	-0.13	-42	1.52	2.2	0.302	1.1	27.4	2.5	0.657	2.2	0.9
OGC.3-1	3179	±168	3475	±33	5	-0.04	-310	1.48	3.7	0.301	2.1	28.1	4.3	0.676	3.7	0.9
OGC.2-2	2994	±86	3494	±17	10	-0.12	-35	1.54	2.3	0.305	1.1	27.2	2.5	0.649	2.3	0.9
OGC.1-2	3655	±809	3480	±36	-2	0.28		1.37	7	0.302	2.3	30.4	7.3	0.73	7	0.9
OGC.2-3	3632	±313	3473	±21	-2	0.33		1.37	2.9	0.301	1.3	30.2	3.2	0.728	2.9	0.9
OGC.1-3	3220	±129	3499	±21	5	-0.03	-328	1.46	2.7	0.306	1.4	28.9	3.1	0.686	2.7	0.9
OGC.2-4	2984	±93	3495	±18	10	0.01	507	1.55	2.5	0.305	1.1	27.2	2.7	0.647	2.5	0.9
PHAL.1-1	1984	±59	1929	±152	-3	-0.2	-285	2.79	3.1	0.118	8.5	5.8	9	0.359	3.1	0.3
PHAL.2-1	1796	±50	2080	±108	14			3.05	2.8	0.129	6.2	5.8	6.8	0.328	2.8	0.4
PHAL.3-1	1838	±61	2122	±110	13			2.97	3.4	0.132	6.3	6.1	7.1	0.337	3.4	0.5
PHAL.2-2	1745	±54	1958	±126	11			3.17	3.3	0.12	7.1	5.2	7.8	0.316	3.3	0.4
PHAL.3-2	1963	±79	1620	±270	-22	0.07	773	2.88	4.3	0.1	14.5	4.8	15.1	0.347	4.3	0.3
PHAL.4-1	2355	±91	1875	±122	-25	1.77	43	2.36	3.7	0.115	6.8	6.7	7.7	0.423	3.7	0.5
PHAL.2-3	1814	±58	2014	±82	10	-0.95		3.03	3.3	0.124	4.6	5.6	5.7	0.33	3.3	0.6
PHAL.3-3	1893	±72	1715	±248	-11	-0.6		2.97	4.1	0.105	13.5	4.9	14.1	0.337	4.1	0.3

Supplementary SHRIMP U-Pb data for Chapter 6 - 1.39 Ga Biberkine dykes, mount CS16-4

Mount CS16-4 Spot	204Pb /206Pb	±%	207Pb /206Pb	±%	208Pb /206Pb	±%	206Pb /238U	±%	% 206Pbc	ppm U	ppm Th	4-corr ppm 206Pb*	4-corr ppm 208Pb*	232Th /238U	±%	(1) 206Pb /238U Age	
15WDS16B2R.258B-1	8.40E-04	58	0.108	3.5	0.029	10.5	0.295	2.5	1.35	53	1.2	12	-0.02	0.023	5	1470	±42
15WDS16B2R.258B-2	1.10E-04	71	0.097	1.7	0.018	6.2	0.298	1.6	0.18	231	11.5	52	0.73	0.052	1.5	1512	±22
15WDS16B2R.266B-1	1.40E-03	41	0.104	3.2	0.053	7	0.253	3.2	2.24	68	6	14	0.06	0.092	2.3	1376	±35
15WDS16B2R.266B-2	3.90E-03	23	0.134	2.8	0.149	4.1	0.326	2.2	6.53	94	6.7	20	0.16	0.073	4.6	1445	±61
15WDS16B2R.266B-3	1.50E-03	38	0.102	3.1	0.051	7.1	0.245	4.4	2.56	71	6.2	15	-0.08	0.091	2.1	1460	±37
15WDS16B1.248B-1	9.70E-04	21	0.103	1.2	0.093	2	0.435	1	1.58	308	52	64	3.83	0.175	2.9	1394	±33
15WDS16B1.248B-2	7.40E-04	19	0.098	1.9	0.137	4.7	0.512	3.9	1.21	330	88.9	74	8.31	0.279	1.9	1493	±20
15WDS16B1.246B-1	2.60E-03	19	0.127	4.8	0.122	11.8	0.201	1.5	4.26	297	29.4	70	2.08	0.102	1.3	1551	±27
PHAL.1-1	3.40E-04	71	0.129	2.5	0.005	18.6	0.408	4.2	0.51	79	0.8	27	-0.18	0.01	6.8	2139	±54
PHAL.2-1	3.50E-04	71	0.126	2.6	0.006	19.5	0.38	3.6	0.53	70	0.9	23	-0.15	0.013	6	2100	±51
PHAL.3-1	9.10E-04	58	0.129	3.4	0.007	20.9	0.171	2.3	1.41	98	1.3	30	-0.77	0.014	6.1	1971	±49
PHAL.3-2	1.90E-03	38	0.127	4.9	0.009	18.6	0.178	2.4	3.02	90	1.3	26	-1.57	0.015	5.5	1865	±48
PHAL.2-2	----	---	0.13	2.2	0.007	16.1	0.358	1.7	--	100	1.2	34	0.23	0.012	5.2	2170	±45
PHAL.2-3	9.60E-04	45	0.127	2.7	0.007	18.9	0.392	4.2	1.48	54	0.7	17	-0.46	0.013	6.3	1998	±95
PHAL.2-4	-1.80E-04	100	0.121	4.8	0.006	18.3	0.395	3.5	--	68	0.9	23	0.27	0.013	6.4	2122	±54
OGC.1-1	7.00E-04	38	0.299	1.5	0.16	2.8	1.515	2.6	0.83	39	22.6	23	3.21	0.606	1.4	3383	±100
OGC.2-1	-1.70E-04	71	0.297	1.4	0.157	6	1.236	2.3	--	60	35.1	35	5.76	0.601	4.3	3345	±85
OGC.2-2	3.50E-05	100	0.302	1.3	0.113	1.9	1.173	2.1	0.04	151	58.4	87	9.81	0.4	2	3308	±57
OGC.3-1	4.90E-05	71	0.298	0.7	0.162	1.4	1.371	5.1	0.06	169	98.2	107	17.25	0.602	1.3	3554	±56
OGC.3-2	----	---	0.297	2.1	0.145	1.8	1.448	3.7	--	97	50.9	58	8.44	0.543	0.9	3386	±64
OGC.4-1	---	---	0.3	0.9	0.141	1.8	1.202	2.8	0	128	65.8	76	10.81	0.532	1.3	3394	±60

Supplementary SHRIMP U-Pb data for Chapter 6 - 1.39 Ga Biberkine dykes, mount CS16-4

Mount CS16-4 Spot	(2) 206Pb /238U Age		(1) 207Pb /206Pb Age		% Dis-cor-dant	7corr 208Pb* /232Th	±%	(1) 238U /206Pb*	±%	(1) 207Pb* /206Pb*	±%	(1) 207Pb* /235U	±%	(1) 206Pb* /238U	±%	err corr
15WDS16B2R.258B-1	1463	±44	1557	±152	6	-0.15	-99	3.91	3.2	0.096	8.1	3.4	8.7	0.256	3.2	0.4
15WDS16B2R.258B-2	1511	±24	1527	±39	1	0.06	48	3.78	1.7	0.095	2.1	3.5	2.7	0.264	1.7	0.6
15WDS16B2R.266B-1	1380	±36	1320	±197	-5	0.03	97	4.2	2.8	0.085	10.2	2.8	10.5	0.238	2.8	0.3
15WDS16B2R.266B-2	1465	±63	1170	±355	-26	0.14	36	3.98	4.7	0.079	17.9	2.7	18.5	0.251	4.7	0.3
15WDS16B2R.266B-3	1478	±39	1215	±220	-22	0.07	43	3.93	2.9	0.081	11.2	2.8	11.5	0.254	2.9	0.2
15WDS16B1.248B-1	1393	±35	1407	±68	1	0.08	11	4.14	2.6	0.089	3.6	3	4.4	0.241	2.6	0.6
15WDS16B1.248B-2	1503	±22	1365	±61	-10	0.12	7	3.84	1.5	0.087	3.1	3.1	3.5	0.261	1.5	0.4
15WDS16B1.246B-1	1562	±29	1436	±204	-9	0.12	47	3.68	2	0.09	10.7	3.4	10.9	0.272	2	0.2
PHAL.1-1	2159	±65	2029	±64	-6	0.69	93	2.54	3	0.125	3.6	6.8	4.7	0.393	3	0.6
PHAL.2-1	2121	±61	1983	±68	-7	0.59	84	2.6	2.9	0.122	3.8	6.5	4.8	0.385	2.9	0.6
PHAL.3-1	1981	±55	1901	±130	-4	-0.3	-181	2.8	2.9	0.116	7.3	5.7	7.8	0.358	2.9	0.4
PHAL.3-2	1894	±52	1639	±222	-16	-0.44	-183	2.98	2.9	0.101	12	4.7	12.3	0.335	2.9	0.2
PHAL.2-2	2183	±54	2103	±38	-4	0.74	66	2.5	2.4	0.13	2.2	7.2	3.3	0.4	2.4	0.7
PHAL.2-3	2017	±111	1872	±108	-8	-0.05	-1263	2.75	5.5	0.114	6	5.7	8.1	0.363	5.5	0.7
PHAL.2-4	2141	±66	2013	±89	-6	1.07	70	2.57	3	0.124	5	6.7	5.9	0.39	3	0.5
OGC.1-1	3328	±207	3429	±28	2	0.09	173	1.45	3.8	0.292	1.8	27.8	4.2	0.69	3.8	0.9
OGC.2-1	3219	±154	3463	±23	4	0.04	263	1.47	3.3	0.299	1.5	28	3.6	0.68	3.3	0.9
OGC.2-2	3138	±96	3479	±20	6	-0.11	-74	1.49	2.2	0.302	1.3	27.9	2.6	0.671	2.2	0.9
OGC.3-1	0	±76	3460	±12	-4			1.36	2.1	0.298	0.7	30.2	2.2	0.736	2.1	0.9
OGC.3-2	3302	±131	3456	±32	3	0.08	136	1.45	2.4	0.297	2.1	28.3	3.2	0.691	2.4	0.8
OGC.4-1	3300	±118	3472	±14	3	0.06	153	1.44	2.3	0.3	0.9	28.7	2.4	0.693	2.3	0.9

Supplementary SHRIMP U-Pb data for Chapter 6 - 1.39 Ga Biberkine dykes, mounts CS16-2 and CS16-4

Mount CS16-2
Errors are 1-sigma; Pbc and Pb* indicate the common and radiogenic portions, respectively.
Error in Standard calibration was 0.42% (not included in above errors but required when comparing data from different mounts).
(1) Common Pb corrected using measured ^{204}Pb.
(2) Common Pb corrected by assuming $^{206}Pb/^{238}U$-$^{207}Pb/^{235}U$ age-concordance

Mount CS16-4
Errors are 1-sigma; Pbc and Pb* indicate the common and radiogenic portions, respectively.
Error in Standard calibration was 0.46% (not included in above errors but required when comparing data from different mounts).
(1) Common Pb corrected using measured ^{204}Pb.
(2) Common Pb corrected by assuming $^{206}Pb/^{238}U$-$^{207}Pb/^{235}U$ age-concordance

Supplementary SHRIMP U-Pb data for Chapter 7 - 1.13 Ga Bunger Hills dykes, mount CS15-5 (zircon)

Mount CS15-5 Spot	204Pb /206Pb	±%	207Pb /206Pb	±%	208Pb /206Pb	±%	206Pb /238U	±%	% 206Pbc	ppm U	ppm Th	4-corr ppm 206Pb*	4-corr ppm 208Pb*	232Th /238U	±%	(1) 206Pb /238U Age	
BHD1-7A.21Z-1	1.70E-05	71	0.07806	0.65	0.55	0.51	0.465	5.3	0.03	846	1527	141	78	1.86	0.54	1142	±14
BHD1-7A.21Z-2	-2.50E-04	50	0.07832	1.76	0.27	1.69	0.47	3.4	--	101	92	16	5	0.94	0.46	1111	±18
BHD1-7A.21Z-3	7.90E-05	50	0.07786	1	0.47	0.75	0.43	5.8	0.13	365	565	59	28	1.6	0.77	1112	±13
BHD4-7A.104Z-1	---	---	0.07718	1.39	0.17	1.62	0.433	4	0	188	103	31	5	0.57	0.95	1117	±15
BHD4-7A.104Z-2	9.60E-05	50	0.07716	1.1	0.33	4.38	0.444	4.3	0.16	286	329	46	15	1.19	2.88	1112	±13
BHD4-7A.104Z-3	-2.10E-04	58	0.0764	1.87	0.28	3.01	0.421	3.8	--	106	96	18	5	0.94	0.47	1134	±18
BHD1-7A.19Z-1	2.70E-05	71	0.07806	0.83	0.5	0.61	0.443	6	0.05	518	857	84	43	1.71	0.29	1120	±12
BHD1-7A.19Z-2	9.00E-05	100	0.08025	2.12	0.2	2.32	0.439	5.7	0.15	76	50	12	2	0.68	1.01	1085	±19
BHD1-7A.19Z-3	-3.30E-05	100	0.07786	2.05	0.41	1.04	0.445	5.5	--	209	281	34	14	1.39	0.74	1105	±19
BHD4-7B.81Z-1	4.20E-05	50	0.07812	0.73	0.67	0.47	0.485	5.2	0.07	634	1429	105	71	2.33	0.48	1141	±12
BHD4-7B.81Z-2	-3.80E-05	71	0.07877	0.97	0.56	0.75	0.424	4.9	--	387	712	66	37	1.9	0.57	1161	±13
BHD4-7B.81Z-3	----	---	0.07786	0.93	0.75	0.98	0.383	4.8	--	510	1266	84	64	2.56	0.32	1134	±13
BHD1-7B.36Z-1	6.20E-05	45	0.07812	0.79	0.5	0.58	0.447	6.5	0.1	550	915	89	45	1.72	0.82	1119	±17
BHD1-7B.36Z-2	-8.30E-05	71	0.0792	1.44	0.37	1.21	0.42	5.9	--	184	220	30	11	1.23	0.71	1108	±15
BHD1-7B.36Z-3	-3.20E-05	100	0.08062	1.25	0.42	1.67	0.417	3.9	--	222	303	37	16	1.41	0.29	1140	±14
BHD4-7B.66Z-1	1.10E-04	38	0.07923	0.87	0.52	0.63	0.437	5.4	0.18	491	844	81	42	1.78	0.61	1129	±12
BHD4-7B.66Z-2	3.20E-04	21	0.08276	0.82	0.47	0.63	0.43	6.3	0.54	541	832	89	41	1.59	1.12	1132	±12
BHD4-7B.66Z-3	2.90E-05	71	0.07871	1.59	0.63	0.57	0.454	3.7	0.05	445	921	74	47	2.14	0.38	1139	±12
BHD1-7B.41Z-1	4.20E-06	100	0.07639	0.46	0.84	0.28	0.501	6.2	0.01	1551	4390	267	225	2.92	0.85	1177	±15
BHD1-7B.41Z-2	1.20E-04	24	0.07914	0.6	0.64	0.4	0.457	6.4	0.2	987	2046	167	107	2.14	0.89	1156	±15
BHD1-7B.41Z-3	-2.00E-05	100	0.07778	1.01	0.31	1.49	0.415	6.4	--	385	390	63	19	1.05	0.42	1121	±13
BHD1-7A.19Z-4	1.30E-04	58	0.07899	1.47	0.38	1.2	0.428	6.6	0.22	170	216	28	11	1.31	0.58	1122	±15
BHD1-7A.19Z-5	-1.90E-04	58	0.07935	1.76	0.31	1.61	0.406	6.2	--	128	132	21	7	1.06	0.43	1109	±17
BHD1-7A.19Z-6	-3.60E-04	58	0.08099	2.45	0.21	4.26	0.438	6.8	--	59	40	9	2	0.71	1.03	1082	±21
BHD1-7B.66Z-4	1.90E-05	71	0.07641	0.69	0.55	0.75	0.462	4.9	0.03	701	1288	116	65	1.9	0.25	1136	±12
BHD1-7B.66Z-5	5.20E-05	38	0.07829	0.62	0.69	0.44	0.436	6.1	0.09	971	2198	163	113	2.34	1.24	1148	±12

Supplementary SHRIMP U-Pb data for Chapter 7 - 1.13 Ga Bunger Hills dykes, mount CS15-5 (zircon)

Mount CS15-5 Spot	(2) 206Pb /238U Age		(1) 207Pb /206Pb Age		% Dis-cor-dant	7corr 208Pb* /232Th	±%	(1) 238U /206Pb*	±%	(1) 207Pb* /206Pb*	±%	(1) 207Pb* /235U	±%	(1) 206Pb* /238U	±%	err corr
BHD1-7A.21Z-1	1142	±15	1142	±14	0	0.0568	1.6	5.16	1.3	0.0778	0.7	2.079	1.5	0.1938	1.3	0.9
BHD1-7A.21Z-2	1105	±18	1243	±54	12	0.0532	2.9	5.31	1.7	0.0819	2.7	2.125	3.2	0.1882	1.7	0.5
BHD1-7A.21Z-3	1112	±13	1115	±25	0	0.0548	1.7	5.31	1.2	0.0767	1.3	1.992	1.8	0.1883	1.2	0.7
BHD4-7A.104Z-1	1117	±15	1126	±28	1	0.0573	3	5.29	1.4	0.0772	1.4	2.013	2	0.1892	1.4	0.7
BHD4-7A.104Z-2	1113	±14	1090	±29	-2	0.0527	5.4	5.31	1.3	0.0758	1.4	1.968	1.9	0.1883	1.3	0.7
BHD4-7A.104Z-3	1131	±19	1180	±55	4	0.0579	3.8	5.2	1.7	0.0793	2.8	2.103	3.3	0.1923	1.7	0.5
BHD1-7A.19Z-1	1119	±13	1139	±18	2	0.0555	1.4	5.27	1.2	0.0777	0.9	2.032	1.5	0.1897	1.2	0.8
BHD1-7A.19Z-2	1081	±20	1172	±53	8	0.0516	4.1	5.46	1.9	0.079	2.7	1.996	3.3	0.1833	1.9	0.6
BHD1-7A.19Z-3	1102	±20	1155	±42	5	0.0547	2.6	5.35	1.9	0.0783	2.1	2.018	2.9	0.1869	1.9	0.7
BHD4-7B.81Z-1	1141	±13	1135	±16	-1	0.0558	1.4	5.17	1.2	0.0775	0.8	2.069	1.4	0.1936	1.2	0.8
BHD4-7B.81Z-2	1160	±14	1180	±21	2	0.0585	1.6	5.07	1.2	0.0793	1.1	2.158	1.6	0.1974	1.2	0.8
BHD4-7B.81Z-3	1134	±13	1143	±19	1	0.0566	1.6	5.2	1.2	0.0779	0.9	2.065	1.5	0.1924	1.2	0.8
BHD1-7B.36Z-1	1119	±18	1127	±19	1	0.055	2	5.28	1.6	0.0772	1	2.019	1.9	0.1896	1.6	0.9
BHD1-7B.36Z-2	1104	±16	1206	±34	9	0.0545	2.2	5.33	1.5	0.0804	1.8	2.079	2.3	0.1876	1.5	0.6
BHD1-7B.36Z-3	1135	±15	1223	±27	7	0.0569	2.3	5.17	1.4	0.0811	1.4	2.161	1.9	0.1934	1.4	0.7
BHD4-7B.66Z-1	1128	±13	1140	±23	1	0.0559	1.6	5.23	1.2	0.0777	1.2	2.05	1.7	0.1914	1.2	0.7
BHD4-7B.66Z-2	1131	±13	1152	±30	2	0.0551	1.8	5.21	1.2	0.0782	1.5	2.071	1.9	0.192	1.2	0.6
BHD4-7B.66Z-3	1138	±13	1155	±33	1	0.0568	1.5	5.18	1.2	0.0783	1.6	2.086	2	0.1932	1.2	0.6
BHD1-7B.41Z-1	1181	±15	1104	±9	-7	0.0578	1.6	4.99	1.4	0.0763	0.5	2.108	1.4	0.2003	1.4	0.9
BHD1-7B.41Z-2	1158	±16	1132	±16	-2	0.0585	1.8	5.09	1.4	0.0774	0.8	2.098	1.7	0.1965	1.4	0.9
BHD1-7B.41Z-3	1120	±14	1149	±21	3	0.055	2.2	5.26	1.3	0.0781	1.1	2.045	1.6	0.19	1.3	0.8
BHD1-7A.19Z-4	1121	±16	1125	±41	0	0.0549	2.2	5.26	1.5	0.0772	2	2.022	2.5	0.1901	1.5	0.6
BHD1-7A.19Z-5	1102	±18	1246	±50	12	0.054	2.7	5.33	1.7	0.082	2.5	2.122	3	0.1877	1.7	0.5
BHD1-7A.19Z-6	1069	±22	1339	±79	21	0.0506	5.7	5.47	2.2	0.086	4.1	2.168	4.6	0.1827	2.2	0.5
BHD1-7B.66Z-4	1138	±12	1099	±15	-4	0.0564	1.4	5.19	1.1	0.0761	0.7	2.023	1.4	0.1927	1.1	0.8
BHD1-7B.66Z-5	1149	±12	1135	±14	-1	0.0575	1.7	5.13	1.1	0.0775	0.7	2.085	1.3	0.195	1.1	0.8

Supplementary SHRIMP U-Pb data for Chapter 7 - 1.13 Ga Bunger Hills dykes, mount CS15-5 (zircon)

Mount CS15-5 Spot	204Pb /206Pb	±%	207Pb /206Pb	±%	208Pb /206Pb	±%	206Pb /238U	±%	% 206Pbc	ppm U	ppm Th	4-corr ppm 206Pb*	4-corr ppm 208Pb*	232Th /238U	±%	(1) 206Pb /238U Age	
BHD1-7B.36Z-4	9.10E-05	50	0.07859	1.08	0.48	0.79	0.432	4	0.15	305	475	51	25	1.61	0.6	1149	±14
OGC.1-1	6.30E-06	100	0.30005	0.36	0.35	0.48	1.625	4.4	0.01	294	385	175	61	1.35	0.43	3402	±34
OGC.2-1	-1.00E-05	100	0.29877	0.42	0.13	0.97	1.527	4.4	--	186	88	114	15	0.49	0.41	3472	±39
OGC.2-2	---	100	0.29716	0.51	0.14	1.87	1.525	4.7	0	124	66	76	11	0.55	0.92	3464	±43
OGC.3-1	3.20E-05	71	0.29777	0.53	0.12	2.42	1.416	6.1	0.04	123	51	73	9	0.43	1.65	3398	±42
OGC.4-1	9.90E-06	100	0.29841	0.41	0.13	0.92	1.26	4.1	0.01	266	133	166	22	0.52	0.62	3519	±37
OGC.5-1	-3.80E-05	50	0.30015	0.4	0.3	0.63	1.616	4.1	--	199	226	120	36	1.17	0.32	3439	±38

Mount CS15-5 Spot	(2) 206Pb /238U Age		(1) 207Pb /206Pb Age		% Dis-cor-dant	7corr 208Pb* /232Th	±%	(1) 238U /206Pb*	±%	(1) 207Pb* /206Pb*	±%	(1) 207Pb* /235U	±%	(1) 206Pb* /238U	±%	err corr
BHD1-7B.36Z-4	1150	±14	1129	±28	-2	0.0588	1.7	5.12	1.3	0.0773	1.4	2.08	1.9	0.1952	1.3	0.7
OGC.1-1	3316	±69	3470	±6	3	0.1337	15	1.44	1.3	0.3	0.4	28.745	1.3	0.695	1.3	1
OGC.2-1	3484	±102	3464	±7	0	0.2032	53.7	1.4	1.4	0.2989	0.4	29.406	1.5	0.7136	1.4	1
OGC.2-2	3478	±114	3456	±8	0	0.201	54.1	1.41	1.6	0.2972	0.5	29.154	1.7	0.7115	1.6	1
OGC.3-1	3326	±87	3457	±8	2	0.068	117.8	1.44	1.6	0.2974	0.5	28.467	1.7	0.6941	1.6	0.9
OGC.4-1	3641	±150	3461	±6	-2	0.3592		1.38	1.4	0.2983	0.4	29.872	1.4	0.7263	1.4	1
OGC.5-1	3391	±85	3473	±6	1	0.1508	21.5	1.42	1.4	0.3005	0.4	29.206	1.5	0.7048	1.4	1

Supplementary SHRIMP U-Pb data for Chapter 7 - 1.13 Ga Bunger Hills dykes, mount CS15-6 (baddeleyite)

Mount CS15-6 Spot	204Pb /206Pb	±%	207Pb /206Pb	±%	208Pb /206Pb	±%	206Pb /238U	±%	% 206Pbc	ppm U	ppm Th	4-corr ppm 206Pb*	4-corr ppm 208Pb*	232Th /238U	±%	(1) 206Pb /238U Age	
BHD1-4.193B-1	1.30E-03	32	0.086	2.6	0.038	13.5	0.132	2.4	2.3	67	1.1	10	-0.12	0.017	2.1	1068	±35
BHD1-4.193B-2	2.70E-04	71	0.081	3.9	0.008	14.2	0.119	2	0.45	76	1.1	11	-0.02	0.015	2.2	1006	±21
BHD4-1.205B-1	1.70E-03	24	0.104	2	0.104	3.3	0.142	1.1	2.86	107	6	17	0.75	0.058	1.1	1123	±17
BHD4-1.205B-2	3.70E-03	17	0.129	1.9	0.165	4.1	0.169	1.1	6.27	81	4.5	14	0.44	0.058	6	1173	±31
BHD1-4.164B-1	1.30E-04	35	0.08	0.9	0.036	2.2	0.167	0.5	0.21	480	37.3	80	2.59	0.08	0.6	1146	±18
BHD1-4.167B-1	3.20E-04	50	0.083	2	0.028	5.9	0.157	1.6	0.53	92	1.3	15	0.25	0.014	1.9	1138	±15
BHD1-4.167B-2	5.50E-04	27	0.083	1.4	0.029	3.8	0.164	1.1	0.93	168	2.3	28	0.27	0.014	5.3	1155	±13
BHD1-4.179B-1	8.10E-04	25	0.085	2.6	0.029	8.6	0.191	2.4	1.38	110	2.4	20	-0.01	0.022	2.9	1251	±16
BHD1-4.179B-2	1.50E-04	23	0.08	0.6	0.04	3.1	0.196	2.7	0.26	692	63.3	127	4.34	0.094	0.9	1243	±15
BHD1-4.181B-1	2.50E-05	71	0.078	0.8	0.036	1.9	0.147	0.6	0.04	690	61.5	114	4.04	0.092	0.5	1132	±11
BHD1-4.181B-2	1.60E-04	28	0.077	0.8	0.051	5	0.204	4.6	0.27	679	83	127	5.83	0.126	3.9	1268	±23
BHD4-1.209B-1	1.40E-03	20	0.082	3	0.073	7.5	0.221	0.9	2.42	135	13.5	25	0.56	0.103	3.3	1253	±17
BHD4-1.209B-2	2.70E-04	25	0.078	1	0.037	2.2	0.151	1.8	0.45	683	58.8	113	3.11	0.089	1.5	1136	±14
BHD4-1.209B-3	2.10E-04	26	0.08	0.9	0.04	2	0.155	0.8	0.35	703	62.2	116	3.81	0.091	0.7	1137	±14
BHD4-5.115B-1	5.20E-04	38	0.088	2	0.054	4	0.17	3.7	0.87	72	4.9	12	0.43	0.071	6.9	1159	±16
BHD4-5.115B-2	2.70E-03	19	0.125	1.9	0.187	4.2	0.193	1.2	4.49	56	4.3	10	0.91	0.079	1	1190	±20
BHD4-5.117B-1	7.10E-05	50	0.08	1	0.031	2.5	0.164	2.5	0.12	343	20.2	52	1.52	0.061	0.8	1055	±13
BHD4-5.125B-1	1.00E-03	24	0.087	2.9	0.034	4.4	0.163	1.7	1.78	95	2.9	17	-0.07	0.032	1.2	1205	±25
BHD1-4.157B-1	6.30E-05	45	0.078	0.8	0.028	2.2	0.254	1.2	0.11	368	28.5	61	1.61	0.08	0.6	1143	±12
BHD1-4.157B-2	4.40E-05	50	0.078	0.8	0.027	4.7	0.252	1.4	0.07	409	29.8	68	1.75	0.075	0.4	1143	±11
BHD1-4.157B-3	1.50E-04	32	0.079	0.9	0.033	2.2	0.247	1.7	0.25	388	34.3	63	1.72	0.091	0.4	1112	±16
BHD4-1.205B-3	2.20E-04	71	0.081	2.4	0.029	13	0.15	2.3	0.36	69	2.7	11	0.24	0.041	24.8	1107	±16
BHD4-1.209B-4	1.20E-03	23	0.084	1.8	0.067	5.7	0.206	2.9	2.08	127	12.5	21	0.5	0.102	2.4	1163	±16

Supplementary SHRIMP U-Pb data for Chapter 7 - 1.13 Ga Bunger Hills dykes, mount CS15-6 (baddeleyite)

Mount CS15-6 Spot	(2) 206Pb /238U Age		(1) 207Pb /206Pb Age		% Dis-cor-dant	7corr 208Pb* /232Th	±%	(1) 238U /206Pb*	±%	(1) 207Pb* /206Pb*	±%	(1) 207Pb* /235U	±%	(1) 206Pb* /238U	±%	err corr
BHD1-4.193B-1	1078	±37	832	±205	-31	0.113	75	5.55	3.6	0.067	9.8	1.66	10.5	0.18	3.6	0.3
BHD1-4.193B-2	1001	±22	1118	±108	11	-0.144	-77	5.92	2.3	0.077	5.4	1.79	5.9	0.169	2.3	0.4
BHD4-1.205B-1	1119	±16	1204	±154	7	0.112	20	5.25	1.6	0.08	7.8	2.11	8	0.19	1.6	0.2
BHD4-1.205B-2	1176	±30	1107	±256	-7	0.132	26	5.01	2.9	0.076	12.8	2.1	13.1	0.2	2.9	0.2
BHD1-4.164B-1	1146	±19	1142	±25	0	0.078	9	5.14	1.7	0.078	1.2	2.09	2.1	0.195	1.7	0.8
BHD1-4.167B-1	1136	±16	1169	±71	3	0.176	39	5.18	1.4	0.079	3.6	2.1	3.8	0.193	1.4	0.4
BHD1-4.167B-2	1160	±14	1074	±65	-8	0.255	21	5.09	1.3	0.075	3.2	2.04	3.5	0.196	1.3	0.4
BHD1-4.179B-1	1264	±17	1028	±102	-24	0.225	30	4.67	1.4	0.074	5.1	2.17	5.2	0.214	1.4	0.3
BHD1-4.179B-2	1249	±16	1141	±18	-10	0.102	6	4.7	1.3	0.078	0.9	2.28	1.6	0.213	1.3	0.8
BHD1-4.181B-1	1131	±12	1146	±18	1	0.07	7	5.21	1.1	0.078	0.9	2.06	1.4	0.192	1.1	0.8
BHD1-4.181B-2	1281	±24	1052	±24	-23	0.119	8	4.6	2	0.074	1.2	2.23	2.3	0.217	2	0.9
BHD4-1.209B-1	1283	±18	686	±161	-91	0.163	13	4.66	1.5	0.062	7.6	1.84	7.7	0.215	1.5	0.2
BHD4-1.209B-2	1140	±15	1048	±33	-9	0.079	8	5.19	1.3	0.074	1.6	1.97	2.1	0.193	1.3	0.6
BHD4-1.209B-3	1137	±15	1123	±27	-1	0.071	8	5.19	1.4	0.077	1.3	2.05	1.9	0.193	1.4	0.7
BHD4-5.115B-1	1157	±16	1201	±81	4	0.086	18	5.08	1.5	0.08	4.1	2.18	4.4	0.197	1.5	0.3
BHD4-5.115B-2	1181	±18	1357	±174	13	0.187	12	4.93	1.8	0.087	9	2.43	9.2	0.203	1.8	0.2
BHD4-5.117B-1	1049	±14	1183	±23	12	0.045	16	5.62	1.4	0.079	1.2	1.95	1.8	0.178	1.4	0.8
BHD4-5.125B-1	1216	±26	996	±127	-23	0.115	44	4.87	2.2	0.072	6.2	2.05	6.6	0.205	2.2	0.3
BHD1-4.157B-1	1144	±12	1125	±20	-2	0.068	8	5.15	1.1	0.077	1	2.06	1.5	0.194	1.1	0.7
BHD1-4.157B-2	1143	±12	1141	±17	0	0.066	9	5.15	1.1	0.078	0.9	2.08	1.4	0.194	1.1	0.8
BHD1-4.157B-3	1111	±17	1128	±25	2	0.053	10	5.31	1.6	0.077	1.3	2.01	2	0.188	1.6	0.8
BHD4-1.205B-3	1105	±16	1134	±75	3	0.084	42	5.34	1.6	0.078	3.8	2	4.1	0.187	1.6	0.4
BHD4-1.209B-4	1179	±16	826	±135	-45	0.108	11	5.06	1.5	0.067	6.5	1.82	6.7	0.198	1.5	0.2

Supplementary SHRIMP U-Pb data for Chapter 7 - 1.13 Ga Bunger Hills dykes, mount CS15-6 (baddeleyite)

Mount CS15-6 Spot	204Pb /206Pb	±%	207Pb /206Pb	±%	208Pb /206Pb	±%	206Pb /238U	±%	% 206Pbc	ppm U	ppm Th	4-corr ppm 206Pb*	4-corr ppm 208Pb*	232Th /238U	±%	(1) 206Pb /238U Age	
PHAL.1-1	-1.40E-04	50	0.128	1.2	0.005	9.1	0.287	1.6	--	122	1.1	39	0.39	0.009	2.2	2061	±24
PHAL.2-1	8.20E-05	58	0.129	1	0.005	20.5	0.321	0.7	0.12	170	1.5	59	0.14	0.009	2	2178	±24
PHAL.3-1	4.20E-05	100	0.131	1.3	0.007	8.7	0.266	1.3	0.06	103	1.2	30	0.17	0.012	2	1900	±23
PHAL.4-1	-1.00E-04	71	0.128	1.4	0.005	11.5	0.3	3.1	--	71	0.9	22	0.19	0.013	2.3	1986	±26
PHAL.4-2	1.60E-04	50	0.125	1.3	0.006	8.4	0.304	2.6	0.25	81	1.2	26	0.02	0.015	1.9	2034	±25
PHAL.4-3	4.10E-05	100	0.129	1.2	0.006	8.5	0.319	2.4	0.06	84	1.3	26	0.13	0.016	1.8	2022	±25
PHAL.5-1	8.30E-05	71	0.128	1.2	0.006	8.6	0.294	0.8	0.12	103	1.4	33	0.11	0.014	1.9	2036	±25
PHAL.5-2	1.30E-04	58	0.128	1.3	0.006	9	0.291	1.8	0.19	97	1.3	31	0.06	0.013	2	2047	±25
PHAL.5-3	----	---	0.133	1.3	0.005	10.4	0.296	1.6	--	94	1	29	0.15	0.011	2.3	1989	±31
PHAL.5-4	-4.20E-05	100	0.126	1.3	0.006	8.9	0.29	0.8	--	97	1.2	30	0.24	0.013	2	2016	±26
PHAL.6-1	1.00E-04	58	0.127	1.1	0.006	7.8	0.25	1.8	0.15	117	1.5	36	0.1	0.014	1.7	1972	±22
OGC.1-1	1.50E-05	58	0.299	0.3	0.138	0.7	1.442	3	0.02	203	106.8	124	17.09	0.543	0.8	3451	±60
OGC.2-1	6.60E-05	35	0.297	0.4	0.133	0.9	1.356	3.6	0.08	124	60.8	72	9.51	0.506	0.3	3320	±34
OGC.2-2	9.60E-05	33	0.299	0.5	0.155	0.9	1.292	3.5	0.11	94	53.7	55	8.54	0.589	0.4	3371	±36
OGC.3-1	4.20E-05	27	0.299	0.3	0.316	1.4	1.313	3.6	0.05	350	421.4	212	67.36	1.244	1	3441	±35
OGC.4-1	---	---	0.298	0.4	0.153	0.8	1.349	4.1	0	114	64.6	70	10.81	0.584	0.4	3476	±36
OGC.4-2	4.20E-05	45	0.299	0.4	0.265	0.7	1.156	3.4	0.05	122	111.4	68	18.12	0.945	0.3	3226	±46

Supplementary SHRIMP U-Pb data for Chapter 7 - 1.13 Ga Bunger Hills dykes, mount CS15-6 (baddeleyite)

Mount CS15-6 Spot	(2) 206Pb /238U Age		(1) 207Pb /206Pb Age		% Dis-cor-dant	7corr 208Pb* /232Th	±%	(1) 238U /206Pb*	±%	(1) 207Pb* /206Pb*	±%	(1) 207Pb* /235U	±%	(1) 206Pb* /238U	±%	err corr
PHAL.1-1	2056	±28	2091	±24	2	0.132	215	2.65	1.4	0.129	1.3	6.73	1.9	0.377	1.4	0.7
PHAL.2-1	2200	±30	2064	±20	-7	1.286	35	2.49	1.3	0.128	1.1	7.07	1.7	0.402	1.3	0.8
PHAL.3-1	1872	±26	2099	±24	11	-0.965		2.92	1.4	0.13	1.4	6.15	2	0.343	1.4	0.7
PHAL.4-1	1970	±30	2085	±27	6	-0.357	-63	2.77	1.5	0.129	1.5	6.42	2.2	0.361	1.5	0.7
PHAL.4-2	2040	±29	1999	±28	-2	0.198	89	2.7	1.4	0.123	1.6	6.29	2.1	0.371	1.4	0.7
PHAL.4-3	2014	±29	2071	±23	3	-0.128	-127	2.71	1.4	0.128	1.3	6.5	1.9	0.368	1.4	0.7
PHAL.5-1	2032	±29	2062	±25	1	-0.059	-325	2.69	1.4	0.127	1.4	6.52	2	0.371	1.4	0.7
PHAL.5-2	2046	±29	2052	±26	0	0.022	943	2.68	1.4	0.127	1.5	6.52	2.1	0.374	1.4	0.7
PHAL.5-3	1966	±36	2134	±22	8	-0.88		2.77	1.8	0.133	1.3	6.61	2.2	0.361	1.8	0.8
PHAL.5-4	2010	±30	2055	±24	2	-0.019	-1095	2.72	1.5	0.127	1.3	6.42	2	0.367	1.5	0.7
PHAL.6-1	1962	±26	2035	±23	4	-0.274	-61	2.8	1.3	0.125	1.3	6.19	1.8	0.358	1.3	0.7
OGC.1-1	3435	±144	3462	±5	0	0.157	87	1.41	2.2	0.298	0.3	29.14	2.3	0.708	2.2	1
OGC.2-1	3188	±60	3449	±7	5	-0.006	-602	1.48	1.3	0.296	0.4	27.48	1.4	0.674	1.3	1
OGC.2-2	3269	±69	3459	±8	3	0.057	76	1.46	1.4	0.298	0.5	28.21	1.5	0.687	1.4	0.9
OGC.3-1	3411	±80	3462	±4	1	0.161	18	1.42	1.3	0.298	0.3	29.02	1.3	0.705	1.3	1
OGC.4-1	3505	±100	3459	±7	-1	0.222	42	1.4	1.3	0.298	0.4	29.35	1.4	0.715	1.3	1
OGC.4-2	3023	±69	3463	±7	9	0.036	54	1.54	1.8	0.299	0.4	26.74	1.9	0.649	1.8	1

Supplementary SHRIMP U-Pb data for Chapter 7 - 1.13 Ga Bunger Hills dykes, mounts CS15-5 (zircon) and CS15-6 (baddeleyite)

Errors are 1-sigma; Pbc and Pb* indicate the common and radiogenic portions, respectively.
Error in Standard calibration was 0.32% (not included in above errors but required when comparing data from different mounts).
(1) Common Pb corrected using measured ^{204}Pb.
(2) Common Pb corrected by assuming $^{206}Pb/^{238}U$-$^{207}Pb/^{235}U$ age-concordance

Errors are 1-sigma; Pbc and Pb* indicate the common and radiogenic portions, respectively.
Error in Standard calibration was 0.43% (not included in above errors but required when comparing data from different mounts).
(1) Common Pb corrected using measured 204Pb.
(2) Common Pb corrected by assuming 206Pb/238U-207Pb/235U age-concordance